From high-pressure to migmatisation:

On orogenic evolution of the Southern Lepontine (Central Alps of Switzerland/Italy)

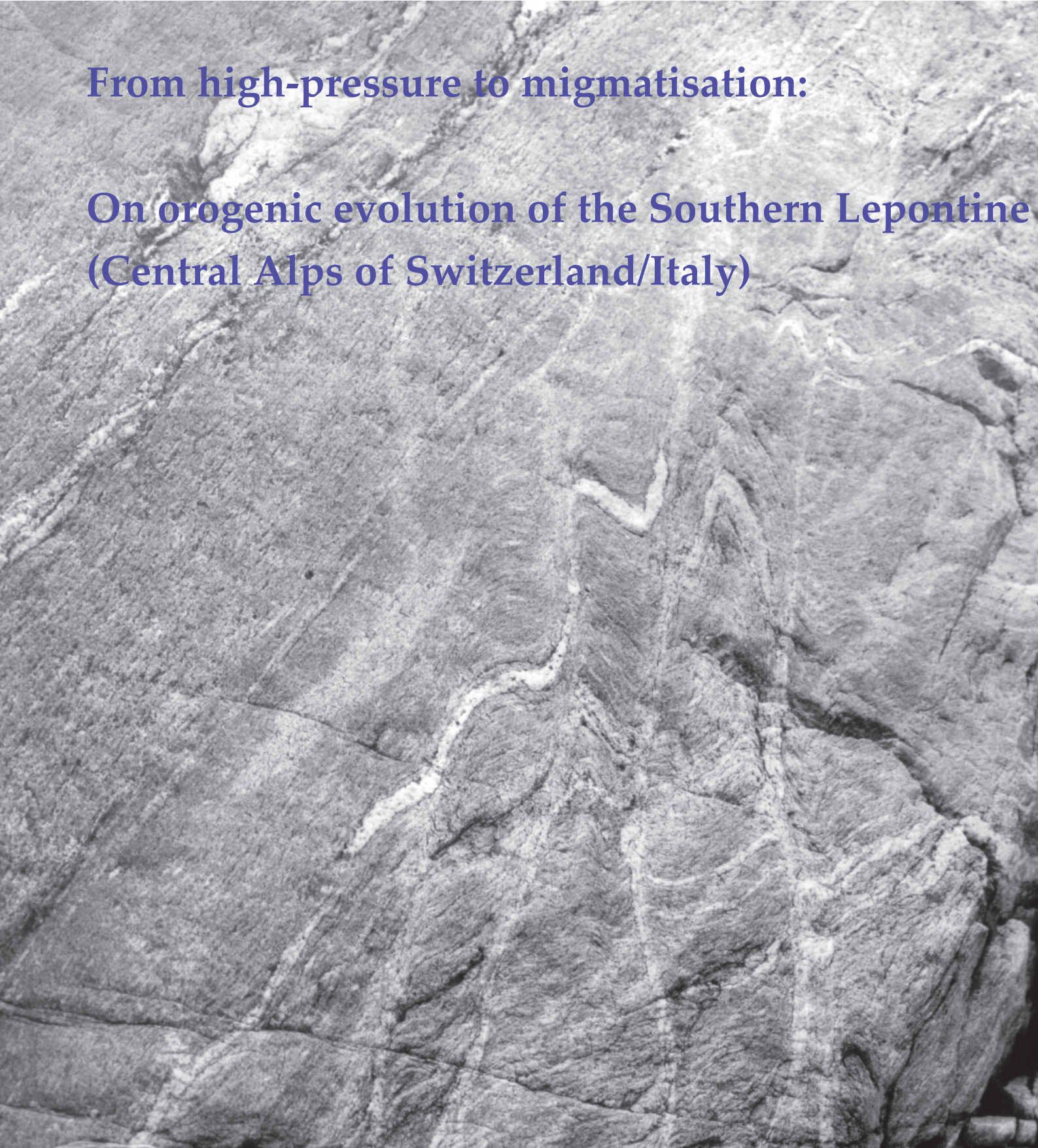

Inauguraldissertation
der Philosophisch-naturwissenschaftlichen Fakultät
der Universität Bern

Thomas Burri, 2005

Verdankungen

Während der inzwischen doch recht langen Zeit am Institut für Geologie haben mir die verschiedensten Leute vom Institut wie auch von ausserhalb des Institutes immer wieder mit Rat, Tat und Zuspruch zur Seite gestanden. Es ist unmöglich alle diese Leute entsprechend zu würdigen, umso mehr möchte ich mich an dieser Stelle bei Ihnen allen recht herzlich bedanken.

Trotzdem möchte ich es nicht versäumen einigen Personen, welche mich im Laufe meiner Arbeit ganz besonders unterstützt haben, einen speziellen Dank zukommen zu lassen:
Zuerst möchte ich mich sehr herzlich bei meinem Arbeitsleiter Alfons Berger bedanken, der sehr viel zu dieser Arbeit beigetragen hat. Sei es im Feld, sei es in den fast täglichen Diskussionen und Streitgesprächen, sei es im durchackern und kommentieren meiner Manuskripte, sei es in überraschenden, scharfsinnigen Kommentaren zum Weinbau oder zum „meaning of life", Alfons war immer mit Rat und Tat zur Stelle.
Martin Engi sei gedankt dass seine Tür immer offen stand für Fragen zur Geologie, insbesondere zur Thermodynamik und dazugehörigen Programmen . Ebenso danke ich Ihm für die sorgfältige Überarbeitung meiner Manuskripte die viel zu deren Verbesserung beigetragen hat.
Ebenfalls bedanken möchte ich mich bei Edwin Gnos, der jede, mir noch so exotische und unbekannte Phase in meinen Dünnschliffen und Gesteinen bestimmen konnte, der immer eine gute Antwort zu all meinen geologischen Fragen wusste, und der mich mit viel Weitblick und Geduld durch das Mysterium „Mikrosonde" geführt hat. Danke auch für deine Menschlichkeit. Fraukje Brouwer sei gedankt für Ihre Diskussionsfreudigkeit und Ausdauer (Capoli), für ihre Tips wenn am Komputer wieder was nicht geklappt hat, und vor allem für Ihre unglaublich sorgfältige und durchdachte Überarbeitung meiner Manuskripte.

Dank geht an meine Kollegen, welche mich auch in meinen stressigen (für mich bisher unbekannt abgelöschten) Stunden ertragen und aufgemuntert haben. Besonders bedankt seien Andreas Ebert, Nadim Scherrer, Dani Traber, Mats Rickli, Ulrich Linden, Valérie Grandjean, Marco Herweg, Guido Schreuers und Werner Zaugg, welche mir auch immer wieder bei den unterschiedlichsten wissenschaftlichen und Informatik-Problemen unter die Arme gegriffen haben. Einen speziellen Dank auch an Urs Eggenberger, der mir bei vielen durchschwitzten Badminton Stunden und dazugehörigen Fehlschlägen und Misstritten ein guter Lehrer und psychologischer Betreuer war. Möge Dir auch in Zukunft der Wind in deine Segel blasen.
Dank gebührt auch Leuten von ausserhalb des Institutes, welche mir mit thermodynamischen Tips (Philip Hunziker und Christian de Capitani), mit Hilfe beim durchforsten von Sammlungen (Ruedi Hänni) und beim Organisieren und Durchführen unserer Ticino-meetings mitgeholfen haben (Hansruedi Pfeifer). Ebenfalls danke ich Roger Rütti, für den regen wissenschaftlichen wie auch persönliche Austausch, und hoffe dass wir wieder einmal im Tessin zusammen Steine klopfen können.

Einen speziellen Dank auch an Paul Gräter und Peter Knup, für ihr immer noch enormes Interesse, für ihre Begeisterungsfähigkeit, und vor allem für Ihre tollen menschlichen Seiten.

Gedankt sei auch dem technischen Team Jüre Megert, Vreni Jakob, Adrian Liechti und Ruth Maeder fürs diskutieren und Rätsel raten, und natürlich auch für die erstklassigen Dünschliffe.

Auch meinen Eltern sei gedankt, die mich immer nach besten Kräften und ohne lange zu fragen unterstützt haben und die auch meine angespannteren Phasen ertragen haben.

Liebe Trix, wir haben es uns wahrlich nicht immer einfach gemacht. Beide eingeklemmt zwischen Arbeit und sehr wenig gemeinsamer Freizeit, einmal angenagt von Selbstzweifel, andererseits wieder top-motiviert wenn endlich was geklappt hat. Ich würde mich sehr glücklich schätzen wenn es uns vergönnt wäre auch einmal eine entspanntere Zeit zusammen zu erleben.

Last but not least danke ich dem Schweizerischen Nationalfond für die finanzielle Unterstüzung dieser Forschungsarbeit (Projekt "Metamorphic Evolution, SNF 2000-063'593)

TOM Burri, im Juli 2004

Zusammenfassung

"Curiosity kills the cat" hiess eine Gruppe aus den 80'Jahren (welche übrigens nie zu meinen Lieblingsgruppen gehörte). Während Neugier für Katzen durchaus gefährlich werden kann (was ist wohl auf der anderen Seite der Stras….) , so sollten sich Forscher jeglicher Gattung zur Neugier verpflichtet führen. Neugier und der Wunsch etwas zu begreifen sind denn auch der wichtigste rote Faden dieser Arbeit. Ein weiterer roter Faden ist sicher die intensive Nutzung von thermodynamischen Programmen; obwohl eine grosse Hilfe um Gesteine und deren Geschichten „verstehen zu lernen", sind sie immer eine grosse Herausforderung und allzuoft Grund grosser Frustration (fight amphiboles!!). Ein letzter Roter Faden stellt das Arbeitsgebiet dar, die Zentralalpen, oder etwas genauer gesagt das Tessin und anschliessende Gebiete. Auch wenn die Zentralalpen nicht in jedem Kapitel von gleicher Wichtigkeit sind, so waren sie doch immer Anlass zu den in dieser Arbeit angestellten Überlegungen und Untersuchungen. In geologischer Hinsicht sind die Zentralalpen noch immer der „Playground of Europe" und werden ihn hoffentlich noch lange bleiben.

Die vorliegende Arbeit gliedert sich in verschiedene Kapitel, deren grosser Zusammenhang nicht immer leicht herauszufinden ist, denen aber immer die drei oben erwähnten roten Fäden zugrunde liegen. Leider, aber wie so oft, konnte nicht alles was man sich vorgenommen hatte auch beendet werden. So ist eine Studie an den Selten-Erden-Mineralien (REE-Mineralien) Monazit, Allanit und Apatit ohne Abschluss geblieben. Eigentlich hätte nur noch wenig zur Vollendung gefehlt, schliesslich lag es aber an der drängenden Zeit dass diese Arbeit wahrscheinlich nie beendet werden wird. Bei anderen Kapiteln dieser Arbeit hat es ebenfalls nicht gereicht alle brennenden Fragen umfassend und abschliessend zu beantworten. Manchmal kam dabei das Gefühl auf, dass eine beantwortete Frage durch zwei neue ersetzt würde. Trotzdem gelang es die Kernpunkte der jeweiligen Problematik einzuengen und zukünftiger Forschung eine erweiterte Grundlage zu bieten. Im nun folgenden Text möchte ich nur ganz kurz und stichwortartig auf die einzelnen Kapitel eingehen. Da ein umfangreiches Inhaltsverzeichnis wenig bis nichts zur Übersichtlichkeit beitragen würde, wird auf ein solches verzichtet.

Kapitel 1 (S 1-27) **On the Alpine migmatite belt of the Central Alps** (*Über den Alpinen Migmatitgürtel der Zentralalpen*)
In diesem Kapitel beschäftigten wir uns mit der schon lange andauernden Diskussion ob in den Zentralalpen ein Migmatitgürtel Tertiären Alters tatsächlich existiert, und wenn ja, in welcher Beschaffenheit. Wie waren die Vorstellungen und Theorien früherer Generationen von Geologen und wie haben sie sich seither verändert? Wie kam es zur Bildung eines Migmatitgürtels, wie ist seine Ausdehnung und in welchem Zusammenhang steht er zur regionalen Tektonik.

Kapitel 2 (S 28-45) **Restite formation by water assisted partial melting in the Central Alps** *(Restit-Bildung durch wasser-saturiertes Schmelzen in den Zentralalpen)*
Dieses Kapitel beschäftigt sich mit der Genese einer auffälligen Gesteinsassoziation in der Valle Onsernone Gegend. Mineral-Pargenesen, Reaktionstexturen und thermodynamische Berechnungen zeigen dass es sich bei den untersuchten Gesteinen um Restite von partiell geschmolzenen pelitischen Gesteinen handelt. Überraschend ist die Erkenntnis das die Gesteine eher ein Produkt von wassersaturiertem Schmelzen sind als ein Produkt von dehydratations-Schmelzen.

Kapitel 3 (S 46-65) **Processes of partial melting in collisional settings** *(Prozesse partiellen Auschmelzens in Kollisions-Orogenen)*
Dieses Kapitel untersucht das Verhalten von drei verschiedenen Gesteinstypen während einer Phase partiellen Aufschmelzens. Die Diskussion benutzt das neue Schmelzmodelle von Holland&Powell, welches erlaubt Phasendiagramme in Schmelz-führenden Systemen zu berechnen. Die Diskussion fokussiert auf die Frage ob und wann partielles Aufschmelzen während eines Subduktions-Zyklus möglich und auch wahrscheinlich ist, und was dabei die massgebenden Prozesse sind.

Kapitel 4 (S 66-82) **Melt segregation and rheology in anatectic collisional systems: a critical review and new concepts** *(Schmelz-Segregation und Rheologie in anatektischen Umgebungen von Kollisionsgürteln: Eine kritische Besprechung und neue Konzepte)*
Schmelzbildung und Segregation, sowie deren Auswirkung auf ein Gestein sind Grundfragen dieses Kapitels. Nach einer Besprechung bestehender Konzepte untersuchen wir Gemeinsamkeiten und Unterschiede von wassersaturiertem- und dehydratations-Schmelzen. Mittels einer ausgedehnten Mohr-Kreis Diskussion wird versucht die Bildung von konkordanten und diskordanten Leukosomen zu ergründen.

Kapitel 5 (S 83-105) **Relics of eclogite facies metamorphism in the southwestern Lepontine area (Central Alps of Switzerland/Italy). A combined discussion on petrology, structures and thermodynamic computation** *(Relikte Eklogit-fazieller Metamorphose im Gebiet des südwestlichen Lepontins (Schweizerische und Italienische Zentralpen: Eine kombinierte Diskussion mittels Petrologie, Strukturen und thermodynamischen Berechnungen)*
Dieses Kapitel untersucht verschiedene Eklogit-Vorkommen im südwestlichen Lepontin. Es untersucht kritisch wie gut die thermodynamischen „state of the art" Modelle sind, und benutzt thermodynamische Berechnungen um komplizierte Reaktionstexturen, verschiedenes Verhalten von Gesteinen während der Exhumation und die PT-Geschichte von ausgewählten Handstücken zu ergründen. Aufgrund der neu untersuchten Eklogit-Vorkommen wird eine neue Verbreitung von Hochdruckgesteine im Lepontin vorgestellt und deren Bedeutung diskutiert.

Kapitel 6 (S 106-126) **Metamorphic evolution of pelitic rocks of the Monte Rosa nappe: Constraints from petrology and single grain monazite age data** *(Metamorphe Entwicklung pelitischer Gesteine der Monte Rosa Decke: Petrologische Befunde und Einzelkorn-Monazit Altersdatierungen) Publiziert in Schweiz. Mineral. Petrogr. Mitt., 81, 305-328, 2001*
In diesem Kapitel wird die Geochronologie der Monte Rosa Decke kritisch durchleuchtet und es werden neue U-Th-Pb-Monazit Alter von Metapeliten präsentiert. Zusätzlich werden neue PT-Abschätzungen der Equilibrierungs-Bedingungen der Gesteine, mittels Multi-Equilibriums-Berechnungen durchgeführt. Diese zeigen zum Teil überraschend hohe Temperaturen für die Monte Rosa Decke, dafür aber keinen Hinweis auf Drücke deutlich über 12 kbar. Eine kombinierte Betrachtung von Mineral-Paragenesen, Altern und PT-Abschätzungen deutet auf eine lange, polyzyklische Metamorphose Geschichte der Monte Rosa Decke hin, im Einklang mit dem Feldbefund.

Kapitel 7 (S 127-142) **Field-relations, deformation and geochemistry of the nappe stack between the Leventina- and Verzasca-Valley** *(Feldbeziehungen, Deformation und Geochemie des Deckenstapels zwischen Valle Leventina und Valle Verzasca)*
In diesem Kapitel besprechen wir die Geologie im weiteren Umfeld des Pizzo Vogorno. Wie lassen sich die verschiedenen tektonischen Einheiten voneinander abgrenzen, wie verhalten sich verschiedene Lithologien derselben tektonischen Einheit während der Alpinen Metamorphose, existieren Hochdruck-Relikte in der Cima-Lunga Einheit auch im Untersuchungsgebiet? Um diese Fragen zu beantworten benutzen wir petrographische, geochemische, strukturelle und thermodynamische Informationen. Ein Resultat der Arbeit ist eine neue Abgrenzung der Maggia-Decke, welche sich im Untersuchungsgebiet weiter nach Norden erstreckt als bisher kartiert.

Kapitel 8 (S 143-150) **Structures of the southwestern Lepontine: A working report** *(Strukturen des südwestlichen Lepontins: Ein Arbeitsbericht)*
Dieses Kapitel untersucht die Strukturen im südwestlichen Lepontin. Das Gebiet ist gekennzeichnet durch verschiedene Syn- und Antiformen, welche in der Gegend von Locarno in der südlichen Steilzone konvergieren. Die verschiedenen Strukturen können im wesentlichen 4 verschiedenen Deformationsphasen zugeordnet werden: (1) Subduktion (2) Delamination und Deckenbildung (3) Rückfaltung (4) Rückaufschiebung. Mehrere geologische Profile helfen die Strukturen besser zu visualisieren.

Summary

„Curiosity kills the cat“ was the name of a band from the 80's (not may favourite band by the way). While curiosity can indeed be dangerous for cats (what's again on the other side of the stre….), curiosity must be an obligation for all types of scientists. Curiosity as well as the wish to understand something, are in fact the most important "file rouge" of the present work. Another file rouge of this study is certainly the intensive use of thermodynamic computation; although a big help to get a better understanding of a rocks history, computation always remains a big challenge, and still too often cause of frustration (fight amphibole!!). A last file rouge represents the study area, the Central Alps, or more correctly stated, the Ticino and adjacent areas. Even though the Central Alps are not in every chapter of the same importance, the always were the cause of reflection and investigation in this study. From a geological point of view, the Central Alps have remained the "Playground of Europe", and hopefully will remain it for another long time.

The presented study is organised into different chapters, the larger context of which cannot always be easily found, which are however all based on the three file rouge mentioned above. Unfortunately, but as usual, not everything could be finished as desired. Notably a study on the rare earth minerals (REE-Minerals) monazite, allanite and apatite has remained unfinished. Although almost finished, the decreasing time has prevented the study from being accomplished. Moreover in other chapters, certain questions of "burning" interest could not be answered in a comprehensive and concluding manner. Sometimes it occurred to me that, having one question answered, I got back two new ones. Nevertheless, we arrived to set the focus on the essential points of the respective subjects and to provide a base for future research. In the following text I will only shortly summarise the different chapters. I have renounced setting up a detailed table of contents, since it would not improve the overview.

Chapter 1 (P 1-27) **On the Alpine migmatite belt of the Central Alps**
In this chapter we deal we the already long-lasting debate on the existence or non-existence of a Tertiary migmatite belt in the Central Alps. How did former generations of geologists interpret the migmatites, and how did concepts change since then? What was the cause of migmatite formation, how extended is the belt, and what is its regional-tectonic context?

Chapter 2 (P 28-45) **Restite formation by water assisted partial melting in the Central Alps**
This chapter deals with the genesis of a suite of conspicuous rocks in the Valle Onsernone area. Mineral assemblages, reaction textures and thermodynamic computation suggest that the rocks represent restites of partially molten pelitic rock. Of some surprise is the recognition that the rocks must have formed during water assisted partial melting rather than by dehydration melting.

Chapter 3 (P 46-65) **Processes of partial melting in collisional settings**
This chapter investigates the behaviour of three different rock types in the course of a phase of partial melting. The discussion takes use of the new melt-model of Holland&Powell, that allows the computation of phase diagrams in melt-bearing systems. We set the focus on the question if and when partial melting is possible or even likely to occur during a subduction-cycle, and which processes are of importance.

Chapter 4 (P 66-82) **Melt segregation and rheology in anatectic collisional systems: a critical review and new concepts**
Melt formation and their bearing on a solid rock are the key questions of this chapter. After a review of current concepts, we investigate similarities and differences of water assisted- and dehydration melting. Using an extended Mohr-circle discussion we try to explain the formation of concordant and discordant leucosomes.

Capter 5 (P 83-105) **Relics of eclogite facies metamorphism in the southwestern Lepontine (Central Alps of Switzerland/Italy). A combined discussion on petrology, structures and thermodynamic computation**
This chapter investigates several eclogite-occurrences in the southwestern Lepontine area. It critically addresses the question how good current thermodynamic models are and it uses thermodynamic computation to investigate complicate reaction textures, the contrasting behaviour of rocks during exhumation and the PT-history of selected samples. Because of the new investigated metaeclogite samples, we propose a new distribution of high-pressure rocks in the Lepontine and discuss their significance.

Chapter 6 (P 106-126) **Metamorphic evolution of pelitic rocks of the Monte Rosa nappe: Constraints from petrology and single grain monazite age data** (Published in Schweiz. Mineral. Petrogr. Mitt. 81, 305-328, 2001)
In this chapter we critically address the geochronology of the Monte Rosa nappe and we present new U-Th-Pb-monazite ages of several metapelites. In addition we estimate conditions of final equilibration of these rocks, using a multi-equilibrium approach. The results indicate in part surprisingly high temperatures for the Monte Rosa nappe, but now evidence of pressures in excess of 12 kbar. Combined observation of mineral assemblages, ages and PT-estimates suggest a protracted, polycyclic metamorphic history for the Monte Rosa nappe, in line with observed field relations.

Chapter 7 (P 127-142) **Field-relations, deformation and geochemistry of the nappe stack between the Leventina- and Verzasca-Valley**
In this chapter we discuss the geology in the wider surrounding of Pizzo Vogorno. How can different tectonic units be separated from each other, how behave different lithologies of the same unit during Alpine metamorphism, do there exist any high-pressure relics also in the Cima-Lunga unit of the study area? To answer these questions, we use petrographic, geochemical, structural and thermodynamic information. One result of the study is a new outline of the limit of the Maggia-nappe, which extends further north then previously suggested.

Chapter 8 (P 143-150) **Structures of the southwestern Lepontine: A working report**
This chapter investigates the structures of the southwestern Lepontine area. The area is characterised by several syn- and antiformal structures, which appear to converge in the Southern Steep Belt near Locarno. The different structures can be attributed to 4 different phases of deformation: (1) subduction (2) delamination and nappe-formation (3) backfolding (4) backthrusting. Several geological profiles allow a better visualisation of the structures of the study area.

On the Alpine migmatite belt of the Central Alps

Thomas Burri, Alfons Berger, Martin Engi

Abstract

This study investigates the Tertiary migmatite belt of the Central Alps of Switzerland and Italy. It starts with a review of concepts and observations on the migmatites from the classical Lepontine nappe stack performed during the last 100 years. We discuss field relations, age and distribution of the Alpine migmatites, using structural, textural and petrologic arguments. Alpine migmatites are generally confined to the Southern Steep Belt (SSB), a regional scale shear-zone of the Central Alps. Migmatites surfacing in the northern part of the Lepontine area are related to pre-Alpine, probably Variscan or older phases of migmatisation, connected to the intrusion of large bodies of granitic to quartz-dioritic composition as well as mafic and granitic dykes. Except for the Bergell and Novate plutons, Alpine igneous activity in the Central Alps is limited to *in situ* migmatisation and to the intrusion of aplitic and pegmatitic dykes and smaller granitoid bodies. Metamorphic conditions had allowed water-assisted melting of granitoid rocks in a large part of the Lepontine, and dehydration melting of muscovite in the eastern part of the study area. PT-conditions were, however, clearly below the limit of dehydration melting of biotite.
We use published data on the Tertiary temperature and pressure field of the Central Alps to delimit the location of various solidi. These calculated predictions were then compared with the observed distribution of migmatites. The resulting patterns indicate that migmatisation and dyke intrusion were possible in an area substantially larger than the muscovite dehydration melting zone, but are in generally limited to the area where fluid-assisted partial melting has potentially occurred. The spatial relationship between the occurrence of migmatites and the SSB indicates that migmatisation and deformation were coupled processes. We suggest that the focused deformation in the SSB led to episodically enhanced fluid flow and this in turn to water-assisted partial melting. The formation of the migmatite belt and its spatial extent were thus delimited by favourable thermal conditions, focused deformation and enhanced fluid flow.

> ***Partielle Anatexis in Teilgebieten des Lepontinischen Gneisskomplexes ist also nach den heutigen experimentellen und nach der Felderfahrung eine vertretbare, noch nicht schlüssig bewiesene Interpretation. Das Thema ist überreif und muss gründlich und kritisch neu bearbeitet werden.***[1]
> *Eduard Wenk (1975)*

Introduction

Migmatisation of the middle crust is usually associated with high ambient temperatures that may lead to the dehydration melting of muscovite, biotite or amphibole. Much effort of the last thirty years has been put into the study of high-temperature migmatite terranes, where migmatisation is related to extended intrusions or to unusually high heat flow. However, in the context of continental collision, particularly high temperatures may not be the main reason for the formation of extensive migmatite terranes. The common association of migmatisation with regional scale shear zones suggests that migmatisation and deformation may be genetically related (Mogk, 1992; Brown and Solar, 1998). Because deformation and fluid flow are often coupled (Etheridge *et al*., 1983; Kerrich, 1986; Ferry, 1994), water-assisted partial melting along such large scale shear-zones may offer a viable explanation for the genesis of these migmatite terranes at comparatively low metamorphic grade.
A migmatite belt, situated to the north of the main tectonic boundary of the Central Alps (the Insubric Lineament), has been recognised for a long time and was attributed to Alpine and/or pre-Alpine metamorphism.
(*Note that we use the word "Alpine" only in its temporal sense; thus the expressions "of Tertiary age" and "of Alpine age" are used as equivalent throughout this study.)*
The obvious spatial relationship between the migmatites and the Southern Steep Belt (SSB) of the Central Alps was already recognised by several of the earlier authors, but was subject to fervent debate in more recent times (see historical review below). The concept of granitisation, which has since been abandoned, brought much confusion into the migmatite debate, also in the Central Alps. In this

[1] *"Concerning the current experimental and field experience, partial anatexis in the Lepontine Gneiss Complex is a viable, but not yet unambiguously proven interpretation. The subject is overripe and must be resumed thoroughly and critically."*

paper we review the migmatite research performed over the last 100 years in the Central Alps, and the evolution of concepts that attempted to explain the observed migmatisation features and the evolution of the migmatite belt.
Despite a wealth of publications on the migmatites of the Central Alps, no attempt has been made previously to describe the migmatite-types and their field relations on the scale of the whole migmatite belt. Several older studies do, however, exactly portray the migmatites occurring in a particular section of the belt (Kobe, 1956; Knup, 1958; Blattner, 1965; Sharma, 1969; Hänny, 1972; Hänny *et al*., 1975; Hafner, 1993).
The present study provides an inventory of the types and spatial distribution of Alpine migmatites in the Central Alps. Using published data on the regional temperature and pressure field in the Central Alps (Engi *et al*., 1995; Todd and Engi, 1997), we construct the predicted regional distributions of water-assisted- and dehydration melting and compare these with the field-inventory. In order to constrain conditions of partial melting in the migmatite belt, we apply amphibole thermobarometry on amphibole-bearing leucosomes.
This information leads to new conclusions on the genesis of the migmatites of the Central Alps and on their relation to the metamorphic and structural evolution of the area.

Geology of the SSB and adjacent areas

The Swiss and Italian Central Alps form an Alpine Barrovian-type metamorphic belt (Niggli and Niggli, 1965; Niggli, 1970; Wenk, 1975; Engi *et al*., 1995). Temperature generally increases from north to south (Trommsdorff, 1966; Frey *et al*., 1980; Engi *et al*., 1995; Todd & Engi, 1997; Nagel *et al*., 2002) reflecting the south-vergent subduction of the European plate below the Apulian plate and the subsequent uplift during continent-continent collision. In detail, PT-relations are complicated due to the relaxation of the isotherms that accompanies deformation and exhumation of the nappe stack (see in Engi *et al*., 2001a). In the internal part of the Central Alps, a moderately dipping nappe-stack is exposed, which forms the metamorphic core of that part of the mountain belt, the so called Lepontine Dome (Fig. 1). The Lepontine nappes consist of basement units, dominated by Variscan granitoids that intruded the metamorphic basement. Several of these nappes also contain migmatites, which are probably genetically related to these intrusives. The most important units in the study area are the classical basement nappes (units) Monte-Rosa, Maggia, Antigorio, Simano and Leventina and the very heterogeneous Adula, Cima-Lunga and Orselina units, which contain abundant HP-metamorphic relics. These latter units were recently interpreted as TAC-units (Tectonic Accretion Channel), thus as exhumed parts of a subduction channel (Engi *et al*., 2001a). The Lepontine Dome structure is bordered to the north and south by elongate steep belts. The east-west striking Southern Steep Belt (SSB), which is a crucial structure in the context of this study, is the location of km-scale back-folding and back-thrusting of the Alpine nappe stack (Milnes, 1974a; Heitzmann, 1987). The whole nappe stack swings from its moderately dipping orientation into upright and even overturned orientations (Fig. 2). The SSB itself has classically been divided into different units, historically called "Zonen" or "Züge" (= elongate, sometimes discontinuous trails) (see e.g. in Kern, 1947; Zawadynski, 1952; Knup, 1958). The SSB bears most convincing evidence of Alpine anatexis and intrusion. The migmatite belt, where pegmatitic and aplitic dykes, meter to decametre-sized granitic bodies as well as *in situ* migmatites are widespread, stretches from the Bergell in the east to Domodossola in the west. Whereas the eastern end is sharply delimited by the Muretto Line (normal fault) (Berger, 1995), the western end is of a more gradual type.
In the south, the belt is truncated by the main shear zone of the Central Alps, the ductile to brittle E-W running Insubric Line (termed Tonale-Line east of Locarno, and Canavese-Line west of Locarno (Schmid *et al*., 1989; Steck and Hunziker, 1994; Schärer *et al*., 1996). This shear zone separates the low-grade (Alpine) metamorphic and only moderately deformed southern block (Apulian plate, Southern Alps) from the high-grade metamorphic area (European plate, Central Alps) to the north. North of the Insubric Line, metamorphic grade reached amphibolite-facies conditions on a regional scale (Trommsdorff, 1966; Wenk, 1970; Niggli, 1970; Engi *et al*., 1995), but relics of eclogite and granulite facies occur inside the TAC-units (Droop and Bucher-Nurminen, 1984; Trommsdorff, 1990; Pfeifer *et al*., 1991; Tóth *et al*., 2000; Brouwer, 2000; Grandjean, 2001; Engi *et al*., 2001a; Dale and Holland, 2003). West of Locarno the Insubric Line bends towards the southwest, whereas the SSB maintains its roughly E-W direction (Steck, 1984; Heitzmann, 1987; Schmid *et al*., 1989) (Fig. 1). The opening gap between the SSB and the Insubric Line is taken up by the Sesia-unit.
The Insubric Line did not correspond to the main boundary during subduction and back-thrusting, but rather transects this older element (Schärer *et al*., 1996). The ductile main shear-zone during back-thrusting parallels the SSB and will be termed Arcegno-Palanzeno Shear-zone in this work (Fig. 1). Due to major displacements along the younger ductile to brittle Insubric and Centovalli Lines, amphibolite-facies fabrics and assemblages in the SSB were locally severely overprinted by greenschist-facies brittle deformation.

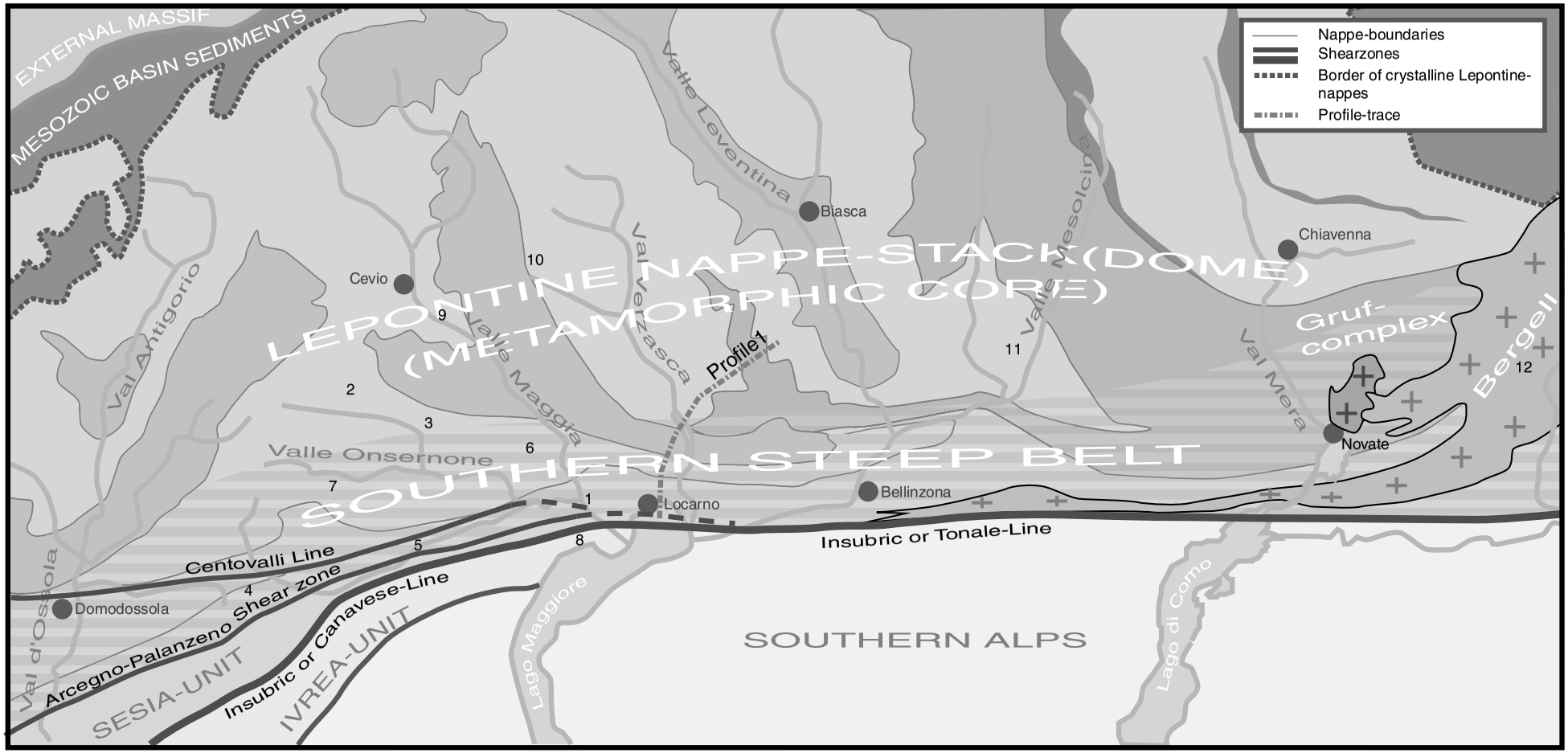

Fig. 1) Tectonic overview of the Central Alps. Numbers refer to localities described in the text: 1-Ponte Brolla, 2-Alpe Ribia, 3-Gresso, 4-Santa Maria Maggiore, 5-Camedo, 6-Capoli, 7-Bagni di Craveggia, 8-Arcegno, 9-Riveo, 10-Alpe Sambucco, 11-Verdabbio, 12-Bagni di Masino. Tectonic units are denoted as thin continuous lines for orientation.

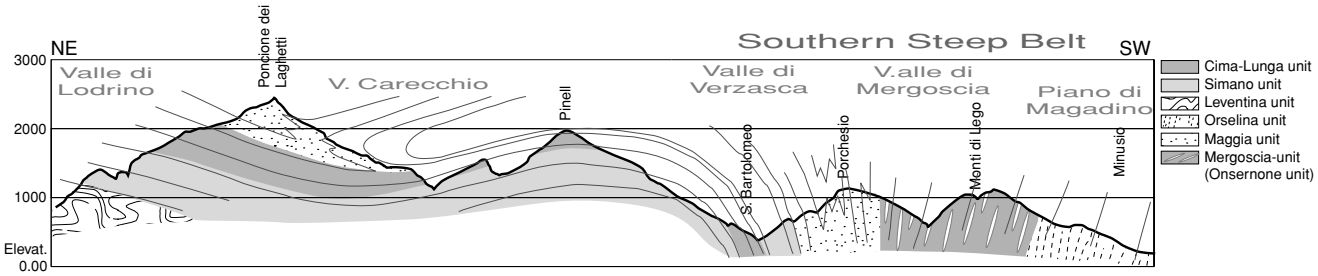

Fig. 2) Profile through the Southern Steep Belt. See figure geologic overview for profile-trace. The profile is partly based on an unpublished sketch by E. Wenk and improved with data from recent studies (Gruskovnjak, 2002; Leonardi, 2003).

Historical aspects of Alpine migmatisation

"We define granitisation widely as the process by which solid rocks are converted to rocks of granitic character; this includes all such processes as Palingenesis, Syntexis, Transfusion, Permeation, Metasomatism, Migmatization, Injection, Assimilation and Contamination, as used by various authors, but rarely with well defined meanings".

Malcom Mac Gregor and Gilbert Wilson (Mac Gregor and Wilson, 1939, p. 194)*), cited in* (Read, 1957).

See also the glossary of historical migmatite terms in the Appendix.

Preface

There has been a long and fascinating debate on the age and genesis of granitic and migmatitic rocks of the Central Alps, for more than a hundred years now. In the course of the evolution of thought, individual interpretations reflected the knowledge of the time, or the preferred hypothesis of the respective working groups (and usually of their leaders). The study of migmatitic rocks in the Central Alps mirrors the hot discussion on granite genesis held at the same time in the rest of the world, and which culminated in the well known "granite controversy" (Read, 1957; or see review in Pitcher, 1997).

As elsewhere, different concepts existed in the Alps to explain the genesis of the migmatitic and granitic rocks that were found in the pertinent study areas. Whereas the Basel school, under M. Rheinhard and E. Wenk who were inspired by fieldwork performed in extensive migmatite terranes of Greenland, became defenders of granitisation theory (transformists), other prominent protagonists like P. Niggli of the Zürich-working group held a more conservative, magmatic view (magmatists).

However, when reading the above quotation from Mac Gregor & Wilson (1939), it appears that granitisation was an almost universal concept that could include processes as different as metasomatism and magmatic injection. In the absence of experimental data, ideas on the genesis of migmatitic rocks remained vague and contradictory. The academic trench that divided Switzerland at that time, and which was symptomatic for the dispute elsewhere in the world, was ironically described as part of the Swiss federalistic system by Eduard Wenk (1966).

The migmatisation-debate declined after the retirements of the main actors from the stage of (Alpine) migmatisation. Max Reinhard retired in 1952, Paul Niggli in 1953 and Eduard Wenk as the last actor (officially) in 1973. *(Final conclusions of P. Niggli can be found in his speech to the Schweizerische Mineralogisch-Petrographische Gesellschaft in 1950* (Niggli, 1950)*, those of Wenk are summarised in* (Wenk, 1975)*, again a speech to the same society, but 25 years later.*

Historical review

Probably the first geologists to describe the migmatites from the SSB were G. Klemm and U. Grubenmann in the first decade of the 20th century (Klemm, 1906/1907; Grubenmann, 1910). The first thesis on the subject was written but a few years later by one of Grubenmann's students (Gutzwiller, 1912). These early authors clearly recognised the exceptional nature of the migmatitic rocks, and described them as "Injektionsgneise"," Lagen und Adergneise", "Bändergneise" and "Mischgneise" (injection gneisses, veinites and arterites, banded gneisses and mixed gneisses; see glossary in the appendix for explanations of no longer used expressions). They also mentioned the abundance of aplitic and pegmatitic dykes occurring in the "root-zone" (i.e. the SSB) of the Alps. Gutzwiller recognised the distinct structural position of the "Injektiongneise" when he stated that: "...herrschen im Verzasca- und im Maggiatal, hauptsächlich in deren südlichen

[2] *"...pronounced banded gneisses predominate especially in the southern parts of Valle Verzasca- and Valle Maggia. In Valle Ticino near Bellinzona, they are restricted to the small area between S. Crocifisso and Pedivilla. Because of the striking contrast between the northerly adjacent orthogneisses (Alpine basement nappes) and the southerly adjacent schists of the Seegebirge (only weakly metamorphic Southern Alps), and because of their unique character, these banded gneisses appear to be special formations."*

Teilen, ausgeprägt gebänderte Gneise, welche im Tessintal, in der Umgebung von Bellinzona, nur auf die kleine Strecke zwischen S. Crocifisso und Pedivilla beschränkt sind. Infolge der auffallenden Differenz gegenüber den nördlich davon gelegenen Orthogneisen sowie den südlich sich anschliessenden Schiefern des Seegebirges und ihres höchst eigenartigen, individuellen Charakters scheinen diese gebänderten Gneise besondere Bildungen zu sein..." [2]. Note that the Insubric Line was not yet recognised as the main suture between Europe and the Adriatic indenter. Gutzwiller thus described the existence of distinct migmatitic rock types (banded gneisses or injection gneisses) mainly in the southern parts of the larger Ticino Valleys, the area now termed Southern Steep Belt, but did not address their formation-age. An extraordinary explanation for the youngest magmatic activity (mainly in the Bergell area) was proposed by (Hugi, 1922), who concluded that the intrusive rocks originated from granitic liquids, that were extracted from not yet fully crystallised Variscan magmas. A few years later, an Alpine age was proposed for pegmatitic and aplitic dykes in the SSB and the southern parts of Valle Mesolcina and Val Calanca based on structural arguments (Kündig, 1926). When in the 1930's the relationships between the Alpine pegmatites and the probably Mesozoic calcsilicates and marbles (at Castione) were studied (Mittelholzer, 1936), the clear cross-cutting of metasediments by pegmatites were taken as proof that the dykes could be no older than Mesozoic, and probably dated from the Tertiary.

In the same period, several statements favouring an Alpine migmatite belt were given in textbooks and papers. H. Preiswerk, who mapped an exceptionally large part of the Ticino area, stated that unequivocally Mesozoic sediments at Castione and on Alpe Drosina sura (Val Drosina) were discordantly cut by pegmatitic dykes and "am Kontakt mit den Gängen sind die Marmorschichten oft in auffälliger Weise emporgebogen"[3] (Preiswerk, 1925a). P. Niggli confirmed that Alpine to post-Alpine pegmatites and "dyke-injections" occurred on a regional scale in the root-zone (=SSB) of the Central Alps (Niggli, 1950), but he rejected the view that these dykes where produced *in situ* ("keineswegs als Exsudate an Ort und Stelle zu deuten"[4]). However, an unequivocal formulation of the migmatite forming processes in the SSB obviously troubled him very much: "Mehr unregelmässiges, fast schlierenartiges Auftreten massiger bis pegmatitischer Strukturen (Entstehung interner Exsudate) und nur lokal vorhandenes, wenig weitreichendes Abquetschen von an molekulardisperser, schmelzartiger Phase angereichertes Material in das Nebengestein darf nicht fehlen, selbst wenn von einer allgemeinen Umschmelzung keine Rede ist ..."[5] (Niggli, 1950). It becomes evident from these lines how vague the concepts of migmatite formation were at that time, when few experimental data were available, and the granitisation theory was at its climax. Niggli's seemingly bewildering description probably reflects his insecurity. It was not until the 1960's, that experimental data of Winkler and of Willy started to clarify the confusion (reviews in Winkler, 1979; Pitcher, 1997). Reading between the lines, we suppose however that P. Niggli held a relatively conservative view on the extent and distribution of Alpine migmatisation, similar to the conclusions of Gutzwiller. Although approving the existence of Alpine dykes and probably of Alpine *in situ* leucosomes in the SSB, he clearly rejected extensive granitisation of the Lepontine area, as it was at the time proposed by the Basel group. The latter group, led by Max Reinhard and Eduard Wenk, started research in the Lepontine area in the forties and fifties of the last century. Influenced by the concepts of granitisation theory and by fieldwork performed in extensive migmatite terranes of Greenland, they interpreted large tracts of the Lepontine as (metasomatically) granitised old basement units (Wenk, 1953; Günthert, 1956; Wenk, 1962). In 1953 E. Wenk stated: "Im Bereich des tieferen Penninikums wurde die praetriadische Gesteinsunterlage im Verlaufe der Alpenfaltung umgeformt und z.T. auch metasomatisch verändert. Die Gesteinsumwandlung erreichte im Unterbau das Ausmass einer Ultrametamorphose: reaktivierte, möglicherweise auch juvenile, granitische und pegmatitische Schmelzlösungen wurden aus dem Untergrund ausgepresst, stiegen während der Gebirgsbildung als kristallbreiartige Kernmasse in die sich entwickelnden Antiklinalstrukturen empor und kamen so in Kontakt mit alpin-metamorphen praetriadischen Hüllgneissen und auch mit Mesozoikum."[6] (Wenk, 1953). This theory was partly based on the important reconnaissance work of E. Wenk, in which he recognised that the whole Lepontine area had experienced intense recrystallisation during Alpine deformation and metamorphism. He concluded that structures ob-

[3] *"..at the contact with the dykes, the marble layers are often bent up in a conspicuous fashion."*

[4] *"...should in no way be interpreted as in situ exsudates"*

[5] *" The occurrence of more irregular, almost schlieren-like massive to pegmatitic structures (development of internal exsudates (see glossary in the Appendix)) and of only locally occurring and locally produced material, which is enriched in a (molecular) dispersive, melt-like phase and was squeezed out into the country rock, are ubiquitous, even though one cannot call it complete fusion."*

[6] *"In the domain of the lower Pennine nappes, the pre-Triassic basement has been transformed and also in part metasomatically alterated in the course of the Alpine orogenesis. Metamorphism in the deepest domains reached the degree of ultrametamorphism: reactivated, probably also juvenile, granitic and pegmatitic melts were squeezed out of the underground, moved upwards during orogenesis as cores made of a crystal-mush into the developing anticlinal structures, and thus came into contact with Alpine metamorphic pre-Triassic mantle-gneisses and also with Mesozoic sediments."*

served inside the nappes dominantly reflect Alpine orogenic processes. This led him to interpret the Maggia-nappe as an Alpine granitised area with two main intrusives complexes, the Cocco- and Ruscada-granitoids (Wenk, 1962). The interpretation is also based on additional structural and petrographic arguments: Like the SSB, the Maggia-nappe forms a steep zone (Maggia-Synform), trending however roughly NW-SE, as opposed to the E-W striking SSB. The association of steep structures, intrusion and migmatisation in the Maggia steep zone as well as in the SSB, led Wenk to conclude that the Maggia-Steep-Zone is comparable in origin to the SSB and that the Maggia intrusives (Cocco, Ruscada and Matorello) are genetically linked to the intrusives of the SSB (Bergell and Novate). Wenk argued that the steep structures of the SSB and the Maggia-Steep-Zone had enhanced thermal fluxes which, as a consequence, caused migmatisation and granitisation (Wenk, 1970). These interpretations were (apparently) confirmed by and in part dependent on studies performed by some of his students (Günthert, 1954; Günthert, 1956; Sharma, 1969).

Wenks view did not remain undisputed. Although Niggli (in Cadisch, 1953) and Niggli&Niggli (1965) agreed with the possibility of Alpine migmatisation in the SSB, they rejected Wenk's ideas regarding the Maggia nappe when realising that its migmatites and intrusives had been deformed during the Alpine orogeny. The same holds for the migmatite outcrops at Lavertezzo, which were interpreted as Alpine (Sharma, 1969). Other authors completely denied the existence of Alpine migmatites (Zwart, 1967; Milnes, 1969). These authors, both structural geologists, based much of their interpretation on the petrographic study of Niggli&Niggli (1965). In light of the actual statements of the latter authors however, it seems plausible that Milnes and Zwart may have misinterpreted some of the arguments, probably because of the confusing terminology used in the migmatite debate at the time.

The rise of isotopic age determinations, from the 1960's, first could not contribute much to the migmatisation problem. Many analyses were performed using the Rb-Sr and K-Ar methods on whole rocks powders or on mica and feldspar aliquots. Results from mineral aliquots were interpreted in terms of cooling ages. These could therefore only provide a minimum age for the Alpine migmatisation, which must have occurred above the isotopic closure temperatures of the investigated systems (see review of available data in Hunziker *et al*., 1992).

However, Wenk's conclusions were severely challenged by the studies of Blattner (1965) and of Hänny (1972) and Hänny *et al*. (1975), who concluded that Alpine anatexis could not be responsible for the schollen-type migmatites of their study area (Valle Bodengo, Italy). In their view Alpine anatexis was restricted to the intrusion of small granitoid bodies and dykes and to leucocratic veins and pods, because they observed clear discordances between these and the Alpine structures. U-Pb monazite and Rb-Sr whole-rock and mineral age determinations, yielded a pre-Alpine age for the schollen-migmatites (discordant Variscan and pre-Variscan ages) and an Alpine age (22-23 Ma) of metamorphism (Hänny *et al*., 1975). An Alpine age of the veins and pods could neither be definitely confirmed nor rejected, due to inadequacies inherent in the Rb-Sr isotopic system.

Over time, Eduard Wenk, without explicitly stating it, changed his mind regarding the extent of Alpine granitisation in the Central Alps. His distribution-maps of Alpine intrusives and migmatites (Wenk, 1970) drew a picture far different from the "ultrametamorphosed" Lepontine Dome of his earlier studies (Wenk, 1953; Wenk, 1962; Wenk, 1966). Influenced by the new experimental and isotopic studies, he no longer explicitly mentioned granitisation, but more often spoke of anatectic processes (Wenk, 1970; Wenk, 1975). Wenk's late interpretations were no longer very different from those of other authors or even from P. Niggli's interpretations, 25 years prior. Whether migmatite areas outside the SSB were an Alpine product appeared no longer so unequivocal (see first citation of this contribution Wenk, 1975). It was probably this turn around in Wenk's-thinking that finally led to his rather resigned statement: " Ich habe von Haus aus keine Aversion gegen Anatexis und Migmatite, und das ist in der Schweiz viel, fast zu viel!"[7] (Wenk, 1975).

In the light of new experimental results and age determinations, granitisation theory had to be discarded as an explanation for the migmatites in the Central Alps. The final blow to granitisation theory was probably dealt by Mehnert (see discussion in Winkler, 1979)) who stated that "granitisation...took place, on the whole, without the addition of alkalis", thus without the need of any metasomatic process, that was the fundament of the granitisation concept.

Fig. 3) Discordant aplite, crosscutting deformed pre-Alpine migmatites at Lavertezzo (Valle Verzasca). Hammer for scale.

[7] *"Based on my scientific formation, I carry with me no aversion against anatexis and migmatites. This is much, almost too much in Switzerland."*

In the following years, other geochronologic studies performed on retentive minerals such as monazite and zircon indicated a mainly Variscan age for the granitoid bodies of the Lepontine nappes (Köppel *et al*., 1980, and references therein). For the intrusives of the Maggia nappe (Cocco, Ruscada and Matorello granitoids), discordant U-Pb ages of monazite and zircon indicated an intrusive age of ca. 300 Ma (upper intercept), and Alpine metamorphism at 20-27 Ma (lower intercept and concordant ages of monazite and zircon) (Köppel and Grünenfelder, 1975; Köppel *et al*., 1980).
Köppel & Grünenfelder (1975) provided the first unequivocal time-mark for intrusive processes in the SSB. Based on concordant U-Pb monazite ages they concluded that the emplacement of the Bergell intrusion had occurred at 30 Ma, and the intrusion of the smaller Novate granite at 26 Ma (In contrast to other authors, they interpreted the obtained monazite ages as crystallisation ages and no longer as cooling ages). Because migmatisation processes appear to be coupled with the emplacement of these plutonic bodies, ages in the order of 30-26 Ma could now be suggested for the age of migmatisation. More recently, an age of ca. 31 Ma (U-Pb and Th-Pb ages on zircon and allanite) was obtained by von Blanckenburg (1992).
Unambiguous confirmation of the Alpine age of the discordant pegmatitic and aplitic dykes in the SSB and adjacent areas has since been published. Oligocene ages were obtained for discordant dykes and veins of the SSB (26-29 Ma), and a Miocene age of 20 Ma for a discordant dyke at Lavertezzo (lower intercept age, see Fig. 3) (Schärer *et al*., 1996; Romer *et al*., 1996). The same studies demonstrated that the migmatites of Lavertezzo, interpreted earlier as Alpine anatectic products (Sharma, 1969), yielded an age of 280-290 Ma, and are therefore related to the Variscan orogeny. An age of 32 Ma was obtained for a leucosome in the Alpe Arami area, and an age of 25 Ma for a pegmatite a few kilometres NE of Bellinzona (summarised in Gebauer, 1999). Dykes are therefore similar in age to the Novate intrusive body (Köppel *et al*., 1980). These results unequivocally established that Alpine migmatisation processes had indeed taken place in the SSB.

Migmatites in the Central Alps

General overview

Migmatitic rocks of the Central Alps crop out in the External Massifs (Aar, Gotthard), the Lepontine nappes, the Southern Alps and the Sesia-unit. Metamorphic studies, performed over the 20th century, revealed that Alpine migmatisation did not occur in the External Massifs, the Sesia-unit or in the Southern Alps, because only moderate temperatures were reached during the Alpine metamorphic overprint in these areas (overview in Frey *et al*., 1999). In recent decades, isotopic age determinations have confirmed Variscan to Caledonian ages for metamorphism and associated migmatitic and intrusive activity in the External Massifs and the Southern Alps. Even though Alpine metamorphism was pressure accentuated in the Sesia-unit, metamorphic temperatures did not reach conditions of partial melting, and isotopic results again indicate pre-Alpine ages for its intrusive activity (comprehensive reviews can be found in von Raumer and Neubauer, 1993; Frey *et al*., 1999)).
Based on structural and petrologic arguments, it has been known for a long time that the intrusive and magmatic history of the External Massifs must be of pre-Alpine age. It was therefore no surprise to find a similar history in the southward adjacent basement units. However, the high degree of deformation and metamorphism in the Lepontine area, as well as the very reduced and fragmentary sedimentary record, complicate the discrimination of old migmatitic basement from "young" Alpine migmatites.
Despite the generally high grade of deformation and metamorphism, the pre-Alpine history of the Lepontine nappes can be deciphered to some extent in the field. Some nappes like the Leventina and Antigorio units are dominated by granitoid gneisses (Variscan intrusives) which locally exhibit intrusive relationships with an older basement. Other nappes like the Maggia, Simano, Tambo and the Suretta units are composite nappes, consisting of a probably pre-Variscan basement, intruded by Variscan granitoids. Stromatic to nebulitic or melt-rich agmatic migmatites are associated with these intrusives and are locally well preserved as for example in the Simano and Maggia units (Sharma, 1969; Wenk, 1970; Wenk, 1975), in the Suretta unit (Nussbaum *et al*., 1998) and in the SSB (Blattner, 1965; Hänny, 1972)).

Features of migmatisation and intrusion

In this paragraph we document the different types of migmatites and intrusive rocks attributable to Tertiary metamorphism in the Central Alps. We describe rocks characteristics and evidence of partial melting that can be observed from the outcrop to the thin section scale.
Migmatites in the SSB can be divided into three classes, from small to large:

a) Small-scale melt-segregation into *in situ* leucosomes (centimetres to decimetres).
b) Medium-scale melt-segregation into pods, zones or small bodies (decimetre to metre-scale).
c) Dykes (pegmatites and aplites) and larger granitoid bodies.

Note that transitions between these types are often gradual and that evidence of former melt may also be found on the grain scale.

a) Small scale melt-segregation of in situ leucosome

Small-scale melt-segregation processes are observable from the segregation into melt pools between adjacent grain boundaries up to the segregation into centimetre to decimetre size pockets and veins. In the last few years several authors have demonstrated how the presence of former melt can be inferred from the study of thin sections (Vernon, 2000; Sawyer, 2000; Rosenberg and Handy, 2000; Sawyer, 2001; Rosenberg, 2001). Straight grain boundaries may indicate undisturbed growth of a mineral into a melt. Thin films of quartz or K-feldspar along two-grain boundaries or triple junctions may reflect the localities of final crystallisation of melt. Another characteristic is the filling of transgranular fractures by quartz and K-feldspar, interpreted as a former filling of melt subsequent to grain fracturing.

Many examples of such features can be found in stromatic migmatites like sample Bor1 (Fig. 4). A scan of a circular rock slab (Ø 2.5 cm) shows that the rock is differentiated into a leucosome-rich domain, consisting mainly of Kfs + Pl + Qtz, and a gneissic domain consisting of Pl + Qtz + Kfs + Bt (Fig. 4). Biotite in the leucocratic domain appears refractory, except for a few small, hypidiomorphic grains, which are interpreted as neoformations in the melt. Gneissic domains are only slightly enriched in plagioclase, while Kfs as well as Qtz remain present. Figure 4A shows the relatively coarse grained and only slightly deformed leucocratic domain, which we interpret as crystallised melt. The white arrow points to an idiomorphic K-feldspar corner, lined by a thin film of quartz-grains on the lower straight grain boundary. The rest of the grain has more irregular grain boundaries, locally affected by myrmekitisation. Similar textures (except for myrmekites) can be observed for plagioclase. Except for slightly undulose extinction of quartz, deformational features are absent from this leucocratic domain.

Figures 4B and 4C are from the gneissic domain, where grains are typically smaller, but still remain in the order of millimetres, due to enhanced recovery at high temperatures. Micas, feldspar and quartz show a clear SPO, which defines the main foliation (Fig. 4B, foliation from lower left to upper right). At higher magnification, evidence of former melt can also be found in the gneissic domains (Fig. 4C). Arrows indicate sites of former melt, now present as small grains of mainly K-feldspar and quartz, which are situated along two-grain boundaries and triple junctions. Note the rounded habit of many grains, which may be an effect of their disso-

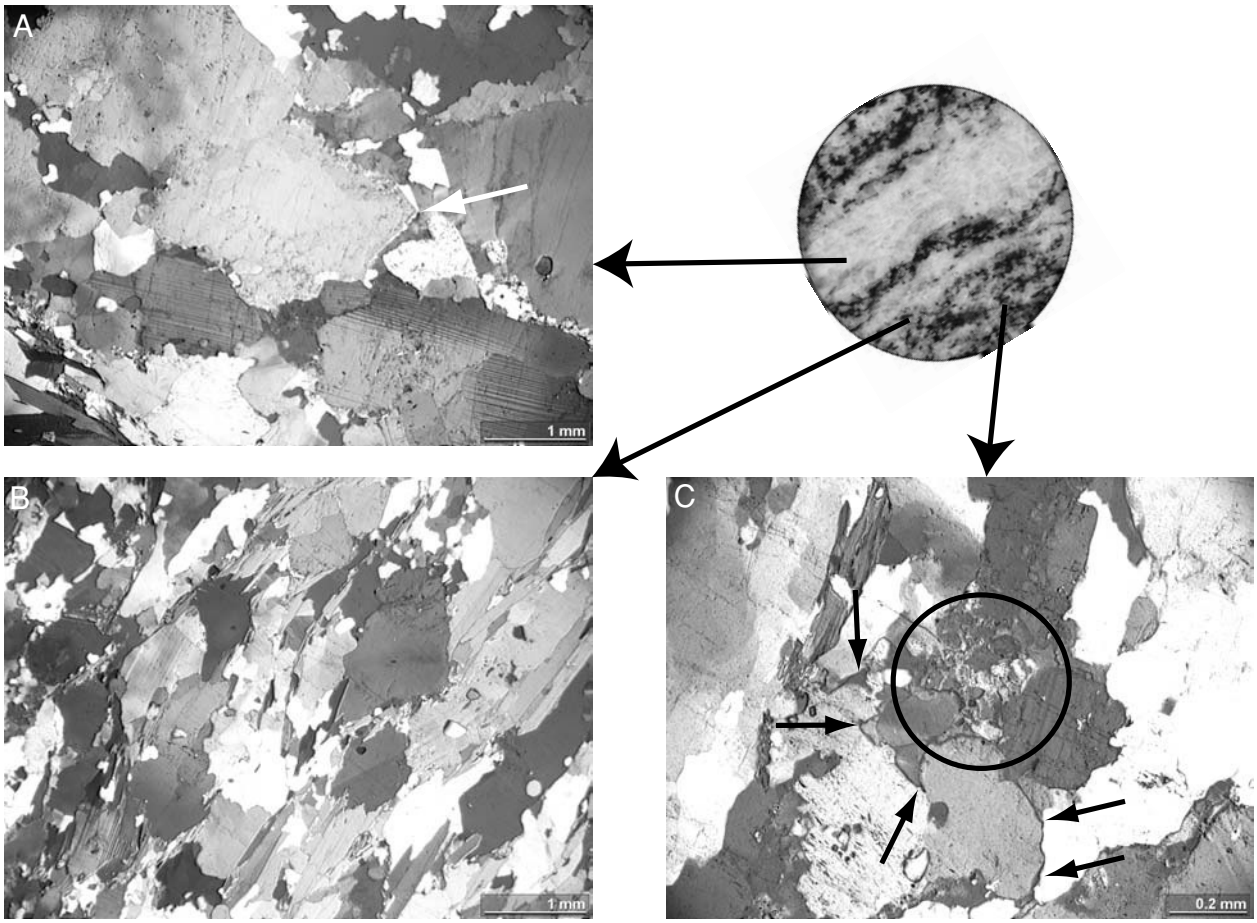

Fig. 4) Migmatites in thin section (Bordoglio, Valle Onsernone). Figures A-C depict different domains of the sample (see text for explanation). Width of circular slab is 2.5cm.

lution during partial melting. The circle indicates an area, where a K-feldspar grain was cataclastically deformed, after which the voids were filled with melt.

Whereas grain scale segregations are usually too small to be detected in the field, melt pockets and veins are frequently observed in the SSB. Figure 5 displays a typical sample from stromatic migmatites from the Valle Onsernone area. Whereas some leucosome was able to segregate into coarser grained patches (right hand side of photograph), others remained near the very site of melting, forming elongate quartz and feldspar-enriched areas parallel to the foliation (white arrows). This indicates that melt was present throughout the rock, but that only a certain fraction has segregated on the sample scale. Note that the transition from leucosome to host rock is often diffuse (upper part of larger segregation to the right). Leucosome segregations are often rimmed by elongate or more lump-like aggregates of biotite (black arrows), which suggests that the melt was locally-derived, and has left behind refractory biotite. Figure 6 shows the appearance of such small-scale melt segregations inside a stromatic migmatite in outcrop. Melt has segregated into mainly foliation parallel, elongate patches and veins. Again, leucosomes are rimmed by biotite-rich areas and are typically coarser grained than the host rock. We emphasise that often observed foliation parallel segregation of melt is not an evidence for the pre-Alpine age of migmatite formation. The typically coarser grain size and the preservation of subtle transitions between leucosome and hostrock reveals the Alpine age of migmatisation. The feasibility of syn-deformative creation of foliation parallel melt segregation has been demonstrated in several studies (Brown *et al*., 1995, and references therein; Barraud *et al*., 2004).

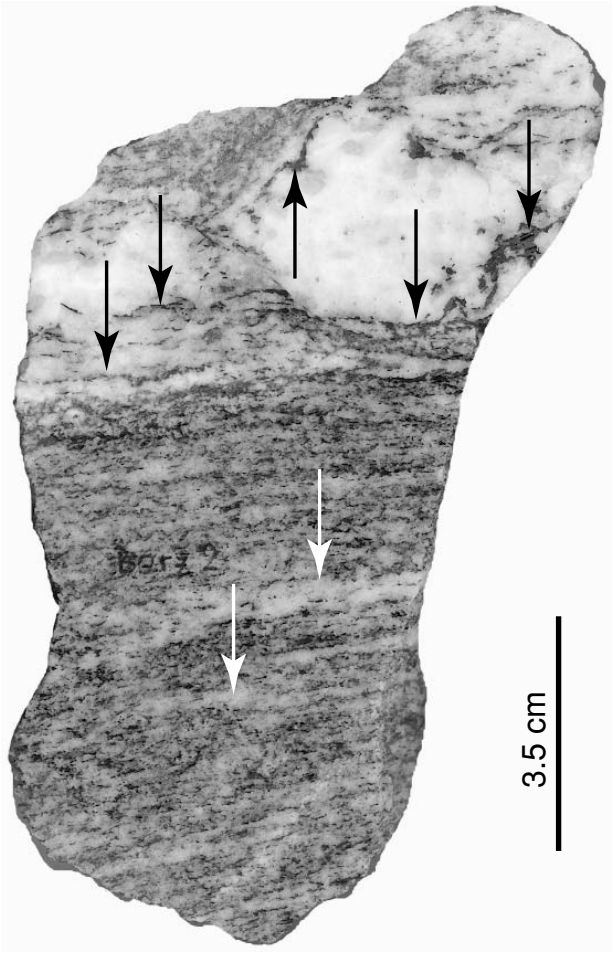

Fig. 5) Polished slab showing small-scale melt segregations in a granitoid orthogneiss of the Onsernone-unit (Berzona, Valle Onsernone). On the right-hand side of the slab, cm-scale melt segregation into irregular patches is observed. Note that the transition to the host rock is often diffuse and that biotite is arranged in elongate and heap-like aggregates along the leucosome rim (black arrows). On the left-hand side of the slab, smaller scale melt segregations indicate the presence of melt throughout the rock (white arrows). Width of sample 14 cm.

Fig. 6) Migmatite outcrop with small scale melt segregations (Gordevio, Valle Maggia). Melt has segregated into mainly foliation parallel patches and veins. Estimated melt fraction using image editing ca. 20% (min 15, max 24%). Width of photograph ca 30 cm.

Other outcrops are however better suited to demonstrate the temporal link of deformation and melt segregation, thus of the Alpine age of migmatisation. In figure 7 melt filled shear zones form an en echelon pattern, indicating sinistral sense-of-shear. Note that conjugate dextral and sinistral sets have been found in the same locality, indicative of a dominance in the pure shear component (Mancktelow, 2002). The occurrence of entirely undeformed veinlets which crosscut the strong Alpine fabric was observed in several localities (Fig. 8). They indicate that locally, deformation had ceased while melt was still present in the system. Typically, such veinlets are of only local extent.

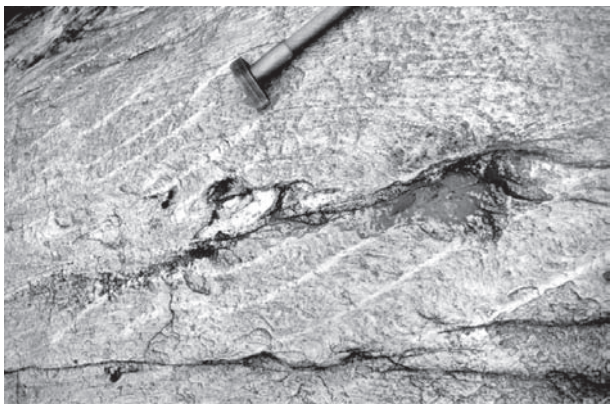

Fig. 7) En echelon melt filled shear zones displace the main Alpine fabric (Ponte Brolla, entrance of Valle Maggia). Hammer for scale.

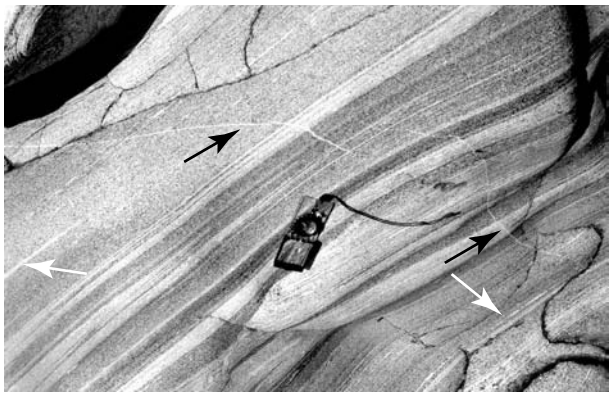

Fig. 8) Discordant melt-veins (black arrows), about 5-10 mm thick, crosscut mylonitic gneiss (Avegno, Valle Maggia). Note concordant leucosome (white arrows). Compass for scale.

b) Medium scale melt-segregation into local melt zones or small bodies (dm-m scale).

The small-scale segregations described in the previous section are often associated with, or grade into larger segregations. We assign migmatites to the second type if a disintegration of the fabric on the decimetre to metre-scale is observed or if melt was able to accumulate on the metre-scale. Figure 9 shows an example of type b migmatites, where the pervasive Alpine fabric becomes undulatory and grades into a more massive to igneous fabric. Rocks in such localities can be differentiated into a pervasively foliated melanosome, a mesocratic domain (mesosome), which typically contains relics of the old foliation, and into leucosome which occurs as patches inside the mesosome. We interpret the melanosome as a melt depleted restite, the mesosome as a mix of refractory minerals and (former) melt, and the leucosome as (former) segregations of pure melt. The black phenocrysts visible in such leucocratic pods in figure 9 are magnetite octahedra, which may indicate a relatively elevated oxygen fugacity. The occurrence of similar but finer grained magnetite in the surrounding gneisses indicates that oxygen fugacity in the melt and the host rock did not differ much. At several localities a gradual transition into the common stromatic migmatites or into virtually unmolten orthogneisses occurs within a few meters. Such unmolten gneisses, interpreted as unaffected protoliths, are usually more leucocratic than the melanosome in neighbouring migmatites, indicating melt subtraction from the melanosome.

At several localities in the SSB distinct granitoid bodies up to several meters in size occur, displaying sharp contacts with host rock and the main Alpine fabric (Fig. 10). Frequently, schollen of the host rock were enclosed in the granitoid magma. A striking characteristic of such granitoid bodies are the often observable leucocratic rims at the contact with the host rock or with enclosed schollen (Fig. 11). These rims may have formed due to enhanced melting along the borders as a result of an increased H_2O-activity of the melt. Such an increase may occur during ascent of the rock, because the equilibrium water content of a melt may decrease during exhumation, depending on the respective PT-path (see excellent discussions in Holtz and Johannes, 1994; Johannes and Holtz, 1996; Holtz *et al*., 2001). Alternatively, these rims may represent migration of melt from the partially molten host rock into the magma body. Indeed, a melt-filled shear zone that ends at such a body, appears to expel melt into the granite, once more indicating the contemporaneousness of deformation and igneous activity in the SSB.

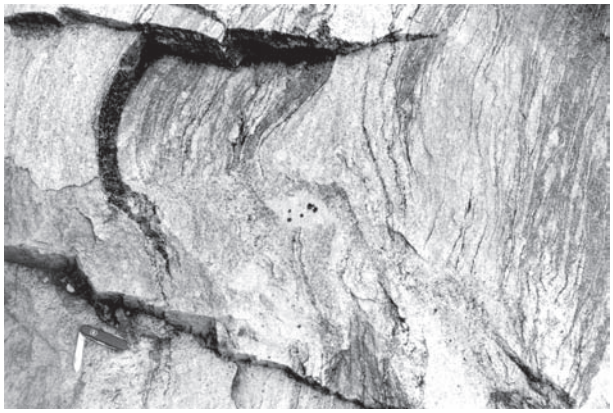

Fig. 9) Melt-rich zone in relatively homogeneous granitoid gneiss (Auressio, Valle Onsernone, road outcrop, pocket knife for scale). The main Alpine foliation grades into an igneous fabric, where a" ghost" foliation is locally still visible. Magnetite-bearing leucocratic pods in the centre of the picture, indicate complete separation of the melt from the partially molten rock.

Fig. 10) Discordant granitoid body, cutting the Alpine main foliation (Ponte Brolla, entrance to Valle Maggia). Note leucocratic rims along the contact with the host rock. Compass for scale.

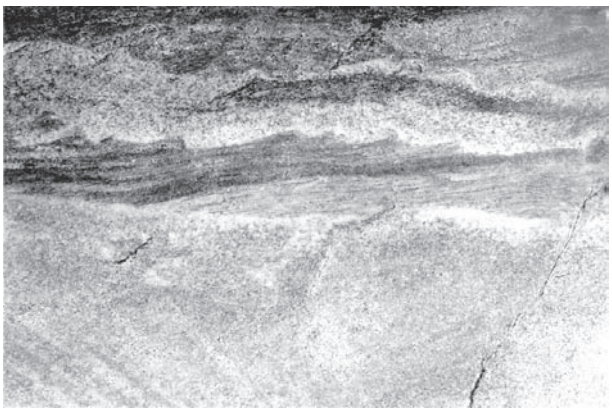

Fig. 11) Detachment of a metre scale scholle from the host rock (Ponte Brolla, entrance to Valle Maggia). The Alpine foliation and lithologic borders remain well preserved. Note leucocratic rim around the host rock and the scholle where in contact with the granitoid leucosome. Width of picture ca. 70 cm.

c) Dykes (pegmatites and aplites)

Granitoid dykes are omnipresent in the SSB (e.g. Fig. 3) and were therefore recognised and described as Alpine products early on (Gutzwiller, 1912; Preiswerk, 1925b; Kündig, 1926; Mittelholzer, 1936; Kern, 1947; Niggli, 1950; Paraskevopoulos, 1953; Knup, 1958; Stern, 1966; Reinhardt, 1966; Sharma, 1969; Wenk, 1970; Niggli, 1970). Whereas some dykes can be traced for hundreds of meters, many dykes seem to quickly die out laterally.

Dykes can be divided into granitoid pegmatites and aplites, although transitions from one into the other may locally be observed. The majority of pegmatites are muscovite (± garnet) -bearing, whereas biotite-pegmatites are less frequent. Aplites on the other hand, are dominantly biotite or two mica aplites. The mineral-chemistry of white micas (Stern, 1966) and feldspars (Paraskevopoulos, 1953) has been studied, but no systematic geochemistry of the intrusive rocks has been done so far. The dykes are usually composed of quartz, microcline and an albite-rich plagioclase, with variable modes of muscovite and biotite, and often garnet. Typical pegmatite minerals like tourmaline or beryl are less common. but were described as accessory phases at several localities (Gutzwiller, 1912; Preiswerk, 1925b; Kündig, 1926; Mittelholzer, 1936; Taddei, 1938; Taddei, 1940; Knup, 1958; Bächlin *et al*., 1981). At several localities, schollen from the immediate country-rock or of unclear origin are found inside dykes.

Dykes generally occur in increasing abundance towards the south, although accumulations of Alpine pegmatites were reported as far north as Verdabbio in Valle Mesolcina (Kündig, 1926). Where several dykes intersect, larger pegmatoid bodies are created, as for example in the riverbed outcrops NW of Camedo. The Centovalli-Pedemonte area between S. Maria Maggiore and Ponte Brolla is intensely intruded by pegmatites, with dykes up to 50 meters wide (Kern, 1947).Whereas to the north dykes exhibit often straight margins and are clearly discordant to the main Alpine fabric, many dykes in the south are deformed, often in a characteristic "megaptygmatic" way (irregular open folds on a centimetre to metre scale). This spatial contrast in dyke emplacement style indicates that deformation in the south of the SSB was still ongoing during intrusion of the dykes, whereas deformation may have already ceased in the north (or north) of the SSB at the same time.

Although a decrease in grain size towards the host gneiss was reported, chilled margins (s.s.) have not been found nor reported to date (Mittelholzer, 1936). This suggests that temperatures of host rocks and intruding dykes did not differ much. Keeping in mind the water-saturated solidus of granitoid systems (e.g. in Johannes & Holtz, 1996), we estimate that temperatures during crystallisation of the dykes must have been in the order of 600-650°C. Lower crystallisation temperatures could only be suggested, if the pegmatites had been rich in fluxing volatiles like lithium, beryllium, boron or fluorine. Despite a few known occurrences of tourmaline and/or beryl bearing pegmatites, the majority of dykes are quit unspectacular, coarse grained granites (also stated in Knup, 1958) (some uncertainty remains in the fact that neither fluorine nor lithium contents of micas have been reported so far).

The general lack of pegmatites enriched in such volatile bearing phases argues against a genetic interpretation of the pegmatites as late stage magmatic liquids. A similar conclusion results from the observed REE-depletion, because most dykes contain only a few allanite grains, and other REE-phases were not observed. This suggests that dykes formed by liquid extraction in the course of partial melting (Stern, 1966), leaving back accessory phases in the restite. This conclusion is supported by isotopic investigations performed on the Bergell intrusive suite (von Blanckenburg *et al*., 1992). Spidergrams for pegmatites and aplites show a significant depletion of REE and a negative Eu-anomaly compared to the main tonalite and granodiorite bodies. Furthermore, ε_{Nd} vs ε_{Sr}-plots indicate an only modest mantle influence, if at all. REE-depletion and the Eu-anomaly were explained as either due to fractionation of REE and Eu-bearing phases (accessories, feldspar), or to partial fusion of a country rock that retained the accessories in the residue. Published $^{87}Sr/^{86}Sr$ ratios of 0.712-0.718 favour the latter hypothesis (Hänny *et al*., 1975; von Blanckenburg *et al*., 1992). All of the above facts argue against enriched late stage pegmatites, which may crystallise at temperatures as low as 475°C (London, 1992), and rather suggest crystallisation temperatures of 600-650° for the dykes in the Central Alps. Additional arguments for relatively high temperatures during dyke intrusion comes from a study who proposes that dyke propagation of granitic magmas should be halted by freezing soon after the magma encounters rocks at temperatures below the magma solidus (Rubin, 1995). Therefore, intrusion of the pegmatites at tem-

peratures much below the respective solidus appears not very likely.

On the basis of Rb-Sr muscovite cooling ages, Schärer et al (1996) claimed that temperatures of the host rock did not exceed 500°C during intrusion of the dykes (500°C were adopted as the closure temperature). Based on recent research, Villa (1998) suggests a (pure) diffusive closure temperature of 600-650°C for this system. The author emphasises however that (fluid-assisted) recrystallisation mechanisms, which may also occur at lower temperatures, are more effective and more likely to occur than pure diffusive closure. Given the uncertainty inherent in the interpretation of Rb-Sr-cooling ages, we hesitate to follow the conclusions of Schärer et al. and classify these particular ages as not very conclusive, in contrast to the U/Pb-Mnz+Xen-ages of the same study, which we interpret as formation ages.

In addition to dykes, several larger scale intrusive bodies of Alpine age occur in the study area. Whereas the Adamello pluton (to the east of the study area) and the Bergell pluton are usually explained as mixed source plutons with a strong mantle-signature, rocks from the smaller Novate intrusive are classified as crustal melts, due to their major element and isotopic composition (von Blanckenburg *et al*., 1992; von Blanckenburg *et al*., 1998). Comparatively high $^{87}Sr/^{86}Sr$ ratios of 0.7098 indicate an important crustal contribution for the Novate granite (von Blanckenburg *et al*., 1992). Two other smaller granitoid intrusives, the Soe and Garzelli domes, are of uncertain age but have compositions similar to the Novate granitoid (Hänny *et al*., 1975). Both granites are structurally situated in the hinge of kilometre-scale antiforms (the Cressim and Garzelli-antiforms), and both yield high $^{87}Sr/^{86}Sr$ ratios, from 0.712 up to 0.836, indicative of a high crustal contribution (Hänny *et al*., 1975). Petrographic and structural evidence, as well as U-Pb-monazite ages of 22.9-23.5 Ma point towards Tertiary ages, yet U-Pb zircon and Rb-Sr whole-rock errorchrones indicate a Variscan origin for these rocks. It remains unclear whether or not the Soe and Garzelli granitoids are related to the Alpine intrusive activity, but at least local anatectic remobilisation is very likely (R. Hänny, pers. com., see also Fig. 6 in Hänny *et al*., 1975).

Rock-melt interaction

Interaction between granitic melt and different types of host rock can be observed at several sites in the SSB. Certain localities exhibit spectacular reaction textures on the thin section to sample scale. Petrographically most interesting interactions may be observed where leucocratic melts interact with mafic or ultramafic rocks, as for instance at Capoli (Valle Maggia), where melts interact with a body of metaeclogites. Rock-melt interaction is there generally restricted to the immediate vicinity of centimetre-scale veins which succeeded to intrude along the rims of the body. A larger scale melt-rock interaction was observed in riverbed outcrops near Camedo (Centovalli) and will be described in some detail, because of their unique nature. The area around Camedo is intensely intruded by pegmatitic dykes, which in the gorge NW of Camedo intersect to form a larger igneous body. A metre-scale enclave of mafic to ultramafic composition is conspicuous due to its ovoid textures (Fig. 12). The "eggs" are mainly composed of a pale, probably Mg-rich amphibole, with in certain domains abundant clinopyroxene. Clinopyroxene is locally replaced by amphibole, but may in some cases be part of the stable mineral assemblage. Plagioclase occurs between the amphibole and clinopyroxene grains. Pegmatite material in direct contact with the ultramafic eggs is fine-grained and exceptionally rich in biotite compared to the only muscovite bearing pegmatitic liquid. Leucocratic veins crosscutting the ovoids may reflect later ingress of pegmatite liquid. Based on the uncommon association of pegmatite and ultramafic rocks and on the spectacular (microscopic) reaction textures, we suggest that the ovoids were formed by the interaction between the ultramafic rock and the pegmatoid melt. The origin of the mafic inclusion is uncertain but roughly three scenarios are possible:

a) The enclave is a piece of an ultramafic cumulate, entrained from a larger magma chamber during the ascent of the dykes.

b) The enclave represents a piece of country rock, incorporated during intrusion of the dyke.

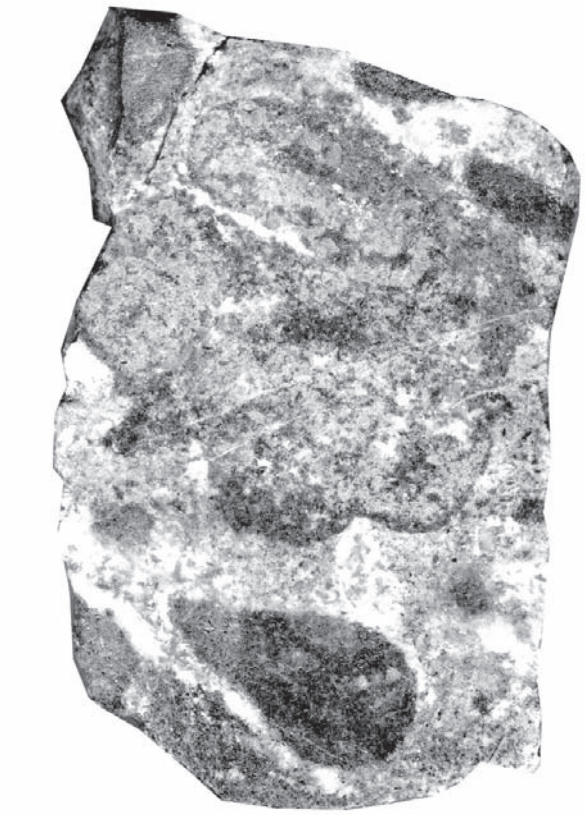

Fig. 12) Interaction between pegmatite-melt and an included ultramafic enclave (Camedo, Centovalli). Ultramafic areas separate into elliptical domains with roughly concentric zoning. Long axes 8 cm.

c) The enclave was part of a mafic dyke that mingled with the pegmatite.
Due to the lack of large scale intrusive bodies in the Camedo area and due to the general absence of mafic dykes except in the immediate surrounding of the major intrusives Bergell and Adamello, we exclude scenarios a) and c) as likely explanations. On the other hand, the occurrence of several ultramafic bodies in the direct vicinity, and the proposed origin of the pegmatites as segregated partial melts support the second hypothesis. In addition, similar textures where observed in the Bagni di Masino area, where melt from migmatitic orthogneisses interacts with a neighbouring ultramafic body.

Extent of Alpine migmatisation

It has been postulated for a long time that at least locally partial melting had occurred during the Tertiary. Concepts diverged mainly with respect to the extent of migmatisation. In order to establish the distribution of Alpine migmatisation in the Central Alps, we performed extensive field work in combination with a review of the relevant literature. In the field we used mainly structural and textural criteria to distinguish between Alpine and Pre-Alpine migmatites. The generally strong and pervasive Alpine deformation facilitated discrimination to some extent, because many of the observed migmatites are discordant to this strong Alpine fabric. Nevertheless ambiguity remained in some cases. We took the following criteria as indicative of Alpine migmatite formation:

- Discordance of dykes, veins or small-scale melt segregations with the observed main Alpine foliation.
- Coarse-grained and almost undeformed leucosomes inside highly deformed finer grained rocks.
- Melt-filled shear zones or boudin necks, attributable to Alpine deformation.

As demonstrated by other authors, age-relationships are not always unequivocal, especially where several generations of migmatites coincide (Blattner, 1965; Hänny, 1972; Schärer *et al*., 1996; Romer *et al*., 1996). In such localities unequivocal Alpine intrusives or *in situ* leucosomes can typically be identified. The pre-Alpine age of the older and stronger deformed migmatites, though probable, can not always be unambiguously approved (Hänny, 1972; Hänny *et al*., 1975). Therefore, we probably mapped a minimum extent of *in situ* partial melting when applying the above listed criteria. Due to the very characteristic features of Alpine migmatites, we are however convinced that Alpine partial melting took place inside the mapped (minimum) border. In contrast to *in situ* migmatisation, the extent of Alpine dyke intrusion is easily mapped.
Field work and study of relevant literature allow us to delineate three major limits (Fig. 13):

Limit of aplitic and pegmatitic dykes:

Aplites and pegmatites often crosscut the main Alpine foliation, especially towards the north of the SSB, where they are good structural and temporal markers. Towards the south they often occur in intersecting swarms, which can give rise to larger bodies, tens of meters in size (e.g. at Camedo, in the riverbed below the custom office, see also in Knup, 1958; Reinhardt, 1966). Discordant, tube-like or circular granitoid bodies are restricted to the SSB.

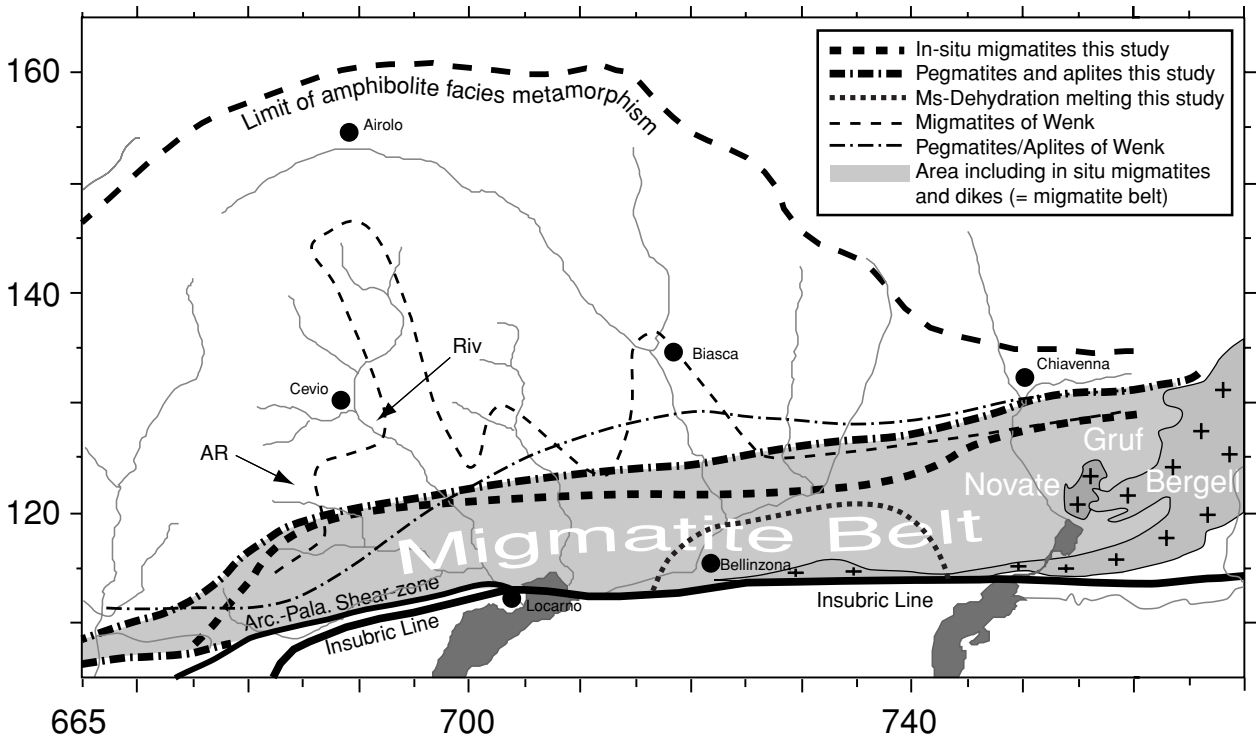

Fig. 13) Distribution of Alpine migmatites in the Lepontine area. Massive dashed lines depict limits established in this study, thin dashed lines are from Wenk (1970). Continuous lines are major shear zones. AR = Alpe Ribbia, Riv = Riveo

Dykes and granitoid bodies are abundant in the south, and decrease in number towards north. Our mapped border comprises all observed and reported dykes of unequivocal Alpine age.

Limit of in situ migmatisation

In situ migmatisation is often observed in the form of concordant and discordant leucosomes (veins or pods), which are generally coarser grained than the country rock. Leucosomes are also observed inside dm- to m-scale shear zones. Melt segregations in spatially limited localities reach the extent of diatexis, where the Alpine fabrics become diffuse to even disintegrate. In many cases, unambiguous evidence for dehydration melting is lacking, but textural evidence for partial melting is unequivocal. Typical reaction products of dehydration melting like Sil+Kfs, Opx, Crd or Grt are completely absent from strongly migmatitic orthogneisses. This suggests that partial melts in the orthogneiss must have formed by fluid assisted partial melting if they show evidence of a high former melt fraction.
We delimited the border of *in situ* migmatisation using the widespread occurrence of unequivocal Alpine leucosomes (according to the above listed criteria). Spatially limited occurrences of concordant and more ambiguous leucosomes (some of which are discussed in some detail below) to the north of our mapped limit where not included, because of their ambiguity.

Limit of dehydration melting of white mica

This limit outlines the area where phengite breakdown led to the production of K-feldspar, sillimanite (or kyanite) and melt, according to the model reaction
Ms + Qtz = Kfs + Sill + Melt
For several reasons this border is not easy to map: Many sillimanite bearing rocks from the study area do not contain K-feldspar and are therefore more likely related to subsolidus reactions (first sillimanite isograd). Thus the field recognition of sillimanite alone, does not allow to map out the limit of muscovite dehydration melting. In addition, sillimanite + K-feldspar could also be produced through the subsolidus reaction
Ms + Qtz = Kfs + Sill + H_2O
(second sillimanite-isograd). As a further complication, muscovite may become stable again along the retrograde path, thereby disguising its former breakdown.
Our limit encloses localities where partial melting can be observed at the outcrop and where samples contain Sill+Kfs. The Sill+Kfs+Melt-isograd has not previously been mapped out in the Alps, and our limit represents a first rough attempt (Fig. 13). Besides of our own sample collection, we used data from the literature (Thompson, 1976; Nagel, 2000; Brouwer, 2000) and field observations to delineate this limit. Further complications exist because the SSB is in part composed of TAC units, which contain various HP-HT relics. Such exceptionally high PT-conditions are however only reported for distinct mafic to ultramafic relics and evidence of HP-metamorphism is lacking in the majority of rocks from the SSB.

Possible occurrence of biotite dehydration melting

There exist few known occurrences of cordierite-bearing assemblages in the Lepontine (Wenk, 1975; Irouschek, 1980; Brouwer, 2000) as well as a single example of a sapphirine-orthopyroxene-cordierite-bearing assemblage (Gruf-complex, Droop & Bucher-Nurminen, 1984). The latter study proposed the production of melt due to Bt-dehydration reactions like
2Bt + 6Ky = 3Saph + 3Qtz + 2Kfs + Melt
and
Bt + Ky + H2O = Saph + Qtz + Melt
The survival of biotite was explained by the complete consumption of Al-silicate, at conditions below the upper thermal stability limit of biotite at metamorphic conditions of are around 830°C/ 10kbar. The proximity of these outcrops with the large Bergell intrusion (Fig. 1 or 13) may however suggest that their formation could be related to the emplacement of the hot Bergell pluton and is not representative for the majority of rocks in the SSB. Beside this exceptional occurrence, biotite appears as a stable main phase in all granitoid and pelitic to semipelitic gneisses of the study area, and evidence of biotite-dehydration melting is missing in the vast majority of such rocks. Because cordierite was also detected in rocks far north of the study area (Irouschek, 1980) where Alpine partial melting can be excluded, the occurrence of sparse cordierite is not necessarily linked to partial melting but may instead indicate unusual (Mg-rich) rock compositions.
Biotite dehydration melting may have occurred in a few exceptional localities, but is overall very rare in the SSB.

Special migmatite associations

A few local occurrences of probable Alpine leucosomes were documented to the north of our limit of *in situ* migmatisation, for example in a quarry at Riveo (Valle Maggia, fig. 13). Here, a few coarser grained small-scale melt segregations in the form of cm-dm sized irregular pockets and veins are observed. Because of their small size, such veins would not have retained their coarseness during solid state mylonitic deformation, which suggests an Alpine origin for these leucosomes. The melt fraction in these rocks must have been very low, as no other indications of anatexis were found. We suggest that mylonitic deformation may have enhanced melt segregation and that post-kinematic crystallisation of the leucosome resulted in the observed coarser fabric.
Another special migmatite association was documented near Alpe Ribia (Valle Vergeletto, Fig. 13),

where migmatitic orthogneisses, a few tens of meter long, occur inside otherwise non-migmatitic, mylonitic orthogneisses (Fig. 14). Borders between migmatite and orthogneiss are blurred, indicating a common protolith for the two rocks. The migmatites are stromatic and leucosome occurs in the form of irregular, foliation parallel pods. Although the migmatites were deformed by some decimetre to metre scale folds (Fig. 14), leucosomes retained their typical coarseness. Intriguingly, the migmatites are situated in the top of an inhomogeneous trail, comprising amphibolites and metasediments (Häuselmann, 1997; Burri, 1999). Rocks from this trail may have released volatiles through continuous dehydration reactions. Liberated fluids did not induce partial melting in the Pl + Qtz bearing amphibolites and metasediments, but induced local partial melting upon entering the overlying Kfs + Pl + Qtz-bearing gneisses.

Similar relations between heterogeneously composed trails and enhanced rates of partial melting in associated orthogneisses were observed in the metasedimentary trails below Gresso (Valle Vergeletto, inside the limit of *in situ* migmatisation). Here, the contact between metasediments and adjacent orthogneisses is delineated by a several decimetre thick, melt enriched orthogneiss layer. Again, partial melting has occurred in the K-feldspar bearing orthogneisses due to the release of volatiles from the adjacent metasediments.

These occurrences indicate that in special circumstances, partial melting may have occurred outside our limit of *in situ* partial melting. Such rocks appear to be of local importance only and are dependent on the availability of volatiles. These occurrences where therefore not included inside our limit of *in situ* partial melting, which delimits the area were partial melting was widespread.

Results

Our approach reveals several important features:

- Alpine *in situ* migmatisation and intrusive activity roughly coincide, but the limit of dyke intrusions generally extends beyond that of *in situ* partial melting by a few hundred metres to several kilometres.
- Alpine migmatisation is generally restricted to the SSB and areas immediately adjacent to the north. To the south it is sharply delimited by the Insubric line, west of Locarno, by the Saas-Zermatt-zone s.l. immediately south of the Monte-Rosa-unit. Between Santa Maria Maggiore and Domodossola, the number of dykes decreases, and the border of intrusive activity shifts towards the northern limit of the Monte Rosa-unit (Reinhardt, 1966). The occurrence of an Alpine dyke was however reported from the western side of Valle d'Ossola, inside the Moncucco-unit (Locality Tappia, L. Keller pers. comm.). Towards north, the border of migmatisation is more diffuse, although the occurrence of Alpine migmatites and intrusives decreases rapidly north of the SSB.
- Alpine migmatisation commonly led to stromatic migmatites (Fig. 15) and only rarely produced metre-scale diatexitic structures (Fig. 9). Alpine migmatisation did not lead to extensive agmatitic (schollen-type) migmatites (see also Blattner, 1965; Hänny, 1972; Hänny *et al*., 1975). Occurrences of extended agmatitic migmatites are therefore regarded as pre-Alpine formations.
- Migmatites are not only observed in "fertile" lithologies like metasediments, but also in rather "unfertile" granitoid orthogneiss. Furthermore, migmatisation locally appears linked to the occurrence of heterogeneous, metasediment-bearing trails (e.g. at Alpe Ribia and at Gresso, Valle Vergeletto).
- Evidence for dehydration melting of white mica is mainly observed in the area around Bellinzona and disappears between Locarno and Bellinzona to the west, and between Novate and Bellinzona to the east. Outside this area, reaction products of muscovite dehydration melting (Al-silicate + K-feldspar) are generally lacking or appear related to subsolidus processes rather then partial melting.
- Evidence of biotite dehydration-melting is constrained to a few outcrops near the Bergell intrusion. Reaction products of biotite dehydration melting like orthopyroxene, sapphirine, spinel or cordierite are generally lacking (Opx, Sp and Spr) or are often related to subsolidus reactions (Crd).
- In contrast to the restricted evidence of dehydration melting, phengite and biotite are omnipresent in leucosomes and country rocks.

Fig. 14) Migmatitic granitoid gneisses overlying a heterogeneous trail of amphibolites and metasediments (Alpe Ribbia, Valle Vergeletto).

Comparison with other studies

A previous distribution map of Alpine migmatisation was published by Wenk (1970), and his proposed limits are included in figure 13. Wenk's limit of Alpine migmatisation differs from ours, whereas the two limits for Alpine dykes roughly coincide. Based on structural and isotopic arguments dis-

Fig. 15) Typical stromatic migmatite in granitoid orthogneisses of the Mergoscia-zone. Note euhedral amphibole in the leucosome. Estimated melt fraction using image editing ca. 27% (min 25, max 30%). Width of picture ca. 1.5m. (Mergoscia, Valle Verzasca)

cussed above, we conclude that several migmatites, considered as Alpine by Wenk, are actually of pre-Alpine age. For instance, revealing structural observations can be made at Alpe Sambucco (Val d'Osura in Valle Verzasca), where migmatitic rocks from the Maggia nappe were transformed into banded gneisses during mylonitic deformation along the Alpine Pertusio shear zone. Except for outcrops inside the SSB, the often-cited migmatites of the Maggia and Simano units most certainly reflect a pre-Alpine period of intrusion and migmatisation.

On the other hand, our interpretation concurs with that of Niggli (1950) and Niggli & Niggli (1965) and other authors (see review above), who proposed that Tertiary magmatic activity was restricted to the "root-zone" (SSB). In addition, our interpretation is in line with the interpretation of other authors who have worked in the eastern part of the study area (R. Hänny, pers. comm.).

Arcegno-Palanzeno shear zone

As detailed above, anatexis and intrusion are sharply delimited to the south, and the limit is more gradual in the north. East of Locarno, Alpine magmatic activity is truncated along the Insubric Line (termed Tonale Line in that area). West of Locarno, *in situ* migmatisation and intrusive activity occur no further south than in the ophiolitic Zermatt-Saas zone. In contrast, the Sesia zone in the eastern Centovalli area shows no sign of Alpine *in situ* migmatisation and intrusion of pegmatites and aplites, but it does carry characteristic Tertiary porphyritic dykes of mafic composition, which are absent in the northerly adjacent Lepontine units. We note, however, that migmatites of yet unresolved ages have been reported from the Sesia unit in Val Grande (Reinhardt, 1966). Because we did not visit this area, the significance of these migmatites remains unsolved also after this study. Nevertheless, the sharp break in Alpine migmatisation between the Sesia and northerly adjacent units suggests that the Sesia-unit and the Lepontine-nappes were juxtaposed after intrusion and migmatisation, which had finished at last around 20 Ma ago (discordant dyke at Lavertezzo). We therefore postulate a shear zone situated between the Sesia-unit to the south and the back-thrusted Lepontine nappes to the north. Considering the extreme deformation of the Monte-Rosa-unit in the Centovalli area, the Monte Rosa unit and probably also the Orselina- and Zermatt-Saas units may be integral parts of this shear zone, which we call Arcegno-Palanzeno shear zone, named after two villages laying along the inferred border (Fig. 1 and 13). In the area around Arcegno, pegmatitic dykes often show a strong mylonitic overprint, whereas dykes in the adjacent Orselina unit are undeformed or show an irregular, "mega-ptygmatic" fold style. This change in deformation style of Alpine dykes indicates an increase in strain from north to south. Further to the west, we suppose that the Arcegno-Palanzeno shear zone continuous along the contact between the Sesia unit and the Saas-Zermatt ophiolites. It further appears that the Arcegno-Palanzeno shear-zone may be genetically linked to the east with the Tonale-line. In map view, the combined Tonale- and Arcegno-Palanzeno shear-zones (and the latter's westward continuation) form one continuous, generally east-west striking shear zone, which was the location of backfolding and back-thrusting during continent collision.

We note that the proposed Arcegno-Palanzeno shear-zone does not coincide with a similar shear-zone, termed (Rhône-) Simplon shear-zone (Steck & Hunziker, 1994; Schärer *et al*., 1996; Romer *et al*., 1996). Although the Simplon- and the Arcegno-Palanzeno shear-zones coincide in their eastern part, our interpretation of the westward continuation diverges from that of the Simplon shear -one. The Simplon shear zone is interpreted to bend towards the north, thus towards the Simplon area (see Fig. 3 in Schärer *et al*., 1996), and is interpreted to be related to the unroofing of the Central Alps. Further movement along this extensional normal fault during decreasing temperatures became more localised inside the ductile to brittle Simplon-line (Mancktelow, 1992; Schärer *et al*., 1996). By contrast,

due to its tectonic position, the proposed Arcegno-Palanzeno shear-zone is interpreted to have accommodated movements during backthrusting of the Central Alps and may thus be slightly older then the Simplon shear zone.
We admit however that our interpretation is mainly, though not exclusively, based on Alpine features of migmatisation and intrusion. Further fieldwork is necessary to better constrain the direction of the Arcegno-Palanzeno shear zone west of Valle d'Ossola.

Modelling of the regional distribution of Alpine migmatites

The pressure and temperature distribution for the Barrovian overprint of the Central Alps was recently represented in terms of P and T-contours (Engi *et al*., 1995; Todd & Engi, 1997) (top of Fig. 16). In this section, we use this model to map out the traces of different solidus curves of granitoid rocks in the Lepontine area and to compare these model-maps with the observed field distribution of migmatites and dykes. Before discussion of the results, we need however to shortly review the main features of the Engi et al.-model, to be able to discuss limits of the model and potential problems when applying it to our questions.
PT-data for the Barrovian overprint were estimated using program TWQ (Brown et al., 1988) together with the internally consistent thermodynamic database of (Berman, 1988, update 92). To smooth out irregularities in the spatial PT-estimates, they used kriging. PT-estimates were interpreted to represent the pressure at the maximum temperature reached during the Tertiary metamorphism (P at T_{max}). This suggestion is based on the assumption that rocks reach their maximum entropy and their minimum water content in general near the highest temperatures along a PT-path. Problems in using these contour maps may raise due to several reasons:

- *The use of different databases may lead to slightly different results and all estimates as well as our own results are thus clearly a function of the applied database.*
- *The data-distribution in the study area is not uniform. Especially in the eastern part of the SSB the sample density is not very high.*

Keeping in mind these potential problems, we represented several water-saturated solidus curves, as well as the muscovite and biotite dehydration melting reactions onto the PT-contoured maps. We chose the water saturated granite solidus of (Holtz et al., 2001, Fig. 4), the water saturated tonalite solidus of (Schmidt, 1993, Fig. 4) and the muscovite and biotite dehydration reactions of (Mogk, 1992, Fig. 9). The pegmatite-solidus is taken to be some 25°C lower than the granite solidus at a given pressure, to consider possible effects of enrichment in fluxing elements. A lower solidus would be at odds with the fact that the relatively few tourmaline and beryl bearing pegmatites show no strong enrichment. The pegmatite solidus used may yield a lower estimate for the distribution of these dykes. Projected solidus points were interpolated and smoothed by hand.
The projected water-saturated solidi delineate the area where water-assisted partial melting of rocks of pegmatitic, granitic or tonalitic composition could have occurred, provided an aqueous fluid had access. Furthermore the limits should approximately outline the border where dyke intrusions of the respective compositions should be arrested due to the rapid crystallisation of the dykes upon intrusion of a host rock with a temperature below their solidus (Rubin, 1995).
Results of this exercise are illustrated in figure 16, which shows that almost the entire area where *in situ* partial melting and dyke intrusion was observed (grey shading) is enclosed within the water saturated granite solidus field. Substantial differences compared to the mapped-out distribution (Fig. 13) occur in the easternmost part of the area, were the sample density used for the PT-contours was rather low. Indeed, recent thermobarometric results (Nagel, 2000) indicate higher PT-conditions in this area where partial melting is widespread. The misfit on the western edge of the map is small and may be explained by the uncertainties in the P and T distributions. For example, the calculated border of *in situ* partial melting in the western part of the study area neatly coincides with the mapped distribution. The limit of the pegmatite solidus encloses nearly the whole area where Alpine dykes were observed. The misfit in the eastern part of the area is again attributable to the low sample density. The discrepancy in the western part may indicate that the chosen pegmatite solidus was slightly too high, or that the dykes arrived to intrude host rocks which were slightly cooler than their solidus. Additionally, because of the occurrence of a narrow sillimanite bearing belt that stretches beyond Valle d'Ossola (Niggli, 1970; Keller, 2004), we put forward the possibility of an enhanced thermal flux in this narrow belt, the effects of which (in respect to PT-contouring) may not have been resolved by the statistical kriging method (which used 10 kilometre gridding). Recent estimates of metamorphic conditions for this area suggest in fact higher temperatures and pressures (Engi *et al*., 2001b; Keller, 2004)
An important result of the comparison of field and model distribution is the notion that water-assisted partial melting and dyke intrusion may have been possible more then ten kilometres north of the mapped limit of *in situ* migmatisation (Fig. 16). It is thus possible that partial melting has occurred outside the SSB, but that resulting melt fraction have been too small to be recognised in the field (see also conclusions in White *et al*., 2001; White and Powell, 2002).
The mapped and calculated limits of muscovite dehydration melting are in good agreement, both be-

ing restricted to an area near Bellinzona. According to the model used, biotite-dehydration melting reaction should not have occurred at the present level of exposure, which is again in agreement with its exceedingly rare occurrence in the field.
Overall, the comparison demonstrates that the distribution of *in situ* migmatisation exceeds the calculated area of dehydration melting, but is enclosed within the limits of fluid-saturated melting. This suggests that water-assisted partial melting was an important process in the SSB, as was already deduced above on the basis of phase relations. The presence of pore fluids may in addition have led to the creation of a small melt fraction (<10%) in areas outside the limit of dehydration melting. Where a higher melt fraction or an inhomogeneous distribution of leucosomes inside a homogenous host rock was observed, infiltration of external fluids was probably the cause of migmatisation. The fact that partial melting occurred almost exclusively in the SSB suggests a genetic link, as is discussed below.

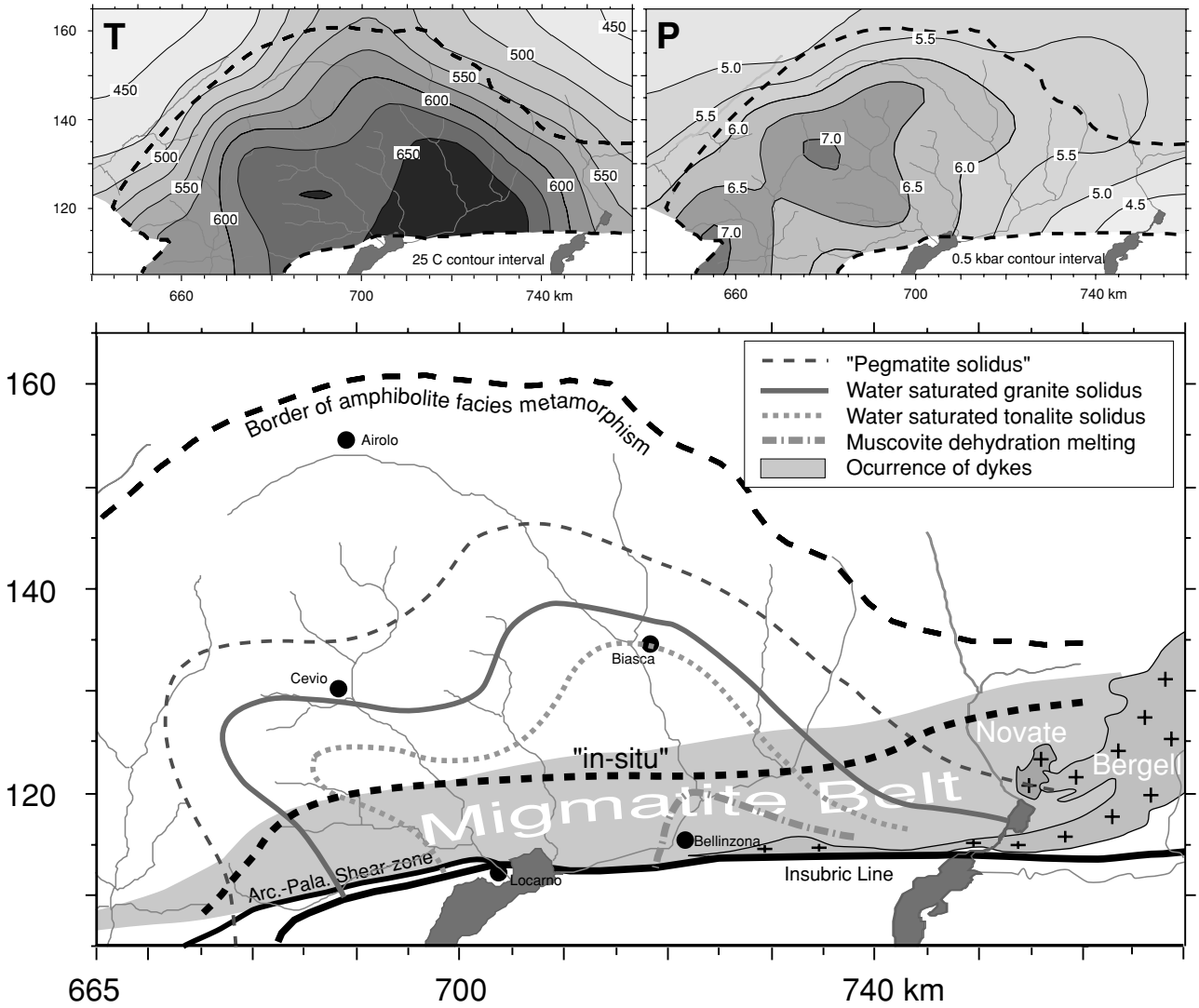

Fig. 16) Projection of the water saturated pegmatite-,granite- and tonalite solidi, and of the trace of the muscovite dehydration reaction onto a map of the Central Alps. The two smaller insets at the top are the P and T-contour maps taken from (Engi et al., 1995; Todd & Engi, 1997). See text for further explanation.

Al-in hornblende thermobarometry

The occurrence of amphibole in anatectic melts is of interest for two reasons:

- Experiments performed in granitic and tonalitic systems indicate that addition of an external fluid is necessary to stabilise amphibole during partial melting of granitoid rocks (Naney, 1983; Gardien *et al*., 2000). Thus amphibole-bearing leucosomes of granitoid composition are a strong indication of water-assisted partial melting.
- Amphibole in partial melts may be used for thermobarometric purposes and may thus help constrain the PT conditions of migmatisation.

In this paragraph we concentrate on the second objective. In migmatite terranes like the Central Alps, where migmatisation has dominantly occurred in granitoid orthogneiss, it is difficult to determine the PT conditions of partial melting, because mineral assemblages in granitoid gneisses are not suitable for thermobarometry. Thus, amphibole thermo-

barometry provides a good means for establishing conditions of migmatisation in the SSB, where amphibole-bearing leucosomes occur frequently (e.g. Fig 15). We collected samples from amphibole-bearing leucosomes and veins or from smaller granitoid bodies or dykes; table 1 lists localities and provides a brief description. In general, the samples lack evidence of deformation or strong retrograde overprint. Domains exhibiting signs of retrograde reactions or alteration in thin section were excluded from thermobarometry. Generally the complete mineral assemblage was analysed, in several samples however only the composition of amphibole and plagioclase. Measured amphibole profiles always showed but weak chemical zoning. All analysed amphiboles yield relatively high K_2O-contents of 1-2 wt%. Representative mineral compositions of the studied samples are given in table2 (Appendix).

Methods: Minerals were analysed on a Cameca SX50 electron microprobe, equipped with 4 wavelength dispersive spectrometers, at the microprobe lab at Bern University, using natural silicate standards. Analysis conditions were 15 kV and 20 nA. We analysed the compositions of small scale local assemblages to avoid the problems resulting from variations in mineral and effective bulk compositions.

To estimate pressure, we applied the Al-in-hornblende barometer of Anderson and Smith (1995), a calibration which takes into account the effects of temperature on the amphibole Al-content. The required mineral assemblage of hbl + bio + pl + Kfs + qtz + tit + Fe-Ti-ox +liq + fl (Schmidt, 1992) was always observed. Textural evidence was taken as proof for the presence of former melt and a fluid phase must have been present at least during crystallisation of the melt. The authors proposed that the barometer may only be applied if the ratio of $Fe_{tot}/(Fe_{tot}+Mg)$ in amphibole varies between 0.4 and 0.65. Most analysed amphibole grains fulfil this requirement or are only slightly outside this range by 0.03 at most. An additional limit is X_{An} in plagioclase, which must be between 0.25 and 0.35. Again, most analysed grains fulfil this requirement or are less than 0.03 outside. The only exceptions are two samples collected at Bagni di Craveggia (MAP), where X_{An} is only 0.08-0.13. Anderson and Smith (1995) suggest, however, that only a plagioclase too high in anorthite or a K-feldspar too low in orthoclase should influence the accuracy of the barometer. Both phases in the Bagni di Craveggia samples are within reasonable limits, and calculated pressures should be reliable. To estimate temperatures we applied the two amphibole-plagioclase thermometers of Holland and Blund (1994). All criteria regarding mineral composition were met.

One problem inherent to amphibole-thermobarometry in partially molten systems is the significance of the calculated PT-conditions. Because amphibole in anatectic granitoid systems is a reaction product of a water-assisted melting reaction, it is not clear whether the amphibole composition reflects the conditions of nucleation and growth, or the condition of crystallisation of the entire melt. As suggested by (Schmidt, 1992), hornblende may re-equilibrate as long as a melt phase is present in the system and hornblende compositions should therefore reflect conditions close to the crystallisation of the (partial) melts along the water saturated solidus. Further reequilibration of hornblende might occur if the fluid released from the crystallising melt does not immediately escape the system. We argue that several of the observed retrogressed domains are due to such stagnant fluids. We

Locations of samples used for Amphibole-Thermobarometry

Sample	X-ccord.	Y-coord	Location	Description	Additional comment
7A101	722.500	118.775	Mövenpick-highway-restaurant, near Bellinzona	Amphibole-bearing leucosomes in migmatitic gneiss	
7A86	722.500	118.775	Mövenpick-highway-restaurant, near Bellinzona	Amphibole-bearing leucosomes in migmatitic gneiss	
7A96	722.500	118.775	Mövenpick-highway-restaurant, near Bellinzona	Amphibole-bearing leucosomes in migmatitic gneiss	
7A97	722.500	118.775	Mövenpick-highway-restaurant, near Bellinzona	Amphibole-bearing leucosomes in migmatitic gneiss	
8A19	725.225	120.250	Roadturn NE of Arbedo, Valle Mesolcina	Amphibole-bearing leucosomes in migmatitic amphibole-rich-gneiss	
Ar9902	725.125	119.325	Road-tunnel below Aragno, Valle d'Arbedo	Amphibole-bearing leucosomes in migmatitic gneiss	
Ave5	701.260	118.160	Avegno, Valle Maggia	Amphibole-bearing synconcordant vein in migmatitic gneiss	
Bag4a	685.300	116.750	Bagni di Craveggia, Valle Onsernone	Amphibole-bearing discordant vein in migmatitic gneiss	
Bag6	685.300	116.750	Bagni di Craveggia, Valle Onsernone	Amphibole-bearing discordant vein in migmatitic gneiss	
Fon7	690.625	118.225	Ponte Oscuro, Valle Vergeletto	Amphibole-bearing leucosomes in migmatitic gneiss	
Merg2B	708.550	117.750	Fressino near Mergoscia, Valle Verzasca	Amphibole-bearing leucosomes in migmatitic gneiss	
Pon3	701.750	115.920	Ponte Brolla, Pedemonte	Amphibole bearing pegmatitic vein	
Pon5a	701.750	115.920	Ponte Brolla, Pedemonte	Amphibole bearing pegmatitic vein	
Vz470	709.400	117.700	S. Cazza, Valle Verzasca	Amphibole-bearing leucosomes in migmatitic gneiss	Collection of MPI-Basel, samplefrom E. Wenk
Vz578	714.250	118.550	S of Forcola, Valle di Cugnasco	Amphibole-bearing leucosomes in migmatitic (Cocco) gneiss	Collection of MPI-Basel, samplefrom E. Wenk
Wurz129	700.000	119.500	Road between Dunzio-Aurigeno, Valle Maggia	Amphibole bearing aplite	Collection of MPI-Basel, samplefrom E. Wenk
Wurz251a	724.650	119.700	Road between Arbedo-Traversagna	Amphibole-bearing leucosomes in migmatitic gneiss	Collection of MPI-Basel, samplefrom E. Wenk

Table 1) Short description and localities of amphibole bearing leucosomes and small dykes used for thermobarometry in this study.

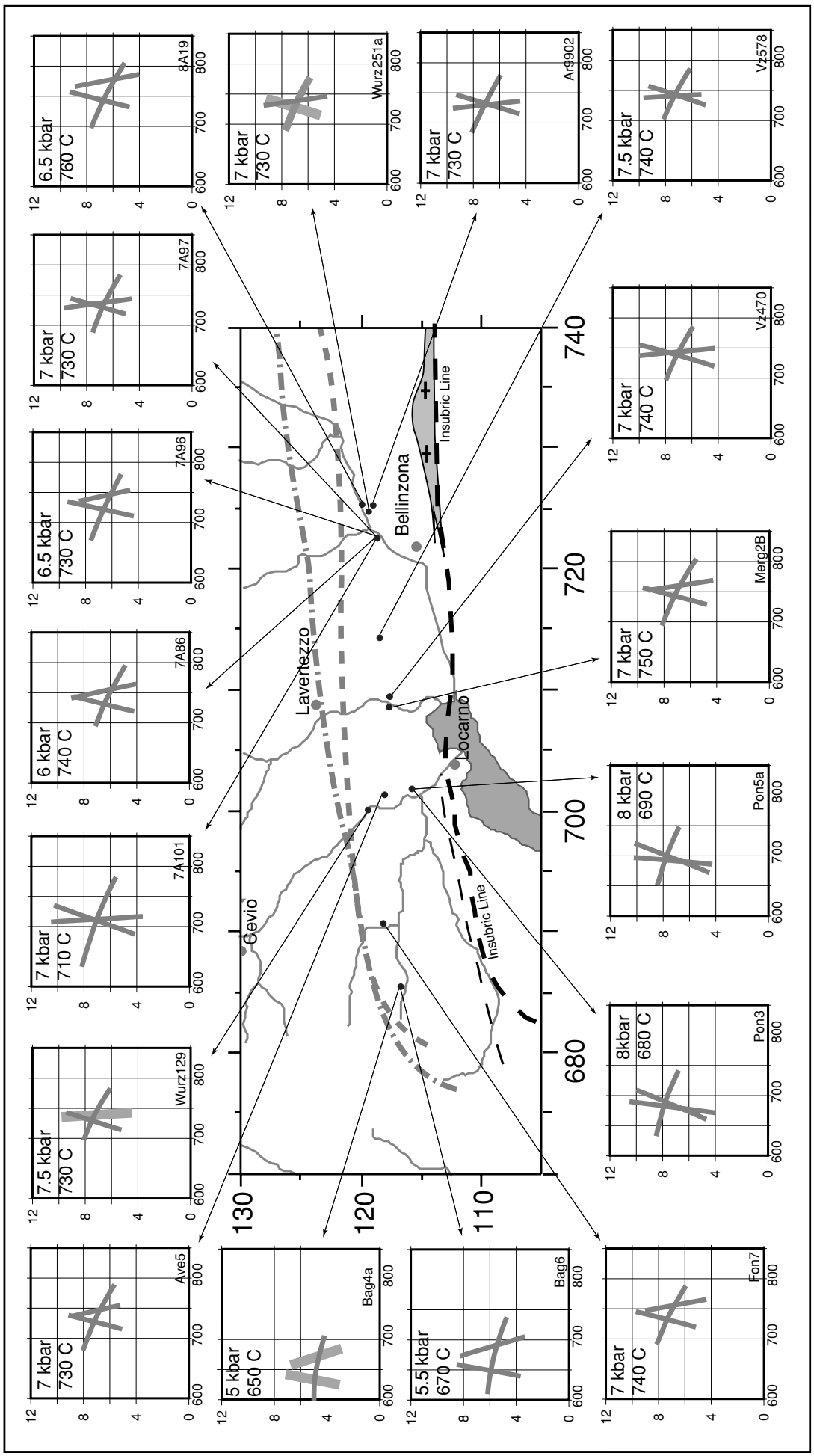

Fig. 17) Compilation of PT-estimates for Alpine migmatisation in the SSB. P and T of amphibole bearing leucosomes were estimated using the Hbl-barometer of (Anderson & Smith, 1995) and the Amp-Pl-thermometers of (Holland & Blundy, 1994).

avoided analysing such domains, hence estimated PT conditions should reflect the final crystallisation of leucosomes. In several samples plagioclase grains included in amphibole were also analysed to track a possible change in PT-conditions during amphibole growth. Differences between matrix or inclusion pairs of amphibole and plagioclase were always smaller than 25°C within a single sample, thus within error. This suggests that amphibole continuously equilibrated with the melt, or that they recorded only a short section of the PT path of a single sample.

Results of thermobarometry are collected in figure 17. Most results indicate that the veins and leucosomes crystallised at 700-750°C and 6-8 kbar. Two samples from Ponte Brolla (Pon3 and Pon5a) indicate slightly lower temperatures of 680-690°C at 8 kbar. Samples from Bagni di Craveggia (Bag4a and Bag6) exhibit even lower temperatures of 650-670°C at pressures around 5-5.5 kbar, which could reflect a real PT difference of these two samples or a bias introduced by the low anorthite contents of plagioclase.

Several conclusions can be drawn from figure 17:

- At every locality the water saturated solidus of granitic to tonalitic rocks was reached or even overstepped by up to 100°C. This overstepping appears to question the postulate that amphibole reflects conditions during final crystallisation of the melt, because this should occur along the water saturated solidus.
- At several localities, muscovite dehydration melting has been possible.
- At no locality biotite dehydration melting has been possible.
- The data indicate no apparent PT gradient from east to west nor from north to south (the latter also due to the small N-S spread of samples). We note, however, that the lowest temperatures are found in the western part of the migmatite belt.
- Except for the samples from Bagni di Craveggia, Al-in-hornblende thermobarometry consistently led to 20-80°C higher temperature estimates and of 0.2-1.5 kbar higher pressure estimates than the TWQ multiphase equilibrium approach (Engi *et al*., 1995; Todd & Engi, 1997).

Discussion of thermobarometric results

Observed discrepancies between PT conditions estimated using amphibole thermobarometry and those calculated with TWQ may be explained differently:

Reported errors of the calibrations are ± 40°C for the thermometer (Holland & Blundy, 1994) and ± 0.6 kbar for the barometer (Anderson & Smith, 1995). Assuming similar P and T uncertainties for the TWQ-approach, one might conclude that all results are identical within the error. However, in this study, amphibole-thermobarometry consistently yields higher temperatures and pressures than the multi-equilibria approach, hence one method may slightly over- or underestimate the actual PT conditions

Own investigations and similar observations (Engi et al., 2001b; Carrupt, 2003) indicate that the database used to determine the P and T distributions (Berman 1992) may lead to slightly lower temperature and pressure estimates compared to more recent databases (e.g Berman & Aranovich, 1996; Holland and Powell 1998).We argue that the simple binary biotite model of the B92-database may have underestimated P and T, because it does not consider effects of the Tschermak-exchange. Biotite analyses from the study area commonly contain non-negligible Al on the M-site of biotite. We performed however no further runs to test this hypothesis

Aside of these possible inconsistencies inherent to the TWQ-results, there exist petrologic arguments to explain the apparent discrepancies: Most of our PT- estimates indicate conditions considerably above the water-saturated solidus of granitic to tonalitic rocks. According to Schmidt (1992), amphibole should equilibrate as long as melt is present, thus until the solidus of the system is reached. Temperatures in excess of ~670°C, as indicated by many of the investigated samples, are however clearly outside any reasonable range for the solidus at 6-10 kbar. The obtained higher temperatures may thus indicate a larger error associated to the Holland & Blundy (1994) calibration, or alternatively, crystallisation of the leucosomes above their actual water-saturated solidus. The latter may for instance be reasonably explained by the injection of a hydrous melt into a fluid undersaturated rock. Upon injection, and provided that the melt is stagnant for a considerable time, the hydrous melt and the water-undersaturated solid rock strive towards equilibration, tending to flatten out the gradient in fluid-activity between melt and solid rock with time. Water-undersaturated host rocks would act as a sponge and extract water from the melt until equilibrium is achieved. This must induce crystallisation of the melt as soon as the water content of the melt drops below its minimum (e.g. Johannes & Holtz, 1996)). Further equilibration of amphibole is then inhibited due to the lack of melt. We note that such a process may only occur along the retrograde path, where rocks most likely become fluid-undersaturated, due to retrograde hydration reactions. By contrast, rocks should always be close to fluid-saturation along the prograde path, due to the continuous and discontinuous breakdown of hydrous phases with increasing temperatures. The apparently too high PT estimates may therefore reflect conditions of melt-crystallisation of the melt upon injection into water undersaturated melt. We argue that the crystallisation of *in-situ* leucosomes may be similarly explained, thus most likely when migmatites cool-down during exhumation, and retrograde hydration reactions in the solid rocks are initiated. As a consequence, partial melts observed

at one outcrop may have formed and crystallised at different conditions. The complete melt fraction observed at an individual outcrop would thus overestimate the melt fraction present at a single point in time. Similarly, Mogk (1992) suggested for a migmatite terrain in the Gallatin Range (USA) that at any one time there is only a small melt fraction present in any part of the system, and melt will be constrained to localised envelopes around shear zones. Although the above sketched scenario may explain why temperatures during crystallisation of the leucosomes may have been higher than those suggested by TWQ-modelling, such high temperatures are again at odds with the suggestion that the TWQ-modelling portrays conditions near P at T_{Max}. We suggest that only improved thermodynamic standard state data and solution models, especially for biotite and amphiboles, may help resolve these problems.

Discussion and conclusions

This study shows that evidence of Alpine migmatisation and dyke intrusion in the Central Alps is unequivocal, but that it is constrained to the Southern Steep Belt and immediately adjacent areas. Thus, besides of being the location of strong deformation, the SSB is also the location of a migmatite belt of Tertiary age. Estimated PT-conditions suggest that dehydration melting was not the only migmatite forming process. Instead, water-assisted partial melting occurred and had been possible in a much larger area than actually observed. Partial melting and dike intrusion occurred over a protracted time, as indicated by the presence of locally deformed as well as completely undeformed dykes and leucosomes. The period can be bracketed between 32 Ma (intrusion of Bergell and related dykes) and 20 Ma (undeformed dyke at Lavertezzo). Most data indicate however ages around 25-28 Ma.

The SSB is the most important structure of the Central Alps and includes several stages of the orogenic history of the Alps: a) It represents a deep part of the Alpine TAC (Engi *et al*., 2001a); b) It is the location of backfolding and backthrusting (Milnes, 1974b; Milnes, 1974a; Heitzmann, 1987; Schmid *et al*., 1989); c) The SSB grades into the mylonites of the Insubric Line which accommodated much strain related to dextral strike slip movements (Schmid *et al*., 1989). All this demonstrates that the SSB was the location of major deformation over a protracted time interval. The coincidence of this structure with Alpine migmatisation suggests a genetic link between deformation and migmatisation, such as enhanced heat-, fluid- or melt-flow along this structure. For instance, dynamic coupling of deformation and enhanced fluid flow has often been invoked (Etheridge *et al*., 1983; Kerrich, 1986; Mogk, 1992; Ferry, 1994; Oliver, 1996). Rock anisotropy may additionally have contributed to this coincidence, with fluid, melt or heat flow parallel to the foliation of a rock being preferred and faster than across the foliation (Wenk, 1970; Manning and Ingebritsen, 1999) (see also chapter 4).

For the SSB we propose that, besides of PT conditions, the present extent of the migmatite belt was largely controlled by the focused deformation, which promoted enhanced heat-, melt- and fluid-flow and associated water-fluxed partial melting. Therefore, the already developed and developing steeply dipping structures of the SSB may have allowed for a faster upward heat and fluid flux than was possible in the flat lying nappes adjacent to the north (Fig. 2). It is worth noting that similar steep structures occur in other migmatite belts that were in part produced by water-assisted partial melting (Mogk, 1992). Other studies performed in the SSB similarly proposed that fluid flow may have been responsible for the formation of some of the migmatites (Schärer *et al*., 1996; Gebauer, 1999). Other authors emphasised the localised deformation and the steeply inclined planar structures in the SSB that had likely enhanced the local heat flow and resulted in the partial fusion of the rocks (Stern, 1966; Wenk, 1970; Romer *et al*., 1996). We note that the coupling of heat and fluid flow is likely, as migrating aqueous fluids or silicate liquids may advect heat up into higher levels of the Crust.

The coincidence of migmatisation and deformation may also have been important for the tectonic evolution of the Central Alps, as the presence of melt causes effective weakening, resulting in increased strain rates and exhumation velocities in the Central Alps. Late orogenic back-thrusting of the Lepontine over the Southern Alps was thus likely accompanied and accelerated by the presence of melt in the SSB. An estimate of its significance for the Central Alps is however complicated by several factors: a) The amount of melt present at different localities varies considerably as a function of bulk composition and the amount of infiltrating fluid. b) It remains uncertain whether all leucosomes were in the liquid state at the same time and PT-conditions (see discussion above). c) Strain accommodated inside melt-rich zones may not be visible after crystallisation of the melt. For example, in many of the stromatic orthogneisses (which exhibit melt fractions > 20%) inside the so called Mergoscia-zone (former Injektionsgneisszone von Mergoscia), fabrics appear magmatic rather than metamorphic. Rocks from this zone typically lack a tight and pervasive foliation or lineation. As a consequence, some areas of the SSB may have behaved as a crystal-rich mush, whereas other areas behaved as essentially solid rocks. Because strain partitions into the weakest rheology, considerable strains may have been taken up by the more pervasively molten rocks of the Mergoscia-zone, although after the crystallisation of the melt, such high strains are no longer apparent.

References

Anderson, J. L. & Smith, D. R. (1995): The effects of temperature and fO2 on the Al-in-honblende barometer. American Mineralogist 80, 549-559.

Ashworth, J. R. (1985): Migmatites. In: Ashworth, J. R. : Migmatites. Blackie, , 1-31.

Bächlin, R., Bianconi, F., Codoni, A., Vesco, E. D., Knoblauch, P., Kündig, E., Reinhard, M., Spaenhauer, F., Spicher, A., Trommsdorff, V. & Wenk, E. (1981): Blatt 1313 Bellinzona. Geologischer Atlas der Schweiz ed. Schweizerische Geologische Kommission.

Barraud, J., Gardien, V., Allemand, P. & Grandjean, P. (2004): Analogue models of melt-flow networks in folding migmatites. Journal of Structural Geology 26, 307-324.

Berger, A. (1995): Magmatic and solid state flow during the syntectonic emplacement of the Bergell pluton (southeastern part): field studies and microstructural analysis. Dissertation, Basel.

Berman, R. G. (1988): Internally consistent thermodynamic data for minerals in the systen Na_2O-K_2O-CaO-FeO-Fe_2O_3-Al_2O_3-SiO_2-TiO_2-H_2O-CO_2. Journal of Petrology 29, 445-522.

Blattner, P. (1965): Ein anatektisches Gneissmassiv zwischen Valle Bodengo und Valle di Livo (Prov. Sondrio und Como). Schweiz. Mineral. Petrogr. Mitt. 45/2, 973-1071.

Brouwer, F. M. (2000): Thermal evolution of high-pressure metamorphic rocks in the Alps. Doctoral Thesis, Universiteit Utrecht, Geologica Ultraiectina 199, 224 pp.

Brown, M., Averkin, Y. A. & McLellan, E. L. (1995): Melt segregation in migmatites. Journal of Geophysical Research 100/B8, 15655-15679.

Brown, M. & Solar, G. S. (1998): Shear-zone systems and melts: feedback relations and self-organization in orogenic belts. Journal of Structural Geology 20/2/3, 211-227.

Brown, T. H., Berman, R. G. & Perkins, E. H. (1988): GEØ-CALC: Software package for calculation and display of pressure-temperature-composition phase diagrams using an IBM or compatible personal computer. Comp. Geosci. 14, 279-289.

Burri, T. (1999): Metamorphism and tectonics within the Vergeletto "Spoon" (Southern Valle Maggia, Ticino). Diploma Thesis, University of Berne, 112 pp.

Cadisch, J. (1953): Geologie der Schweizer Alpen. Wepf&Co Publishers, Basel, 480 pp.

Carrupt, E. (2003): New stratigraphic, structural and geochemical data from the Val Formazza - Binntal area (Central Alps). Dissertation, Université de Lausanne, Mémoires de Géologie (Lausanne), No. 41, 2003, 118 pp.

Dale, J. & Holland, T. J. B. (2003): Geothermobarometry, P-T paths and metamorphic field gradients of high-pressure rocks from the Adula Nappe, Central Alps. Journal of Metamorphic Geology 21, 813-829.

Droop, G. T. R. & Bucher-Nurminen, K. (1984): Reaction textures and metamorphic evolution of sapphirine-bearing granulites from the Gruf Complex, Italian Central Alps. Journal of Petrology 25/3, 766-8031.

Engi, M., Berger, A. & Roselle, G. T. (2001a): Role of the tectonic accretion channel in collisional orogeny. Geology 29/12, 1143-1146.

Engi, M., Scherrer, N. C. & Burri, T. (2001b): Metamorphic evolution of pelitic rocks of the Monte Rosa nappe: Constraints from petrology and single grain monazite data. Schweiz. Mineral. Petrogr. Mitt. 81/3, 305-328.

Engi, M., Todd, C. S. & Schmatz, D. R. (1995): Tertiary metamorphic conditions in the eastern Lepontine Alps. Schweiz. Mineral. Petrogr. Mitt. 75, 347-369.

Etheridge, M. A., Wall, V. J. & Vernon, R. H. (1983): The role of the fluid phase during regional metamorphism and deformation. Journal of Metamorphic Geology 1, 205-226.

Ferry, J. M. (1994): A historical review of metamorphic fluid flow. Journal of Geophysical Research 99/B8, 15487-15498.

Frey, M., Bucher, K., Frank, E. & Mullis, J. (1980): Alpine metamorphism along the Geotraverse Basel-Chiasso-a review. Eclogae geol. Helv. 73/2, 527-546.

Frey, M., Desmons, J. & Neubauer, F. (1999): The new metamorphic map of the Alps. Schweiz. Mineral. Petrogr. Mitt. 79. Stäubli Verlag AG, Zürich, 230 pp.

Gardien, V., Thompson, A. B. & Ulmer, P. (2000): Melting of Biotite + Plagioclase + Quartz Gneisses: the role of H2O in the stability of amphibole. Journal of Petrology 41/5, 651-666.

Gebauer, D. (1999): Alpine geochronology of the Central and Western Alps: new constraints for a complex geodynamic evolution. Schweiz. Mineral. Petrogr. Mitt. 79/1, 191-208.

Grandjean, V. (2001): Petrographical evolution of mafic relics and their implication for the geodynamics of the Central Alps. Dissertation, University of Berne, 103 pp.

Grubenmann, U. (1910): Über einige tiefe Gneise aus den Schweizeralpen: C.R.X1 Congr. Geol. Int. Stockholm, 625.

Gruskovnjak, A. (2002): Geologische und petrographische Untersuchungen im Lepontin im Grenzbereich von Maggia- und Simanodecke (Ticino). Diplomarbeit, Universität Bern, 87 pp.

Günthert, A. W. (1954): Beiträge zur Petrographie und Geologie des Maggia-Lappens (NW-Tessin). Schweiz. Mineral. Petrogr. Mitt. 34/1, 159.

Günthert, A. W. (1956): Ueber das alpine Alter der penninischen Deckengesteine des WTessins und der angrenzenden Simplon-Region. Geologische Rundschau 45/2, 194-202.

Gutzwiller, E. (1912): Injektionsgneisse aus dem Kanton Tessin. Dissertation, Universität Zürich, 64 pp.

Hafner, M. (1993): Strukturgeologische und geochemische Untersuchungen von leukokraten Granit-Gängen und Migmatiten der südlichen Adula am Monte Peschiera (It). Diplom, Basel..

Hänny, R. (1972): Das Migmatitgebiet der Valle Bodengo (östliches Lepontin). Beiträge zur geologischen Karte der Schweiz. Neue Folge 145.

Hänny, R., Grauert, B. & Soptrajanova, G. (1975): Paleozoic migmatites affected by high-grade tertiary metamorphism in the Central Alps (Valle Bodengo, Italy). Contrib. Mineral. Petrol. 51, 173-196.

Häuselmann, P. (1997): Zur Geologie des Val Vergeletto (Ti). Diplomarbeit, Bern, 98 pp.

Heitzmann, P. (1987): Evidence of late Oligocene/early Miocene backthrusting in the central alpine "root zone". Geodinamica Acta 1/3, 182-192.

Holland, T. & Blundy, J. (1994): Non-ideal interactions in calcic amphiboles and their bearing on amphibole-plagioclase thermometry. Contrib. Mineral. Petrol. 116, 433-447.

Holtz, F. & Johannes, W. (1994): Maximum and minimum water contents of granitic melts: implications for chemical and physical properties of ascending magmas. Lithos 32, 149-159.

Holtz, F., Johannes, W., Tamic, N. & Behrens, H. (2001): Maximum and minimum water contents of granitic melts generated in the crust: a reevaluation and implications. Lithos 56, 1-14.

Hugi, E. (1922): Das Aarmassiv ein Beispiel alpiner Granitintrusion: Hauptversammlung der Schweizerischen Naturforschenden Gesellschaft. Verhandlungen der Schweizer. Naturforschenden Gesellschaft 2. Bern, 86-109.
Hunziker, J. C., Desmons, J. & Hurford, A. J. (1992): Thirty-two years of geochronological work in the Central and Western Alps: a review on seven maps. Mémoire de Géologie (Lausanne) 13. , Lausanne.
Institute, A. G. (1957): Dictionary of geological terms. Third ed. Dolphin Books, New York, 545 pp.
Irouschek, A. (1980): Zur Verbreitung von Cordierit im zentralen Lepontin. Schweiz. Mineral. Petrogr. Mitt. 60/2-3, 137-144.
Johannes, W. & Holtz, F. (1996): Petrogenesis and experimental petrology of granitic rocks. Minerals and Rocks. Springer Verlag, Berlin, 335 pp.
Keller, L. M. (2004): Relationships between metamorphism and deformation: Examples from the Western Alps (Camughera-Moncucco unit and Monte Rosa Nappe, N'Italy). Dissertation, University of Basel, 133 pp.
Kern, R. (1947): Zur Petrographie des Centovalli. Dissertation, ETH-Zürich, 95 pp.
Kerrich, R. (1986): Fluid infiltration into fault zones: Chemical, isotopic and mechanical effects. PAGEOPH 124/1/2, 225-268.
Klemm, G. (1906/1907): Bericht über Untersuchungen an den sog. Gneisen und den metamorphen Schiefern der Tessiner Alpen: K.pr.Akad.d.Wissensch..
Knup, P. (1958): Geologie und Petrographie des Gebietes zwischen Centovalli-Valle Vigezzo und Onsernone. Schweiz. Mineral. Petrogr. Mitt. 38/1, 236.
Kobe, H. (1956): Geologisch-Petrographische Untersuchungen in der Tessiner Wurzelzone zwischen Vergeletto-Onsernone und Valle Maggia. Schweiz. Mineral. Petrogr. Mitt. 36/1,
Köppel, V. & Grünenfelder, M. (1975): Concordant U-Pb ages of monazite and xenotime from the Central Alps and the timing of the high temperature Alpine metamorphism, a preliminmary report. Schweiz. Mineral. Petrogr. Mitt. 55/1, 129-132.
Köppel, V., Günthert, A. W. & Grünenfelder, M. (1980): Patterns of U-Pb zircon and monazite ages in polymetamorphic units of the Swiss Central Alps. Schweiz. Mineral. Petrogr. Mitt. 61, 97-119.
Kündig, E. (1926): Beiträge zur Geologie und Petrographie der Gebirgskette zwischen Val Calanca und Misox. Schweiz. Mineral. Petrogr. Mitt. 6, 1-96.
Leonardi, U. (2003): Zur Abgrenzung und Entwicklung der Cima Lunga und angrenzende Einheiten im Gebiet von Valle di Drosina - Valle di Lodrino (Kanton Tessin). Diplomarbeit, Universität Bern, 105 pp.
London, D. (1992): The application of experimental petrology to the genesis and crystallization of granitic pegmatites. Canadian Mineralogist 30/3, 499-540.
Mac Gregor, M. & Wilson, G. (1939): On granitization and associated processes. Geol. Mag. 76, 193.
Mancktelow, N. S. (1992): Neogene lateral extension during convergence in the Central Alps: Evidence from interrelated faulting and backfolding around the Simplonpass (Switzerland). Tectonophysics 215, 295-317.
Manktelow, N. S. (2002): Finite-element modelling of shear zone development in viscoelastic materials and its implications for localisation of partial melting. Journal of Structural Geology 24, 1045-1053.
Manning, C. E. & Ingebritsen, S. E. (1999): Permeability of the continental crust: Implications of geothermal data and metamorphic systems. Reviews of Geophysics 37/1, 127-150.
Mehnert, K. R. (1968): Migmatites and the origin of granitic rocks. Elsevier, Amsterdam, 393 pp.
Milnes, A. G. (1969): On the orogenic history of the central alps. Journal of Geology 77, 108-112.
Milnes, A. G. (1974a): Post-Nappe Folding in the Western Lepontine Alps. Eclogae geol. Helv. 67/2, 333-348.
Milnes, A. G. (1974b): Structure of the Pennine Zone (Central Alps): A new working hypothesis. Geol.Soc.Amer. Bulletin 85, 1727-1732.
Mittelholzer, A. E. (1936): Beitrag zur Kenntnis der Metamorphose in der Tessiner Wurzelzone. Schweiz. Mineral. Petrogr. Mitt. 16, 182.
Mogk, D. W. (1992): Ductile shearing and migmatization at mid-crustal levels in an Archaean high-grade gneiss belt, northern Gallatin Range, Montana, USA. Journal of Metamorphic Geology 10, 427-438.
Nagel, T. (2000): Metamorphic and structural history of the southern Adula nappe (Graubünden, Switzerland). Doctoral thesis, Universität Basel, 3 chapters.
Nagel, T., Capitani, C. d. & Frey, M. (2002): Isograds and P-T evolution in the eastern Lepontine Alps (Graubünden, Switzerland). Journal of Metamorphic Geology 20, 309-324.
Naney, M. T. (1983): Phase equilibria of rock forming ferromagnesian silicates in granitic systems. American Journal of Science 283, 993-1033.
Niggli, E. (1970): Alpine Metamorphose und alpine Gebirgsbildung. Fortschr. Miner. 47/1, 16-26.
Niggli, E. & Niggli, C. R. (1965): Karten der Verbreitung einiger Mineralien der alpidischen Metamorphose in den Schweizer Alpen. Eclogae geol. Helv. 58, 335-368.
Niggli, P. (1950): Probleme der alpinen Gesteinsmetamorphose. Schweiz. Mineral. Petrogr. Mitt. 30/2, 500-538.
Nussbaum, C., Marquer, D. & Biino, G. G. (1998): Two subduction events in a polycyclic basement: Alpine and pre-Alpine high-pressure metamorphism in the Suretta nappe, Swiss Eastern Alps. Journal of Metamorphic Geology 16, 591-605.
Oliver, N. H. S. (1996): Review and classification of structural controls on fluid flow during regional metamorphism. Journal of Metamorphic Geology 14, 477-492.
Paraskevopoulos, G. M. (1953): Beitrag zur Kenntnis der Feldspäte der Tessiner Pegmatite. Tschermaks Min. u. Petr. Mitt. 3/3, 191.
Pfeifer, H. R., Colombi, A., Ganguin, J., Hunziker, J. C., Oberhänsli, R. & Santini, L. (1991): Relics of high-pressure metamorphism in different lithologies of the Central Alps, an updated inventory. Schweiz. Mineral. Petrogr. Mitt. 71, 441-451.
Pitcher, W. S. (1997): The nature and origin of granite. 2nd ed. . Chapman and Hall, London, 387 pp.
Preiswerk, H. (1925a): Tessinergneiss. Eclogae geol. Helv. 19/1, 177-187.
Preiswerk, H. (1925b): Vom Gestein im Tessin. Die Alpen 12, 441-461.
Read, H. H. (1957): The granite controversy. Thomas Murby & Co, London, 430 pp.
Reinhardt, B. (1966): Geologie und Petrographie der Monte-Rosa-Zone, der Sesia-Zone und des Canavese im Gebiet zwischen Valle d'Ossola und Valle Loana (Prov. die Novara, Italien). Schweiz. Mineral. Petrogr. Mitt. 46/2, 553-.
Romer, R. L., Schärer, U. & Steck, A. (1996): Alpine and pre-Alpine magmatism in the root-zone of the western Central Alps. Contrib. Mineral. Petrol. 123, 138-158.
Rosenberg, C. L. (2001): Deformation of partially molten granite: a review and comparison of experimental and natural case studies. Int. J. Earth Science (Geol. Rundsch.) 90, 60-76.
Rosenberg, C. L. & Handy, M. R. (2000): Syntectonic melt pathways during simple shearing of a partially molten rock analogue (Norcamphor-Benzamide). Journal of Geophysical Research 105/B2, 3135-3149.
Rubin, A. M. (1995): Getting granite dikes out of the source region. Journal of Geophysical Research 100/B4, 5911-5929.

Sawyer, E. W. (2000): Grain-scale and outcrop-scale distribution and movement of melt in a crystallising granite. Transactions of the Royal Society of Edinburgh: Earth Sciences 91, 73-85.
Sawyer, E. W. (2001): Melt segregation in the continental crust: distribution and movement of melt in anatectic rocks. Journal of Metamorphic Geology 19, 291-309.
Schärer, U., Cosca, M., Steck, A. & Hunziker, J. C. (1996): Termination of major ductile strike-slip shear and differential cooling along the Insubric Line (Central Alps); U-Pb, Rb-Sr and (super 40) Ar/ (super 39) Ar ages of cross-cutting pegmatites. Earth and Planetary Science Letters 142/3-4, 331-351.
Schmid, S. M., Aebli, H. R., Heller, F. & Zingg, A. (1989): The role of the Periadriatic Line in the tectonic evolution of the Alps. In: Coward, M. P., Dietrich, D. & Park, R. G. : Alpine tectonics Geological Society Special Publication 45. Geological Society of London, , 153-171.
Schmidt, M. W. (1992): Amphibole composition in tonalite as a function of pressure: an experimental calibration of the Al-in-hornblende barometer. Contrib. Mineral. Petrol. 110, 304-310.
Schmidt, M. W. (1993): Phase relations and compositions in tonalite as a function of pressure: An experimental study at 650°C. American Journal of Science 293, 1011-1060.
Sharma, R. S. (1969): On banded gneisses and migmatites from Lavertezzo and Rozzera (Valle Verzasca, canton Ticino). Schweiz. Mineral. Petrogr. Mitt. 49/2, 199-276.
Steck, A. (1984): Structures de deformations tertiaires dans les Alpes centrales. Eclogae geol. Helv. 77/1, 55-100.
Steck, A. & Hunziker, J. C. (1994): The Tertiary structural and thermal evolution of the Central Alps; compressional and extensional structures in an orogenic belt. In: Seranne, M. & Malavieille, J. : Late orogenic extension. 238. Tectonophysics, 229-254.
Stern, W. B. (1966): Zur Mineralchemie von Glimmern aus Tessiner Pegmatiten. Schweiz. Mineral. Petrogr. Mitt. 46, 137-181.
Taddei, C. (1938): Notizie mineralogiche ticinesi: berillo e prenite di Cresciano sul Sasso (Riviera). Schweiz. Mineral. Petrogr. Mitt. 18, 437-440.
Taddei, C. (1940): Pegmatiti della Svizzera Italiana e minerali in esse contenuti. Schweiz. Mineral. Petrogr. Mitt. 20, 247-252.
Thompson, P. H. (1976): Isograd patterns and pressure-temperature distributions during regional metamorphism. Contrib. Mineral. Petrol. 57, 277-295.
Todd, C. S. & Engi, M. (1997): Metamorphic field gradients in the Central Alps. Journal of Metamorphic Geology 15, 513-530.
Tóth, T. M., Grandjean, V. & Engi, M. (2000): Polyphase evolution and reaction sequence of compositional domains in metabasalt; a model based on local chemical equilibrium and metamorphic differentiation. Geological Journal 35/3-4, 163-183.
Trommsdorff, V. (1966): Progressive Metamorphose kieseliger Karbonatgesteine in den Zentralalpen zwischen Bernina und Simplon. Schweiz. Mineral. Petrogr. Mitt. 46, 431-460.
Trommsdorff, V. (1990): Metamorphism and tectonics in the Central Alps: The Alpine lithospheric mélange of Cima Lunga and Adula. Mem. Soc. Geol. It. 45, 39-49.
Vernon, R. H. (2000): Review of microstructural evidence of magmatic and solid-state flow. Electronic Geosciences 5/2,
Villa, I. M. (1998): Isotopic closure. Terra Nova 10, 42-47.
von Blanckenburg, F. (1992): Combined high-precision chronometry and geochemical tracing using accessory minerals: applied to the Central-Alpine Bergell intrusion (central Europe). Chemical Geology 100, 19-40.
von Blanckenburg, F., Früh-Green, G., Diethelm, K. & Stille, P. (1992): Nd-, Sr-, O-isotopic and chemical evidence for a two-stage contamination history of mantle magma in the Central-Alpine Bergell intrusion. Contrib. Mineral. Petrol. 110, 33-45.
von Blanckenburg, F., Kagami, H., Deutsch, A., Oberli, F., Meier, M., Wiedenbeck, M., Barth, S. & Fischer, H. (1998): The origin of Alpine plutons along the Periadriatic Lineament. Schweiz. Mineral. Petrogr. Mitt. 78/1, 55-66.
von Raumer, J. & Neubauer, F. (1993): Pre-Mesozoic geology in the alps . Springer Verlag, Heidelberg, 677 pp.
Wenk, E. (1953): Prinzipielles zur geologischen Gliederung des Penninikums im zentralen Tessin. Eclogae geol. Helv. 46, 9-21.
Wenk, E. (1962): Das reaktivierte Grundgebirge der Zentralalpen. Geologische Rundschau 52, 754-766.
Wenk, E. (1966): Einige Probleme des anatektischen Unterbaus der Alpen.: Etages tectonique. Colloque de Neuchâtel, 83-87.
Wenk, E. (1970): Zur Regionalmetamorphose und Ultrametamorphose im Lepontin. Fortschr. Miner. 47/1, 34-51.
Wenk, E. (1975): Zur alpinen Metamorphose. Schweiz. Mineral. Petrogr. Mitt. 55/1, 116-125.
White, R. W. & Powell, R. (2002): Melt loss and the preservation of granulite facies mineral assemblages. Journal of Metamorphic Geology 20, 621-632.
White, R. W., Powell, R. & Holland, T. J. B. (2001): Calculation of partial melting equilibria in the system Na_2O-CaO-K_2O-FeO-MgO-Al_2O_3-SiO_2-H_2O (NCKFMASH). Journal of Metamorphic Geology 19, 139-153.
Winkler, H. G. F. (1979): Petrogenesis of metamorphic rocks. 5′th ed. . Springer Verlag, New York, 348 pp.
Zawadynski, L. (1952): Geologisch-petrographische Untersuchungen in der Valle Onsernone (Tessin). Schweiz. Mineral. Petrogr. Mitt. 32/1,
Zwart, H. J. (1967): The duality of orogenic belts. Geologie en Mijnbouw 46/8, 283-309.

Appendix

Selected analyses of amphiboles (All Fe as FeO)

Reference	Fon7	Merg2B	Ave5	Wurz251a	Wurz129	Vz578	Vz470	Pon3	Pon5a	Bag6	Ar9902-1	8A19-109-1	7A86.2-h6-1	7A97-38-1	7A96-49-1	7A101-7-1
assemlage	1.3	1.1	3.2	5	6	2.2	1.1	point113	point7	point68	1	1	1	1	1	1
compund	wt%	wt%	wt%	wt%	wt%	wt%	wt%	wt%	wt%	wt%	wt%	wt%	wt%	wt%	wt%	wt%
F-	0.18	0.13	0.12	0.04	0.12	0.17	0.23	0.18	0.17	0.28	n.d.	n.d.	n.d.	n.d.	n.d.	n.d.
Na2O	1.41	1.45	1.37	1.28	1.41	1.17	1.34	1.28	1.32	1.74	1.13	1.38	1.09	1.15	1.24	1.27
MgO	6.30	7.18	7.00	8.24	7.11	6.96	7.92	8.98	8.98	7.91	8.16	9.52	8.49	7.58	7.84	8.98
Al2O3	12.76	13.24	12.56	12.77	13.49	13.28	13.17	13.14	13.15	10.48	13.31	12.86	11.81	12.52	11.95	12.12
SiO2	39.36	39.44	39.59	41.12	40.22	40.53	40.43	42.16	41.98	42.75	41.20	40.55	41.19	40.42	40.09	41.35
Cl-	0.02	0.02	0.03	0.00	0.01	0.01	0.02	0.01	0.00	0.01	n.d.	n.d.	n.d.	n.d.	n.d.	n.d.
K2O	1.81	1.90	1.80	1.48	1.65	1.74	1.85	1.68	1.68	1.57	1.43	1.70	1.39	1.77	1.53	1.51
CaO	11.14	11.26	11.15	11.69	11.41	11.52	11.49	11.50	11.74	10.68	11.56	11.70	11.69	11.66	11.27	11.52
TiO2	0.72	1.10	1.00	0.79	0.92	0.88	1.14	0.87	0.79	0.89	1.01	1.10	0.98	1.15	1.11	0.88
Cr2O3	0.06	0.00	0.00	0.00	0.00	0.00	0.00	0.00	0.00	0.00	0.00	0.00	0.12	0.04	0.04	0.04
MnO	0.55	0.66	0.87	0.41	0.63	0.52	0.49	0.65	0.62	0.56	0.71	0.45	0.41	0.53	0.64	0.73
FeO	23.06	20.94	21.49	20.10	21.08	21.95	20.38	17.89	17.38	22.06	20.07	17.80	20.12	20.39	20.18	18.61
BaO	0.04	0.03	0.06	0.03	0.02	0.01	0.00	0.03	0.07	n.d.	n.d.	n.d.	n.d.	n.d.	n.d.	n.d.
Total	97.42	97.35	97.04	97.95	98.07	98.74	98.44	98.37	97.90	98.94	98.57	97.05	97.29	97.21	95.89	97.01
-O as F+Cl	0.08	0.06	0.06	0.02	0.05	0.07	0.10	0.08	0.07	0.12	0.00	0.00	0.00	0.00	0.00	0.00
Total	97.34	97.29	96.98	97.93	98.02	98.66	98.34	98.30	97.83	98.82	98.57	97.05	97.29	97.21	95.89	97.01

Selected analyses of plagioclase

Reference	Fon7	Merg2B	Ave5	Wurz251a	Wurz129	Vz578	Vz470	Pon3	Pon5a	Bag6	Ar9902-1	8A19-107-1	7A86-f7-1	7A97-43-1	7A96-46-1	7A101-8-1
assemblage	1.3	1.1	3.2	5	6	2.2	1.1	point116	point8	point70	1	1	1	1	1	1
compound	wt%	wt%	wt%	wt%	wt%	wt%	wt%	wt%	wt%	wt%	wt%	wt%	wt%	wt%	wt%	wt%
Na2O	8.67	8.45	8.58	8.09	8.10	7.08	7.52	7.36	7.16	10.56	8.10	7.66	7.52	7.52	8.19	0.54
MgO	0.00	0.00	0.01	0.01	0.01	0.01	0.01	0.00	0.01	0.01	0.00	0.01	0.00	0.01	0.00	0.01
Al2O3	24.13	25.19	24.35	25.12	25.72	25.89	25.86	26.76	26.92	21.90	25.76	26.41	25.35	24.45	24.43	18.18
SiO2	61.49	60.32	60.88	61.18	60.73	58.04	59.56	59.92	59.78	67.35	61.17	58.65	59.17	60.10	61.19	64.56
K2O	0.27	0.13	0.23	0.29	0.22	0.23	0.99	0.26	0.24	0.25	0.39	0.17	0.22	0.28	0.32	15.92
CaO	5.17	5.97	5.37	6.22	6.60	7.47	6.21	7.60	7.92	2.41	6.67	7.07	7.43	7.23	5.76	0.01
MnO	0.00	0.07	0.01	0.01	0.00	0.00	0.03	0.01	0.00	0.01	0.02	0.02	0.00	0.00	0.00	0.04
Fe2O3	0.15	0.14	0.13	0.32	0.10	0.31	0.25	0.00	0.00	0.18	n.d.	n.d.	n.d.	n.d.	n.d.	n.d.
SrO	0.05	0.00	0.09	0.03	0.01	0.00	0.00	n.d.	n.d.	n.d.	n.d.	n.d.	n.d.	n.d.	n.d.	n.d.
BaO	0.00	0.04	0.00	0.00	0.02	0.00	0.02	0.08	0.06	n.d.	0.07	0.23	0.34	0.19	0.13	0.26
Total	99.94	100.30	99.65	101.26	101.51	99.05	100.46	102.08	102.22	102.68	102.18	100.20	100.05	99.79	100.03	99.53
xK [Or]	0.02	0.01	0.01	0.02	0.01	0.01	0.06	0.01	0.01	0.01	0.02	0.01	0.01	0.02	0.02	0.95
xNa [Ab]	0.74	0.71	0.73	0.69	0.68	0.62	0.65	0.63	0.61	0.88	0.67	0.66	0.64	0.64	0.71	0.05
xCa [An]	0.24	0.28	0.25	0.29	0.31	0.36	0.30	0.36	0.37	0.11	0.31	0.33	0.35	0.34	0.27	0.00

Table 2) Representative compositions of amphibole and plagioclase used for thermobarometry.

Appendix

Glossary of old fashioned migmatite expressions.

The classic literature concerned with anatectic processes is often confusing, due to the use of now obsolete expressions. These have been abandoned largely because they were part of a specific concept or theory, which has since been superseded.
Explanations are partially taken from the "Dictionary of Geological Terms " (Institute, 1957), from (Mehnert, 1968) and from (Ashworth, 1985).

- Palingenesis: "Rebirth". The process of formation of new magma by the melting or fusion of country rocks with heat from another magma, with or without addition of granitic material (the latter is also termed granitisation).
- Granitisation: A term used with somewhat different connotations by different authors. Usually denotes the production of *in situ* granitoid bodies by metasomatic processes. Granitisation does not necessarily involve partial melting or melt injection, but may also be a purely metasomatic process. "Granitised" rock bodies usually contain abundant enclaves of host rock and are interpreted to have directly evolved from them.
- Ultrametamorphism: Similar to granitisation, but connected to partial anatexis rather than pure metasomatism. Extensively used to explain migmatitic areas inside the Lepontine by Wenk and co-workers.
- Ichor (proposed by J.J. Sederholm) "Juice or liquor" derived from a granitic magma, which is capable of granitising solid rocks. Synonyms: emanation, mineraliser, residual magma
- Exsudation: Nicely invokes that even rocks sweat under amphibolite facies conditions. Describes matter extracted from a solid rock and deposited elsewhere. Genesis or origin are usually unclear or explained in diverging manners as either fluid- or liquid-derived.
- Arterite: A banded migmatite with leucosomes interpreted to have intruded from outside.
- Veinite: A banded migmatite with the leucosomes interpreted to be *in situ* partial melts.
- Injection gneiss: a gneiss with banding being wholly or partly due to (layer parallel) lit-par-lit injection of granitic magma. Synonyms: composite gneiss, similar to arterites
- Mischgneiss or mixed gneisses: Synonymous to migmatite in so far that they represent a composite of leucocratic (igneous) and of meso- to melanocratic (metamorphic) rocks. Genetically, however, they were interpreted to represent a transitional state during subsolidus "orthogneissification".
- Neosome-paleosome: Still used in the recent literature, but should be abandoned due to their over-simplistic view. Neosome comprises leuco and melanosome (see definitions below). Paleosome is equivalent to mesosome and denotes the unmolten part of a rock.

Expressions used in this study

Much of the following terms are based on the nomenclature originally proposed by (Mehnert, 1968) and reviewed in (Ashworth, 1985).

- Migmatite: A rock, found in medium- to high-grade metamorphic areas, that is pervasively inhomogeneous on a macroscopic scale, one part being pale-coloured and consistently of quartzofeldspathic of feldspathic composition. Commonly, these leucocratic domains show a magmatic fabric.
- Anatexis: *In situ* partial melting of a rock.
- Leuco-, meso- and melanosome: Description of the different domains of an in situ migmatite in terms of their relative colours and implied genetic origin. Leucosomes are the bright parts, mesosomes the intermediate, and melanosomes the dark parts of a migmatite. Leucosome is also frequently used to denote the segregated melt fraction of a partially molten rock and melanosome as the restitic part of a migmatite. Mesosome is interpreted as the unmolten equivalent of the migmatite.
- Metatexis and diatexis: Denotes the degree of partial melting in migmatites. Metatexis characterises a moderate degree of partial melting (< 30-50%) with leucosome subordinate to the rest of the rock. Structures of the protolith do not rupture.

Diatexis describes a high degree of partial melting (>30-50%). Structures of the protolith are often disintegrated or only survive as "ghost" structures or schollen.

- Structural terms used to describe observed outcrop features.

Stromatic-type: layered to banded migmatites with often "undulating" foliation. The common type of metatexite.

Agmatic-type: Breccia-like migmatite with small or large amounts of leucosome.

Schollen-type: Schollen of host-rock inside leucosome.

Schlieren or nebulitic-type: Leucosome-dominated migmatite with many transitions of host rock into leucosome.

Schollen, schlieren/nebulitc and in part agmatitic types are typical representants of diatexitic migmatites.

Restite formation by water assisted partial melting in the Central Alps.

Thomas Burri

Abstract

We document observations made on a local suite of metapelitic restites sampled from the late Alpine migmatite belt of the Central Alps. Using thermodynamic computation, we infer that the investigated samples have formed in the course of water assisted partial melting rather than by dehydration melting. Associated partially molten orthogneiss lacking any trace of dehydration melting reaction products like sillimanite, garnet, cordierite or orthopyroxene sustain this interpretation. The measured bulk rock composition indicates that a melt fraction in the order of 0.3 was drained from the rock. Thermodynamic modelling suggests that the rock was effectively resetted during partial melting, in contrast to other metapelitic rocks of the area which have preserved a more complete history. Formation of the restite took place inside the local km-scale Onsernone-antiform, which formed coeval with partial melting. Deformation lead to enhanced fluid flow inside the antiformal structure, especially in areas composed of different rock types, where deformation may become localised. Localisation of deformation and fluid flow may then have triggered partial melting at conditions below dehydration-melting of muscovite.

Introduction

Migmatisation in the Lepontine area (Ticino, Switzerland) in the course of the Alpine orogeny has been controversial since the beginning of the last century. The relatively weak Alpine overprint in the external massifs has allowed an early recognition of pre-Alpine periods of intrusive and migmatitic activity. Since it has been recognised that also the crystalline basement nappes in the Lepontine-area had undergone a pre-Alpine phase of intrusion and metamorphism, discussion has centred on the age and extent of the Alpine part of migmatisation. Due to the complicate pre-Alpine history and due to the lack of isotopic age data in the Central Alps up to the 1970's, any statement on the age and significance of the migmatites and plutonic rocks in the Lepontine was associated with ambiguity. Today, it can be stated with some certainty that Alpine migmatisation was confined to the so called Southern Steep Belt (SSB) of the Central Alps and has occurred in the period between 35-25 Ma (see chapter 1).

Restite and migmatite formation are commonly interpreted as high-temperature processes. Restitic rocks are usually formed by the extraction of a fluid enriched partial melt, leaving behind a melt and water depleted restite, commonly enriched in refractory phases such as biotite, garnet, cordierite or orthopyroxene. Based on their characteristic coarse grain size and low mode of hydrous phases, such restites are usually termed granulites, though this term usually implies high temperatures (granulite facies conditions). Partial melting may occur through dehydration melting of hydrous phases like phengite, biotite or amphibole at relatively high temperatures, or through water assisted partial melting at any temperature above the water saturated solidus. In the former case the melt fraction depends on the mode of the decaying hydrous phases, in the latter case on the amount of fluid present in the system: If the fluid stems exclusively from the pore space of a rock, melt fractions are limited to a 1-2% (e.g. Spear *et al*., 1999). If a hydrous fluid infiltrates a rock at conditions above the respective water saturated solidus, the melt fraction is largely a function of the amount of infiltrating fluid. Due to recent progress in the field of computational thermodynamics (de Capitani and Brown, 1987; Holland and Powell, 2001), dynamic anatectic settings can be investigated in terms of phase diagrams and/or calculated mineral compositions. This allows a better understanding of observed textures or phase assemblages and to more reliably decipher a rocks history.

This paper is part of a regional-scale study on Alpine migmatisation in the Central Alps of Switzerland and Italy (chapter 1). It discusses features and processes of partial melting as observed in the Alpine migmatite Belt of the Central Alps, with a special emphasis on partial melting triggered by the infiltration of fluid. We focus on a local suite of conspicuous metapelitic restites, sampled in the Valle Onsernone area (Ticino). To better constrain the evolution of theses rocks, we make extensive use of thermodynamic computation. Segments of the complex Alpine history of this rock can be reliably traced using measured bulk-rock and mineral compositions in combination with thermodynamic computation.

Geologic overview

The Lepontine area consists of the classical Alpine nappe stack that has undergone greenschist to amphibolite facies metamorphism. The flat-lying central part of the Lepontine is delimited by steep E-W-oriented structures, forming a northern and a southern steep belt. The sample locality in the Valle Onsernone area is part of the Southern Steep Belt (SSB, formerly termed root-zone of the Lepontine nappes) (Fig. 1). The SSB is characterised by steeply inclined or even overturned structures, attributed to Tertiary phases of backfolding and backthrusting of the Lepontine nappe stack during continent collision. In the south, the SSB is truncated by the ductile to brittle Insubric Line, and in the western part of the area by the ductile Arcegno-Palanzeno Shear-zone (ductile Simplon-Line of Steck (1984), Steck and Hunziker (1994) and Schärer *et al*. (1996)). The SSB was thus a zone of major deformation of the Central Alps during collision, while at the same time the flat lying central part became only slightly bent by local syn- and antiforms (Fig. 2). The studied samples were collected inside the Onsernone-unit in the core of the local km-scale Onsernone-antiform, which forms here the northern limit of the SSB. In the same unit several relics of high pressure rocks have been reported (Forster, 1947; Kobe, 1956; Colombi and Pfeifer, 1986; Pfeifer *et al*., 1991), and a few new metaeclogitic samples have been found in the last few years in the same area (chapter 5). This has lead to the working hypothesis, that parts of the area could be related to the TAC-units (Tectonic Accretion Channel) of the Central Alps (Engi *et al*., 2001). These relatively well constrained units, which surface further east (Adula, Cima-Lunga, Mergoscia-Arbedo and Orselina-units), are composed of a mélange comprising metasediments, metamafics, meta-ultramafics and orthogneisses.

Most of the Onsernone unit consists of quite unspectacular biotite-gneisses (migmatitic towards the south and east), which are locally transected by heterogeneous trails composed of metasediments, metamafics and orthogneisses (Kobe, 1954; Wenk, 1955; Kobe, 1956; Kobe, 1966). The occurrence of several metaeclogitic rocks inside these trails indicates an affinity with established TAC-units of the Central Alps.

Towards the south and east of Valle Onsernone, Bt-gneisses are increasingly migmatitic. At the sample locality, melt filled shear-zones and other melt segregations inside the homogeneous Bt-gneisses indicate melt production during the formation of the Onsernone-antiform (Fig. 3).

PT-estimates for the research area indicate temperatures near 650°C at a pressure of 6-7 kbar for peak conditions (i.e. P at T_{max}) (Engi *et al*., 1995; Todd and Engi, 1997; Burri, 1999). These estimated tempera-

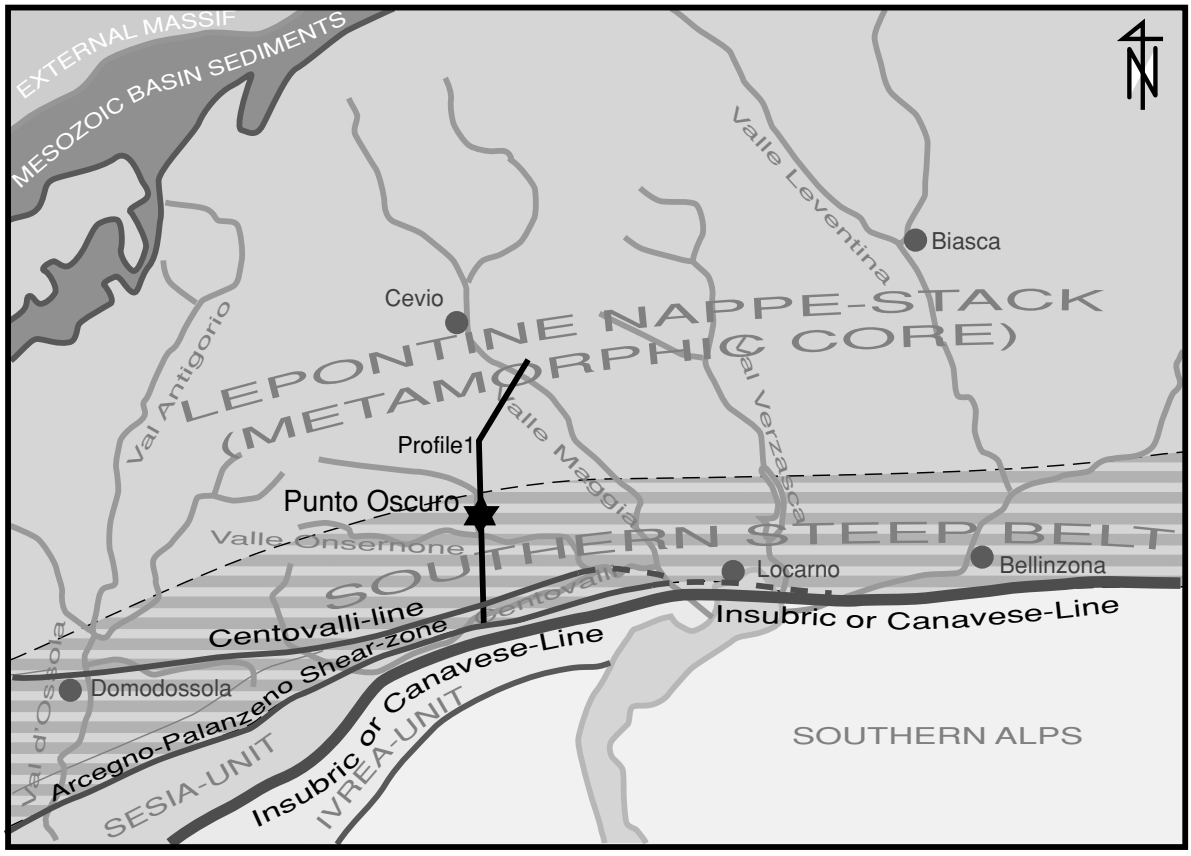

Fig. 1: Tectonic overview of the Lepontine Alps. The Lepontine nappe stack consists of several basement/cover-nappes (schematically outlined by thin grey lines)), which experienced greenschist to amphibolite facies metamorphism. Horizontally striped areas (SSB) largely coincide with the occurrence of the Tertiary migmatite belt. Towards the west, the migmatite-belt narrows compared to the SSB.
Star = Sample locality Ponte Oscuro. The trace of the profile shown in figure 2 runs through the sample locality.

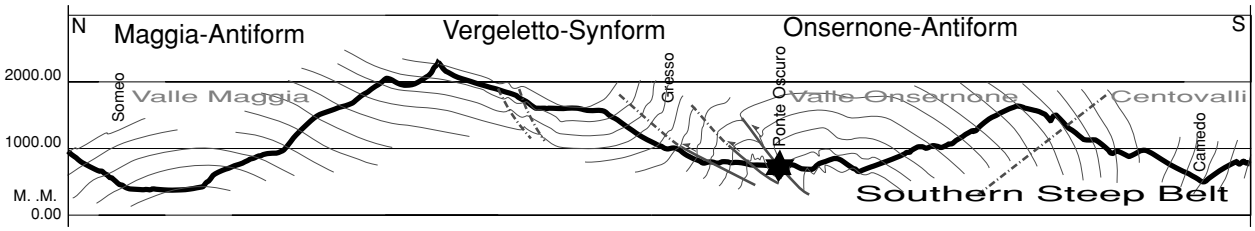

Fig. 2 Structural N-S profile through the study area. Units are not differentiated. Sample locality at Ponte Oscuro is outlined by a star. See figure 1 for location of the profile.

tures suggest conditions not much above the water-saturated solidus of granitic or pelitic rocks. Some 30 km to the east of the study area, temperatures in the order of 700-750°C at 6-8 kbar are proposed (Engi *et al*., 1995; Tóth *et al*., 2000; Nagel, 2000; Nagel *et al*., 2002). This is also in line with textural evidence for the overstepping of the second sillimanite-isograd (Sill+Kfs).

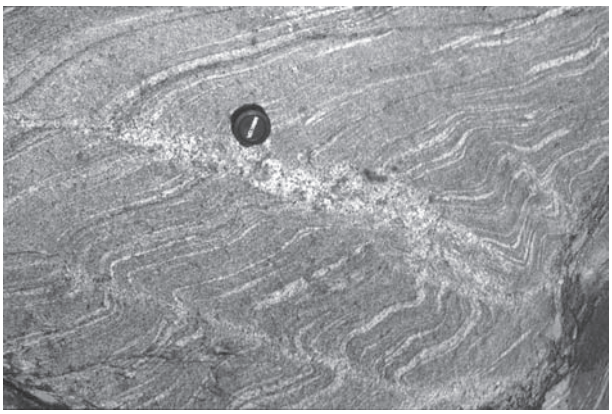

Fig. 3: Synkinematic melt-filled shear zone inside migmatitic orthogneiss in the core of the Onsernone antiform. Locally, conjugate shear zones indicate dominantly compressive deformation inside the antiform. Cover of camera-objective for scale.

Sample description

Riverbed outcrops of Ponte Oscuro (entrance of Valle Vergeletto) host a garnet-rich pale-green rock among migmatitic Bt-gneisses. The rock is part of an inhomogeneous trail of metasedimentary and metamafic rocks. HP-relics were found inside similar trails in the area. The rock stands out from the country rocks due to its massive appearance and its extreme tenacity, and due to its modal composition. A chemical analysis of this rock (sample FON1, performed using standard XRF-techniques at the University of Friburg), reveals the extraordinary rock composition (table 1): Sample Fon1 has a very low SiO_2-contents of 44%, indicative of ultrabasic rocks. Compared to mafic or ultramafic compositions however (table 1), the Al_2O_3 (27%) and the K_2O-contents are much higher, and the MgO and CaO contents much lower. Even compared to common metapelites of the Lepontine (TN307 and TN47a in table 1), the Al2O3 content of the sample is exceptionally high. The sample is additionally enriched in TiO2, Fe2O3, CaO and Na2O compared to the common metapelites and is depleted in K2O. Discrimination diagrams depicting the unique composition of this rock are shown in figure 4.

The rock consists, in the order of decreasing abundance, of plagioclase, garnet, kyanite, biotite, rutile/ilmenite, staurolite and phengite. K-feldspar has not been observed, quartz seems to be confined to a few quartz veinlets of uncertain significance. The high-alumina assemblage suggests a metapelitic rock, although extraordinarily rich in plagioclase and relatively poor in micas compared to "common" metapelites.

Sample	restite	metaeclogite	metaeclogite	UM-eclogite	metapelite	metapelite	metapelite
wt%	FON1	BOR2	PORC1	CAP5	TN307	TN47a	TN205(Proxy)
SiO2	44.13	48.82	47.67	39.01	53.24	56.42	49.99
TiO2	2.11	2.33	1.84	3.40	0.74	0.77	0.80
Al2O3	27.36	16.00	19.39	18.75	22.25	22.03	25.72
Fe2O3	13.28	13.86	9.92	20.20	7.26	7.40	7.39
MnO	0.30	0.18	0.10	0.33	0.11	0.14	0.21
MgO	2.70	5.92	6.14	9.03	2.32	3.31	1.64
CaO	4.58	8.48	10.51	7.35	0.55	1.23	0.99
Na2O	2.96	2.74	2.55	0.72	0.76	1.80	2.37
K2O	1.24	0.19	0.74	0.08	5.34	2.84	3.68
P2O5	0.04	0.29	0.16	0.22	n.d.	n.d.	n.d.
GV=H2O	0.68	0.46	0.32	-0.14	n.d.	n.d.	n.d.
total	99.37	99.28	99.33	98.95	92.57	95.94	92.79

Table1 Rock compositions of the Ponte Oscuro sample compared to selected basic to ultrabasic and metapelitic rocks of the SSB. Fon1 is the restite sample from Ponte Oscuro, ALZ74 and Bor2 are metaeclogites, and Cap5 is an ultramafic rock, all from the study area. TN307 and TN47a are typical metapelites from the Lepontine area, and TN205 is the metapelite used as a proxy in this study. All TN-numbers are from Nagel (2000). Note that iron in metapelites is measured as FeO and not as Fe2O3.

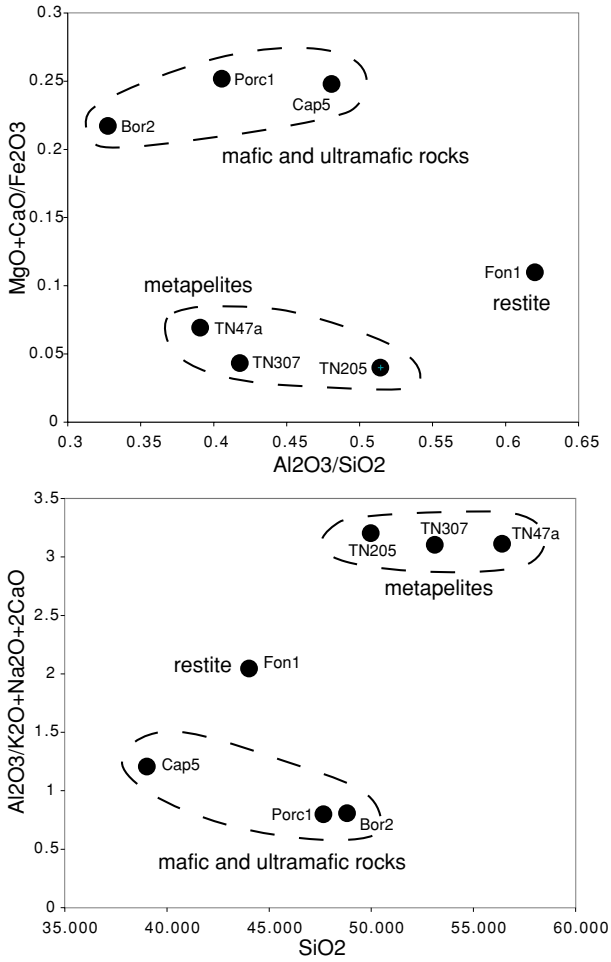

Fig. 4 Element wt.% discrimination diagrams depicting compositional differences between mafic, ultramafic and pelitic rocks compared to sample fon1.

Garnet occurs in two generations of similar compositions, contrasting grain size: Large mm-cm sized garnets are transected by several cracks (Fig. 5). Inside the cracks a texturally well equilibrated typical amphibolite facies assemblage is observed (Bt-Pl-Stau-Ilm), apparently formed at similar metamorphic conditions as the rest of the sample. These cracks show an enrichment in staurolite compared to the matrix, suggesting garnet dominated local domains inside the cracks. A second generation of smaller garnet grains (Fig. 6) is characterised by an abundance of small inclusions (too fine grained to be analysed but in part probably graphite). Chemical zoning of coarse grained garnet is generally weak (Fig. 5+7), with slight (locally almost rhythmic) variation in the element profile, but without a general gradient from core to rim. The smaller garnet fraction also exhibits relatively weak chemical zoning (Fig. 6+8), but have a clear tendency from rim to core. X_{Alm} increases, whereas X_{Py} and X_{Gr} decrease towards the rims and X_{Sps} remains constant at a low concentration. Although both garnet types are similar in composition (see table 2), the finer fraction

Fig. 7 Analysed garnet profile through coarse grained garnet. Not rhythmic alternations and the lack of a clear zoning. Lower figure denotes the profile trace.

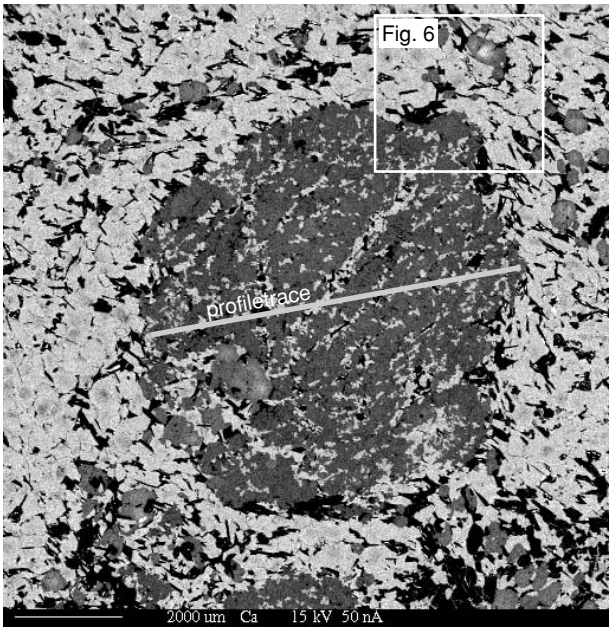

Fig. 5 Ca-Kα element map (EMPA). The bright phase are plagioclase grains, garnet is medium bright, and dark phases are kyanite and biotite. Note that the Ca-zoning is very weak in the large garnet, whereas zoning can be observed in the second (smaller) garnet generation (see upper right). A second generation grain is intergrown with the larger garnet in the lower left, recognised due to the stronger Ca-zoning.

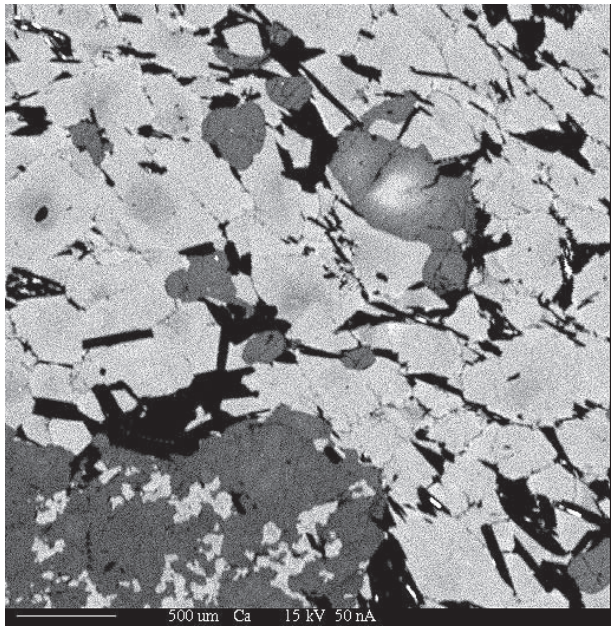

Fig. 6 Cut from figure 5 (upper right). Ca-zoning is visible in the smaller garnet generation as well as in the plagioclase grains, whereas almost no zoning is visible in the larger grt-grain to the lower left.

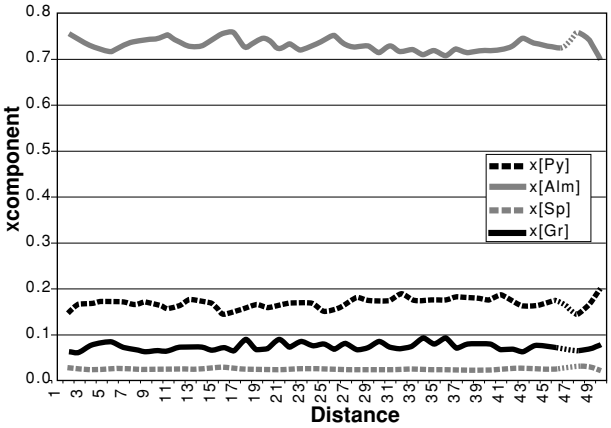

seems slightly lower in X_{Alm} (0.7 vs. 0.73) and slightly higher in X_{Gr} (0.13 vs. 0.07).
The reason for the only insignificant zoning in the coarse garnet fraction is unclear. These grains either grew during a short time and PT-interval (segregation of several small garnets into one larger garnet?), or a former chemical zoning was destroyed due to element-diffusion at high temperatures. The pseudorhythmic pattern might be indicative for garnet segregation processes. Alternatively, the observed zoning could reflect cracking and annealing of garnet clasts. The observed transgranular structures in the garnet (Fig. 5) are interpreted as such former cracks, partially annealed during amphibolite facies metamorphism. Garnet compositions along rims or cracks may therefore be slightly different from the ones in unaffected domains. Other metapelitic rocks near the study area also contain two garnet fractions, the coarser of which is interpreted as early Alpine or pre-Alpine (probably Variscan), based on textural (Rütti, 2003) and/or isotopic evidence (monazite U-Th/Pb ages, unpublished data, Burri (1999). We therefore emphasise the possibility, that only the finer grained garnet fraction was produced during the Alpine cycle. To what extent the recrystallisation and reequilibration of the older clasts has been accomplished, remains an open question.
Plagioclase (always andesin, X_{An} 0.29-0.44) (table 2) is relatively weakly zoned (Fig. 6+8), but several features are visible. The profile shown in figure 8 documents such a complete zoning. A relatively An-poor central plateau shows an abrupt increase in An, followed by a slight decrease in An, and again followed by a more pronounced increase in An towards the rim. Other grains only show an increase in An towards the rim, where it remains constant at a higher level. Many grains show polysynthetic twins which are not continuous throughout the relatively low-An cores, suggesting that the later are relics and belong to another growth phase.
Kyanite grains often show a homogeneous core, followed by a poikilitic rim, again followed by a homogeneous but almost xenomorphic outermost rim

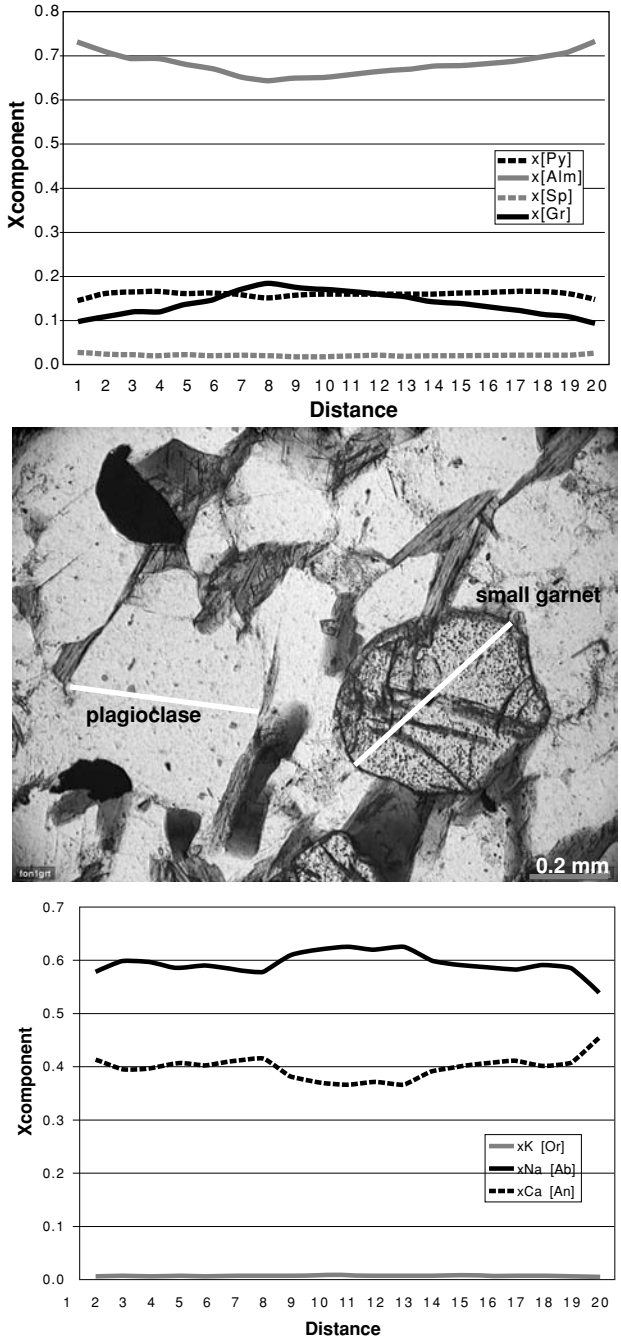

Fig. 8 Analysed profiles through small garnet grain and matrix plagioclase. Picture in the middle denotes the profile traces.

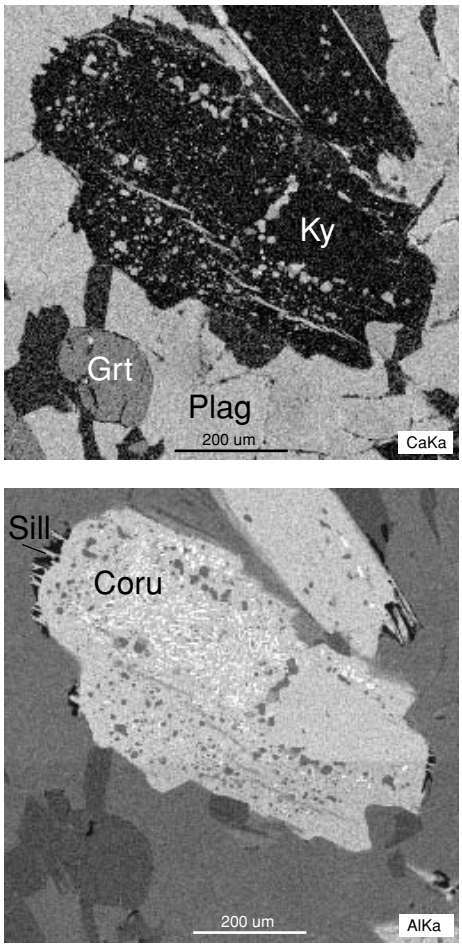

Fig. 9 SEM-elementmaps of a larger kyanite grain. Cores are rich in corundum inclusions, whereas the rims are characterised by numerous inclusions of plagioclase grains.

(Fig. 9). SEM-observations reveal that several kyanite cores are full of tiny corundum inclusions. The majority of inclusions in the poikilitic rims exhibit compositions similar to the matrix-plagioclase grains and are thus interpreted as plagioclase inclusions, in part again interspersed among corundum inclusions (Fig. 9).

The relatively few observed grains of (euhedral) staurolite may be associated with a late garnet consuming reaction, because staurolite occurs preferentially inside the mentioned garnet cracks. The typical staurolite composition is X_{Mg} 0.23, X_{Fe} 0.65, X_{Zn} 0.12, manganese is very low (< 0.1 wt.%).

Replacement textures: Rutile is commonly rimmed or replaced by ilmenite. A few larger kyanite grains show fine-grained acicular crystals along their borders, probably of sillimanite (see lower right in Fig.9). Other kyanite grains show partial replacement by phengite along their rims, mainly in areas of stronger retrogression. Biotite frequently displays sagenite structures, which are locally associated with chloritisation of the biotite. This may indicate a release of Ti during cooling (Henry and Guidotti, 2002), possibly followed by the decomposition of biotite to chlorite. Highest Ti-contents found in (sagenite-free) biotite are 2.4 wt.%.

Abundant chloritisation of biotite, and sericitisation of plagioclase occurs in zones of higher retrogression, which are often connected to small-scale brittle fractures.

Equilibration conditions of the samples

In order to establish metamorphic conditions during formation of the rock, we applied program TWQ (Berman, 1992) in combination with the internally consistent database of Berman and Aranovich (1996). In addition, we used the staurolite model of Nagel *et al*. (2002), which includes new standard state data for Mg-staurolite and a regular solution model with one symmetric Margules term (W_H = – 20 kJ).

Mineral compositions of local assemblages were measured in domains devoid of late hydration reactions and brittle fracturing. Figure 10 displays PT-estimates thus obtained. This figure is representative of all calculated assemblages which all lead to very similar estimates. Calculated reactions are listed in the appended table. No endmember was discarded. Note, however, that the staurolite-end/members as well as siderophyllite and eastonite involve larger uncertainties. We therefore depicted reactions dominated by these endmembers as dashed lines. In fact, two of three reactions of this type show the largest offset. The estimated equilibration pressure is around 7-7.5 kbar, temperatures around 650°C. Sillimanite as well as kyanite were used for calculation of the diagram, and reaction number 3 is the polymorphic ky-sill-transition. Excluding either of the two polymorphs does not lead to a different PT-estimate, thus implying that equilibration occurred very close to the ky-sill-transition. Inserting either rutile or quartz into the calculation lead to extreme scatter. Obviously, neither quartz nor rutile were in equilibrium with the measured assemblage, in line with the petrographic observation. Using corundum as an additional phase leads to a less pronounced scatter compared to rutile or quartz, indicating that corundum was not far from equilib-

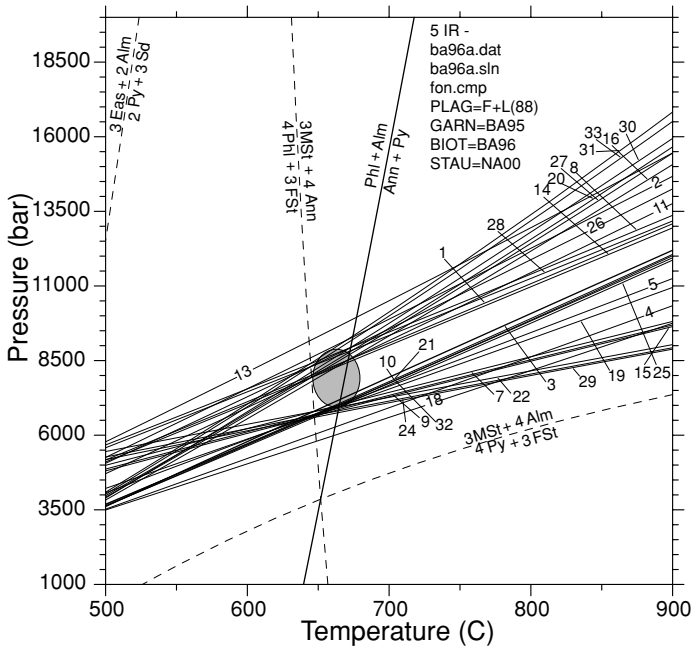

1): 12Ky + 4Gr + 3Ann = Alm + 12An + 3Sd
2): 24Ky + 8Gr + 3Eas + 6Ann = 24An + 2Py + 9Sd
3): Ky = Si
4): 3Sd + 6Phl + 24Ky + 8Gr = 2Alm + 24An + 9Eas
5): 2Phl + 12Ky + 4Gr + Ann = Alm + 12An + 3Eas
6): 3Eas + 2Alm = 2Py + 3Sd
7): 2Py + 12Ky + 4Gr + 3Ann = 3Alm + 12An + 3Eas
8): 3Ann + 4Gr + 12Si = 3Sd + 12An + Alm
9): 3MSt + 24Ky + 8Gr + 6Ann =2 Alm + 24An + 6Eas + 3FSt
10): 3Phl + 12Ky + 4Gr = 12An + 3Eas + Py
11): Phl + 12Ky + 4Gr + 2Ann = 12An + Py + 3Sd
12): 3MSt + 4Ann = 4Phl + 3FSt
13): 6Ann + 3Eas + 8Gr + 24Si = 9Sd + 2Py + 24An
14): 3MSt + 48Ky + 16Gr + 12Ann = 48An + 4Py + 12Sd + 3FSt
15): 9MSt + 48Ky + 16Gr + 12Ann = 48An + 12Eas + 4Py + 9FSt
16): 3Phl + 12Ky + 4Gr + 2Alm = 12An + 3Py + 3Sd
17): Phl + Alm = Ann + Py
18): 24Si + 3Sd + 6Phl + 8Gr = 2Alm + 24An + 9Eas
19): 12Si + 2Phl + 4Gr + Ann = Alm + 12An + 3 Eas
20): 16Gr + 48Ky + 12Phl + 9FSt = 9MSt + 12Sd + 48An + 4Alm
21): 16Gr + 48Ky + 12Phl + 3FSt = 3MSt + 12Eas + 4nAn +4 Alm
22): 12Si + 2Py + 4Gr + 3Ann = 3Alm + 12An + 3Eas
23): 3MSt + 4Alm = 4Py + 3FSt
24): 3MSt + 24Si + 8Gr + 6Ann = 2Alm + 24An + 6Eas + 3FSt
25): 4Gr + 3Phl + 12Si = Py + 3Eas + 12An
26): 2Ann + 4Gr + Phl + 12Si = 3Sd + Py + 12An
27): 8Gr + 24Ky + 6Phl + 3FSt = 3MSt + 6Sd + 2Py + 24An
28): 3MSt + 48Si + 16Gr + 12Ann = 48An + 4Py + 12Sd + 3FSt
29): 9MSt + 48Si + 16Gr + 12Ann = 48An + 12Eas + 4Py + 9FSt
30): 2Alm + 4Gr + 3Phl + 12Si = 3Sd + 3Py + 12An
31): 9FSt + 48Si + 12Phl + 16Gr = 4Alm + 48An + 12Sd + 9MSt
32): 16Gr + 12Phl + 48Si + 3FSt = 3MSt + 12Eas + 48An + 4Alm
33): 3FSt + 24Si + 6Phl + 8Gr = 24An + 2Py + 6Sd + 3MSt

Fig. 10 Multi-equilibrium calculation for sample Fon1 using program TWQ and the internally consistent database of Berman & Aranovich (1996). Dashed reactions are dominated by staurolite or the biotite endmembers siderophyllite and eastonite. Elipse indicates inferred equilibration conditions for the sample. See text for discussion.

rium with the assemblage. Indeed, using activities of 0.6-0.7 for corundum significantly improved the convergence.
As a first conclusion, the TWQ-approach indicates final equilibration-conditions close to, or slightly above the water saturated solidus of the haplogranitic (or of the pelitic) system. Although surrounding orthogneiss is clearly migmatitic, unambiguous textural evidence of former melt in the restite sample is scarce.

From a single equilibrium condition towards a PT-path

TWQ-modelling estimates the conditions of final equilibration of the rock sample. To investigate on the samples Alpine (PT) history (using mineral compositions and reaction textures), phase diagrams were calculated using program DOMINO (de Capitani & Brown, 1987) together with the internally consistent databases of Berman (1988, upgrade JUN92, with various updates, preserving the internal consistency). For information on used models see Appendix.
The XRF-analysis of sample Fon1 (table 1) was used as bulk composition. Oxygen fugacity was assumed to be buffered by QFM and neither quartz nor fluid saturation was imposed. In fact, to approach the observed assemblage H2O-contents was the only variable allowed to change. The fluid phase was initially assumed to be pure H2O.
Because the Berman-database does not comprise endmembers for silicate melts, it cannot be used to compute phase diagrams involving melts. As long as the conditions remain below the water saturated solidus, the phase diagram is (thermodynamically) correct. Above the solidus, calculated phase assemblages and compositions deviate stronger from "reality" with increasing melt fraction. Given the low contents of hydrous phases in the rock, melt fractions below muscovite dehydration melting should be low and hardly affect computed phase relations.
The calculated phase diagram (shown in fig. 11) again suggests conditions of around 7 kbar and 600-650°C for the observed assemblage, assuming both, kyanite and sillimanite as part of the stable assemblage (which must be near or along the Sill-Ky join). Maximum pressures during final equilibration could have been no higher than 8.5 kbar, else corundum (present as inclusion in kyanite only) and rutile (now mantled by ilmenite) would be stable. Pressure was not below 6 kbar, else quartz should be stable and phengite should have reacted out. The phengite stability limit has an uncommon shape compared to common metapelitic rock (almost horizontal below 700°C), which is however a function of the bulk composition.
Equilibrium conditions calculated using program TWQ are consistent with the result of DOMINO-modelling. All observed phases (at the estimated equilibrium conditions) are present in the phase diagram at the same conditions (Fig. 11). Phengite is calculated to be present in minor amounts (ca. 3 vol.%). This may indicate that in contrast to the first interpretation based on microscopy, phengite was not produced at a later stage, but is part of the observed assemblage. Computed mineral modes and compositions at 7 kbar/650°C (using Program THERIAK) are shown in Table 2, together with data from EMP-analyses.

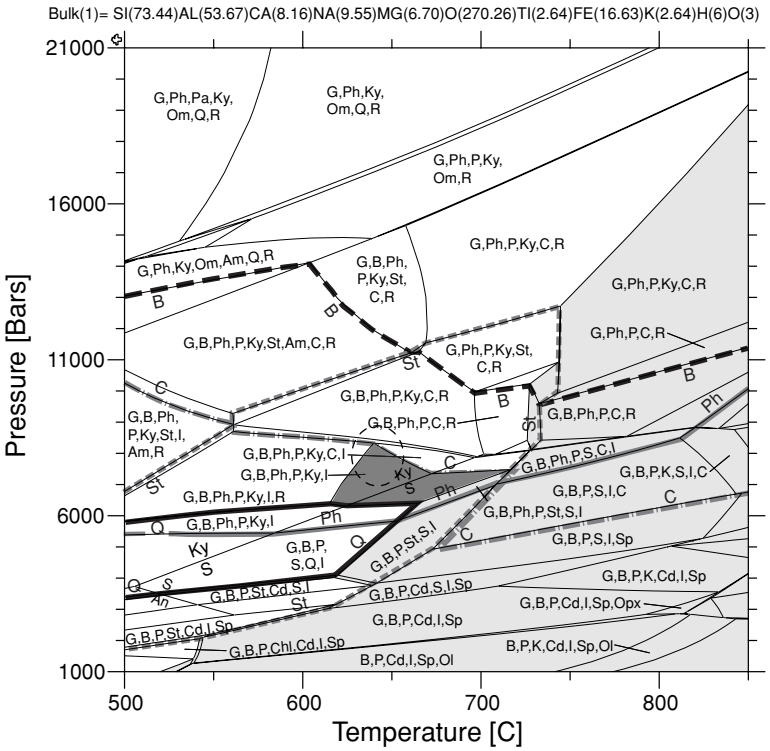

Fig. 11 Calculated phase diagram for sample fon1, using the internally consistent database of Berman (1988). The light shaded area depicts fluid oversaturation (fluid coexists with solids), the dark shaded area represents the observed stable mineral assemblage. Dashed ellipses denotes estimated equilibration conditions using TWQ. Stability limits of several phases are depicted.
Abbreviations in all diagrams: Am=amphibole, B=biotite, C=corundum, Cd=cordierite, Chl=chlorite, G=garnet, I=ilmenite, K=K-feldspar, Ky=kyanite, Ol=olivine, Om=omphacite, OPX=orthopyroxene Ph=phengite, P=plagioclase, Q=quartz, R=rutile, S=sillimanite, Sp=spinel, St=staurolite.

P = 7000.00 bar		P(Gas) = 7000.00 bar			T = 650.00 C = 923.15 K	
Fon1	Calculated			Measured		
	Vol%	component	X		X (range)	X(medium)
GARNET(coarse)		GROSSULAR			0.06-0.09	0.08
		PYROPE			0.14-0.18	0.17
		ALMANDINE			0.7-0.75	0.73
		SPESSARTINE			0.02	0.02
GARNET(small)	20.19	GROSSULAR	0.09		0.18(c)-0.09(r)	
		PYROPE	0.19		0.17(c)-0.13(r)	
		ALMANDINE	0.71		0.64(c)-0.75(r)	
		SPESSARTINE	n.c.		0.02	
BIOTITE	8.45	PHLOGOPITE	0.61	(XMg(M))	0.40-0.49	0.47
		ANNITE	0.39	(XFe(M))	0.31-0.36	0.34
				(XAl(M))	0.13-0.19	0.14
PHENGITE	3.00	MUSCOVITE	0.84		n.d.	
		PARAGONITE	0.07		n.d.	
		MCELADONITE	0.04		n.d.	
		FCELADONITE	0.04		n.d.	
PLAGIOCLASE	52.97	ALBITE	0.57		0.69(c)-0.55(r)	0.57
		ANORTHITE	0.41		0.29(c)-0.44(r)	0.42
		K-FELDSPAR	0.02		0.002-0.007	0.005
STAUROLITE	5.06	FE-STAUROLITE	0.74	(XFe)	0.64-0.67	0.65
		MG-STAUROLITE	0.26	(XMg)	0.17-0.23	0.22
				(XZn)	0.11-0.15	0.12
ILMENITE	2.79	ILMENITE	0.92	(XFe)	097-0.99	0.98
		GEIKELITE	0.08	(XMg)	<0.01	<0.01
				(XMn)	0.01-0.02	0.015
KYANITE	7.53					

n.c. =not calculated (no Mn in the bulk system), n.d. = not determined, (c) = core, (r) = rim

Table 2 Calculated and measured modes and mineral compositions for sample Fon1.

Computed mineral compositions are all reasonably close to the measured ones except for biotite and ilmenite. The biotite model in the JUN92-database consists only of the two endmembers phlogopite and annite. Tschermaks exchange $(Fe/Mg)_1Si_1Al_{-2}$ leading to the endmembers eastonite and siderophyllite is not considered in the model (but is contained in the BA96 database used for TWQ). However, observed $X_{Al}(M)$ ranges from 0.13-0.19, and is thus not negligible. Ti-exchange in biotite is not considered either in the model. As a result, the calculated X_{Mg}/X_{Fe}-ratio is slightly higher (1.6) than the measured (1.4). These limitations may also slightly influence compositions of phases coexisting with biotite. Discrepancies in the composition of ilmenite are due to the simple ideal solution approach used for the geikielite-ilmenite binary.

Note that use of an XRF-analysis provides an average chemical bulk system. Local chemical domains were not considered here. To account for such local domains a different approach would be needed (see e.g. in (Tóth et al., 2000; Nagel, 2000; Grandjean, 2001; Rütti, 2003; Brouwer and Engi, 2004). Given this restriction, calculated compositions are in very good agreement with measured compositions.

To test for the influence of quartz and fluid saturation (or undersaturation) we slightly increased and decreased the SiO_2- and H_2O-contents of the bulk system. This test demonstrate, that stability relations and modes of corundum, quartz and phengite are significantly influenced by even slight fluctuations of these two system components. A decrease of the H_2O-contents leads to stabilisation of corundum and to a destabilisation of phengite. Increasing the SiO_2-content has the opposite effect and additionally increases the mode of kyanite.

The phase diagram further suggests that at the conditions obtained in the TWQ-run, the assemblage is quartz-undersaturated, though close to saturation (Fig. 11). Quartz saturation is reached at lower pressures and temperatures. To obtain the observed assemblage at the estimated PT-conditions, the rock must be (slightly) fluid deficient at 7 kbar/650°C (no free fluid phase), else the observed aluminosilicate phase would not be stable at that conditions.

Figure 12 depicts several isopleths and isolines (moles) calculated for garnet and plagioclase. If we accept that volume diffusion in plagioclase and garnet at the estimated PT-conditions is of minor importance, we may interpret the compositional data (table 2 and fig. 7+8) as growth zoning and use them to infer the PT-path prior to equilibration of the rock. Using calculated garnet and plagioclase isopleths for analysed rim compositions, equilibration conditions are estimated at 580-630°C and 6-7 kbar, thus at slightly lower temperatures than indicated by the TWQ results. To infer the PT-path reported in the garnet zoning from core to rim, we use intersections of garnet isopleths. Mineral analysis had to be normalised to the three endmembers Alm-Py-Gr, because manganese was excluded from the model-system. The obtained PT-path is shown in the lower right of figure 12, together with estimated TWQ-conditions and phase relations as observed in figure 11. According to computation, garnet zoning reports a clockwise PT-path from 8,5-9 kbar at 560-590°C,

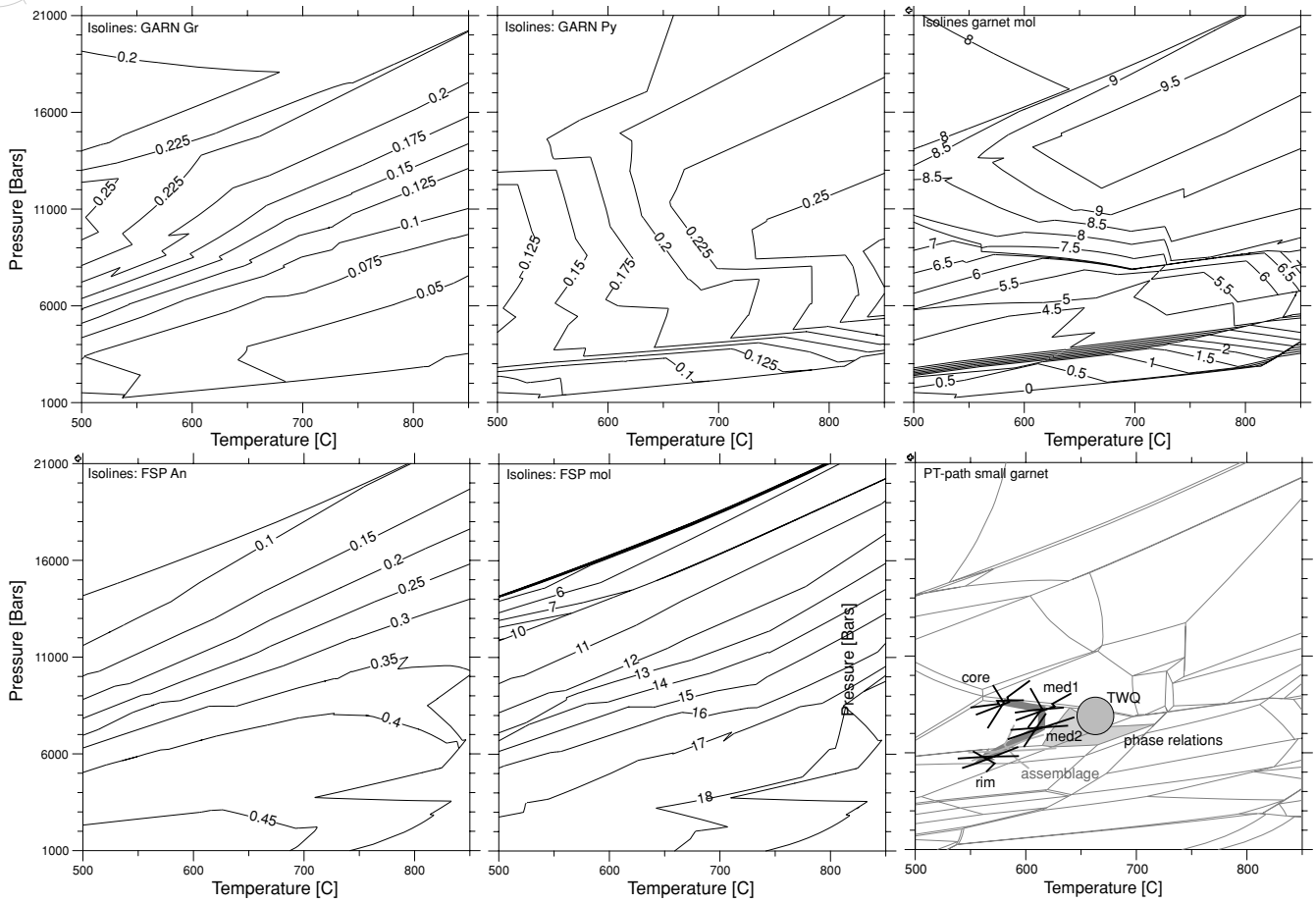

Fig. 12 Isopleths and isolines of moles for garnet and plagioclase calculated with the Berman database. To the lower right, a PT-path is inferred from the comparison of the small garnet profile (Fig. 8) and the intersections of calculated garnet isopleths. "Assemblage" denotes conditions for the mineral composition used in the TWQ-estimate. For comparison, TWQ-estimates and PT-conditions inferred from phase relations are added.

down to 5,5-6 kbar at 550-580°C. Peak temperatures reached are around 620°C at 7-8 kbar, and suggest subsolidus processes rather than partial melting. We note that phase relations (Fig. 11) as well as TWQ-results (Fig. 10) both suggest temperatures higher by some 50°C. Higher temperatures are also indicated because partial melting has occurred in the surrounding rocks. This suggests that the inferred PT-path may be displaced towards lower temperatures, and may only be used qualitatively, probably as a result of the simplified assumptions (e.g. system definition). An interesting point inferred from the documented PT-path, is the fact that the small garnets formed during exhumation, which is associated with bulk-garnet resorption and plagioclase growth (compare with isolines (moles) of garnet in figure 12). This suggests that garnet growth was accompanied by the resorption of an older garnet generation. Relics of this generation are probably the coarse grained garnet fraction. Why such a kind of recrystallisation should occur is uncertain, but we tentatively suggest, that it could be related to partial melting. Element-diffusion through a melt is faster by orders of magnitude compared to migration along (almost dry) grain boundaries. The conspicuous poikilitic growth of kyanite and garnet indicates a sharp increase in growth rates.

Overall, obtained results are in satisfactory agreement with the peak-PT conditions of 640°C / 6.6 kbar proposed for this area (Engi *et al*., 1995; Todd & Engi, 1997). TWQ-results, DOMINO-modelling as well as published data all suggest that the water saturated solidi of granitic and pelitic systems were overstepped in the study area, but that muscovite-dehydration melting should not have occurred.

Calculation of melt bearing systems

The extraordinary rock composition as well as estimated PT-conditions both indicate that partial melting was a probable process in the formation of the studied rocks. To explore effects and mechanisms of partial melting and melt extraction on the metamorphic evolution of the rocks, we applied the internally consistent database of Holland&Powell (1998) in combination with program DOMINO to the same rock composition that was used above. The HP98-database has recently been extended to allow modelling of melt-bearing systems (White *et al*., 2001; Holland & Powell, 2001).

Because this melt-model melt was not fitted for pressures much in excess of 10 kbar (and is therefore no longer very reliable at higher pressures), we computed the diagrams to pressures of "only" 12 kbar. In this PT-window, the model should lead to reliable predictions. An artefact of the model-fit has been found, if it is used at water saturation (excess water to always saturate the system). At these conditions, the solidus bends back (just above 12 kbar) by almost 180° and declines

with a positive slope towards lower temperatures. For example at 6 kbar and 300°C a water enriched melt is predicted by the model assuming water saturation. On a PT-diagram the solidus has the form of a "pseudosolvus". We do not exactly know the reason for this inconsistency, but it appears that the model H_2O_{liq}-component is too stable compared to H_2O_{fluid} at these conditions.

Results of computation are shown in figure 13, and are discussed in the following text. Except for the melt, the diagram is qualitatively identical to figure 11 (because calculated isopleths are similar to those reported in figure 12, we renounce plotting them). Larger differences exist however for the stabilities of corundum, cordierite and paragonite. Corundum remains stable towards lower pressures and temperatures using the Berman-database. On the other hand, cordierite remains stable towards higher pressures using the HP-database (e.g. at 700°C, cordierite decays at 5.5 kbar (HP) and 4 kbar(Berman)). Paragonite is stable towards lower pressures in the HP-runs. All other phases show reasonable agreement in stability and composition.

Stability relations indicate a limited field at 7.5 kbar and 600-650°C for the final equilibration of the rocks, or at least a passage through this field. At these conditions the rock is very slightly quartz- and fluid-undersaturated. Phengite and rutile would react out while ilmenite and quartz should react in.

Sillimanite is not yet stable and must therefore be interpreted as a post-peak reaction product (P at T_{max}) at lower pressures. In the melt absent field phengite stability shows the same horizontal trend as observed in the figure 11. Corundum reacted out at 10 kbar (at the same T), or at 750°C (at 7 kbar). Final equilibration occurred some 25°C below the solidus (at 7kbar). Calculated isopleths (Fig. 13) for garnet again indicate a clockwise PT-path, however at higher conditions compared to the results using the Berman-database. Core compositions report conditions of ca 640-660°C at 10.5-11 kbar, while rim compositions indicate 560-600°C at 6.5-7 kbar. Highest temperatures reached along the PT-path are in the order of 660°C at 9-10 kbar. Note that an intersection of the PT-path with the predicted solidus requires temperatures higher by some 30°C. Thus, although in much better agreement with observed phase relations and with TWQ-estimates compared to the PT-path reported in figure 12, isopleths-intersections apparently again indicate slightly too low temperatures. Again, reported PT-conditions would have allowed water assisted melting, but not muscovite-dehydration melting.

The solidus of the system shows a fairly complicated PT-outline (Fig 13), mainly due to the intersection of the solidus with areas of water saturation or undersaturation (different water activities). At conditions below 5 kbar, the solidus lies in the fluid absent field at about 800°C, where melt is produced due to the onset of the continuous fluid-absent reaction

Cord+Bio+Plag+Kfs = Grt+Spin+Liq (1)

The upper (terminal) thermal stability limit of biotite is reached only at higher 70°C lower temperatures. Formation of melt at these conditions is thus mainly a function of a continuous bio-consuming reaction. By the same reaction additional fluid is liberated (and at the same time incorporated into the melt) through the consumption of cordierite, which decreases its "hydrous-cordierite" component (according to the HP-model). The melt fraction increases steadily from zero at 820°C to 12% at 880°C

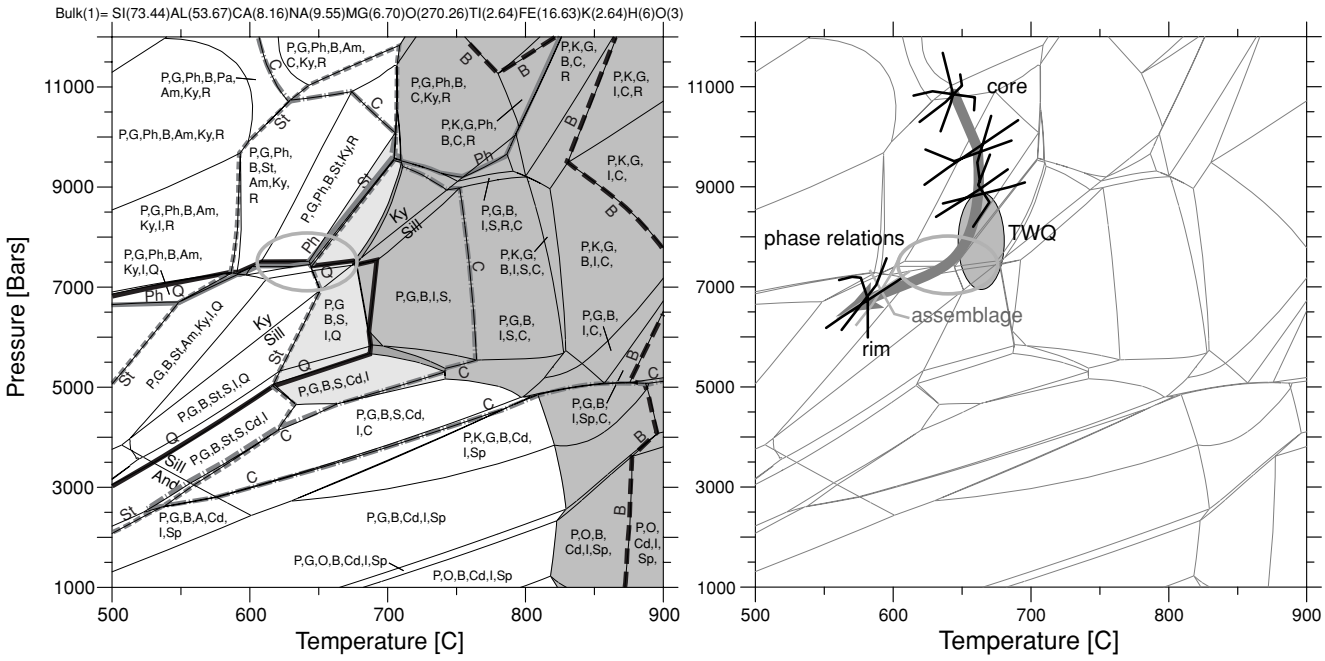

Fig. 13 Left: Calculated phase diagram for sample Fon1, using the extended internally consistent database of Holland & Powell (1998). The melt present field is outlined by medium grey shading, the fluid present field by light grey shading and the melt+fluid present field by dark grey shading. The remaining area is fluid- and melt-undersaturated. Ellipse denotes the observed assemblage. Abbreviations as in figure 11. Right: PT-path inferred from comparison of analysed garnet profile and the intersections of garnet-isopleths. "Assemblage" denotes conditions for the mineral composition used in the TWQ-estimate. For comparison, TWQ-estimates and PT-conditions inferred from phase relations are added.

as a result of dehydration melting of biotite (and cordierite).
At conditions between 5-10 kbar the solidus enters a fluid saturated area and is displaced to lower temperatures of around 670-700°C. Note that further addition of fluid would not result in lowering of the solidus, which appears therefore relatively high, as a function of the bulk composition. At 7.5 kbar/ 675°C, melt is produced through the water assisted melting reaction
Plag+Grt+Bio+*Rt*+H2O = Ky+*Ilme*+Liq (2)
Note that ilmenite and rutile enter only incidentally into the reaction, because breakdown (or creation) of rutile and ilmenite occur at the chosen conditions (see fig. 13). With the chosen bulk composition, the very small melt fraction of ca. 1% is a result only of the consumption of the available hydrous fluid (water assisted melting). As a result the melt fraction increases only to a very minor extent with temperature (2% at 750°C), due to the decreasing equilibrium water content of the melt with temperature (see e.g. Fig. 2.25 in Johannes and Holtz, 1996).
More relevant in the context of this study is the crystallisation-behaviour of the last melt during cooling of the rock below the solidus. The composition of the (last) liquid at 680°C is albite (0.45), SiO_2 (0.34),K-feldspar (0.21), the other components being small. The model predicts only moderate changes in melt composition for changing P (± 2 kbar) or T (± 50°C). At 7.5 kbar, crystallisation of the last liquid should lead to minor plagioclase, garnet and biotite according to reaction (2). Due to the low melt fraction of only 2-3%, neither plagioclase nor garnet are predicted to change their compositions abruptly during crystallisation of the melt. Recrystallisation along the decompression path may additionally have lead to an effective destruction of textural evidence for former melt at the grain scale. This may explain why such textural evidence is scarce. The small amount of fluid released during crystallisation of the melt is predicted to be consumed completely some 30°C below the solidus (at 7.5 kbar), to form retrograde hydrous phase.
A revealing feature of the rock is the lack of quartz and K-feldspar, the presence of muscovite and the abundance of plagioclase. Assuming "standard" partial melting of metapelitic rocks, the first important melting starts through a (water absent) dehydration melting reaction such as
Ms + Qtz = Sil + Kfs + melt (3)
The reaction, which occurs at temperatures e" 700°C at pressures above 6 kbar, consumes quartz, which could explain the lack of quartz in the rock if much melt had left the system. On the other hand, according to computation, a considerable amount of K-feldspar is produced in reaction (3) (e.g. 17% at 6 kbar), which has not been observed in the rock. Provided that the melt-model is correct and that the K-feldspar component does not completely dissolve into the melt, K-feldspar should remain in the rock as a refractory phase if melt is drained from the rock. This suggests that reaction (3) cannot be responsible for the formation of melt in the studied sample.
As the studied rock represents a melt-depleted restite, its composition is no longer appropriate to help decipher the rocks history prior to partial melting. Therefore a proxy-metapelite was used to explore the different processes of partial melting occurring in metapelitic rocks (composition of metapelite taken from Nagel (2000)). The used composition (given in table 1 (TN205)) is close to our samples in contrast to the majority of metapelites from Nagel (2000), which have compositions closer to the ones of TN307 and TN47a.
This proxy-metapelite was used to test the influence of increasing temperature or increasing water content of the system on the melt fraction, the melt composition, as well as on the melting reactions and phase relations.

Dehydration melting vs. water assisted melting

For the following discussion, binary T-X diagrams instead of the usual PT-diagrams are used, because phase relations and phase compositions are a function of the chosen water content of the system. Figure 14 is such a diagram, calculated for the proxy-metapelite at a constant pressure of 7 kbar (equilibration conditions) and an increasing water content of the bulk system along the X-axis. Note that common metapelitic rocks along a prograde PT-path should be only very slightly fluid saturated, hence situated along a vertical axes of about 0.15 on the binary diagram (ca. 0.5 vol.% of fluid). Higher X-values should only be encountered if fluid infiltrates from an external source, and are only reasonable for melt-bearing systems.

First we briefly discuss a few important features of the binary:
At conditions of water undersaturation the solidus lies at a temperature of ca. 710°C (dehydration melting), while it decreases to ca. 650°C in fluid saturated areas (water assisted melting). At relatively dry conditions, K-feldspar is produced through the decomposition of phengite at a temperature of ca. 710°C. With increasing water contents of the system, K-feldspar dissolves into the melt and is no longer present at an X > 0.4 of the binary. Similarly, quartz and phengite react out with increasing H_2O-content of the bulk system, due to their dissolution into the melt phase. Figure 15 shows that once temperatures of 670°C are reached, the melt fraction is mainly a

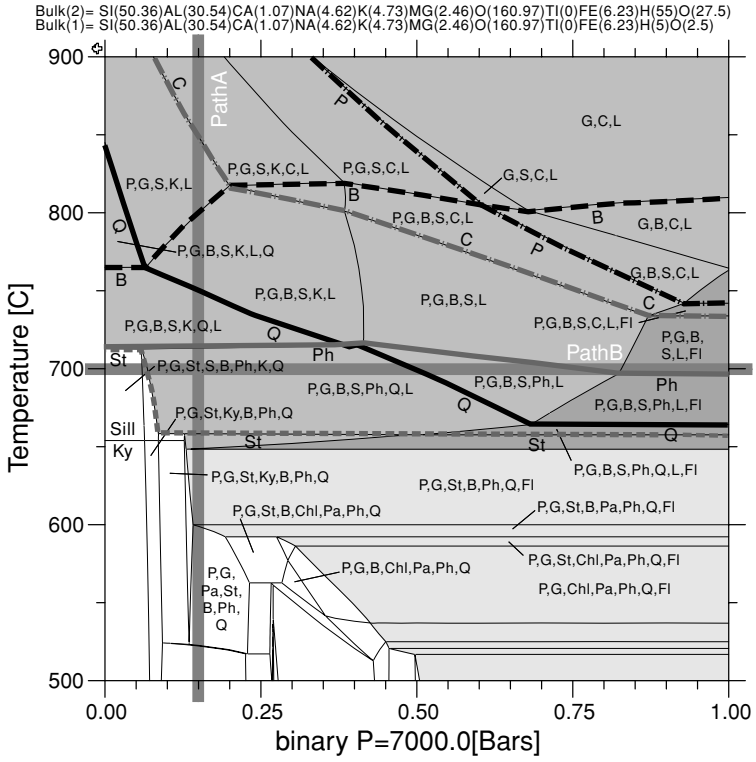

Fig. 14 Binary T-X diagram of composition TN205 (table 1) at a pressure of 7 kbar and increasing amount of water in the bulk system with increasing value of the X-axis. Shading and abbreviations as above. The amount of free fluid in the system at 640°C, slightly below the water saturated solidus of 650°C, changes from 0.14 wt.% (=0.47 vol.%) at X=0.15, to 2.8 wt.% (=8.9 vol.%) at X=0.5 and to 6.44 wt.% (=18.7 vol.%) at X=1.

function of the system water content (until the melt becomes water oversaturated) and only to a lesser degree a function of temperature.

Corundum, which was observed as inclusion in kyanite, becomes stable towards lower temperatures with increasing H2O-content. Nevertheless, for the chosen composition, temperatures of at least 750°C are necessary to form corundum at all (at 7 kbar). Note, however, that corundum becomes stable towards lower temperatures with increasing pressure (Fig. 11+13). Staurolite is predicted to intersect with the solidus and is the first phase to react out after the onset of partial melting. The intersection of staurolite with the water saturated solidus was correctly predicted by Spear *et al*. (1999) and its stability during partial melting was experimentally confirmed by García-Casco *et al*. (2003). Staurolite and the aluminosilicate phases (ky+sill) are only predicted to coexist at water-undersaturated conditions. Figure 15 shows the influence of increasing temperature or water content on mineral composition (anorthite and almandine). The anorthite content of plagioclase increases strongly with increasing water content of the system (and decreasing amount of plagioclase), and to a lesser degree with increasing temperature. By contrast, almandine in garnet varies mainly as a

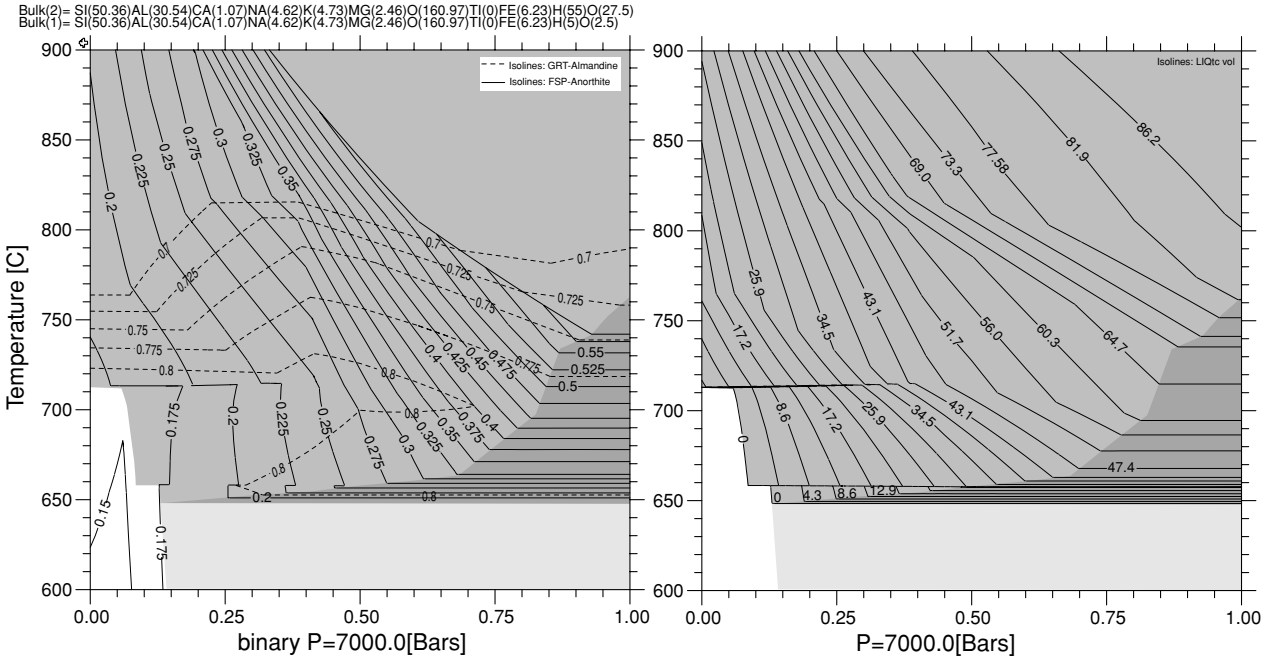

Fig. 15 Left: Isopleths for almandine and anorthite components in garnet and plagioclase. Right: Volumes of melt in vol.%. Shading as in figure 13.

function of temperature and is not much influenced by a change in the water content.

The above computed phase diagrams demonstrate that dehydration- or water assisted melting must lead to different types of restites, phase relations and compositions of solids and melts. Below, we investigate on two different scenarios (depicted in fig. 16 and 14). We once follow an isobaric heating path from 630 to 850°C, at a constant water content of the system (X = 0.15, in fig. 14, Path A). Path A thus simulated partial melting mainly as an effect of heating and related dehydration melting. Along a second path (path B), we assume infiltration of fluid (equals a path parallel to the X-axes of fig. 14) at a constant temperature of 700°C.

Following the heating path A from 630-850°C the following reaction sequence can be read of diagram A1 of figure 16. *(Note that in all reactions given below only absolute volume changes are depicted. Exchange of components in solid phases or in the melt are not considered in the equations).* At ca. 645°C the first melt is produced as a result of the small amount of free fluid (0.5 vol.%) present in the system via the reaction

Plag+Stau+Phen+Qtz+Bio+Fluid = Grt+Liq (4)

The complete consumption of the fluid only leads to a small melt fraction in the order of 2%. Shortly thereafter, the upper thermal stability limit of staurolite is encountered, which leads to the production of melt via the discontinuous reaction

Plag+Stau+Phen+Qtz+Bio = Grt+Sill+Liq (5)

In the course of this reaction the melt fraction increases to 6%, and it further increases to 11% upon heating to 710°C, due to the continuous reaction

Phen+Qtz+Grt = Plag+Sill+Bio+Liq (6)

Between 710 and 720°C the discontinuous reaction

Plag+Phen+Bio+Qtz = Sill+Grt+Kfs+Liq (7)

leads to a large increase in the melt fraction to 25%. This is actually the complete formulation of the phengite breakdown reaction (3). The melt fraction increases further to 33% until quartz is completely consumed by 750°C owing to the continuous reaction

Plag+Sil+Bio+Qtz = Grt+Kfs+Liq (8)

The melt fraction further increases to 38%, until all biotite is consumed by 800°C, owing to the continuous reaction

Plag+Sill+Bio = Grt+Kfs+Liq (9)

The remaining assemblage at this point is Grt+Sill+Kfs+Plag+Liq. If melt at this point left the system (e.g. as a consequence of the volume increase of the melting reaction and resulting hydrofracturing), K-feldspar should remain in the rock as a refractory phase. Figures 16-A2 and A3 illustrate that during the increase of temperature the albite contents in plagioclase decreases, while the orthoclase and anorthite components increase. Similarly, garnet should become poorer in almandine and richer in pyrope components, contrary to the observed garnet-zoning. Note that during the entire sequence of partial melting, the melt remains at its minimum (or equilibrium) water content and does not reach saturation.

A similar discussion for the sequence along path B (figure 16-B1-3) does not make much sense, because we do not assume a continuous increase in fluid, but rather a single or a pulsed infiltration during geologically brief time spans. However it is readily visible in the diagram that plagioclase, phengite, biotite and quartz are always resorbed between 0.1-0.5 X, while garnet remains nearly constant and sillimanite and liquid increase in mode. The anorthite content of plagioclase strongly increases with increasing water content (and with decreasing mode of plagioclase), while garnet composition remains almost constant. Hence, plagioclase, phengite and quartz are increasingly dissolved into the melt, while biotite is largely converted garnet. By X=0.5, the melt fraction rises to 48% and quartz is completely dissolved into the melt. As a result, a further increase in water content leads to further consumption of phengite and plagioclase, and the melt becomes poorer in quartz. Thus, even though temperatures remain clearly below those of phengite-breakdown, phengite is gradually consumed with increasing H_2O-content of the system and finally vanishes by X = 0.8 of the binary (melt fraction 60%). At X > 0.5, biotite is stabilised over garnet, due to the increasing water content of the melt (=increasing water activity), which by this point had risen to above the minimum water content.

Note that in contrast to path A, the water content of the melt does not remain at its minimum. Instead, three evolutionary steps can be distinguished: At low water contents of the system, once equilibrium

Melt added to sample Fon1 with melt-composition calculated at 7.5 kbar/700°C

melt fraction	Al/Si	Ca/Na	Ca/K	Al/Ca	Fe/Mg	Ca/Fe
fon1	0.731	0.855	3.097	6.574	2.481	0.491
0.02	0.723	0.844	3.013	6.598	2.481	0.491
0.08	0.695	0.801	2.717	6.696	2.481	0.493
0.15	0.665	0.754	2.422	6.816	2.480	0.495
0.20	0.648	0.729	2.275	6.888	2.480	0.497
0.31	0.614	0.676	1.996	7.054	2.480	0.500
0.40	0.589	0.637	1.808	7.194	2.479	0.502
0.50	0.564	0.597	1.631	7.356	2.478	0.505

Table 3 Change in select cation-ratios of sample Fon1 upon addition of melt.

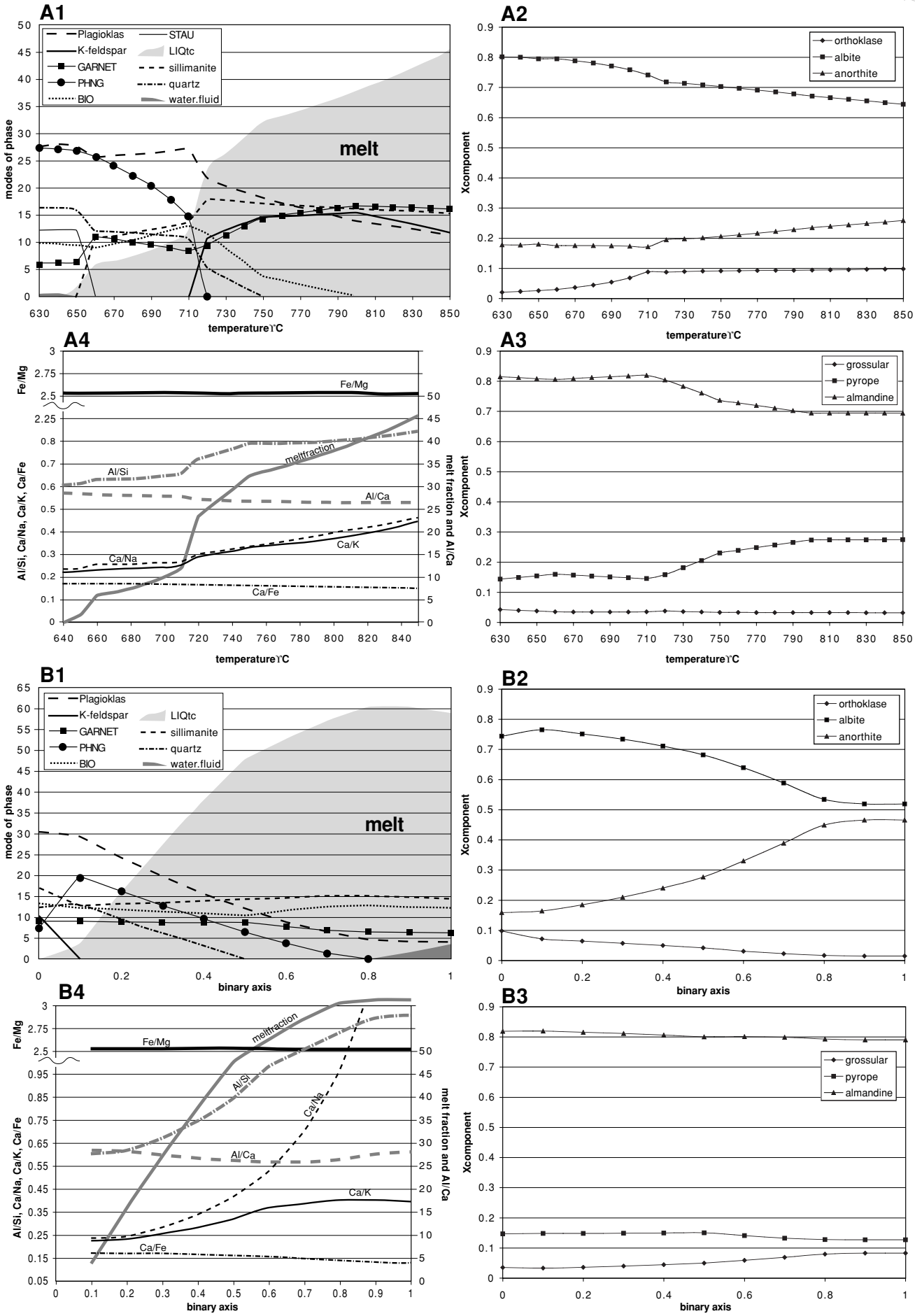

Fig. 16 Figures A1-3 depict the modes and compositions of the main phases along a value of 0.15 of the binary X-axes with increasing temperature. Figures B1-3 depict the same but with increasing water content of the system at a constant temperature of 700 °C. See text for discussion. Figure A4 and B4 visualise the change in element-ratios along path A and B, assuming complete extraction of the melt from the restite.

between infiltrating fluid and rock is reached, the melt remains at its minimum water content as long as X < 0.5. If 0.5 < X < 0.8, the water contents of the melt exceeds the necessary minimum amount and increases continuously until at X > 0.8, a free fluid phase coexists. A further increase in water would not lead to any further change of the assemblage.
Figures 16-A4 and B4 visualise the change in select element ratios along paths A and B if the produced melt is always completely subtracted from the bulk composition. A general tendency in both dehydration and fluid assisted melting is the general increase of Ca/Na- and Ca/K-ratios with increasing melt fraction due to the preferential dissolution of the albite-component in plagioclase, and of phengite, respectively. Indeed relatively high ratios are observed for these elements in the sample studied (table 3). Because the concentrations of the anorthite, fayalite and forsterite components in the melt remain very low, the restite gets enriched in Fe, Mg and Ca. A very important element ratio in the context of partial melting is the Al/Si ratio which rises with increasing extraction of melt. A melt depleted restite must therefore become enriched in alumina and depleted in silica, as actually observed in the studied sample (compare composition of fon1 with TN-samples in table 1).
We therefore use the Al/Si-ratio as a proxy to estimate the amount of extracted melt. An average Al/Si-ratio of 0.47 was calculated from 10 typical metapelite-samples from the Lepontine area (Nagel, 2000) (which are not reported to have undergone partial melting). A maximum Al/Si-ratio of 0.61 (= ratio of our proxy) was nowhere overstepped, and the Al/Si-ratio of 0.73 of the studied sample is still considerably higher. To approximate this ratio, a minimum melt fraction of 0.25-0.30 must be extracted from the proxy-metapelite. Because the proxy has the highest Al/Si-ratio of all metapelites reported in Nagel (2000), the estimated extraction of a melt fraction of 0.25-0.3 is a minimum: At an initial Al/Si-ratio of 0.47 of the protolith (average, see above), extraction of a melt fraction in the order of 0.5 would be necessary!

Discussion

The above observations rely on the assumption that the metapelite used as a proxy behaves similar to the protolith of the restite sample. Comparing calculated element-ratios (and absolute wt.%) of our used proxy with those of the studied restite, it becomes obvious that the studied sample is slightly enriched in CaO and that it shows a relatively high Fe/Mg ratio compared to the proxy and the other metapelites. The CaO-enrichement may indicate the presence of carbonate in the protolith, which might thus have been slightly marly.

To test for the influence of these inconsistencies we added different amounts of melt to sample fon1. The melt added had the composition calculated close to the solidus (at 7.5 kbar/700°C). The change in element ratios is shown in table 3. As predicted above, addition of melt leads to a decrease of the Al/Si, Ca/Na and Ca/K ratio, while the Al/Ca ratio slightly increases and the Fe/Mg and Ca/Fe-ratios remain almost constant. The choice of the melt composition and melt fraction is of course somewhat arbitrary, as it depends on the type of melting reaction (water

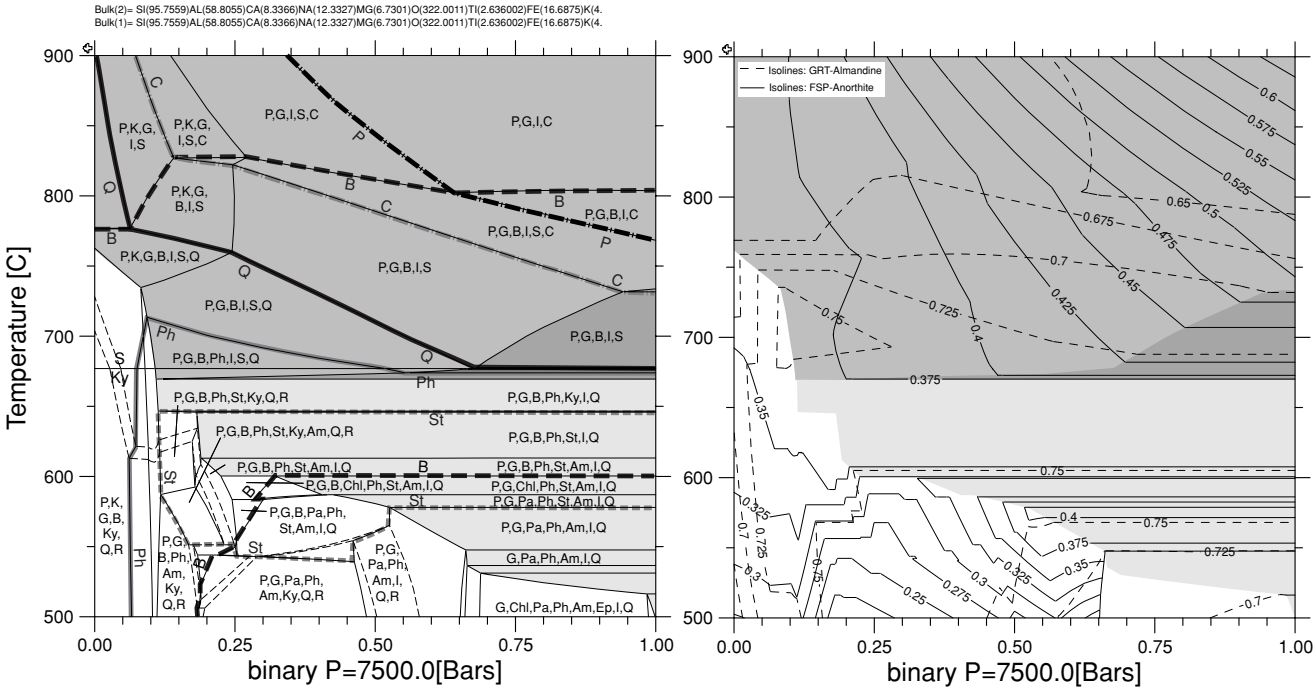

Fig. 17 Left: Binary PT-diagram calculated for sample fon1 assuming an addition of a melt fraction of 0.3. Right: Calculated isopleths for almandine and anorthite components in garnet and plagioclase. Shading as in figure 13.

assisted vs. water absent), on the temperature and pressure and on the amount of fluid in the system (see above). However within reasonable PT-limits, the melt-composition is fairly robust.
In a last step we present a binary TX-diagram computed for a pressure of 7.5 kbar, assuming the addition of 30% of melt. Again, the water content of the system increases along the binary X-axis. Results are depicted in figure 17. Although the recalculated composition is not identical to that of the proxy, the diagram is qualitatively very similar to figure 14. A few important changes are notable: The solidus of the new system is higher by some ten degrees (at 670°C). Phengite reacts out earlier than in the proxy with increasing water content of the system. Plagioclase does not react out completely in this diagram (up to 900°C). Therefore, a probable protolith of sample Fon1A is relatively rich in plagioclase already before the onset of partial melting, and its restite should become even more enriched in plagioclase, which is what we observe in the sample. To demonstrate once more the influence of a changing water contents on phase composition, isopleths were calculated for almandine and anorthite (Fig. 17).

Again, the amount of fluid in the system is critical for the composition of plagioclase, while it bears only a minor influence on the composition of garnet. The calculated isopleths indicate roughly a temperature of 700°C at X ca. 0.4 - 0.5 for the measured mineral compositions. The measured mineral compositions and profiles may provide further insight into the processes working during partial melting. According to figure 17, an increase in anorthite content of plagioclase indicates an increasing amount of hydrous fluid in the system. The initial step around the (relic?) plagioclase cores (increase in X_{An}) may therefore delineate the location where plagioclase dissolution during partial melting was halted. The relatively pronounced increase in anorthite around this core may therefore indicate subsequent crystallisation of plagioclase around these refractory cores (fig. 17). The subsequent slight increase in albite may be attributed to some effects of fractional crystallisation (melt becomes anorthite depleted). The relatively strong increase in anorthite towards the rim may indicate another phase of fluid infiltration, or a decrease in pressure (by ca. 1 kbar)

Conclusion

Thermodynamic modelling (TWQ and DOMINO) suggests a clockwise PT-path from 10-11 kbar/650-700°C down to 6.5-7.5 kbar /580-650°C for the studied sample. Rock composition indicates extraction of melt from a slightly marly metapelitic protolith. A minimum melt fraction in the order of 0.25-0.3 is estimated based on the Al/Si-ratio of the rock. If dehydration melting had been the main cause for restite formation, only a small melt fraction (of the order of < 0.10) had been present at the estimated conditions (Fig. 16), whereas temperatures of at least 750°C would have been indicated to create the estimated minimum melt fraction of 0.25-0.3. In addition, the lack of K-feldspar, the presence of white mica as well as the measured mineral profiles are not consistent with HT-conditions reached during partial melting of the sample. Water assisted partial melting and melt extraction at relatively moderate PT-conditions are in better agreement with the observed mineral assemblages, mineral compositions and zonings, reaction textures and well established Alpine PT-conditions of the Barrovian overprint. This conclusion is further supported by the associated, partially melted granitoid gneisses (Fig. 3), which lack any evidence of dehydration melting reactions (no aluminosilicate, garnet, cordierite or orthopyroxene). Migmatisation of these rocks thus required water assisted partial melting related to fluid infiltration.
It is important to note that based on the K- and Si-depletion of the studied samples alone, muscovite dehydration melting had been the most straight forward explanation for this conspicuous rock. However, detailed information on phase relations and compositions, combined with textural evidence and thermodynamic computation allow delineating a different scenario of partial melting as a result of fluid infiltration. Melt-filled shear-zones, as for example shown in figure 3, indicate that partial melting was a syn-kinematic process and probably took place during the creation of the local kilometre-scale Onsernone-antiform. The strong deformation that partitioned into the SSB and especially in the growing Onsernone Antiform, may have lead to an increase and localisation of fluid flux. The coupling of deformation and enhanced fluid flow has been observed and described repeatedly (Etheridge *et al*., 1983; Kerrich, 1986; Ferry, 1994; Oliver, 1996). As the studied samples are part of a narrow heterogeneous trail (consisting of metasediments and amphibolites), included within predominantly granitoid orthogneiss, strain may have additionally partitioned into this zone, which represents an area of high competency contrast. As a result, fluid flow was probably channelled into this zone of focused deformation, and may have initiated partial melting.
The present study therefore suggest that in orogenic settings, migmatisation may not always be related to very high temperatures and associated dehydration melting of hydrous phases like muscovite or biotite. By contrast, partial melting may be a combined result of increased temperatures and localisation of deformation and fluid flow. Deciphering in detail the history of rocks undergoing such orogenic cycles of subduction and migmatisation, may necessitate a very detailed and almost meticulous discussion, based on field information, phase relations and thermodynamic computation.

References

Berman, R. G. (1988): Internally consistent thermodynamic data for minerals in the systen Na_2O-K_2O-CaO-FeO-Fe_2O_3-Al_2O_3-SiO_2-TiO_2-H_2O-CO_2. Journal of Petrology 29, 445-522.

Berman, R. G. (1992): TWEEQU (version 1.0) Thermobarometry with estimation of equilibration state: .

Berman, R. G. & Aranovich, L. Y. (1996): Optimized standard state and solution proberties of minerals I. Contrib. Mineral. Petrol. 126, 1-24.

Brouwer, F. M. & Engi, M. (2004): Staurolite and other high-alumina phases in alpine eclogites from the Central Swiss Alps: Analysis of domain evolution. The Canadian mineralogist (in press),

Burri, T. (1999): Metamorphism and tectonics within the Vergeletto "Spoon" (Southern Valle Maggia, Ticino). Diploma Thesis, University of Berne, 112 pp.

Colombi, A. & Pfeifer, H. R. (1986): Ferrogabbroic and basaltic meta-eclogites from the Antrona mafic-ultramafic complex and the Centovalli-Locarno region (Italy and Southern Switzerland) - first results. Schweiz. Mineral. Petrogr. Mitt. 66, 99-110.

de Capitani, C. & Brown, T. H. (1987): The computation of chemical equilibrium in complex systems containing non ideal solutions. Geochemica et Cosmochemica Acta 51, 2639-2652.

Engi, M., Berger, A. & Roselle, G. T. (2001): Role of the tectonic accretion channel in collisional orogeny. Geology 29/12, 1143-1146.

Engi, M., Todd, C. S. & Schmatz, D. R. (1995): Tertiary metamorphic conditions in the eastern Lepontine Alps. Schweiz. Mineral. Petrogr. Mitt. 75, 347-369.

Etheridge, M. A., Wall, V. J. & Vernon, R. H. (1983): The role of the fluid phase during regional metamorphism and deformation. Journal of Metamorphic Geology 1, 205-226.

Ferry, J. M. (1994): A historical review of metamorphic fluid flow. Journal of Geophysical Research 99/B8, 15487-15498.

Forster, R. (1947): Geologisch-petrographische Untersuchungen im Gebiete nördlich Locarno. Schweiz. Mineral. Petrogr. Mitt. 27/2, 249.

García-Casco, A., Haissen, F., Castro, A., El-Hmidi, H., Torres-Roldán, R. L. & Millán, G. (2003): Synthesis of staurolite in melting experiments of a natural metapelite: consequences for the phase relations in low-temperature pelitic migmatites. Journal of Petrology 44/10, 1727-1757.

Grandjean, V. (2001): Petrographical evolution of mafic relics and their implication for the geodynamics of the Central Alps. Dissertation, Universität Bern, 103 pp.

Henry, D. J. & Guidotti, C. V. (2002): Titanium in biotite from metapelitic rocks: Temperature effects, crystal-chemical controls, and petrologic applications. American Mineralogist 87, 375-382.

Holland, T. & Powell, R. (2001): Calculation of phase relations involving haplogranitic melts using an internally-consistent thermodynamic database. Journal of Petrology 42, 673-683.

Holland, T. J. B. & Powell, R. (1998): An internally-consistent thermodynamic data set for phases of petrological interest. Journal of Metamorphic Geology 16, 309-343.

Hunziker, P. (2003): The stability of tri-octahedral Fe2+-Mg-Al chlorite. A combined experimental and theoretical study. Dissertation, University of Basel, 121 pp.

Johannes, W. & Holtz, F. (1996): Petrogenesis and experimental petrology of granitic rocks. . Minerals and Rocks . Springer Verlag, Berlin, 335 pp.

Keller, L. M. (2004): Relationships between metamorphism and deformation: Examples from the Western Alps (Camughera-Moncucco unit and Monte Rosa Nappe, N'Italy). Dissertation, University of Basel, 133 pp.

Kerrich, R. (1986): Fluid infiltration into fault zones: Chemical, isotopic and mechanical effects. PAGEOPH 124/1/2, 225-268.

Kobe, H. (1954): Vorläufige Mitteilungen über den Verlauf wichtiger Paragesteinszüge zwischen Vergeletto-Onsernone und Valle Maggia. Eclogae geol. Helv. 47, 167-171.

Kobe, H. (1956): Geologisch-Petrographische Untersuchungen in der Tessiner Wurzelzone zwischen Vergeletto-Onsernone und Valle Maggia. Schweiz. Mineral. Petrogr. Mitt. 36/1.

Kobe, H. (1966): Paragesteinszüge, Struktur und Anatexis im Gebiete zwischen V.Onsernone und V.Maggia. Schweiz. Mineral. Petrogr. Mitt. 46, 461-471.

Mäder, U. K. & Berman, R. G. (1992): Amphibole thermobarometry: a thermodynamic approach. Geological Survey of Canada Current Research Part E/Paper 92-1E, 393-400.

Mäder, U. K., Percival, J. A. & Berman, R. G. (1994): Thermobarometry of garnet-clinopyroxene-hornblende granulites from the Kapuskasing structural zone. Can. J. Earth Sci. 31, 1134-1145.

Meyre, C., Capitani, C. d. & Partzsch, J. H. (1997): A ternary solid solution model for omphacite and its application to geothermobarometry of eclogites from the Middle Adula nappe (Central Alps, Switzerland). Journal of Metamorphic Geology 15, 687-700.

Nagel, T. (2000): Metamorphic and structural history of the southern Adula nappe (Graubünden, Switzerland). Doctoral thesis, Universität Basel, 3 chapters.

Nagel, T., Capitani, C. d. & Frey, M. (2002): Isograds and P-T evolution in the eastern Lepontine Alps (Graubünden, Switzerland). Journal of Metamorphic Geology 20, 309-324.

Oliver, N. H. S. (1996): Review and classification of structural controls on fluid flow during regional metamorphism. Journal of Metamorphic Geology 14, 477-492.

Pfeifer, H. R., Colombi, A., Ganguin, J., Hunziker, J. C., Oberhänsli, R. & Santini, L. (1991): Relics of high-pressure metamorphism in different lithologies of the Central Alps, an updated inventory. Schweiz. Mineral. Petrogr. Mitt. 71, 441-451.

Rütti, R. (2003): The tectono-metamorphic evolution of the northwestern Simano Nappe (Central Alps, Switzerland). Doctoral thesis, ETH-Zürich, 112 pp.

Schärer, U., Cosca, M., Steck, A. & Hunziker, J. C. (1996): Termination of major ductile strike-slip shear and differential cooling anlong the Insubric line (Central Alps): U-Pb, Rb-Sr and Ar/Ar ages of cross-cutting pegmatites. Earth and Planetary Science Letters 142, 331-351.

Spear, F. S., Kohn, M. J. & Cheney, J. T. (1999): P-T paths from anatectic pelites. Contrib. Mineral. Petrol. 134, 17-32.

Steck, A. (1984): Structures de deformations tertiaires dans les Alpes centrales.

Eclogae geol. Helv. 77/1, 55-100.

Steck, A. & Hunziker, J. C. (1994): The Tertiary structural and thermal evolution of the Central Alps; compressional and extensional structures in an orogenic belt. In: Seranne, M. & Malavieille, J. : Late orogenic extension. 238. Tectonophysics, , 229-254.

Todd, C. S. & Engi, M. (1997): Metamorphic field gradients in the Central Alps. Journal of Metamorphic Geology 15, 513-530.

Tóth, T. M., Grandjean, V. & Engi, M. (2000): Polyphase evolution and reaction sequence of compositional domains in metabasalt; a model based on local chemical equilibrium and metamorphic differentiation. Geological Journal 35/3-4, 163-183.
Wenk, E. (1955): Ergebnisse einer Rekognoszierung im Gebirgsdreieck Domodossola-Camedo-P.Porcarescio (Lepontinische Alpen). Eclogae geol. Helv. 48, 125-131.
White, R. W., Powell, R. & Holland, T. J. B. (2001): Calculation of partial melting equilibria in the system Na_2O-CaO-K_2O-FeO-MgO-Al_2O_3-SiO_2-H_2O (NCKFMASH). Journal of Metamorphic Geology 19, 139-153.

Appendix

For computation of phase diagrams and isopleths with program DOMINO, we used the internally consistent databases of (Berman, 1988, update JUN92), or of (Holland & Powell, 1998). For calculation with the HP98-database we used exclusively standard state data and solution models according to this database. For computation with the Berman database we used, in addition to the data provided in the original database, the following recent standard state data and solution models appropriate for this database:
Phengite: (Keller, 2004)
Chlorite: (Hunziker, 2003)
Staurolite and Chloritoid: (Nagel, 2000)
Omphacite: (Meyre *et al*., 1997)
Epidote: Ideal binary between epidote and clinozoisite, this study
Ilmenite: Ideal binary between ilmenite and geikielite, this study
Amphibole: Molecular site mixing model with the activities of the endmembers equal to $(X_{Endm})^2$ and with one symmetric Margules terms of + 20000 J for the pargasite-tremolite join. We used the Mäder (94) dataset for the three endmembers pargasite-tremolite-edenite and their respective Fe-counterparts. Fe-Edenite was new defined as Edenite(1)Fe-Pargasite(1.25)Pargasite(-1.25). This study.
Note that the epidote, ilmenite and amphibole models are only approximate, because no published models exists for the Berman database. A complex activity model for amphibole (Mäder and Berman, 1992; Mäder *et al*., 1994), which includes several site-dependent Margules terms cannot be computed, because it violates some of the fundamental assumptions inherent to program DOMINO. Fortunately the amphibole stability field is outside of our region of interest and does therefore not influence our discussion.

Processes of partial melting in collisional setting

Thomas Burri and Alfons Berger

Abstract

Syn- and post-kinematic migmatisation is a common feature in collisional settings. Anatexis may be caused by dehydration-melting reactions, or by the infiltration of fluid into rocks at temperatures above their water-saturated solidus. We explore processes of partial melting in the course of subduction and collision, using thermodynamic computation. We investigate granitic, semipelitic and mafic systems, discussing partial melting either in closed systems, or in open systems. In the latter, partial melting is triggered by the influx of external fluids.

Whereas syncollisional partial melting in closed systems could account for a melt fraction of some 20% in granitic and pelitic rocks, only minor amounts are predicted for mafic rocks. Natural examples of migmatisation in the latter lithology are therefore better explained by fluid infiltration scenarios as the cause of partial melting. Distinguishing water-assisted partial melting from dehydration-melting in the field is not easy. We suggest several criteria, which may be indicative for fluid-fluxed partial melting. An important indication of water-assisted partial melting are amphibole-bearing leucosomes, which are commonly found within partially molten granitoid gneisses. Melts from fluid-fluxed partial melting are often interpreted to be unable to leave the site of melting due to the negative volume change of the melting reaction. Using recent data on partial molar volumes of oxides in melts in combination with thermodynamic computation, we demonstrate that this statement is only true for closed systems, but not for open systems where fluid infiltration may occur. Our model indicates that volume changes for melting due to fluid infiltration may in fact be highly positive. Water-assisted partial melting may be an important process for amphibolite facies shear zones of regional extent, where enhanced rates of fluid flow may accompany deformation. The decrease in rock strength due to the presence of melt may lead to localised deformation and increased strain rates in partially molten rocks.

Introduction

Partial melting induces major changes in the rheology of a rock. Very generally speaking, increasing amounts of melt lead to a steady decrease in rock strength (Arzi, 1978; Rutter and Neumann, 1995; Vigneresse and Tikoff, 1999; Rosenberg, 2001; Mecklenburgh and Rutter, 2003). If partial melting and deformation coincide, migmatisation may cause strain partitioning into the partially molten rock and a related increase in strain rates (Davidson *et al*., 1994; Brown and Solar, 1998; Vigneresse & Tikoff, 1999; Brown and Solar, 1999; Dimanov *et al*., 2000; Rosenberg and Berger, 2001; Paterson, 2001). Another probable effect of synkinematic migma-tisation is an increasing rate of melt segregation and melt expulsion (Brown *et al*., 1995; Kisters *et al*., 1998; Brown & Solar, 1998; Vigneresse & Tikoff, 1999; Brown & Solar, 1999; Rosenberg and Handy, 2000; Rosenberg, 2001; Barraud *et al*., 2004). Syncollisional partial melting may therefore exert an essential influence on the tectonic evolution of a mountain belt. In the last 20 years migmatite research has focused on high-temperature migmatisation processes, which involve dehydration-melting reactions (DM-reaction) at temperatures in excess of 700-750ºC. In contrast, water-assisted partial melting (WAM) (also called water or fluid-fluxed partial melting (Patiño Douce and Mc Carthy, 1998)) has been largely ignored as a probable cause of migmatisation. This neglect is related to the fact that, in general, only a very modest amount of fluid is present in rocks at amphibolite to granulite-facies conditions. Hence, water-assisted partial melting in a closed system usually creates melt fractions below 2-5 vol.% (e.g. Patiño Douce and Harris, 1998; Thompson, 2001; Whittington and Treloar, 2002). Nevertheless, WAM was occasionally described as a possible cause for migmatite formation (Yardley and Barber, 1991; Mogk, 1992; Brown *et al*., 1995; Butler *et al*., 1997; Patiño Douce & Mc Carthy, 1998; Viruete, 1999; Prince *et al*., 2001; Mogk, 2001; Garlick and Gromet, 2004). Water assister melting can certainly become important if external fluids are able to infiltrate rocks at temperatures above their water-saturated solidus. Because fluid flow and deformation are often associated processes (e.g. Etheridge *et al*., 1983; Ferry, 1994; Oliver, 1996), this type of migmatisation may

be typically found along shear-zones of regional extent (see chapters 1).
In this contribution we discuss migmatisation processes in collisional settings with an emphasis on water-assisted partial melting. Using thermodynamic computation, we explore phase relations and melt productivity of several lithologies undergoing subduction, collision and exhumation along different PT-paths.

General introduction to melting processes

In the following analysis, we constrain the discussion of fluid assisted melting to water-rich fluids, ignoring mixing-effects. Thus, the term fluid will be used below to describe a very dominantly hydrous fluid. The main effect of a mixed H_2O-CO_2 fluid is to shift the fluid-saturated solidus towards higher temperatures, and thus to decrease the melt fraction at any given temperature. In addition, lowering of the water activity decreases the stability fields of hydrous minerals like micas and staurolite, and increases those of dry minerals like feldspars, garnet and pyroxenes.
Melting processes are often discussed in terms of congruent or incongruent melting. In congruent melting, a mineral melts to a liquid of the same composition, whereas in incongruent melting, a mineral breaks down to a new mineral in addition to a melt. Strictly speaking, these terms should only be applied to single minerals and not to natural rocks, where melting of a mineral assemblage is discussed. We therefore define our use of the two terms in the following discussion.
Congruent melting (s.l.) of a mineral assemblage leads to the creation of a melt plus refractory minerals. Congruent melting does not lead to the creation of new mineral phases, but solid solution phases may adjust their composition to maintain equilibrium between solids and melt. Congruent melting reactions (s.l.) in migmatite terrains is generally restricted to water-assisted melting, where the degree of partial melting depends primarily on the amount of fluid present in the system.

Incongruent melting reactions (s.l.) are typically fluid (or vapour) absent melting reactions (dehydration-melting reactions, or DMR), during which the decay of a hydrous phase leads to the creation of a melt and to a new (less hydrous) solid assemblage including one or several neoformed phases. The degree of partial melting is limited by the modal abundance of the phase(s) breaking down.
In addition we introduce the term **mixed mode melting reactions** which denotes water-assisted melting reactions involving the coeval breakdown and crystallisation of hydrous phases and the formation of a melt. Such reactions are important indicators for the involvement of a fluid phase in the migmatisation process. The degree of partial melting is dependent on the modal abundance of the decaying phase (or of any reactant of the melting reaction) as well as on the amount of fluid taking part in the reaction. The biotite-breakdown reaction to form amphibole and melt is discussed below as a typical example of mixed mode reactions.
It is usual to speak of **fluid-saturated** or **under-saturated melting** or to denote melts evolved through water-assisted melting as "fluid-saturated melts" and those produced through dehydration-melting as "water-deficient" or "water-undersaturated melt". We will avoid these terms in the following discussion, because they are misleading. Melts cannot be fluid-undersaturated at equilibrium, because such a condition would immediately give rise to crystallisation. However, melts may contain a minimum water content only, which is their equilibrium water content (Johannes and Holtz, 1996; Holtz *et al*., 2001b; Holtz *et al*., 2001a). Isolines of minimum water contents in granitic systems are depicted in figure 1 as dashed lines. Note that melts at their minimum water content are not fluid-saturated. If a melt contains more water than at equilibrium with the solid constituents (refractory minerals in magma or host rock), then the surplus of fluid may be used to promote further melting or to form hydrous solids in the country rock. A water amount in excess of the minimum may arise for sufficiently large melt segregations, if equilibration with the host rock is no longer main-

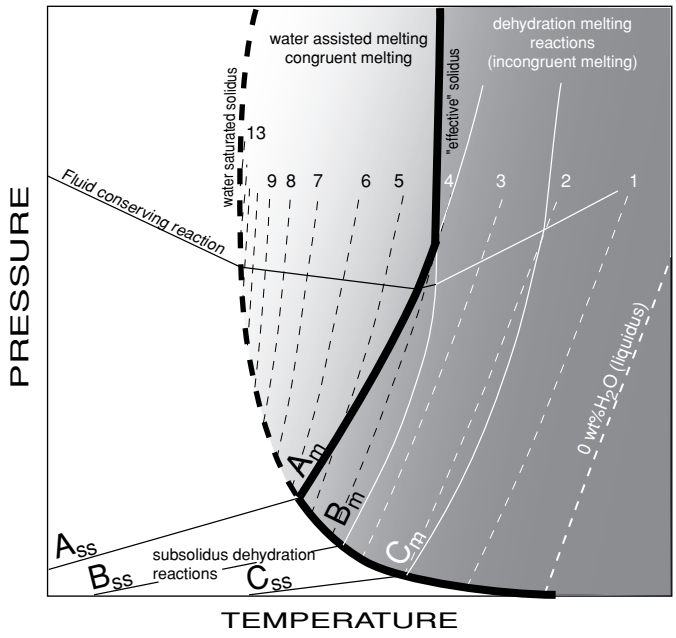

Fig. 1: General phase relations in an anatectic system. See text for discussion. Thick dashed line: water-saturated solidus; thick solid line: effective solidus; A_{SS}-C_{SS}: subsolidus dehydration reactions; A_m-C_m: dehydration-melting reactions. Dashed lines with numbers are isopleths of minimum water content of the melt.

tained. In such cases, melts may even become supersaturated in fluid and a hydrous fluid may start to exsolve. As long as melt segregations remain on the centimetre to decimetre scale, equilibration with the solid constituents (host rock) may however be reached within geologically significant timescales (pers. com. F. Holtz). This behaviour is independent of whether the melt was produced by WAM or DM. Therefore, although speaking of fluid-saturated or fluid-undersaturated melting is correct (saturation in this case refers to the solid system, which may or may not contain a free fluid phase), we propose that the terms "fluid-saturated or undersaturated melts" should be avoided, because they are misleading.

Figure 1 gives a schematic overview of the processes determining the melting relations in a hypothetical system. Two processes are important for the creation of anatectic migmatites (leaving aside the possibility of subsolidus-formation of migmatites):

Depending on temperature, fertile lithologies rich in mica and amphibole, such as metapelites, semipelites and hydrated mafic rocks may undergo dehydration-melting.

Alternatively, water-assisted melting may be initiated as a result of the influx of external fluids. If fluid infiltration occurs, water-assisted congruent melting may take place at any point above the water-saturated solidus (shaded areas).

At closed system conditions, water-assisted partial melting will commonly produce but a small melt fraction along the **water-saturated solidus**, through the consumption of the available pore fluid in a congruent melting reaction. Without fluid infiltration the **effective solidus** (locality where melt fractions overstep 1-2 %) of a given system is located along the first dehydration-melting reaction. As a result, the effective solidus of a specific system is made up of sections of various dehydration melting reactions (thick solid lines in fig. 1) and may have a fairly complicated outline (see also in Schmidt and Thompson, 1996; Vielzeuf and Schmidt, 2001).

At conditions below the water-saturated solidus, subsolidus dehydration reactions A_{ss}-C_{ss} lead to changes in the (solid) mineral assemblage and to the liberation of free fluid. A typical example of such a reaction is

Ms + Qtz = Kfs + Sill + H2O (1)

Where the reaction intersects the water-saturated solidus, the slope of the reaction usually steepens, and the liberating fluids lead to incongruent melting. The expression of reaction (1) in melt-bearing systems would be

Ms + Qtz = Kfs + Sill + melt (2)

The slopes of the dehydration-melting reactions A_m-C_m continuously change with pressure as a function of the changing water activity of the melt, and the slopes change again where they intersect a fluid-conserving reaction of type

Bt + Ab + Als + Qtz = Ms + Grt (3)

Assuming near-isobaric heating, melt fractions abruptly increase each time a dehydration-melting reaction (A_m-C_m) is overstepped, due to the decay of a hydrous phase. Between such reactions, the melt fraction increases slightly and continuously, due to the decreasing minimum water content of a melt with rising temperatures (dashed fluid isopleths in fig. 1). Because of the different slopes of the dehydration-melting reactions, they may intersect, hence melting sequences vary along different PT-paths.

Computation of partial melting in collisional settings

General discussion and setup for computation

The degree of partial melting in subduction and collisional settings depends strongly on the lithology, PT-path, infiltration of fluids and the initial hydration state (the latter denoting the initial bulk-fluid content of a rock in the form of free fluid or hydrous phases). A fluid saturated rock at equilibrium coexists with at least a very minor amount of fluid. Any addition of an identical fluid will not lead to changes in the phase assemblage nor in the modes of the solids. Instead, addition of fluid to an only partially hydrated (fluid-undersaturated) rock must result in a change in the phase assemblage or in the modes of the solids. Dry basement may not be fully water-saturated at the onset of subduction, in contrast to unmetamorphic sediments, which are likely to be fluid-saturated. With the exception of very dry rocks like unaltered granulites and HT-eclogites, most rocks contain at least a very small amount of pore fluid at the beginning of partial melting. In general prograde metamorphism leads to a decrease in the mode of hydrous phases, such that the presence of a hydrous fluid may always be ensured along the prograde path. "Dry" basement rocks may have become partially rehydrated during previous metamorphic cycles or may take up fluids during early stages of subduction. Upon reheating, such units are likely to become fluid-saturated along fractures and shear zones, and may show a variable hydration state in between such structures.

Below we discuss the change of phase assemblages and the occurrence and degree of partial melting along two different collisional-PT-paths (A and B), similar in type to paths reported for the European Central Alps (e.g. in Frey and Ferreiro-Mählmann, 1999; Nagel *et al*., 2002; Rütti, 2003, see also discussion in Engi *et al*., 2001 and Roselle *et al*., 2002)). We investigate three typical crustal lithologies; granites, semipelites and mafic rocks, the chemical compositions of which are given in table 1. The system components used for the calculation of the respective systems are also listed in this table. For discussion, we use phase diagrams and phase variation diagrams computed with program THERIAK and

Composition of rocks used for computation

wt.% oxide	granite	semipelite	basalt
SiO2	70.77	53.24	52.38
TiO2		0.74	
Al2O3	14.83	22.25	16.93
FeO		7.26	10.29
Fe2O3	2.44		
MgO	1.19	2.32	7.13
CaO	1.34	0.55	10.05
Na2O	3.33	0.76	3.21
K2O	6.1	5.34	
total	100	92.46	99.99

table 1: Rock compositions used in thermodynamic computation. Granite from (Naney, 1983), semipelite from (Nagel, 2000), basaltic rock from (Poli, 1993). The semipelite composition was estimated by surface integration using EMP-analysis and was normalised for calculation.

DOMINO (de Capitani and Brown, 1987), in combination with the internally consistent database of Holland and Powell (1998) with updates for melt bearing systems (White *et al*., 2001; Holland and Powell, 2001). We note that the melt-model is not well constrained for pressures in excess of ca. 12 kbar and that calculation in mafic to ultramafic systems would require some refinement of the model (White *et al*., 2001). Therefore, calculations performed at pressures higher than 12 kbar and in mafic systems may involve increasing uncertainties. Complete fluid saturation (pure water) was assumed over the whole PT-field for the computation of PT-phase diagrams. Melt was excluded from calculation of PT-phase diagrams, because the solidus, phase assemblages and modes of minerals vary with the fluid content of the bulk system, which may locally differ as explained above. Isolines of free H_2O (in mol) were then calculated to indicate the location in PT-space where minor and major amounts of fluid are released. Increasing numbers on the isolines (Fig. 2-5) indicate fluid-release from the hydrous solids, and the spacing between the isolines reflects the amount of fluid released in a certain PT-interval. Note that absolute numbers depend on the bulk composition. To visualise the conditions and progress of partial melting, we calculated stable assemblages along two segments of PT-paths typical of collisional settings (figures 2B-4B show location of PT-paths, figures 2C+D - 4C+D show assemblages along the calculated segments). Note that we usually plot melt-bearing segments of the respective PT-paths only, which differ for each lithology. At the onset of partial melting, we assume a small amount of 0.2-0.25 vol.% of hydrous fluid to be present, which simulates the effect of a possible pore fluid. We denote this kind of partial melting, where a small amount of pore fluid may initially be present, as *closed system melting* in the following discussion. Calculated segments of the PT-paths are depicted in PT- diagrams as solid black lines; thick grey lines indicate the presence of melt. Because of the inadequacies of the melt model at high pressure, we excluded melt from calculation in the granitic system at conditions below the experimentally determined water-saturated granite solidus (table 2.1 in Johannes & Holtz, 1996). Else, in fluid saturated systems above ca. 12 kbar, the model predicts a back-bending of the solidus towards lower pressures.
We note that by using thermodynamic computations, we always restrict ourselves to equilibrium scenarios, an assumption which may not be completely adequate to describe natural metamorphic processes, especially in dry protoliths.

Closed system melting (no fluid infiltration)

Granitic systems [1]:

Figure 2A presents the phase diagram computed for the granitic system. Predicted stabilities of amphibole and of clinopyroxene need a short assessment: Computation demonstrated that stabilities of these phases are strongly influenced by oxygen fugacity. The existence of minor amounts of amphibole (< 5%) in a small area of the diagram is in part connected to the assumed QFM (quartz-fayalite-magnetite) buffering. At more oxidising conditions of IMR (ilmenite-magnetite-rutile) or even HM (hematite-magnetite) buffering, amphibole is everywhere replaced by epidote below temperatures of 600ºC. In addition, clinopyroxene stability extends to surprisingly low pressure-conditions. We note, however, that Naney (1983) documented clinopyroxene at 8 kbar between 600-700ºC, thus even at lower pressure then predicted in this study. Stability of clinopyroxene in the experiments was show to increase with increasing water content of the system. On the other hand, the computed stability of clinopyroxene towards lower P and T is again related to the assumed $f(O_2)$ (QFM-buffer). Use of the IMR or HM buffer, which may be more characteristic for lower grade conditions, shifts up the lower limit of clinopyroxene stability by 2-3 kbar because of the increased epidote stability. In experiments performed at higher oxidising conditions of NNO-buffering, epidote was in fact observed (Naney, 1983). Several reactions calculated below may thus involve epidote on the reactant side instead of clinopyroxene at temperatures below 700ºC. Calculated variations of clinopyroxene composition (jadeite isolines in fig. 2A) are however consistent with natural phase relations of HP-metagranitoids, for which a replacement of primary jadeite by more omphacitic clinopyroxene has been reported (Oberhänsli *et al*., 1985). According to our computation, this replacement should occur during decompression of such rocks.
Examination of figures 2A + B shows that a major fluid release (that could induce partial melting) occurs when phengite + clinopyroxene (or epidote) +

[1] *Note, that because we discuss metamorphic processes in a large PT-window, we will usually denote white micas as phengites in the following discussion.*

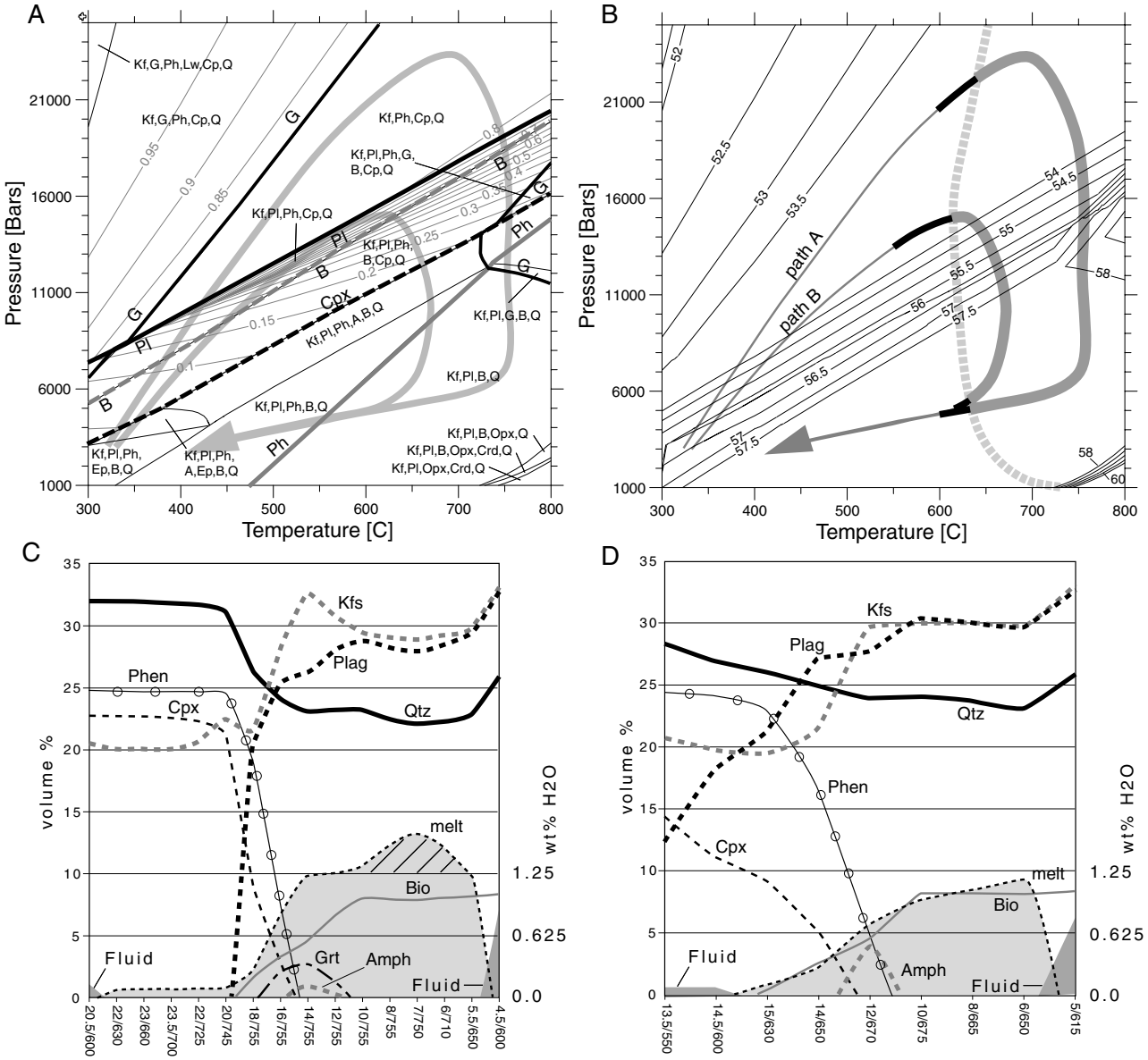

Fig. 2: (A) Melt absent phase diagram calculated for the water saturated granitic system at f(O_2) of QFM buffer. Boundaries of phase assemblages are denoted by thin solid lines. Several phase boundaries important for discussion are additionally outlined by different thicker lines. Associated labels are always situated on the stable side of the boundary, except where a minus sign is prefixed. Light grey lines and numbers are isolines with mole fractions of jadeite in clinopyroxene. Note that at low P and T cpx would be replaced by epidote for realistic f(O_2). (B) Isolines in moles of free fluid (pure water) the water saturated granitic system. Increasing numbers indicate increasing release of fluid from decaying hydrous solids. Dashed grey line is water-saturated granite solidus according to (Johannes & Holtz, 1996). Overlaid are two PT-paths characteristic of collisional settings. Black thick lines denote calculated, melt absent segments, and thick grey lines calculated, melt present segments of the PT-paths. (C) Changes in phase relations and modes for the granite system following the high-pressure path A of figure 2B. The modal abundance (vol.%) is plotted on the y-axis, and calculated PT-points of the PT-path on the x-axis. The volume of free fluid phase at the onset of partial melting is 0.2-0.25 vol.%. The diagonal striped area is explained in the text. (D) Changes in phase relations and modes for the granite system following path B of figure 2B. The volume of free fluid phase at the onset of partial melting is 0.2-0.25 vol.%.
Abbreviations: A/Amph-amphibole, An-andalusite, B/Bio-biotite, Ca-carpholite, Cd-cordierite, Ch-chlorite, Cp/Cpx-clinopyroxene, Ct-chloritoid, Ep/Epi-epidote, F-fluid, G/Grt-garnet, Gl-glaucophane, Kf/Kfs-K-feldspar, Ky-kyanite, Lw-lawsonite, Mt-magnetite, Op/Opx-orthopyroxene, Pa/Para-paragonite, Ph/Phen-Phengite, Pl/Plag-plagioclase, Q/Qtz-quartz, S/Sill-sillimanite, St-staurolite, Zo-zoisite

quartz (± amphibole) break down to produce K-feldspar + plagioclase + biotite (+ fluid or melt). At temperatures below the water saturated solidus, this main fluid-release does not coincide with the location of the final phengite breakdown (compare phengite-out line ("Ph") in figure 2A). Therefore a small amount of phengite remains stable towards lower pressures at these conditions. This indicates that the reaction is not a pure phengite-breakdown reaction, but is more complex in detail. The extent of phengite consumption in the course of this reaction depends on the breakdown of clinopyroxene (or epidote ± amphibole), and not on the upper thermal stability limit of phengite.

As a consequence, the major consumption of phengite is predicted to occur at fairly low temperature, and the water saturated solidus is therefore crossed at higher pressures (see discussion below). Figures 2B, C and D indicate that dehydration-melting of phengite could account for the commonly observed partial melting in granitoid systems at comparatively low temperatures. Another striking

feature is the absence of aluminosilicate phases on the product side of the dehydration reaction, in contrast to muscovite dehydration melting in pelitic systems. The surplus of alumina is probably taken up in the melt and in the eastonite and siderophyllite components of biotite (Tschermaks exchange $(Mg/Fe)_1Si_1 \leftrightarrow Al_{-2}$). Experimental results in granitic systems sustain that Tschermaks exchange may become important at elevated temperatures (Gardien *et al*., 1995; Vielzeuf & Schmidt, 2001). A second major fluid release is visible at low pressure and high temperature due to the breakdown of biotite, leading to the formation of cordierite and orthopyroxene.

Figure 2C shows the development of mineral assemblages and melt fraction along the high-pressure subduction path A. The modal abundance is plotted on the y-axis, calculated PT-points along the PT-path on the x-axis. First congruent melting occurs along the water-saturated solidus at about 22 kbar and 630ºC, due to the consumption of the available pore fluid. The resulting melt volume of < 1% remains nearly constant until the decay of phengite is initiated according to the pseudoreaction

Phen + Cpx/Epi + Qtz >> Kfs + Plag + Bio + Melt (± Grt/Amph) (4)

We use the term pseudoreactions to outline a change in modal abundances over a PT-interval, rather than a stoichiometrically balanced reaction. To point out such reactions, the balancing equations are divided by a different sign (>>). All proposed reactions of this type can be inferred from diagrams 2C+D - 4C+D.

A maximum melt volume of 13-14% is reached during ascent of the rock at 7 kbar/750ºC (fig. 2C). Such a high melt fraction is remarkable, especially because the final solid assemblage does not contain any minerals characteristic for dehydration-melting like orthopyroxene, cordierite or sillimanite (e.g. Patiño Douce & Harris, 1998; Thompson, 2001). The small amount of garnet (~3%) present between 18-11 kbar would only be preserved (stably) if melt escaped at these conditions, inhibiting consumption of garnet due to the lack of fluid necessary to grow biotite. The only mineralogical indication of former partial melting in such rocks is the absence of phengite, which was completely consumed in the course of partial melting. However, the relatively high melt fraction is expected to lead to macroscopic segregation of melt (Laporte and Watson, 1995; Brown *et al*., 1995; Vigneresse & Tikoff, 1999), hence partial melting may be inferred on the basis of textural and structural evidence on the microscopic to outcrop scale. The considerable melt fraction results primarily from phengite-decomposition, but a small amount is also due to the pore fluid that was assumed to be present at the onset of partial melting (0.5-1 vol.% melt in fig. 2C and D). A considerable amount of 3-4 vol.% of melt is additionally due to the decrease in (minimum) water content of melt with decreasing pressure along the HP-path A (assuming equilibrium between melt and solids, see fig. 1). The decrease in water contents of the melt leads to additional partial melting in the rock (in dependence on the PT-path). The hump in the melt fraction between 10 and 5.5 kbar observed in figure 2C (denoted by diagonal stripes) is due to this effect. Even though the initial pore fluid was only in the order of 0.01 wt.%, the amount of fluid released during final crystallisation of the rock amounts to almost 1 wt.%. This pronounced increase results from the breakdown reaction of phengite. A part of its hydrous component is taken up by newly growing biotite, the rest dissolves in the melt. Upon crystallisation, some of the released volatiles may escape from the rock, the rest may be consumed in the formation of secondary phengite at temperatures of ~550ºC.

Figure 2D displays the evolution of granitic rocks along PT-path B. Again, a relatively high melt fraction is created upon complete consumption of phengite according to reaction (4). Although the final assemblage shortly after crystallisation of the melt is equal to the assemblage observed in the HP-loop (Qtz + Kfs + Pl + Bi + fluid), the maximum volume of melt reached along the PT-path is only of the order of 9%. The cause of this lower melt fraction is the lower maximum temperature reached, because melts at lower temperature contain a higher amount of fluid. Rocks following a PT-path that does not reach conditions of partial melting may dry out earlier than rocks following path A or B, because the former cannot store fluid liberated in the course of phengite decomposition in the melt. Rocks that cross the water saturated solidus at pressures below 10 kbar develop no appreciable melt fraction, because much of the white mica is consumed before the water-saturated solidus is overstepped (fig. 2B). In the absence of effective melt segregation, a small melt fraction may hardly be detectable in the (re)solidified rock. We note that along the chosen PT-paths, which are typical for the central parts of the Alpine orogen, no biotite dehydration melting is predicted to occur, and that partial melting is essentially the result of the breakdown of phengite and epidote (in the absence of fluid infiltration).

Semipelitic and pelitic systems

Figures 3A-D display computations performed for these systems. Major amounts of fluid that could induce partial melting are released through the decomposition of paragonite, staurolite, phengite or biotite, depending on the PT-path (fig. 3B). A major fluid (or melt) release in collisional settings occurs through the final decomposition of phengite at the second sillimanite isograd (reactions (1) and (2)). Complete consumption of phengite occurs only along the HP-path A.

Comparison of figures 2A and 3A as well as of 2B and 3B indicates that final phengite breakdown in granitic systems occurs at almost 100ºC lower temperatures than in pelitic systems, and that an important phengite fraction in the granite reacts out at even lower conditions. Obviously this lowering in

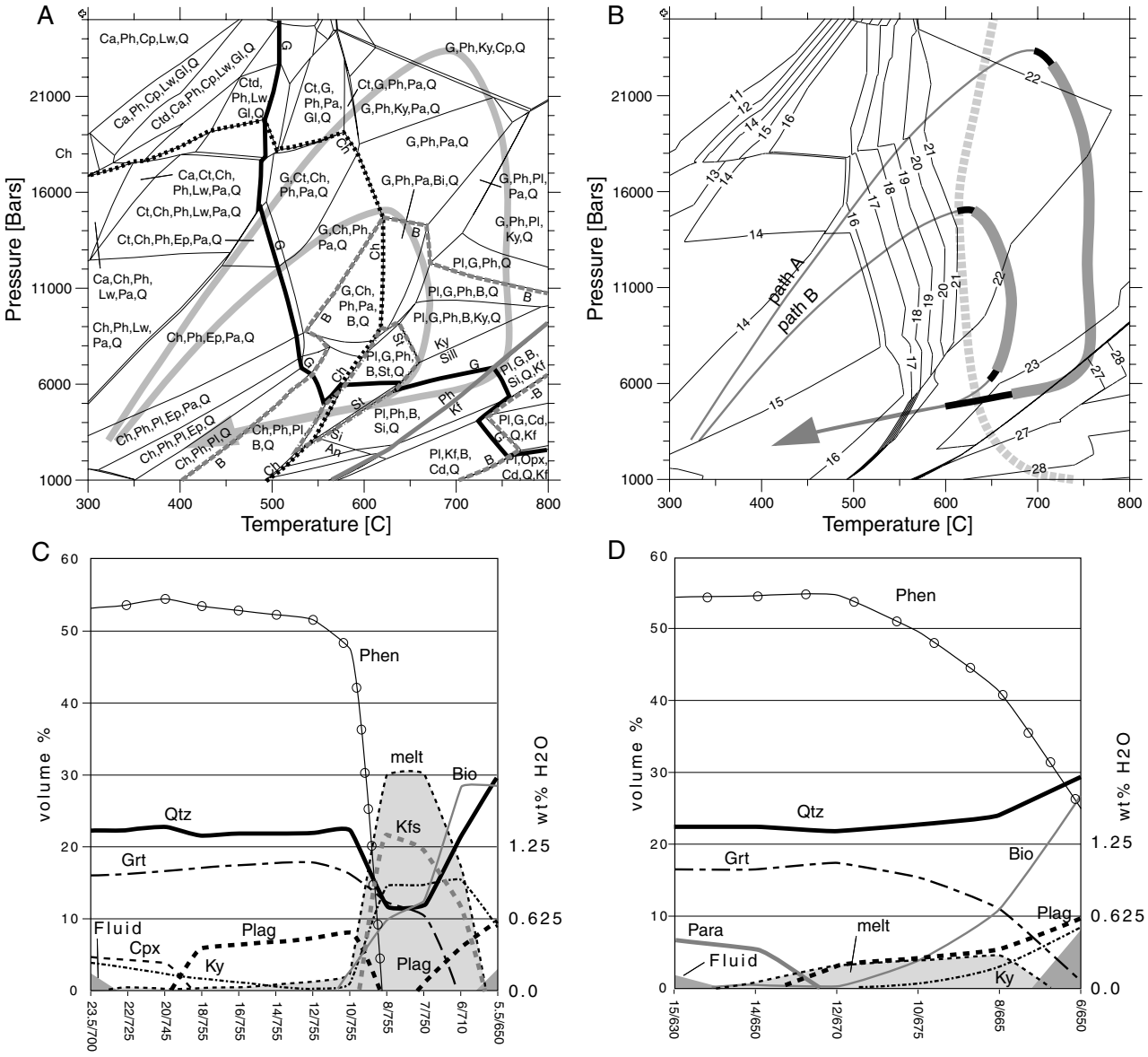

Fig. 3: (A) Computed phase diagram for the water saturated pelitic system. Compare with caption of figure 2A for additional information. (B) Isolines in moles of free fluid (pure water) for the water saturated pelitic system. Dashed grey line is water-saturated solidus of granitic systems according to Johannes & Holtz (1996). See caption of figure 2B for further information. (C) Changes in phase relations and modes for the pelitic system following path A. The volume of free fluid phase at the onset of partial melting is 0.2-0.25 vol.%. (D) Changes in phase relations and modes for the pelitic system following path B. The volume of free fluid phase at the onset of partial melting is 0.2-0.25 vol.%. See caption of figure 2C+D for further information.

temperature of white mica breakdown must be compositionally controlled. This suggests that granitoid rocks which followed a pressure-accentuated path at moderate temperatures (e.g. path B) may exhibit migmatitic features, while associated metapelitic rocks appear largely unaffected by partial melting. Aluminosilicate phases primarily form along the decompression path in water-saturated systems. At lower water activities (water-undersaturation or mixed fluids) or in more aluminous systems ("real" pelites), growth of kyanite may also occur earlier along the prograde path.

Along subduction path A, a first minor amount of melt (< 1 vol.%) is created at 700-725ºC at 22-23 kbar, thus at higher temperatures than in the granite system (compare figures 3C and 2C). This may be a result of the lack of K-feldspar in the pelitic system. Figure 3C indicates that the first melt forms through a congruent fluid-consuming melting reaction

Cpx + Ky +Fluid >> Grt + Phe + Qtz +Melt (5)

Up to the onset of phengite decomposition at 12 kbar/755ºC the melt fraction remains below 2%. A substantial amount of melt is then produced through the incongruent phengite breakdown reaction

Phe + Qtz + Grt + Pl >> Kfs + Bio + Ky/Sill + Melt(6)

The occurrence of garnet on the left hand side of reaction (6) is related the decompression of the rock from 12 to 6 kbar, which leads to (stable) replacement of garnet by biotite. A maximum of over 30 vol.% melt is predicted at 7 kbar/750ºC. Estimates of the melt fraction resulting from muscovite-dehydration-melting of typical metapelites are in the order of < 20% (Le Breton and Thompson, 1988; Spear *et al.*, 1999; Thompson, 2001; Kriegsman, 2001), and

in granitoid systems it is accordingly smaller. Estimates indicate the formation of approximately 88 vol.% melt per volume of decaying muscovite (Patiño Douce & Harris, 1998) or 70 vol.% melt per volume of muscovite (Spear *et al*., 1999). Our computation suggests ca. 60 vol.% melt per volume phengite, which is slightly lower than the above estimates. The predicted high melt fraction of 30% (instead of 20%), is probably composition-dependent (high-K).

A considerably different picture is obtained along path B (figure 3D), where the melt fraction never exceeds 5%. This moderate degree of partial melting is related to the incomplete consumption of white mica along path B. The predicted melt fraction is primarily the result of paragonite dehydration-melting. We emphasise that along the same PT-path in a granitic system phengite breaks down completely to form biotite, plagioclase and K-feldspar (compare with fig. 2A).

Higher melt fractions would be expected only if temperatures along the respective PT-paths reached conditions of biotite dehydration-melting (temperatures > 750ºC at all pressures up to 15 kbars (Stevens *et al*., 1997; Patiño Douce & Harris, 1998; Thompson, 1999; Spear *et al*., 1999). Our results suggest that dehydration-melting of paragonite and phengite are likely to occur during subduction and collision, but that metamorphic conditions along the PT-paths adopted were too cool to enter the field of biotite-DM.

Hydrous MORB systems

Figure 4A show the phase relations computed for the basaltic system. Fluid release to induce partial melting occurs due to the decomposition of epidote, paragonite and amphibole (fig. 4A+B). Note that the chosen bulk system lacks potassium, whereas natural paragonite may in fact be K-bearing. This effect of solid solution may to some extent increase the stability of paragonite. Furthermore, K-bearing systems may contain phengite and biotite in addition to paragonite.

Very different rock evolutions are predicted for rocks following either path A or B. Along the high-pressure path A rocks reach eclogite-conditions, where the assemblage consists entirely of the anhydrous minerals Grt + Cpx + Ky + Qtz. The small amount of fluid assumed to remain in the rock is completely consumed to form amphibole upon initial exhumation. The necessity of fluid consumption is well visible in figure 4B: The post-peak-pressure segment of path A crosses isolines towards lower numbers, indicating incorporation of fluid into the solid assemblage. During exhumation, the amount of hydrous phases never exceeds 5% of the rock volume (fig. 4C). Because of this dry assemblage, partial melting would not even occur if minor amounts of fluid is allowed to infiltrate the rock. Growth of amphibole acts as an effective fluid buffer, inhibiting partial melting in such rocks. To induce partial melting, the rock needs to be flushed with fluid. The metamorphic evolution of a rock following path B contrasts to the above, because hydrous phases remain abundant in the rock also at post peak-pressure conditions (fig. 4D). The persistence of hydrous phases and a small amount of pore fluid lead to congruent partial melting at the water saturated solidus (at temperatures as low as 600ºC at ca. 14.5 kbar) according to

Qtz +Epi + Para + Fluid >> Amph + Cpx + Melt (7)

Partial melting continues through the combined consumption of epidote and paragonite by the incongruent melting reaction

Qtz +Epi + Para + Amph ± Cpx >> Plagi + Grt + Melt (8)

and, after the complete consumption of paragonite, through a mixed mode reaction

Qtz + Epi + Grt >> Amph + Plag (8a)

Reaction (8a) produce only an additional 1-2% of melt. (Note that reactions 8 and 8a would also involve exchange of melt components on either side of the equation, which is neglected for simplificity). A maximum melt volume of ca. 9% is obtained at 12 kbar and 670ºC, thus just before T_{Max} is reached. Again, the occurrence of garnet and clinopyroxene on the left hand side of equations (8) and (8a) implies the consumption of these phases during decompression. The importance of epidote/zoisite as the first hydrous phase to melt along a prograde PT-path between 10-30 kbar was recently recognised (Vielzeuf & Schmidt, 2001).

Note that a significant amount of melt may be produced along PT-paths intermediate between paths A and B, as a result of prograde dehydration-melting of amphibole, epidote/zoisite and paragonite. However, if rocks follow a PT-path at lower pressure than path B, paragonite and epidote decay before the onset of partial melting (fig. 4A), and the resulting melt fraction will be correspondingly smaller.

During ascent of the rock, melt is predicted to quickly crystallise during ascent of the rock along path B between 12-10 kbar near 675ºC according to

Grt + Melt ± Epi >> Amph + Plagi + Qtz ± Fluid (9)

This suggests that the calculated water-saturated solidus is higher by some 20ºC than the experimentally determined solidus. Whereas a large amount of fluid-components from the crystallising melt is taken up in amphibole, the amount of fluid released at the end of crystallisation remains substantial (ca 1.2 wt.%).

The predicted temperature of 600ºC for the first occurrence of partial melt is at odds with the experimentally determined water-saturated solidus, which occurs at 620-650ºC between 10-15 kbar (Rapp, 1995; Johannes & Holtz, 1996; Vielzeuf & Schmidt, 2001). The melt model obviously predicts a water saturated solidus too low by some 20-50ºC. As a consequence, paragonite should intersect the solidus at a higher pressure and its breakdown along path B would result in minor amounts of partial melting only (com-

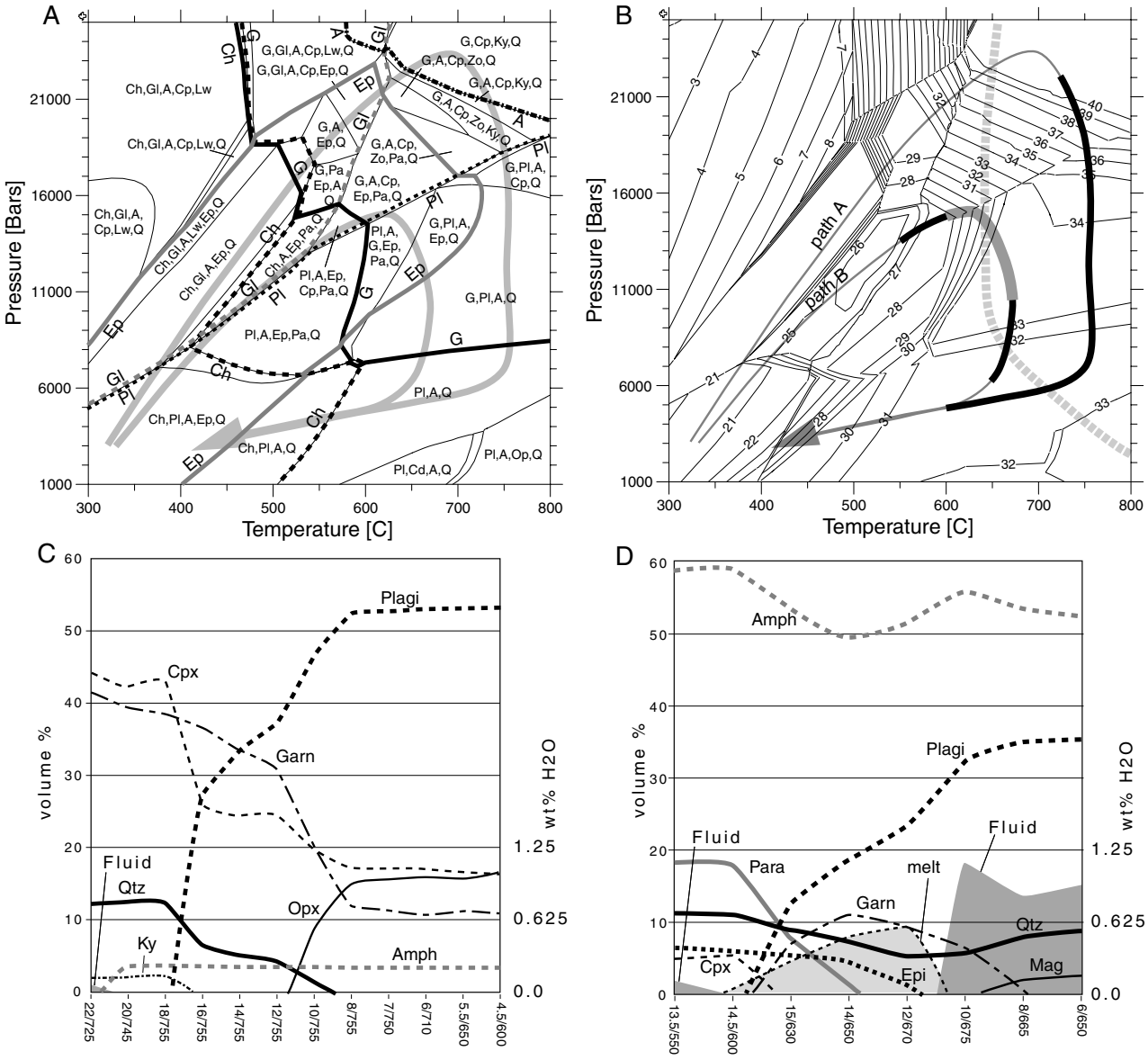

Fig. 4: (A) Computed phase diagram for the water saturated mafic system. See caption of figure 2A for further information. (B) Isolines in moles of free fluid (pure water) for the water saturated mafic system. Dashed grey line is water-saturated solidus of basaltic systems according to (Vielzeuf & Schmidt, 2001). See caption of figure 2B for further information. (C) Changes in phase relations and modes in the mafic system following path A. The volume of free fluid phase at the onset of partial melting is 0.2-0.25%. (D) Changes in phase relations and modes for the mafic system following path B. The volume of free fluid phase at the onset of partial melting is 0.2-0.25%. See caption of figure 2C+D for further information.

pare fig. 4A). We note, however, that incorporation of muscovite-component into paragonite in potassium-bearing mafic rocks may lead to an extension of paragonite stability towards higher temperatures. In addition, phengite at higher, and biotite at lower pressure may be present, and both of them decay at higher temperatures. The stability of phengite towards higher temperature (and pressure) compared to paragonite may thus allow dehydration-melting along paths A or B, while biotite will not melt at any temperatures reached along the two PT-paths.

Discussion and comments on dry melting

The results presented above depend on the thermodynamic database, including solution models, and on the assumption of equilibrium. We mentioned the uncertainties inherent in the computation involving amphibole, which may lead to overestimated amphibole stability in granitoid systems; we also noted that the melt model may become less reliable at (increasing) pressures above 10-12 kbar. Additional calculations performed as a test on granitoid systems confirm that amphibole stability is overestimated in such systems. Thermodynamic computation reproduces the experimentally established influence of bulk water content on amphibole stability (Naney, 1983; Gardien *et al*., 2000), but with unsatisfactory sensitivity. Though dependent on the fluid content of the system, amphibole is predicted to becomes stable in the granite system in a small area at temperatures above 600ºC, which has not been observed in the experiments (Naney, 1983). Despite these reservations, computation allows a reasonable assessment of partial melting processes in the rocks studied. Such computations suggest a very different partial melting behaviour for differ-

ent lithologies which follow identical PT-paths, as well as for a single lithology which follows different PT-paths. Subduction to pressures of 24 kbar and subsequent exhumation at relatively high temperatures may lead to considerable melting in granitoid and pelitic systems, whereas no partial melting is predicted in mafic rocks, due to the complete consumption of hydrous phases during subduction. By contrast, a lower degree of partial melting than along path A is predicted for granitoid and pelitic systems along path B, and significant partial melting is predicted for mafic rocks due to the decomposition of paragonite and epidote. These differences are essentially a consequence of the modes of phengite, paragonite and epidote present when the rock passes the water-saturated solidus, as well as of the maximum PT-conditions reached.

The models presented above indicate that "dry" partial melting during subduction and collision may lead to considerable melt fractions in granitic, pelitic, and to a lesser degree in basaltic rocks. The degree of partial melting is very sensitive to the PT-path followed by the pertinent rocks, because this controls the amounts of volatiles stored in hydrous minerals. Importantly, partial melting in all lithologies is primarily predicted to occur during exhumation, except for a short segment along PT-path A in granitoid systems. This of course reflects the chosen PT-paths, which are typical for the evolution of the Central Alps, but not for all collisional orogens. Nevertheless, for the chosen PT-settings, partial melting should primarily occur during exhumation, thus during the collisional part of the orogenic history. Only along hotter PT-paths, or where fluid infiltration occurs, may partial melting occur already during subduction. Partial melting of granitoid rocks due to water-fluxed melting in an early collisional stage has indeed been proposed by (Patiño Douce & Mc Carthy, 1998; Prince *et al*., 2001).

Open system melting (with fluid infiltration)

Water-assisted partial melting is unlikely to be an important migmatite-forming process in high grade granulite terranes. It may however be important at lower temperature in subduction and collision settings, where fluid infiltration may occur along regional scale shear zones as a result of the focused deformation. At conditions above the water-saturated solidus, infiltration of water-rich fluids may trigger partial melting or increase the melt fraction. In this paragraph we investigate the consequences of various degrees of infiltration of a water dominated fluid at different temperatures and a constant pressure of 8 kbar. This pressure was chosen because partial melting occurred at similar conditions in the Central Alps (see chapter 1). For discussion, we use the same three rock compositions as above (table 1) to compute binary T-X-diagrams with varying compositions from water-poor to water-rich along the X-axes (called X_{Hydr} in the following). Water is added to the "dry" protolith until the system is everywhere supersaturated in fluid, and a maximum melt fraction is reached. Further addition of fluid would not lead to a change in phase relations or in the modes. In the following discussion, rocks that contain a fluid phase at the solidus are denoted as "fluid-saturated (b.s.)" (where b.s. means below solidus), because the melt may completely consume any fluid immediately above the solidus, and the rock is no longer fluid-saturated.

Granitic systems

Water-assisted partial melting ($X_{hydr} > 0.02$) in the granitic system at 8 kbar starts at 605ºC (fig. 5A). In water-undersaturated (b.s) rocks ($X < 0.02$), no melt is predicted up to 800º, where biotite starts to disintegrate. Since phengite is not stable in the water undersaturated granite, phengite dehydration-melting does not occur in such dry rocks. At water-saturated (b.s.) conditions ($X_{hydr} > 0.02$), phengite decays at ~630ºC, but it is stabilised up to 650ºC at conditions of water infiltration ($X_{hydr} > 0.05$). However, because of the minor amount of phengite that remains near the solidus (see discussion above), the effect of final phengite breakdown on the melt fraction is unimportant (see melt isochores in fig. 5A).

Without fluid infiltration ($X_{hydr} < 0.05$), melt fractions will not become larger than ~5-10 % until biotite breaks down, whereas with increasing water content of the systems, the melt fraction raises steadily, until a free hydrous fluid exsolves from the melt. Further addition of fluid no longer results in changes of the phase assemblage nor in the mode of minerals (except for the fluid phase itself). Because the granite chosen is close to a granitic minimum composition, maximum melt fractions of up to 90% are predicted for conditions as low as 630ºC at 8 kbar for the case of massive fluid infiltration. Rocks following paths A or B, may therefore suffer extensive partial melting upon fluid infiltration. Rocks of granodioritic to tonalitic composition likely show a somewhat lower degree of water assisted partial melting at these same conditions.

Below 800ºC, K-feldspar is the first phase to be consumed with increasing water content of the system. Further infiltration leads to the consumption of quartz and then plagioclase. After complete consumption of quartz and feldspars, the system is merely composed of biotite, amphibole and melt (± fluid). The predicted sequence is however at odds with experimental investigations of the same system (Fig. 2A. in Naney, 1983). At temperatures below 800ºC, they observed plagioclase to break down first, followed by quartz and then K-feldspar, and at temperatures above 800ºC, the sequence changed to quartz, then K-feldspar and finally plagioclase. In the granite experiment, clinopyroxene and epidote occurred below 800ºC, while amphibole was not observed. Probably, these inconsistencies are

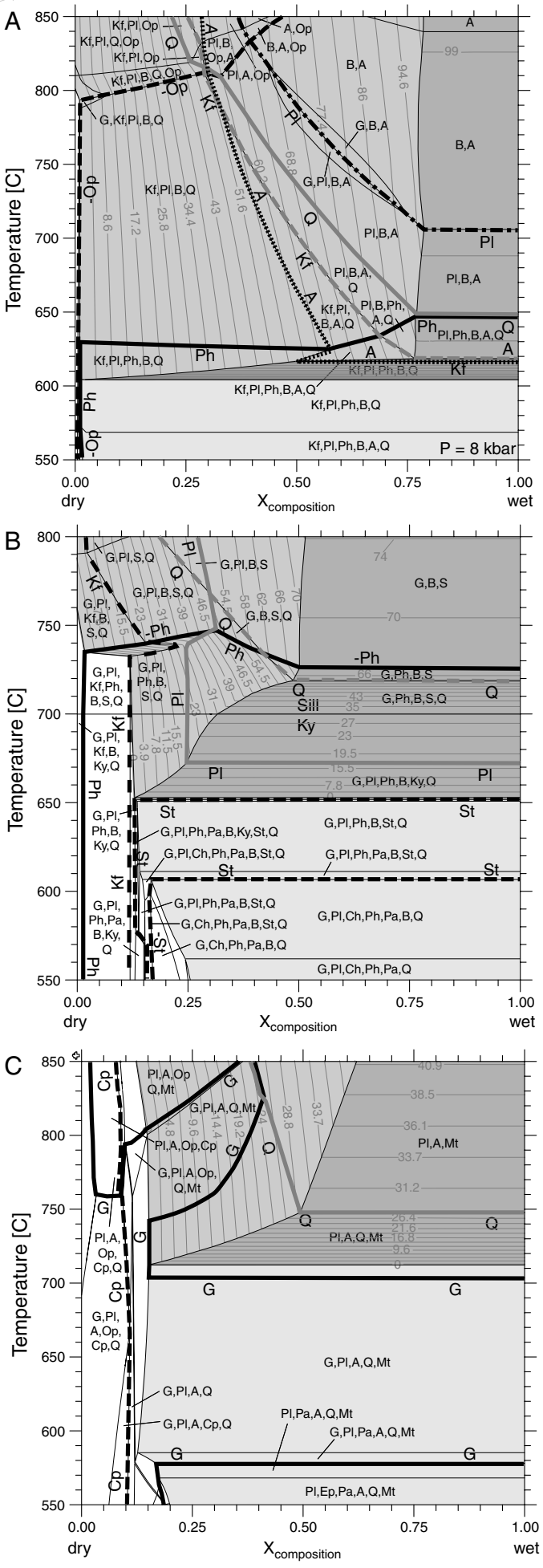

Fig. 5: (A) Binary T-X diagram for the granite system at a pressure of 8 kbar. The water content of the system increases along the X-axis. Grey shaded lines and numbers are isochores of melt volume in vol.%. The water content just below the solidus is 0 wt.% at X=0, 3.25 wt.% at X=0.2, 6.47 wt.% at X=0.4, 9.48 wt.% at X=0.6, 12.31 wt.% at X=0.8 and 14.97 wt.% at X=1. Light grey shading indicates the presence of free fluid, intermediate grey shading a melt, and dark grey shading coexistence of melt and fluid. (B) Binary T-X diagram for the pelite system at a pressure of 8 kbar. The water content of the system increases along X-axis. Grey shaded lines and numbers are isochores of melt volume in vol.%. The water content just below the solidus is 0.97 wt.% at X=0.2, 3.88 wt.% at X=0.4, 6.58 wt.% at X=0.6, 9.22 wt.% at X=0.8 and 11.67 wt.% at X=1. Shading as in figure 5A. (C) Binary T-X diagram for the mafic system at a pressure of 8 kbar. The water content of the system increases along the X-axis. Grey shaded lines and numbers are isochores of melt volume in vol.%. The water content just below the solidus is 0.41 wt.% at X=0.2, 2.11 wt.% at X=0.4, 3.75 wt.% at X=0.6, 5.33 wt.% at X=0.8 and 6.11 wt.% at X=1. Shading as in figure 5A.

attributable to model uncertainties, mainly related to melt and amphibole. Note however, that the melt model reproduces other experimental results for granitoid rocks (Holland & Powell, 2001). It is well known that rapid water-assisted melting may lead to disequilibrium melting (e.g. Rubie and Brearley, 1990; Prince *et al*., 2001; Whittington & Treloar, 2002). Therefore, inconsistencies may also be related to disequilibrium melting, due to the relatively short durations of the experimental runs (3-10 days (Naney, 1983))

Semipelitic systems

Initial partial melting in a fluid-saturated (b.s) metapelitic rock (X > ca. 0.15) at 8 kbar occurs at a temperature of 650ºC (fig. 5B). In fluid-undersaturated (b.s.) systems (X < ca. 0.15), first melting occurs at a temperature of > 730ºC, due to the breakdown of phengite. Note that the final phengite-breakdown in pelitic systems is predicted to occur at temperatures almost 100ºC higher than in the granitic system. Note that K-feldspar is predicted for fluid-undersaturated (b.s.) systems only, except in a small area where K-feldspar growth coincides with phengite breakdown. Without fluid-infiltration (X < 0.15), a maximum melt fraction of ~5% is predicted at temperatures below 730ºC, but a much higher melt fraction of 15-25% above this temperature, due to dehydration-melting of phengite.

Upon infiltration of a water-rich fluid (X > 0.15), a maximum melt fraction of 15% is obtained at 670ºC (peak temperature along path B), 30% at 700ºC, > 60% at 720ºC, and 70% at 750ºC (peak temperature along path C). If melt is essentially removed from the rock at the highest degree of melting, a melt depleted restite composed of garnet, biotite and sillimanite would remain. The order in which the other phases are consumed (at 8 kbar), is primarily a function of temperature, but also of composition. Between 650-670ºC, infiltration of fluid only results in a change of the modal abundance, but not of the phase assemblage. At temperatures between 670-730ºC, plagioclase re-

acts out first, whereas at slightly higher temperatures phengite breakdown occurs first. At temperatures above 770ºC, quartz is completely consumed before plagioclase. The occurrence of water-assisted partial melting of pelitic rocks in amphibolite facies terranes has been reported (see chapter 2 and (Yardley & Barber, 1991).

Basaltic systems

In fluid-undersaturated (b.s.) mafic rocks at 8 kbar, partial melting is not expected to occur below 850ºC (X < ca. 0.15, Fig. 5C). Above 750ºC granulite-facies assemblages, containing Cpx +Opx + Pl ± Grt + a minor amount of amphibole, are observed for fluid-undersaturated conditions, whereas with increasing water contents the assemblage is made up of Grt + Pl + Amph + Qtz + Mt + Melt and finally of Pl + Amph + Mt + Melt. In the presence of a fluid phase (X > 0.15), first water-assisted partial melting is predicted at a temperature of 710ºC. Maximum calculated melt fractions for the case of fluid infiltration are 29% at 750ºC, 35% at 800ºC, and 41% at 850ºC. These calculations demonstrate that even in mafic rocks at comparatively low temperatures, a considerable melt fraction may be formed upon fluid infiltration. The resulting melt fraction depends strongly on the PT-path and on the amount of infiltrating fluid. For example, in rocks following path B (T_{max} = 675ºC), no melt should form at 8 kbar irrespective of the amount of fluid that infiltrates the rock, whereas a maximum of almost 30% of melt may form in rocks following path C (T_{max} = 755ºC). This contrasts strongly with the "dry" melting scenario, where only a minor amount of melt may be produced in mica bearing assemblages (see fig. 4D).
An interesting feature of basaltic systems is the fact that melt may be completely consumed above the water saturated solidus during isothermal ascent: According to several studies (Sen and Dunn, 1994; Rapp, 1995; Vielzeuf & Schmidt, 2001), melt is produced with increasing P and/or T through the vapour-absent melting reaction

Amph + Pl ± Qtz = Grt + Cpx + Melt (10)

Inversion of reaction (10) will thus lead to the formation of plagioclase and amphibole and to the consumption of hydrous melt. In order to test for this effect, we calculated two diagrams which show the change in modal abundance during isothermal uplift from 20 to 4 kbar at 750ºC (fig. 6A+B). In figure 6 A, an initial melt fraction of ca. 30 vol.% is assumed, which could be the result of prograde breakdown of amphibole, epidote and paragonite, or due to the infiltration of fluid. During ascent, the amount of melt decreases, especially between 8 and 4 kbar. Nevertheless, melt remains in the system until it crosses the water saturated solidus at about 4 kbar. In contrast, in rocks with a lower initial melt fraction of ca. 10 vol.% at 20 kbar (fig. 6 B), the melt is consumed completely during ascent to 8 kbar according to the pseudoreactions

Grt + Cpx + Qtz + melt ± Zo >> Amph + Plagi (10a)

between 19-17 kbar, then by

Grt + Qtz + melt >> Amph + Plagi (10b)

between 17- ca 10 kbar, and finally by

Amph + Grt + Liq >> Plagi + Qtz + Magn (10c)

between ca 10-8 kbar. Reaction (10c) is strongly dependent on the assumed O_2-buffering of the system and is not relevant for this discussion.
Consequently, calculations suggest that the solidus of mafic systems must show a sharp bent near the garnet-out border, depending on the water content of the system. Such a shape of the water-saturated solidus has in fact been reported for mafic rocks (Rapp, 1995; Johannes & Holtz, 1996; Vielzeuf & Schmidt, 2001, and references therein).

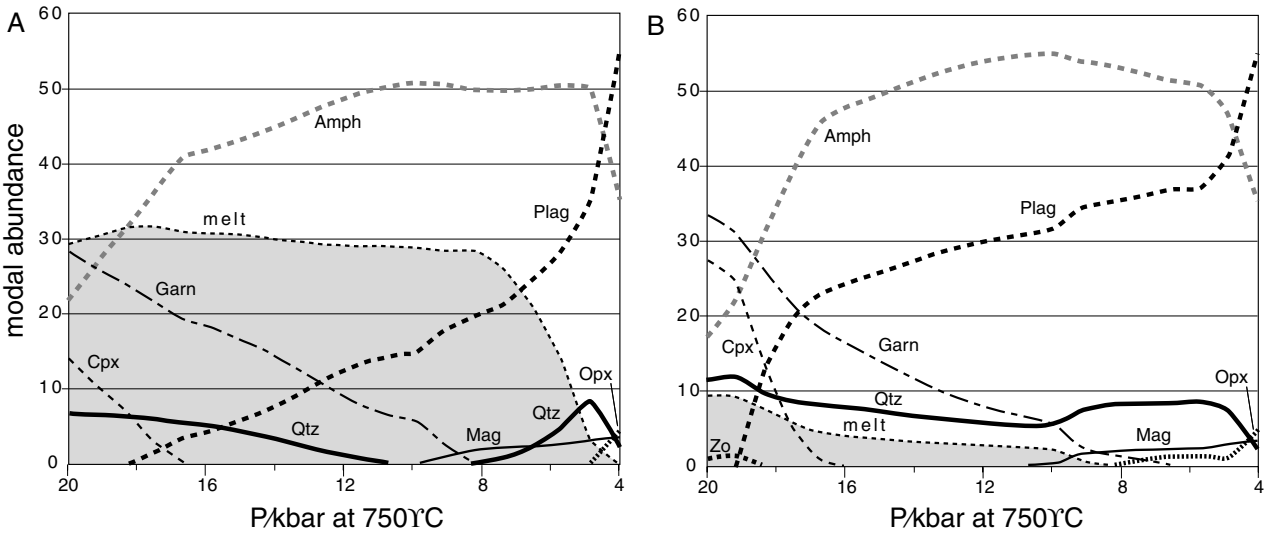

Fig. 6: Change of modal abundance in a mafic system during isothermal ascent from 20 to 4 kbar at a constant temperature of 750ºC. A with a high initial melt fraction of 30%, B with a lower initial melt fraction of 10%. See text for discussion.

Assessment of amphibole stability in water-assisted melting of granitoid rocks

As demonstrated by the above computation, both closed system- as well as open system melting of granitoid rocks may occur during a collisional cycle, and indeed partially molten granitoid gneisses are typical of migmatite terranes (Brown *et al*., 1995; Patiño Douce & Mc Carthy, 1998), even at comparably low grade conditions (Mogk, 1992; Garlick & Gromet, 2004). Such anatectic granitic to granodioritic gneisses are often accompanied by amphibole bearing leucosomes (chapter 1 and Mogk, 1992; Viruete, 1999; Gardien *et al*., 2000, and references therein; Thompson, 2001; Mogk, 2001; Garlick & Gromet, 2004), and these amphiboles may be key to distinguishing dehydration-melting from water fluxed-melting.

In contrast to amphibole-bearing leucosomes, large scale intrusives of granitic and granodioritic composition commonly (though not exclusively) contain epidote and biotite (± ilmenite and hematite) rather than amphibole, and observations suggest a possible partial replacement of primary amphibole by biotite and plagioclase during the crystallisation (Speer, 1987). This led Viruete (1999)to formulate a (incongruent) mixed-mode melting reaction

Bio + Plag + Qtz + H_2O = Hbl + Melt (11)

which is followed at higher temperatures by the biotite dehydration reaction

Bio + Plag + Qtz = Hbl + Kfs + Melt (12)

Both reactions are thought to have a relatively steep positive slope in PT-space (Viruete, 1999) and could therefore be responsible for the observed replacement of amphibole in the course of cooling and crystallisation of granitic intrusives (Speer, 1987). We note that the biotite dehydration-melting reaction (12) is not supported by experimental investigations in granitic and granodioritic rocks (Naney, 1983; Gardien *et al*., 2000). In both studies, amphibole was stabilised only above the water-saturated solidus upon addition of 3-5 wt.% of H_2O, which is clearly in excess of the amount of fluid which can be stored in a reasonable pore space at amphibolite facies conditions. This suggests that amphibole bearing leucosomes should only form in granitic to granodioritic rocks upon fluid infiltration. Gardien et al. (2000) concluded "*that at all pressures relevant for melting within the crust, the addition of external H_2O is required to stabilize amphibole during the anatexis of biotite-plagioclase-quartz assemblages*". Considering, however, the relatively small number of experiments (experiments at 2, 8, 10, 15, and 20 kbar), this conclusion may overestimate the conclusions which can be derived from the available experiments.

In his field-based study, Mogk (1992) proposed the mixed-mode melting reaction

Bio + Plag(1) + Qtz ± Epi + H_2O = Hbl + Plag(2) + Melt (Kfs-rich) (13)

as the cause of amphibole formation in anatectic granites. He suggested that amphibole formed at comparatively low temperatures of 670-730ºC, in response to fluid infiltration (Mogk, 2001). In conclusion, amphibole bearing leucosomes in anatectic granites may be indicative for "wet" melting.

Investigations performed on amphibole-bearing leucosomes in the Central Alps of Switzerland (fig.7) indicate that a reaction similar to (13) was responsible for the formation of partial melts and amphibole. Textural evidence in favour of this reaction is provided by epidote grains, which are euhedral if included in biotite, but have a xenomorphic shape in the quartz-feldspar matrix (Fig. 8). Epidote grains partially included in biotite are euhedral inside biotite, but appear resorbed where in contact with the matrix. A finer-grained second generation of epidote, typically forming aggregates, often rims the partially resorbed older epidote grains or occurs as precipitates in fractures or along grain boundaries (Fig. 8). We interpret this textures as a partial resorption of epidote by incongruent mixed-mode melting (reaction (13)), followed by a partial back-reaction dur-

Fig. 7: Stromatic migmatite with amphibole-bearing leucosome inside granodioritic gneiss (Mergoscia, Switzerland). Width of picture ca. 40 cm.

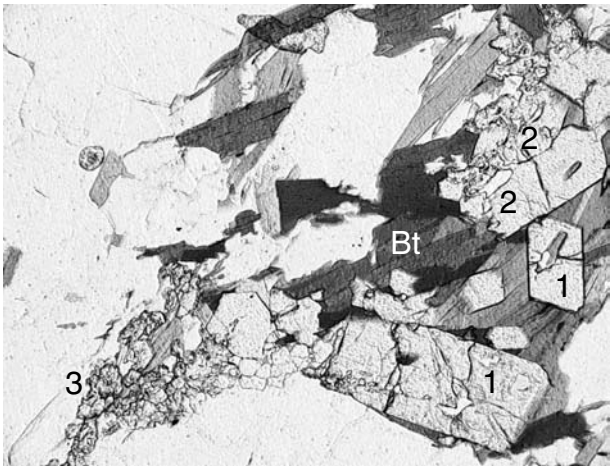

Fig. 8: Epidote phase relations in amphibole-bearing leucosome. Bright low relief phases are feldspar and quartz, dark phase is biotite, bright high relief phase is epidote. Numbers: 1 denotes primary epidote included in biotite grains. Note the idiomorphic shapes of these grains. 2 denotes primary epidote partially resorbed along the upper grain boundary during partial melting. 3 denotes a secondary, finer-grained epidote fraction, probably formed during crystallisation of the melt.

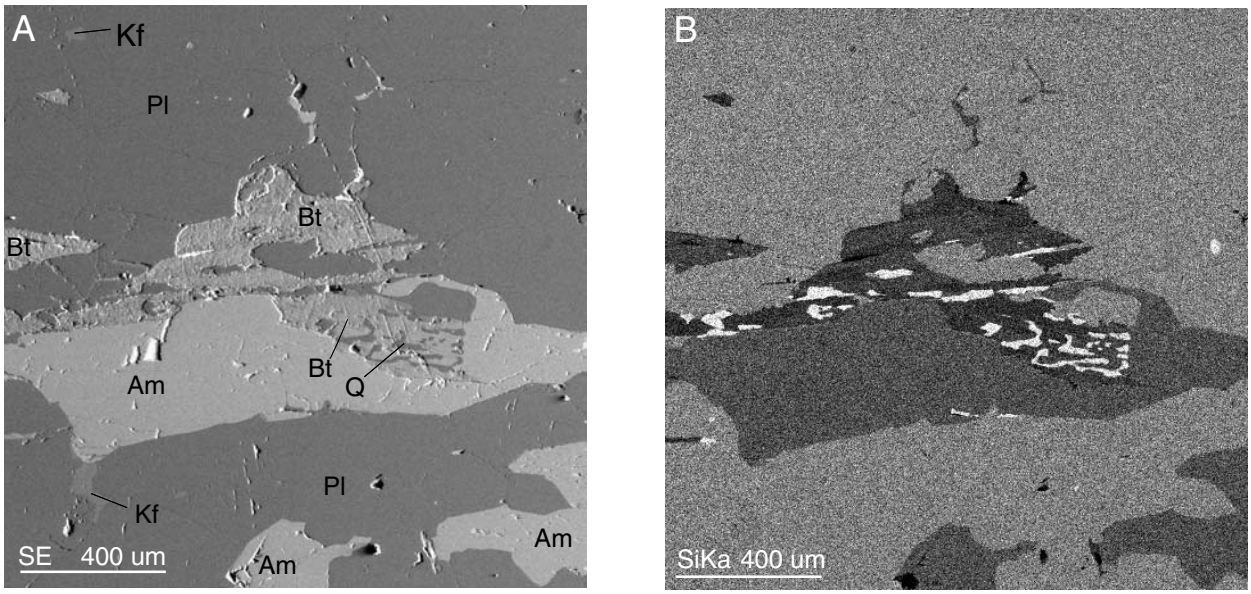

Fig. 9: Quartz-biotite symplectite partially included in amphibole and interpreted as a result of a mixed mode melting reaction leading to the formation of amphibole. A = secondary electron image, B = Si-Kα Xray-map. See text for discussion.

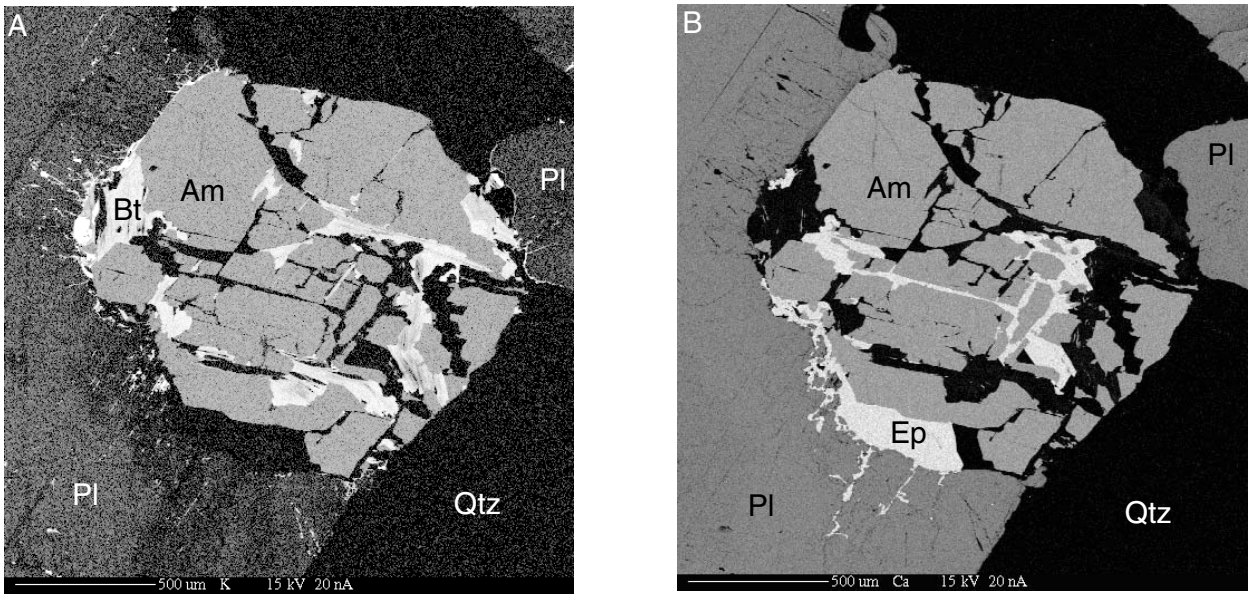

Fig. 10: Ca-Kα and K-Kα Xray-maps showing partial back-reaction of igneous amphibole in granitic leucosome. Amphibole is replaced by epidote, biotite and quartz. Part of the biotite is replaced by secondary chlorite. Replacement of amphibole mainly occurs along its rim or along the mineral cleavage.

ing crystallisation of the melt to form the finer grained epidote fraction. Other conspicuous texture involve quartz-biotite-symplectites enclosed in amphibole (fig. 9). The symplectite is interpreted as a feature of biotite breakdown caused by reaction (13). Inclusion of the symplectite during coeval growth of amphibole may have led to its partial preservation and may have inhibited a complete reaction. Back-reaction of amphibole to form biotite, epidote and quartz during crystallisation of the melt has frequently been observed (Fig. 10). Biotite symplectites are not observed at such sites. Amphibole replacement occurs dominantly along amphibole grain boundaries, or along its cleavage. The observed replacement of amphibole along cleavage plains in figure 10 may be promoted if back-reaction is volume increasing and may cause small scale hydro-fracturing in minerals with good cleavage. Close inspection of figure 10 indeed shows that secondary minerals grew along fractures in amphibole and plagioclase, but not in quartz. If this is related to hydrofracturing as a result of a positive volume change, it indicates that retrograde replacement of amphibole occurred during crystallisation of the melt, at supersolidus conditions. The back-reaction is incomplete, indicating that melt had escaped from the leucosome. Later retrograde reaction, which led to partial replacement of biotite and amphibole by chlorite, probably occurred at subsolidus conditions and resulted in the consumption of the remaining pore fluid. Thermodynamic computation shows that chlorite is not predicted to occur above 400ºC in granitic to granodioritic rocks (Fig. 2A). Chlorite is only observed along or within grains of amphibole or

biotite. Additional calculations suggest that growth of chlorite in granitoid systems may be restricted to the direct replacement of biotite and amphibole in local chemical domains (which are dominated by the presence of biotite and amphibole).

Using the experimental granite composition of Naney (1983), thermodynamic computation predicts the formation of amphibole in a very water rich system. Figure 5A demonstrates that amphibole is stabilised with increasing temperature and water content of the system, and that amphibole in anatectic granitic system (at 8 kbar) may not be stable in the absence of fluid infiltration. Although the computation correctly predicts the dependence of amphibole stability on the fluid content of a system, the prediction is again at odds with experimental results, where epidote (at lower T) or clinopyroxene (at higher T) instead of amphibole were observed at the same pressure of 8 kbar (Naney, 1983). Although the amphibole model may overestimate amphibole stability in granitic systems, the apparent discrepancy might be merely an effect of oxygen fugacity. Reported oxygen fugacities for the experiments are between the Ni-NiO and the HM-buffer, while QFM-buffering was assumed for the computation of figure 5A. In computations using the less-reducing IMR-buffer, epidote and clinopyroxene essentially replace amphibole, and at conditions of the HM-buffer, amphibole is completely replaced.

Open- and closed-system melting in collisional settings

Rocks following PT-paths typical of collisional settings may undergo partial melting as a result of changing pressure and temperature, or due to fluid infiltration. Maximum melt fractions during closed-system melting are predicted to be on the order of 20-30% in metapelites, 10-15% in granites and 0-<10% in mafic rocks. The first melt may develop at different conditions, because saturation states of rocks undergoing subduction and collision may vary strongly. Attainment of fluid-saturation below or at the water-saturated solidus is a reasonable assumption for monocyclic metasediments or for strongly hydrated oceanic crust, but not necessarily for "dry" continental crust, composed of intrusive and high grade metamorphic rocks. Polymetamorphic, continental basement units may be strongly fluid-undersaturated and should not undergo extensive partial melting unless they have rehydrated before or during subduction, or unless fluid infiltration occurs. In nature, melt fractions may therefore be smaller than those proposed above. We note, however, that exposed basement units commonly show evidence of various types of alteration, which are not related to weathering. Ductile or brittle shear-zones or fractures from millimetre to kilometre scales are frequently observed, and the hydration state inside such structures may be considerably higher than in the surrounding unaffected gneisses. Therefore, the formation of a first small melt fraction inside such structures is likely to take place along the water-saturated solidus, while surrounding rocks remain completely solid until they reach conditions of dehydration-melting. This may lead to partitioning of strain into such pre-existing structures as a result of the weakening effect of melt.

Similar localisation of strain and partial melting may occur during open-system melting, because infiltration of fluid will be most effective along pre-existing or syn-kinematic shear zones and fractures or along other anisotropies like lithologic boundaries. Efficient fluid infiltration at such sites may cause melt fractions higher than estimated for "dry" melting. Partially-molten amphibolites of qtz-dioritic composition found in the Central Alps are likely examples of such a process (figure 11A). The degree of partial melting on the outcrop scale varies from virtually unmolten to at least 15-20%, as depicted in figure 11A. Even though the occurrence of such high melt fractions is relatively rare, examples of partially molten amphibolites have been observed in the same area (Southern Steep Belt, Central Alps of Switzerland). Estimated maximum temperatures of the area are 700-750ºC at pressures of 6-8 kbar (Engi *et al*., 1995; Todd and Engi, 1997; Nagel, 2000), which is consistent with the observed paragenesis in the rock (amphibole but no pyroxenes). Computations for the basaltic system (see fig. 5C) indicate that the observed high melt fraction at these conditions must be an effect of the infiltration of a water-rich fluid phase.

In pelitic systems, the occurrence of open-system partial melting in an orogenic setting was documented by (Yardley & Barber, 1991), who attributed it to the infiltration of fluids released from a nearby crystallising pluton. An example where fluid infiltration led to partial melting of biotite-rich metapelites along shear zones was reported from the Himalayan orogen (Butler *et al*., 1997). Additional evidence of partial melting and melt extraction from metapelitic rocks as a result of fluid infiltration is given in chapter 2.

Examples of open-system melting in granitoid rocks are also found in the southern parts of the Central Alps. Melt fractions of at least 20-25 % are observed in granodioritic gneisses, migmatised during the Alpine orogeny (see chapter 1). Again, the distribution of partial melts at outcrops is variable, even where partial melting occurred in a homogeneous protolith (fig. 11B). Virtually unmolten gneisses (left hand side of fig. 11B) may grade into metatexitic, stromatic migmatites (right hand side of fig. 11B) or into meter scale, almost diatexitic migmatites (fig. 11C), where the gneissic fabric of the protolith becomes diffuse or even disintegrated. However, for "dry" melting of granitic rocks, we have shown above that computation predicts some 10-15 vol.%

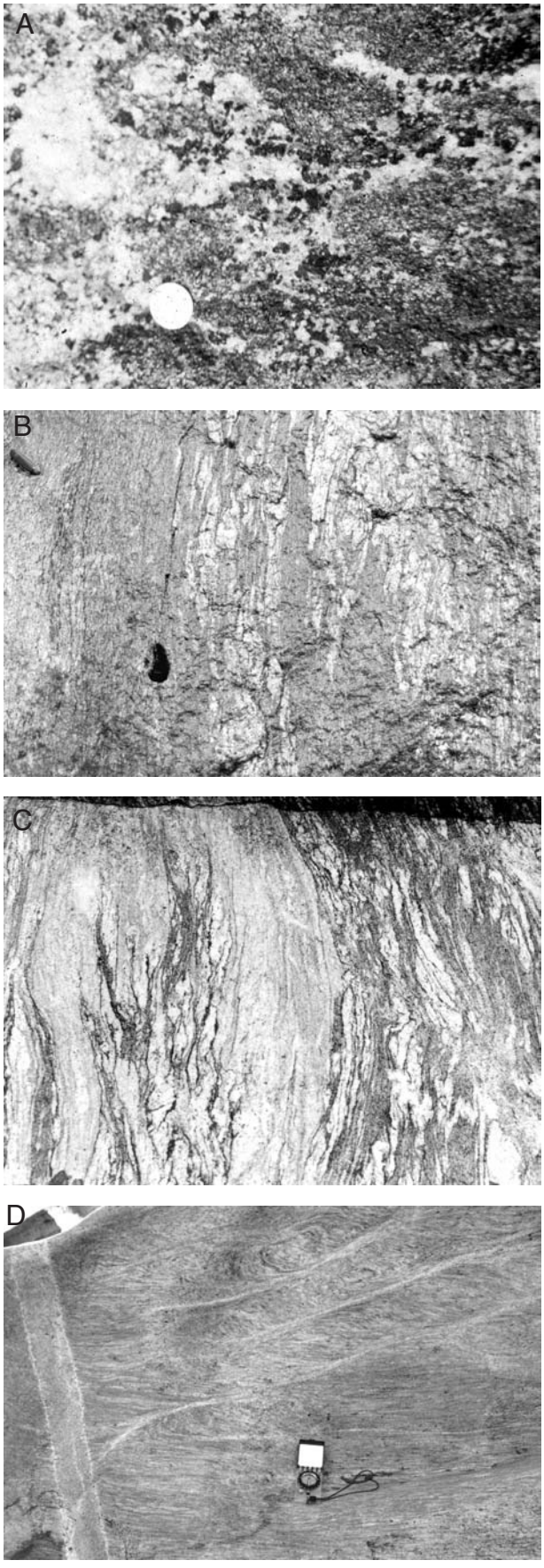

Fig. 11: (A) Anatectic amphibolite (Arbedo, Switzerland). Note neocrystallisation of coarse grained amphibole in the leucosome. Partial melting at relatively moderate temperatures is interpreted to have occurred due to the influx of fluid. Coin for scale. (B) Anatectic granodioritic gneiss (Auressio, Switzerland). The leucosome fraction in the right half of the picture is estimated to be 19-22% using image analyses (program Image SXM). Note inhomogeneous distribution of melt: only a small melt fraction is observed in the dominantly gneissic part to the left, whereas a substantially higher degree of partial melting is observed in the right part of the image. Pocket knife for scale in the upper left corner. (C) Stromatic metatexite in the right part of the picture grades into an almost diatexitic structure to the left (same locality as in Fig. 11B). Note disintegration of gneissic structure to the left. Width of photograph ca. 80 cm. (D) Syn-anatectic, melt filled shear bands in migmatitic biotite-gneiss. The shear bands indicate a sinistral sense of shear (Ponte Brolla, Switzerland). Compass for scale.

of melt at 750ºC, which is higher than the temperatures reached in most of the Central Alps. According to these models, the observed melt fraction of > 20% can only be explained if fluid infiltration occurred above the water-saturated solidus. In other localities, metre-scale melt zones, clearly distinct from Alpine granitic dykes, exhibit an igneous fabric and are composed almost entirely of leucosome with local relic "ghost" foliations of the protolith, visible as parallel biotite-rich schlieren. Because such zones often grade diffusely into the mylonitic host rock, we interpret them as *in-situ* partial melts rather than melt segregated from the surrounding gneisses. We have demonstrated above how massive water influx may result in melt fractions of >90% in granitic gneisses at 750ºC and 8 kbar. The general lack of "granitised" rock-masses larger than a few metres across indicates that such a high degree of partial melting is confined to localities where extensive fluid infiltration occurred, probably supported by deformation. More voluminous "granitisation" in collisional belts appears improbable, since fluid sources are limited and because fluid fluxes may be channelised. We suggest that the observed inhomogeneous distribution of partial melting inside relatively homogeneous protoliths provides a clear indication of fluid-assisted partial melting. Partial melting will dominantly occur in areas where fluid succeeded to infiltrate the rock, such that the observed leucosome distribution to some extent reflects former fluid-pathways.

Segregation and extraction of partial melts

For partial melts to intrude upper crustal levels in the form of dykes or plutons, they must be able to segregate and escape from the site of melting. Melt segregation is favoured by a positive volume change of the melting reaction, which may lead to a build-up of fluid pressure. The resulting pressure gradient may enhance melt escape or initiate hydraulic fracturing in the partially-molten rock or the surrounding solid rocks (Brown *et al*., 1995; Connolly *et al*., 1997; Rushmer, 2001; Whittington & Treloar, 2002; Holyoke-III and Rushmer, 2002). Such a pressure gradient will only relax if some melt escapes from the system, or if the surrounding rocks have sufficient time to respond by ductile flow. A complete escape of melt is not likely and a certain melt fraction may remain in the rock to balance pressure. Therefore, leucosomes in migmatite terrains may not reflect the inability of melt to escape, but may just be the remaining melt fraction needed to maintain the fluid pressure. Melt segregation and escape may also be favoured if partial melting coincides with

deformation. Because partially-molten rocks are much weaker, strain may effectively partition into such rocks and promote further melting, melt segregation or melt escape in a mutual feedback process (Mogk, 1992; Davidson *et al*., 1994; Brown & Solar, 1998; Vigneresse & Tikoff, 1999; Whittington & Treloar, 2002; Garlick & Gromet, 2004).

Because dehydration-melting is usually associated with positive volume changes, it may be effective in promoting melt segregation and escape (Brown *et al*., 1995; Connolly *et al*., 1997; Rushmer, 2001; Whittington & Treloar, 2002; Holyoke-III & Rushmer, 2002). By contrast, water-assisted partial melting is expected to lead to negative volume changes, and efficient melt segregation or extraction are not expected in the absence of deformation (e.g. Clemens and Droop, 1998; Rushmer, 2001; Holyoke-III & Rushmer, 2002). Instead, this process would lead to a collapse of the pore space and result in compaction. In addition, such melts are not suggested to travel far from their source, since the melt would rapidly freeze during ascent, due to the shape of the water-saturated solidus (see fig. 1). However, water-assisted partial melting is only associated with a negative volume change if it occurs in a closed system (no fluid infiltration). This type of partial melting is only representative for partial melting taking place at the water-saturated solidus, due to the consumption of the available pore fluid. Owing to the small pore space, this type of partial melting results in small melt fractions only. If melting occurs below 10-12 kbar, escape and ascent of such melts is unlikely, because they immediately freeze. At pressures above 10-12 kbar, the slope of the solidus changes from negative to positive and consequently melts could rise a considerable distance before crystallising. However, the very low melt fractions may prevent effective segregation of such partial melts.

More importantly, water-assisted partial melting is not constrained to the water-saturated solidus, but may occur at any point above this solidus if infiltration of fluid occurs. Such melts must be capable to escape from the host rock for a considerable distance, since they do not freeze quickly. If water-assisted melting occurs as an effect of fluid infiltration, the fluid is effectively trapped by the melt at the site of partial melting. Over time, the small amounts of fluid that infiltrates the rock may accumulate and may give rise to a considerable melt fraction. Note that the additional volume of infiltrating fluid must be considered in volume change calculations (see chapter 4). Figure 12 graphically depicts this model scenario: Fluid that infiltrates a rock at subsolidus conditions may pass through the rock, while at supersolidus conditions, the fluid is trapped in the forming melt, leading to a considerable increase in rock volume with time, as long as melt does not escape from the system.

Figure 13, calculated for a haplogranite system serves to visualise the space-problem in an open

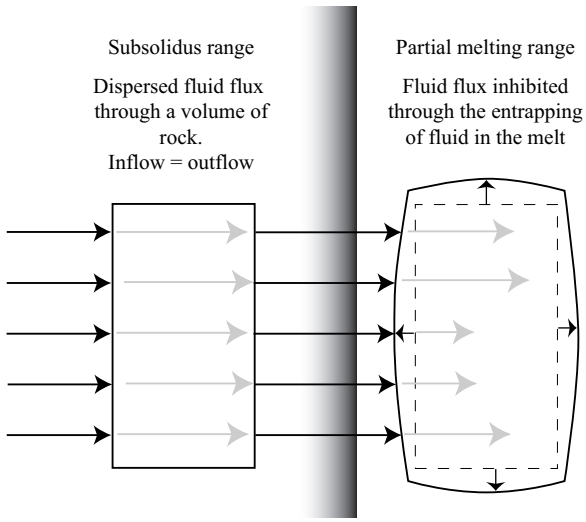

Fig. 12: Model scenarios of volume changes in water fluxed partial melting. See text for discussion.

system. (The construction of the figure is explained in chapter 4). In the computation of the diagram it was assumed that the melt contains the minimum amount of fluid and that all fluid stored in the melt has infiltrated from the surrounding. The minimum amount of fluid was adapted from Holtz *et al*. (2001b). The calculated volume changes represent a complete conversion of solids into melt (eutectic melting) and are thus representative only of that rock fraction which undergoes partial melting. Absolute volume changes therefore depend on the melt fraction and are smaller than the calculated values.

The calculated diagram indicates massive positive volume changes of the order of 5-35 % between 0-8 kbar. The largest changes (35 %) are located along the water-saturated solidus between 5-8 kbar. Volume changes decrease with increasing temperature, but remain positive over the entire diagram, providing an important driving force for melt segregation and escape. Note that the extent of partial melt-

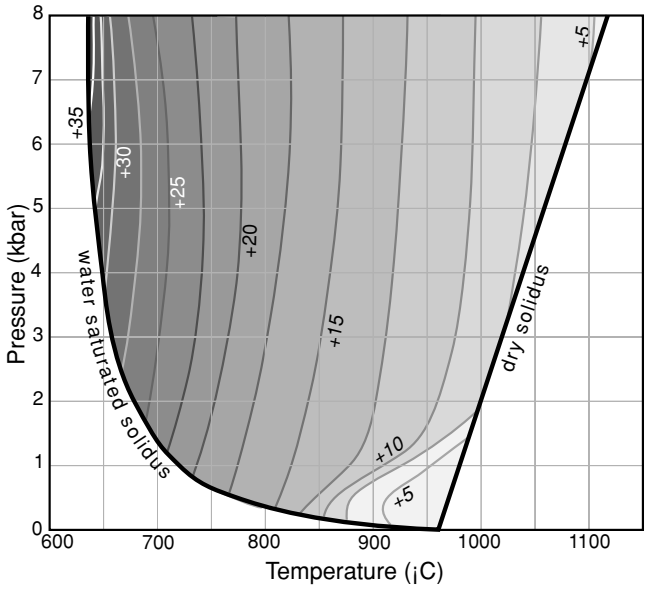

Fig. 13: Volume changes calculated for non-isochemical water-assisted partial melting. See text for discussion and chapter 4 for the construction of the diagram.

ing may remain small, and that associated volume changes on the sample to outcrop scale will be smaller than those reported in figure 13. For example, partial melting at 8 kbar and 750ºC in the haplogranite leads to a positive volume change of ~22%, but assuming a melt fraction of 0.2, the overall volume change will be but 4.4%. Based on these considerations, we conclude that melts formed due to fluid infiltration at temperatures above the water-saturated solidus may effectively segregate and escape from the rock and may rise to the same crustal levels as melts produced by dehydration-melting under similar conditions.

Recognition of water-assisted partial melting in the field

Evidence of anatectic processes is relatively easily recognised in the field or in thin section. Recently, several authors have reviewed and discussed textural evidence of the former presence of melt, from the grain to the outcrop-scale (Vernon, 2000; Sawyer, 2000). However, it is often not as easily established whether "dry" or "wet" partial melting has occurred, especially in granitoid rocks, where the mineralogical record may be unspectacular.
We propose the following characteristic as indicative of WAM caused by fluid infiltration. Note that only the combination of several of these features may provide good evidence for "wet" partial melting and migmatisation.

- Metamorphic conditions may be relatively moderate, but above the water-saturated solidus of the system in question. Usually, PT-conditions do not allow for dehydration-melting of biotite, (Mogk, 1992; Mogk, 2001) (see also chapter 1), but high temperatures do not preclude the possibility of WAM.
- Leucosomes in the form of veins and pockets of different size may be observed in different types of granitoid gneisses, whereas they are rare in metapelites or metamafic rocks (fig. 11B and C).
- Phases typical of dehydration-melting, such as sillimanite + K-feldspar, orthopyroxene, clinopyroxene, garnet, spinel and cordierite, are often absent. In contrast, biotite and muscovite remain abundant, and hornblende may be observed in leucosomes.
- Migmatisation occurs synkinematically and appears associated with regional scale shear zones. Evidence of coeval partial melting and deformation are found at the outcrop (fig. 11D) to regional scale.
- Different degrees of partial melting are observed in similar rocks. Strongly anatectic and almost non-migmatitic rocks of the same protolith occur side by side (figs. 11B and 11C).
- Different generations of leucosomes displaying different amounts of deformation may indicate repeated creation of partial melt. Crosscutting leucosomes show typically a coarser grained fabric compared to the host rock, while folded veins may have partly recrystallised to a smaller size. Folding does not necessarily cause recrystallisation, because it may occur while leucosomes were only partially solid (Barraud *et al*., 2004).

Conclusion

Syntectonic partial melting is commonly observed in collisional settings. Thermodynamic computation, despite inherent uncertainties, allows the thorough investigation of partial melting processes in such settings. Assuming PT-paths typical of collisional orogens, computations suggest that partial melting typically occurs due to dehydration-melting of muscovite, paragonite and epidote, depending on the lithology, and/or through the infiltration of fluids. Incongruent dehydration melting of biotite or amphibole are untypical of collisional settings, because they require overly high temperatures. A mixed mode melting reaction, consuming biotite (± epidote) to form amphibole in granitoid rocks may instead be indicative of fluid fluxed partial melting.
Whereas dehydration-melting occurs mainly during exhumation (during or following collision), "wet" partial melting may happen as soon as the water-saturated solidus of a rock is overstepped, be on the prograde or on the retrograde temperature path. Water-assisted partial melting may be coeval with dehydration-melting, and the two processes are not mutually exclusive, hence, exhumed migmatite terranes may be the result of both processes. Infiltrating fluids may derive from nearby crystallising intrusive rocks, or from subsolidus dehydration reactions at deeper crustal levels. The strong deformation accompanying subduction and collision may generate fluid pathways which allow fluids and melts to migrate. Weak zones that could preferentially act as fluid channels are discontinuities like lithological boundaries, fractures and shear-zones (at any scale). Fluid flow and associated partial melting may promote strain partitioning and localisation of deformation, which, in turn, may enhance rates of fluid flow and partial melting.
Melt extraction is favoured by deformation and by positive volume changes of melting reactions. The presented data reveal that water-assisted partial melting is strongly volume-increasing if it occurs in response to fluid infiltration. Dehydration-melting as well as water-assisted melting may both lead to the efficient segregation and escape of melt through the build-up of a melt pressure in the rock.

In conclusion, heterogeneously composed, regional scale shear zones are areas where enhanced fluid fluxes may occur, and therefore represent preferred sites of large scale migmatisation. Such a situation is observed in the Central Alps of Europe, where a migmatite belt coincides with the Southern Steep Belt, a shear zone of regional extent (chapter 1). Similar interrelationships between migmatisation and regional-scale shear zones have been noted previously, and fluid infiltration is considered as one cause of migmatite formation (Mogk, 1992; Brown *et al*., 1995; Butler *et al*., 1997; Prince *et al*., 2001). Although the limited availability of infiltrating fluids may prevent the formation of volumetrically important granitoid intrusions by "wet" melting, the presence of partial melts significantly influences the bulk rheology in any emerging orogen. The associated decrease in rock strength leads to a strong partitioning of strain into the partially molten rock, which influences strain rates of thrusting, strike slip movements or exhumation.

References

Arzi, A. A. (1978): Critical phenomena in the rheology of partially melted rocks. Tectonophysics 44, 173-184.

Barraud, J., Gardien, V., Allemand, P. & Grandjean, P. (2004): Analogue models of melt-flow networks in folding migmatites. Journal of Structural Geology 26, 307-324.

Brown, M., Averkin, Y. A. & McLellan, E. L. (1995): Melt segregation in migmatites. Journal of Geophysical Research 100/B8, 15655-15679.

Brown, M. & Solar, G. S. (1998): Shear-zone systems and melts: feedback relations and self-organization in orogenic belts. Journal of Structural Geology 20/2/3, 211-227.

Brown, M. & Solar, G. S. (1999): The mechanism of ascent and emplacement of granite magma during transpression: a syntectonic granite paradigm. Tectonophysics 312, 1-33.

Butler, R. W., Harris, N. B. W. & Whittington, A. G. (1997): Interactions between deformation, magmatism and hydrothermal activity during active crustal thickening: a field example from Nanga Parbat, Pakistan Himalayas. Mineralogical Magazine 61, 37-52.

Clemens, J. D. & Droop, G. T. R. (1998): Fluids, P-T paths and the fates of anatectic melts in the earth's crust. Lithos 44, 21-36.

Connolly, J. A. D., Holness, M. B., Rubie, D. C. & Rushmer, T. (1997): Reaction-induced microcracking: An experimental investigation of a mechanism for enhancing anatectic melt extraction. Geology 25/7, 591-594.

Davidson, C., Schmid, S. M. & Hollister, L. S. (1994): Role of melt during deformation in the deep crust. Terra Nova 6, 133-142.

de Capitani, C. & Brown, T. H. (1987): The computation of chemical equilibrium in complex systems containing non ideal solutions. Geochemica et Cosmochemica Acta 51, 2639-2652.

Dimanov, A., Wirth, R. & Dresen, G. (2000): The effect of melt distribution on the rheology of plagioclase rocks. Tectonophysics 328, 307-327.

Engi, M., Berger, A. & Roselle, G. T. (2001): Role of the tectonic accretion channel in collisional orogeny. Geology 29/12, 1143-1146.

Engi, M., Todd, C. S. & Schmatz, D. R. (1995): Tertiary metamorphic conditions in the eastern Lepontine Alps. Schweiz. Mineral. Petrogr. Mitt. 75, 347-369.

Etheridge, M. A., Wall, V. J. & Vernon, R. H. (1983): The role of the fluid phase during regional metamorphism and deformation. Journal of Metamorphic Geology 1, 205-226.

Ferry, J. M. (1994): A historical review of metamorphic fluid flow. Journal of Geophysical Research 99/B8, 15487-15498.

Frey, M. & Ferreiro-Mählmann, R. (1999): Alpine metamorphism of the Central Alps. Schweiz. Mineral. Petrogr. Mitt. 79/Special Issue: The new metamorphic map of the Alps, 135-154.

Gardien, V., Thompson, A. B., Grujic, D. & Ulmer, P. (1995): Experimental melting of biotite + plagioclase + quartz ± muscovite assemblages and implications for crustal melting. Journal of Geophysical Research 100/B8, 15581-15591.

Gardien, V., Thompson, A. B. & Ulmer, P. (2000): Melting of Biotite + Plagioclase + Quartz Gneisses: the role of H2O in the stability of amphibole. Journal of Petrology 41/5, 651-666.

Garlick, S. R. & Gromet, L. P. (2004): Diffusion creep and partial melting in high temperature mylonitic gneisses, Hope Valley shear zone, New England Appalachians, USA. Journal of Metamorphic Geology 22, 45-62.

Holland, T. & Powell, R. (2001): Calculation of phase relations involving haplogranitic melts using an internally-consistent thermodynamic database. Journal of Petrology 42, 673-683.

Holland, T. J. B. & Powell, R. (1998): An internally-consistent thermodynamic data set for phases of petrological interest. Journal of Metamorphic Geology 16, 309-343.

Holtz, F., Becker, A., Freise, M. & Johannes, W. (2001a): The water-undersaturated and dry Qz-Ab-Or-system revisited. Experimental results at very low water activities and geological implications. Contrib. Mineral. Petrol. 141, 347-357.

Holtz, F., Johannes, W., Tamic, N. & Behrens, H. (2001b): Maximum and minimum water contents of granitic melts generated in the crust: a reevaluation and implications. Lithos 56, 1-14.

Holyoke-III, C. W. & Rushmer, T. (2002): An experimental study of grain scale melt segregation mechanism in two common crustal rock types. Journal of Metamorphic Geology 20, 493-512.

Johannes, W. & Holtz, F. (1996): Petrogenesis and experimental petrology of granitic rocks. Minerals and Rocks . Springer Verlag, Berlin, 335 pp.

Kisters, A. F. M., Gibson, R. L., Charlesworth, E. G. & Anhaeusser, C. R. (1998): The role of strain localisation in the segregation and ascent of anatectic melts, Namaqualand, South Africa. Journal of Structural Geology 20/2/3, 229-242.

Kriegsman, L. M. (2001): Partial melting, partial melt extraction and partial back reaction in anatectic migmatites. Lithos 56, 75-96.

Laporte, D. & Watson, E. B. (1995): Experimental and theoretical constraints on melt distribution in crustal sources: the effect of crystalline anisotropy on melt interconnectivity. Chemical Geology 124, 161-184.

Le Breton, N. & Thompson, A. B. (1988): Fluid-absent (dehydration) melting of biotite in metapelites in the early stages of crustal anatexis. Contrib. Mineral. Petrol. 99, 226-237.

Mecklenburgh, J. & Rutter, E. H. (2003): On the rheology of partially molten synthetic granite. Journal of Structural Geology 25/10, 1575-1585.

Mogk, D. W. (1992): Ductile shearing and migmatization at mid-crustal levels in an Archaean high-grade gneiss belt, northern Gallatin Range, Montana, USA. Journal of Metamorphic Geology 10, 427-438.

Mogk, D. W. (2001): Magmatic hornblende relations in migmatitic biotite TTG gneisses, northern Gallatin Range, SW Montanta: Geological Society of America, 2001 annual meeting. Abstracts with Programs, 33. Geological Society of America, 250.

Nagel, T. (2000): Metamorphic and structural history of the southern Adula nappe (Graubünden, Switzerland). Doctoral thesis, Universität Basel, 3 chapters.

Nagel, T., Capitani, C. d. & Frey, M. (2002): Isograds and P-T evolution in the eastern Lepontine Alps (Graubünden, Switzerland). Journal of Metamorphic Geology 20, 309-324.

Naney, M. T. (1983): Phase equilibria of rock forming ferromagnesian silicates in granitic systems. American Journal of Science 283, 993-1033.

Oberhänsli, R., Hunziker, J. C., Martinotti, G. & Stern, W. B. (1985): Geochemistry, geochronology and petrology of Monte Mucrone: an example of eo-alpine eclogitization of Permian granitoids in the Sesia-Lanzo zone, Western Alps, Italy. Chem Geol (Isotope Geosci Sect) 52, 165-184.

Oliver, N. H. S. (1996): Review and classification of structural controls on fluid flow during regional metamorphism. Journal of Metamorphic Geology 14, 477-492.

Paterson, M. S. (2001): A granular flow theory for the deformation of partially molten rocks. Tectonophysics 335/1/2, 51-61.

Patiño Douce, A. E. & Harris, N. (1998): Experimental constraints on Himalayan anatexis. Journal of Petrology 39/4, 689-710.

Patiño Douce, A. E. & Mc Carthy, T. C. (1998): Melting of crustal rocks during continental collision and subduction. In: Hacker, B. R. & Liou, J. G. : When continents collide: Geodynamics and geochemistry of ultrahigh-pressure rocks . Kluwer, Dordrecht(NL), 27-55.

Poli, S. (1993): The amphibolite-eclogite transformation: An experimental study on basalt. American Journal of Science 293, 1061-1107.

Prince, C., Harris, N. & Vance, D. (2001): Fluid-enhanced melting during prograde metamorphism. Journal of the Geological Society of London 158, 233-241.

Rapp, R. P. (1995): Amphibole-out phase boundary in partially melted metabasalt, its control over liquid fraction and composition, and source permeability. Journal of Geophysical Research 100/B8, 15601-15610.

Roselle, G. T., Thüring, M. & Engi, M. (2002): Melonpit: A finite element code from simulating tectonic mass movement and heat flow within subduction zones. American Journal of Science 302, 381-409.

Rosenberg, C. L. (2001): Deformation of partially molten granite: a review and comparison of experimental and natural case studies. Int. J. Earth Science (Geol. Rundsch.) 90, 60-76.

Rosenberg, C. L. & Berger, A. (2001): Syntectonic melt pathways in granitic gneisses, and melt-induced transitions in deformation mechanisms. Phys. Chem. Earth (A) 26/4-5, 287-293.

Rosenberg, C. L. & Handy, M. R. (2000): Syntectonic melt pathways during simple shearing of a partially molten rock analogue (Norcamphor-Benzamide). Journal of Geophysical Research 105/B2, 3135-3149.

Rubie, D. C. & Brearley, A. J. (1990): A model for rates of disequilibrium melting during metamorphism. In: Ashworth, J. R. & Brown, M. : High temperature metamorphism and crustal anatexis Mineralogical Society Series 2. Mineralogical Society, London, 57-86.

Rushmer, T. (2001): Volume change during partial melting reactions: implications for melt extraction, melt geochemistry and crustal rheology. Tectonophysics 342, 389-405.

Rutter, E. H. & Neumann, D. H. K. (1995): Experimental deformation of partially molten Westerly granite under fluid-absent condtitions, with implications for the extraction of granitic magmas. Journal of Geophysical Research 100/B8, 15697-15715.

Rütti, R. (2003): The tectono-metamorphic evolution of the northwestern Simano Nappe (Central Alps, Switzerland). Doctoral thesis, ETH-Zürich, 112 pp.

Sawyer, E. W. (2000): Grain-scale and outcrop-scale distribution and movement of melt in a crystallising granite. Transactions of the Royal Society of Edinburgh: Earth Sciences 91, 73-85.

Schmidt, M. W. & Thompson, A. B. (1996): Epidote in calc-alkaline magmas: An experimental study of stability, phase relationships, and the role of epidote in magmatic evolution. American Mineralogist 81, 462-474.

Sen, C. & Dunn, T. (1994): Dehydration melting of a basaltic composition amphibolite at 1.5 and 2 GPa: implications for the origin of adakites. Contrib. Mineral. Petrol. 117, 394-409.

Spear, F. S., Kohn, M. J. & Cheney, J. T. (1999): P-T paths from anatectic pelites. Contrib. Mineral. Petrol. 134, 17-32.

Speer, J. A. (1987): Evolution of magmatic AFM mineral assemblages in granitoid rocks: The hornblende + melt = biotite reaction in the Liberty Hill pluton, South Carolina. American Mineralogist 72, 863-878.

Stevens, G., Clemens, J. D. & Droop, G. T. R. (1997): Melt production during granulite-facies anatexis: experimental data from "primitve" metasedimentary protoliths. Contrib. Mineral. Petrol. 128, 352-370.

Thompson, A. B. (1999): Some time-space relationships for crustal melting and granitic intrusion at various depths. In: Castro, A., Fern„ndez, C. & Vigneresse, J. L. : Understanding granites: Integrating new and classical Techniques 168. Geological Society, Special publications, London, 7-25.

Thompson, A. B. (2001): Clockwise P-T paths for crustal melting and H_2O recycling in granite source regions and migmatite terrains. Lithos 56, 33-45.

Todd, C. S. & Engi, M. (1997): Metamorphic field gradients in the Central Alps. Journal of Metamorphic Geology 15, 513-530.

Vernon, R. H. (2000): Review of microstructural evidence of magmatic and solid-state flow. Electronic Geosciences 5/2,

Vielzeuf, D. & Schmidt, M. W. (2001): Melting relations in hydrous systems revisited: application to metapelites, metagreywackes and metabasalts. Contrib. Mineral. Petrol. 141, 251-267.

Vigneresse, J. L. & Tikoff, B. (1999): Strain partitioning during partial melting and crystallizing felsic magmas. Tectonophysics 312, 117-132.

Viruete, J. E. (1999): Hornblende-bearing leucosome development during syn-orogenic crustal extension in the Tormes Gneiss Dome, NW Iberian Massif, Spain. Lithos 46, 751-772.

White, R. W., Powell, R. & Holland, T. J. B. (2001): Calculation of partial melting equilibria in the system Na_2O-CaO-K_2O-FeO-MgO-Al_2O_3-SiO_2-H_2O (NCKFMASH). Journal of Metamorphic Geology 19, 139-153.

Whittington, A. G. & Treloar, P. J. (2002): Crustal anatexis and its relation to the exhumation of collisional orogenic belts, with particular reference to the Himalya. Mineralogical Magazine 66/1, 53-91.

Yardley, B. W. D. & Barber, J. P. (1991): Melting reactions in the Connemara schists: the role of water infiltration in the formation of amphibolite facies migmatites. American Mineralogist 76, 848-856.

Melt segregation and rheology in anatectic collisional systems: a critical review and new concepts

Thomas Burri

Abstract

The presence of melt in a partially molten rock leads to a reduction of rock strength. Besides of the weakening effect of the melt due to its considerably lower viscosity, the rock strength is influenced by melt topology and is related to a switch in the dominant deformation mechanism. Whether partial melts are able to segregate is mainly influenced by deformation and hydrofracturing, the latter as a result of the increasing pore pressure if the melting reaction is volume increasing. Using recent models on melt volumes in combination with thermodynamic computation, we propose a new model for the case of non-isochemical, water assisted partial melting. This new model allows concluding that, in contrast to the general statement, water assisted partial melting is volume increasing if it results from the infiltration of fluids. Therefore, water assisted melting may result in hydrofracturing and may be as effective in segregating and draining melts as dehydration melting. The distribution of partial melts on the outcrop may be explained by an extended discussion of the Mohr-Circle. Foliation-parallel as well as discordant leucosomes may be explained as an effect of slip along the foliation or at a specific angle to the maximum stress direction respectively. Increasing pore pressure due to partial melting strongly favours melt segregation processes.

Introduction

Partial melting of crustal rocks may, as an ultimate product, lead to the formation of plutons of predominantly granitoid composition. Accepting that large plutons do not form by *in situ* transformation into igneous rocks (formerly called ultrametamorphism or granitisation), but rather by emplacement of melt or magma that was created at deeper crustal levels, it is evident that the melt has to be extracted out of the melting area. In a first step, melt that forms on the grain scale must accumulate in sample scale segregations, then in outcrop scale segregations until it finally escapes from the local system. Processes that enhance melt segregation and extraction are still under discussion, but recent work proposes that, apart from buoyancy and gravity driven compaction, melt enhanced embrittlement and deformation may be of prime importance for melt segregation and escape (e.g. Davidson *et al*., 1994; Rutter and Neumann, 1995; Rosenberg, 2001). In this contribution we critically review some of these processes and introduce new concepts based on our own investigation. We focus on differences that may occur if partial melting occurs through dehydration melting, or through water assisted melting, with or without the infiltration of fluid.

The formation of partial melts in solid rocks exerts a strong influence on rock strength and on deformation processes, thus it will influence the rheology of a rock. This has been thoroughly discussed in the last decades (Dell'Angelo and Tullis, 1988; Davidson *et al*., 1994; Rutter & Neumann, 1995; Brown *et al*., 1995; Butler *et al*., 1997; Brown and Solar, 1998; Vigneresse and Tikoff, 1999; Brown and Solar, 1999; Dimanov *et al*., 2000; Rosenberg and Berger, 2001; Rosenberg, 2001; Mecklenburgh and Rutter, 2003). Researchers agree that the presence of melt in a rock leads to a reduction of rock strength, the degree of which depends on the melt fraction. If partial melting is a synkinematic process, rocks that are affected by partial melting will be weaker than surrounding solid rocks, and may become sites of focused deformation. Consequently, this may lead to changes in local or even regional scale strain rates, what may strongly influence deformation and exhumation processes in collisional settings.

Model rheology of partially molten rock systems

The presence of partial melt in a rock considerably lowers the rock strength, due to the lower viscosity of the melt (10^4-10^8 Pa s) compared to the rocks viscosity (10^{13}-10^{15} Pa s). Considering a partially molten rock roughly as a two component system made up of low viscosity melt and high viscosity solids, the character of the melt-solid system can be modelled (Vigneresse & Tikoff, 1999). Average viscosity varies between the values of the two components as a function of the solid-melt volume-ratio. An increasing melt fraction leads to a (nonlinear) decrease in viscosity of the bulk system. The mixing behaviour can be constrained between two end-member laws, the Voigt and Reuss values (Fig. 1. in Vigneresse & Tikoff, 1999). Recently, a slightly modified model for partially molten systems, based on

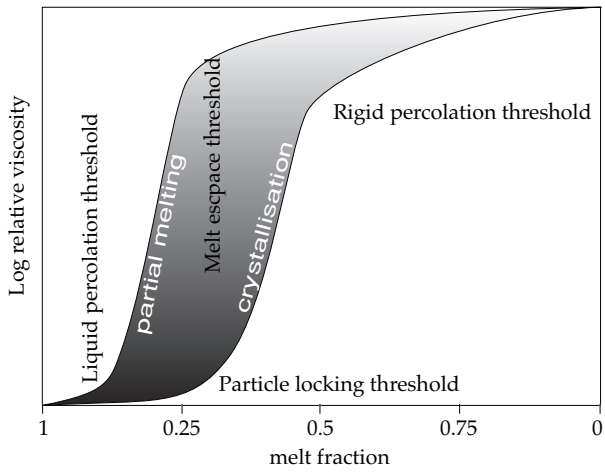

Fig. 1) Variation of magma viscosity with increasing melt fraction according to Vigneresse&Tikoff (1999). A clear nonlinear relationship exists between increasing melt fraction and decreasing system viscosity. Partially melting systems are predicted to have a lower viscosity than crystallising systems at the same melt fraction. Four different thresholds are predicted. The shaded area coincides with experimental data.

percolation theory, was proposed in which partial melting and crystallisation are not considered to be mechanically equivalent mechanisms (Vigneresse & Tikoff, 1999). They proposed four threshold values to be important in static partially molten rock systems (Fig. 1): If rocks crystallise, they first encounter a "rigid percolation threshold" at a melt fraction of about 0.45, a boundary where rigid particles start to strongly interact and to form a framework of touching particles that can support a load. At a melt fraction of about 0.25, a "particle locking threshold" is reached, below which no magma (solid + melt) can escape the system (similar to the Rheologically Critical"Melt Percentage of Arzi (1978)).

On the other hand, if rocks undergo partial melting, a "liquid percolation threshold" is first reached at a melt fraction of around 0.08. There, a continuous connection of the liquid pathways becomes established and a liquid can circulate on a centimetre to decimetre scale. At a melt fraction of 0.2-0.25, a "melt escape threshold" is reached, where melt transport evolves from a diffusion mode to an advection mode and melt can be transported over kilometres. Of importance for the rheology of partially molten system is the suggestion that systems undergoing partial melting are weaker than crystallising systems at the same melt fraction (Fig. 1).

These threshold values, representative for static systems, may however shift if deformation coincides with partial melting or melt crystallisation. This may lower the melt escape threshold and enhance melt-segregation, hence, melt may segregate already at very low melt fractions if partial melting and deformation are simultaneous processes. Melt segregation, however, is influenced also by melt topology, i.e. the distribution of melt in a rock. Whether partial melts are constrained to unconnected melt pockets or form a connected melt-network has a significant influence on melt segregation and rock rheology.

Influence of fluid and melt topology on rock strength in static and deforming systems

Nomenclature: In the following, grain boundaries delineate planar two-phase interfaces, grain edges a linear array of three or more grain edges and grain corners a punctiform three- or more- grain junction.

The creep strength of a partially molten rock depends on the melt fraction and on the grain scale melt distribution, the so called melt topology. For example, rock strength is considerably decreased if a fluid or a melt is distributed along grain boundaries instead of being constrained to grain edges or corners (Tullis *et al*., 1996; Dimanov *et al*., 2000). In both studies, the observed increase in strain rate is related to a switch in the dominating deformation mechanism. Fluid and melt topology may therefore exert a significant influence on rocks strength and strain rates. In addition, topology is important for fluid and melt permeability in a rock and thus for segregation processes. In the following two paragraphs fluid and melt topologies in hydrostatic as well as in more natural dynamic systems are reviewed and discussed.

Fluid and melt topology under static conditions

Under static (litho- or hydrostatic) conditions, melt or fluid distribution strives towards an equilibrium through reduction of the interfacial free energy. The latter is a function of the ratio of the solid-solid grain boundary energy (γ_{ss}) and the energy of the solid-liquid interface (γ_{sl}) and results in an equilibrium solid-liquid dihedral angle θ (or wetting angle) (Philpotts, 1990; Laporte and Watson, 1995; Holness, 1995). In an equilibrium distribution for an isotropic matrix (Laporte & Watson, 1995; Kohlstedt, 2002, and references therein) the relation is given by

$$\gamma_{ss} = 2\gamma_{sl}\cos(\theta/2) \qquad (1)$$

The dihedral angle θ depends on temperature, the type of volatile or liquid phase, and on the type of solid phase(s). Relation (1) holds for a homogeneous monomineralic system, with single valued solid-liquid and solid-solid interfacial energies that is subject to hydrostatic stress. For a dihedral angle > 60°, liquids will form unconnected, isolated pores at grain corners or edges (Fig. 2a1+a2). For angles < 60° liquids will form a three dimensional framework of channels along grain edges and corners (Fig. 2b1+b2), and for angles of 0°, melt will be dispersed along all grain boundaries.

In monomineralic silicate systems, most solid-melt dihedral angles are < 60°, whereas they are usually > 60° in (H_2O-CO_2-) fluid-solid systems (Laporte & Watson, 1995; Holness, 1995; Brown *et al*., 1995). Therefore, in monomineralic solid-volatile systems, volatiles should be largely constrained to pores at grain corners and edges, and transport should only

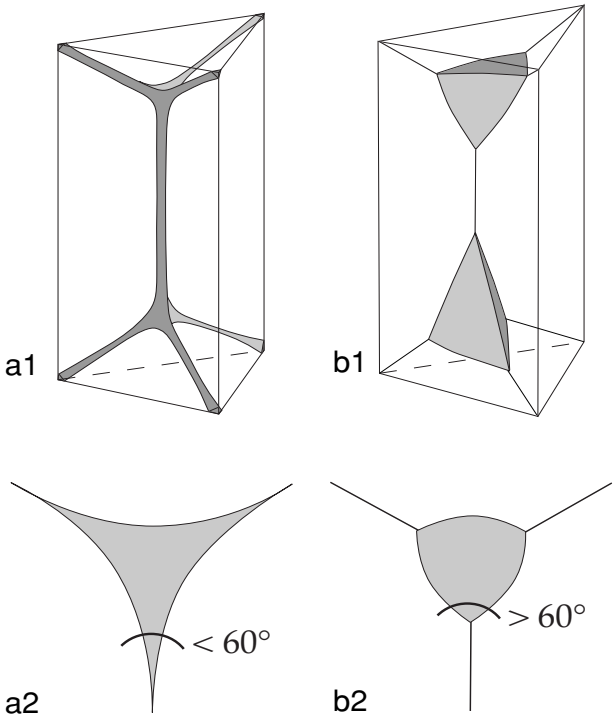

Fig. 2) Equilibrium melt topology in monomineralic rocks. At angles < 60° (Fig. a1+2) melt forms an interconnected channel framework along grain edges and corners. At angles > 60° (b1+2) melt is situated in isolated pores at grain corners. At dihedral angles θ = 0°, melt would wet all grain boundaries (not shown). Modified after Laporte&Watson (1995).

occur through diffusive mechanisms, because no connected pore-network exists. By contrast, an interconnected pore space may exist in monomineralic solid-melt systems, theoretically at infinitely low melt fractions, and melts may circulate by diffusive and advective mechanisms. At which rate melt and fluids circulate is strongly dependent on their viscosity and the effective permeability. Melt viscosity is thought to be the most important factor considering melt segregation processes in hydrostatic systems (Laporte & Watson, 1995). For ideal sources with $\theta < 60°$ an equilibrium melt fraction ϕ_{min} is predicted, which represents a minimum state of interfacial energy per unit volume (Laporte & Watson, 1995). If the melt fraction ϕ is smaller than ϕ_{min}, melt is uniformly distributed along grain edges and corners. If it is larger, small melt pools will catch the melt fraction in excess of ϕ_{min}. Thus the concept of a minimum melt fraction predicts the segregation of melt in a static system, even in the absence of deformation.

Deviations from the described topology are reported for more complex systems like polymineralic aggregates or with changing fluid composition (Laporte & Watson, 1995; Holness, 1995). Several factors contribute to this deviation from the isotropic fluid or melt topology:

- Every crystal has a certain degree of intrinsic anisotropy due to its crystal structure. The above theory, however, is strictly applicable to isotropic systems only. Intrinsic anisotropy leads to anisotropy in the solid-solid and solid-liquid interfacial energies, which depend on the orientation of the crystal lattices of two touching grains and of the bonding mismatch of the crystal melt interface. This may lead to moderate differences in the wetting angle for weakly anisotropic phases, and to more pronounced deviations for strongly anisotropic minerals.
- Additions of a second solid phase may produce a strong decrease of the wetting angle. For the **quartz-H_2O**-system the addition of a small amount of feldspar (microcline-albite), leads to a decrease of >10° in the dihedral quart-quartz-fluid angle at temperatures in excess of 500°C. Final angles in the feldspar-quartz-systems are below 60° at the onset of partial melting. This behaviour was explained by non-ideal mixing properties of feldspar in the fluid phase (Holness, 1995). In addition a change from a non-connected to a partially connected pore space was found in the same system (permeability transition), if temperatures reach > 600°C.
- Fluid composition has a strong influence on the wetting angle in an otherwise constant (solid) system. In contrast to the change in the qtz-fsp-H_2O-system, additions of small amounts of a second solid phase in the **qtz-CO_2**-system did not result in significant changes in dihedral angle (still > 90°) (Holness, 1995). This remarkable contrast may indicate that, in contrast to H_2O-fluids, pure CO_2-fluids are not able to migrate through silicate systems.
- Volume changes in melting reactions may strongly affect equilibrium topology. Positive volume changes may lead to hydrofracturing and to the segregation of melt into extensional fractures. Pathways for fluid or melt percolation are effectively created by this process. In contrast, negative volume changes may lead to a soaking of already present melt towards the sites of melting and to a compaction of the grain aggregate (Connolly *et al*., 1997).

These observations indicate that in natural silicate systems under static conditions, water-rich fluids or silicate melts form a connected pore space and (dependent on the respective viscosity) are able to flow through this porosity-network. In addition, the pore space necessary for circulation of a hydrous fluid or a melt may be created through hydrofracturing processes in volume increasing dehydration reactions. Due to the much lower viscosity, hydrous fluid may be able to flow at a higher rate than a silicate melt. In addition, water may more effectively diffuse along "intact" grain boundaries then melt, due to the much smaller size of these molecules compared to the larger polymerised melt-molecules. In contrast, CO_2-rich fluids may not easily flow through silicate rocks, because no connectivity of the isolated pores should be established.

Fluid and melt topology under deforming conditions

The concepts of wetting angle and minimum melt fraction ϕ_{min}, which are functions of surface energies, are suggested to be of minor importance in deforming systems (Brown *et al*., 1995). As a result of deformation, grain boundaries are transient features, because they are destroyed and created due to dynamic recrystallisation. Therefore, fluid and melt topology may deviate from ideal and may change with deformation. In fact, a switch in the distribution of fluid was observed for experimentally deformed feldspar aggregates (Tullis *et al*., 1996), where deformation lead to new fluid distribution along grain boundaries. The change in topology was accompanied by a change in the dominant deformation mechanism from dislocation creep to diffusion creep, and was connected to a significant reduction in rock strength. As deformation ceded, fluids regained their stable isotropic distribution along grain triple and four grain junctions. Although important sources of information, experiments may not accurately reflect natural processes. For example, melt topology was observed to be different in experiments and in nature: In natural systems a switch in topology from isotropic melt pockets at grain junctions to elongate melt pockets oriented dominantly (sub)parallel but also (sub)perpendicular to the foliation plane was observed (Sawyer, 2001; Rosenberg, 2001). This distribution may favour flow parallel to the foliation.

In experiments, melt is preferentially situated at an orientation subparallel to the maximum compressive stress, or at an angle of ~30° within micro-fractures (Dell'Angelo & Tullis, 1988; Rutter & Neumann, 1995; Rosenberg & Berger, 2001; Rosenberg, 2001). Note, however, that intergranular cracks in muscovite dehydration-melting experiments show often a preferred orientation parallel to the muscovite grains, or are influenced by the existence of neighbouring melt pools (Connolly *et al*., 1997). Melt distribution in experiments may therefore depend on the differential stress (Rosenberg, 2001) or on the strain rate (which are interrelated): Rosenberg (2001) suggests that melt topology in experiments is governed by surface energy at low differential stresses, and by the orientation of the principal stress axes at high differential stresses. Note, however, that partially molten rocks under high applied pressures sustain only small differential stresses before they start to deform (Davidson *et al*., 1994; Handy and Streit, 1999), and that high differential stresses may be associated with high strain rates, which are unimportant in nature. Experiments and nature show that deformation results in redistribution of fluid and melt: Although originally distributed along two (or more) phase boundaries (reactants), melt may move down gradients in effective stress towards places of lower effective stress, such as sites of dilation and microfracturing. As a consequence, the change in fluid or melt topology may lead to a higher degree of fluid or melt connectivity and to enhanced rates of grain boundary diffusion. Experiments on partially molten plagioclase aggregates reveal that rock strength is in fact strongly influenced by melt topology (Dimanov *et al*., 2000). A minor amount of liquid (< 2%) distributed along grain boundaries is sufficient to reduce rock strength 5-10 times compared to rocks with melt confined to grain corners. The observed reduction was explained by enhanced rates of grain boundary diffusion through the melt which allows solution-precipitation processes to become more competitive.

Deformation mechanism

The presence of melt in a rock leads to a significant lowering of rock strength with increasing melt fraction (Arzi, 1978; Rutter & Neumann, 1995; Vigneresse & Tikoff, 1999; Rosenberg, 2001). At relatively low melt fractions (< 20-30 %), which may be typical for syncollisional migmatites, the lowering of rock strength compared to that of the solid rock may not be simply explained by the lubrication effect of the low viscosity melt, because a similar effect is also observed in the solid-fluid system at very low porosities: In deformation experiments, the redistribution of water along grain boundaries leads to a considerable reduction of the system bulk strength, beyond of that induced by hydrolytic weakening of the minerals (Tullis, 2002). In the solid-fluid system, the main reasons for the lowered strength is apparently the redistribution of fluid from grain edges and corners to grain boundaries, and an associated switch in the principal deformation mechanism from mainly dislocation creep to diffusion creep (pressure solution creep) and grain boundary sliding (Tullis *et al*., 1996). In the solid-melt system, a similar switch in deformation mechanism from dislocation-creep to melt-assisted diffusion creep or granular-flow with increasing melt fraction has been proposed by several authors (Dell'Angelo & Tullis, 1988; Paterson, 1995; Tullis *et al*., 1996; Rosenberg & Berger, 2001; Rosenberg, 2001; Paterson, 2001; Mecklenburgh & Rutter, 2003)]. In general, synmigmatic cataclastic flow, as often observed in experimentally deformed rocks, must be of minor importance in natural systems, because average strain rates are very low, and melt may escape at a higher rate than deformation proceeds (Dell'Angelo & Tullis, 1988). As a result, occasional hydrofracturing may concur with melt assisted diffusion creep and granular flow rather than with cataclastic flow.

Thus, the main effect of the presence of melt at low melt fractions may be the establishment of an interconnected melt-network, and an associated increase in intergranular diffusion rates. This may induce a switch in the deformation mechanism and lead to a increase in strain rates.

Melting reactions and associated changes in volume and pore pressure

Melting reactions

In collisional settings, partial melting of solid rock occurs due to two different processes: Rocks may either melt through dehydration melting reactions (DM-reactions) at elevated temperatures or through water-assisted melting (WAM) at or above the water saturated solidus. Both processes are dependent on the availability of fluid. Pore fluids or infiltrating fluids are responsible for WAM, whereas fluid released through the decay of hydrous minerals in DM is taken up to form melt. Resulting melt fractions depend therefore on the amount of available fluid and on PT-conditions. Melt fractions remain small if only the pore fluid is consumed, or if the mode of the decaying hydrous phase is small. In contrast, high melt fractions are obtained if fluid infiltrates a rock, or if the rock contains a high amount of the decaying hydrous phases.

Volume changes in melting reactions are positive or negative, dependent on the type of melting reaction. In closed systems, the change in volume is associated by a change in pore pressure. Pore pressure must increase if $\Delta V_{melting}$ is positive and decrease if it is negative. In the literature it is generally put forward that dehydration melting leads to positive, water assisted melting to negative volume changes (Brown *et al*., 1995; Clemens and Droop, 1998; Rushmer, 2001; Prince *et al*., 2001; Holyoke-III and Rushmer, 2002), due to the positive and negative slopes of the melting curves respectively. The negative volume change of WAM should inhibit the formation of dilational strains (pore pressure), and melt should not escape the site of melting (Clemens & Droop, 1998; Rushmer, 2001; Holyoke-III & Rushmer, 2002). Therefore, melt created by WAM should hardly be extracted from a partially molten rock. In contrast, dehydration melting reactions commonly show positive slopes, favouring a positive volume change. The discussion on the slopes of the melting reactions uses the Clapeyron-equation

$$dP/dT = \Delta_r S/\Delta_r V$$

Statements relying on the Clapeyron-equation alone, may overstress its applicability, especially in water assisted melting reactions, were fluid and liquid phases both contribute considerably to the change in entropy. We further note that the slopes of water saturated solidi in most systems change sign at higher pressures. In addition, the relation may not even hold for DM-reactions, as indicated by calculated volume changes for experimentally determined melting reactions. These show volume changes in the order of –7 to +3 % for different biotite-DM-reactions and +62 % for the only calculated phengite-DM-reaction (Rushmer, 2001) (due to reported inconsistencies of the calculations, absolute values should be considered with caution). Hence, biotite dehydration melting may even lead to negative volume changes, in contrast to the general thinking.

One point usually not discussed is the circumstance that water assisted melting may occur at any point above the water saturated solidus if fluid infiltration occurs. Volume changes at these conditions are however not *a priory* comparable to those occurring at the water saturated solidus. Furthermore, we need differentiating between closed and open system conditions for WAM-processes. If partial melting occurs in a closed system and exclusively by the consumption of the available pore fluid, melting reactions may be volume decreasing or near volume constant. By contrast, in an open system where fluid infiltration occurs, the infiltrating fluid is trapped in the melt at the site of partial melting. This additional volume must be accounted for in the calculation of volume changes. For visualisation, we could imagine a fluid-rock system, where fluid percolates through the rock (Fig. 3). At subsolidus conditions, the influx of fluid equals the outflux, at least if the rock is already water saturated at the moment of fluid infiltration. As a result no volume changes will occur in the system. By contrast, if fluid infiltration occurs in a system above the water saturated solidus, the infiltrating fluid is trapped in the partial melts, and the fluid outflux may be much smaller or even equal zero compared to the influx. Consequently, the bulk volume increases with increasing melt fraction, as a result of the additional volume of the infiltrating fluid.

For the calculation of volume changes in such non-isochemical systems the general volume equation for water assisted partial melting in closed systems

$$\hat{I}V = V_{melt+fluid} - (V_{solid} + V_{porefluid})$$

in the open system fluid infiltration scenario becomes

$$\hat{I}V = V_{melt+fluid} - V_{solid}$$

where $V_{melt+fluid}$ denotes the volume of the melt including the dissolved infiltrated fluid. This new

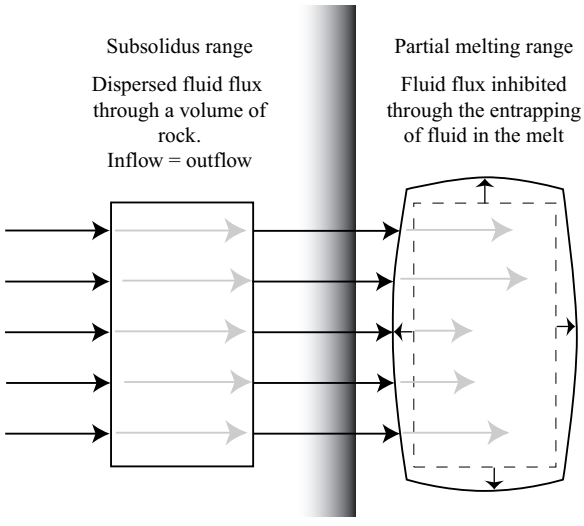

Fig. 3) Sketch depicting dispersed fluid flow through a volume of rock, and associated positive volume change if the fluid is trapped inside the melt if infiltration occurs at conditions above the water saturated solidus of the system.

model on water assisted partial melting clearly suggests a much larger potential volume increase than at closed system conditions. In the following discussion we present calculated volume changes for closed as well as open-system scenarios in a haplogranitic system, and discuss their relevance for melt segregation in natural anatectic systems.

Calculation of volume changes in WAM in the haplogranitic system

The calculation of volume changes of water assisted melting reactions demands precise knowledge of the volume of the solids, the volume and (minimum) amount of the fluid and the volume of the melt at P and T. The minimum water content of a melt is the amount of water required to melt a rock sample completely (at given P and T). We use eutectic compositions of the haplogranite system, which has the big advantage that the solid rock is completely transformed into melt upon addition of the minimum water content. Volumes of refractory minerals therefore cancel out from calculation. A smaller amount of fluid would only result in a smaller melt fraction, but relative volume changes of the melting reaction would remain constant. Volume changes are calculated using the following models and programs:

a) The minimum (or equilibrium) water content of the melt at given P and T is taken from the updated haplogranite-model of (Holtz *et al*., 2001b).

b) Programs THERIAK and DOMINO (de Capitani and Brown, 1987) are used for the calculation of volumes of solids and fluid.

c) For the calculation of melt volumes we use a recent model that sums-up partial molar volumes of oxides and water in a melt (Ochs-III and Lange, 1997).

Description of different models:

The model of Holtz et al. (2001) describes the minimum or equilibrium water content of a melt in haplogranitic systems (Fig. 4). Their model was fitted using experimentally determined eutectic or minimum compositions at different P and T conditions that allowed calculating liquidus curves (equals minimum water contents of a melt) over the investigated PT-space of 0-8 kbar and 550-1150 °C. Eutectic or minimum compositions change with P and T, which should be considered in the calculation of phase diagrams. Because too few eutectic composition are however accurately known, we chose the experimentally determined eutectic composition at 5 kbar and 1% H_2O (Qz32Ab35Or33) (Holtz *et al*., 2001a) *for the whole PT-field of interest, and adjusted the water content of the melt according to the model* (Holtz *et al*., 2001b; Holtz *et al*., 2001a). *This inconvenience should however not much influence calculated volume changes (pers. comm. F. Holtz). In addition, test runs using the few experimentally determined eutectic compositions fitted well with our later calculation.*

Using the eutectic composition mentioned, we employed programs DOMINO and THERIAK (de Capitani & Brown, 1987) *in combination with the internally consistent database of* (Berman, 1988) *to compute phase diagrams, stable assemblages and volumes of solids and fluid at certain PT-points. Phase relations and calculated volumes for the given input are displayed in figure 5. Note that absolute values of calculated isochors are not relevant, because they depend on the definition of the bulk system.*

Because the Berman (1988) database does not include thermodynamic data for melts, melt volumes were calculated using the model of Ochs and Lange (1997), which involves the summation of partial molar volumes of oxides and H_2O to calculate volumes of melts. A similar approach was recently chosen to calculate ΔV of selected dehydration melting reactions (Rushmer, 2001).

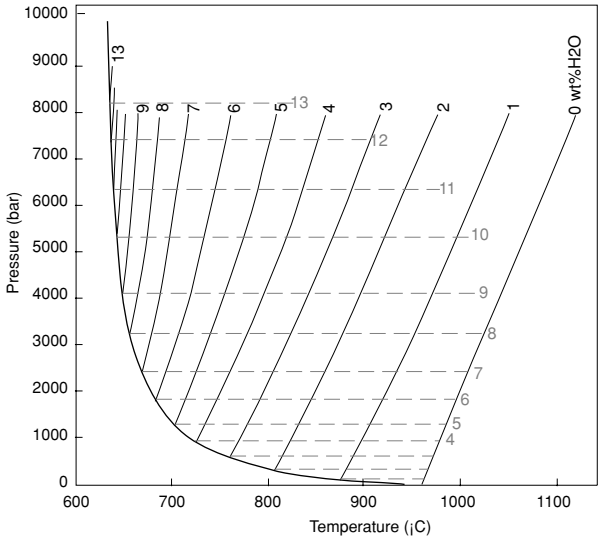

Fig. 4) Haplogranite system according to Holtz et al. (2001). Solid lines are liquidus curves, providing information on the minimum water content of a melt. Water saturation lines (dashed lines) are depicted qualitatively, as they are taken from an older model of Holtz&Johannes (1994).

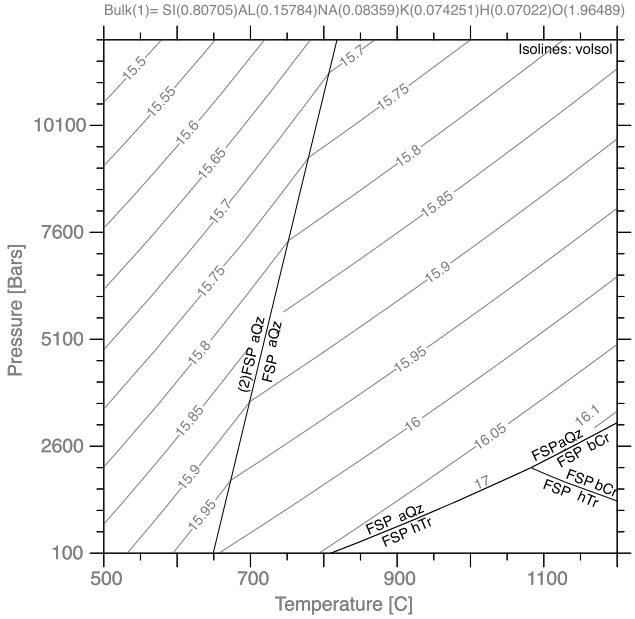

Fig. 5) Calculated phase diagram for eutectic composition of Holtz et al. (at 5 kbar and 1% H_2O (Qz32Ab35Or33) (2001) using program Domino. Headline is chosen bulk system in moles. Isochores (volume of solids in [ccm]), are shown to visualise changes in volume with P and T. Note that values depend on the definition of the bulk system.

"Closed system" melting (partial melting without fluid infiltration)

In a first step volume changes are calculated for isochemical systems devoid of fluid infiltration and where only the available pore fluid is used for partial melting. ΔV of melting is obtained by subtracting $(V_{sol} + V_{fluid})_{THERIAK}$ from $(V_{melt})_{Ochs\&Lange}$, and by recalculating into percents of volume change by comparison to the unmolten state. Although melt fractions will remain small due to the minor amount of fluid

present in the pore space, volume changes may lead to dilational strains on a small scale (grain scale) if the reaction is volume increasing.

Figure 6 shows the results of the volume-change calculations. Volume data were contoured by hand, the large number of calculated PT-points ensuring the accuracy of the fit. Main features of the diagram are the considerably negative values obtained at low pressures near the water saturated solidus (due to the high volume expansion of water at low pressure) and the reasonably high positive values near the dry liquidus (due to high volume expansion and low water contents of the melt). At higher pressure of 4 – 8 kbar, only–small volume changes in the order of ± 1 % were calculated. The line of zero volume change is depicted as a black line. Negative as well as positive volume changes concur with the slopes of the solidus and liquidus respectively. Unfortunately, for lack of data, the model cannot be extended towards higher pressures (e.g. 15 kbar) which are still relevant for anatexis in collisional orogenies. The diagram suggests however, that for pressures up to 12 kbar, volume changes near the water saturated solidus may be small. Thus, only minor volume expansions or contractions are expected to occur during water assisted melting in collisional orogeny. The comparably large negative volume change between 0-4 kbar of up to – 20% would probably lead to collapse of the grain framework and to a compaction of the rock. However, pressures below 4 kbar at temperatures in excess of 600°C are not characteristic of collisional orogeny.

Volume changes along the solidus can easily be interpreted as ΔV of the melting reaction. At higher temperatures however, the significance of the volume change is more difficult to understand because all available fluid is consumed along the solidus and because the minimum water contents varies all over the diagram as a function of P and T. Assuming a constant amount of pore fluid (in mole) over the whole PT-area, calculated volume changes would imply a change in the amount of melt (in moles). As a result, calculated volume changes above the solidus are no longer trivial.

Calculated ΔV-values of -7 - +3% for biotite-DM (Rushmer, 2001) are similar to our estimates (at the same P and T), and it appears that "closed system" partial melting and biotite-DM should create only small tensile stresses through the change in volume. Instead, muscovite-DM leads to much higher positive volume changes (+62% for the only calculated muscovite-DMR (Rushmer, 2001)), and may therefore lead to fracturing of a rock. We emphasize that dilational stresses on the grain scale and on the outcrop scale should be distinguished: Dilational stresses around decaying muscovite grains may be high and lead to microcracking (small scale hydrofracturing, Connolly *et al*., 1997; Holyoke-III & Rushmer, 2002), whereas the imposed stress on the sample or on the outcrop scale depends on the mode of the decaying phase and on its geometric distribution. A small mode leads to small stresses and local microcracking only, and as a result melt connectivity may not be reached. On the other hand, if muscovite is abundant in the rock or is distributed along layers (foliation or chemical banding), microcracks may lock in 2D or 3D. Once connectivity is established, melt may start to segregate and escape on the centimetre to decimetre scale (Connolly *et al*., 1997).

A new model for "open system" melting (partial melting with fluid infiltration)

As noticed above, water assisted partial melting occurring as an effect of fluid infiltration is not isochemical (open system). Our new model proposes that the infiltrating fluid is trapped at the site of melting as it dissolves into the liquid, and that ΔV of the

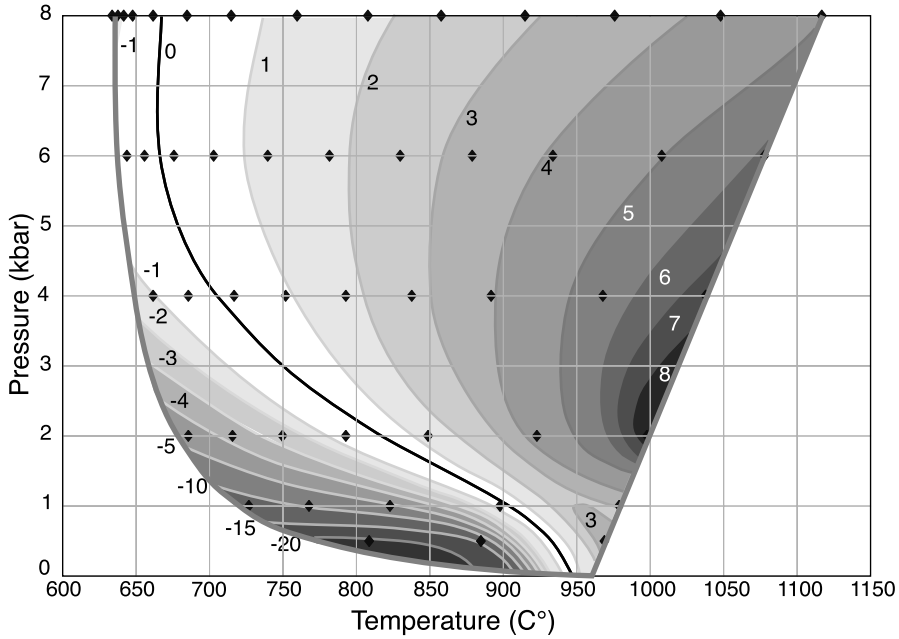

Fig. 6) Calculated volume changes in the haplogranite system Holtz et al. (2001). Negative values indicate that the volume of melt is smaller than the volume of solids + fluid (in vol.%) and vice versa.

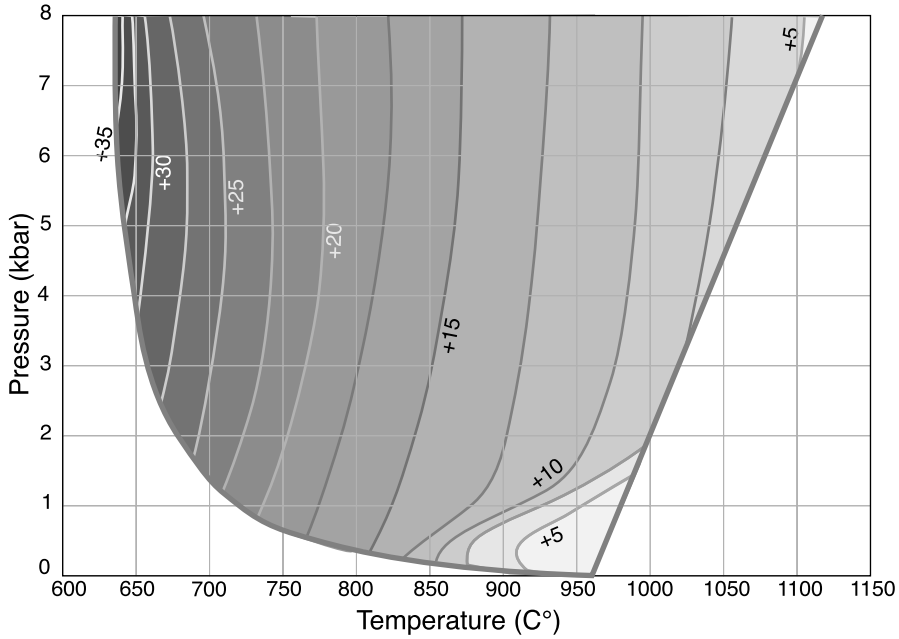

Fig. 7) Volume changes in haplogranite system without incorporating the volume of the fluid phase before the onset of melting (see text)

partially molten system is now obtained by subtracting $(V_{sol})_{THERIAK}$ from $(V_{melt+fluid})_{Ochs\&Lange}$. The volume change is then recalculated into percents of volume change compared to the solid system devoid of fluid ($(V_{melt+fluid})_{Ochs\&Lange}$ already incorporates the infiltrated fluid whereas $(V_{sol})_{THERIAK}$ denotes the dry solid rock, prior to infiltration). Obviously, this type of partial melting must lead to much larger volume changes than calculated above for a dry system, and as long as no melt leaves the system, a high pore pressure and high tensile stresses must build up. Figure 7 shows volume changes calculated for the haplogranite system under the assumption that all fluid infiltrates from outside the local system. Calculated isolines are much more regular than those calculated for "closed system" melting and display a clear situation. Very high positive volume changes of +30 to +35% occur along the water saturated solidus between 4-8 kbar. Similar values are suggested up to 10-12 kbar. The change in volume remains positive all over the calculated diagram but it decreases continuously with increasing temperature. Nevertheless, if fluid infiltration occurs at temperatures below 800°C, positive volume changes on the order of 15-35% are obtained. Although dilational stresses on the sample to outcrops scale depend on melt fraction and thus on the amount of infiltrating fluid, calculated volume changes indicate very high stresses at the site of melting. These may lead to a rapid 3D connection of melt channels on the grain scale, due to hydrofracturing, and probably to rapid segregation and extraction of melt. Assuming a melt fraction of 20% created at 700°C/8 kbar, the overall positive volume change would be in the order of 5%, whilst the volume change on the grain scale (at the site of melting) would be around 25%.

We may thus infer two contrasting scenarios for WAM-processes:

- If WAM occurs solely through the consumption of the available pore fluid, minor positive or negative volume changes occur and the driving force for melt segregation and escape remains small. In such a situation, melt may stay in the rock as long as deformation is of minor importance. If deformation leads to enhanced melt segregation, such melts may yet not be able to escape for a large distance, because they would immediately crystallise upon cooling, as an effect of the shape of the water saturated solidus. Because the solidus bends back above 10-12 kbar, melt produced at higher pressures may be able to rise for a considerable distance before freezing.
- If WAM is triggered by fluid infiltration at or above the water saturated solidus, major positive volume changes may occur and the driving force for melt segregation is large. Relaxation of the resulting high stresses may best occur through the escape of melt from the site of melting. If melts were created at some temperature above the water saturated solidus, they will be able to travel for a considerable distance before they crystallise. Depending on the extent of fluid infiltration, such melts may even segregate on a larger scale to form plutonic bodies of different size.

Melt viscosity revisited

Several authors have critically stated that the leucosomes observed in migmatite terrains were obviously not able to leave the outcrop system and thus remained largely *in situ*. Such leucosomes are often inferred to be related to water assisted melting processes, where melt should be trapped at the local scale, due to the negative volume change of the melting reaction. In addition, the leucosomes should immediately freeze during ascent, due to the shape of the water saturated solidus (negative slope of the reaction). In addition, because partial melting is assumed to have occurred at low temperatures, melt viscosity may be high and may hinder efficient melt segregation.

This criticism may not be justified for several reasons: Above we have proposed a new model for partial melting occurring in open system. According to this model, water assisted melting reactions are volume increasing in fluid infiltration settings. We have additionally noted that water assisted partial melting is not constrained to the water saturated solidus, but may occur at considerably higher temperatures in dependence on the influx of fluids. Furthermore, leucosomes observed on the outcrop may not demonstrate the inability of the melt to escape from the rock, but may just represent that melt fraction left behind after extraction (e.g. Brown *et al.*, 1995). Note that for the segregation into local leucosomes, melt must be able to escape at least from the site of melting, and it may thus be able to move at a larger scale. Furthermore, recent investigations document that the apparently unconnected 2D-distribution of leucosome pockets and veins may in fact form an interconnected 3D-network (Sawyer, 2000; Sawyer, 2001). Thus, melt may percolate through veins and pockets in a 3D-space and may crystallise away from where it has formed. Once such an interconnected network is established, melt may effectively drain from the site of formation and may segregate into larger bodies and dikes from where it can leave the system. Whether the relatively low temperatures near the water saturated solidus really lead to the formation of very viscous melts unable to escape from the system, is the topic of this paragraph.

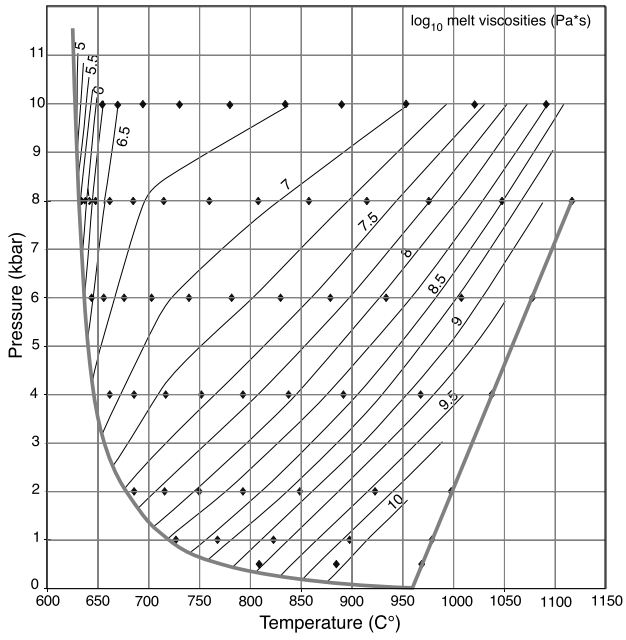

Fig. 8) Melt viscosity calculated for the haplogranite-system using minimum water content of melt according to Holtz et al. (2001). Melt viscosity was calculated according to Dingwell (1999).

For the following discussion we again make use of the haplogranite model (Holtz *et al.*, 2001a, Fig. 4), and discuss the viscosity of granitoids at their minimum (or equilibrium) water content. This assumption may be justified for melts in migmatites, which have a comparatively long residence time to equilibrate with the host rock. Fluid in excess of the minimum may promote further partial melting in the host, rather than accumulate in the melt. This scenario is not adequate for rising plutonic bodies, which are unable to equilibrate with the host, due to their large volumes. Depending on the PT-path, the water content of rising magma may change during ascent and crystallisation (excellent discussion in Johannes and Holtz (1996)). For the calculation of melt viscosity, we use the recent model of Dingwell (1999). Melt viscosity is calculated according to

$$\log K = ((-3.545+0.833\ln(w))+(9601-2368\ln(w))) / (T-(195.7+32.25\ln(w)))$$

where K is viscosity and w is weight percent of water in melt. The equation is therefore essentially dependent on the water content of the melt and on temperature. The influence of pressure is assumed to be of minor importance for melt viscosity and is neglected.

Figure 8 displays calculated isolines of melt viscosity (in units of $\log_{10}$K (Pa*s)) for the haplogranite system. Comparison of the diagram with the haplogranite-model of Holtz *et al.* (2001b) shows that viscosity is mainly dependent on the water content, and only to a lesser degree on temperature. The lowest viscosity coincides with highest water contents of the melt, independent of temperature. Estimated melt viscosity of natural systems is in the order of $10^{8\text{-}9}$ Pa*s (dry) and $10^{6\text{-}7}$ Pa*s (wet) (Brown *et al.*, 1995). Values lower than 10^7 Pa*s are calculated near the water saturated solidus above 3 kbar in the haplogranite system, and the viscosity decrease to 10^5 Pa*s at 11 kbar near the solidus. In fact, the border between values higher or lower than 10^7 Pa*s appears to coincide with the area where muscovite dehydration melting occurs. Because we assumed a minimum water content of the melt, the calculated melt viscosity represents a maximum value, and actual viscosity may be lower. Therefore, melt viscosity at the PT-conditions important for partial melting collisional orogenies, thus below 750° C and above 4-5 kbar, is lower than those expected in muscovite- or biotite dehydration-melting. As a result,

the low melt viscosity calculated for water assisted partial melting in collisional settings should not inhibit but enhance melt segregation.
We have proposed that dehydration melting as well as melting due to fluid infiltration may lead to important positive volume changes, and that melt viscosity does not counteract segregation of partial melts produced through infiltrating fluids. In the next chapter we address the consequences of volume changes on pore pressure, hydrofracturing and melt segregation, using primarily the Mohr-circle for discussion.

Development of high pore pressures: A discussion of the Mohr-Circle

The rheology and deformation-behaviour of a rock under high grade (migmatisation) conditions can be qualitatively described by use of the extended Mohr-circle diagram. The main point of our discussion concerns the formation of a high pore pressure, due to partial melting. The increasing pore pressure may induce hydraulic fracturing when the pressure oversteps certain rock intrinsic threshold values (e.g. tensile yield). An understanding of the concept of **hydraulic fracturing** may be very much improved through a discussion of the Mohr-circle.
Much of the following concepts is based on discussions in Kerrich (1986), Ramsay and Huber (1987), Twiss and Moores (1992), Davidson *et al*. (1994) and Handy & Streit (1999). We use the nomenclature of Twiss&Moores (1992), who discuss the relationship between the maximal stress δ_1 and the normal of the fracture or foliation plane (not with the fracture or foliation plane itself).
Our discussion starts with the general concepts of the Mohr-circle, proceeds with simple cases of hydrofracturing in isotropic rocks and then advances to a discussion of more complex, anisotropic, migmatitic rocks.

General application to isotropic rocks:

The following discussion first deals with an ideal case of an isotropic rock, i.e. a chemically homogeneous rock devoid of cleavages, fissilities, foliations or fractures. Likely candidates for such a scenario are, for example, homogeneous mikritic limestone, monomict quartzite, or a homogeneous and fresh igneous rock, devoid of fractures, enclaves, differences in grain size and so on.
Figure 9 shows the setup for a Mohr-Circle discussion and the related physical situations in a rock (9a-c). The abscissa contains the **normal stress (δ_n)**, the ordinate the **shear stress (τ)**. δ_1 and δ_3 are the **maximal and minimal normal stresses** (usually compressive) respectively, which define the size of the Mohr circle. The **differential stress δ_D** ($\delta_1 - \delta_3$) is thus equal to the diameter of the Mohr-Circle. The **mean stress** is given by $(\delta_1+\delta_3)/2$, if $\delta_2 = \delta_3$, (or $(\delta_1 + \delta_2 + \delta_3)/3$ when δ_2 is $\neq \delta_3$) and is the midpoint of the Mohr-circle. The failure envelope is given by the linear Mohr-Coulomb-Criterion at positive normal stresses and by the parabolic Griffith-Criterion at tensile stresses (negative normal stresses). At high positive normal stresses, deformation is defined by the von Mises-Criterion, paralleling the abscissa. At positive normal stresses, deformation is compressive, at negative normal stresses it is extensional and if the shear stress (τ) equals zero, it is purely tensional. If the Mohr-Circle touches the Griffith or Mohr-Coulomb failure criteria, the rock fails brittle under an angle θ (angle between the maximal normal stress δ_1 and the normal to the failure plane). If deformation occurs according to the von Mises-Criterion, deformation is controlled by some kind of ductile flow. In the following discussion, we will call this specific envelop the **isotropic failure envelope (T_{iso})** as it holds only for isotropic rocks. This envelope is characteristic or accurate only for a certain rock type of specific grain size, at a given tempera-

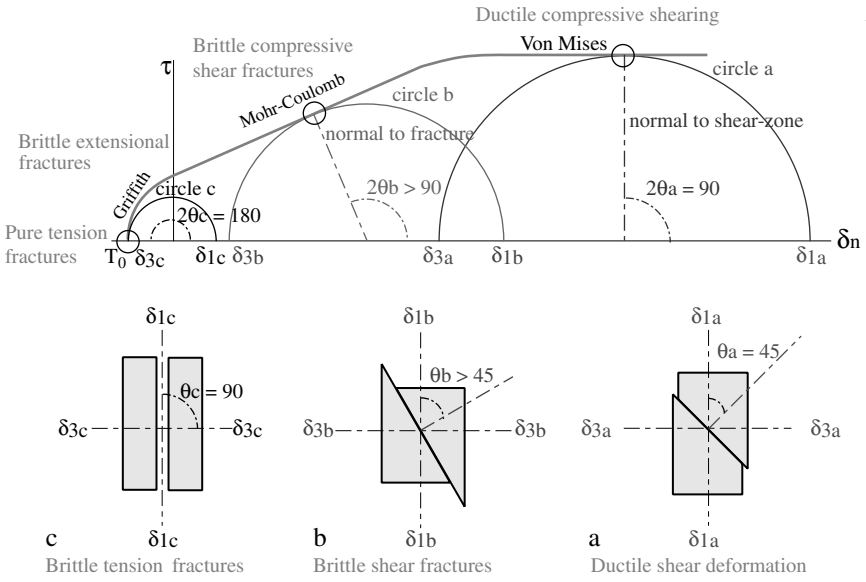

Fig. 9) Three different Mohr-Circles and their related physical situations in an ideal, isotropic rock. See text for discussion.

ture and strain rate. Thus the failure envelope depends on mineral content and temperature, and it is strain rate and grain size sensitive. Changing any of these variables leads to a change in the failure envelope. As an example, we could imagine that rising temperatures, smaller grain sizes, and smaller strain rates may all contribute to an enlargement of the von Mises-Criterion at the expense of the Mohr-Coulomb-Criterion, as a result of increasing importance of grain boundary diffusion. If the circle touches the envelope along the von Mises-Criterion, ductile deformation occurs along compressive shear-zones at an angle θ of 45° to δ_1 (Fig. 9a and circle a). Actually two planes with angle ± θ and different sense of rotation are possible, giving rise to conjugate sets of shear zones or fractures at an angle 2θ = 90°. If the Mohr-Coulomb-Criterion is touched, compressive deformation gives rise to brittle shear fracturing, in general at an angle θ of around 60° in most types of rocks (Fig. 9b and circle b, or the well known 30° between the fracture plain and δ_1). Touching the Griffith-Criterion gives rise to mixed mode tensile-shear fractures (or extensional shear fractures), except for the case when 2θ is 180° and the fracturing is purely tensile (no shear stress at this angle) and occurs parallel to the maximum compressive stress direction (Fig. 9c and circle c).

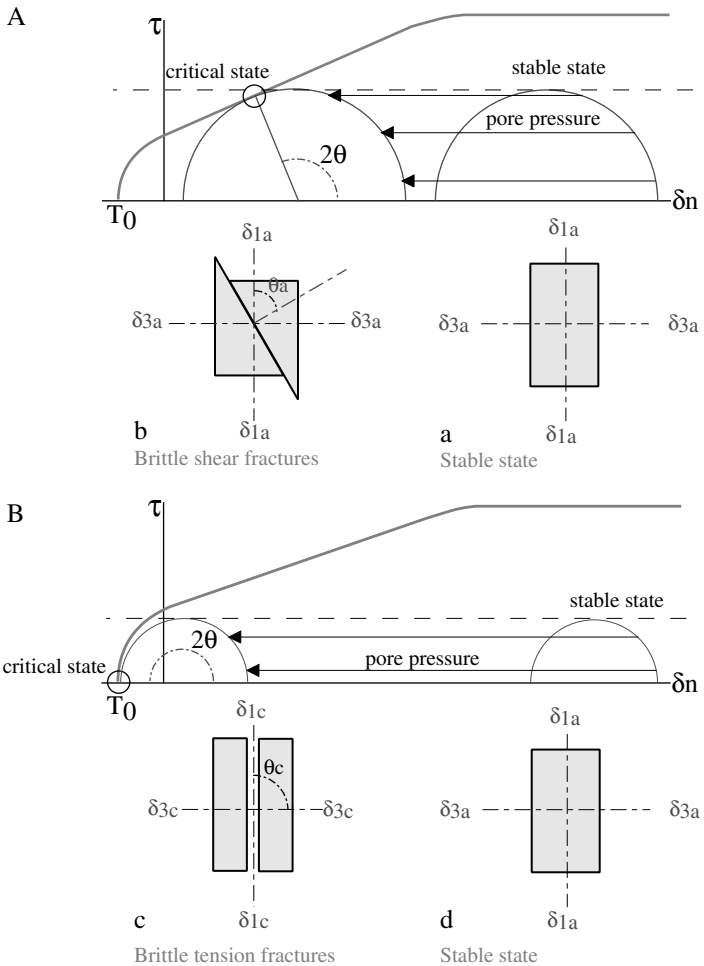

Fig. 10) Influence of fluid pressure on Mohr-Circle discussion and deformation. Figure a-d visualise the physical situation. See text for discussion.

Influence of pore fluid and fluid pressure

The above discussion strictly applies to isotropic dry rocks, neglecting the influence of pore fluid. In most real rocks however, the pore space is filled with a fluid phase, standing under a certain pressure. At the Earth surface, fluid pressure is close to hydrostatic, whereas deeper in the Crust it reaches lithostatic, or even higher pressures (overpressuring). In sedimentary basins, hydrostatic pressure was observed to approach lithostatic pressure at about 6 km depth (Woods and Walther, 1986). Reasons for this change are the decrease in pore space with depth and the related decrease in permeability. In addition, the liberation of fluids or liquids through dehydration and decarbonation reactions, or the take up of infiltrating fluid by the melt may lead to a build up fluid pressure (e.g. Dell'Angelo & Tullis, 1988; Davidson *et al*., 1994; Connolly *et al*., 1997; Rushmer, 2001; Labotka *et al*., 2002; Holyoke-III & Rushmer, 2002).

The influence of pore pressure on rock deformation can again be explained by the use of the Mohr-Circle. The main effect of the development of a fluid pressure is the reduction of the **applied stress** by an amount equal to the fluid pressure. The new **effective stress is** thus:

$$\delta_{eff} = \delta_{app} - P_f$$

(where P_f is fluid pressure and δ_{app} is the applied stress, thus one of the principal normal stresses $\delta_{1\text{-}3}$). As a consequence, the Mohr-Circle shifts towards the left, while the differential stress and the shear stress remain constant (i.e. no change of the size of the Mohr circle, see Fig. 10). The shift of the Mohr-Circle from a stable state towards the left may lead to brittle fracturing as the circle touches the failure-envelope (critical state) (Fig. 10A), even though deformation might be generally ductile at the pertaining conditions. This type of fracturing-process is called **hydrofracturing**. At middle to lower Crustal conditions (which may be important for anatectic processes in collisional setting), effective stresses may be very low because fluid pressures are close to lithostatic (equal δ3). In addition, fluid may not be able to flow rapidly due to the low permeability of rocks at these conditions (e.g. Davidson *et al*., 1994; Connolly *et al*., 1997; Manning and Ingebritsen, 1999). Both, high fluid pressures and low permeabilities favour hydraulic fracturing deep in the Crust, even at the conditions of partial melting. Whether hydrofracturing leads to compressive (Fig. 10A), or to extensional shear fractures (Fig. 10B) is dependent on the relative size of the Mohr-Circle, thus on the differential stress. At high pressure and temperature, differential stresses may

become low (e.g. Davidson *et al*., 1994), and a build-up of fluid pressure may therefore lead to extensional fracturing according to the Griffith-Criterion, or even to purely tensile fractures (Fig. 10B).
The discussion can also be applied to melt bearing systems, where the pore space is filled by a silicate liquid instead of a hydrous fluid. In this case we might speak of **melt induced fracturing** (or melt enhanced embrittlement (Davidson *et al*., 1994)) rather than hydrofracturing. In nature, melt induced fracturing may become important if melt formation is rapid and volume increasing as for example in muscovite dehydration melting or in fluid fluxed melting. If the additional volume of melt is formed more rapidly than the rock is able to accommodate (e.g. by melt drainage or by ductile deformation of the surrounding rocks), pore pressure will build up and eventually lead to melt induced fracturing (Davidson *et al*., 1994; Connolly *et al*., 1997; Rushmer, 2001; Holyoke-III & Rushmer, 2002). Melt induced fracturing may also occur as a result of deformation if strain rates are faster than migration (or escape) rates of fluids or liquids (Dell'Angelo & Tullis, 1988; Connolly *et al*., 1997). It may be especially important at the onset of partial melting (low melt fractions), because a connected melt network may not yet have established, and permeabilities are low. Once liquid pathways are established, the build-up of fluid pressure during on-going partial melting may result in a continuous drainage of melt (on geologic timescales). In detail, the process may be episodic, because deformation may destroy fluid pathways and fluid pressure may again rise until new fractures and connectivities are established (Davidson *et al*., 1994). Note that hydrofracturing may lead to brittle fractures in the partially molten rock itself as well as in the surrounding solid rocks: As long as melt is not able to drain from the local system the build up of liquid pressure may lead to fracturing of the unmolten host rock. Therefore, melt enhanced fracturing helps to accommodate the space problem created at the onset of partial melting.

Fracturing and hydrofracturing in anisotropic rocks

High grade gneisses, which are typical for collisional settings, have little in common with isotropic rocks. They are usually made up of different minerals with contrasting grain sizes and show anisotropy due to foliation or schistosity. Fracturing and hydrofractturing are therefore influenced by additional factors and cannot be explained by the above simple discussion of an isotropic rock.
Rock intrinsic anisotropies like foliations or schistosities in high grade gneisses are the weakest elements of a rock and are represented in the Mohr-Circle discussion by **anisotropic failure envelopes ($\mathbf{T_{aniso}}$)** (fracture reactivation curve of Ramsay & Huber (1987)), which are displaced towards lower shear stresses (Fig. 11). If deformation occurs along these secondary envelopes, **slip or failure happens parallel to the foliation**, instead of deforming at a certain critical angle θ. As in the isotropic case, ductile flow occurs along the von Mises part of the envelope and compressive or extensional shear fractures develop along the Mohr-Coulomb and along the Griffith parts respectively. $\mathbf{T_{aniso}}$ is similar in shape to $\mathbf{T_{iso}}$ but is displaced to lower shear stresses (at the same normal stress). It has been suggested that the von Mises-Criterion may be more strongly displaced at higher confining pressures than the other failure criteria (Ramsay & Huber, 1987). Thus, the shape of anisotropic envelopes may differ to some extent from the isotropic envelope (Fig. 11 and 12). The relative position of a secondary envelope depends on the development (intensity) of a foliation.
Figure 11 displays three envelopes, each representative for a foliation of differing intensity. For discussion we imagine a single protolith showing different intensities of foliation development; the rock with the strongest overprint (most effective foliation) shows the largest displacement towards lower shear stress. The orientation of the three foliation planes is assumed to be identical and is represented by the normal to the foliation in figure 11. However, the discussion of anisotropic failure envelops differs from that of the isotropic case: At a given differential stress, the normal cuts the innermost envelope (effective foliation) inside the Mohr circle and the rock is in an unstable state. Displacement then takes place **parallel to the foliation** (Fig. 11). The intermediate secondary envelope cuts the normal exactly at the intersection with the Mohr circle. The rock remains in a critical state and deformation parallel to the foliation may start as soon as one factor changes (change in orientation of the foliation or change in differential stress). The third envelop (ineffective foliation) is cut by the normal outside the Mohr circle. As a consequence, the rock remains in a stable state and no displacement occurs. Thus, if the development of the foliation is weak, the Mohr circle may touch $\mathbf{T_{iso}}$ before the foliation is in a critical position. Failure will then occur at an angle θ to δ_1 according to the isotropic failure envelop.
Note that first slip parallel to the foliation plane occurs if the foliation (or in this case also its normal) is at exactly 45° to δ_1 ($2\alpha a = 90°$). At this condition, flow occurs as soon as the circle touches the anisotropic envelope. If the foliation is at an angle < 45° > to δ_1, slip will occur correspondingly later. In this case, the circle cuts T_{aniso}, until the normal (dashed line in figure 12) reaches an unstable state (see e.g. circle A in figure 12). Therefore deformation parallel to the foliation will only occur if the normal is at an angle $\geq 2\alpha$ and $\leq 2\beta$ to δ_1, which corresponds to the shaded area in figure 12. For example, in a situation as depicted by circle A (and inset 12a), a rock would undergo ductile flow parallel to the foliation, because its normal is in an unstable state. Instead, in the situation depicted by circle B (and inset 12b), failure occurs along the isotropic envelop at an angle θb between the normal (point-dashed line in figure

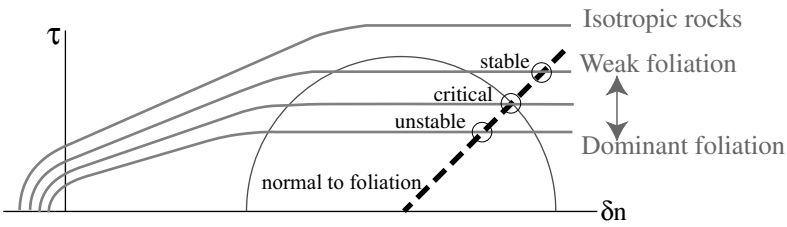

Fig. 11) Influence of rock anisotropy on Mohr-Circle discussion and deformation. See text for discussion.

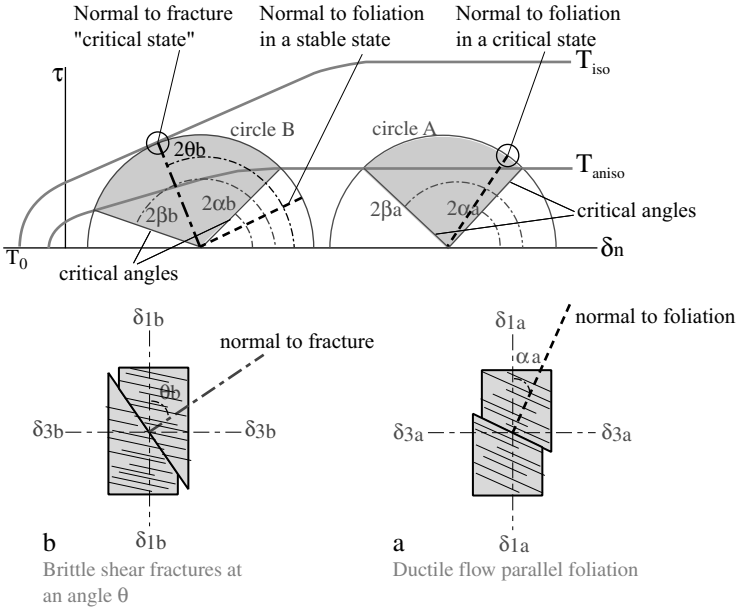

Fig. 12) Mohr-Circle discussion of anisotropic rocks. Figures a and b visualise the physical situation. See text for discussion.

12) and δ_1, because the orientation of the foliation is still in a stable state while the circle already touches the isotropic envelop. Note that in both situations the circle has considerably cut the anisotropic failure criterion before deformation occurs.
Hence, fracturing according to the anisotropic criterion is dependent on the differential stress, on the effectiveness of the foliation and on its orientation. In contrast to the isotropic case, $\mathbf{T}_{aniso}$ does not allow predicting the angle θ at which the rock fails, but it may allow a rough evaluation of the stress directions, if fracturing or rock-flow has occurred parallel to the foliation. The influence of fluid pressure is analogous to the isotropic case (shift of Mohr circle), and will not be discussed here. Instead we continue with the application of the above discussion to natural migmatites.

Application of the Mohr-Circle discussion to natural rocks.

In this paragraph we discuss how the distribution of partial melts in outcrop may be related to the Mohr-Circle. We focus on three typical features of synkinematic partial melting: a) foliation parallel leucosomes (Fig. 13, b) foliation discordant leucosomes (Fig. 14), c) melt filled shear zones (Fig. 15).
In natural anatectic rocks deformation depends on the relative sizes of the failure envelops and the Mohr-Circle. The size of the Mohr-circle is defined by the differential stress, which is supposed to be low in high grade terrains (e.g. Davidson *et al.*, 1994; Handy & Streit, 1999). Therefore the circle may tend to intersect the envelopes along the Mohr-Coulomb- or the Griffith-criteria (if pore pressure increases), rather than along the von Mises-Criterion (Fig. 16, circles A and B). On the other hand, increasing temperature and pressure should decrease the size of the envelopes, which therefore approach again the Mohr-Circle. Because deformation at high grade conditions generally occurs by ductile flow, the circle in unmolten rocks will generally intersect the envelope along the ductile von Mises Criterion. Whether flow occurs parallel to the foliation or at an angle θ to δ_1 depends on the distance between the isotropic and the anisotropic failure envelops. Note that a small distance increases the likelihood of failure along the isotropic envelope because only a small section of the circle intersects with the anisotropic envelop (shaded areas in fig. 16). We suggest that an increasing melt fraction may reduce the effect of the foliation, because slip will be preferentially partitioned into the melt rather than in the otherwise easily deforming micas. Therefore the isotropic failure envelope may again become more important with increasing melt fraction.
As the circle shifts to the left due to increasing pore pressure (melt fraction), the shaded area increases because of the slope of the Mohr-Coulomb-Criterion

Fig. 13) Foliation-parallel leucosomes in orthogneiss. Ticino, Switzerland. Pocket knife for scale.

Fig. 14) Leucosomes of different sizes crosscut the foliation. No displacement is observed, indicating pure tensional fracturing. Ticino, Switzerland. Shadow of right arm in upper left corner for scale.

Fig. 15) Near vertical, melt-filled shear-zones displace the main foliation of the mylonitic orthogneiss. Shear-sense indicates right side up movement. Width in the centre of the photograph is approximately 1.2 metre.

(increase of left part of the shaded area), and failure along the anisotropic envelope becomes more likely (compare different size of shaded areas of circles A and B in fig. 16). Therefore, increasing pore pressure due to partial melting may favour brittle fracturing parallel to the foliation. Circle B in figure 16 serves as an example: Failure parallel to the foliation does not occur if the normal to the foliation is situated in the unshaded sections of the circle, thus at angles of ca. 0-30° and 85-90° to δ_1 (or of 60-90° and 0-5° in respect to the foliation). Therefore failure parallel to the foliation would not occur at very low or at high angles of δ_1 to the foliation, but at all intermediate angles.

As long as slip occurs in the ductile domain (von Mises-Criterion), melt segregation parallel to the foliation may be unimportant (circle A in fig. 16) since melt fractions must be low (else the circle had shifted to the left into the brittle domain) and because deformation is ductile and compressive. Melt segregation parallel to the foliation may however become more important with increasing melt fraction and pore pressure, because the circle increasingly intersects the brittle Mohr-Coulomb-Criterion (circle B). Although still in the compressive field, brittle fracturing may result in the creation of voids, which favour melt segregation. Extensional fracturing (along the Griffith-Criterion), which is the most efficient way to enhance melt segregation (dilational sites!), is unlikely to occur parallel to the foliation for circles A and B in figure 16, because of their large sizes (compare small section of circle B that intersects with the envelop in the extensional domain). However, it may occur if the size of the Mohr-Circle is small compared to the size of the envelope, thus at low differential stresses (Fig. 16, circles C and D). Again, brittle extensional or even pure tensional fracturing parallel to the foliation is favoured with increasing distance between the two envelopes (circles C and D). Using circle D as an example, extensional fracturing parallel to the foliation (before the isotropic envelope is touched) occurs if the normal to the foliation is situated at ca 35-90° to δ_1 (or at 0-55° in respect to the foliation). Thus foliation parallel tensional fracturing is favoured by lower angles of the foliation to δ_1. Note that circles with a size intermediate between A and C may first touch the isotropic envelop in the extensional domain, what results in the formation of brittle extensional shear zones at an angle θ to δ_1.

With this background, we may now infer how concordant and discordant leucosomes and melt bearing shear zones are interpreted in terms of the Mohr-Circle:

Foliation-parallel leucosome: Foliation parallel leucosomes might be simply explained by rotation of discordant leucosome into parallelism with the foliation during ongoing deformation. However, the

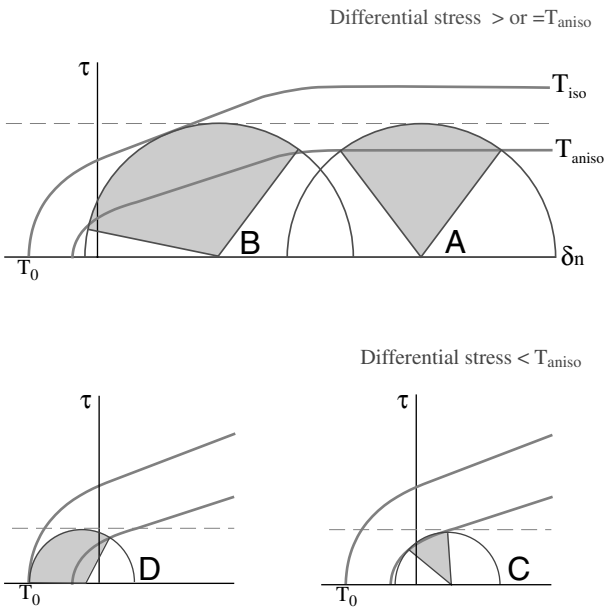

Fig. 16) Influence of differential stress on deformation processes. See text for discussion.

above discussion has shown that foliation parallel slip and related segregation is favoured with increasing distance between the isotropic and the anisotropic failure envelops. Thus, pervasive foliations favour foliation parallel segregation. In addition, an increasing melt fraction will favour this type of segregation, as it shifts the circle into the brittle domain, where the creation of voids may assist melt segregation. Note however, that with increasing melt fraction the effect of the foliation may decrease, because deformation partitions into the melt domains (see discussion above). Foliation-parallel melt segregation is in addition favoured by angles near 45° of the foliation to δ_1 in the compressive domain, and by an increasing spectrum towards lower angles in the extensional domain. Small differential stresses, as they are probably characteristic for the middle- to lower crust (Davidson *et al*., 1994; Handy & Streit, 1999), favour melt segregation in general, because the lead to extensional brittle deformation, which enhances segregation through dilatancy.

Foliation discordant leucosomes: Discordant leucosomes are favoured if no or only a weak rock-anisotropy exists, and at high melt fractions. Both factors lead to a decrease in distance between the isotropic and the anisotropic envelops, and therefore increase the likelihood of deformation according to the isotropic criteria. Discordant melt segregation is in addition favoured by angles ≠ 45°of the foliation to δ_1 in the compressive domain, and by high angles in the extensional domain. Purely tensional fractures parallel to δ_1, which do not result in slip along the failure plane (shear stress τ equals 0), are favoured by low differential stresses (see fig. 16).

Melt filled shear-zones: Melt filled shear zones are favoured by brittle and extensional deformation. As noted above, it is not yet clear if compressive ductile shear-zones may result in melt segregation (Mancktelow, 2002). Like discordant leucosomes, melt filled shear zones are favoured by angles ≠ 45°of the foliation to δ_1 in the compressive domain, and by high angles in the extensional domain.

The shear-zones must originally have developed at an angle of 45-30° to δ_1, and are often observed as conjugate sets with opposing shear-sense in the field (Oliver and Barr, 1997; Butler *et al*., 1997; Kisters *et al*., 1998; Mancktelow, 2002). Usually, the conjugate shear-zones show a near symmetric distribution in respect to the foliation, with one set of shear zones at an angle + ϕ, and the other with —ϕ. This geometry may be explained by two scenarios:

In **pure shear**, the foliation develops at 90° to the principal stress direction. If pore pressure increases, shear-zones at an angle ϕ = ± 30-45° to δ_1 develop, thus at 45-60° to the foliation (Fig. 17A). If the angle between the shear-zone and the foliation is < 45°, as

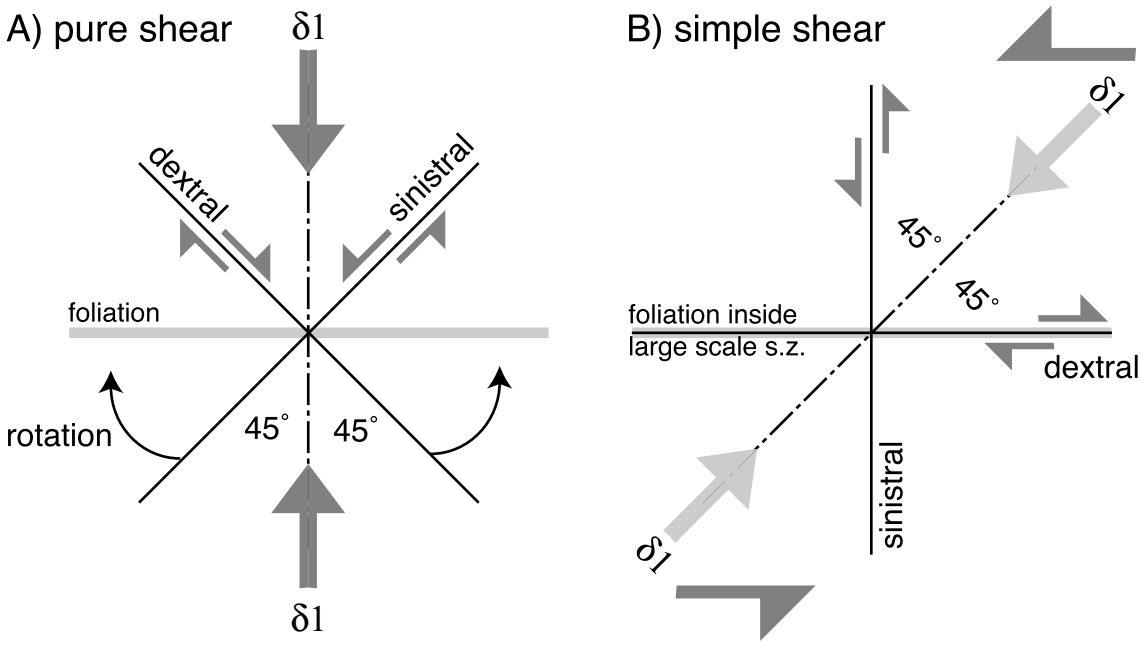

Fig. 17) Development of shear-zones as a result of pure or simple shear. See text for discussion.

is often observed (chapter 1), the shear-zone must have rotated towards the foliation during ongoing compression.
If local-scale shear-zones develop during **simple shearing** (Fig. 17B), δ_1 must be at an angle of 45° to the large scale shear-zone boundary. Due to progressive rotation, the dominant foliation inside this shear-zone becomes near by parallel to the shear-zone boundary. Therefore, if the shear-zones are themselves oriented at 45 or 30° to δ_1, they will be parallel and perpendicular to the dominant foliation, or at an angle of 15 and 75°, respectively (see Mancktelow, 2002). For perfect simple shear this initial orientation does not change with deformation. However, with an increasing pure shear component of deformation, the asymmetric distribution of the shear-zones gets increasingly symmetric and is finally indistinguishable from the distribution obtained in perfect pure shear deformation (Mancktelow, 2002). Therefore, conjugate shear-zones at an equal angle to the foliation, but with opposite sign and sense of rotation imply a high component of overall pure shear (compressive) deformation.
Note that those shear-zones which are oriented parallel to the foliation in simple shear, may be an alternative explanation for the occurrence of foliation-parallel leucosomes. In large scale shear-zones (e.g. regional scale), foliation parallel melt segregation may be an expression of the simple shear component. The conjugate set that should form at 75-90° to the foliation may be inhibited, because the foliation is at 45° to δ_1 and deformation parallel to this plane is preferred.

Conclusions

Review of relevant literature demonstrates that the rheology of a solid rock is strongly influenced by the occurrence of partial melting. The presence of melt leads to a general weakening of a solid rock, the extent of which is governed by the melt fraction, the melt distribution (topology) and the deformation mechanism. Melt topology on the other hand is influenced by surface energies of melt and solids, and by deformation.
Whether melt produced through water assisted melting is stagnant and remains in the local system, or if it in contrary is able to leave the systems, has been discussed quite controversially in the past. Based on a new model, we propose that water assisted melting, triggered by the influx of fluid in an open system, is strongly volume increasing. In order to accommodate the developing space problem and melt-overpressure, this must result in hydrofracturing and melt drainage, or in a more continuous type of melt drainage. Furthermore, estimated melt viscosity is lowest near the water saturated solidus, which should effectively promote movement and escape of melt from a partially molten rock. Thus, if migmatites developed as a result of fluid infiltration at some temperature above the water saturated solidus, the melt observed in outcrop must not necessarily originate from the immediate surrounding. The widespread dikes or smaller granitic bodies that often accompany such migmatite terrains (see chapter 1) suggest that melt segregation and escape may really have been effective.
The macroscopic distribution of melt on the outcrops may be explained by an extended discussion of the Mohr-circle. The base of discussion is the suggestion that partial melting may often be volume increasing, giving rise to melt overpressure and hydrofracturing (melt enhanced embrittlement). The discussion shows that the melt distribution is mainly influenced by the orientation of the principal stress axes and by the existence and orientation of rock anisotropies like foliations. In general, strongly developed foliations with an orientation near 45° to the principal stress increase the occurrence of foliation parallel melt segregation. By contrast, high angles between foliation and principal stress axes favour fracturing at an angle near 45° to the foliation, giving rise to discordant leucosomes or discordant melt filled shear-zones.

References

Arzi, A. A. (1978): Critical phenomena in the rheology of partially melted rocks. Tectonophysics 44, 173-184.

Berman, R. G. (1988): Internally consistent thermodynamic data for minerals in the systen Na_2O-K_2O-CaO-FeO-Fe_2O_3-Al_2O_3-SiO_2-TiO_2-H_2O-CO_2. Journal of Petrology 29, 445-522.

Brown, M., Averkin, Y. A. & McLellan, E. L. (1995): Melt segregation in migmatites. Journal of Geophysical Research 100/B8, 15655-15679.

Brown, M. & Solar, G. S. (1998): Shear-zone systems and melts: feedback relations and self-organization in orogenic belts. Journal of Structural Geology 20/2/3, 211-227.

Brown, M. & Solar, G. S. (1999): The mechanism of ascent and emplacement of granite magma during transpression: a syntectonic granite paradigm. Tectonophysics 312, 1-33.

Butler, R. W., Harris, N. B. W. & Whittington, A. G. (1997): Interactions between deformation, magmatism and hydrothermal activity during active crustal thickening: a field example from Nanga Parbat, Pakistan Himalayas. Mineralogical Magazine 61, 37-52.

Clemens, J. D. & Droop, G. T. R. (1998): Fluids, P-T paths and the fates of anatectic melts in the earth's crust. Lithos 44, 21-36.

Connolly, J. A. D., Holness, M. B., Rubie, D. C. & Rushmer, T. (1997): Reaction-induced microcracking: An experimental investigation of a mechanism for enhancing anatectic melt extraction. Geology 25/7, 591-594.

Davidson, C., Schmid, S. M. & Hollister, L. S. (1994): Role of melt during deformation in the deep crust. Terra Nova 6, 133-142.

de Capitani, C. & Brown, T. H. (1987): The computation of chemical equilibrium in complex systems containing non ideal solutions. Geochemica et Cosmochemica Acta 51, 2639-2652.
Dell'Angelo, L. & Tullis, J. (1988): Experimental deformation of partially melted granitic aggregates. Journal of Metamorphic Geology 6, 495-516.
Dimanov, A., Wirth, R. & Dresen, G. (2000): The effect of melt distribution on the rheology of plagioclase rocks. Tectonophysics 328, 307-327.
Dingwell, D. B. (1999): Granitic melt viscosities. In: Castro, A., Fernàndez, C. & Vigneresse, J. L. : Understanding granites: Integrating new and classical techniques Geological Society, London, Spezial publications 168. Geological Society, London, 27-38.
Handy, M. R. & Streit, J. E. (1999): Mechanics and mechanisms of magmatic underplating: inferences from mafic veins in deep crustal mylonite. Earth and Planetary Science Letters 165/3-4, 271-286.
Holness, M. B. (1995): The effect of feldspar on quartz-H_2O-CO_2 dihedral angles at 4 kbar, with consequences for the behaviour of aqueous fluids in migmatites. Contrib. Mineral. Petrol. 118, 356-364.
Holtz, F., Becker, A., Freise, M. & Johannes, W. (2001a): The water-undersaturated and dry Qz-Ab-Or-system revisited. Experimental results at very low water activities and geological implications. Contrib. Mineral. Petrol. 141, 347-357.
Holtz, F., Johannes, W., Tamic, N. & Behrens, H. (2001b): Maximum and minimum water contents of granitic melts generated in the crust: a reevaluation and implications. Lithos 56, 1-14.
Holyoke-III, C. W. & Rushmer, T. (2002): An experimental study of grain scale melt segregation mechanism in two common crustal rock types. Journal of Metamorphic Geology 20, 493-512.
Johannes, W. & Holtz, F. (1996): Petrogenesis and experimental petrology of granitic rocks. . Minerals and Rocks . Springer Verlag, Berlin, 335 pp.
Kerrich, R. (1986): Fluid infiltration into fault zones: Chemical, isotopic and mechanical effects. PAGEOPH 124/1/2, 225-268.
Kisters, A. F. M., Gibson, R. L., Charlesworth, E. G. & Anhaeusser, C. R. (1998): The role of strain localisation in the segregation and ascent of anatectic melts, Namaqualand, South Africa. Journal of Structural Geology 20/2/3, 229-242.
Kohlstedt, D. L. (2002): Partial melting and deformation. In: Karato, S.-i. & Wenk, H.-R. : Plastic deformation of minerals and rocks Reviews in Mineralogy & Geochemistry 51. Mineralogical Society of America, , 121-135.
Labotka, T. C., Anovitz, L. M. & Blencoe, J. G. (2002): Pore pressure during metamorphism of carbonate rock: effect of volumetric properties of H2O-CO2 mixtures. Contrib. Mineral. Petrol. 144, 305-313.
Laporte, D. & Watson, E. B. (1995): Experimental and theoretical constraints on melt distribution in crustal sources: the effect of crystalline anisotropy on melt interconnectivity. Chemical Geology 124, 161-184.
Mancktelow, N. s. (2002): Finite-element modelling of shear zone development in viscoelastic materials and its implications for localisation of partial melting. Journal of Structural Geology 24, 1045-1053.
Manning, C. E. & Ingebritsen, S. E. (1999): Permeability of the continental crust: Implications of geothermal data and metamorphic systems. Reviews of Geophysics 37/1, 127-150.
Mecklenburgh, J. & Rutter, E. H. (2003): On the rheology of partially molten synthetic granite. Journal of Structural Geology 25/10, 1575-1585.
Ochs-III, F. A. & Lange, R. A. (1997): The partial molar volume, thermal expansivity, and compressibility of H_2O in $NaAlSi_3O_8$ liquid: new measurements and an internally consistent model. Contrib. Mineral. Petrol. 129, 155-165.
Oliver, N. H. S. & Barr, T. D. (1997): The geometry and evolution of magma pathways through migmatites of the Halls Creek orogen, Western Australia. Mineralogical Magazine 61, 3-14.
Paterson, M. S. (1995): A theory for granular flow accommodated by material transfer via an intergranular fluid. Tectonophysics 245, 135-151.
Paterson, M. S. (2001): A granular flow theory for the deformation of partially molten rocks. Tectonophysics 335/1/2, 51-61.
Philpotts, A. R. (1990): Principles of igneous and metamorphic petrology. . Prentice Hall, New Jersey, 498 pp.
Prince, C., Harris, N. & Vance, D. (2001): Fluid-enhanced melting during prograde metamorphism. Journal of the Geological Society of London 158, 233-241.
Ramsay, J. G. & Huber, M. I. (1987): The techniques of modern structural geology. Volume 2: Folds and fractures. 1997 ed. 2. Academic Press, London, 700 pp.
Rosenberg, C. L. (2001): Deformation of partially molten granite: a review and comparison of experimental and natural case studies. Int. J. Earth Science (Geol. Rundsch.) 90, 60-76.
Rosenberg, C. L. & Berger, A. (2001): Syntectonic melt pathways in granitic gneisses, and melt-induced transitions in deformation mechanisms. Phys. Chem. Earth (A) 26/4-5, 287-293.
Rushmer, T. (2001): Volume change during partial melting reactions: implications for melt extraction, melt geochemistry and crustal rheology. Tectonophysics 342, 389-405.
Rutter, E. H. & Neumann, D. H. K. (1995): Experimental deformation of partially molten Westerly granite under fluid-absent condtitions, with implications for the extraction of granitic magmas. Journal of Geophysical Research 100/B8, 15697-15715.
Sawyer, E. W. (2000): Grain-scale and outcrop-scale distribution and movement of melt in a crystallising granite. Transactions of the Royal Society of Edinburgh: Earth Sciences 91, 73-85.
Sawyer, E. W. (2001): Melt segregation in the continental crust: distribution and movement of melt in anatectic rocks. Journal of Metamorphic Geology 19, 291-309.
Tullis, J. (2002): Deformation of granitic rocks: Experimental studies and natural examples. In: Karato, S.-i. & Wenk, H.-R. : Plastic deformation of minerals and rocks Reviews in Mineralogy and Geochemistry 51. Mineralogical Society of America and Geochemical Society, , 51-96.
Tullis, J., Yund, R. & Farver, J. (1996): Deformation enhanced fluid distribution in feldspar aggregates and implications for ductile shear zones. Geology 24/1, 63-66.
Twiss, R. J. & Moores, E. M. (1992): Structural geology. W.H. Freeman and Company, New York, 532 pp.
Vigneresse, J. L. & Tikoff, B. (1999): Strain partitioning during partial melting and crystallizing felsic magmas. Tectonophysics 312, 117-132.
Woods, B. J. & Walther, J. V. (1986): Fluid flow during metamorphism and its implication for fluid-rock ratios. In: Walther, J. V. & Wood, B. J. : Fluid-rock interactions during metamorphis. Springer Verlag, New York, 89-108.

Relics of eclogite-facies metamorphism in the southwestern Lepontine area (Central Alps of Switzerland/Italy). A combined discussion on petrology, structures and thermodynamic computation

Thomas Burri

Abstract

High-pressure rocks in the Central Alps reflect the subduction of the European Margin below the northwards drifting Apulian plate. Although many rocks must have reached eclogite-facies conditions, only some have (partly) preserved eclogite-facies assemblages. Thermodynamic computation indicates that the preservation of eclogite-facies assemblages is strongly dependent on the amount of water stored in a rock at eclogite-facies conditions, on the amount of water that infiltrates during ascent, and on the conditions along a PT-path where the minimum water content is reached. Whereas mafic rocks reach their minimum water content at eclogite-facies conditions, pelitic rocks may reach this point only during ascent of a rock, which explains why pelitic rocks only rarely preserve evidence of eclogite-facies conditions.

Several new eclogite samples, found in the southwestern Lepontine area, suggest that eclogite-facies metamorphism in the Central Alps was more widespread than previously thought. Metaeclogites have typically developed chemical subdomains as a result of a varying degree of fluid-undersaturation reached during ascent. Three samples, which were studied in detail, suggest that pressures in excess of 20 kbar were reached during the Tertiary. Phase assemblages and reaction textures in several other samples suggest similar high-grade conditions. These new occurrences allow identification of a new Mergoscia-Onsernone-unit, which underlies the Maggia nappe in the Maggia-Onsernone area. This indicates that Maggia-, Tambo- and Suretta nappes belong to the Briançonnais domain, whereas the underlying units belong to the Alpine TAC (Tectonic Accretion Channel) or to the Southern European Margin.

Introduction

In a collisional orogenic cycle, rocks experience very different PT-conditions until they are finally exhumed to the earth surface and can be studied by geologists. It is a common feature of collisional mountain belts that much of the high-pressure (HP) history is preserved as sparse eclogite-facies relics that escaped retrogression, whereas the vast majority of the rocks enclosing such relics only testify for amphibolite-facies or lower-grade conditions.

HP-information is most often found in mafic to ultramafic rocks, probably because their high-pressure assemblages are almost entirely composed of anhydrous phases like clinopyroxene, garnet, olivine, orthopyroxene, kyanite and rutile. Triggering retrograde reactions in mafic and ultramafic rocks along the exhumation path then requires significant infiltration of external fluids. As a consequence, HP-relics are often found to be armoured by a mantle of amphibolite-facies rocks of similar composition but higher water-content (Heinrich, 1983; Terry *et al*., 2000). In addition, the relics frequently display different types and degrees of retrogression, as an effect of restricted fluid influx. Although the discovery and recognition of such relics in the field is often a problem, a correct interpretation of their history from observed phase assemblages and mineral compositions is even more complicated. In theory, thermodynamic computation provides an elegant approach to investigate the significance of the observed phase relations. In reality, however, modelling of amphibole-bearing assemblages is associated with relatively large uncertainties, due to inconsistencies inherent in available thermodynamic data (including solution models) for amphibole. These are mainly related to the sparse experimental data, and the complexity of amphibole mineral-chemistry. Nevertheless, thermodynamic computation of phase diagrams may provide a good means to investigate observed phase relations and reaction textures. In this study, we apply thermodynamic computation, using the internally consistent dataset of Holland and Powell (1998), to investigate

in detail the history of three (meta) high-pressure rocks from the Lepontine area of the Central Alps of Switzerland. Using computed phase diagrams we investigate observed phase relations and reaction textures. We then use this information to interpret the history and significance of several other rocks from the southwestern Lepontine area that display phase relations and reaction textures similar to the ones observed in the three samples. This leads to a new inventory of Alpine high-pressure rocks and to a new concept of high-pressure metamorphism in the Central Alps.

Geology of the study area

The European Central Alps have formed as a result of late Cretaceous and Tertiary subduction and continent-continent collision. The Lepontine area, which is part of the Central Alps, forms the highest-grade metamorphic core of the Alpine chain (also called Lepontine Dome). The Lepontine is composed of a stack of continental basement nappes, separated from each other by shear zones and / or post-Variscan sediments, the latter usually very reduced and discontinuous in the south. The metamorphic grade generally increases to the south and complicates discrimination of pre-Variscan (polymetamorphic), from post-Variscan (monometamorphic) sediments. The central part of the Lepontine area is defined by roughly flat-lying structures, whereas the northern and southern limits are defined by structural steep belts. The Southern Steep Belt (SSB), which is important in the context of this study, was formerly known as the root-zone of the Central Alps, because the nappe stack turns into a vertical or even overturned position, interpreted as the root of the orogen (Fig. 1B). Towards the south, the SSB grades into the Insubric Line, which is the locality where the high grade metamorphic area of the Lepontine is juxtaposed with the Southern Alps, an area that has only undergone low grade metamorphism during the

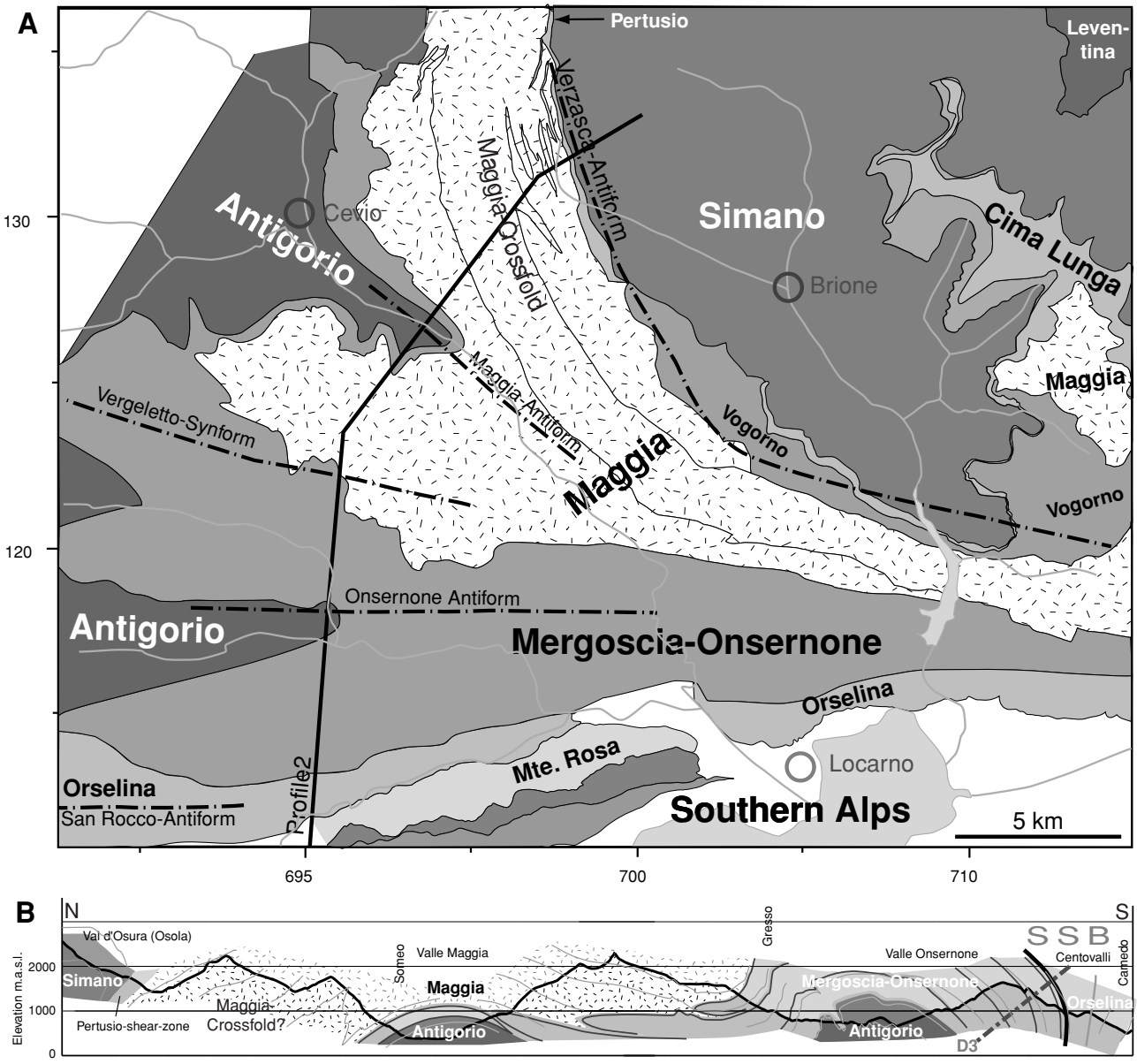

Fig. 1 A) Tectonic overview of the study area. Limits of tectonic units in part taken from published and unpublished geological maps and own data. B) Profile through the study area. For Location of profile trace see fig. 1A. SSB = Southern Steep Belt.

Tertiary. Structural work has demonstrated that the formation of the SSB is related to a phase of backfolding and backthrusting (Milnes, 1974; Heitzmann, 1987; Schmid *et al*., 1989). The metamorphic grade in the Lepontine area varies from upper greenschist in the north, to upper amphibolite-facies in the south (Niggli and Niggli, 1965; Wenk, 1975; Trommsdorff, 1980; Engi *et al*., 1995). Although amphibolite-facies metamorphism is dominant in this area, relics of high-pressure and (sparse) granulite-facies metamorphism are found as well (see reviews in Frey and Ferreiro-Mählmann, 1999; Frey *et al*., 1999). High-pressure relics do not occur throughout the Lepontine, but are constrained to a few distinct units, the Adula-, the Cima-Lunga-, the Orselina- and Mergoscia-Arbedo units (further to the west, the Saas Fee-Zermatt-, and the Antrona units also contain HP-relics). It is as yet unclear how closely these units are related, and if they should be considered as separate units. The strong correspondence in lithostratigraphy as well as tectonic position suggests a close genetic relationship. Although HP-relics are relatively frequent in these units, the majority of rocks displays amphibolite-facies assemblages, attributed to a Barrovian-type overprint of the Central Alps. It is questionable whether the dominance of amphibolite-facies rocks is merely a result from the strong Barrovian overprint, or if only a minority of rocks have in fact undergone high-pressure metamorphism. Recent research interprets the high-pressure units of the Central Alps as a lithospheric mélange (Trommsdorff, 1990) or as a Tectonic Accretion Channel (TAC) (Engi *et al*., 2001): Slices of continental and oceanic crust may delaminate from subducting units and become part of the subduction channel, which may also incorporate mantle fragments. This process leads to the formation of heterogeneous units with a very fragmentary character, remarkable for the presence of high-pressure rocks. The size of individual fragments may be on the order of decimetres to kilometres. Internal deformation of the TAC and differential back-flow of included fragments may lead to different PT-paths, each characteristic for the pertinent fragment (Engi *et al*., 2001). Slices of the TAC may delaminate from the subduction channel and become emplacement as a heterogeneously composed nappe onto the "common" nappe stack. The high-pressure Adula and Cima-Lunga units, which are inhomogeneous composites of metaigneous and meta-sedimentary rocks as well as mafic and ultramafic fragments, are examples (and theoretical basis) of such processes.

The study area contains two units with typical TAC-characteristics, the Cima-Lunga and the Orselina units (Fig. 1A), both composed of a heterogeneous mélange of continental, ophiolitic and mantle fragments (e.g. Knup, 1958; Fumasoli, 1974; Pfiffner and Trommsdorff, 1998). It has been noted in the past that high-pressure rocks in the study area may not be restricted to these two units, but also occur in the Mergoscia-Onsernone unit (Fig. 1A and B, Forster, 1947; Kobe, 1956; Colombi and Pfeifer, 1986; Pfeifer *et al*., 1991). There, however, their occurrence is restricted to several bodies of variable size, that are part of heterogeneous trails. The latter are commonly wedged-in between larger masses of granitoid orthogneiss. The present study, which mainly focuses on the Megoscia-Onsernone unit, investigates on several already known localities and new occurrences.

Set-up of thermodynamic computation

Thermodynamic computation of phase diagrams has become a frequently applied tool in petrology. Unfortunately, computation of phase assemblages in mafic systems is in general associated with larger uncertainties, due to the very complex amphibole solid solution. As a result of the low number of experiments in chemically complicated amphibole-bearing systems, standard-state data and solution models for amphiboles are relatively poorly constrained. Although complex activity models and calibrations for amphiboles have been published (Mäder and Berman, 1992; Mäder *et al*., 1994; Dale *et al*., 2000; Okamoto and Toriumi, 2004), or are part of internally consistent thermodynamic databases (Berman, 1988; Holland & Powell, 1998), amphibole is usually computed by the use of simplified subsystems like calcic-amphiboles (tremolite-pargasite-tschermakite) and alkali-amphiboles (glaucophane) (e.g. López Sánchez-Vizcaíno *et al*., 2003). As a result, thermodynamic computation of amphibole-bearing systems is still associated with substantial uncertainty. Predicted amphibole compositions, and thus also those of the coexisting phases, must be considered with reasonable caution. Nevertheless, thermodynamic computation may provide important information on the evolution of studied samples.

For thermodynamic computation we used programs Theriak and Domino of de Capitani and Brown (1987) in combination with the internally consistent dataset of Holland & Powell (1998) (HP98). Models used for computation are all from the HP98 database, except for ilmenite, computed as an ideal binary ilmenite-geikielite solution, and glaucophane, computed as a one-site glaucophane - Fe-glaucophane solid-solution, with a_{glau} equal to $(X_{Mg})^3$. According to HP98, Ca-amphibole was calculated as non-ideal tremolite-ferrotremolite-tschermakite-ferrotschermakite-pargasite-ferropargasite solid-solution. Glaucophane and Ca-amphibole solid-solutions show commonly overlap in PT-space at blueschist-facies conditions. Furthermore, Ca-amphibole is predicted to unmix into two amphiboles at lower pressures. For simplicity, areas with two stable Ca-amphiboles are not separately indicated in the computed phase diagram.

Correspondence between thermodynamic computation and experiments

To test the applicability of the thermodynamic data, we apply thermodynamic computation to published experimental data on high-pressure phase relations in basaltic systems (Poli, 1993; Liu *et al*., 1996). Bulk compositions of these two experiments and of the other computed rocks are given in table 1. For computation we assumed complete fluid-saturation over the entire diagram (fluid being pure H_2O). Oxygen-fugacities are similar to those reported for the experiments (QFM_{Calc}vs. QFM_{Exp} in Liu *et al*. (1996), IMR_{Calc} vs. NNO_{Exp} in Poli (1993)). Figures 2 and 3 show the computed phase relations, with the location of phases of interest outlined by different patterns and lines. Experimental data points, labelled with the observed experimental assemblage, are added for comparison. Note that calculated phase relations at temperatures above ca. 700-750˚C must be considered with caution, because a melt phase may be present at these conditions (at 800˚C in the experiment of Liu *et al.* (1996)). At low melt fractions, however, calculated phase relations do not differ much from that of the melt bearing systems (except for the melt phase itself).

Overall, agreement between experimental data and computed phase relations is reasonable, but several discrepancies are notable: (A) Chloritoid is not computed for either of the two studied compositions, in contrast to the experimental results. We note, however, that chloritoid present in the experiment of Liu et al. (1996) is considered as metastable by the authors. Stable chloritoid, as obtained in the experiment of Poli (1993), was again not predicted. Instead excess alumina is attributed to kyanite rather than chloritoid. As a test we varied the symmetric Margules term of the molecular chloritoid solution model (+1000 J in HP98). A relatively small Margules term of -20 kJ was adequate to reproduce the experimental data. (B) Neither zoisite nor epidote occurred in the experiments of Liu et al. (1996), in line with the computed phase relations. Poli (1993) reported epidote-group phases for all of his experimental data points, in contrast to the computed predictions. This suggests that zoisite stability is underestimated in the computation by nearly 4 kbar at 650˚C. Note that no attempt is reported from Poli to differentiate zoisite from epidote (clinozoisite). (C) The calculated chlorite-stability field is very restricted between 7-12 kbar. Instead, a mixed-layer smectite-chlorite phase was reported to occur in the experiments of Poli (1993). We suggest, that amphibole-stability may be overestimated at the expense of chlorite in the above pressure range. (D) A minor discrepancy further exists between computed and observed stability of plagioclase. Plagioclase stability in the experiments of Liu et al. (1996) at 700˚C appears unrealistically low. The lack of plagioclase from this temperature upward may however be related to the dissolution of plagioclase into a melt phase.

Despite these inconsistencies, overall agreement between experiment and computed phase relations is reasonable. Bearing in mind the reported shortcomings in computation, calculated phase-diagrams may be used to infer PT-paths and to interpret reaction textures observed in thin section.

Sample	Poli	Liu	TN307	BOR2	Cap6	PORC1
SiO2 wt.%	52.38	50.1	53.24	48.82	43.12	47.67
TiO2 wt.%		1.25	0.74	2.33	1.64	1.84
Al2O3 wt.%	16.93	14.8	22.25	16.00	16.77	19.39
Fe_{Tot} wt.%	11.43	13.89	8.0663	13.86	15.38	9.92
MnO wt.%		0.22	0.11	0.18	0.29	0.10
MgO wt.%	7.13	7	2.32	5.92	9.76	6.14
CaO wt.%	10.05	11.1	0.55	8.48	12.18	10.51
Na2O wt.%	3.21	2.57	0.76	2.74	1.01	2.55
K2O wt.%		0.14	5.34	0.19	0.02	0.74
P2O5 wt.%			n.d.	0.29	0.07	0.16
SUM wt.%	101.13	101.07	93.38	98.82	100.24	99.01
Ba ppm	n.d.	n.d.	n.d.	42.80	20	158.50
Cr ppm	n.d.	n.d.	n.d.	115.46	103	37.88
Cu ppm	n.d.	n.d.	n.d.	91.57	18	33.89
Nb ppm	n.d.	n.d.	n.d.	7.96	5	8.97
Ni ppm	n.d.	n.d.	n.d.	53.75	62	16.95
Pb ppm	n.d.	n.d.	n.d.	<7	<5	<7
Rb ppm	n.d.	n.d.	n.d.	<3	<5	11.96
Sr ppm	n.d.	n.d.	n.d.	59.72	76	897.14
V ppm	n.d.	n.d.	n.d.	311.54	n.d.	402.72
Y ppm	n.d.	n.d.	n.d.	61.71	42	30.90
Zn ppm	n.d.	n.d.	n.d.	113.47	66	73.76
Zr ppm	n.d.	n.d.	n.d.	213.00	24	103.67

table 1) Chemical composition of used samples. Samples "Poli" from (Poli, 1993), "Liu" from (Liu et al., 1996), "TN307" from (Nagel, 2000). Other samples are from this study, with chemical analysis using standard XRF-techniques.

Fe_{Tot} calculated as Fe_2O_3

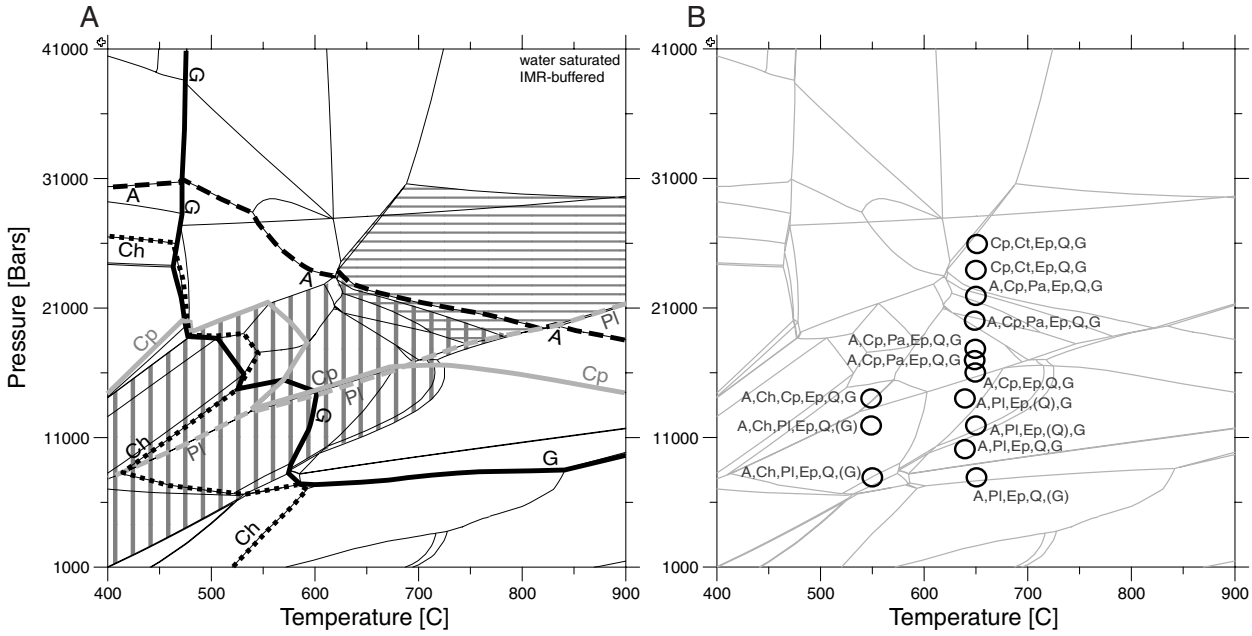

Fig. 2) Computed phase relations (A) and experimental data points (B) for the experimental composition of Poli (1993). Several phase-stability limits are denoted by different types of lines. Vertically striped area denotes presence of epidote or zoisite, horizontal stripes the presence of kyanite.
Abbreviations used in this and the following diagrams: A=Amphibole, B/Bt=Biotite, Cd=Cordierite, Ch=Chlorite, Coe=Coesite, Cp=Clinopyroxene, Ct=Chloritoid, Ep=Epidote, G=Garnet, Gl=Glaucophane, IL=Ilmenite, Kf=K-feldspar, Ky=Kyanite, Lw=Lawsonite, m=melt, Mt=Magnetite, Op=Orthopyroxene, Pa=Paragonite, Ph=Phengite, Pl=Plagioclase, Q=Quartz, Rt=Rutile, Si=Sillimanite, Tc=Talc, Ti=Titanite, Zo=Zoisite

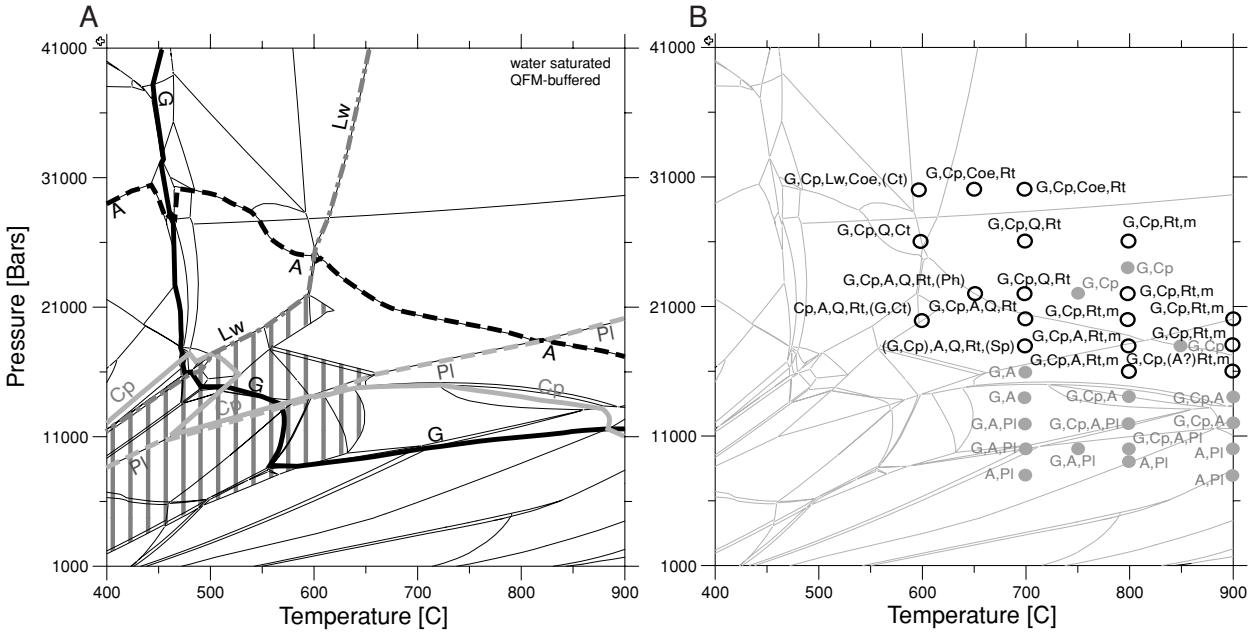

Fig. 3) Computed phase relations (A) and experimental data points (B) for the experimental composition of Liu et al. (1996). Several phase-stability limits are denoted by different types of lines. Vertical striped area denotes presence of epidote or zoisite. Abbreviations as in Fig. 2.

Contrasting evolution of pelitic and basic rocks during subduction and collision

The mineralogical evolution of mafic rocks undergoing subduction and subsequent exhumation is mainly dependent on the bulk composition and on the PT-path. Of great importance are characteristics like the fluid content of the system (e.g. Rubie, 1990), fluid composition and oxygen fugacity. Fluid-undersaturated rocks portray a very different mineralogical evolution compared to water-saturated rocks for several reasons: (a) The limited amount of fluid in the system leads to a decrease in the mode of hydrous phases and to a related increase in less hydrous or anhydrous phases. This may also significantly influence phase compositions of coexisting phases. (b) In the absence of a interstitial fluid phase, reaction rates may become very sluggish, especially in the absence of notable deformation and with declining temperatures. Incomplete reactions and formation of subdomains may be the result of such undersaturation (Burri, 1999; Zeming *et al*., 2000; Tóth *et al*., 2000; Nakamura, 2002; Brouwer and Engi, 2004). Hence, depending on the initial fluid content of a rock (at the onset of subduction), and

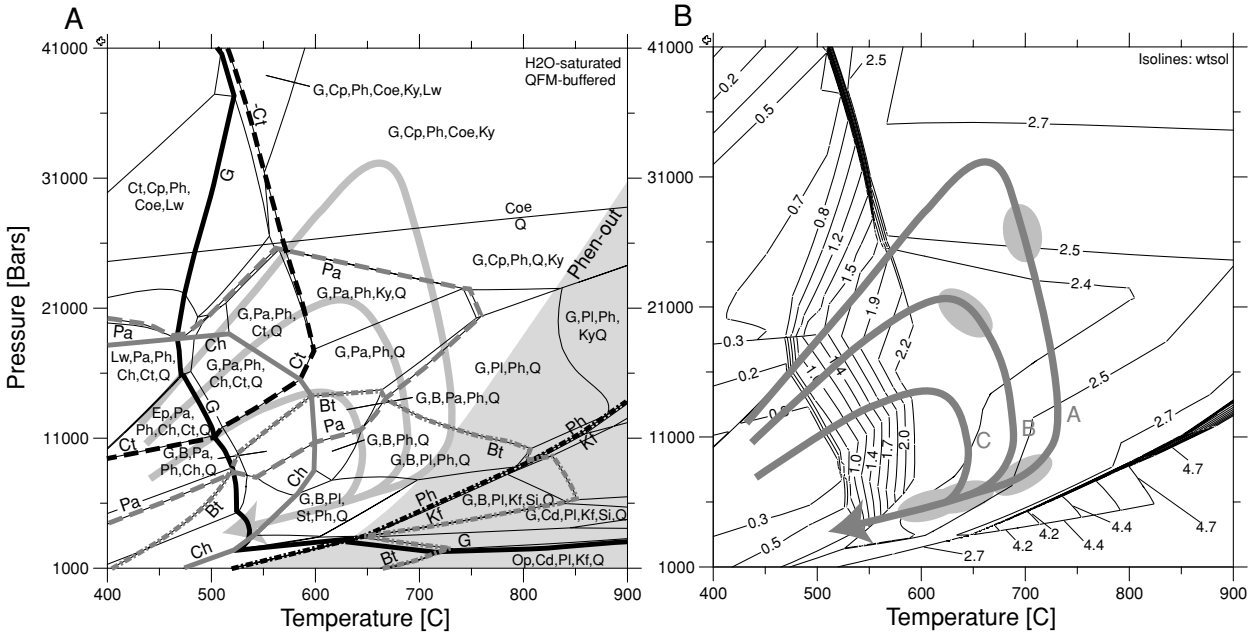

Fig. 4) (A) Phase relations calculated for the pelitic rock composition of Nagel (2000) (table1). Shaded area (Phen-out) denotes the presence of melt as a result of phengite dehydration melting (taken from experimentally determined phengite dehydration-melting of Hermann & Green (2001)). Several phase-stability limits are denoted by different types of lines. (B) Isolines of H_2O-change in wt.% in respect to the assemblage with the highest water contents. Positive numbers denote loss of fluid from the hydrous solids. See text for discussion. Shaded ellipses denote localities where fluid undersaturation is reached along the PT-path, assuming closed system.

depending on if, and when a rock becomes fluid undersaturated during a collisional cycle, its mineralogical evolution may be very different.

Assuming fluid-saturation at the onset of subduction, the PT-point where fluid-undersaturation is reached depends mainly on the PT-path, on the chemical system and on porosity, the latter typically being very low in high-grade metamorphic rocks. As a consequence and in the absence of fluid infiltration, rocks may become fluid-undersaturated (very) soon after the first (retrograde) hydration reaction is encountered. In general, retrograde hydration reactions occur with decreasing temperatures during exhumation, but the exact location depends on the bulk composition and on the PT-path. Below, we compare a pelitic (Fig. 4A and B, rock composition given in table 1) and a mafic system (Fig. 5A and B, composition of Poli (1993), see table 1) in respect to fluid-escape and fluid-consumption. Figures 4+5A are the phase diagrams calculated for the respective systems, figures 4+5B the corresponding isolines for the weight of solids, which reflect the release or consumption of fluid. For better overview, the isolines are recalculated into change in weight-%

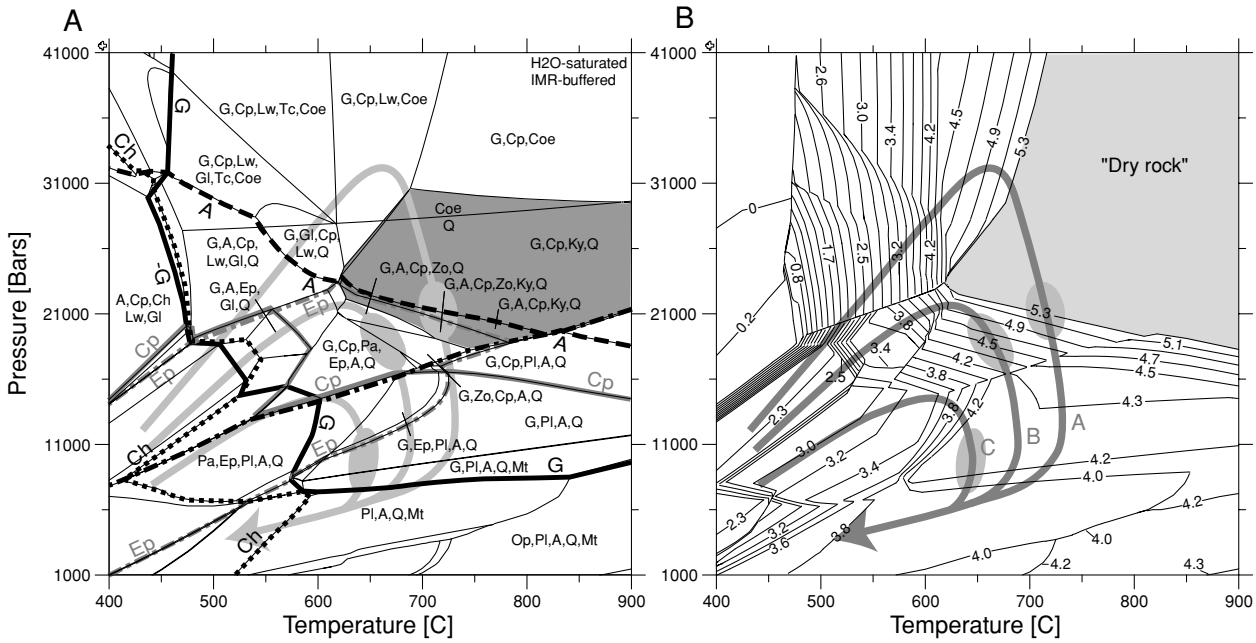

Fig. 5) A) Phase relations calculated for the mafic rock composition of Poli (1993) (table1). Dark shaded area denotes the presence of kyanite. Several phase-stability limits are denoted by different types of lines. B) Isolines of H_2O-change in wt.% in respect to the assemblage with the highest water contents. Positive numbers denote loss of fluid from the hydrous solids. See text for discussion. Shaded ellipses denote localities where fluid undersaturation is reached along the PT-path, assuming closed system. Shaded field denotes the area where fluid is restricted to grain boundaries only.

of solids, in respect to the most hydrated (heaviest) assemblage (positive numbers depict release of fluid from the hydrous solids). Loss or consumption of water (in wt.%) along a PT-path can thus be directly read from the diagrams. Three different PT-paths are inserted for discussion.

(a) Pelitic rocks:

Assuming an initial very small amount of fluid in the system, pelitic rocks following any of the three PT-paths remain fluid saturated along the whole prograde path as a consequence of the crossing of continuous and discontinuous dehydration reactions (fig. 4A and B). The hydrous phases phengite and paragonite remain stable in the system towards high to very high-pressures. Due to the positive slope of the phengite dehydration-melting reaction, phengite in pelitic rocks remains stable towards high temperatures at high-pressures, and phengite breakdown may only occur during a late phase of exhumation (Patiño Douce and McCarthy, 1998; Hermann and Green, 2001). The field where partial melt is present as a result of phengite breakdown is depicted as a shaded area in figure 4A. Because the melt-present area only slightly interferes with the PT-paths considered, the discussion is not affected by the occurrence of partial melting. We note, however, that paragonite dehydration-melting may occur at lower temperatures, and that fluid liberated by this reaction is consumed by the melt. Disregarding dehydration-melting, it is evident from figure 4B that retrograde reactions are likely to occur during ascent of pelitic rocks: Rocks following path A become very slightly fluid-undersaturated shortly after P_{Max} is reached (upper ellipses in fig. 4B). During further exhumation, they again reach fluid saturation between ca. 16 to10 kbar. A similar scenario holds for rocks following paths B and C. This indicates that retrograde attainment of fluid-saturation may be the reason why metapelitic rocks usually show a dominant amphibolite-facies overprint. The reappearance of fluid in the system again enhances reaction rates, leading to effective resetting of the high-grade assemblage. Furthermore, prograde loss of fluid is much less extensive than in basic systems (compare fig. 4B with 5B), and the amount of H_2O remaining in the system is thus larger. Fluid-conserving reactions may therefore be important during exhumation of metapelites. In this context it is revealing that garnet zoning in metapelitic rocks from the Cima-Lunga high-pressure unit document an exhumation path (see chapter 7).

(b) Mafic rocks

Similar to the pelitic rocks, mafic rocks remain fluid buffered along the whole prograde path as a consequence of the prograde overstepping of continuous and discontinuous dehydration reactions (Fig. 5A and B). Along the prograde path much fluid is released through continuous reactions, which is apparent in the figure because fluid is usually released over a considerable PT-interval rather then by abrupt steps like in the pelitic system. In contrast to pelitic rocks, hydrous phase do not remain stable over the entire PT-range.

On the retrograde path, two scenarios are found: rocks not reaching eclogite-facies conditions (paths B and C) retain fluid in the system, the amount of which largely depends on the mode of amphibole at amphibole-eclogite-facies conditions (Fig. 5A and B). The mode of amphibole is essentially a function of the maximum pressure reached along the PT-path. If no fluid-infiltration occurs, fluid-undersaturation is reached between P_{Max} and T_{Max} along the decompression path (ellipses on paths B and C in fig. 5B). Rocks that reach eclogite-facies conditions contain the anhydrous assemblage garnet-omphacite-rutile ± kyanite. As soon as such rocks leave the eclogite field during exhumation, any small amount of fluid that has remained in the system is immediately consumed to form amphibole along garnet-omphacite contacts (ellipse on path A in figure 5B). This reaction texture is often observed in eclogites (see below or in Heinrich (1983)). Due to the lack of fluid, further retrograde reactions are inhibited, and the next reaction that may occur is the fluid absent reaction

Grt + Omph + Qtz = Plag + diopside-rich Cpx (1)

The common preservation of the HP-assemblage in rocks unaffected by fluid infiltration or deformation demonstrates that retrograde reactions may be extremely sluggish in completely dry systems, even at high temperatures and pressures.

To demonstrate the effect of fluid-undersaturation we have calculated two diagrams each for the retrograde part of the PT-paths (Fig. 6), assuming (1) complete fluid saturation along the PT-path ("wet"), (2) only a small amount of fluid present along the grain boundaries ("dry", ca. 0.2 wt%). This means that rocks that encounter the first hydration reactions will soon run out of fluid in the "dry" scenario. We calculated each path from the maximum pressure reached along the path, until the three paths join at 6 kbar/625°C. As a consequence, all fluid-saturated systems contain the same phase assemblage at the end of the calculated path (compare A-B-C-wet in fig. 6).

Path A: In the water-saturated case ("wet"), the change in the phase assemblage along the PT-path reflects the changing metamorphic facies, from the assemblage Grt-Cpx-Qtz(Coe) at eclogite-facies conditions, to Am-Grt-Cpx-Qtz at amphibole-eclogite-facies conditions, Grt-Am-Pl-Qtz at garnet-amphibolite conditions, and finally Am-Pl-Qtz at amphibolite-facies conditions. In the absence of fluid infiltration ("dry"), the assemblage along the PT-path differs strongly from the wet case: Amphibole never becomes an important constituent of the rock, whereas Cpx and Grt remain stable at all conditions along the retrograde PT-path. Furthermore, orthopyroxene becomes stable with decreasing pressure. Three major reactions can be read from the diagram:

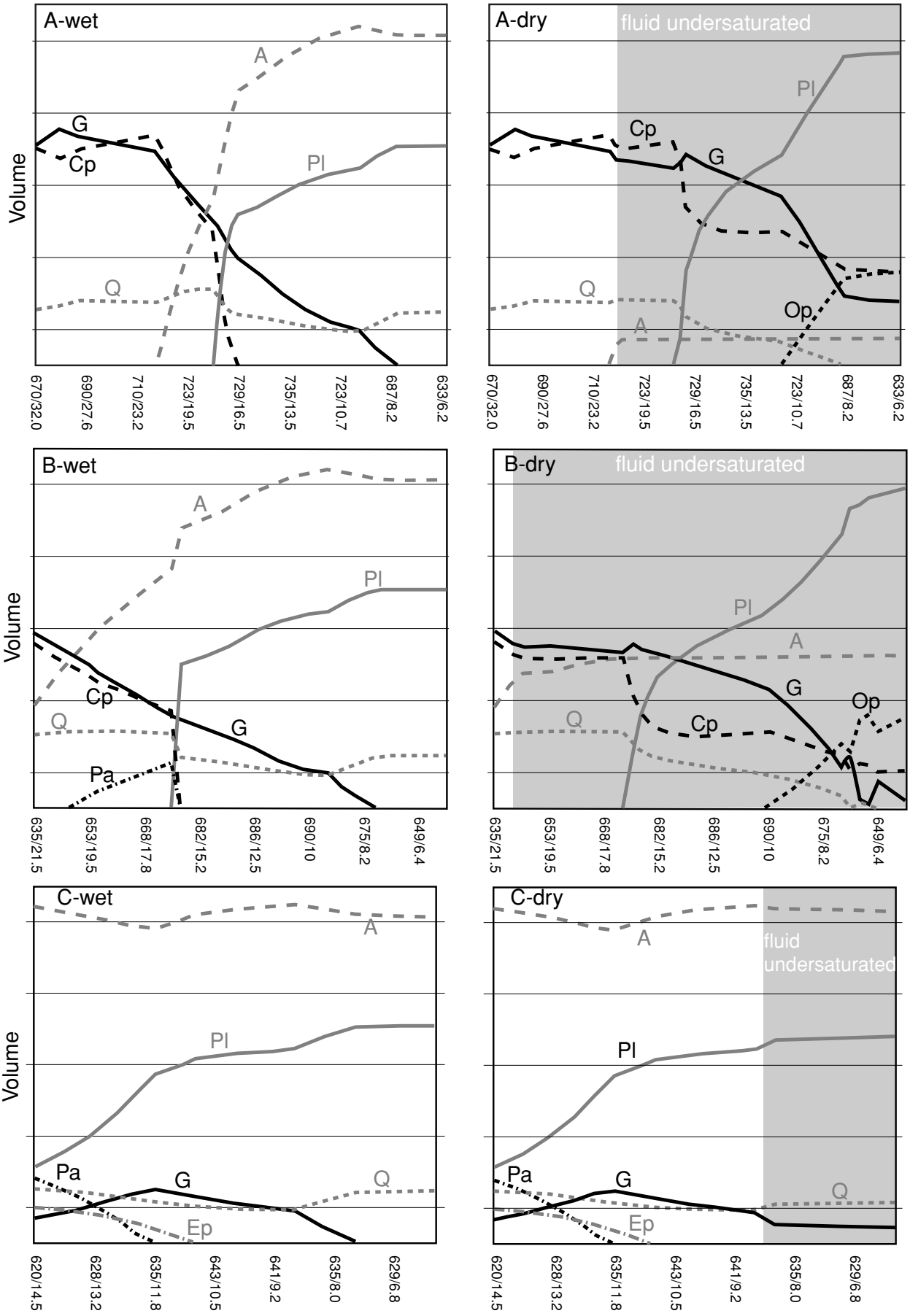

*Fig. 6) Changes in modal composition along PT-paths A-C of fig. 4 and 5. Only main phases are shown. Diagrams labelled A-C-**wet** were calculated assuming complete water saturation. Diagrams termed A-C-**dry** were calculated assuming only a small amount of fluid in the pore space. See text for further discussion.*

(a) The small amount of pore fluid assumed to be present when leaving eclogite-facies conditions is used up in the reaction

Cpx + Grt = Am + Qtz (2)

which leads to rims of amphibole along Cpx-Grt-grain boundaries. (b) During further decompression, plagioclase becomes stable, and a reaction similar to

Cpx1 + Qtz = Pl + Cpx2 + Grt (3)

may occur. The amount of garnet used up in this reaction is minor. This reaction is responsible for the formation of diopside(Cpx2) + plagioclase-symplectites replacing former omphacite (Cpx1). In a next step, garnet and quartz are continuously replaced by plagioclase, which may produce the well known plagioclase coronas around garnet. Decreasing temperatures may then inhibit a fourth major reaction

Grt + Qtz + Cpx = Pl + Opx (4)

that would give rise to a typical granulite-facies assemblage Cpx + Grt + Pl + Qtz + Opx + Am, at temperatures well below 700˚C!

Path B: The general relations along path B are similar to the evolution described for path A. The main difference is the persistence of amphibole as a major phase over the whole calculated PT-path, in the "wet" as "well" as in the dry case. Again, garnet and clinopyroxene remain stable towards much lower conditions in the water-undersaturated case compared to water-saturation, and again orthopyroxene becomes stable with decreasing pressure. Fluid-undersaturated rocks at the end of the cycle display an assemblage typical of upper amphibolite to granulite facies conditions (Cpx + Opx + Pl + Am ± Grt).

Path C: The water-saturated and undersaturated cases are very similar to each other. Under dry conditions the lack of fluid allows the survival of a small amount of garnet. Because pressures nowhere oversteps 15 kbar, clinopyroxene stability is not reached and amphibole remains the most abundant phase in the rock throughout the PT-cycle.

Some conclusions: In system where fluid is only allowed to escape but not to infiltrate (actually our "dry" case), the amount of volatiles stored in a mafic rock is essentially a function of the amount of amphibole that remains in the system. The calculated amount of zoisite is insignificant and was not shown in figure 6 for simplification). The mode of amphibole is directly related to the pressure reached along a PT-path, so that rocks following path C retain the highest amount of amphibole (and thus of H_2O stored in hydrous solids), whereas rocks following path A become almost anhydrous. Similarly, fluid-undersaturation along all three "dry" PT-paths is related to the growth of amphibole, which acts as an effective fluid sink. Because reaction rates may become very sluggish at fluid-undersaturated conditions, we suggest that the mineral assemblage observed in mafic rocks reflects the conditions at which fluid undersaturation was reached along the PT-path. Therefore, the PT-conditions documented by different mafic rocks depends essentially on the pertinent PT-path. Further retrogression is limited to rocks affected by (a) fluid infiltration, (b) deformation, (c) fluid conserving reactions at increased temperatures.

As an effect of fluid-undersaturation, retrograde reactions may be limited to restricted chemical subsystems or subdomains (Grandjean, 2001; Brouwer & Engi, 2004). The evolution of such domains may be computed by choosing a new representative bulk composition. In dry eclogites for example, omphacite may form such a chemical subsystem, producing diopside-rich clinopyroxene and plagioclase. Other subdomains may be related to the replacement of the high-pressure phases lawsonite, garnet, kyanite, zoisite and phengite (e.g. Rubie, 1990; Zeming *et al*., 2000; Tóth *et al*., 2000; Terry *et al*., 2000; Grandjean, 2001; Nakamura, 2002; Brouwer & Engi, 2004). The kinetic barrier for retrograde reactions to occur, may be overcome if exhumation is accompanied by differential stresses, which could deliver the activation energy necessary. Since retrograde reactions during exhumation are generally volume increasing, incipient retrograde reaction may impose an internal stress. Once initiated, retrograde reactions may thus result in small-scale deformation processes, which may allow fluid-infiltration along grain boundaries or microfractures. Infiltration of fluid then leads to intense resetting of the high-grade assemblage (Engvik *et al*., 2001).

Typical textures found in partially retrogressed eclogites are very spectacular symplectites (see below). The formation of these symplectites is likely related to fluid-deficiency and/or metastable overstepping of a reaction. Fluid-deficiency leads to only localised reactions inside specific domains. Local-scale *in-situ* replacement with no or only very restricted addition of external components (from outside the domain) is thus favoured. The metastable overstepping of a reaction increases the difference in Gibbs-free energy between the metastable high-grade assemblage and the actual stable assemblage. In very dry eclogite systems, overstepping may thus be large. Then, as soon as deformation or limited fluid infiltration triggers a reaction, the reaction is driven by the associated large decrease in Gibbs-free energy. Therefore, symplectites may evolve quickly until the fluid is consumed and reaction rates become sluggish again.

Case studies

All studied samples are parts of variable-sized mafic bodies, which are situated inside larger masses of unspectacular orthogneiss. Commonly, the mafic bodies are part of inhomogeneous trails of metasedimentary, mafic and ultramafic rocks. Except for the larger mafic body at Capoli, which stretches some tens of metres, the eclogite relics are no larger than a few meter across. Below, we present detailed data on three selected suites of samples. To evaluate the metamorphic history of the samples, we have computed phase diagrams and isopleths of garnet composition. Because manganese was excluded from computation, analysed garnet-compositions were normalised to the three components almandine, pyrope and grossular. Analysed garnet-profiles were then compared with the computed garnet composition, and the respective PT-paths were deduced. The bulk composition of the studied samples, shown in table 1, was determined using standard XRF-analyses.

Capoli

Sample description

The mafic to ultramafic body at Capoli has been mentioned for a considerable time. A few authors even mention the occurrence of ultramafic samples with assemblages similar to Alpe Arami near Bellinzona (Kobe, 1956; Pfeifer *et al*., 1991). The investigated samples show different degrees of retrogression, with some samples preserving the eclogite-facies assemblage Cpx + Grt + Rt, others showing extensive development of Cpx-Pl, or Amph-Pl-symplectites, and still others showing only the stable amphibolite-facies assemblage Amph-Pl-Qtz-Sph/Ilm. Figure 7 shows products of early retrograde reactions among a relatively well-preserved eclogite-facies assemblage consisting of garnet, omphacite and rutile. Three types of retrograde reactions are observed: a) Formation of an amphibole rim of some µm to some tens of µm along Grt-Cpx and Grt-Grt grain boundaries. b) Formation of plagioclase-clinopyroxene symplectites along Cpx-Cpx grain boundaries. c) Formation of ilmenite at the expense of rutile grains in the matrix.
Formation of amphibole-rims requires the presence of pore water, or the infiltration of water along grain boundaries. The restricted extent of amphibole formation indicates an only very limited influx of fluid or the survival of a grain boundary fluid during HT-HP-metamorphism. Figure 8 displays spectacular details of the Cpx-Pl-symplectite: A very fine-grained symplectite starts to form at the contact with the decaying omphacite grain, and gets increasingly coarser grained with increasing distance from the contact. This suggest continuous recrystallisation of (relatively) "older" symplectite while nucleation of the fine grained symplectite continues. With time, the worm like structures may coalesce into larger grains and may form more characteristic mineral shapes. Clinopyroxene changes composition from omphacite in the preserved grains, to diopside-rich compositions in the symplectite. In only weakly retrogressed domains (fig. 7), omphacite and symplectite-clinopyroxene show a considerable overlap in composition whereas two clearly distinct populations occur in stronger retrogressed domains (fig. 8). Amphibole occurs as inclusions in garnet as well as along garnet grain boundaries (see figs. 7 and 8). Amphibole composition of inclusions varies from magnesiohornblende to pargasite, while retrograde amphibole varies between pargasite to edenite. Additional inclusions in garnet are omphacite (identical composition as matrix grains), as well

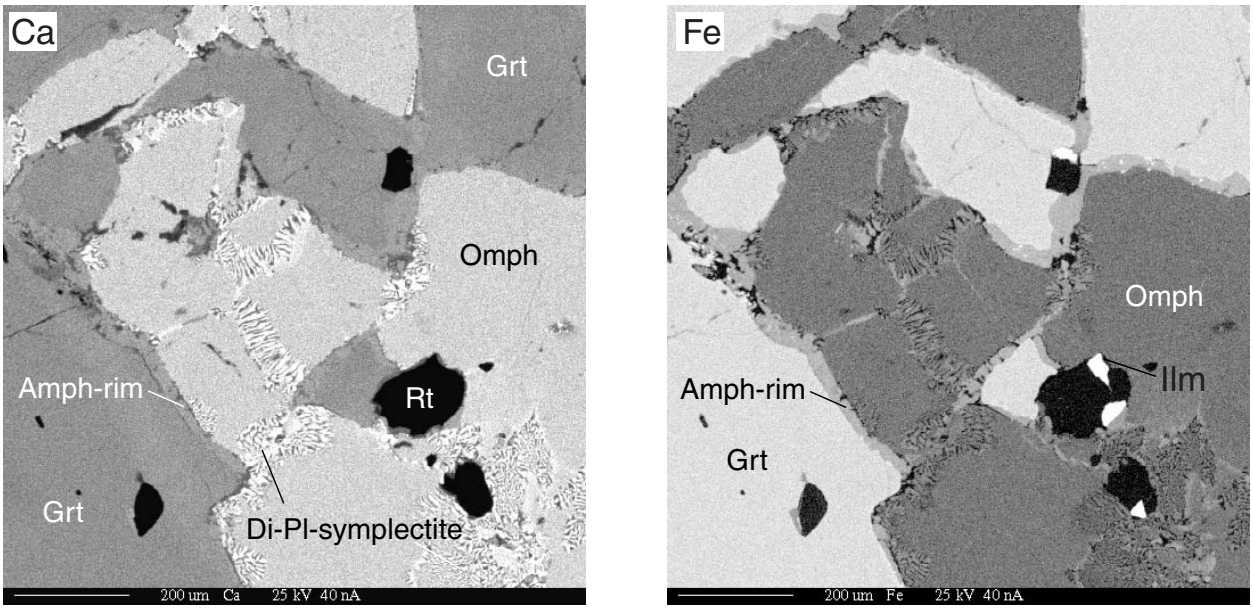

Fig. 7) X-ray maps for Ca (left) and Fe (right) in sample Cap7. The maps show products of incipient retrograde reactions during decompression. Amphibole rims grow along Grt-Grt and Grt-Cpx grain boundaries. Fine-grained symplectites of Di-rich clinopyroxene and plagioclase grow along Grt-Cpx and Cpx-Cpx grain boundaries.

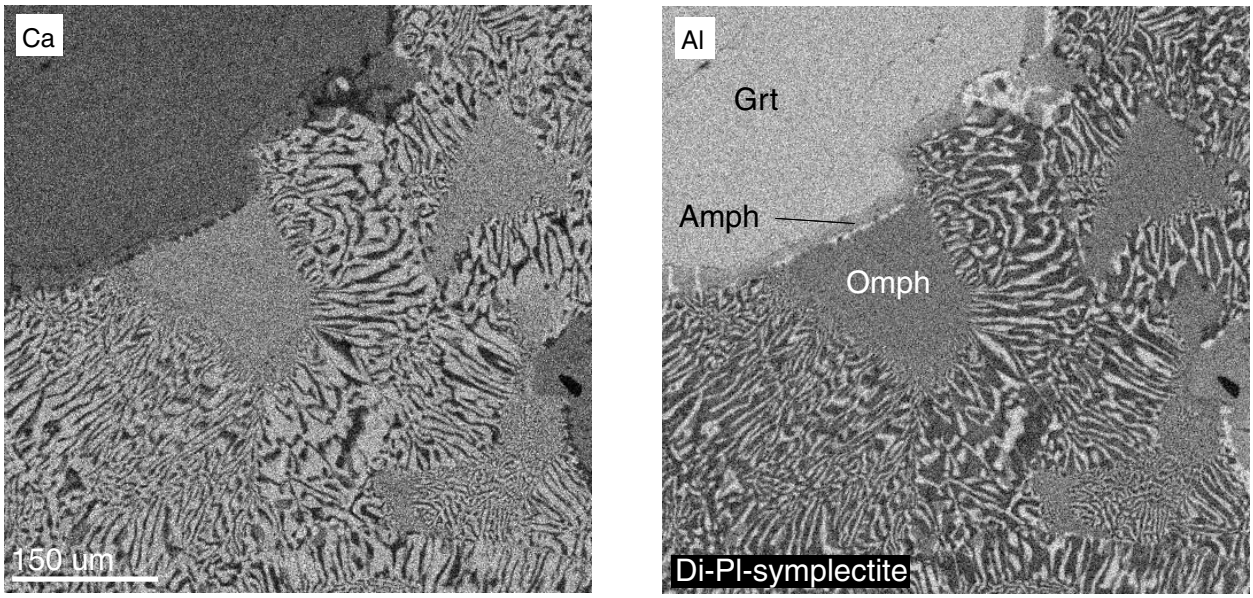

Fig 8) X-Ray maps for the elements Ca (left) and Al (right) in sample Cap7. Symplectites of Di-rich clinopyroxene and plagioclase. Note coarsening of the symplectites from the site of nucleation towards the former grain boundaries, probably as a result of recrystallisation.

as a few grains of zoisite ($X_{pist} = 0.1$), allanite, pyrite and chalcopyrite. Conspicuously, garnet cores show countless inclusions of rutile needles (similar to those reported from the Adula nappe Heinrich, 1983), usually without preferred orientation. Such rutile-rich garnet cores are typical for many high-pressure rocks of the area and are probably a critical indicator of high-pressure. Due to lack of experimental data, we can only speculate about the significance of the rutile needles (as Heinrich (1983) some twenty years ago). If the Ti-content of garnet would increase with pressure, the rutile needles could result from exsolution from an originally high-Ti garnet. On the other hand, small rutile needles may be typical for the conditions of early subduction, and may simply be inclusions.

Figure 9 shows a back-scattered electron image (BSE) of sample Cap6. Although garnet zoning is roughly concentric, irregularities indicate a complicated growth history. Notable is the frequent, discordantly cut garnet zoning, which indicates resorption of particular grains. Because no garnet should be resorbed in the eclogite facies field, this feature indicates a (continuous?) recrystallisation of a garnet-omphacite-rutile matrix. Although zoning is clearly visualised by BSE-acquisition, analysed garnets show slightly irregular, but essentially flat profiles in major elements (fig. 10A). Nevertheless, cores are slightly enriched in grossular, whereas almandine shows a slight increase towards the rim and pyrope and grossular a slight decrease. Fe/Mg-ratios have a tendency to increase from 1.1-1.15 in the core to 1.25-1.45 at the rims. Like garnet, omphacites show

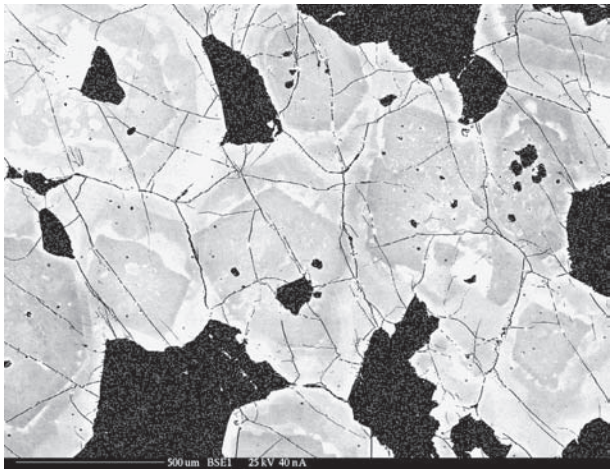

Fig. 9) Back-scattered electron BSE-Image in sample Cap6. Light phase with internal zoning is garnet. The zoning indicates several stages of garnet growth and garnet resorption, interpreted as continuous recrystallisation at eclogite-facies conditions.

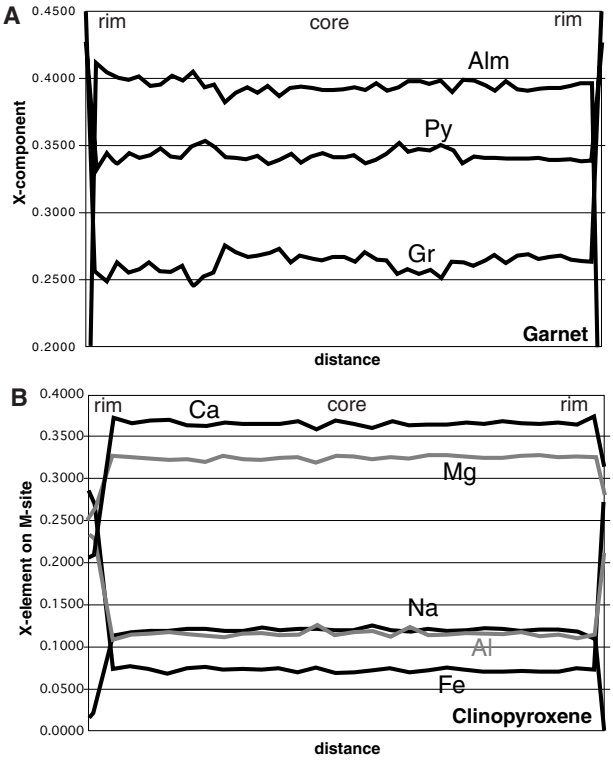

Fig. 10) EMP-element profiles through garnet and clinopyroxene in sample Cap6. Both profiles are essentially flat, garnet shows however some irregular fluctuations, which are not consistent with element diffusion.

a dominantly flat zoning (fig. 10B). Since X_{Na} and X_{Al} on the M-site almost coincide, tschermaks- or aegirine-substitutions are apparently subordinate to the jadeite-component. Estimation of ferric iron (calculated according to Droop (1987)), confirmed the very low aegirine content.

The combined information from BSE-mapping and flat element-profiles suggest that a continuous recrystallisation of the high-pressure assemblage has occurred. Although high temperatures may have been reached (see below), the clear steps in the garnet profiles as well as in the BSE-image argue against flattening of the profiles through extensive volume diffusion. This indicates that most of the garnet grew at similar conditions but over a protracted period, and that part of the garnet results from recrystallisation rather than net-transfer reactions.

Thermodynamic computation

To estimate the peak metamorphic conditions registered by the rock, we applied program TWQ (Berman, 1991), in combination with the internally consistent dataset of Berman (1988, update 1992) (omphacite according to the recent omphacite solution model of Meyre *et al*. (1997)). Furthermore we computed a phase diagram and garnet isopleths using program Domino and the internally consistent dataset of Holland & Powell (1998). Results are shown in figure 11. Because of the relatively complicated diagram, especially at amphibolite-facies conditions, we have only labelled fields significant for the history of the rock. The complicated pattern at amphibolite-facies conditions is mainly related to changing stability of kyanite, staurolite, margarite and chloritoid.

Although the prograde PT-path is relatively poorly constrained, included amphibole and zoisite grains as well as the absence of quartz inclusions suggest a relatively "hot" subduction (Fig. 11). Using TWQ, the eclogite-facies assemblage Grt + Omph + Rt allows only an estimate of temperatures reached during eclogite-facies metamorphism, based on Mg/Fe-exchange between coexisting garnet and pyroxene grains. An estimate of the peak pressure requires the presence of phengite and quartz/coesite, which are, however, absent due to the potassium and silica-poor rock composition. Combining calculated phase relations with estimated TWQ-temperatures for Grt-Omph-rim pairs, minimum conditions of 750˚C at 20 kbar are obtained (Fig. 11 B). Using TWQ, a maximum pressure cannot be inferred for this assemblage. Calculated isopleths for garnet (almandine, using program Domino), lead to almost identical temperature estimates (see black lines fig. 11). Note however that almandine-content in garnet cores decreases to 0.39, indicating temperatures in the order 900˚C or more. Garnet zoning cannot be used to improve constraints on pressures reached along the PT-path, because the calculated grossular component remains constant all over the eclogite field (Grt-Cpx-Rt). This constancy may however be an artefact of the lack of a Ca-Tschermaks component in the Cpx-solution models used in both databases. Calculated garnet isopleths indicate that almandine and pyrope content in the eclogite field is extremely sensitive to changing temperatures. Almandine e.g. shows only a variation of 0.42 to 0.38 between 600 and 1100˚C. Thus, slight inaccuracies in microprobe analyses may result in considerable errors in estimated temperatures. The almost coincidence of cal-

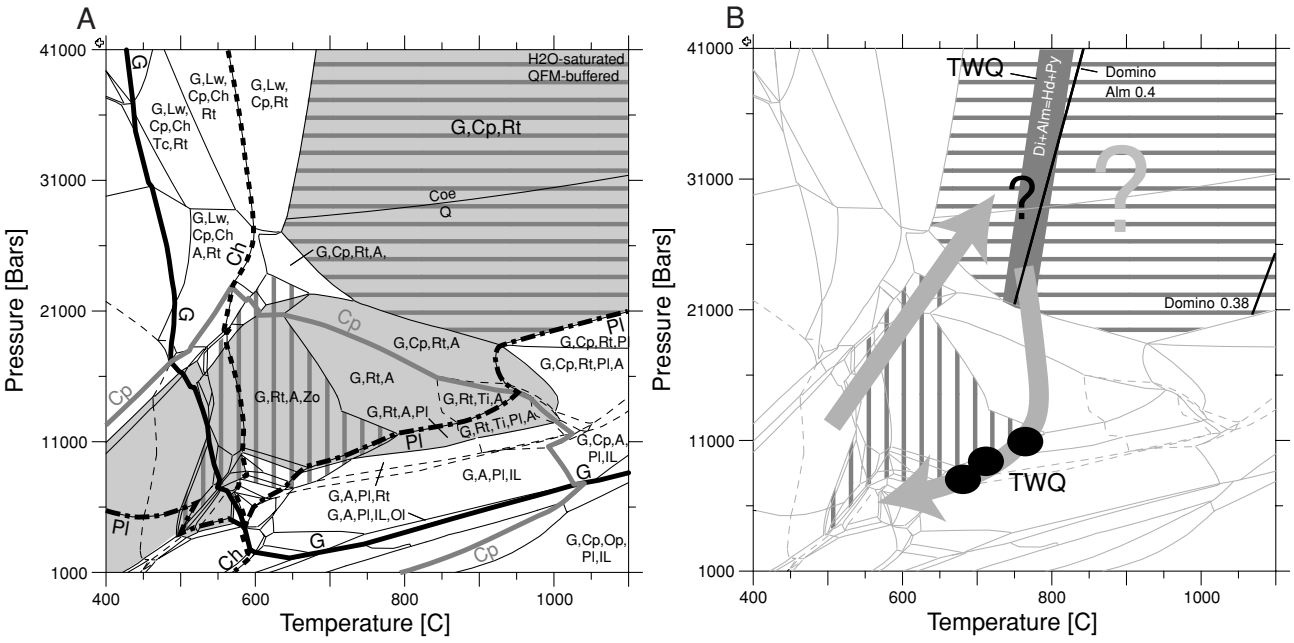

Fig. 11) (A) Computed phase relations for sample Cap6, assuming fluid saturation and QFM-buffering. Grey shading indicates presence of quartz (very small at eclogite conditions), vertical stripes the presence of zoisite and horizontal stripes the eclogite-facies field with the assemblages Grt-Cpx-Rt±Qtz/Coe. Due to the too numerous Pt-fields, only assemblages of importance for this study are noted. (B) TWQ-results (dark shaded area and black ellipses) and calculated isopleths for almandine (black lines) using Domino. Grey arrows indicate approximate PT-path for the sample. Maximum pressure reached is uncertain.

culated garnet isopleths and the TWQ-equilibrium indicates that the "effective bulk composition" does not significantly deviate from the bulk rock composition, suggesting that chemical fractionation due to garnet-growth is unimportant. Based on the above information, we suggest temperatures >750˚C at pressures >20 kbar as a minimum estimate for the peak metamorphic conditions registered by the Capoli-eclogites.

Garnet composition and zoning indicates that it formed at eclogite-facies conditions, thus in the presence of the assemblage Grt-Cpx-Rt. This confirms the above suggestion that garnet is largely a product of recrystallisation rather than of net-transfer reactions along the prograde path. The exhumation path is reasonably well constrained, due to additional TWQ-calculations using the assemblage Cpx-Amph-Grt (black ellipses in Fig. cap61HP). The inferred PT-path suggests hot exhumation from eclogite-facies to 750-800˚C at 10.5-11.5 kbar, followed by cooling during ongoing exhumation to 670-720˚C at 7.5-8.5 kbar, until the rock reaches conditions of 625-650˚ at 6-6.5 kbar (the latter according to Engi *et al*., 1995). During ascent of the sample, initial small amphibole rims may have formed around garnet at ca. 20 kbar, followed by breakdown of omphacite to plagioclase and diopside, when plagioclase stability was reached around 11 kbar (or at higher pressure at water undersaturated conditions). Ilmenite started to partially replace rutile at around 8-9 kbar.

The PT-path suggests delamination of a hot mafic body from a subducting unit, rapid exhumation with only minor associated cooling inside the subduction channel, and final emplacement into a colder unit, where it is quenched rapidly during ongoing exhumation.

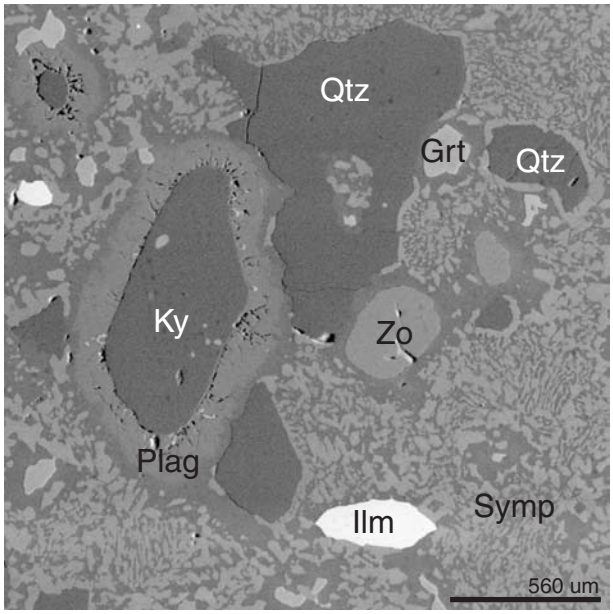

Fig. 12) Secondary electrons (SE) images of reaction textures in sample Porc1. Note zoned plagioclase corona around kyanite, Cpx-rim around Qtz and fine-grained symplectite, consisting of Cpx, Pl and Amph.

Porcaresc

Sample description

Field relations of the samples from Porcaresc are not very clear. Again, the mafic rocks are situated within large masses of granitoid gneiss. The rocks could be part of a narrow trail wedged in between the gneiss, or may represent a part of a budinaged mafic dyke. The samples show complex reaction textures, indicative for the breakdown of phengite, kyanite, zoisite, garnet and omphacite. Kyanite typically has a rounded shape, due to partial resorption, and is surrounded by anorthite-rich plagioclase, which becomes increasingly richer in albite with increasing distance from kyanite (fig. 12 A). A similar reaction texture in retrograde eclogites has recently been described by Nakamura (2002), and was explained as a result of developing gradients in chemical potentials. Former phengite has broken down to form aggregates of acicular biotite and plagioclase (fig. 13). Garnet typically shows rims consisting of plagioclase or amphibole, and several grains contain cores with accumulations of fine rutile needles (compare with Capoli samples), while other inclusions are lacking. Zoisite (X_{pist} = 0.1) is usually relatively coarse grained, appears partially resorbed, and exhibits characteristic hour-glass structures (Fig.

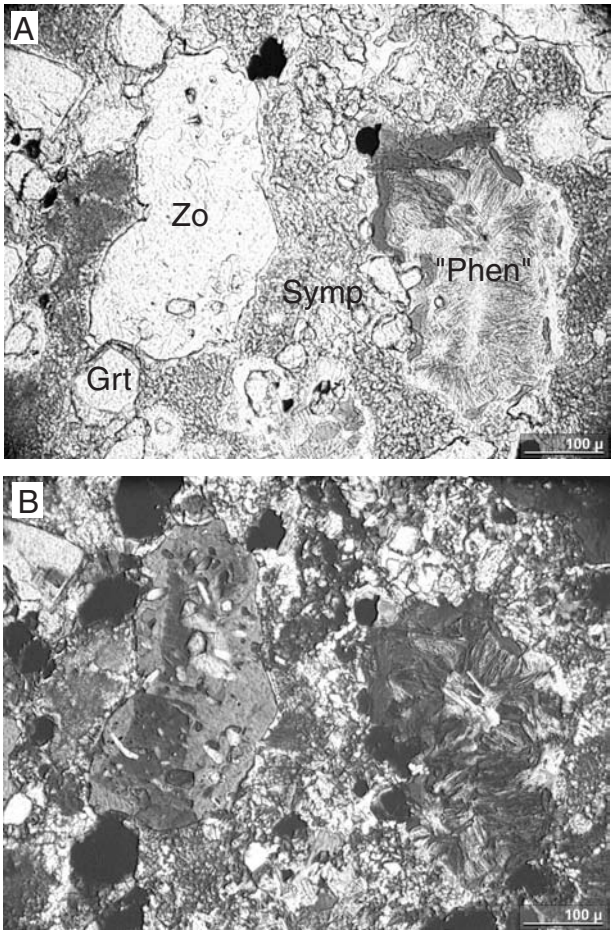

Fig. 13) Photomicrograph of reaction textures in thin section of sample Porc1 (A = PPL, B =XPL). Note phengite breakdown domain ("Phen"), resorbed shape and hour-glass structure in zoisite (visible under crossed nichols).

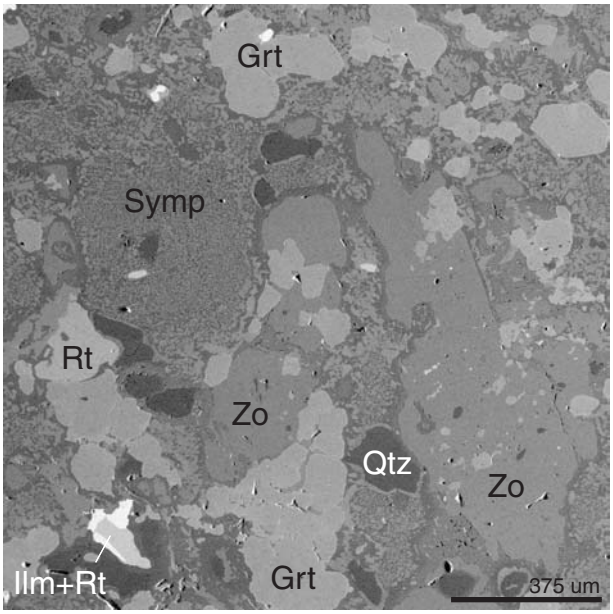

Fig. 14) Secondary electrons (SE) image of reaction textures in sample Porc1. See text for discussion.

13 + 14). It contains inclusions of kyanite, garnet and clinopyroxene, suggesting that growth occurred along the exhumation path. Omphacite breakdown led to formation of a globular symplectite consisting of diopside-rich Cpx, amphibole and plagioclase (Fig. 14). Larger poicilitic amphibole grains that appear to overgrow the older matrix are of magnesiohornblende to edenitic composition. Because they contain inclusions of zoisite, kyanite, (retrogressed) phengite, rutile and garnet, and because of their composition, amphibole is interpreted as retrograde reaction product in domains where fluid infiltration occurred. Whether amphibole was part of the high-pressure assemblage remains unclear. The presence of kyanite argues against this, because amphibole and kyanite coexist only in a small PT-area, at least at water saturated conditions (see Fig. 16). Quartz is often rimmed by a Al-poor clinopyroxene, probably due to stabilisation of Cpx in the presence of quartz, and rutile is often partially replaced by ilmenite. Other phases present in the rock are pyrite and apatite.

Analysed garnet profiles are somewhat irregular, but generally depict a decrease in pyrope and an increase

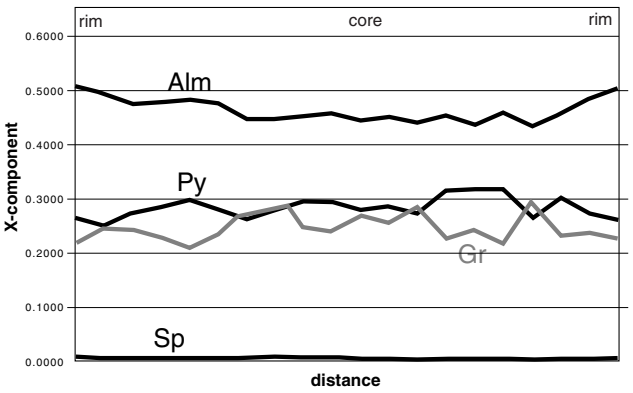

Fig. 15) EMP-element profile through garnet in sample Porc1. See text for discussion.

in almandine from core to rim (Fig. 15). A plateau in the core of the garnet shows the highest pyrope-content (X_{Py}> 0.32, right half of the profile).

Thermodynamic computation

Figure 16 shows the phase diagram calculated for sample Porc1. Due to the lack of inclusions in garnet (except for rutile), the prograde path of the sample is not well defined. According to the calculated garnet-isopleths, garnet-zoning indicates exhumation from 37 kbar to 23 kbar, followed by burial to 28 kbar (see inset in fig. 16B). Core compositions indicate extremely high-pressures of around 37 kbar at 670˚C, mainly determined by the high X_{Py}. These high estimates are however not sustained by the presence of coesite-relics or other UHP-indicators. We suggest that the very high pressure estimates may result from the presence of a high-Mg precursor like glaucophane, chloritoid and lawsonite, which had a buffering effect on the chemical bulk system. Such sample-scale disequilibrium for certain elements in garnet has recently been reported by Carlson (2002). Garnet growth may therefore have mainly occurred on the prograde path between 23-28 kbar around 620˚C (compare with inset in fig. 16). In detail, the path appears rather complicated, which may also be related to fluctuations in effective chemical bulk, rather then by abrupt changes in PT-conditions. Garnet growth at the inferred conditions appears reasonable, because it is related to a major change in phase relations. According to computed phase diagrams, garnet growth was the result of the reaction

$$Glau + Lw = Grt + Omph + Qtz + H_2O \quad (5)$$

probably followed by

$$Lw = Grt + Omph + Ky + Zo + H_2O \quad (6)$$

One uncertainty remains in the fact that chloritoid is not predicted for the estimated conditions of garnet growth, although observed at similar conditions in the experiments of Poli (1993). To test for this factor, we applied the above noted test-Margules parameter of - 20 kJ to the chloritoid solution model of HP98. This approach showed that chloritoid may have been stable at these conditions, and that garnet growth may have been related to a reaction like

$$Omph + Law + Ctd = Grt + Qtz + H_2O \quad (7)$$

followed by

$$Lw + Ctd = Grt + Omph + Ky + Zo + H_2O \quad (8)$$

Recalculation of the garnet isopleths however showed that the conditions of garnet formation remain almost unaffected by the presence of chloritoid. It is notable that garnet zoning reflects a relatively short episode of garnet growth according to reactions (5)-(8). Whereas later growth-zoning may simply be resorbed, the path prior to the reported growth-phase is not recorded in garnet-zoning. Provided that this feature is not a mere cutting effect, it suggests resorption of early garnet during formation of a second generation of garnet, probably because the compositions of the first generation got out of equilibrium with the new assemblage. We can

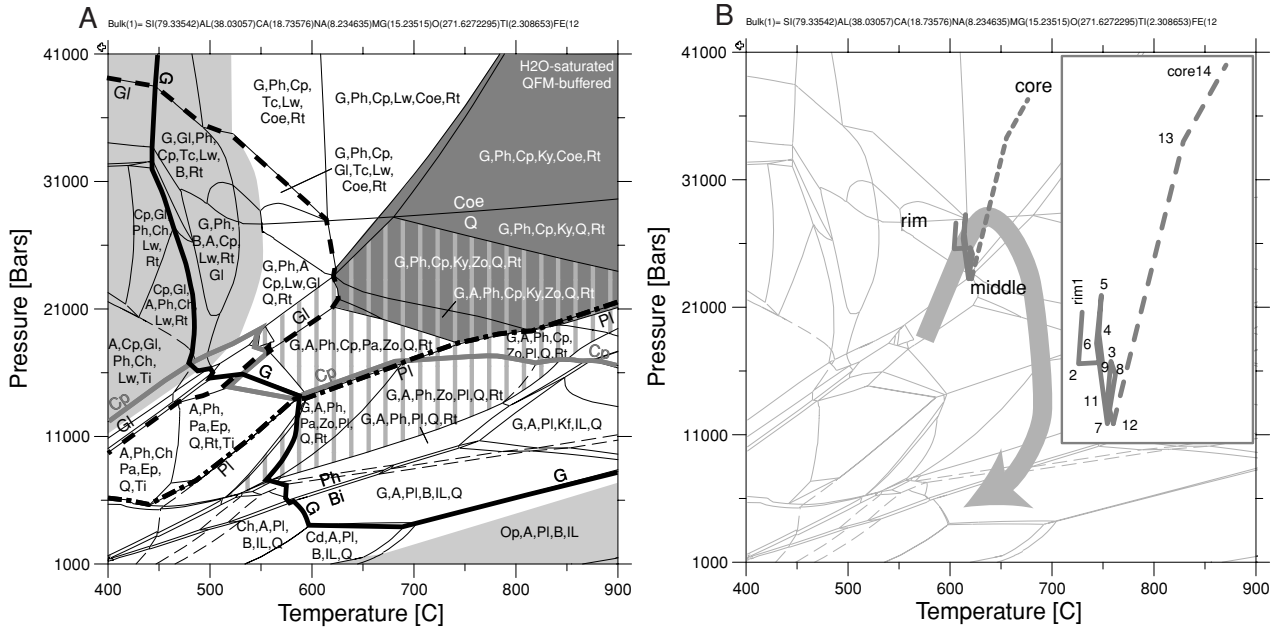

Fig. 16) (A) Computed phase relations for sample Porc1, assuming fluid saturation and QFM-buffering. Light shaded area denotes absence of quartz/coesite, dark shading the presence of kyanite, vertical striped area presence of zoisite. (B) Thin grey line indicates intersections of garnet isopleths using garnet compositions according to the analysed garnet profile in fig. 15. Inset is enlargement of the PT-path derived from garnet zoning. Grey thick arrow indicates approximate PT-path for the sample.

exclude effects of volume diffusion, due to the low reported temperatures.

The high-pressure assemblage Grt + Ky + Omph + Qtz + Ph + Rt ± Zo is depicted in figure 16A by a dark shading combined with vertical stripes (overlap of kyanite and zoisite field). Assuming temperatures not much in excess of 700˚C for the HP-stage, minimum pressures for this assemblage are 19 to 21 kbar. Breakdown of primary omphacite during decompression must have occurred when the stability limit of plagioclase was encountered at approximately 17 kbar (at 700˚C). Phengite breakdown, which has resulted in the formation of biotite and plagioclase, must have occurred at around 8-9 kbar and temperatures between 650-700˚C˚C. Lower temperatures are unlikely, since biotite would not have grown along the retrograde path, and metamorphic conditions of 650˚C at 6-6.5 kbar, as estimated for the Barrovian overprint of the area (Engi *et al*., 1995), would not have been reached (see fig. 16B). Decomposition of phengite was accompanied by partial consumption of rutile to form ilmenite at similar PT-conditions.

Bordoglio

Sample description

Samples from Bordoglio were collected along a road cut. They belong to a narrow trail of metasedimentary and mafic rocks, embedded in orthogneiss. Samples from Bordoglio show a complete suite from weakly retrogressed Ky-Phen-eclogites to almost completely equilibrated Bt-Ttn-Ilm-amphibolites. In addition, these samples show different types from coarse-grained homogeneous, to fine-grained and laminated. Some of the laminae are obviously enriched in aluminium, because they contain abundant kyanite. Although breakdown of kyanite and phengite occurs in samples from Porcaresc as well, retrograde reactions in samples from Bordoglio are partly of a different type. Kyanite, for example, shows unequivocal evidence of resorption and a similar plagioclase-corona as in samples from Porcaresc (Fig. 12), however the plagioclase is intensely intergrown with hercynitic spinel (Fig. 17). Kyanite locally contains inclusions of garnet. Breakdown of phengite occurs in two different types of reactions. One type is the same as observed in samples from Porcaresc, and occurs in relatively weakly overprinted samples. Type 2 occurs in relatively strongly retrogressed samples and shows a domain, armoured by plagioclase, which mainly consists of a felt of celadonite-poor white mica (Si = 3.0-3.1, Fig. 18). Other phases present inside this domain are an anorthite-rich plagioclase, ilmenite, K-feldspar and biotite, intergrown with the plagioclase rims. Another brownish, acicular phase, occurring mainly in the core of the domain, is composed of Al, Fe, Mg and Ti, and is probably hoegbomite (fig. 18).

Sample Bor2, which was used for calculation, is a relatively strongly retrogressed eclogite, containing coarse-grained garnet with inclusions of zoisite, anorthite-rich plagioclase, amphibole of pargasitic to magnesiohornblende composition and clinopyroxene. Again, rutile-rich cores are observed frequently. Garnet-zoning shows a generally almandine rich composition with the core relatively enriched in grossular and low in pyrope (fig. 19). The innermost core shows a hump in pyrope and almandine content, while grossular decreases. Pyrope-content increases towards the rim, whereas grossular decreases and almandine shows at most a very small increase. The outermost rim is defined by a small increase in almandine and a small de-

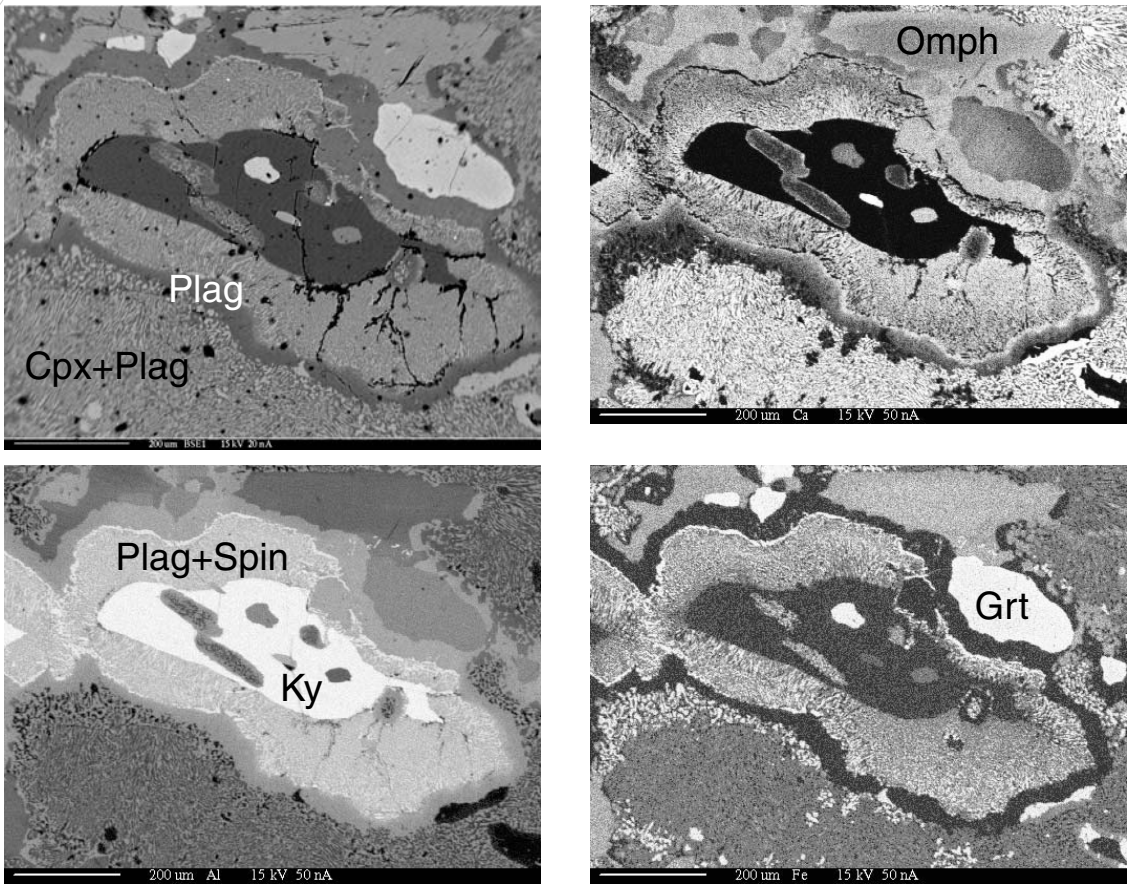

Fig. 17) BSE-image and X-Ray maps of kyanite decay in sample Bor4. The partially resorbed kyanite grain is surrounded by a plagioclase-spinel corona. A second chemically zoned corona of plagioclase, devoid of spinel, rims the inner corona. Note partially back-reacted omphacite, that has decayed to a symplectite of Di-rich clinopyroxene and plagioclase (see also inclusion in kyanite). Phases included in kyanite are omphacite, rutile and garnet.

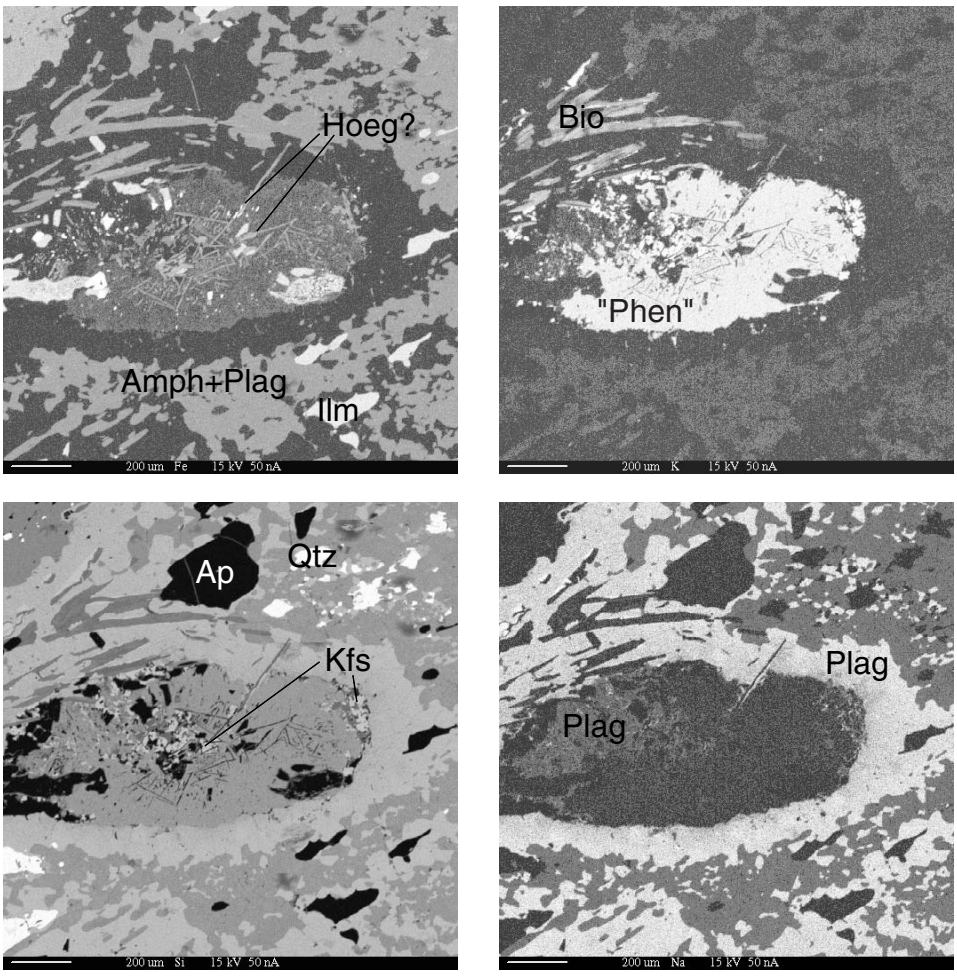

Fig. 18) Reaction texture in sample Bor2, probably related to the breakdown of phengite. An inner core, mainly consisting of low-Si muscovite, plagioclase, K-feldspar and possibly hoegbomite needles is rimmed by a corona of plagioclase. Biotite is also present in the upper left of the texture. The texture is surrounded by a recrystallised amphibole-plagioclase symplectite.

crease in pyrope, likely related to diffusional re-equilibration or resorption.

Thermodynamic computation

Figure 20 shows calculated phase relations for sample Bor2. Calculated isopleths suggest that garnet growth-zoning developed due to prograde consumption of glaucophane, talc and lawsonite between 26-32 kbar at 550-600˚C. Again, the core composition (hump in pyrope) yields higher pressure estimates of around 32-33 kbar, followed by exhumation to 26 kbar. We suggest that a similar effect of local chemical buffering as proposed for the Porcaresc samples as cause of this jump in pressure, rather than exhumation with subsequent burial. The sharp bend of the outermost point may be related to effects of diffusion or resorption.

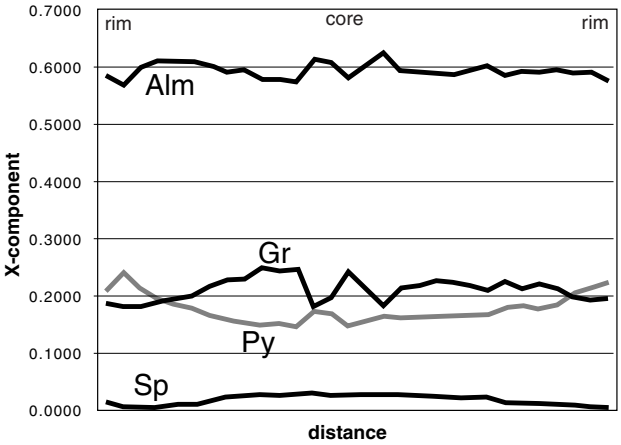

Fig. 19) EMP-element profile through garnet in sample Bor2. See text for discussion.

Like in the discussion of sample Porc1, chloritoid may have been part of the prograde assemblages. Recalculation of the isopleths using the "test"-Margules parameters again showed that the calculated PT-path remains almost unchanged.

One inconsistency between computation and observation is the pargasitic to magnesiohornblende composition of included amphibole instead of the predicted glaucophane-type. Provided that the calculated path is qualitatively correct, which appears reasonable because formation of garnet is predicted for a location where major garnet-growth occurs, two alternative interpretations are possible: (a) Included amphiboles continued to react as a result of increasing temperature, also after being included in garnet. (b) Prograde growth of pargasitic amphibole was followed by growth of glaucophane. This would imply a relatively steep course for the inferred PT-path (light grey arrow), inline with the predicted limited occurrence of zoisite at the border of amphibolite to blueschist facies (vertically striped area in fig. 20).

Additional uncertainty stems from the absence of coesite inclusions, despite of its predicted stability on the basis of garnet zoning. Although polygonal quartz inclusions occur in garnet, the typical radial cracks around these inclusions are missing. We note, however, that such inclusions predominantly occur in the inner parts of garnet, which, as argued above, may have formed below the quartz-coesite boundary. Nevertheless, these facts may indicate that the predicted PT-path could be displaced towards pressures somewhat too high, for example as the result of garnet fractionation from the effective bulk.

The retrograde path is associated with the consumption of garnet and omphacite to form plagioclase and amphibole, at conditions below 18 kbar. The relatively strong retrogression suggests that fluid must have infiltrated the rock during decompression. Breakdown of phengite started probably at ca. 11

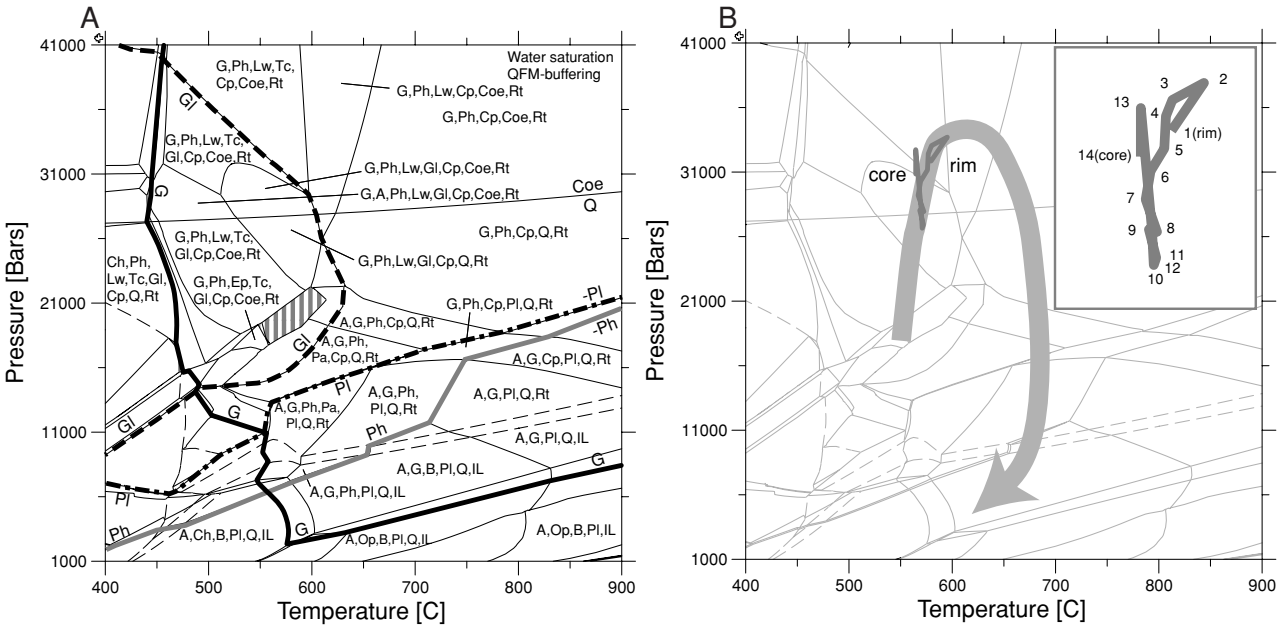

Fig. 20)) (A) Computed phase relations for sample Bor2, assuming fluid saturation and QFM-buffering. Vertically striped area denotes presence of zoisite. (B) Thin grey line indicates intersections of garnet isopleths using garnet compositions according to the analysed garnet profile in fig. 15. Inset is enlargement of the PT-path derived from garnet zoning. Grey thick arrow indicates approximate PT-path for the sample. See text for further discussion.

kbar, followed by growth of ilmenite at around 10 kbar. A final PT-point along the path is the Barrovian overprint of this area, estimated to be in the order of 650°C at 6-6.5 kbar (Engi *et al*., 1995; Todd and Engi, 1997).

Distribution of high-pressure rocks in the Central Alps: An updated inventory

The main occurrences of high-pressure rocks in the Central Alps are well known and thoroughly investigated (e.g. Wang, 1939; Forster, 1947; Heinrich, 1983; Pfeifer *et al*., 1991; Frey & Ferreiro-Mählmann, 1999; Engi *et al*., 2001). Relatively coherent high-pressure units (TAC) from the Central Alps are the Orselina, Adula and Cima-Lunga units, which have an equivalent tectonic position and lithologic content (Fig. 1). Although internally fragmented and composed of a variety of rock types, these nappes form distinct units, which can be differentiated from the surrounding "common" nappes. Additional evidence of high-pressure metamorphism is found in the Orselina- and in the Mergoscia-Arbedo-zone (see Spicher (1980) or Bächlin *et al*. (1981) for location of these units), but was not systematically investigated with modern methods (see however Grandjean (2001)). Between Locarno and Domodossola (to the west of the study area) evidence of high-pressure metamorphism is sparse but has been described by several authors (Kobe, 1956; Colombi & Pfeifer, 1986; Pfeifer *et al*., 1991). More widespread evidence of high-pressure is again found west of Valle d'Ossola, in the Saas-Zermatt and in the Antrona zones, the latter of which interpreted as equivalent to the ophiolite-bearing Orselina-zone (Colombi & Pfeifer, 1986), which stretches towards Locarno.
Recent high-pressure research, except for the contributions of Colombi & Pfeifer (1986, Pfeifer *et al*. (1991) and Grandjean (2001), has dominantly concentrated on the Adula and Cima-Lunga units as well as on the famous Alpe Arami outcrops (e.g. Heinrich, 1983; Trommsdorff, 1990; Pfiffner & Trommsdorff, 1998; Trommsdorff *et al*., 2000; Brouwer, 2000). Due to our investigation, it has become possible and necessary to update the inventory of relics of high-pressure metamorphism in the Central Alps, and to discuss its implications.
In figure 21 we have compiled all published and new occurrences of high-pressure rocks in the area between Valle Verzasca and Valle d'Ossola. Coordinates and a short description of all samples are summarised in table 2. In the map we have indicated two tectonic units: the Maggia nappe, which does not contain evidence of high-pressure metamorphism, and the Cima-Lunga nappe, which is a typical high-pressure unit from the Central Alps. Occurrences of high-pressure rocks are denoted by filled circles if evidence is unequivocal, and by open circles where textures and mineral relics are suspicious of former high-pressure metamorphism, but unequivocal evidence is lacking. We take several types of textural and mineralogical evidence as indicative of high-pressure metamorphism:
a) Persistence of at least relics of the high-pressure assemblage omphacite, garnet and rutile.
b) Symplectite of diopside and plagioclase or of amphibole and plagioclase, obviously replacing HP-omphacite or garnet. Often relic grains of omphacite or garnet are still visible.

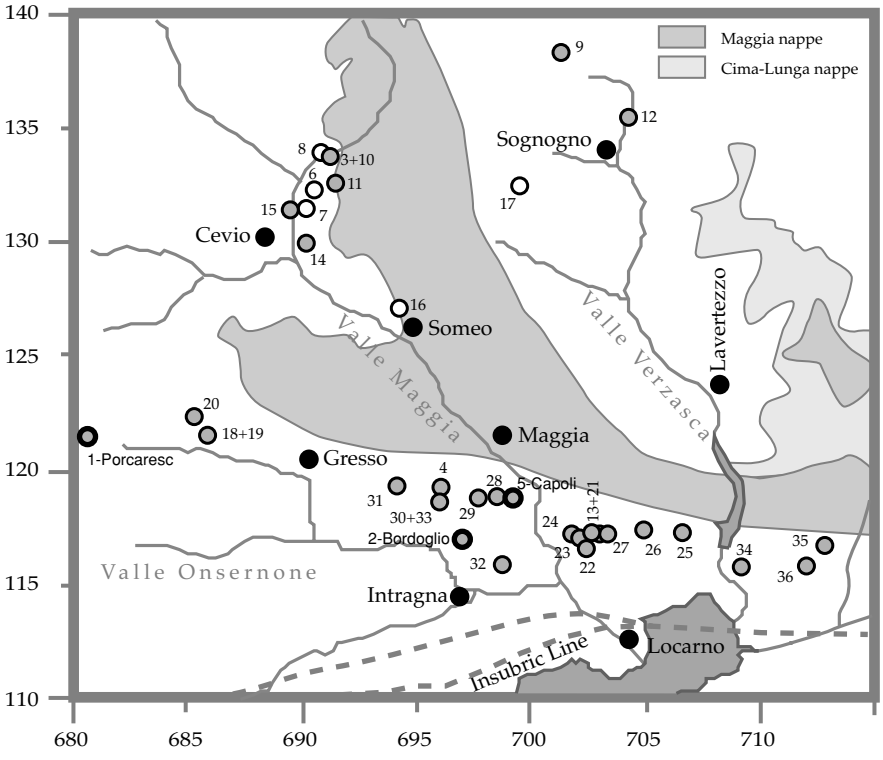

Fig. 21) Occurrences of high-pressure relics in the Maggia-Onsernone area. Filled circles indicate occurrences with unambiguous evidence of high pressure metamorphism, open circles such with possible, but not unambiguous textural evidence.

		coordinates		phases			textures					remarks	source
	sample	X	Y	grt	cpx	Rt	fine sympl.	recry.sympl	rt-rimmed	rt-rich-core	plagi only in coronas and symplectites		
1	Porc1a	680550	121525	!	x	x	!	0	x	x	yes	phengite, zoisite and kyanite breakdown, kyanite still present, but resorbed, zoisite with hourglass structures	t.s.
2	Bor2+4	696975	116960	!	!	x	!	!	x	x	yes	Every stage from pure eclogite facies to amphibolite facies present	t.s., Kobe
3	Mag286	691150	133850	!	relics	x	!	x	x	0	yes	phengite breakdown, px-rims around quartz	t.s., Gräter
4	Gari2	696075	119350	!	x	x	!	0	x	x	yes	poygonal quartz, px-rims around qtz, kyanite and zoisite breakdown	t.s., Kobe
5	Capoli	699200	118840	!	!	x	!	!	x	x	yes	Every stage from pure eclogite facies to amphibolite facies present	t.s., Kobe, Pfeifer
6	Big8	690525	132325	x	0	x	0	x	x	x	-	zoisite-breakdown, atoll-garnets	t.s.
7	Big6	690175	131525	x	x	x	0	x	x	0	yes	zoisite with hourglass structure, plagioclase only present where it replaces zoisite, carbonate present	t.s.
8	Bron6	690825	134000	0	0	x	incl. in hbl!	0	x	0	-	strongly recrystallised, but fine symplectite included in hornblende, zoisite relics	t.s.
9	Tenc1	701300	138300	x	x	x	x	x	x	(x)	yes	symplectite still relatively fine	t.s.
10	Mag177	691150	133850	relics	0	x	0	x	x	0	-	plagi-coronas around grt, biotite cluster possibly pseudomorphic after phengite	t.s., Gräter
11	Mag296	691530	132590	x	0	x	0	0	x	0	0	zoisite consumption by plagioclase, paragonite clusters?	t.s., Gräter
12	Vz854	704250	135450	x	incl. in grt	x	!	x	x	0	yes	amphibole is smaragdite, phengite-breakdown, zoisite with hourglass structure,	t.s., Basel
13	Wurz152	703000	117270	!	!	x	!	!	x	0	yes	eclogite assemblage visible, possible coexistence with amphibole	t.s., Basel
14	Grü475a	690200	~130000	!	incl. in ky	x	!	0	x	!	yes	kyanite breakdown, zoisite present, amphibole smaragdite	t.s., Basel
15	Grü497	~689500	~131450	x	x	x	0	x	x	x	yes	symplect. relatively fine, zoisite, kyanite is in part replaced by staurolite, two amphiboles present	t.s., Basel
16	Som8+9	694275	127120	x	0	x	o	x	x	(x)	yes	symplect. relatively fine, biotite pseudom. after phengite?	t.s.
17	Vz136	699500	132500	!	0	0	0	0	0	0	yes	plagioclase exclusively where it replaces grt together with epi. Amphbole is smaragdite	t.s., Basel
18	PD80	685960	121600	!	x	x	x	0	x	x	yes	phengite breakdown, potash-rich-rock	t.s., Häuselmann
19	Alz74	685960	121600	x	0	x	0	x	0	!	yes	typical garnet resorbtion	Burri
20	PD74	685300	122290	x	0	x	x	x	x	0	yes	phengite-breakdown, potash-rich-rock	t.s., Häuselmann
21	Monteggia	702700	117300	!	x	x	!	-	-	-	-	phengite-breakdown	Forster
22	Frunt	702400	116600	!	x	0	!	-	0	0	-	atoll-garnet, phengite-breakdown	Forster
23	Valeggia	~702050	~117100	!	x	x	!	-	-	x	-	phengite and kyanite-breakdown, cpx-rims around quartz	Forster
24	Gallinee	701800	117250	!	x	x	!	-	-	x	-	one sample with vesuvian-breakdown	Forster
25	Fontai	706600	117250	!	x	x	!	-	-	x	-	phengite-breakdown	Forster
26	Cardada	704950	117400	!	x	x	!	-	-	x	-		Forster
27	Mont1	703300	117250	!	x	-	-	-	-	-	-	metaeclogitic sample, not studied in thin section	t.s.
28	Corte della Cima	698500	118850	-	-	-	-	-	-	-	-	metaeclogitesample, similar to Capoli	Kobe, Pfeifer
29	Salmone	697750	118800	-	-	-	-	-	-	-	-	metaeclogite	Kobe, Pfeifer
30	Pedesen	696050	118650	-	-	-	-	-	-	-	-	metaeclogite	Kobe, Pfeifer
31	Ledrima	694200	119350	-	-	-	-	-	-	-	-	metaeclogite	Kobe
32	Cavigliano	698760	115900	x	x	0	x	-	0	-	-	metaeclogite	Kobe, Colombi
33	Auressio	696000	118680	x	x	0	x	-	0	-	-	metaeclogite	Kobe, Colombi
34	Gordemo,OS46+54	709200	115800	x	x	x	(x)	x	x	0	x	zoisite in matrix, blueish amphibole in grt	Gutzwiler, Wang, Basel
35	Monti di Ditto	712600	116700	-	-	-	-	-	-	-	-	Metaperidotite with chlorite-nests after grt	Wang
36	Monti di Motti	~712000	~115850	x	x	x	x	x	0	-	x	probably phengite-breakdown	Wang

table 2) Localities and short description of rocks preserving evidence of high pressure metamorphism from the Onsernone-Maggia area. See also Fig. 21.

c) Rock matrix defined by a fine to very fine-grained intergrowths of amphibole and plagioclase with grain-size typically below 0.1 mm. Considering the high grade of metamorphism of the study area (amphibolite to upper amphibolite-facies), an interpretation of these textures as more completely recrystallised symplectites as described under b) appears plausible.
d) Relic, resorbed garnet grains, often in combination with a corona enriched in plagioclase and amphibole (kelyphite).
e) Plagioclase occurs only in garnet-coronas or in symplectite domains, and apparently resulted from the break-down of a former high grade assemblage.
f) Occurrence of partially-resorbed or back-reacted phengite, kyanite and zoisite.
g) Reaction of rutile to ilmenite and/or titanite.
h) Garnet-cores incorporating numerous rutile-needles. Although their exact significance is unclear, such cores are typically observed in high-pressure rocks from the Central Alps.
We note that most listed samples are characterised by a combination of several of the above arguments. The updated inventory of high-pressure rocks, shown in figure 21, displays a fairly simple picture for the Lepontine area: High-pressure rocks lack in the Maggia nappe, but are numerous in the underlying and southward-adjacent Orselina and Mergoscia-Onsernone units. Furthermore, the Cima-Lunga nappe, which also underlies the Maggia nappe in the Verzasca area, shows abundant relics of high-pressure. Unfortunately, the continuation of the Cima-Lunga west of Valle Verzasca has remained almost unstudied, and the present study does not mend this unsatisfying circumstance. Besides of the occurrences of HP-rocks surrounding the Maggia nappe, a second, less-well defined group exists in the upper Valle Verzasca area. Because no systematic research of these high-pressure relics has been performed in the context of this study, we refrain from interpretation of their occurrence, but mention their existence. We note, however, that occurrences 9 and 12 are located at an internal boundary of the Simano nappe, which divides the Simano nappe (s.s.) from the Campo Tencia unit. In a recent investigation, conditions of 10-15 kbar at 750°C were proposed for similar samples from this area (Grandjean, 2001). A more in-depth discussion would necessitate a profound investigation on structures in this area, which lies beyond the scope of this study.
The observed distribution of high-pressure rocks in the Maggia-Onsernone area needs some additional comments: Most of the high-pressure rocks reported here were collected in the Mergoscia-Onsernone unit, which is defined by a predominance of granitoid, in part migmatitic gneisses, with only local intercalation of inhomogeneous series, characterised by the occurrence of metasediments, mafic and ultramafic rocks. Thus the lithological characteristic of the Mergoscia-Onsernone unit contrast with those observed in the southward-adjacent Orselina unit, as well as with the Cima-Lunga unit. Surprisingly though, an almost identical bimodal distribution was recently reported from the Central Unit of the Ossa-Morena shear-zone in Spain (López Sánchez-Vizcaíno *et al*., 2003). Like the SSB, the HP-bearing Central unit is divided into a subunit dominated by orthogneiss, and another dominated by metasediments. A similar bimodal distribution is observed in the Adula-unit, the upper part of which is dominated by a very heterogeneous and fragmentary character, while its lower part is dominated by orthogneiss. We note that both parts contain evidence of high-pressure metamorphism.
The observed distribution of relics of HP-metamorphism therefore suggests that the Maggia unit is underlain by HP-bearing units in the Verzasca as well as in the Maggia and Onsernone areas. In contrast to the very inhomogeneous and fragmentary character of the upper Adula, Cima-Lunga and Orselina units, TAC-units in the Onsernone-Maggia area are dominated by orthogneissic sheets, separated from each other by inhomogeneous trails of variable thickness and extent. These relations can best be studied in the so called Cardada trail (Mergoscia-Onsernone unit), which is situated to the north of Locarno and contains several HP-relics. Recent geological mapping in the Onsernone-Maggia area has demonstrated that similar trails are also present in the top of the Antigorio unit

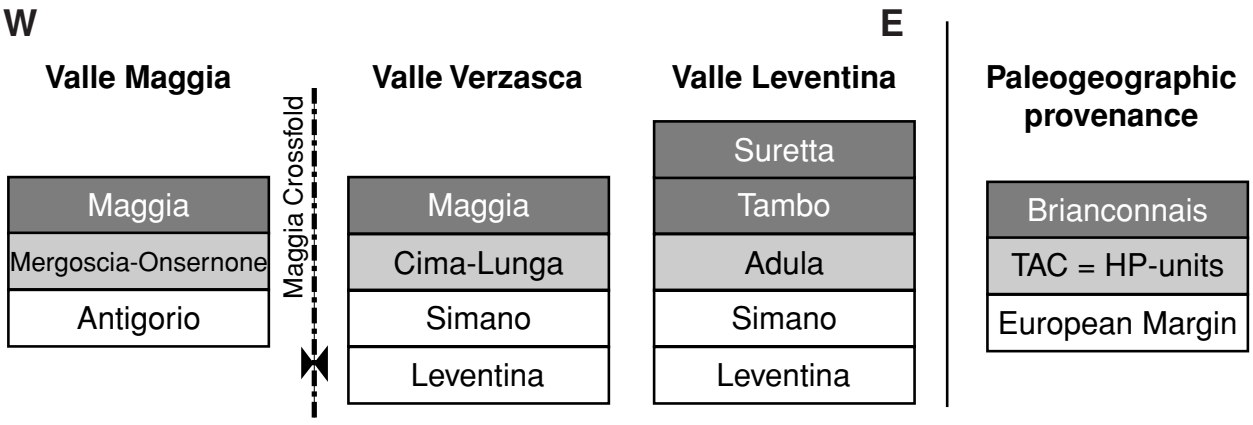

Fig. 22) Sequence of the nappe-stack between the Leventina and Maggia area. See text for discussion.

(Häuselmann, 1997; Gräter and Wenk, 1998; Burri, 1999). The very similar appearance of the granitoid Antigorio-gneiss and the overlying orthogneisses from the Mergoscia-Onsernone TAC-unit has probably hindered earlier recognition of the TAC. Furthermore, the top of the unit currently known as Antigorio nappe, may consist of slices of Antigoriogneiss, intercalated with inhomogeneous Orselina-type trails. Because of this intercalation, a strict distinction between Antigorio and the Mergoscia-Onsernone units cannot be made. This is also the reason why the contact between the two units on the tectonic map (Fig. 1A) and on the constructed profile (Fig. 1B) is hold schematically. It remains uncertain whether the orthogneiss sheets from the Mergoscia-Onsernone units also experienced high-pressure metamorphism, or only the wedged in inhomogeneous TAC-material.

Discussion and conclusions

For a better visualisation of the consequences of this study, we three schematic profiles through the nappe stack in which we tentatively attributed the tectonic units to paleogeographic domains (Fig. 22):
East of Valle Leventina the nappe stack is defined from the bottom up by the Leventina nappe, the Simano nappe, the Adula nappe and the Tambo and Suretta nappes. Except for the Adula nappe and its enclosing sediments, no evidence of Alpine high-pressure metamorphism is found in this section. In Valle Verzasca the nappe stack is defined by the Leventina nappe, Simano nappe, Cima-Lunga nappe and Maggia nappe. Again, high-pressure relics are restricted to a single unit, the Cima-Lunga nappe. Still further west, the nappe stack in Valle Maggia is defined by the Antigorio nappe, the Onsernone-Mergoscia unit and the Maggia nappe.
We tentatively attribute the high-pressure bearing units to the same tectonic level. This leads to a fairly simple picture for the tectonostratigraphy of the Central Alps: We attribute the Maggia, Tambo and Suretta nappes to the Briançonnais domain; the Adula, Cima-Lunga and the Mergoscia-Onsernone units to the Alpine TAC; and finally the Simano, Leventina and Antigorio units to the European margin. The designation of the Antigorio and Simano nappes to the same tectonic level bases on the assumption that these two units formed one lager unit, folded around the hinge of the Maggia-Crossfold (Steck, 1998), which is a SE-NW-striking structure of the Lepontine area (Fig 1). Although the interpretation of this crossfold is still a matter of debate (Grujic and Mancktelow, 1996; Maxelon and Mancktelow, 2002), we note that the Maggia nappe overlies the Antigorio nappe to the west, and the Simano nappe to the east of the crossfold (Fig. 22). This suggests that Antigorio and Simano nappes represent equivalent structural levels. Furthermore, the Maggia nappe is underlain in both areas by HP-bearing TAC-units. This makes a correlation of Maggia and Antigorio units, as suggested by Maxelon & Mancktelow (2002), implausible, because the two units are separated by a TAC-unit.
We therefore propose a relatively simple scenario for the development of the observed nappe-stack in the Central Alps: The Leventina, Simano and Antigorio units are attributed to the southern European margin, the Adula, Cima-Lunga and Mergoscia-Onsernone units to the TAC, and the Maggia, Tambo and Suretta units to the overriding Briançonnais unit. The significance of the Orselina unit, which is also part of the Alpine TAC, is more complicated, because it is not directly connectable with the Cima-Lunga or Adula nappes. We propose that the Orselina, Cima-Lunga and Adula units have a common genetic origin as TAC units, but represent different levels of the subduction channel, juxtaposed during rapid exhumation of the Central Alps along the main backthrust (Tonale-Arcegno-Palanzeno Line, see chapter 1).

References

Bächlin, R., Bianconi, F., Codoni, A., Vesco, E. D., Knoblauch, P., Kündig, E., Reinhard, M., Spaenhauer, F., Spicher, A., Trommsdorff, V. & Wenk, E. (1981): Blatt 1313 Bellinzona. Geologischer Atlas der Schweiz ed. Schweizerische Geologische Kommission.

Berman, R. G. (1988): Internally consistent thermodynamic data for minerals in the systen Na_2O-K_2O-CaO-FeO-Fe_2O_3-Al_2O_3-SiO_2-TiO_2-H_2O-CO_2. Journal of Petrology 29, 445-522.

Berman, R. G. (1991): Thermobarometry using multi-equilibrium calculations:A new technique, with petrological applications. Canadian mineralogist 29, 833-855.

Brouwer, F. M. (2000): Thermal evolution of high-pressure metamorphic rocks in the Alps. Doctoral Thesis, Universiteit Utrecht, Geologica Ultraiectina 199, 224 pp.

Brouwer, F. M. & Engi, M. (2004): Staurolite and other high-alumina phases in alpine eclogites from the Central Swiss Alps: Analysis of domain evolution. The Canadian Mineralogist (in press).

Burri, T. (1999): Metamorphism and tectonics within the Vergeletto "Spoon" (Southern Valle Maggia, Ticino). Diploma Thesis, University of Berne, 112 pp.

Carlson, W. D. (2002): Presidental Address: Scales of disequilibrium and rates of equilibration during metamorphism. American Mineralogist 87, 185-204.

Colombi, A. & Pfeifer, H. R. (1986): Ferrogabbroic and basaltic meta-eclogites from the Antrona mafic-ultramafic complex and the Centovalli-Locarno region (Italy and Southern Switzerland) - first results. Schweiz. Mineral. Petrogr. Mitt. 66, 99-110.

Dale, J., Holland, T. & Powell, R. (2000): Hornblende-garnet-plagioclase thermobarometry: a natural assemblage calibration of the thermodynamics of hornblende. Contrib. Mineral. Petrol. 140, 353-362.

De Capitani, C. & Brown, T. H. (1987): The computation of chemical equilibrium in complex systems containing non ideal solutions. Geochemica et Cosmochemica Acta 51, 2639-2652.

Droop, G. T. R. (1987): A general equation for estimating Fe^{3+} concentrations in ferromagnesian silicates and oxides from microprobe analyses, using stoichiometric criteria. Mineralogical Magazine 51, 431-435.

Engi, M., Berger, A. & Roselle, G. T. (2001): Role of the tectonic accretion channel in collisional orogeny. Geology 29/12, 1143-1146.

Engi, M., Todd, C. S. & Schmatz, D. R. (1995): Tertiary metamorphic conditions in the eastern Lepontine Alps. Schweiz. Mineral. Petrogr. Mitt. 75, 347-369.

Engvik, A. K., Austrheim, H. & Erambert, M. (2001): Interaction between fluid flow, fracturing and mineral growth during eclogitisation, an example from the Sunnfjord area, Western Gneiss region, Norway. Lithos 57/2-3, 111-141.

Forster, R. (1947): Geologisch-petrographische Untersuchungen im Gebiete nördlich Locarno. Schweiz. Mineral. Petrogr. Mitt. 27/2, 249.

Frey, M., Desmons, J. & Neubauer, F. (1999): The new metamorphic map of the Alps. Schweiz. Mineral. Petrogr. Mitt. 79. Zürich, 230 pp.

Frey, M. & Ferreiro-Mählmann, R. (1999): Alpine metamorphism of the Central Alps. Schweiz. Mineral. Petrogr. Mitt. 79/ Special Issue: The new metamorphic map of the Alps, 135-154.

Fumasoli, M. W. (1974): Geologie des Gebietes nördlich und südlich der Jorio-Tonale Linie im Westen von Gravedona (Como, Italia). Dissertation, Zürich.

Grandjean, V. (2001): Petrographical evolution of mafic relics and their implication for the geodynamics of the Central Alps. Dissertation, University of Berne, 103 pp.

Gräter, P. & Wenk, E. (1998): Blatt 1292 Maggia, draft version. Geologischer Atlas der Schweiz. Schweizerische Geologische Kommission.

Grujic, D. & Mancktelow, N. S. (1996): Structure of the northern Maggia and Lebendun nappes, Central Alps, Switzerland. Eclogae geol. Helv. 89/1, 461-504.

Häuselmann, P. (1997): Zur Geologie des Val Vergeletto (Ti). Diplomarbeit, Bern, 98 pp.

Heinrich, C. A. (1983): Die regionale Hochdruckmetamorphose der Aduladecke, Zentralalpen, Schweiz. Dissertation, ETH Zürich, 214 pp.

Heitzmann, P. (1987): Evidence of late Oligocene/early Miocene backthrusting in the central alpine "root zone". Geodinamica Acta 1/3, 182-192.

Hermann, J. & Green, D. H. (2001): Experimental constraints on high pressure melting in suducted crust. Earth and Planetary Science Letters 188/1, 149-168.

Holland, T. J. B. & Powell, R. (1998): An internally-consistent thermodynamic data set for phases of petrological interest. Journal of Metamorphic Geology 16, 309-343.

Knup, P. (1958): Geologie und Petrographie des Gebietes zwischen Centovalli-Valle Vigezzo und Onsernone. Schweiz. Mineral. Petrogr. Mitt. 38/1, 236.

Kobe, H. (1956): Geologisch-Petrographische Untersuchungen in der Tessiner Wurzelzone zwischen Vergeletto-Onsernone und Valle Maggia. Schweiz. Mineral. Petrogr. Mitt. 36/1.

Liu, J., Bohlen, S. R. & Ernst, W. G. (1996): Stability of hydrous phases in subducting oceanic crust. Earth and Planetary Science Letters 143, 161-171.

López Sánchez-Vizcaíno, V., Gómez-Pugnaire, M. T., Azor, A. & Fernández-Soler, J. M. (2003): Phase diagram sections applied to amphibolites: a case study from the Ossa-Morena/Central Iberian Variscan suture (Southwestern Iberian Massif). Lithos 68, 1-21.

Mäder, U. K. & Berman, R. G. (1992): Amphibole thermobarometry: a thermodynamic approach. Geological Survey of Canada Current Research Part E/Paper 92-1E, 393-400.

Mäder, U. K., Percival, J. A. & Berman, R. G. (1994): Thermobarometry of garnet-clinopyroxene-hornblende granulites from the Kapuskasing structural zone. Can. J. Earth Sci. 31, 1134-1145.

Maxelon, M. & Mancktelow, N. S. (2002): Regional correlation of polyphase fold structures in the Central Alps - An approach based on 3D geometric modelling: Penrose Conference: Three-Dimensional Flow, Fabric Development, and Strain in Deformed Rocks and the Significance for Mountain Building Processes:New Approaches. Monte Verita, Switzerland .

Meyre, C., de Capitani, C. & Partzsch, J. H. (1997): A ternary solid solution model for omphacite and its application to geothermobarometry of eclogites from the Middle Adula nappe (Central Alps, Switzerland). Journal of Metamorphic Geology 15, 687-700.

Milnes, A. G. (1974): Post-Nappe Folding in the Western Lepontine Alps. Eclogae geol. Helv. 67/2, 333-348.

Nagel, T. (2000): Metamorphic and structural history of the southern Adula nappe (Graubünden, Switzerland). Doctoral thesis, Universität Basel, 3 chapters.

Nakamura, D. (2002): Kinetics of decompressional reactions in eclogitic rocks - formation of plagioclase coronas around kyanite. Journal of Metamorphic Geology 20, 325-333.

Niggli, E. & Niggli, C. R. (1965): Karten der Verbreitung einiger Mineralien der alpidischen Metamorphose in den Schweizer Alpen. Eclogae geol. Helv. 58, 335-368.

Okamoto, A. & Toriumi, M. (2004): Optimal mixing properties of calcic and subcalcic amphiboles: application of Gibbs' method to the Sanbagawa schists, SW Japan. Contrib. Mineral. Petrol. 146, 529-545.

Patiño Douce, A. E. & McCarthy, T. C. (1998): Melting of crustal rocks during continental collision and subduction. In: Hacker, B. R. & Liou, J. G. : When continents collide: Geodynamics and geochemistry of ultrahigh-pressure rocks . Kluwer, Dordrecht(NL), 27-55.

Pfeifer, H. R., Colombi, A., Ganguin, J., Hunziker, J. C., Oberhänsli, R. & Santini, L. (1991): Relics of high-pressure metamorphism in different lithologies of the Central Alps, an updated inventory. Schweiz. Mineral. Petrogr. Mitt. 71, 441-451.

Pfiffner, M. & Trommsdorff, V. (1998): The high-pressure ultramafic-mafic-carbonate suite of Cima Lunga-Adula, Central Alps: Excursions to Cima di Gagnone and Alpe Arami. Schweiz. Mineral. Petrogr. Mitt. 78, 337-354.

Poli, S. (1993): The amphibolite-eclogite transformation: An experimental study on basalt. American Journal of Science 293, 1061-1107.

Rubie, D. C. (1990): Role of kinetics in the formation and preservation of eclogites. In: Carswell, D. A. : Eclogite facies rocks. Blackie, Glasgow, 111-140.

Schmid, S. M., Aebli, H. R., Heller, F. & Zingg, A. (1989): The role of the Periadriatic Line in the tectonic evolution of the Alps. In: Coward, M. P., Dietrich, D. & Park, R. G. : Alpine tectonics Geological Society Special Publication 45. Geological Society of London, 153-171.

Spicher, A. (1980): Tektonische/Geologische Karte der Schweiz 1:500'000. Schweizerische Geologische Kommission.

Steck, A. (1998): The Maggia cross-fold; an enigmatic structure of the Lower Penninic nappes of the. Eclogae geol. Helv. 91/3, 333-343.

Terry, M. P., Robinson, P. & Krogh-Ravna, E. J. (2000): Kyanite eclogite thermobarometry and evidence for thrusting of UHP over HP metamorphic rocks, Nordøyane, Western Gneiss Region, Norway. American Mineralogist 85, 1637-1650.

Todd, C. S. & Engi, M. (1997): Metamorphic field gradients in the Central Alps. Journal of Metamorphic Geology 15, 513-530.

Tóth, T. M., Grandjean, V. & Engi, M. (2000): Polyphase evolution and reaction sequence of compositional domains in metabasalt; a model based on local chemical equilibrium and metamorphic differentiation. Geological Journal 35/3-4, 163-183.

Trommsdorff, V. (1980): Alpine metamorphism and Alpine intrusion. In: Trümpy, R. : Geology of Switzerland, a guide book . Wepf & Co. Publishers, Basel, 82-87.

Trommsdorff, V. (1990): Metamorphism and tectonics in the Central Alps: The Alpine lithospheric mélange of Cima Lunga and Adula. Mem. Soc. Geol. It. 45, 39-49.

Trommsdorff, V., Hermann, J., Muentener, O., Pfiffner, M. & Risold, A.-C. (2000): Geodynamic cycles of subcontinental lithosphere in the Central Alps and the Arami enigma. Journal of Geodynamics 30, 77-92.

Wang, H. S. (1939): Petrographische Untersuchungen im Gebiet der Zone von Bellinzona. Schweiz. Mineral. Petrogr. Mitt. 19/1, 19-200.

Wenk, E. (1975): Zur alpinen Metamorphose. Schweiz. Mineral. Petrogr. Mitt. 55/1, 116-125.

Zeming, Z., Zhiqin, X. & Huifen, X. (2000): Petrology of ultrahigh-pressure eclogites from the ZK703 drillhole in the Donghai, eastern China. Lithos 52, 35-50.

Metamorphic evolution of pelitic rocks of the Monte Rosa nappe: Constraints from petrology and single grain monazite age data

by Martin Engi, Nadim C. Scherrer, Thomas Burri

Abstract

A suite of metapelites from the pre-granitic basement of the Monte Rosa nappe was collected and investigated to gain insight into the evolution of this important upper Penninic thrust sheet. Careful sampling at mesoscopic to microscopic scale allowed the identification of relics of distinctly pre-Alpine origin, of assemblages formed in the early Alpine high pressure history of the nappe, and of features due to the Meso-Alpine thermal overprint. Variscan structural relics, e.g. large monazite grains with relic cores, or monazite inclusions within garnet porphyroblasts, were recognized in the field and at thin section scale. Alpine features include high pressure and younger thermal phases; these are not readily separable in the field, but they are usually distinctly identifiable at thin section scale.

Combined chemical Th-U-Pb dating of monazite by electron microprobe and novel XRF-microprobe analysis, verified and enhanced by isotopic laser ablation PIMMS analysis, was performed on single monazite grains selected in thin section, with the full context information preserved. Based on electron microprobe data for assemblages from these same thin sections, TWQ thermobarometry indicates metamorphic conditions preserved along the P-T-t path of a polyorogenic evolution. In only two samples monazite inclusions in old garnet were found to record ages of 330 Ma, corresponding to the intrusion of the main Mote Rosa granodiorite mass. High-grade Permian metapelites appear variably affected - in isolated cases even unaffected - by all Alpine activity, retaining mineral assemblages, consistent P-T-information, and monazite grains (even within the sample matrix) formed some 270 Ma ago in response to the intrusion of granitic masses in the Monte Rosa nappe. This same stage of low to medium pressure metamorphism was detected in monazite inclusions in garnet from numerous samples taken at various localities. Reaching sillimanite+Kspar grade, this stage is evident in migmatic restites as well and is suggested to represent either a regional event, at 10-20 km depth, associated with the generation and emplacement of an extensive suite of acid dykes and small stocks; alternatively, and more or less equivalently, one may think of this phase as indicating widespread contact metamorphism.

No evidence whatsoever could be found supporting a questionable Cretaceous high-pressure phase. Consistent TWQ pressures between 9.2 ± 1.8 and 12 ± 1.5 kbar, with temperatures ranging from 595 ± 25 to 755 ± 65°C, represent the dominant Alpine overprint documented in samples containing assemblages kyanite + garnet + phengite ± staurolite. Median conditions are 11.0±1.2 kbar and 652±41°C, with no significant regional gradient, Monazite single grain dates range from 46 to 31 Ma, but with most of the accurate ages lying between 38 and 32 Ma. Several petrological observations suggest that this stage probably represents (partial) re-equilibration upon decompression, rather than the maximum depth reached by the Monte Rosa nappe. Late Alpine thermal overprinting is evidenced by only very few monazite ages of <30 Ma obtained, and no precise P-T-brackets could be obtained for that retrograde stage.

Recent paleogeographic models for the Alpine evolution derive the Monte Rosa nappe from the southern European continental margin. Our results demand that the subduction system implicated this nappe sufficiently early to yield peak metamorphic temperatures near 700°C at 35-30 km depth in the Eocene, probably during extrusion following subduction and slab breakoff. Higher pressure relics are known from several areas along the margin of the Monte Rosa nappe, including the UHP-fragments of Lago Cignana. These relics appear to be restricted to the immediate periphery of the Monte Rosa nappe, outlining a discontinuous mantle of highly strained fragments of ophiolitic and metasedimentary trails. Whether the Furgg Zone, at least its northern parts, may also represent a tectonic mélange, is currently controversial. It seems likely that strain concentration in marginal zones of the Monte Rosa thrust sheet enabled the tectonic emplacement of the several massive granitic sheets that make up the bulk of the nappe. These were left largely intact, thus preserving pre-Alpine and early Alpine assemblages in metapelites protected within less deformed portions of the metagranitoids.

Introduction

The Monte Rosa nappe is a classic crystalline basement nappe situated at the tectonic junction between the Central and the Western Alps. Despite impressive insights from many eminent Alpine geologists (e.g. ARGAND, 1911; BEARTH, 1939; BEARTH, 1952; DAL PIAZ, 1964; DAL PIAZ, 1966; FRANCHI, 1903; FREY et al., 1976; HUNZIKER, 1970; MATTIROLO et al., 1913; REINHARDT, 1966), the evolution and paleogeographic provenance of the Monte Rosa nappe remain controversial. It contains widespread evidence of a protracted polymetamorphic history: Voluminous Variscan granitoids intruded a high-grade gneiss basement, including deformed migmatites, causing contact metamorphism; subsequent regional metamorphism affected this complex, still during the Permian; the Alpine orogeny first produced prominent eclogites and other high-pressure rocks, followed by a widespread Barrovian overprint reaching greenschist facies in the West and amphibolite facies in the eastern portions of the nappe. In terms of tectonic position in the Alpine nappe stack, the Monte Rosa nappe (Fig.1) lies at a level corresponding, in the West, to the Gran Paradiso and Dora Maira "massifs" and, further East, to the Adula nappe, all of which contain Alpine eclogites as well. For the Adula nappe, for example, rapid exhumation from depths in excess of 70 km during the mid Tertiary is well established (e.g. FREY and FERREIRO MÄHLMANN, 1999; NAGEL, 2000). To what extent the high pressure relics in all of these tectonic units may be interpretable in terms of one coherent subduction/emplacement history is a key question in Alpine geodynamics and is relevant in the context of collisional orogeny in general. Current understanding of the kinematic sequence of events and their thermal consequences, in particular, is certainly far from complete in any orogen, including the Alps.

Progress on these questions depends to no small degree on reliable temporal links between several stages of evolution documented by petrological and structural studies for each of these units. For the Monte Rosa nappe, petrographic work by BEARTH (1952, 1958) and DAL PIAZ (1971) documented that, due to localized strain within the nappe, plurifacial assemblages are not just locally preserved, but occur in several km2-size domains. Previous efforts to constrain the temporal evolution of the Monte Rosa nappe (BEARTH, 1952; CHOPIN and MONIÉ, 1984; DAL PIAZ and LOMBARDO, 1986; FREY et al., 1976; HUNZIKER, 1970; HUNZIKER and BEARTH, 1969; HUNZIKER et al., 1992; HUNZIKER and MARTINOTTI, 1984; KÖPPEL and GRÜNENFELDER, 1975; MONIÉ, 1985; ROMER et al., 1996; RUBATTO AND GEBAUER, 1999) indicated Alpine, Variscan, and older ages. Substantial disagreement remains regarding the significance of many of the metamorphic ages in these studies and the discrepancies between dates obtained (e.g. PAQUETTE et al., 1989). The difficulty of interpretation is partly due to problems with specific isotopic systems used (such as excess argon, partial thermal resetting), but a major shortcoming has to do with the selection and documentation of mineral phases used to date the samples. Unfortunately, the loss of structural context incurred when separating mineral fractions from polymetamorphic samples renders a reliable integration of petrologic information impossible. Particularly controversial are age data indicating metamorphism in the Cretaceous, based on Rb-Sr and Ar-Ar dating (CHOPIN and MONIÉ, 1984; HUNZIKER, 1970; MONIÉ, 1985) obtained on samples from peripheral parts of the Monte Rosa nappe, including the Furgg Zone and the Gornergrat Zone. For the latter, recent results by RUBATTO and GEBAUER (1999), who made use of the high spatial resolution of the ion microprobe (SHRIMP) to date multiphase zircons from a

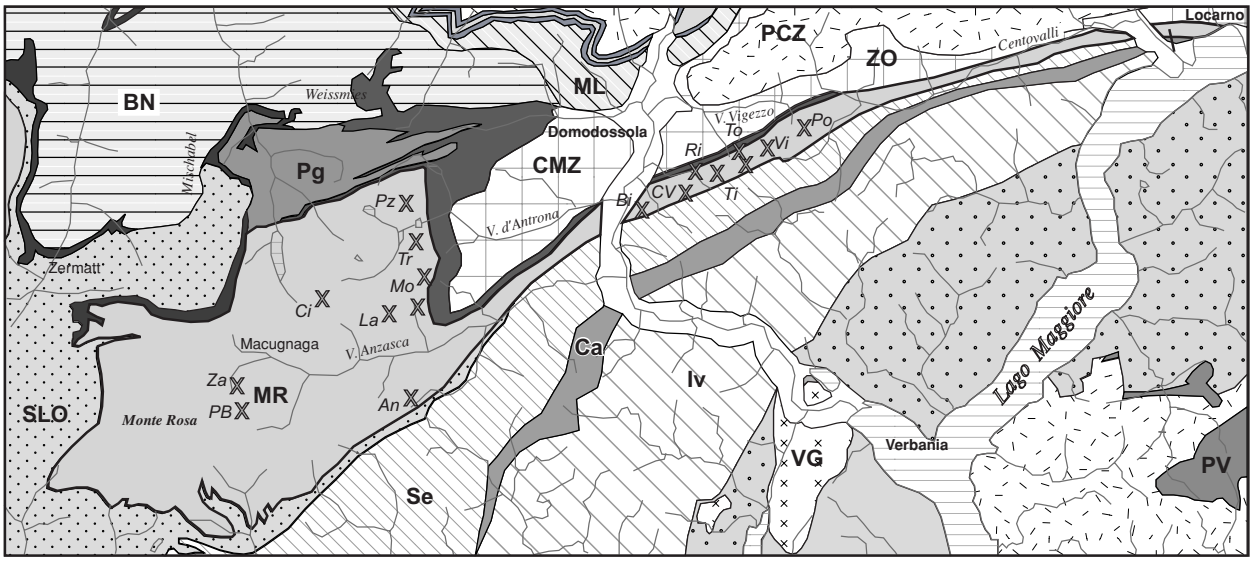

Figure 1: Tectonic overview of the Monte Rosa (MR) nappe, with major tectonic units from the Tectonic Map of Switzerland (SPICHER, 1980): BN: Bernhard nappe, SLO: Schistes lustrés - Ophiolite zone, VG: late Variscan granites, Ca: Canavese zone, Iv: Ivrea zone, MoZ: Moncucco zone, ML: Monte Leone nappe, Pg: Portjengrat unit, PV: Permian volcanics, Se: Sesia Zone, ZO: Zone of Orselina. Sample locations shown by X

metaquartzite, indicated a long sequence of events (from ~700 to 34 Ma), but with no indication of activity leading to zircon growth in the Cretaceous. These authors concluded that the most external zircon zones, dated at 35 Ma, correspond to high pressure conditions for the metaquartzite, estimated at P<14-15 kbar and T<550°C. It is difficult, however, to ascribe the dates obtained on a few individual rims of zircon grains to a specific petrogenetic stage of the metamorphic evolution of their host rock. In addition, the regional significance of these data in not clear, since Masson et al. (2000) have voiced doubt whether the Gornergrat slice belongs to the Monte Rosa nappe (see also DAL PIAZ, this volume). For the main part of the latter, no corresponding age dates are available, but it is worth noting that high-pressure garnet from Dora Maira gave a Lu-Hf age of 32.8±1.2 Ma (DUCHÊNE et al.,1997).

Granitoid rocks predominate the Monte Rosa nappe. A pioneering study by FREY et al. (1976) combined petrology, oxygen isotope thermometry, and geochronology to investigate granitic samples. While substantiating the complex polyorogenic history, with Variscan and Alpine parts, the results of that study lacked in resolution to document the evolution in detail, both with respect to the temporal and metamorphic conditions. CHOPIN and MONIÉ (1984) and by DAL PIAZ and LOMBARDO (1986) added quantitative detail to the Alpine metamorphic high-pressure conditions by studying, respectively, pelitic and mafic samples. However, both of these studies obtained their samples from mélange zones near the margin or roof of the Monte Rosa nappe, and it is not clear when and how these fragments became incorporated in the main mass of the thrust sheet.

To overcome some of the limitations of granitic samples, the present investigation put its focus on pelitic schists and subpelitic paragneisses. These make up a good part of the pre-Variscan basement complex and occur, more sparsely, within the large granitoid masses as well (BEARTH, 1952; DAL PIAZ, this volume). We report on pelitic samples collected from central and eastern parts of the Monte Rosa nappe, where paragneiss units had been mapped notably by MATTIROLO et al. (1913), BEARTH (1952), and REINHARDT (1966).

Following an account of the geological setting and previous results, we present microstructural and petrologic evidence used to constrain the metamorphic evolution of our metapelite samples. Wherever possible, we obtained thermobarometric results for the same samples, from which single grains of monazite had been selected and separated from thin section, using a set of consistent selection criteria. Chemical Th-U-Pb dates and isotopic Th-Pb ages (obtained using laser ablation PIMMS) for these monazite grains are presented (SCHERRER et al., 2001a). Because our approach utilizes the full context information about the grains we dated, and because monazite has such a high closure temperature for Pb-diffusion (PARRISH, 1990), the results obtained afford a reliable interpretation of several stages of the metamorphic evolution. Implications are addressed in two chapters, first in terms of the polymetamorphism of pelites and the behaviour of monazite in these, and then in terms of the evolution of the Monte Rosa nappe as a whole. Finally, the significance of this nappe in the Alpine collision belt, its emplacement and the exhumation of high-pressure rocks are discussed.

Geological framework

Figure 1 shows the Monte Rosa nappe in its present tectonic context, at the same level as the Gran Paradiso nappe of the Western Alps (Dal Piaz and Lombardo, 1995) and the Adula nappe of the Central Alps further east (PFIFFNER and TROMMSDORFF, 1998). The Monte Rosa nappe is immediately rimmed by several Pennine thrust sheets comprising Mesozoic ophiolites and metasediments, and showing abundant evidence of high-pressure Alpine metamorphism. The pre-Variscan metamorphic basement of the Monte Rosa unit is of sillimanite-Kspar-grade, includes migmatites and was intruded by massive granites (initial 87Sr/86Sr: 0.712) and granodiorites during the late Paleozoic, as interpreted by HUNZIKER (1970; Rb-Sr isochron: 310±50 Ma), KÖPPEL and GRÜNENFELDER (1975; U-Pb monazite: 260±5 Ma) and recently confirmed by LANGE et al. (2000; U-Pb data on magmatic zircon and monazite) and LIATI et al. (2001; U-Pb SHRIMP data on zircon: 272±4 Ma). Deformed Monte Rosa granite dated by HUNZIKER (1970; Rb-Sr isochron: 260±10 Ma, initial 87Sr/86Sr: 0.713) and ages near 250 Ma obtained on the regionally widespread foliation-forming white micas (HUNZIKER and BEARTH, 1969) lead these authors to propose a late-Variscan (Permian) metamorphic event. Its character remains ill constrained (FREY et al., 1976; HUNZIKER et al., 1992) but it seems to correlate in time with magmatic activity that produced both granitic stocks and dykes (aplites and pegmatites), but no mafic dykes. Changes produced during the Alpine orogenic cycle differ in intensity, leaving relics in many areas and rock types. The overprint is strongest near shear zones, in peripheral part ("Schieferhülle"; BEARTH, 1952) of the Monte Rosa granite, and in the easternmost section of the nappe, i.e. the Southern Steep Belt between Valle d'Ossola and Locarno. While in the latter area an amphibolite facies overprint effaced most of the high-pressure characteristics of the earlier Alpine metamorphism, this overprint diminishes in intensity and pervasiveness towards the West. Low-temperature eclogite facies relics thus occur far more fre-

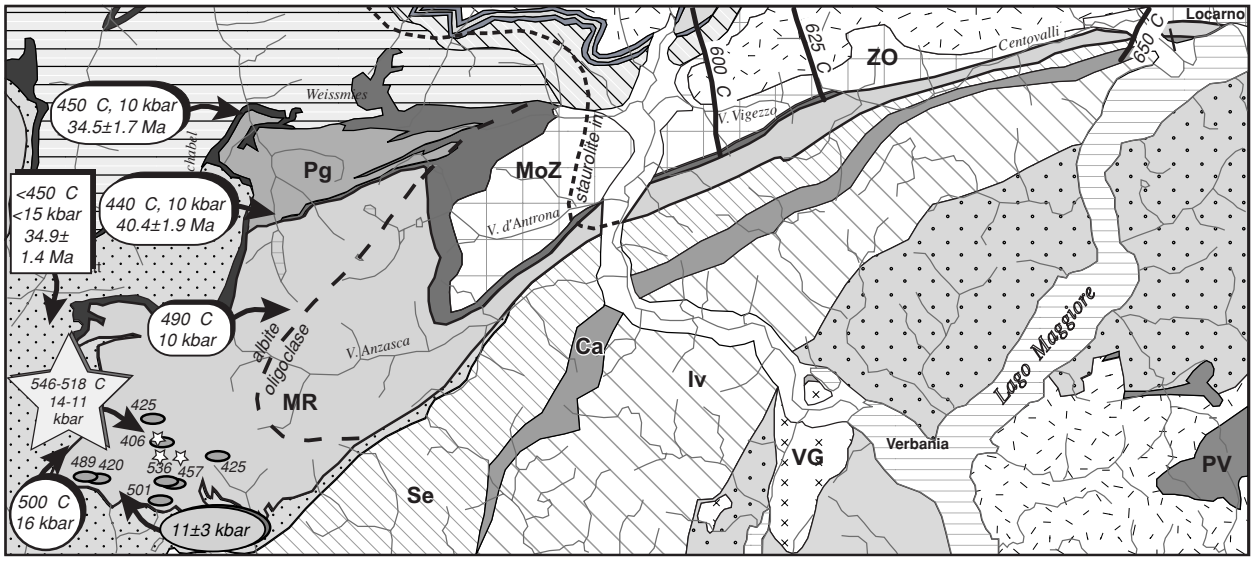

Figure 2: Metamorphic conditions compiled for the Monte Rosa nappe. Note two distinct stages of evolution:
1. Thermobarometric data in boxes refer to conditions of early Alpine high-pressure (eclogite) stage. Data symbols: For eclogites: oval - DAL PIAZ and LOMBARDO (1986); star - BORGHI et al. (1996); for metagranites: oval - FREY et al. (1976); for metapelite: circle - CHOPIN and MONIÉ (1984); for phengite-quartzite: rectangle - RUBATTO and GEBAUER (1999).
2. Mineral zone boundaries and isotherms (600°, 625°, 650°C) characterize Barrovian overprint (the "meso-Alpine" stage of HUNZIKER et al., 1992), the thermal structure of which crosscuts major tectonic boundaries. Albite-oligoclase isograd from BEARTH (1958), staurolite zone boundary from NIGGLI (1970), Barrovian isotherms from TODD and ENGI (1997). For tectonic units refer to Figure 1.

quently to the West of Valle d'Ossola, despite the regionally characteristic postkinematic albitization (BEARTH, 1952) that may be linked to late Alpine hydrothermal activity (PETTKE et al., 1999). Notably, in the abundantly undeformed portions of Monte Rosa granite, no evidence has been reported of the high-pressure breakdown of plagioclase to sodic pyroxene + zoisite + quartz, which is a widespread assemblage in the adjacent Sesia-Lanzo zone (e.g. Monte Mucrone; COMPAGNONI and MAFFEO, 1973; OBERHÄNSLI et al., 1985). As outlined above, the age of Alpine high-pressure conditions in the Monte Rosa nappe is still being debated (mid-Cretaceous or Eo-/Oligocene?), whereas the age of the later thermal overprint is constrained to 34-28 Ma (KÖPPEL et al., 1981; ROMER et al., 1996; PETTKE et al., 1999). Looking at the polymetamorphic history of the entire nappe in some more detail, a number of limits in the present state of understanding emerge, to which the present study may contribute:

- Peak metamorphic conditions reached during the pre-Variscan evolution are not quantitatively known. However, assemblages and local textures were meticulously documented by (BEARTH, 1952) and show the following reaction sequence to be regionally widespread in metapelites: Cordierite first formed at the expense of biotite and was then pseudomorphosed by sillimanite; garnet + sillimanite + biotite occur as a restite assemblage veined by a quartz-feldspar-metatectites; K-feldspar is abundant, with much of the muscovite (and sericite) appearing texturally late. Jointly, these observations indicate partial melting under upper amphibolte facies conditions at medium to low pressures. The absence of andalusite and orthopyroxene, as well as the sparsity of kyanite indicate temperatures near 700°C and pressures of 3-6 kbar. No regional metamorphic gradients have been documented for this pre-Variscan stage. While early studies ascribed kyanite to a late (but pre-granitic!) stage, subsequent workers (DAL PIAZ, 1971; DAL PIAZ and LOMBARDO, 1986) reinterpreted kyanite to be part of early Alpine assemblages.

- The Permian metamorphism is even less well constrained, presumably because it reached conditions of a lower grade than both the earlier metamorphism and the subsequent Alpine high-pressure stage. In granitoids regionally widespread assemblages include oligoclase, orthoclase, and 2M1 muscovite (in contrast to to Alpine HP-assemblages with microcline, (2M1 or 3T) phengite plus either oligoclase or albite + epidote); oxygen isotope temperatures for muscovite indicate temperatures between 520 and 560°C (FREY et al., 1976). Pressures estimated in that same study are given as 2-4 kbar, but the precise basis is not clear. No studies of mafic or pelitic rocks have been conducted so far to derive pressure conditions for the Permian metamorphism or to document the spatial variability of its intensity and character, hence possible tectonic implications remain mysterious. Temporally, the relation between Variscan magmatism and the Permian metamorphic overprint is certainly close. Spatially, the situation is not so clear, since no discrete thermal aureoles have been recognized away from the intrusive contacts (e.g. in the W and SW parts of the nappe), though these are undisturbed in several areas (BEARTH, 1952). (We interpret the high grade gneiss schollen described in that study from within undeformed portions of the Monte Rosa granite as fragments of the pre-Variscan metamorphic basement.) Evenso, it

Sample	X-Coord	Y-Coord.	Alt.(m)	Sample location	Rocktype	Major mineral constituents	Minor	Accessories
An9901	649'850	87'200	2095	W of P. Tignaga, just E of small lake	Grt-bearing mica gneiss	Qtz, Bt, Ms, Grt, Chl	Tur	Ilm, Rt, Mnz
Bi9801	667'200	102'600	640	Alpe Bisoggio, SE Beura	Grt±St-Bt-Ms gneiss	Grt, St, Bt, Ms, Chl, Qtz, Kfs, Pl,		Ilm, Tu, Mnz
Bi9802	667'200	102'600	640	Alpe Bisoggio, SE Beura	Grt±St-Bt gneiss	Grt, ± St, Bt, Ms, Chl, Qtz, Kfs, Pl		Ilm, Tu, Mnz, Zrn
Ci9901	644'500	97'050	2920	between Ofentalpass and P. Cingino Sud	Grt-bearing Ms gneiss			
CV9801	670'400	103'050	1785	NE A. Corte Vecchia	Grt±St-Bt gneiss			
La9901	648'300	94'550	2645		Grt-Bt-Ms schist			
La9903	649'900	95'650	2690	Just SW of Pt 2713 along Cresta di Lareccio	Grt-Bt-Ms schist			
La9904	649'900	95'650	2690	Just SW of Pt 2713 along Cresta di Lareccio	Grt-Bt-Ms schist			
La9905	650'025	95'600	2635	block within few meters of original position	Grt-bearing Ms gneiss			
La9906	650'350	95'700	2620	SE of P. San Martino on S face of SW ridge off Pt. 2733	Grt-bearing mica gneiss			
La9907	647'900	94'750	2785	between P. Lame and Passo delle Lonze along ridge	Grt-Bt-Ms schist			
La9908	647'800	94'700	2707	Psso delle Lonze	Grt-Bt-Ms schist			
Mo9801	652'250	97'600	2385	W Pso. del Mottone	Grt-bearing mica gneiss	Grt, Qtz, Ms, Bt, Chl, Ilm, Plag, K-feld,	Aln	Rt, Mnz
Mo9802	652'250	97'600	2385	W Pso. del Mottone	Grt-bearing mica gneiss	Grt, Qtz, Ms, Chl, Plag, K-feld, Ilm, Rt, Bt	Hem	Mnz, Aln
Mo9803	651'000	95'950	2265	E P. San Martino	Grt-bearing mica gneiss	Ms, Qtz, Bt, Grt, Ap,		
Mo9804	651'050	95'950	2120	E P. San Martino	Grt-bearing mica gneiss	Qtz, Bt, Ms, Chl, Grt, Kfs,		Ilm, Rt, Mnz
PB9901	638'850	87'750	3175	Just below Pt 3180 (NW) on Pizzo Bianco	Grt±St-Bt gneiss			
PB9902	638'850	87'750	3175	Just below Pt 3180 (NW) on Pizzo Bianco	Grt±St-Bt gneiss			
PB9904	638'350	88'400	2610	Just SE of Pta C. Battisti on N side of Locciechiuse	Grt±St-Bt gneiss			
Pi9701	670'900	104'800	1860	NW Pta I Pisoui, along steep trail just below peak	Grt-Bt-Ms schist	Qtz, Plag, Ms, Bt, Grt1, Grt2, Ilm, Ap		Zr, Mz, Rt, Aln
Po9701	678'300	105'950	1750	NE La Porcella	Grt-St-Bt-Ms schist			
Po9702	678'300	105'950	1750	NE La Porcella	Grt-St-Bt-Ms schist			
Po9703	678'300	105'950	1750	NE La Porcella	Grt-St-Bt-Ms schist	Qtz, Grt, Bt, Ms, St		Mnz, Zr
Pz9702	650'350	100'750	1080	NE L. di Antrona	Grt-bearing Sil-Bt gneiss			
Pz9703	651'250	103'200	1940	E of Forcola	Grt-bearing Sil-Bt gneiss			
Pz9704	651'250	103'200	1940	E of Forcola	Grt-bearing Sil-Bt gneiss			
Pz9905	649'325	103'075	2490	N of Cime di Pozzuoli (Pt 2602) on ridge to N.	Grt±St-Bt gneiss			
Pz9906	649'325	103'075	2490	N of Cime di Pozzuoli (Pt 2602) on ridge to N.	Grt±St-Bt gneiss			
Pz9907	650'200	100'350	1080	SW of Lago di Antrona along trail	Grt±St-Bt gneiss			
Ra9701	675'600	105'550	2200	S side P. Ragno-Nona	Grt-St-Bt-Ms schist			
Ra9703	675'250	105'050	2200	S P. Nona, W Costa Nera	Grt-Hbl-Bt schist			
Ri9801	670'600	104'300	1450	NW A. Rina	Grt±St-Bt gneiss	Bt, Ms, Chl, Grt, Qtz, Kfs, Ilm		Ap, Tur, Mnz
Ri9802	670'600	104'300	1450	NW A. Rina	Grt±St-Bt gneiss	Qtz, Kfs, Chl, Ms, Bt, Chl, Grt, Pl	St, Ap	Ilm, Mnz, Aln
Ti9701	672'125	103'900	2110	S P. Tignolino	Grt-Bt-Ms schist			
Ti9801	671'300	103'550	1740	SW P. Tignolino	Grt±St-Bt gneiss	Qtz, Ms, Chl, Grt, St, Ilm	Bt	Zr, Mz, Aln
To9801	673'750	105'650	1895	NE of M. Togano, S of P. Marcio	Grt-Tur-Bt-Ms schist	Qtz, Bt, Ms, Tur, Grt, Ilm, Plag	Hem	Zr, Mz
To9802	673'850	104'550	2190	S of M. Togano	Grt±St-Ms gneiss	Qtz, Ms, Ilm, Grt, St, Chl, Plag		Zr, Mz
Tr9902	651'000	99'050	1800	east of A. Larticcio where trail crosses main creek gully	Grt-Bt-Ms schist	Qtz, Ms, Bt, Grt, Ap	Ilm, Chl	Rt, Mnz
Tr9903	651'800	98'800	2247	Point 2247 N of Psso di Trivera, SW of Punta di Trivera	Grt-Bt-Ms schist			
Tr9904	651'900	98'150	2300	just to the NE of Psso di Trivera	Grt-bearing mica gneiss			
Vi9702	674'220	104'900	2195	SE M. Togano	Grt-bearing mica schist	Grt, ±St, Bt, Ms, Pl, Qtz, Chl	Aln, Ilm, Tur	Xen, Zrn, Rt, Mnz
Za9701	637'500	89'300	2140	E A. Pedriola, block (of local origin)	Ky-bearing Grt-Ms schist	Grt, Cld, Qtz		Mnz
Za9702	637'300	89'450	2070	E A. Pedriola	Grt-bearing Sil-Bt gneiss	Sil, Phe, Qtz, Grt(1+2)		Mnz
Za9703	637'350	89'675	2045	NE A. Pedriola, block (of local origin)	Ky-bearing Grt-mica schist	Sil, St? Pheñ> Bt	Rt, Ilm, Chl, Pl	
Za9705	637'900	89'900	2070	NE A. Pedriola, block (of local origin)	Ky-bearing Grt-mica schist			

Table 1: Metapelite samples from the Monte Rosa nappe studied. Coordinates refer to Swiss topographic maps; mineral abbreviations according to KRETZ (1983).

seems entirely possible that the Permian event essentially represents contact metamorphism, i.e. that heating was due mostly to acid magmatism rather than crustal thinning.
- The early Alpine phase, apart from the age uncertainty mentioned, is fairly well established as a high pressure overprint. Evenso, the number of samples documented by modern methods is quite limited: FREY et al. (1976) derived oxygen isotope temperatures of 440-490°C from five phengite samples of Monte Rosa metagranite. Using this range and the compositions of phengite (3.3-3.4 Si per formula unit) reported in that same study, the calibration by MASSONNE and SCHREYER (1987) indicates maximum pressures of 9-10 kbar. A similar range, bracketed between 9±1 and <14 kbar was delimited from low-temperature eclogites by DAL PIAZ and LOMBARDO (1986), with temperatures between 402 and 536°C based on garnet-clinopyroxene thermometry. (Note that these temperatures were obtained using the calibration by ELLIS and GREEN (1979). The more recent version by KROGH (1988) yields 337-488°C.) For three garnet mica schists studied by BORGHI et al. (1996), thermobarometry gave 515-545°C and 11-14 kbar for what these authors identified to be "first generation assemblages" on textural grounds, buth with no mineral age data available. On the basis of three samples from each of the Internal Pennine "Massifs" (Monte Rosa, Gran Paradiso, and Dora Maira), these authors also inferred a PT-path for the Alpine HP-evolution, supposed to be valid for all of the units. The regional distribution of all of the PT-data available so far for this stage is shown in Figure 2. It would be hazardous to infer a metamorphic field gradient from these data, owing to likely systematic differences between the methods used and the possibility of partial re-equilibration following emplacement.
Higher pressures, at temperatures near 500°C, have been reported from peripheral parts in the SW of the Monte Rosa nappe. Thus, CHOPIN and MONIÉ (1984) obtained 16 kbar from an unusual metapelite sample, and LE BAYON et al. (2001) derived pressures as high as 23 kbar from whiteschists (see PAWLIG and BAUMGARTNER, this volume); the latter conditions are said to reflect the peak of Alpine eclogite facies metamorphism in that area.
- Conditions for this ("meso-") Alpine lower-pressure overprint reached only greenschist facies in the western portion of the Monte Rosa nappe, with a well defined albite-oligoclase isograd (BEARTH, 1958) and, some kilometers further to the NE, the staurolite zone boundary (DAL PIAZ, 1971; NIGGLI, 1970) indicating a field gradient (Fig. 2) that mimics the pattern of regional isotherms for the Central Alps (TODD and ENGI, 1997). Only for this last overprint is it clear that P-T-conditions within the Monte Rosa nappe are comparable to those of neighbouring tectonic units; for the early Alpine and previous phases of the polymetamorphic evolutions, this has not been established and indeed appears unlikely to be the case. The age and duration of tha last Alpine thermal overprint are difficult to delimit precisely. A decreased in intensity and age from East to West is probable, but the time interval over which mineral transformations took place probable increased in the same direction. This pattern is indicated by available isotopic and fission track ages (discussed by ZINGG and HUNZIKER, 1990, HUNZIKER, 1992, and ROMER et al., 1996), and such a pattern is also expected on the basis of thermal models (ENGI et al., 2001; ROSELLE et al., 2001) for the thermal relaxation following peak regional metamorphism.
Paleogeographic reconstructions for the Monte Rosa nappe have come to widely differing conclusions, with some authors attributing the slice of continental crust to paleo-Africa, to the Briançonnais, or to the European margin. Though the debate is ongoing, recent suggestions (FROITZHEIM, 2001; DAL PIAZ, this volume) favor the latter scheme, based on the high pressure metamorphism (FROITZHEIM, 1997; GEBAUER, 1999; RUBATTO and GEBAUER, 1999) having reached its maximum depth on subduction during Eo- to Oligocene times.

Selection and analysis of single grain monazite

Samples collected for the present study are listed in Table 1, which also gives summary of minerals observed. Monazite grains occur in most of the paragneiss samples of the Monte Rosa nappe, but their abundance, size, and structural context are quite variable (SCHERRER et al., 2001a).
The microscopic context, e.g. monazite inclusions in garnet versus single monazite grains or clusters within the matrix, permits a clear separation of two phases of monazite growth in the metapelites. Well shielded monazite inclusions in garnet are compositionally homogeneous and range in size from <10 µm to >100 µm. In pelites and subpelites, such inclusions are found in large garnet porphyroblasts. A texturally different type of monazite inclusions, displaying symplectic textures (SCHERRER et al., 2001a) occurs as well, and these have been attributed to rapid decompression following high pressure conditions during Eo- to Oligocene times (SCHERRER et al., this volume). Far more abundant than either of these types are monazite grains in the matrix, occurring either at grain boundaries or, quite commonly, within biotite, white mica, or one of the aluminosilicate phases. These matrix monazites display many different morphologies, from fine grained trails or single grains to porphyroblastic relics. Texturally, they commonly appear partially recrystallised in between matrix minerals or fully recrystallized with these.
For the purpose of dating specific stages of the polymetamorphic evolution, we selected samples

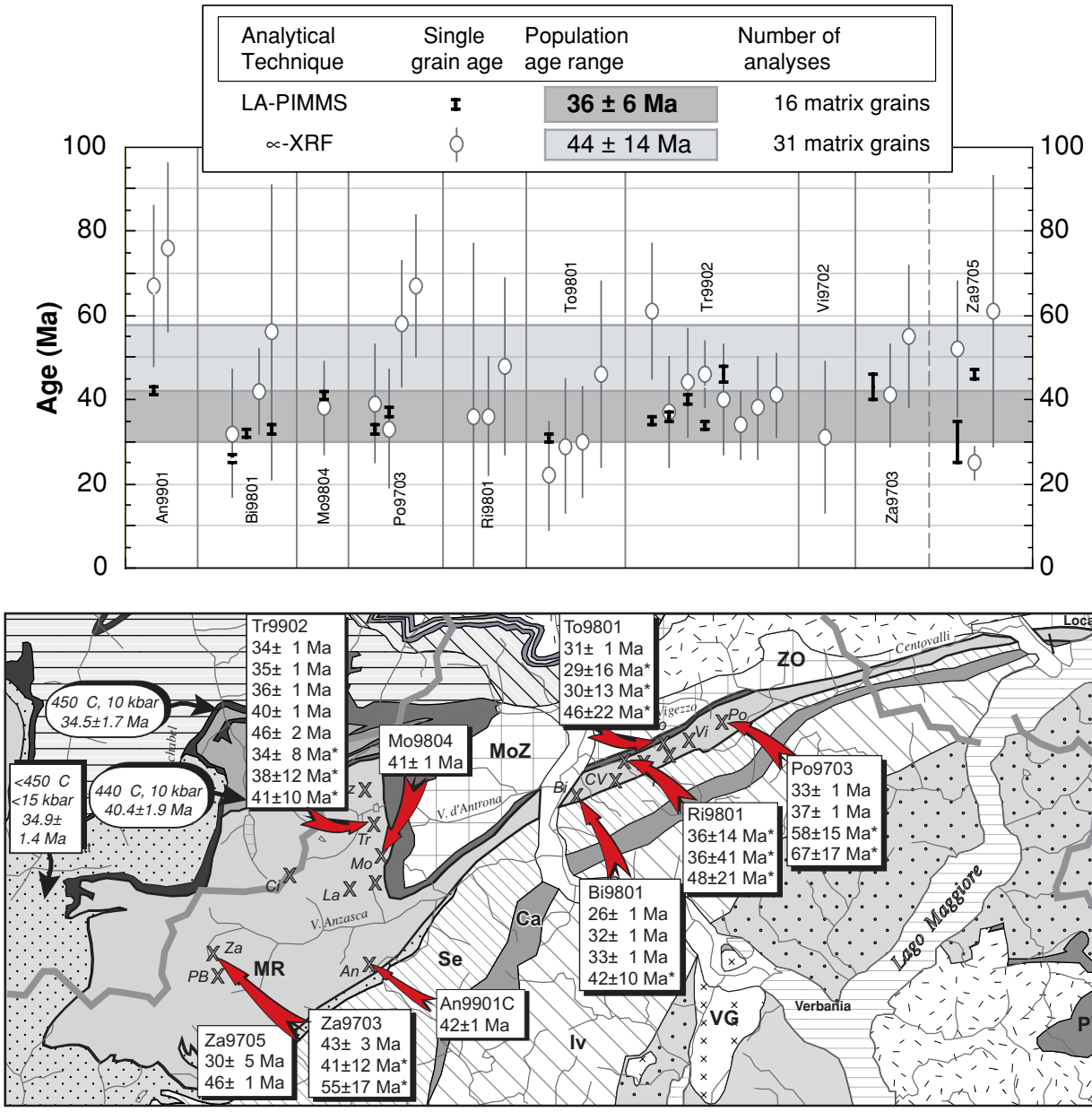

Figure 3: Age data for single monazite grains obtained by chemical and isotopic dating methods applied to the same grains. ?-XRF data denoted by asterisks; all others are LA-PIMMS data (SCHERRER et al., 2001 a).
(A) Data for Permian monazite population: 9 inclusions in garnet, 3 zoned matrix grains with inherited cores, 10 pre-Alpine matrix grains; (B) regional distribution of Permian ages. Data in brackets refer to cores of monazite grains from the matrix; all other grains were included in garnet porphyroblasts. 2?-error on PIMMS data is smaller than symbol size; uncertainty given for population of electron microprobe ages is nominal scatter, ignoring the error of individual EMP ages (60-100 Ma).

with sufficiently large monazite grains (>50 µm if possible) from texturally interpretable contexts, i.e. inclusions in garnet porphyroblasts, equilibrated metamorphic assemblages within the matrix, or reaction textures attributable to a specific breakdown reaction. The approach used in this study for Th-U-Pb dating of monazite is described by SCHERRER et al. (2000, 2001a). A combination of techniques was applied to document microstructures and select grains for dating. Besides the petrographic microscope, SEM and electron microprobe images (BSE and X-ray maps) proved most useful. The selection criteria required by the geochronological methods available set limits on what types of monazite could be dated and did not allow, for example, the analysis of certain fine grained reaction products, such as symplectitic monazite. Where the size and homogeneity of grains were sufficient, single monazite grains were first analyzed by electron microprobe and then painstakingly extracted from specially prepared thin sections, using techniques detailed by SCHERRER et al. (2000). Drilled out monazite grains were then analyzed (SCHERRER et al., 2001a) by XRF microprobe (at University of Bern) to obtain chemical Th-U-Pb ages, and a subset of the samples was subsequently dated by PIMMS (laser-ablation Plasma-Ionisation Multi-collector Mass Spectrometry, at NIGL, British Geological Survey).

Chemical and isotopic age data obtained from monazite grains extracted from our metapelite samples of the Monte Rosa nappe (Table 1) fall into three classes: Chemically homogeneous monazite inclu-

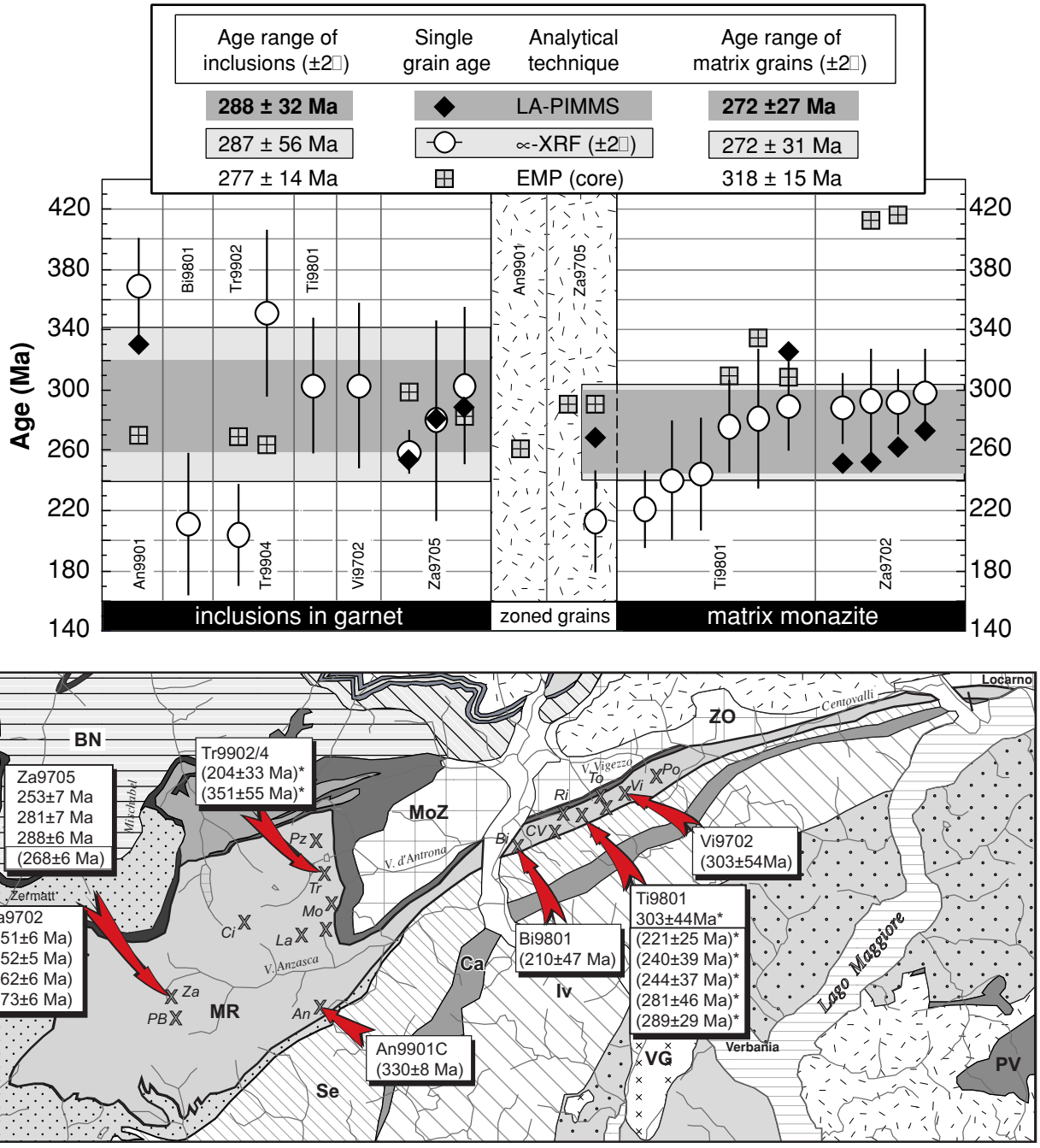

Figure 3: (cont) (C) Alpine monazite population: all 36 grains from matrix; (D) regional distribution of Alpine ages. Data in westernmost box from RUBATTO and GEBAUER (1999) for ophiolitic units adjacent to Monte Rosa nappe; data in oval boxes from FREY et al. (1976) for Monte Rosa metagranites.

sions in large garnet porphyroblasts are of Permian origin (Fig. 3a, b). Matrix monazite generally indicate Alpine ages (Fig. 3c, d), or they have a Permian core surrounded by an Alpine rim. Heterogeneous grains, some with clear core-rim structures and others with complex resorption features, seem to be more common to the west of the Antrona ophiolite and rare in the easternmost part of the nappe, i.e. the Southern Steep Belt. Monazite of Permian age only was observed in one sample, which apparently has escaped the effects of Alpine metamorphism.

Details of the age distribution in each sample are discussed in the subsequent chapter, in the context of the local textures and metamorphic assemblages to which the dated monazite grains belong. In the following, age results shown are those with the lowest analytical uncertainty available for any monazite grain. Errors (SCHERRER et al., 2001a) are quoted in the text at the 2 Sigma-level and, to identify the technique used, chemical XRF-dates are identified by an asterisk (e.g. 260 ± 25 Ma*), whereas PIMMS-ages are shown without a symbol (e.g. 325 ± 8 Ma).

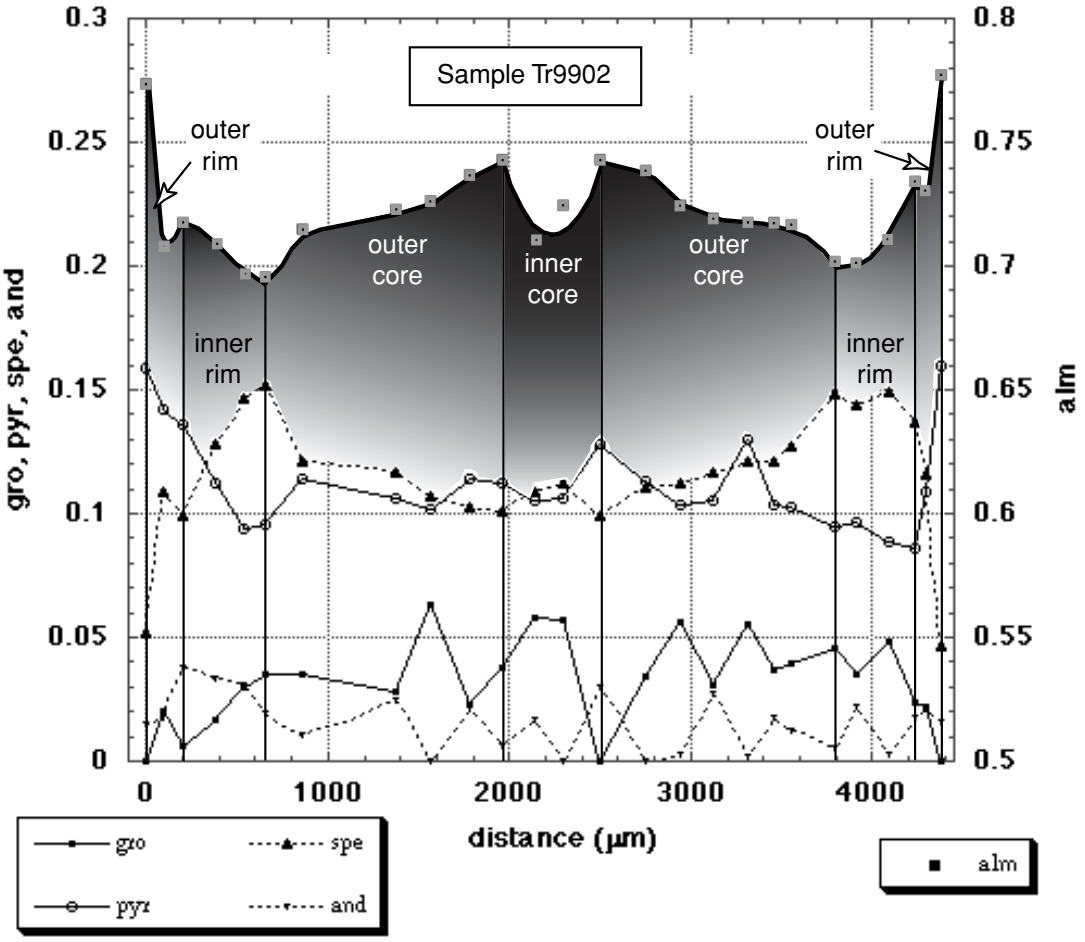

Figure 4: Compositional profile across large garnet porphyroblast in sample Tr9902, arguably representing three generations of garnet. A monazite inclusion within the core of similar Za9705 garnet indicates a uniform age of 259 ± 14 Ma, whereas large monazite grains in the matrix display a core-rim structure with a Permian core and an Alpine rim.

Petrologic evolution

Petrographic characteristics of Monte Rosa metapelites

Thorough petrographic investigations of metapelites were previously reported by BEARTH (1952), DAL PIAZ (1963), DAL PIAZ (1964), DAL PIAZ (1966), DAL PIAZ (1971), REINHARDT (1966), WETZEL (1972), and BORGHI et al. (1996). Typical constituents of Monte Rosa paragneisses include quartz, white mica (phengite and/or muscovite), biotite, garnet, ilmenite, rutile, apatite, monazite and zircon, with staurolite, kyanite and/or sillimanite, chlorite, plagioclase (albite or oligoclase), and allanite ocurring in some samples only. Local textural and mineralogical observations indicate that some metapelites retain partial evidence of their polymetamorphic history, whereas others apparently re-

Tab.2: Single crystal monazite ages (Tab. 1) and multi--equilibriums thermobarometry (TWQ) for metapelites from the Monte Rosa nappe

Sample	Bi9801a	Mo9801c	Pb9901c	Ri9801b2	Ri9801c4	Po9703b	Pz9905b
# rxn	3	3	3	4	3	3	3
P /kbar	11.0±1.0	11.7±1.3	9-12	12.1±1.6	12.0±1.5	10.0±1.0	9.2±1.8
T /∞C	610±25	755±65	730±30	735±55	730±50	595±25	620±60
P /kbar			17-21 *				
T /∞C			770±30 *				
Age range /Ma	33±1 to 26±1	41±1				37±1 to 33±1	
# grains	3	1				2	

rxn: number of independent equilibria used by TWQ (Berman, 1988)
grains: number of matrix grains dated (208Pb/232Th)
* relic higher pressure stage (?) indicated by some equilibria

set completely at some stage of their evolution. Hence it is essential to characterize assemblages at the grain scale, to check for local mineral (dis)equilibria and interpret the state of resetting prior to performing thermobarometry or mineral chronometry.

Within most of the samples analysed, garnet is Fe-rich (Alm60-85) and commonly occurs in (at least) two generations and with some grains showing typical prograde zonation or multiple overgrowth profiles (Fig. 4). Staurolite is regionally most abundant east of Val d'Ossola, particularly in the Southern Steep Belt, where generally few relics of high pressure metamorphism have been reported for the Monte Rosa nappe. However, staurolite of an earlier generation is present also in several samples from further West, outside the staurolite zone boundary (NIGGLI and NIGGLI, 1965; NIGGLI, 1970), in samples retaining high pressure assemblages. On the other hand, chloritoid, phengitic mica (3.3-3.4 Si p.f.u.), rutile, plus kyanite or silliminanite, have been found only to the west of the Antrona trough (Fig. 2). Plagioclase is sparse and where analyzed is of oligoclase composition (~An30). Three types of white mica could be distinguished, with paragonitic and phengitic mica being restricted to the western samples, whereas muscovite (<3.1 Si p.f.u.) is widespread throughout the nappe. Where rutile occurs, it is commonly rimmed by ilmenite, except where protected within in porphyroblasts of gar1 or stau1. Chlorite appears mostly linked to late greenschist facies over-

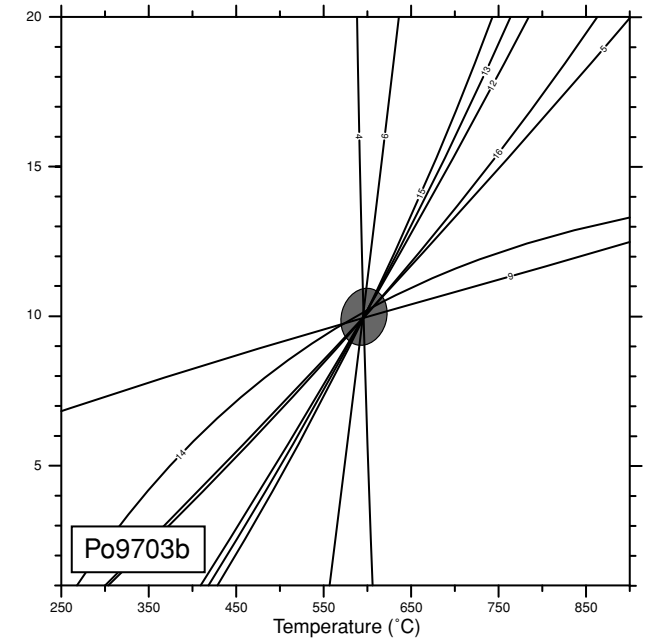

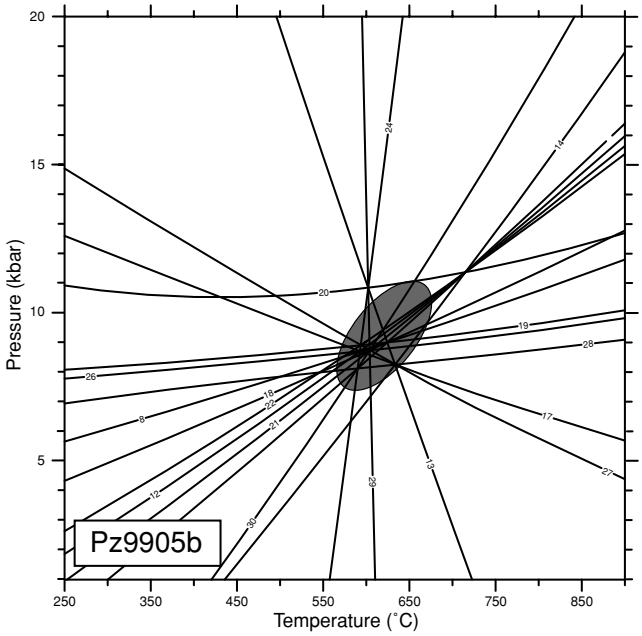

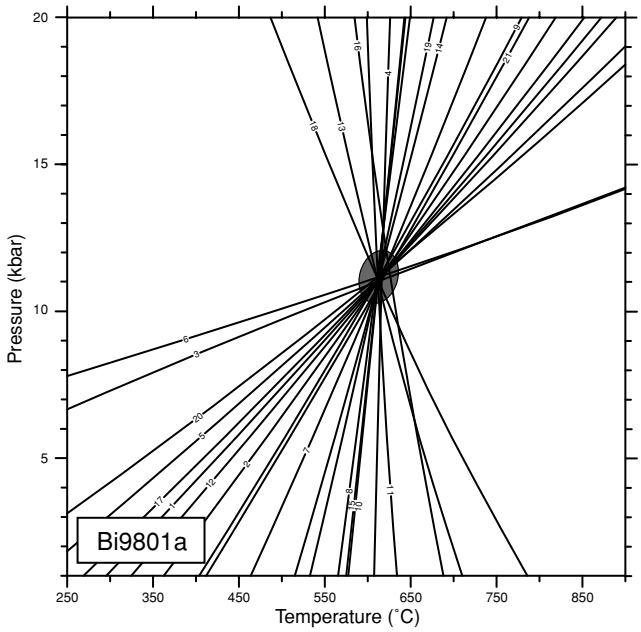

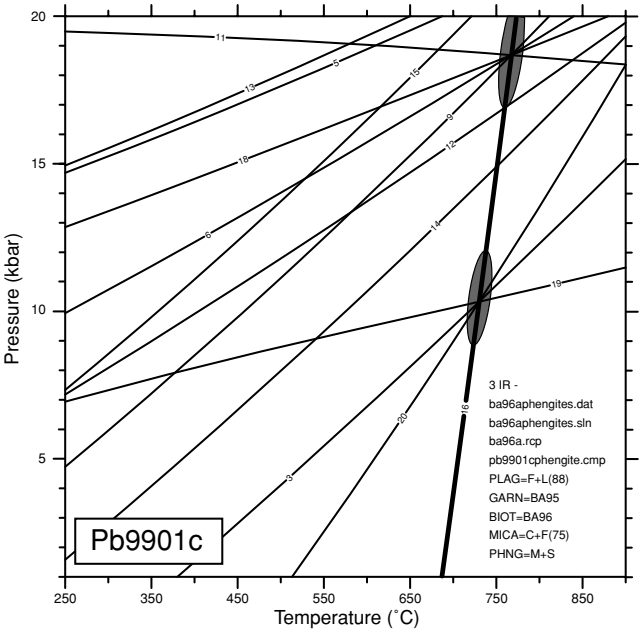

Figure 5: P-T-diagram showing location of fluid-absent equilibria computed using TWQ for phase compositions measured in samples Po9703 and Bi9801. P-T-uncertainty shown by ellipse. Thermodynamic models used and restrictions applied are discussed in text. Individual equilibria are numbered, for reactions see Appendix.

Figure 6: P-T-diagram showing location of fluid-absent equilibria computed using TWQ for phase compositions measured in samples Pz9905 and Pb9901c. See text and Fig. 5 for further details.

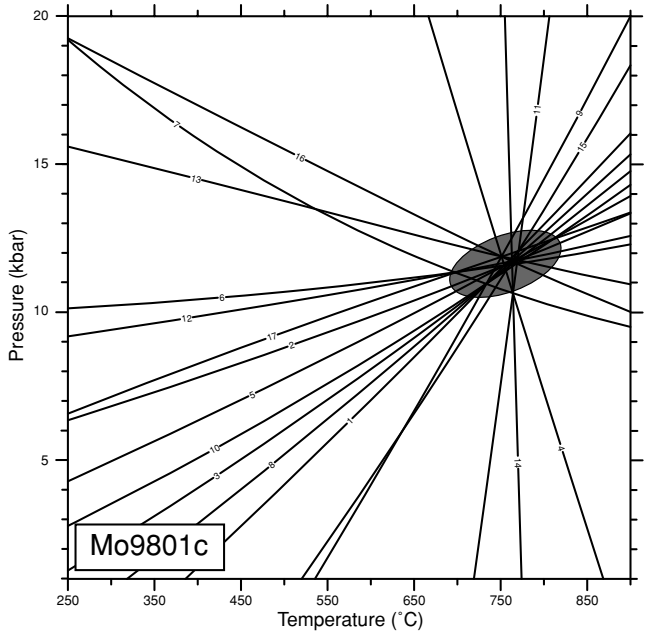

Figure 7: P-T-diagram showing location of fluid-absent equilibria computed using TWQ for phase compositions measured in samples Mo9801 and in two domains of sample Ri9801. See text and Fig. 5 for further explanations.

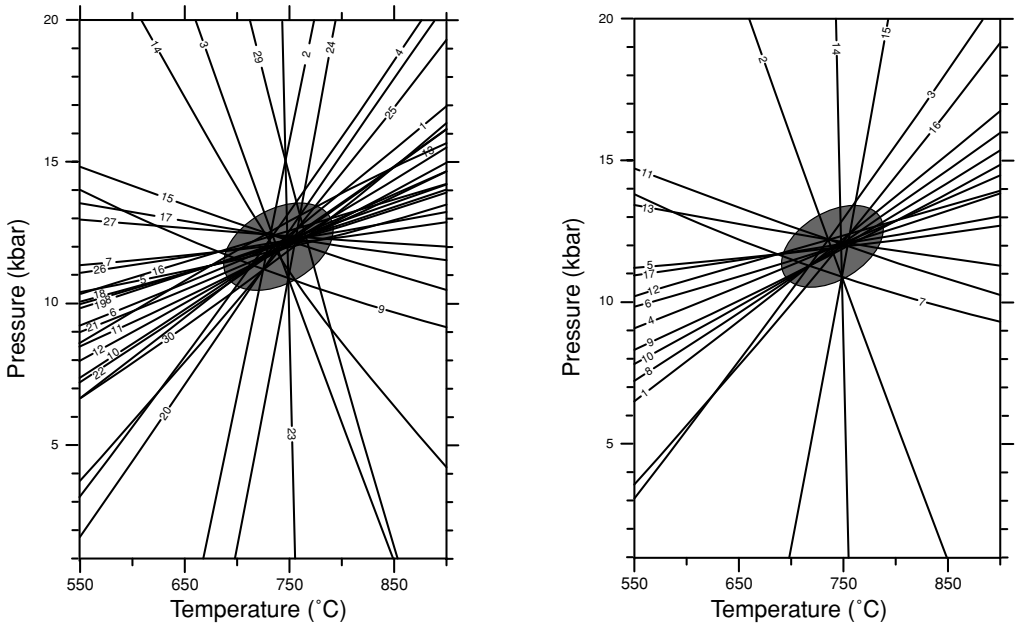

printing, but in some samples it is clearly part of the higher pressure assemblages.

Based on textural relationships, Alpine metamorphic assemblages can be divided into higher and lower pressure assemblages, as previously discussed by BORGHI et al. (1996). At higher pressure the assemblages include Qtz-Ph-Cld-Chl1-Grt1-Ky-Rt±Ilm-±Pg±St1 and at lower pressure Qtz-Ms-Bt-Grt2±St2-±Olig/Ab+Ep.

A select set of individual samples (Table 2) and groups thereof are presented below according to petrological criteria and monazite age data.

Methods used

The characterization and interpretation of polymetamorphic samples demands particular attention to microstructural characteristics, such as relics and domains containing neoblasts of one or more phases overgrowing older assemblages. Apart from careful petrography and comparison to suitable petrogenetic grids, the availability of monazite ages from several individual structural domains of a sample has proven most helpful. Assemblages used in this study to constrain metamorphic P-T-conditions were selected after monazite grains from the same domain had been age-dated with credible results. The aim was thus to obtain thermobarometric data for a particular stage in the metamorphic evolution of the sample. Of course the simultaneity of monazite growth (or complete recrystallization) and of chemical equilibration of the silicate-oxide assemblage used for P-T-determinations cannot be guaranteed. However, criteria such as the chemical homogeneity of monazite and of the major constituent phases analyzed, their alignment in one and the same penetrative foliation, as well as clean boundaries indicative of textural equilibrium, have been used to support (or reject) the hypothesis. Despite these precautions, the thermo-

barometric multiequilibrium approach used indicates that we were not always successful in avoiding disequilibrium assemblages. In a few samples, mineral disequilibria were thus detected only when computing phase diagrams based on microprobe data.
All phases of potential equilibrium assemblages, selected from dated samples, were analyzed by electron microprobe (Cameca SX50, 15 kV, 20 nA; WDS mode, using synthetic and natural standards). Analyses were obtained within small domains selected in thin section, where possible on grains in direct contact. Data were screened to ensure sufficient quality of analyses used. Probe data were normalized according to the requirements of the thermodynamic analysis, using TWQ (BERMAN, 1991) with the dataset by BERMAN and ARANOVICH (1996). In addition, we adopted the revised phengite model by MASSONNE and SZPURKA (1997), the improved thermodynamic properties for staurolite by NAGEL et al. (2001), and an ideal activity model for Mg-Fe-chlorite. To avoid large uncertainties in activities, we excluded mineral components present in very low concentration, i.e. Xcomponent < 0.05 (TODD, 1998). To evaluate the P-T-conditions preserved in any analyzed assemblage we considered all of the (fluid-absent) equilibria computed to be stable anywhere in the P-T-domain [200-1200°C, 1-20 kbar]. The intersection pattern of all of the stable and metastable branches of these possible equilibria was inspected as a first indication of the suitability of the complete assemblage. Depending on the number of phase components involved, the number of independent equilibria turned out usually between 4 and 2. In the latter case, a unique P-T-intersection results, reflecting merely the paucity of the assemblage, the quality of which then cannot be evaluated using TWQ alone. In such cases, it was sometimes possible to check the quality of the P-T-result by comparing the observed assemblage against a suitable petrogenetic grid and by performing the following experiment: Assume that the activity of TiO2 and/or Al2SiO5 equals unity, i.e. that the assemblage was in fact saturated in rutile and/or kyanite (or sillimanite), compute the P-T-diagram again. Then evaluate all of the additional equilibria generated as limiting the space for which a(TiO2) < 1 and/or a(Al2SiO5) < 1. This approach thus utilizes not only the phases present, but also includes the observed absence of the respective titanium or aluminosilicate phase(s). Judging by the consistency of P-T-intersections and the narrow P-T-fields obtained using this approach, we conclude that many of the metapelites investigated appear to be only very slightly undersaturated in the respective phases. In such cases, this experiment sets very useful additional limits in thermobarometry. Its application is, of course, not restricted to "poor" assemblages, i.e. with only two independent reactions. Where 3 or 4 equilibria were independent, the dispersion of invariant points in P-T-space was inspected and, in some cases, overall equilibrium appeared to be well preserved (e.g. Fig. 5, 7). In other cases, all but a few equilibria seemed well behaved, and outliers involved one particular phase component (Fig. 6). This was commonly found to be siderophyllite or rutile. In the former case, the discrepant results may well be caused by an inadequacy in the thermodynamic model, whereas for rutile petrographic evidence usually indicated an irreversible reaction, such as partial replacement by ilmenite. In either case, the hypothesis of a completely intact equilibrium assemblage could not be maintained, the violating mineral species or component was eliminated, and TWQ analysis continued without it. Results shown in the subsequent paragraphs indicate that completely convincing equilibrium assemblages are indeed rather rare in the samples we investigated, but reliable thermobarometric constraints can be derived from a few of them.

Permian metamorphism

In several areas, including the central portion of the nappe to the West of Macugnaga, BEARTH (1952) had mapped metasediments showing little or no Alpine overprint. A suite of metapelites, sandwiched between the main mass of Macugnaga augengneiss and granitic tectonites of the Stelli zone, was sampled near Alpe Pedriola, NW of Pizzo Bianco. Most of these samples (Za-suite in Tables 1 and 2; cf. Fig.1) show the early stages well preserved. In particular, Za9702 displays no signs of a high pressure or retrograde greenschist facies overprint, i.e. the sample appears to have largely escaped Alpine metamorphism. In contrast to samples of chloritoid bearing garnet-mica gneisses (Za9703, Za9705) from the same area, Za9702 also lacks a penetrative foliation. It contains exceptionally abundant fibrolite and K-feldspar, three generations of garnet, and unusual textural characteristics of biotite and white mica. The earliest generation of garnet is present as subidiomorphic grains (~5 mm in diameter), with no evidence of corrosion or overgrowth on them, but with random needles (sillimanite? up to 3 mm in length) crosscutting the grains. Surrounding this earliest generation of garnet is a fine grained felt of fibrolite plus quartz. This sillimanite-rich felt is thickest at opposing ends of garnet porphyroblasts, suggesting the replacement of previous pressure shadows. A dense cluster of roundish garnet grains overgrew the felt and partially replaced it. The only hint at a weak foliation in this sample is given by corroded platelets of coarse biotite that surround the felt rimming the first generation garnet. Biotite is conspicuously reddish-brown, may show delicate symplectic fringes and was replaced, near its margin to fibrolite, by elongate poikilitic garnet containing quartz, K-feldspar, and abundant tiny ilmenite grains as inclusions. These textural and mineralogical features, notably the extreme enrichment in sillimanite, lead us to interpret this sample as a restitic metapelite. In view of the regional homogeneity of the metapelites (BEARTH, 1952), it appears that a significant portion of the leucosome was lost of from its pelitic protolith dur-

ing or following partial melting. Millimeter-size pockets dominated by quartz and K-feldspar, containing some 30% randomly oriented muscovite and biotite, with only traces of sillimanite, may represent seggregates of such leukosome.

Four monazite grains from the matrix of sample Za9702 were dated, yielding a median age of 252 ± 9 Ma (PIMMS data, Table 1). These ages are but slightly younger than those obtained from monazite enclosed in garnet in sample Za9705 taken a few hundred meters away, for which 281 ± 16 Ma resulted. These data represent maximum ages for the garnet from which the respective monazite inclusions were extracted, hence no significant age difference between the porphyroblasts and the matrix monazite can be detected. In sample Za9705, however, monazite grains in the matrix indicate that it has been partially reset, probably due to recrystallization of monazite in the matrix. Ages obtained gave a bimodal distribution: Three monazite grains evidently recystallized at Alpine times (30 ± 5, 46 ± 1, 61 ± 32 Ma*[1]); two grains are zoned, one of which gives an intermediate age (145 ± 5 Ma) probably due to overgrowth of a Permian core by an Alpine rim, the other one appears unaffected (268 ± 6 Ma), as does another matrix monazite (290 ± 120[2] Ma). In a third sample of that suite (Za9703), all of the monazites from the matrix show Alpine ages between 43 ± 3 and 55 ± 17 Ma. Evidently this suite of high-grade metapelites experienced unequal amounts of recrystallization in post-Permian times, with some samples showing Alpine chloritoid ± staurolite ± chlorite, but Za9702 does appear remarkably unaffected by Tertiary events.

Even more exceptional is sample Ti9801 from taken just SW of Pizzo Tignolino, some 8 km SE of Domodossola. Despite the strong strain evident in the Southern Steep Belt portion of the Monte Rosa nappe, this staurolite-chlorite-tourmaline bearing garnet-biotite-muscovite schist indicates the preservation of Permian (and possibly older) ages of monazite within garnet porphyroblasts and in the matrix! For the latter, the median age is 260 ± 25 Ma* from XRF chemical dating, whereas one grain dated by PIMMS gave 325 ± 8 Ma; only one monazite inclusion in garnet could be dated, yielding 303 ± 44 Ma*. As in the previous suite, we infer that the Alpine metamorphism, which in this locality reached lower amphibolite facies conditions, did not reset the Permian ages even in the matrix. Yet the silicate assemblage in this case does not look particularly different from those in neighbouring samples, many of which demonstrably did equilibrate during Alpine times (below). We cannot be sure whether the silicate assemblage in Ti9801 does retain the characteristics of the Permian metamorphism. However, since this sample as well as Za9702 discussed above were taken but a few hundred meters away from intrusive contacts to major granitic bodies, it seems likely that the assemblages were formed by Variscan contact metamorphism and not by a Permian regional event. The P-T-conditions of formation or equilibration were not investigated further.

In several other samples (Tr9902, Tr9904, Vi9702) monazite inclusions in garnet indicate Permian ages, but in all of these the matrix assemblages, including monazite, had evidently recrystallized in Alpine times. Though garnet (gar1) in these samples typically contains numerous inclusions, none of them had sufficiently complete inclusion assemblages to warrant thermobarometry. For this reasons, no precise P-T-conditions could be determined for the Permian regional metamorphism.

Alpine high pressure overprint

A group of our samples shows complex zoning in garnet porphyroblasts and characteristic overgrowth textures that document the transition from pre-Alpine to early-Alpine conditions. Typical in metapelites is a mica-rich matrix dominated by white mica - commonly muscovite and phengite - but with only subordinate biotite, kyanite overgrowing and partially replacing fibrolite, small and commonly roundish garnet of a a second generation, stubby to long-prismatc staurolite, bands of mosaic quartz with sporadic oligoclase and, in mica-free domains, K-feldspar.

In samples showing tectonite fabrics, however, the high-pressure overprint is extensive and obvious. In Monte Rosa metagranites affected (DAL PIAZ and LOMBARDO, 1986; FREY et al., 1976), phengite has Si-contents of 3.35-3.41 p.f.u., Ti-biotite typically shows Mg/(Mg+Fe2+)=0.36 ± 0.06, and assemblages include albite + epidote (or oligoclase), microcline, quartz, as well as accessory titanite, garnet, tourmaline, and magnetite. Phengite in metapelites show Si-contents similar to these, except where subsequent exsolution (discussed below) lead to a new generation of low-celadonite micas. Thermobarometric and age data for metagranitoids, based on FREY et al. (1976), are shown in Figure 2. Included are only those samples, for which Fe/Mg exchange data for phengite and biotite, as well as oxygen isotope temperatures, indicate the attainment and preservation of equilibrium (i.e. #366, 377, 405); pressure values shown for these samples are based on the calibration of MASSONNE and SCHREYER (1987) and Si-values reported by FREY et al. (1976); all ages shown from that study are Rb-Sr isochron results. Results from metabasites studied by DAL PIAZ and LOMBARDO (1986) and BORGHI (1996) are also shown. All three studies indicate a low temperature eclogite stage, with preserved equilibria showing mostly 500±50°C, 10±2 kbar, dated at 35-40 Ma.

In the metapelites we studied, assemblages differ somewhat from eastern to western parts of the Monte Rosa nappe. In the East, two samples from Valle Vigezzo (Po9703 and Bi9801; cf. Fig.1, 5; Tab.1, 2) deserve detailed characterization:

[1] Where no PIMMS-data are available, XRF-data are quoted and denoted by an asterisk.

[2] Large error due to low Th-contents of grain

- Po9703 is a banded, tightly foliated garnet-biotite-muscovite-staurolite-schist sampled NE of Porcella. Grain boundaries are clean and commony straight, aligned monazite grains occur abundantly throughout the matrix that contains recrystallized intergrowths of muscovite and minor biotite. Roundish grains of garnet do not appear to represent more than one generation; similarly pale staurolite is present only in one idiomorphic habitus, as stubby prisms. The Ti-phase is ilmenite only, neither rutile nor titanite have been found. Aluminosilicates are missing, but adjacent samples commonly contain kyanite. TWQ analysis indicates equilibration at conditions close to 600°C and 10 kbar (Fig.5) which appear consistent with the assemblage observed, and the field delimited by the location of equilibria involving kyanite (not shown) includes the three invariant points computed for the observed assemblage. Hence the P-T-result appears credible. Matrix monazite dated from this assemblage indicates an age of 35 ± 2 Ma which is interpreted as the age of equilibration.
- Bi9801 was collected at Alpe Bisoggio, SE of Beura (E of Villadossola) and is very similar to Po9703, both texturally and mineralogically, except that a few larger grains of garnet (gar1) occur and minor fibrolitic sillimanite (but no kyanite) are observed in the mica-rich matrix. Calculated equilibration conditions (Fig.5) are shown for mineral compositions excluding siderophyllite equilibria. The remaining three independent reactions indicate similar P-T-conditions, near 600°C and 11 kbar, reflecting conditions well within the kyanite field. A single monazite grain from a garnet porphyroblast could be extracted and dated, giving an age of 211 ± 47 Ma*, i.e. indicating that gar1 may represent a Permian relic. Monazite from the matrix occurs in two textural types, as single grains and clusters (SCHERRER et al., 2001a). Our age data indicate recrystallization between 33 ± 1 and 32 ± 1 Ma, and possibly (partial?) resetting at 26 ± 1 Ma. One way to interpret all of these data is to invoke decompression from =11 kbar, starting around 34-31 Ma, into the fibrolite field (~5 kbar, assuming isothermal decompression) by 27-25 Ma.

Samples studied from part of the Monte Rosa nappe to the West of Valle d'Ossola include those to the North and South of the upper Val d'Antrona (localities labelled Pz, Ri, Mo; Fig. 1, 6, 7; Tables 1 and 2). Many of these contain overgrowth textures and mineralogical evidence of their polymetamorphic evolution, e.g. chloritoid + kyanite near sillimanite + K-feldspar. Attempts to use TWQ for any of these samples produced highly dispersed patterns with P-T-intersections commonly outside the stability fields of the observed assemblages. Two samples do appear well equilibrated, however:

- Tr9902 is a fine-grained micaschist containing garnet (gar1) porphyroblasts of >5 mm diameter, sprinkled with tiny inclusions of epidote(?) and with coarse biotite + phengite + quartz in adjacent pressure shadows. Abundant roundish, small grains of garnet (gar2) with dark cores appear in the mica matrix which contains subordinate quartz, K-feldspar, chlorite, apatite, and rutile rimmed by ilmenite. The matrix and the rock as a whole are not foliated, and the mica assemblage displays pale biotite as rims around muscovite and lamellar patches within coarse white mica. These are interpreted as exsolution features from phengite breakdown (FERRARIS et al., 2000), and the microstructural evidence does not suggest extensive recrystallization during or following that process. Thermobarometric results for three sets of local mineral compositions suggests equilibration conditions between 550-610°C and 9 ± 2 kbar. The stability field of the observed assemblage and the kyanite-absent field appear to be consistent with the TWQ-intersections, but with only two independent mineral equilibria being usable, the control on the P-T-data is not great. - Monazite occurs both as discrete grains in the matrix and as inclusions in gar1. Ages obtained for the former indicate a range (from XRF-data only) of 34 ± 8 to 50 ± 17 Ma*, consistent with the only PIMMS date available of 46 ± 2 Ma. Monazite inclusions in early garnet yielded 204 ± 33 and 212 ± 35 Ma* as a maximum age for gar1 - again seen as evidence of the persistence of Permian (?) garnet. In an adjacent sample (Tr9904) early garnet porphyroblasts contain monazite suggesting an even older age (Table 2), as well as xenotime too small to be dated by the techniques used in this study.
- Pz9905 is a staurolite bearing garnet-biotite-white mica gneiss collected on the ridge N of Cime di Pozzuoli. It shows similar characteristics to Tr9902, and despite soome P-T-scatter TWQ indicates similar equilibration conditions as well, 620 ± 60°C and 9.2 ± 1.8 kbar (Fig.6). No monazite grains from this sample have been dated, but the consistency between ages obtained for similar samples (Tr9902, Tr9904, and Mo9804) from the NE-portion of the Monte Rosa nappe indicates that these P-T-conditions probably pertain to a similar time segment, i.e. ~40-35 Ma ago. Phengite breakdown textures such as those described above have been observed in many samples from the northeastern and central parts of the Monte Rosa nappe, including those of the Mo- and Pb-suites (Fig. 1, Tables 1 and 2). A typical example is shown for Pb9901c (Fig. 6), with pressure-sensitive equilibria scattering broadly for a single assemblage, as well as from one sample or microscopic domain to the next. Fe-Mg exchange equilibria, notably for garnet - biotite, yield far more consistent temperatures, ehce it is tempting to regard the scatter in pressure intersections as indicating a possible decompression path. Though no quantitative pressure bounds can be extracted, it may be safe to interpret the P-T patterns for such samples as representing some stages along their Alpine decompression paths. None of the assemblages for which reliable P-T intersection patterns have been documented indicate the preservation of pressures beyond 12 ± 1.5 kbar, but the textures described make it likely that the nappe had in fact reached somewhat higher pressure conditions previously. The lack of complete recrystallization dur-

ing the decompression stage may also be responsible for at least part of the dispersion among thermobarometric results of other samples than those described here in detail.

Thermal overprint and retrograde features

Many samples from the portion of the Monte Rosa nappe to the East of Valle d'Ossola are dominantly characterized by extensive re-equilibration under medium pressure amphibolite facies conditions, as evidenced by the abundance of muscovite and the appearance of a new generation of idiomorphic staurolite and/or small almandine-rich garnet. Relic phengite is but locally preserved in masses of celadonite-poor muscovite that contain ill defined patches or lamellae of phlogopite in minor amounts (<5%), presumably again due to exsolution from phengite. In more recrystallized samples, such intergrowths developped discrete grain boundaries between muscovite and biotite; thin lamellae (from <1 to 5 µm) of pale biotite are observed even in idiomorphic muscovite grains >200 µm in size. Kyanite is the stable aluminosilicate polymorph, by contrast to some pelites in tectonic units adjacent to the Monte Rosa nappe, especially in eastern parts of Valle Vigezzo and in Centovalli, where sillimanite occurs (NIGGLI and NIGGLI, 1965; TODD and ENGI, 1997). As outlined for sample Bi9801 (see previous section), the Monte Rosa nappe may have been exhumed rapidly enough, such that eastern portion of the nappe experience decompression in the sillimanite field, leading to the local formation of fibrolite (around 26 Ma ago?).

In addition some metapelites show late greenschist facies retrogression, both East and West of Valle d'Ossola. In the former case, this is probably linked to a late imprint after the amphibolite facies thermal maximum, bot outside the Alpine staurolite field, it is impossible to discern two stages. Neither P-T-data not monazite ages interpretable as a specific stage of retrogression could be documented.

Implications

Tectono-metamorphic evolution of the Monte Rosa nappe

The pre-Variscan metamorphic evolution cannot be defined clearly on the basis of the present results. Sporadic monazite ages found along the southern margin of the nappe (yielding 325±8 Ma in the matrix of Ti9801; 330±8 Ma in An9901 inclusions from texturally old garnet porphyroclasts) agree, within error, with the Rb-Sr isochron age of 310 Ma (±50 Ma according to HUNZIKER, 1970; ±20 Ma according to FREY et al., 1976), interpreted as the age of formation or emplacement of the Monte Rosa granodiorite pluton. Present knowledge, unfortunately, does not constrain the depth of emplacement of this major magmatic body. The isolated garnet grains containing the oldest monazite dated here are interpreted as contact-metamorphic in origin.

The late Variscan phase of magmatism, dated by HUNZIKER (1970) and HUNZIKER and BEARTH (1969) at 260±10Ma, produced lesser but widespread volumes of granitic magmas. Permian contact metamorphism is thought to have caused well equilibrated assemblages to form in metapelites such as the Za-suite described in this study. In most samples of that suite sillimanite and K-feldspar are abundant, and only samples demonstrably affected by the Alpine event contain texturally younger kyanite, an approximate pressure bracket of 5 ± 2 kbar may be

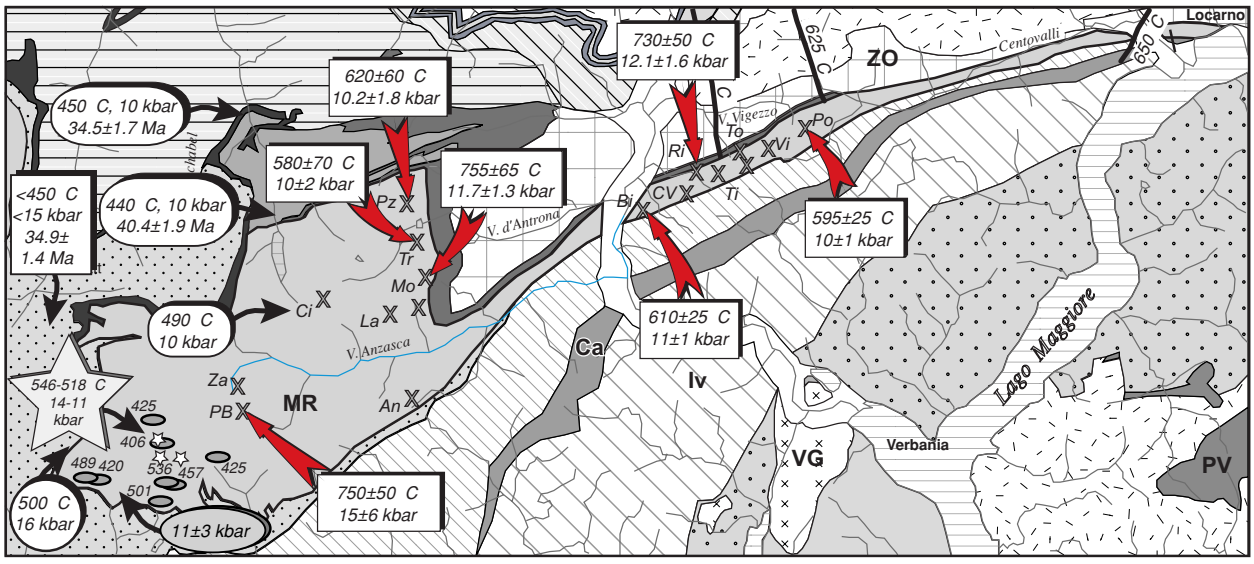

Figure 8: Comparison of metamorphic conditions derived for Alpine high-pressure (exhumation) stage in present study of metapelites, with data from the literature for other rock types. New data shown in rectangular boxes with broad arrows indicating sample locations; other symbols as in Figure 2.

estimated for the intrusive activity around 260 Ma. Monazite grains from many garnet porphyroblasts and a few matrix assemblages, covering a very large portion of the Monte Rosa nappe, indicate ages within error of this magmatic phase. It appears likely, therefore, that one cannot separate the thermal effects of contact metamorphic from those of a regional metamorphic phase with associated penetrative deformation (HUNZIKER, 1970; HUNZIKER and BEARTH, 1969). In view of the indicated intrusive depth of 10-20 km, advective heating during the extended Variscan magmatic activity may well have raised the geothermal gradient regionally. Upper amphibolite facies assemblages, such as those documented in the present study, including restitic migmatite portions, would thus have possibly resulted from partial melting during that phase. This is not to suggest that the granitic magmatism in the nappe at that time resulted from in-situ partial melting, but the absence of thermal aureoles, the paucity of skarn-like features, and the high grade overprint evident in metapelites at least suggest a close link in space and time.

For the Alpine time period, no early subduction-related prograde metamorphism is evident in metapelites, except possibly in a few chloritoid-bearing assemblages in the central part of the nappe (e.g. Za 9705). It seems unlikely that the P-T-t-relations derived from the Alpine assemblages correspond to the deepest subduction stage, given the widespread evidence of phengite (partial) breakdown observed. Probably, partial re-equilibration occurred during ascent or extrusion of the Monte Rosa nappe. Remarkably, however, the pressures obtained are almost always around 9-11 kbar, and for a time segment near 35-40 Ma. No significant regional pressure gradient could be documented for the exhumation stage (Fig.8), nor is a regional age progression discernible, within the uncertainty of the available data for that stage (Fig.3d) of the Monte Rosa thrust sheet.

Whether the higher pressures found by CHOPIN and MONIÉ (1984) and LE BAYON et al. (2001) reflect marginal fragments of the thrust sheet that attained somewhat deeper levels, or whether these conditions reflect the (maximum?) depth reached by the entire nappe, is not clear at the moment. The temperatures obtained in these two studies (~500°C) are remarkably low, compared to our thermometric results. One certainly cannot rule out the possibility of substantial heating during emplacement of the thrust sheet to mid-crustal levels (e.g. BROUWER, 2000; ENGI et al. 2001), but it is also possible that fragmentation of the Monte Rosa nappe occurred in the subduction channel, with some parts reaching greater depth. Evidence for deep extrusion of fragments is available from the ultra-high pressure (UHP) conditions reported from the nearby Lago di Cignana area (REINECKE, 1998; VAN DER KLAUW et al., 1997).

In samples taken to the East of Valle d'Ossola, the Barrovian overprint is strong and has traditionally been assumed to have obliterated most of the earlier high-pressure effects. However, the P-T-conditions indicated by the best-equilibrated of the samples presented in this study indicate a clear discrepancy to the Barrovian conditions (TODD and ENGI, 1997) established for metapelites of adjacent tectonic units (Fig.8), for which pressures are at least 2-3 kbar lower. Assuming that the conditions documented by the multi-equilibrium thermobarometry correspond approximately to Tmax and P(Tmax), this discrepancy in pressure indicates that the Monte Rosa nappe reached its Tmax-conditions during emplacement into the surrounding units, and somewhat earlier (i.e. at a deeper level) than these. Because the temporal constraints are not tight for this phase in adjacent units, no precise inference on the dynamics of emplacement can be derived. However, the emplacement suggests a tempting explanation for the remarkable "protrusion" of the isotherms (FREY et al., 1999) to the SW of the Lepontine dome, in that the rapid extrusion of the Monte Rosa nappe may have introduced advective heat and possibly generated additional shear heating. This heat source would then have perturbed the simple geometry of the regional thermal anomaly depicted by the isotherm pattern further east (ENGI et al., 1995; TODD and ENGI, 1997). The temporal constraints available for the transition from high-pressure to Barrovian conditions in the Monte Rosa nappe certainly permit such an interpretation.

Relevant in this respect are also recent age data by ROMER et al. (1996) for a suite of dykes from eastern parts of the Monte Rosa nappe, which were very accurately dated for two localities. U-Pb ages were obtained from zircon at 30 to 28 Ma, and from xenotime at 26 Ma, all interpreted as dating the postkinematic emplacement of late magmatic aplites and pegmatites under waning metamorphic conditions.

Behaviour of metapelites and monazite within these during polymetamorphism

One of the samples studied retains only Permian characteristics, presumably because it was not exposed to significant deformation or fluid-rock interaction during the Alpine cycle. In this case, both the assemblage of the rock forming minerals (see previous section) and the U-Th-Pb system in monazite are interpreted as having preserved a Variscan state (Table 2). These are remarkable results, as there is no doubt that these samples experienced subsequent subduction to at least lower crustal depth, involving reheating to 550-650°C and rapid extrusion in a convergent setting. We note that the classical study by KÖPPEL and GRÜNENFELDER (1975) reported dates on monazite separates from Monte Rosa granite and one of the metapelites (from Camplicciolli), and that both of these gave U-Pb ages of 260±5 Ma!

Many other samples retain partial Permian characteristics, including undisturbed monazite in porphyroblasts and -clasts, even where matrix recrystallization caused complete resetting of the

monazite grains in the micaschist portion of these samples. Rather few monazite grains indicate "mixed" ages, presumably due to old cores or domains having been overgrown by Alpine monazite. Such intragrain zoning in monazite has commonly been visualized by means of backscatter images in the EMP, and the main chemical cause is due to heterogeneity in Th contents. However, because EMP techniques are inadequate to date young monazite chemically (the limit being <100-200 Ma, depending on Th contents), and the spatial resolution of the µ-XRF and LA-ICPMS instruments is insufficent to resolve different age zones (Fig. 3) in single grains of the size available, "mixed ages" cannot be avoided in some cases (SCHERRER et al., 2001a).

The occurrence of old monazite inclusions in garnet is best explained if the garnet cores are also assumed to be of Permian age. This hypothesis is supported by chemical zoning patterns observed in some of the large garnet grains that show a homogeneous core surrounded by one or more growth rims (chemical profile in Fig. 4). We thus think that the cores of such garnet grains are Permian in age, with the rim being due to Alpine metamorphism. It is not impossible, of course, that the entire garnet might be Alpine in age, but with its core portion simply having included old monazites. This interpretation would require garnet growth at an early Alpine stage prior to the recrystallization of monazite. Because garnet shows a compositional change between core and the overgrowth rim, the Alpine growth of garnet would have had to be polyphase. The observed zoning patterns are thus more in agreement with a Permian origin.

Even in a sample with strong retrogression (Ti9801), monazite in a garnet retains a Permian age, whereas monazite in the chlorite-mica matrix yield mixed ages (Table 2; Fig. 2). The preservation of Permain monazites in matrix (see also sample Za9702), as well as the occurrence of mixed ages in a "Alpine" chorite-mica matrix indicate that the presence of fluid and certain metamorphic conditions are not the only factors controlling the "resetting" of monazite. A process related to growth and/or recrystallization of monazites are necessary to reset the monazite. Understanding monazite forming reactions is needed to use such data in deciphering the P-T-t evolution. Reactions of monazite are indicated by symplectites described in SCHERRER et al. (2001b) and can be also inferred from element compositions. For example, zoning patterns of yttrium in monazite, with enriched cores and depleted rims within the heterogeneous grains, support the observation and idea put forward by PYLE and SPEAR (1999) and FOSTER et al. (2000), i.e. that high yttrium monazite growth precedes garnet growth, whereas monazite growing after garnet nucleation tends to be depleted in yttrium. Xenotime has been observed in a few samples of the metapelite suite investigated here, but its grain size is insufficient for single grain dating by the methods employed.

Conclusions

New P-T-t data have been derived from the polymetamorphic basement rocks of the Monte Rosa nappe. 'In-situ' micro-dating of monazite by PIMMS and µ-XRF technology combined with thermobarometry has been successfully applied to improve the understanding of the complex polymetamorphic history of the Monte Rosa nappe. Two distinct phases of monazite growth emerged, first in the Permian (around 260 Ma ago), related to the intrusion of the Monte Rosa granite; then during Alpine orogeny, around 35 Ma ago, associated with high pressure metamorphism during Tertiary subduction/obduction.

As in other internal units of the Eastern, Central, and Western Alps, a prominent high pressure phase of Alpine age has been documented in the Monte Rosa nappe, reaching eclogite facies conditions during a narrowly constrained period of 40-35 Ma. The record is remarkably similar to that in the adjacent Zermatt-Saas Fee zone, to the Adula nappe, Cima Lunga complex, and the Mergoscia-Arbedo zone further East, and to the Gran Paradiso and Dora Maira further to the Southwest. These units show substantial differences in the internal structure, rock contents, and their pre-Alpine evolution. Similarities in the tectonic and temporal setting of the Alpine metamorphism does, however, suggest a coherent Alpine evolution. The present study contributes new constraints for its reconstruction. Given the present tectonic situation of the Monte Rosa nappe with respect to the Southern Steep Belt and the Insubric Line, it appears that this lineament, or its precursor, acted as a guiding structural element in the hangingwall of the Alpine subduction channel, along which the nappe stack was exhumed. Unlike the highly fragmented and internally attenuated character of other units extruded from eclogite facies depth, such as the Adula nappe, the Cima Lunga complex, and the Mergoscia-Arbedo zone including Alpe Arami (ENGI et al., 2001), the Monte Rosa nappe shows that a rather massive, coherent tectonic body could be also exhumed along this same channel within the same time segment and, most likely, a similar overall transpressional regime.

We conclude that the Alpine subduction channel acted as a conduit for extrusion not only of highly attenuated fragments, as in the case of the Southern Steep Belt of the Alps (ENGI et al., 2001), but also to guide the exhumation of rather more massive upper crustal fragments from depths >40 km back to upper crustal levels.

References

ARGAND, E. (1911): Les nappes de recouvrement des Alpes Pennines et leurs prologements structuraux. Matériaux pour la Carte Géol. Suisse; nouv. série, 31.
BEARTH, P. (1939): Über den Zusammenhang von Monte Rosa- und Bernhard-Decke. Eclogae geol. Helv., 32(1), 101-111.
BEARTH, P. (1952): Geologie und Petrographie des Monte Rosa. Beitr. Geol. Karte Schweiz, Neue Folge, 96. Liefg., 94.
BEARTH, P. (1958): Über einen Wechsel der Mineralfazies in der Wurzelzone des Penninikums. Schweiz. mineral. petrogr. Mitt., 38, 363-373.
BERMAN, R. G. (1991): Thermobarometry using multi-equilibrium calculations: a new technique, with petrological applications. Can. Mineral., 29, 833-855.
BERMAN, R. G. and ARANOVICH, L. Y. (1996): Optimized standard state and mixing properties of minerals: I. Model calibration for olivine, orthopyroxene, cordierite, garnet, and ilmenite in the system FeO-MgO-CaO-Al2O3-SiO2-TiO2. Contrib. Mineral. Petrol., 126, 1-24.
BORGHI, A., COMPAGNONI, R. and SANDRONE, R. (1996): Composite P-T paths in the internal Penninic massifs of the western Alps: Petrological constraints to their thermo-mechanical evolution. Eclogae geol. Helv., 89(1), 345-367.
BROUWER, F.M. (2000): Thermal evolution of high-pressure metamorphic rocks in the Alps. Doctoral thesis, Utrecht University, 146 p.
CHOPIN, C. and MONIÉ, P. (1984) A unique magnesiochloritoid-bearing, high-pressure assemblage from the Monte Rosa, Western Alps; petrologic and 40Ar-39Ar radiometric study. Contrib. Mineral. Petrol., 87, 388-398.
COMPAGNONI, R. and MAFFEO, B. (1973): Jadeite-bearing metagranites s.l. and related rocks in the Mount Mucrone area (Sesia-Lanzo Zone, western Italian Alps). Schweiz. mineral. petrogr. Mitt., 53, 355-378.
DAL PIAZ, G. V. (1964): Il cristallino antico del versante meridionale del Monte Rosa. Paraderivati a prevalente metamorfismo alpino. Rend. Soc. It. Min. Petr., 20, 101-136.
DAL PIAZ, G. V. (1966): Gneiss ghiandoni, marmi ed anfiboliti antiche del ricroprimento Monte Rosa nell'alte Val d'Ayas. Boll. Soc. Geol. It., 85, 103-132.
DAL PIAZ, G. V. (1971): Nuovi ritrovamenti di cianite alpina nel cristallino antico del Monte Rosa. Rend. Soc. It. Min. Petr., 27(2), 437-477.
DAL PIAZ, G. V. (2001): Geology of the Monte Rosa massif: historical review and personal comments. Schweiz. mineral. petrogr. Mitt., this issue.
DAL PIAZ, G. V. and LOMBARDO, B. (1986): Early Alpine eclogite metamorphism in the Penninic Monte Rosa-Gran Paradiso basement nappes of the northwestern Alps. In: Blueschists and eclogites (eds. Evans, B. W. and Brown, E. H.), pp. 249-265, Geol. Soc. Am., Boulder, CO.
DAL PIAZ, G. V. and LOMBARDO, B. (1995): Alpine Tectonics and Metamorphism of the Western Alps. Guidebook for the Pre-Symposium Field Excursion. In: VII Internat. Symp. Antarctic Earth Sci., pp. 61 p., Siena (Italy).
DUCHÊNE, S., BLICHERT-TOFT, J., LUAIS, B., TELOUK, P., LARDEAUX, J.M., ALBAREDE, F. (1997): The Lu-Hf dating of garnets and the ages of the Alpine high-pressure metamorphism. Nature, 387, 586-589.
ELLIS, D. J. and GREEN, D. H. (1979): An experimental study of the effect of Ca upon garnet-clinopyroxene exchange equilibria. Contrib. Mineral. Petrol., 71, 13-22.
ENGI, M., BERGER, A. and ROSELLE, G. T. (2001): The role of the tectonic accretion channel (TAC) in a collisional orogen. Geology, (in press).
ENGI, M., TODD, C. S. and SCHMATZ, D. R. (1995): Tertiary metamorphic conditions in the eastern Lepontine Alps. Schweiz. mineral. petrogr. Mitt., 75(3), 347-369.
FERRARIS, C., GROBÉTY, B. and WESSICKEN, R. (2000): Phlogopite exsolutions within muscovite: a first evidence for a higher-temperature re-equilibration, studied by HRTEM and AFM techniques. Europ. J. Mineral. 13, 15-26.
FOSTER, G., KINNY, P., VANCE, D., PRINCE, C., and HARRIS, N. (2000): The significance of monazite U-Th-Pb age data in metamorphic assemblages; a combined study of monazite and garnet chronometry. Earth Planet. Sci. Lett., 181, 327-340.
FRANCHI, S. (1903): Sul rinvenimento di nuovi giacimente di roccie giadeitiche nelle Alpi occidentali e nell'Appennino ligure. Boll. Soc. Geol. It., 22, 130-134.
FREY, M., DESMONS, J. and NEUBAUER, F. (1999): The new metamorphic map of the Alps. Schweiz. mineral. petrogr. Mitt. 79, 1-230.
FREY, M., HUNZIKER, J. C., O'NEIL, J. R. and SCHWANDER, H. (1976): Equilibrium-disequilibrium relations in the Monte Rosa granite, Western Alps: Petrological, Rb-Sr and stable isotope data. Contrib. Mineral. Petrol., 55, 147-179.

FREY, M. and FERREIRO MÄHLMANN, R. (1999): Alpine metamorphism of the Central Alps. Schweiz. mineral. petrogr. Mitt., 79, 135-154.
FROITZHEIM, N. (2001): Origin of the Monte Rosa nappe in the Pennine Alps - A new working hypothesis. Geol. Soc. Amer. Bull. 113, 604-614.
GEBAUER, D. (1999): Alpine geochronology of the Central and Western Alps: new constraints for a complex geodynamic evolution. Schweiz. mineral. petrogr. Mitt., 79, 191-208.
HUNZIKER, J. C. (1970): Polymetamorphism in the Monte Rosa, Western Alps. Eclogae geol. Helv., 63(1), 151-161.
HUNZIKER, J. C. and BEARTH, P. (1969): Rb-Sr-Altersbestimmungen aus den Walliser Alpen; Biotitalterswerte und ihre Bedeutung für die Abkühlungsgeschichte der alpinen Metamorphose. Eclogae geol. Helv., 62, 205-222.
HUNZIKER, J. C., DESMONS, J. and HURFORD, A. J. (1992): Thirty-two years of geochronological work in the Central and Western Alps; a review on seven maps. Mém. Géol. Lausanne, 13.
HUNZIKER, J. C. and MARTINOTTI, G. (1984): Geochronology and evolution of the Western Alps: a review. Mem. Soc. Geol. It., 29, 43-56.
KRETZ, R. (1983): Symbols for rock-forming minerals. Amer. Mineral.68, 277-279.
KÖPPEL, V. and GRÜNENFELDER, M. (1975): Concordant U-Pb ages of monazite and xenotime from the Central Alps and the timing of high temperature metamorphism, a preliminary report. Schweiz. mineral. petrogr. Mitt., 55, 129-132.
KÖPPEL, V., GÜNTHERT, A. and GRÜNENFELDER, M. (1981): Patterns of U-Pb zircon and monazite ages in polymetamorphic units of the Swiss Central Alps. Schweiz. mineral. petrogr. Mitt., 61, 97-120.
KROGH, E. J. (1988): The garnet-clinopyroxene Fe-Mg geothermometer - a reinterpretation of existing experimental data. Contrib. Mineral. Petrol., 99, 44-48.
LANGE, S., NASDALA, L., POLLER, U., BAUMGARTNER, L. P. and TODT, W. (2000): Crystallization age and metamorphism of the Monte Rosa Granite, Western Alps. In: 17th Swiss Tectonic Studies Group Meeting, ETH Zürich, 51.
LE BAYON, R., SCHMID, S.M. and DE CAPITANI, C. (2001): The metamorphic evolution of the Monte Rosa nappe and its relation to exhumation by fore- and back-thrusting in the Western Alps. Geol. Paläont. Mitt. Innsbruck, 25, 132-133.
LIATI, A., GEBAUER, D., FROITZHEIM, N. and FANNING, M. (2001): U-Pb SHRIMP geochronology of amphibolitized eclogites and orthogneisses from the Furgg zone (Western Alps) and implications for its geodynamic evolution. Schweiz. mineral. petrogr. Mitt., this issue.
MASSONNE, H.-J. and SCHREYER, W. (1987): Phengite geobarometry based on the limiting assemblage with K-feldspar, phlogopite, and quartz. Contrib. Mineral. Petrol., 96, 212-224.
MASSONNE, H.-J. and SZPURKA, Z. (1997) Thermodynamic properties of white micas on the basis of hifh-pressure experiments in the systems K2O-MgO-Al2O3-SiO2-H2O and K2O-FeO-Al2O3-SiO2-H2O. Lithos, 41, 229-250.
MATTIROLO, E., NOVARESE, V., FRANCHI, S. and STELLA, A. (1913): Carta Geologica d'Italia, Foglio 29 Monte Rosa (1:100'000), Serv. Geol. Ital.
MONIÉ, P. (1985): La methode 39Ar-40Ar appliquée au metamorphisme alpin dans le massif du Mont-Rose (Alpes occidentales); chronologie detaillée depuis 110 Ma. Eclogae geol. Helv., 78, 487-516.
NAGEL, T. (2000): Metamorphic and structural history of the southern Adula nappe (Graubünden, Switzerland). Unpub. Ph.D. Thesis, University of Basel, Basel.
NAGEL, T., DE CAPITANI, C. and FREY, M. (2001): Isograds and PT-evolution in the eastern Lepontine Alps, Switzerland. J. Metam. Geol., (in press).
NIGGLI, E. (1970): Alpine Metamorphose und alpine Gebirgsbildung. Fortschr. Mineral., 47, 16-26.
NIGGLI, E. and NIGGLI, C. (1965): Karten der Verbreitung einiger Mineralien der alpidischen Metamorphose in den Schweizer Alpen (Stilpnomelan, Alkali-Amphibol, Chloritoid, Staurolith, Disthen, Sillimanit). Eclogae geol. Helv., 58, 335-368.
OBERHÄNSLI, R., HUNZIKER, J. C., MARTINOTTI, G. and STERN, W. B. (1985): Geochemistry, geochronology and petrology of Monte Mucrone: an example of eo-alpine eclogitization of Permian granitoids in the Sesia-Lanzo zone, western Alps, Italy. Chem. Geol., 52, 165-184.
PAQUETTE, J.-L., CHOPIN, C. and PEUCAT, J.-J. (1989): U-Pb zircon, Rb-Sr and Sm-Nd geochronology of high- to very-high-pressure meta-acidic rocks from the western Alps. Contrib. Mineral. Petrol., 101, 280-289.
PARRISH, R.R. (1990): U-Pb dating of monazite and its application to geological problems. Canad. J. Earth Sci., 27, 1431-1450.
PAWLIG, S. and BAUMGARTNER, L.P. (2001): Geochemistry of a talc-kyanite-chloritoid shear zone within the Monte Rosa granite, Val d'Ayas, Italy. Schweiz. mineral. petrogr. Mitt., this issue.
PETTKE, T., DIAMOND, L. and VILLA, I. (1999): Mesothermal gold veins and metamorphic devolatilisation in the NW Alps: The temporal link. Geology, 27, 641-644.

PFIFFNER, M. and TROMMSDORFF, V. (1998): The high-pressure ultramafic-mafic-carbonate suite of Cima Lunga-Adula, Central Alps: Excursions to Cima di Gagnone and Alpe Arami. Schweiz. mineral. petrogr. Mitt., 78, 337-354.
PYLE, J.M. and SPEAR, F.S. (2000): An empirical garnet (YAG) - xenotime thermometer. Contrib. Mineral. Petrol., 138, 51-58.
REINECKE, T. (1998): Prograde high- to ultrahigh-pressure metamorphism and exhumation of oceanic sediments at Lago di Cignana, Zermatt-Saas Zone, western Alps. Lithos, 42(3-4), 147-189.
REINHARDT, B. (1966): Geologie und Petrographie der Monte-Rosa Zone, der Sesia-Zone und des Canavese im Gebiet zwischen Valle d'Ossola und Valle Loana. Schweiz. mineral. petrogr. Mitt., 46, 553-678.
ROMER, R. L., SCHÄRER, U. and STECK, A. (1996): Alpine and pre-Alpine magmatism in the root-zone of the western central Alps. Contrib Mineral Petrol, 123(2), 138-158.
ROSELLE, G. T., THÜRING, M. and ENGI, M. (2001): MELONPIT: A finite element code for simulating tectonic mass movement and heat flow within subduction zones. Amer. J. Sci., in press.
RUBATTO, D. and GEBAUER, D. (1999): Eo/Oligocene (35 Ma) high-pressure metamorphism in the Gornergrat Zone (Monte Rosa, Western Alps): implications for paleogeography. Schweiz. mineral. petrogr. Mitt., 79, 353-362.
SCHERRER, N. C., ENGI, M., GNOS, E., JAKOB, V. and LIECHTI, A. (2000): Monazite analysis; from sample preparation to microprobe age dating and REE quantification. Schweiz. mineral. petrogr. Mitt., 80(1), 93-105.
SCHERRER, N. C., ENGI, M., CHEBURKIN, A., PARRISH, R. R. and BERGER, A. (2001a): Non-destructive chemical dating of young monazite using XRF: 2. Context sensitive microanalysis and comparison with Th-Pb laser-ablation mass spectrometric data (LA-PIMMS). Chem. Geol. (accepted for publication).
SCHERRER, N. C., GNOS, E. and CHOPIN, C. (2001b): Retrograde monazite-forming reactions in bearthite bearing high pressure rocks. Schweiz. mineral. petrogr. Mitt., this issue.
SPICHER, A. (1980): Tektonische Karte der Schweiz, 1:500'000, Schweizerische Geologische Kommission.
STECK, A., BIGIOGGERO, B., DAL PIAZ, G.V., ESCHER, A., MARTINOTTI, G. and MASSON, H. (2001): Carte tectonique des Alpes de Suisse occidentale et des régions avoisinantes, 1:100'000. Serv. hydrol. géol. nat., Carte spéc. no. 123, 4 maps.
TODD, C. S. (1998): Limits to GASP-thermobarometry in Ca-poor rocks such as metapelites. Amer. Mineral., 83, 1161-1167.
TODD, C. S. and ENGI, M. (1997): Metamorphic field gradients in the Central Alps. Jour. Metam. Geol., 15(4), 513-530.
VAN DER KLAUW, S. N. G. C., REINECKE, T. and STOCKHERT, B. (1997): Exhumation of ultrahigh-pressure metamorphic oceanic crust from Lago di Cignana, Piemontese zone, western Alps: the structural record in metabasites. Lithos, 41(1-3), 79-102.
ZINGG, A. and HUNZIKER, J. C. (1990): The age of movements along the Insubric Line West of Locarno (northern Italy and southern Switzerland). Eclogae geol Helv, 83, 629-644.

Appendix: Mineral reactions used in TWQ thermobarometry

Figure 5
Sample: Po9703b 3 linearly independent reactions
TWQ results: P = 10.0±1.0 kbar T = 595±25 °C
Reactions

2): 2 Alm + 2 Msp + Phl = 3 Sd + 6 aQz + Py
3): 3 FSt + 4 Phl + 8 Msp + 4 Alm = 24 aQz + 12 Sd + 3 MSt
4): 4 Ann + 3 MSt = 3 FSt + 4 Phl
5): 2 Msp + Ann + Alm = 6 aQz + 3 Sd
6): Alm + Phl = Py + Ann
9): Py + 2 Msp + 2 Ann = Phl + 6 aQz + 3 Sd
15): 3 FSt + 2 Py + 2 Phl + 4 Msp = 12 aQz + 6 Sd + 3 MSt
16): 3 FSt + 4 Py + 8 Msp + 4 Ann = 24 aQz + 12 Sd + 3 MSt

Sample: Bi9801a 3 linearly independent reactions
TWQ results: P = 11.0±1.0 kbar T = 610±25 °C
Reactions

1): Alm + Ann + 2 Msp = 3 Sd + 6 aQz
2): 6 FSt + 5 Phl + 30 Msp + 46 Ann = 3 Clh + 117 aQz + 81 Sd
3): 2 Ann + 2 Msp + Py = 3 Sd + 6 aQz + Phl
4): 53 Ann + 10 Phl + 12 FSt = 45 Sd + 18 Msp + 6 Clh + 39 Alm
5): 62 Msp + 3 Clh + 46 Alm = 5 Phl + 159 aQz + 57 Sd + 6 FSt
6): 27 Alm + 3 Clh + 24 Msp = 6 FSt + 45 aQz + 5 Phl + 19 Ann
7): 31 Ann + 5 Phl + 6 FSt = 36 Sd + 27 aQz + 3 Clh + 15 Alm
8): Alm + Phl = Py + Ann
9): 2 Alm + 2 Msp + Phl = 3 Sd + 6 aQz + Py
10): 14 Ann + 49 Phl + 12 FSt = 45 Sd + 39 Py + 18 Msp + 6 Clh
11): 12 Sd + 23 Py + 16 Msp + 3 Clh = 28 Phl + 21 aQz + 6 FSt
12): 6 FSt + 5 Py + 40 Msp + 56 Ann = 3 Clh + 147 aQz + 96 Sd
13): 8 Ann + 3 Clh + 24 Msp + 27 Py = 6 FSt + 45 aQz + 32 Phl
14): 16 Ann + 20 Phl + 6 FSt = 36 Sd + 27 aQz + 15 Py + 3 Clh
15): 12 FSt + 63 Phl + 14 Alm = 6 Clh + 18 Msp + 53 Py + 45 Sd
16): 49 Alm + 6 Clh + 18 Msp + 45 Sd = 12 FSt + 10 Py + 63 Ann
17): 56 Alm + 3 Clh + 72 Msp = 6 FSt + 72 Sd + 189 aQz + 5 Py
18): 8 Alm + 3 Clh + 24 Msp + 19 Py = 6 FSt + 45 aQz + 24 Phl
19): 6 FSt + 36 Phl + 16 Alm = 3 Clh + 31 Py + 27 aQz + 36 Sd
20): 32 Alm + 3 Clh + 24 Msp = 6 FSt + 45 aQz + 5 Py + 24 Ann
21): 6 FSt + 5 Py + 36 Ann = 20 Alm + 3 Clh + 27 aQz + 36 Sd

Figure 6
Sample: Pz9905b 3 linearly independent reactions
TWQ results: P = 9.2±1.8 kbar T = 620±60 °C
Reactions
5): Alm + Ann + 2 Msp = 3 Sd + 6 aQz
8): 3 Alm + 6 mcel = 3 Sd + 18 aQz + 2 Phl + Ann
12): 5 Alm + 6 mcel = 3 Sd + 18 aQz + 2 Py + 3 Ann
13): 3 Sd + 3 mcel = 2 Ann + 3 Msp + Phl
14): 4 Ann + 5 Msp + Py = 6 Sd + 6 aQz + 3 mcel
17): 2 Ann + 6 mcel + 3 Py = 3 Sd + 18 aQz + 5 Phl
18): 2 Alm + Msp + 3 mcel = 3 Sd + 12 aQz + Phl
19): Alm + 3 mcel = 6 aQz + Phl + Msp + Ann
20): 3 Sd + 3 mcel + Alm = 3 Ann + 3 Msp + Py
21): 4 Alm + 3 Msp + 3 mcel = 6 Sd + 18 aQz + Py
22): 2 Alm + 3 mcel = 6 aQz + Py + Msp + 2 Ann
24): Alm + Phl = Py + Ann
25): 2 Alm + 2 Ms + Phl = 3 Sd + 6 aQz + Py
26): Py + 6 mcel + 2 Alm = 3 Phl + 18 aQz + 3 Sd
27): 3 mcel + Py = 6 aQz + 2 Phl + Msp
28): 2 Ann + 2 Msp + Py = 3 Sd + 6 aQz + Phl
29): 3 Sd + 2 Py + 3 mcel = 2 Alm + 3 Msp + 3 Phl
30): 2 Alm + 2 Msp + Phl = 3 Sd + 6 aQz + Py

Sample: Pb9901c 3 linearly independent reactions
TWQ results: P(1) = 17-21 kbar T(1) = 770±30 °C
P(2) = 9-12 kbar T(2) = 730±30 °C
Reactions
3): Alm + Ann + 2 Msp = 3 Sd + 6 aQz
5): 3 mcel + Alm = Ann + Ms + Phl + 6 aQz
6): 6 mcel + 3 Alm = Ann + 2 Phl + 18 aQz + 3 Sd
9): 5 Alm + 6 mcel = 3 Sd + 18 aQz + 2 Py + 3 Ann
11): 3 Py + 6 mcel + 2 Ann = 5 Phl + 18 aQz + 3 Sd
12): 2 Alm + Msp + 3 mcel = 3 Sd + 12 aQz + Phl
13): 3 mcel + Alm = Ann + Msp + Phl + 6 aQz
14): 4 Alm + 3 Msp + 3 mcel = 6 Sd + 18 aQz + Py
15): 2 Alm + 3 mcel = 6 aQz + Py + Msp + 2 Ann
16): Phl + Alm = Ann + Py
18): 2 Alm + 6 mcel + Py = 3 Sd + 18 aQz + 3 Phl
19): Py + 2 Msp + 2 Ann = Phl + 6 aQz + 3 Sd
20): 2 Alm + 2 Msp + Phl = 3 Sd + 6 aQz + Py

Figure 7
Sample: Mo9801c 3 linearly independent reactions
TWQ results: P = 11.7±1.3 kbar T = 755±65 °C
Reactions
1): 2 Msp + Ann + Alm = 6 aQz + 3 Sd
2): 6 mcel + 3 Alm = Ann + 2 Phl + 18 aQz + 3 Sd
3): 6 mcel + 5 Alm = 3 Ann + 2 Py + 18 aQz + 3 Sd
4): 3 mcel + 3 Sd = Phl + 3 Msp + 2 Ann
5): 2 Alm + Msp + 3 mcel = 3 Sd + 12 aQz + Phl
6): Alm + 3 mcel = 6 aQz + Phl + Msp + Ann
7): Alm + 3 mcel + 3 Sd = Py + 3 Msp + 3 Ann
8): 4 Alm + 3 Msp + 3 mcel = 6 Sd + 18 aQz + Py
9): Py + 5 Msp + 4 Ann = 3 mcel + 6 aQz + 6 Sd
10): 2 Alm + 3 mcel = 6 aQz + Py + Msp + 2 Ann
11): Phl + Alm = Ann + Py
12): Py + 6 mcel + 2 Alm = 3 Phl + 18 aQz + 3 Sd
13): 3 Py + 6 mcel + 2 Ann = 5 Phl + 18 aQz + 3 Sd
14): 3 mcel + 2 Py + 3 Sd = 3 Phl + 3 Msp + 2 Alm
15): Phl + 2 Msp + 2 Alm = Py + 6 aQz + 3 Sd
16): Py + 3 mcel = Msp + 2 Phl + 6 aQz
17): Py + 2 Msp + 2 Ann = Phl + 6 aQz + 3 Sd

Sample: Ri9801b (left) 4 linearly independent reactions
TWQ results: P = 12.1±1.6 kbar T = 735±55 °C
Reactions
1): Alm + Ann + 2 Msp = 3 Sd + 6 aQz
2): Msp + Ab = Pg + Kfs
3): 3 Sd + 3 mcel = 2 Ann + 3 Msp + Phl
4): 4 Ann + 5 Msp + Py = 6 Sd + 6 aQz + 3 mcel
5): Alm + Ann + 2 Pg + 2 Kfs = 3 Sd + 6 aQz + 2 Ab
6): 2 Alm + Msp + 3 mcel = 3 Sd + 12 aQz + Phl
7): Alm + 3 mcel = 6 aQz + Phl + Msp + Ann
8): 3 Alm + 6 mcel = 3 Sd + 18 aQz + 2 Phl + Ann
9): 3 Sd + 3 mcel + Alm = 3 Ann + 3 Msp + Py
10): 4 Alm + 3 Msp + 3 mcel = 6 Sd + 18 aQz + Py
11): 2 Alm + 3 mcel = 6 aQz + Py + Msp + 2 Ann
12): 5 Alm + 6 mcel = 3 Sd + 18 aQz + 2 Py + 3 Ann
13): 3 Sd + 3 mcel + 3 Ab = 2 Ann + 3 Pg + Phl + 3 Kfs
14): 4 Ann + 5 Pg + 5 Kfs + Py = 6 Sd + 6 aQz + 3 mcel + 5 Ab
15): 3 mcel + Py = 6 aQz + 2 Phl + Msp
16): 2 Ann + 2 Msp + Py = 3 Sd + 6 aQz + Phl
17): 2 Ann + 6 mcel + 3 Py = 3 Sd + 18 aQz + 5 Phl
18): 2 Alm + 3 mcel + Pg + Kfs = 3 Sd + 12 aQz + Phl + Ab
19): Ab + Alm + 3 mcel = 6 aQz + Kfs + Phl + Pg + Ann
20): 3 Sd + 3 mcel + Alm + 3 Ab = 3 Ann + 3 Pg + 3 Kfs + Py
21): 4 Alm + 3 mcel + 3 Pg + 3 Kfs = 6 Sd + 18 aQz + Py + 3 Ab
22): Ab + 2 Alm + 3 mcel = 6 aQz + Py + Kfs + Pg + 2 Ann
23): 3 Sd + 2 Py + 3 mcel = 2 Alm + 3 Msp + 3 Phl
24): Alm + Phl = Py + Ann
25): 2 Alm + 2 Msp + Phl = 3 Sd + 6 aQz + Py
26): 2 Alm + 6 mcel + Py = 3 Sd + 18 aQz + 3 Phl
27): Ab + 3 mcel + Py = 6 aQz + Kfs + 2 Phl + Pg
28): 2 Ann + 2 Pg + 2 Kfs + Py = 3 Sd + 6 aQz + Phl + 2 Ab
29): 3 Sd + 2 Py + 3 mcel + 3 Ab = 2 Alm + 3 Pg + 3 Phl + 3 Kfs
30): 2 Alm + 2 Pg + Phl + 2 Kfs = 3 Sd + 6 aQz + Py + 2 Ab

Sample: Ri9801c (right) 3 linearly independent reactions
TWQ results: P = 12.0±1.5 kbar T = 730±50 °C
Reactions
1): Alm + Ann + 2 Msp = 3 Sd + 6 aQz
2): 3 Sd + 3 mcel = 2 Ann + 3 Msp + Phl
3): 4 Ann + 5 Msp + Py = 6 Sd + 6 aQz + 3 mcel
4): 2 Alm + Msp + 3 mcel = 3 Sd + 12 aQz + Phl
5): Alm + 3 mcel = 6 aQz + Phl + Msp + Ann
6): 3 Alm + 6 mcel = 3 Sd + 18 aQz + 2 Phl + Ann
7): 3 Sd + 3 mcel + Alm = 3 Ann + 3 Msp + Py
8): 4 Alm + 3 Msp + 3 mcel = 6 Sd + 18 aQz + Py
9): 2 Alm + 3 mcel = 6 aQz + Py + Msp + 2 Ann
10): 5 Alm + 6 mcel = 3 Sd + 18 aQz + 2 Py + 3 Ann
11): 3 mcel + Py = 6 aQz + 2 Phl + Msp
12): 2 Ann + 2 Msp + Py = 3 Sd + 6 aQz + Phl
13): 2 Ann + 6 mcel + 3 Py = 3 Sd + 18 aQz + 5 Phl
14): 3 Sd + 2 Py + 3 mcel = 2 Alm + 3 Msp + 3 Phl
15): Alm + Phl = Py + Ann
16): 2 Alm + 2 Msp + Phl = 3 Sd + 6 aQz + Py
17): 2 Alm + 6 mcel + Py = 3 Sd + 18 aQz + 3 Phl

Field-relations, deformation and geochemistry of the nappe stack between the Leventina- and Verzasca-Valley

Alfons Berger, Thomas Burri, Astrid Gruskovnjak and Ugo Leonardi

Abstract

The Cima-Lunga unit represents an inhomogeneous mélange-type unit, situated along a former plate-boundary. The geometry and geodynamic evolution of the mélange and its surrounding are key to the understanding of the Tertiary evolution of the Central Alps. The nappe sequence in the study area is defined from bottom to top by the Leventina-, Simano-, Cima-Lunga- and Maggia-nappe. Our interpretation of the Cima-Lunga unit as an accreted tectonic mélange (TAC) implies that this unit marks the location of a former plate-boundary between the down going European units (Leventina- and Simano-nappe) and the overriding Briançonnais (Maggia-nappe). The individual nappes contain evidence of Variscan plutonic activity. The Maggia-nappe contains a calc-alkaline series (Cocco-gneis) including late-stage leucogranitic dykes and larger bodies (Ruscada-gneis). The Simano and the Leventina-nappes are dominated by leucogranitic gneisses exhibiting a typical S-type character.

The Cima-Lunga unit encloses several oceanic- and mantle-fragments, which underwent HP-metamorphism, but usually show a strong amphibolite-facies overprint. We investigate in detail the P-T evolution of some metapelitic and metabasic fragments in the southern Cima-Lunga unit. It can be shown, that type of equilibration is strongly influenced by the availability and composition of the fluid. By combining textural information with information from thermodynamic computation, we can show that mafic rocks report a HP-pressure history from at least 1.8 GPa at T > 650˚C down to 0.6 GPa at 550˚C, whereas metapelite only document from 1.1 GPa down to 0.6 GPa at similar temperatures.

Introduction and geological setting

The area between Pizzo Vogorno and Poncione dei Laghetti is key to the understanding of the Central Lepontine nappe stack. Except for the geological map 1:25'000 (Blatt Bellinzona, Bächlin et al. 1974), which coincides with the southern part of the study area, no detailed geological mapping has been carried out so far. This has led to a large degree of freedom for the tectonic interpretation of the study area, and, as a result, of the whole Lepontine nappe stack. Especially the lack of unambiguous nappe dividers in the study area (e.g. Preiswerk 1918, Preiswerk et al. 1934) has led to some new interpretations of the geometry of the Lepontine area (Rütti 2003; Maxelon & Mancktelow 2003). Nappe dividers, which are easily recognised in the northern Lepontine area, are classically interpreted to gradually thin out towards the south. Answering the question if the lack of such clear nappe dividers is related to increasing boudinage and thinning out towards the south, or if their tectonic significance should be questioned, may lead to very contrasting tectonic interpretations. On top of the stack of relatively coherent Alpine nappes, another major limit is found, separating not only single nappes, but previous plate boundaries. Along this limit a lithospheric mélange accumulated during subduction and continent collision (e.g. Trommsdorff 1990, Engi et al. 2001a). Although well known and described, the significance of these mélange units as tectonic markers has not been used to decipher the geometry of the Lepontine nappe stack. Mélange units are represented by the Adula- and Cima-Lunga nappe in the flat lying nappe stack and by similar mélange-type units which constitute a considerable part of the Southern Steep Belt (SSB). The SSB is one of two roughly east-west striking steep belts that occur to the north and to the south of the more or less flat lying nappe stack. Both belts are defined by steep to overturned structures, and are related to a late stage of backfolding and backthrusting in the south and north, respectively. The SSB has therefore acted as a regional scale shear zone, taking up vertical as well as horizontal movements. Due to the intense refolding, thrusting and shearing in the SSB, a tectonic interpretation of this area has become very complicate. Just north of this area, were structures turn back into a gently dip-

ping orientation, the original tectonic geometry or nappe-sequence remained better preserved. Consequently, nappe geometry and tectonic processes along former plate boundaries can be more thoroughly investigated. This is especially true for the area of the Cima-Lunga, where several oceanic- and mantle-type-fragments preserve evidence of a subduction stage (e.g. Heinrich 1986). In this area, petrography and deformation of the northern Cima-Lunga unit has already been investigated in detail (e.g. Grond et al. 1995, Pfiffner & Trommsdorff 1998, Pfiffner 1999, Nimis & Trommsdorff 2001). In contrast, the southern part of the Cima-Lunga unit has not gained much attention and has remained almost unstudied (e.g. DalVesco 1953).

In the last few years, detailed geological mapping on the scale 1:10'000 has been carried out in the latter area to better constrain its tectonic arrangement. In addition to the geological mapping, we use lithostratigraphic, geochemical and petrographic-metamorphic evidence to further constrain the evolution of this part of the Lepontine Alps.

Description of the main units

In the southern Lepontine area two different types of units can be distinguished (see also Fig. 1):

- Group 1 units are coherent continental basement units, which partially preserve features of a pre-Alpine orogenic history. Several outcrops in the study area and many more localities in the Ticino valleys allow to deduce a probably Variscan history of granite intrusion into an older basement of ambiguous age. Available isotopic age determinations are indefinite, because of mixing ages (pre-Alpine and Alpine growth rims), but tentatively indicate a mainly Variscan and in part even older history for these units. Structural remnants of the pre-Alpine history are primarily recognised in areas of weaker Alpine overprint (e.g. Nussbaum et al. 1998, Engi et al. 2001b).
- Group 2 units are tectonic mélange units, thus are defined by a fragmented character, with individual fragments from the meter- to kilometre-scale. An important feature is the frequent preservation of alpine high pressure (HP)-rocks and oceanic fragments. In addition this group is characterised by the occurrence of marbles and other types of metasediments, by metamafic rocks and by ultramafic mantle fragments, the latter often associated with metarodingites. Granitoid gneisses from meter- to kilometre-scale are included as well (e.g. Trommsdorff 1990, Engi et al. 2001a).

The lowest exposed unit of the study area is the Leventina-nappe, mainly characterised by the Leventina gneiss, a leucocratic granitoid two mica gneiss, with biotite commonly dominating over

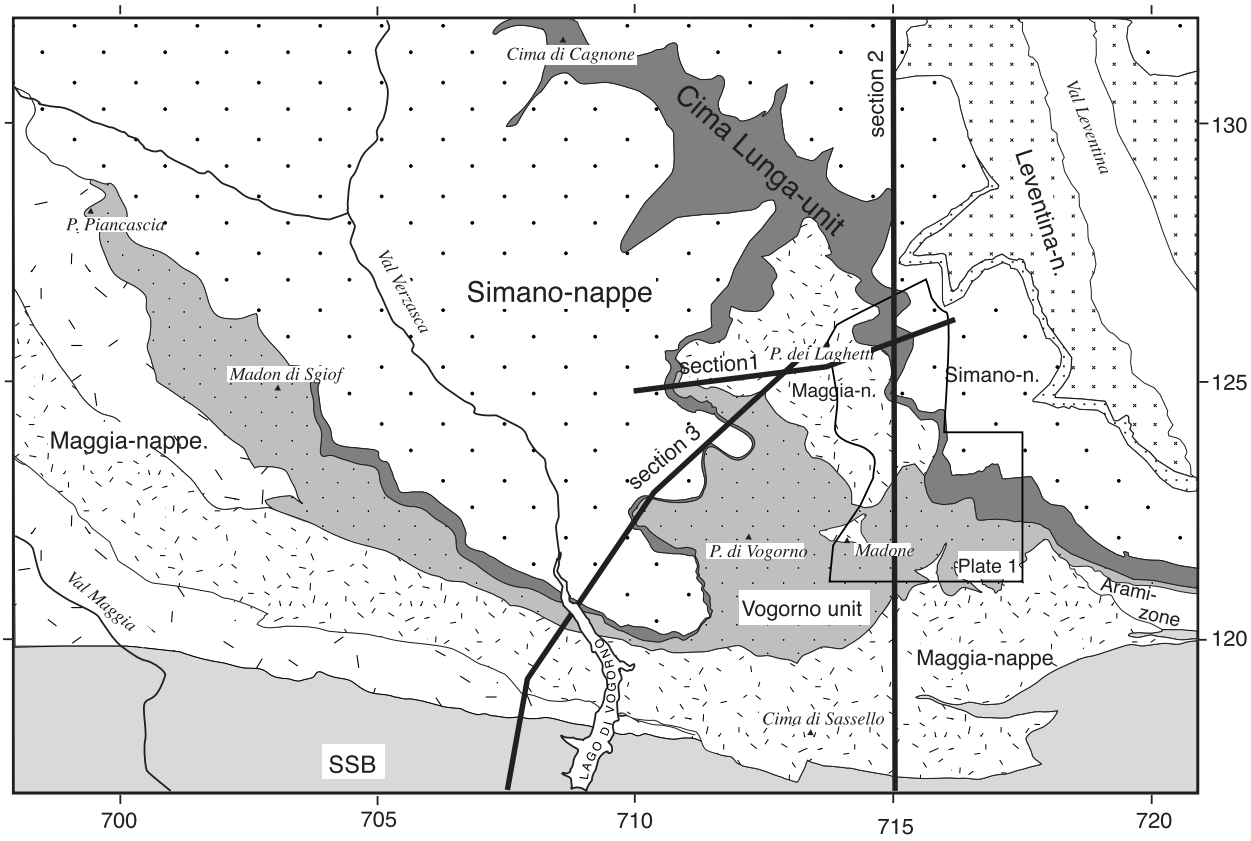

Fig. 1: Geologic-tectonic overview of the area between Val Leventina and Val Verzasca. The map is constructed using own survey-data, and data from Bächlin et al. (1974); Preiswerk et al. (1934) and Gräter (unpublished)

muscovite. Even though relatively homogeneous, grain size and mode of muscovite of the Verzasca-gneiss vary on the map scale. A detailed description of the Leventina gneiss is found in Casasopra (1939). The border of the Leventina nappe to the overlying Simano-nappe is defined by a relatively inhomogeneous series of metasediments, amphibolites and orthogneisses (own observations and Casasopra 1939, Rütti 2003). The often cited quartz-mylonites are locally missing or are in part better interpreted as strongly sheared leucogranites, due to their quartzo-feldspatic composition (Rütti 2003). Nevertheless, some quartzites were confirmed in this study as well, and the main feature of the boundary, a shear horizon of several tens of meter thickness, (interpreted as the thrust plane of the Simano-nappe) was found to always accompany the nappe border.

The investigated part of the Simano nappe consists of metasedimentary polycyclic basement gneisses and Variscan migmatites, both intruded by a leucocratic Variscan two-mica granite (=Verzasca-gneiss; Fig 2a). Locally, mafic dykes crosscut the larger intrusives. Towards the north, the Verzasca-gneiss as the main intrusive of the Simano-nappe is replaced by a coarser grained porphyric K-feldspar-granite (Simano-augengneiss). Smaller and larger bodies of basement gneisses included by the intrusives might be interpreted as former schollen. Such basement-schollen are locally found to preserve pre-Alpine structures (Fig. 2a). Preservation of such structural remnants demonstrates that, despite of the intensity of Alpine metamorphism, pre-Alpine structures have locally survived. Although Alpine structures are dominant in the general case, care must be taken to recognise such structural relics, because they may else lead to erroneous structural interpretations.

The Cima-Lunga unit, which overlies the Simano unit in the study area, is defined by a heterogeneous series of marbles, ultramafic bodies, eclogites, calcareous schist and several gneiss-types (e.g. Pfiffner 1999, Pfiffner & Trommsdorff 1998). Near the base of the Cima-Lunga unit, one or several marble horizons are usually present (Plate 1; Grond et al. 1995; Leonardi 2003, Gruskovnjak 2001). Inside the Cima-Lunga unit large boulders of ultramafic rocks are found, mainly containing olivine, tremolite, cummingonite, enstatite and chlorite. Round chlorite aggregates in ultramafic rocks are interpreted as pseudomorphic after garnet (Fig. 2b). Structure, lithologic content and metamorphic history of the Cima-Lunga unit were well investigated in a northern section of the Cima-Lunga unit (e.g. Dal Vesco 1953, Heinrich 1978, 1983, Grond et al. 1995, Pfiffner 1999, Trommsdorff & Nimis 2001), and a HP- metamorphic history was documented for several locations of this area. This HP-history of the Cima-Lunga unit strongly contrast with the Alpine evolution of the underlying Simano nappe and the overlying Maggia nappe, which both lack evidence for a high-pressure stage. Similarly, the fragmentary mélange-type character of the Cima-Lunga units is clearly different from the more coherent Maggia and Simano units, although common granitic gneisses and garnet-bearing schist occur in the Cima-Lunga as well (e.g. Grond et al. 1995; Preiswerk et al. 1934).

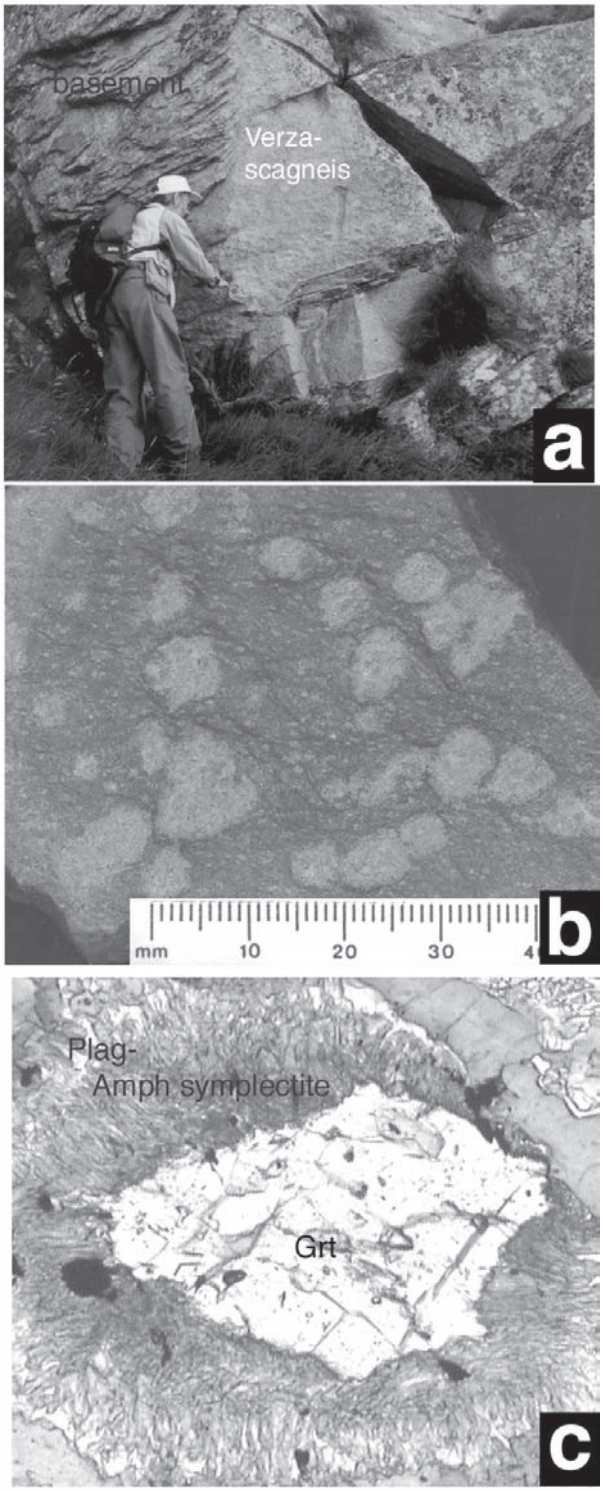

Fig. 2: Field and microphotographs from the investigated rocks: (a) Field photograph of Verzasca-gneiss. Despite of the Alpine structural overprint, intrusive relations between pre-granitoid basement and intruding granitoids are still preserved. (b) Meta-ultramafic rock with round chlorite aggregates pseudomorphic after garnet. Scale is in mm. (c) Microphotograph of metaeclogite. Note symplectite-rim around garnet and plagioclase-clinopyroxene symplectite in the upper part of the picture. Coarser grained mineral in the upper right is retrograde amphibole. Size of figure ca. 2 mm.

We further define a Vogorno unit, which is not differentiable in lithologic content from the Simano-nappe, but which is situated above the Cima-Lunga unit. The Vogorno unit also shears certain similarities with the overlying Maggia nappe, which consists of a pre-Variscan-basement, including different types of metasedimentary gneisses (in part migmatitic), amphibolites and granitoid layers. The inhomogeneous Maggia-basement of uncertain age was intruded by the probably Variscan Cocco- and Ruscada-granitoids. The Alpine orogeny led to the deformation of the whole sequence, but larger granitoid bodies often acted as structural monadnocks, while the surrounding migmatites and sediments became strongly deformed. The Cocco-gneiss is a mesocratic biotite-two feldspar gneiss of granodioritic to quartz-dioritic composition, containing characteristic biotite nests (e.g. Preiswerk 1931; Wenk 1982). The Cocco-granitoids were subsequently intruded by the leucocratic Ruscada granites. Associated metasediments are often strongly migmatitic and may even show diffuse transitions into the granitoids (Preiswerk 1925). Though the Ruscada intrusives are observed to intrude the Cocco-granitoids at several localities, they may both belong to the same calc-alkaline evolution. Ruscada-leucogranites may simply represent the late granitic stage of this evolution.

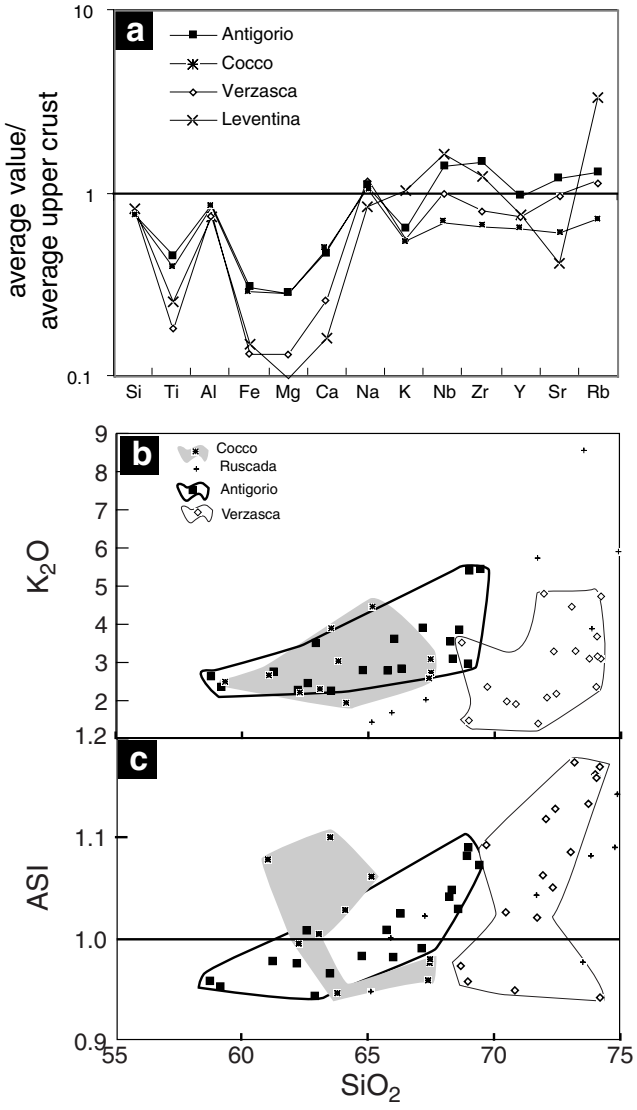

Fig. 3: Geochemical characterisation of orthogneisses from the study area: (a) Spiderdiagrams of averaged rock-suites, normalised to average upper crust (Taylor & McLellan 1985, see also http//:georef.org). Note differences in absolute values in the more compatible elements; (b) SiO_2 versus K_2O diagram of analysed rocks. Si-rich leucogranites are clearly distinguishable from the spread in data of the calc-alkaline suites. (c) SiO_2 versus Aluminium Saturation Index (ASI) of the investigated samples.

Geochemistry of the Variscan intrusives

Major elements and Sr, Rb, Ba, Pb, Ni, V, Zr, Zn, Y were determined using standard X-ray-fluorescence techniques on glass pellets. We analysed samples of granitic to granodioritic compositions from the Antigorio-nappe (= Antigorio-gneiss), Maggia-nappe (Cocco- and Ruscada-gneiss), Simano nappe (= Verzasca-gneiss), Vogorno unit (= Vogorno-gneiss), and the Leventina nappe (Leventina-gneiss). Additional data from the literature (XRF and standard solution techniques) were included in the data set of together 78 analysis (60- own and 18-literature data; Hunziker 1966, Preiswerk 1936). In a first approach standard covariant diagrams and element-ratio diagrams are plotted (Fig. 3). To further refine the results we applied cluster analysis to the data set. Cluster analysis has proofed to be an effective tool to point out differences or similarities of data series by the simultaneous processing of all measured elements (Toth & Engi 1997).

For visualisation purposes, an average of each rock type was calculated and plotted in a spider diagram normalised to the average upper crust (Fig. 3; average upper crust of Taylor and McLennan, 1985; http://earthref.org). The spider-diagram allows differentiation of the Cocco- and Antigorio-gneiss from the Leventina, Vogorno and Verzasca gneiss. Cocco- and Antigorio-gneiss define a calc-alkaline suite, whereas the other metagranitoids represent SiO_2-rich leucogranites (Fig. 3). The first group is dominated by granodiorites, but varieties of quartz-dioritic or leucogranitic compositions (aplites) are observed too. The Cocco- and Antigorio-gneiss overlap in major elements, but can be clearly differentiated in their trace element composition (Fig. 3). As a result, these two rock types can be distinguished using Cluster-analysis (for detail see Gruskovnjak 2001). The second group, the Leventina-, Verzasca- and Vogorno-gneisses are leucogranitic rocks, characterised by an elevated aluminium saturation index (ASI) and a high SiO_2 contents (Fig. 3). Again using cluster analysis, the Leventina-gneiss can be distinguished from the Vogorno- and Verzasca-gneisses. In contrast, Verzasca- and Vogorno-gneisses overlap completely in their chemical signature and seem therefore closely associated. In summary, the granitoid gneisses of the study-area were part of a Variscan calc-alkaline and leuco-granitic igneous activity (compare Bonin et al. 1993,

Schermaier et al. 1997). Because individual nappes contain relatively distinct chemical signatures, it appears possible that the segmentation into different nappes during subduction was influenced by the presence and shape of the Variscan Plutons. Furthermore, the classical differentiation into different nappes based mainly on petrographic and structural reasoning, is sustained by geochemical arguments.

Structure of the nappe stack

Summary of the major deformation phases

Based on overprinting relationships, three main Alpine ductile deformation phases can be distinguished in the southern Central Alps (Table 1; Berger et al. 1996, Pfiffner 1999, Nagel et al. 2002a). In addition, brittle and semibrittle structures are widespread and are often referred to as D4 (e.g. Grond et al. 1995).

The oldest (pre-Alpine) structures of the study area are found in the abovementioned local Variscan basement schollen, which are included in the late Variscan granitoids (see above). Confusion must arise if such structures are interpreted as Alpine. The oldest Alpine structures are preserved inside non-retrograded high-pressure rocks (e.g. Grond et al. 1995, Toth et al. 2001, Brouwer 2000; Table 1). As these structures have lost their framework during fragmentation (they are discordant to the surrounding Alpine structures) they cannot be followed over a large distance. The dominant structure occurring in all units is a pervasive composite S1/S2 foliation

	main effects	where	already reported by:
$D_{variscan}$	development of banding and foliations in old basement	parts of Maggia, Simano	2?
D_{HP}	foliation relcits in HP-rocks, producin melange zone	(Ultra)Basica in Cima Lunga, SSB	4, 5
D1	nappe thrusting and foliation development	all units	1,3,4
D2	tight folding, new penetrative foliation	all units	1,3,4; 2 as D3
D3a	open, partly assymmetric, folding	all flat lying nappes	1,3,4; 2 as D4
D3b	dextral transpression and backthrusting	SSB	3
D4	cataclastic faults	all units	4

1: Nagel et al. 2002, 2: Steck 1998, 3: Berger et al. 1996, 4: Grond et al. 1995 & Pfiffner 1999 5: Brouwer 2000

Table 1: Compilation of deformation-phases

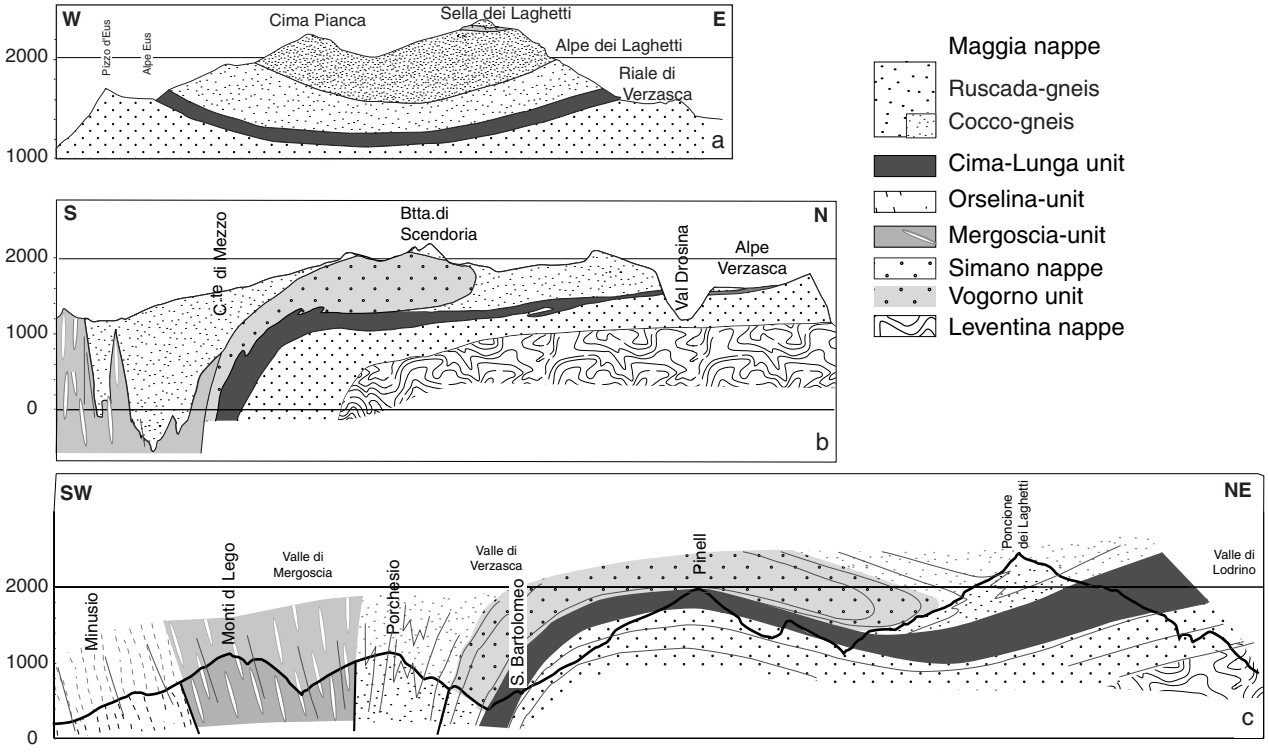

Fig. 4: Different sections through the study area, see figure 1 for section tracing (a) E-W section between Val Leventina and Val Verzasca constructed using own survey data. The open D3 antiform is further supported by section of Preiswerk (1921) (b) N-S section between Magadino plain and Alpe Verzasca. (c) Oblique section, always near-perpendicular to strike of the main foliation. Topography and some structural data from Wenk (unpublished) .

developed during D1/D2 of the respective unit. The geodynamic significance of the tight to isoclinal D2 folding, which refolds the D1 foliation is not fully solved (e.g. Grond et al. 1995, Pfiffner 1999, Nagel et al. 2002a), but a connection to thrusting and nappe-stacking appears plausible. Intense D2-folding is often associated with lithologic contacts or nappe boundaries, where metasedimentary rocks are associated with metagranitoids. Small scale D2-folds are however less frequent inside the large masses of granitic gneisses. The youngest Alpine main deformation phase D3 changes the geometry of an already existing nappe stack. D3 structures are characterised by open, sometimes asymmetric folds which can be followed over larger distances (Fig. 1; see Nagel et al. 2002a). Because D3-folds refold the D1/D2-main schistosity, they are the main large-scale structures recognized on the map-scale (Fig. 1, 4). Parasitic folds, though rare in general, can be locally observed. In the south, D3 folds have the orientation of backfolds, characterised by a steep southern limb, north dipping fold axial planes and a strong asymmetry. It was recently demonstrated, that some of the D3 folds swing from an E-W strike into an N-S strike (i.e. Verzasca-; Cressim-fold, Steck 1998; Nagel et al. 2002a).

Geometry of the study area

The area between Cima del Uomo and Val Lodrino was mapped in detail on a scale 1:10'000 (Plate 1). In the northern part of this area the foliation generally dips gently to the WSW and the nappe stack is only overprinted by late brittle faults. As mentioned above, the nappe stack in the study area is defined from bottom to top by the following nappe sequence: Leventina-, Simano-, Cima-Lunga-, (Vogorno) and Maggia-units (Fig. 1, 4).

In the upper Val Moleno, the folding of the main schistosity suggests a tight fold closing toward NNE, which is interpreted as a D2 fold (Fig. 4d). In the core of the fold, pre-Alpine intrusive structures are preserved (see section on the pre-Alpine history). The folded unit is characterised by two groups of rocks: (1) Granitoid Vogorno-gneiss, which is identical in petrography and field occurrence with the Verzasca-gneiss (see also section on geochemistry); (2) inhomogeneous basement rocks, which are called Gaggia-unit (Wenk 1982). These basement rocks were intruded by the Vogorno-granitoids, a presumably Variscan intrusion. The top of this unit is defined by the bottom of the Cocco and Ruscada gneisses, both characteristic for the Maggia-nappe. Towards the contact, the Maggia rocks are strongly sheared and form a horizon of banded gneisses. The Vogorno sheet may be interpreted as a part of the Maggia nappe, or alternatively, as a tectonic slice of the Simano-nappe, thrusted onto the Cima-Lunga unit. The strong geochemical affinity between the Vogorno and the Verzasca-gneisses may favour the latter hypothesis.

Metamorphic evolution

Based on lithologic and metamorphic arguments, we above divided the southern Lepontine area into two groups. This is also true for the study area, where contrasting lithostratigraphies and metamorphic evolutions are found inside the different units.

The metamorphic evolution of the Leventina, Simano and Maggia-units apparently followed a conventional Barrovian-type metamorphic evolution, and neither elevated pressures nor temperatures have been documented for these units. Recently, peak pressures of 1.0-1.1 GPa at 550°C, and peak temperatures of 650°C at 0.7-0.8 GPa have been estimated for the Simano nappe (Rütti 2003). In another study, slightly higher conditions varying between 600-650°C at 0.8-1.0 GPa (Allaz 2003). In contrast, many high-pressure relics have been described for the fragmented Cima-Lunga unit (Trommsdorff & Nimis 2001, Heinrich 1986, Pfiffner 1999). The Cima-Lunga unit in the study area is defined by a large variety of different rock types, including peridotites, metarodingites and metaeclogites.

In order to better constrain the metamorphic evolution of the study area, several samples of pelitic and mafic composition were studied in detail (Gruskovnjak 2001, Leonardi 2003). In the following sections, we investigate the metamorphic evolution of the southern Cima-Lunga unit and compare the petrologic record preserved in metabasic and metapelitic rocks. We omit further investigations on the polycyclic basement rocks of the Simano-nappe, partly because problems may arise due to an incomplete resetting of the Variscan assemblages, and partly because metamorphic conditions of the Simano-nappe were only recently investigated in some detail by (Grandjean 2000, Rütti 2003, Allaz 2003).

Mafic rocks

Mafic rocks in the Cima-Lunga unit occur as amphibolites devoid of HP-relics or as metaeclogites having suffered different degrees of amphibolite-facies overprints (Fig. 2c). Whether the amphibolites were submitted to HP-conditions too and were just completely resetted during decompression remains an open question. Different stages of the retrograde history from garnet-pyroxene-rutile-, to garnet-amphibole-plagioclase-ilmenite-, and finally to amphibole-plagioclase-titanite paragenesis are preserved in metaeclogites (Fig. 2). Similar eclogitic rocks have been recently reported for the SSB (Brouwer 2000, Grandjean 2001, Toth et al. 2001, Brouwer & Engi in press) and the northern Cima-Lunga unit (Nimis and Trommsdorff 2001, Pfiffner 1999).

A characteristic feature of these rocks are the individual chemical domains that developed during ret-

rogression, caused by the different and restricted mobility of components during retrograde reactions (e.g. Brouwer & Engi, in press). The restricted mobility was probably a combined effect of fluid undersaturation and the generally only minor deformation of these rocks during exhumation. Fluid undersaturation is very likely for rocks having reached eclogite facies conditions, because there, the phase assemblage consists almost entirely of the anhydrous phases garnet-pyroxene-rutile. Even though these different domains indicate disequilibrium on the sample- or even on the thin section scale, local equilibration inside such domains may have been achieved. We use this approach of local equilibrium to test for equilibration-conditions of such local domains in several samples from the study area. Local assemblages of garnet, clinopyroxene, plagioclase and amphibole were analysed and equilibrium PT-conditions were estimated using multiphase equilibrium methods (program TWQ; see Appendix for further details).

A retrograde stage of around 1.2 GPa and 750˚C was calculated for the two samples OS094AD and OS023AD and relatively low conditions of around 550˚C at 0.45 GPa for sample OS022AD using TWQ. The latter result is not very well constrained and would imply very low H_2O-activities in order to stabilise clinopyroxene at these conditions. Based on thermodynamic computation using program Domino, and based on observed phase relations, conditions near 625˚C and 0.75 GPa were obtained for sample OS042AD (Appendix 1).

The locally still observable former HP-assemblage pyroxene-garnet-rutile indicates that pressures of at least 1.8-2.0 GPa (at 700˚C) were reached during the HP-stage (compare experimental results of Liu et al., 1996 Poli, 1993), and that amphibole growth must have occurred during decompression of the samples. Reaction textures further demonstrate that plagioclase has exclusively grown during exhumation, on the behalf of garnet and pyroxene (Fig. 2). Therefore, the metaeclogites record a decompression history from at least 1.8 GPa down to 0.6 GPa. Estimated PT-conditions are considerably higher than those reported for the underlying Simano nappe (Rütti 2003, Allaz 2003).

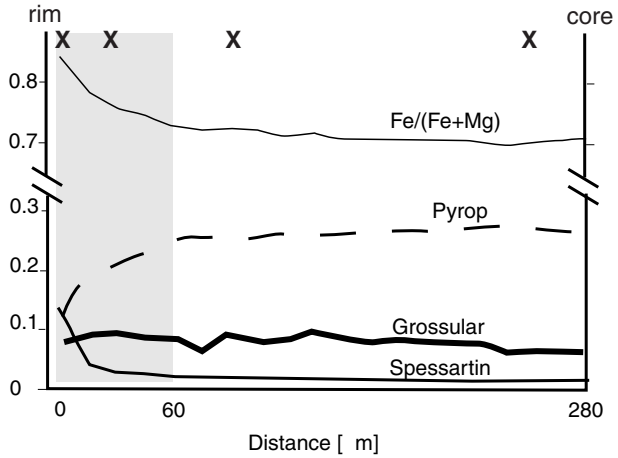

Fig. 5: Microprobe-profile through one garnet-grain in sample P88. Garnet-zoning is symmetric and only one half of a grain is shown. Compositions used for deduction of the PT-path are denoted by crosses.

Metapelitic rocks

Typical metapelites from the Cima-Lunga unit contain kyanite, sillimanite, garnet, biotite, quartz, and plagioclase as major minerals, and rutile, ilmenite, titanite and graphite as major accessories. Element-profiles of garnets in these rocks typically show a plateau in the core, in combination with a ~40µm large rim displaying a near constant Ca-content, an increasing Fe/Mg ratio and an increase in the Mn-content (Fig. 5). In contrast to the metaeclogites of the Cima-Lunga, metapelites show usually a pervasive overprint and lack extensive division into chemical domains. This indicates that metapelites generally more thoroughly reequilibrated than rocks of mafic composition.

In two samples we have analysed two assemblages each, consisting of garnet, biotite, plagioclase, white mica, quartz and aluminosilicate. In a first run, only solid-solid reactions were calculated and PT-conditions estimated from these reactions. In a second step, we approached the fluid composition by varying the mole fractions of H_2O and CO_2 in a T-X_{CO2}-diagram until a best fit was reached, and then recalculated the PT-diagram, using the estimated fluid composition. Estimated fluid compositions are relatively enriched in CO_2 and values range between 0.4-0.8 X_{H2O}. Estimated equilibrium conditions are 0.55-0.65 GPa/610-650˚C for assemblage A in sample P85, 0.65-0.75 GPa/610-650˚C for assemblage B in sample P85, and 0.7-0.75 GPa at 620-660˚C for sample P88 (Appendix 1). Both assemblages in sample P88 yield identical results, indicating that equilibration on the sample scale was reached. Instead, estimated conditions of assemblages A and B of sample P85 diverge by 0.1 GPa, indicating that equilibration may have only be reached on a smaller scale. Both assemblages overlap however within their uncertainty. Estimated conditions lay close to the kyanite-sillimanite boundary. Indeed textural relations indicate a partial replacement of kyanite by sillimanite (see below). To better constrain the respective PT-paths of the metapelitic samples, we computed phase diagrams (Fig. 6) and garnet isopleths using program DOMINO (see Appendix). The presence of graphite in both samples indicates relatively reducing conditions near the QFM-buffer. In addition, pore fluids will contain an important CO_2-component, in line with the above TWQ-estimates. For calculation of the diagram, we therefore assumed QFM-buffering and added CO_2 to the bulk composition. The H_2O/CO_2-ratio defined by the bulk composition is 2/3 (or $X_{CO2} = 0.6$). Assemblages observed in the thin sections (Grt + Phen + Bio + Plag + Ky + Rt and Grt + Phen + Plag + Bio + Si + Ilm) are outlined in the calculated phase diagram (Fig. 6, 8). The diagram indicates conditions of 625-

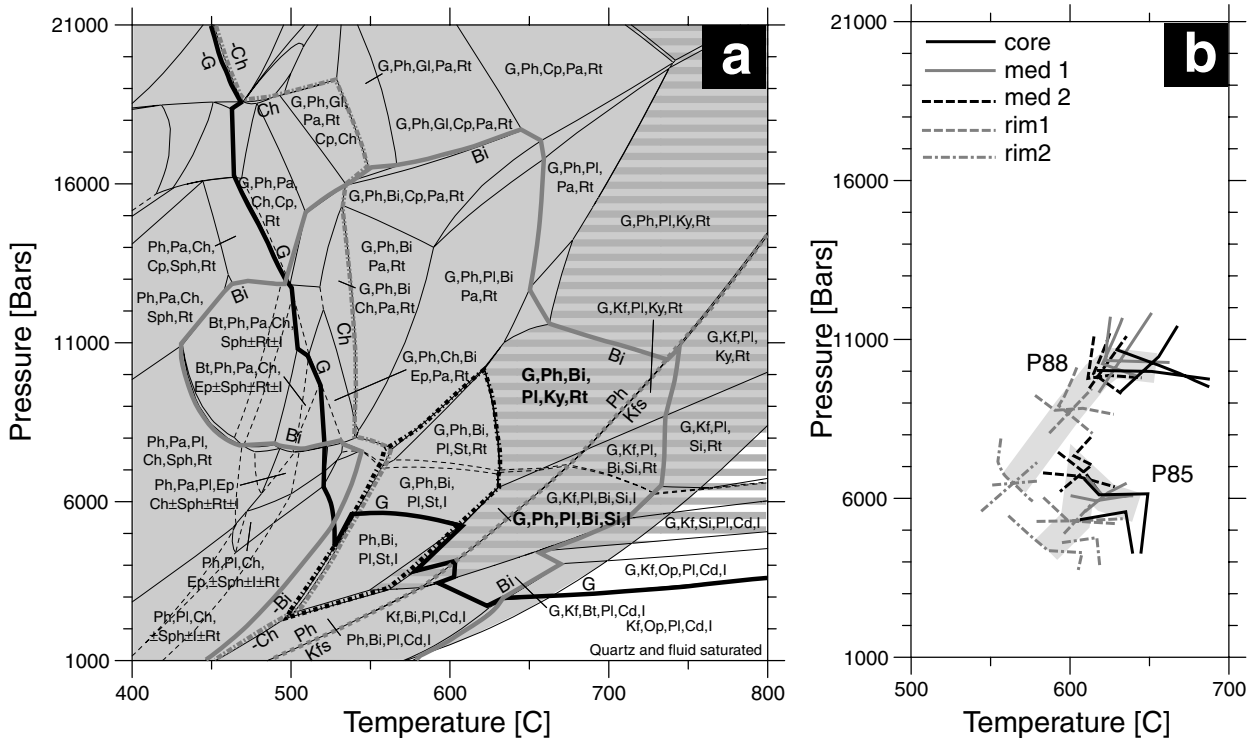

Fig. 6: (a) Phase diagram calculated for metapelite samples P88 and P85. Shaded area denotes stability of graphite. Horizontal stripes indicate the presence of aluminosilicate phases. Observed mineral assemblages are denoted by bold letters. The bold black line denotes the stability field of garnet, the stippled line that of staurolite. Note that staurolite stability depends strongly on water activity (see also figure 8). Abbreviations: Bi-biotite, Cd-cordierite, Ch-chlorite, Cp-clinopyroxene, G-garnet, IL-ilmenite, Kfs-Kfeldspar, Ky-kyanite, Op-orthopyroxene, Pa-paragonite, Ph-phengite, Pl-plagioclase, Q-quartz, Rt-rutile, Sil-sillimanite, Sph-sphene, St-staurolite.
(b) P-T-paths inferred using intersections of garnet isopleths and the analysed garnet profile shown in figure 5. Points are constructed from intersection of garnet isopleths for sample P88 and P85. Five points along the respective profiles from core to rim are plotted.

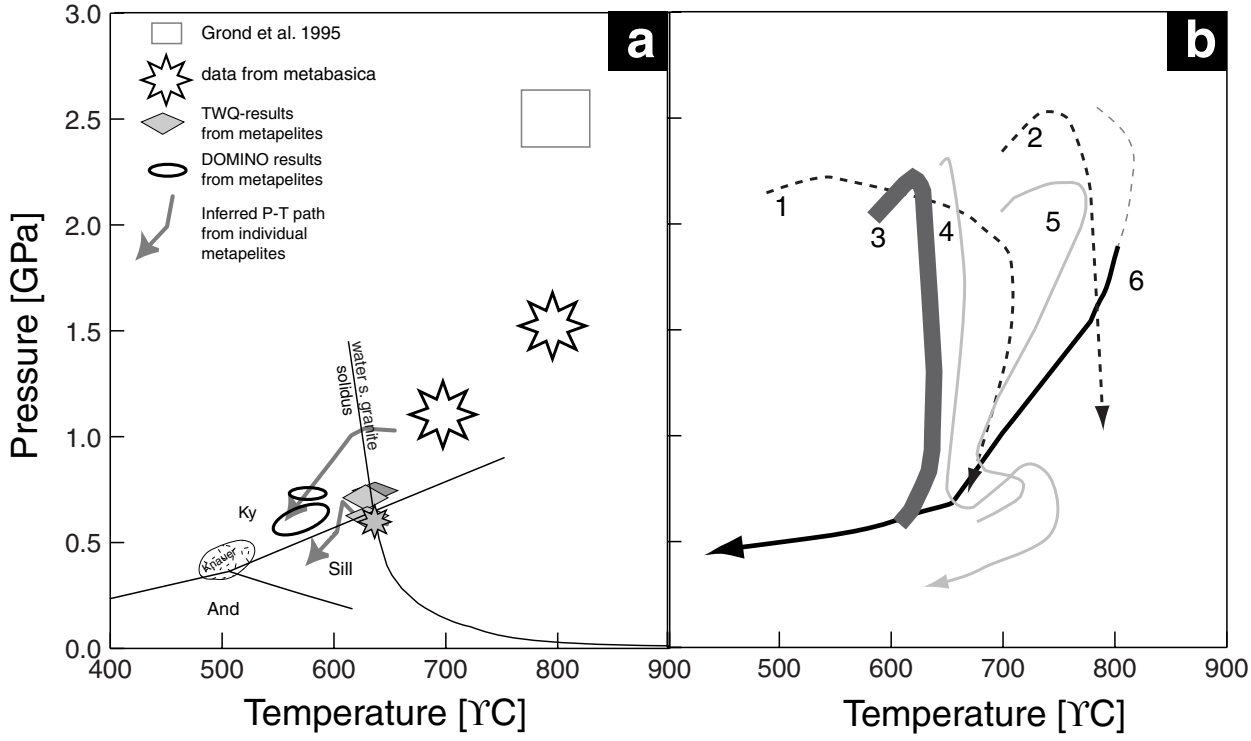

Fig. 7: Compiled information on the P-T evolution of the Cima-Lunga. (a) dat from the Cima Lunga itself. Grey boxes are data from Grond et al. (1995, see also Pfiffner 1999), diamonds are TWQ results (metapelites) from this study. Ellipses are estimated conditions using calculated garnet and plagioclase isopleths. Arrows outline PT-paths inferred for both samples. TWQ results of metaeclogites are shown as stars and conditions of final equilibration of the metabasica inferred from phase assemblages are shown in grey star. All data may be parts of common P-T path or local equilibration of individual P-T paths. (b) different P-T path from the Cima Lunga-, Adula- and SSB-units: 1 and 2: Adula, Dale & Holland (2003); 3: Adula, Nagel et al. (2002a); 4: SSB, Brouwer & Engi (in press); 5: SSB: Toth et al. (2001); 6 possible combined path from this study(southern Cima Lunga).

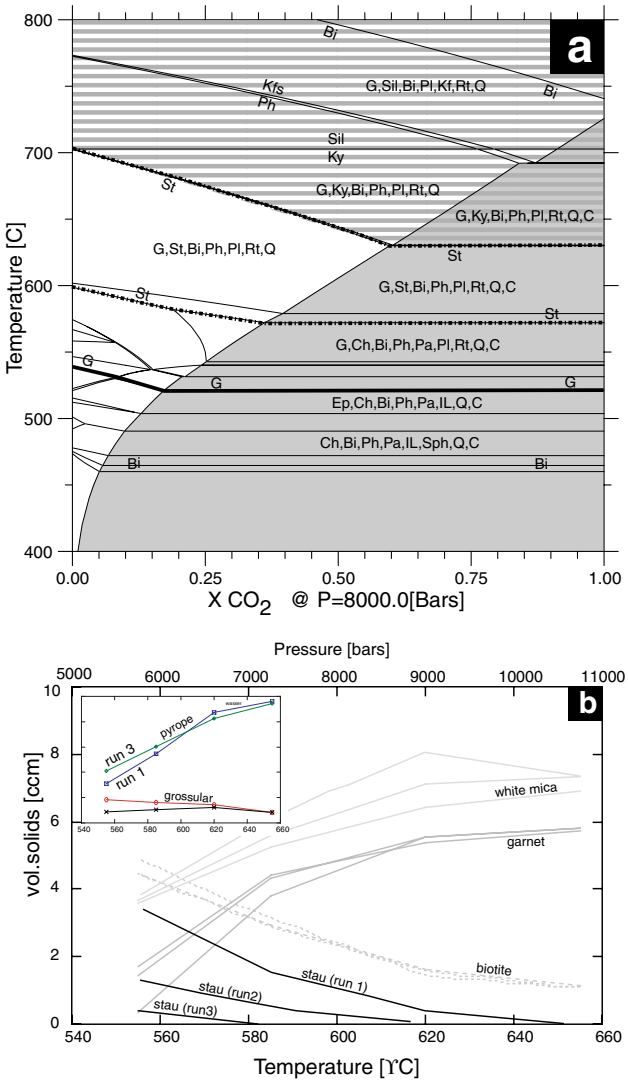

Fig. 8: Effects of fluid on estimated phase-relations and composition: (a) T-XCO_2 diagram at P = 0.8 GPa, denoting the influence of fluid composition on phase relations. At X = O the rock contains pure water as fluid, at X = 1 the amount of H_2O and CO_2 in the system is equal. Shaded area indicates graphite as stable solid phase, striped area denotes stability of aluminosilicate phases. Staurolite stability decreases with increasing CO_2, whereas the stability of the anhydrous aluminosilicates increases at the same time. As soon as graphite gets stable, stability of staurolite is no longer influenced by the fluid composition. Note that the stability of other hydrous phases shows a similar behaviour (see e.g. biotite; see Appendix for further informations on database, Abbreviations as in figure 6). (b) Volume fraction of phases along the inferred path of sample P88. Note the change in pressure and temperature along the path. The different paths are related to changing bulk H_2O-content of the system: Run 1: water saturated; Run 2: intermediate water conditions, Run 3: water is only sufficient to saturate the paragenesis at starting conditions. Small inset shows the relatively weak effect of different water contents on garnet composition.

675°C at 0.7 GPa for the growth of sillimanite and ilmenite. Since ilmenite and sillimanite replace rutile and kyanite respectively, a decompression path leading through these estimated conditions is proposed. To better define respective PT-paths of the two samples, we compare analysed garnet profiles with calculated isopleths for the garnet endmembers grossular, almandine and pyrope. For comparison, analysed garnet compositions were normalised to these three endmembers. Figure 6b displays the results of this approach. Garnet zoning in sample P88 indicates core formation at 1.0 GPa/650°C, followed by a first phase of isobaric cooling of some 50°C, followed by decompression and cooling to 0.7 GPa/570°C. For sample P85, apossible garnet growth at 0.6 GPa/630°C, followed by possible path to 0.7 GPa/610°C and final uplift and cooling to 0.45 GPa/590°C (Fig. 6b, 7). Rather surprisingly, the observed garnet zoning was formed during exhumation, which is generally related to garnet resorption. This implies a very effective garnet-recrystallisation mechanism during exhumation.

The first order information of the phase diagram (Fig. 6a) as well as of garnet zoning agree with the TWQ results, but a displacement of some 50°C towards lower temperatures is visible. In addition, the computed phase diagram suggests that staurolite would just have become stable in all assemblages during exhumation. Staurolite was however not observed in either sample, and the predicted staurolite stability (see Fig. 6) appears inconsistent with the observed phase relations. Lack of staurolite can however be simply the result of fluid under-saturation (see also in discussion-section). Fluid undersaturation likely occurs in closed systems during decompression and cooling, because hydration reactions start to consume the remaining pore fluid. Phase relations, garnet isopleths and TWQ data consistently indicate a decompression P-T path for the two metapelite samples (Fig. 7). Observed reaction textures indicate that the path has crossed the kyanite-sillimanite join twice: The main aluminosilicate-phase kyanite, which is oriented parallel to the foliation, was partially replaced by fine grained sillimanite during decompression (the occurrence of sillimanite was affirmed by in situ micro-Raman analysis). A third generation of aluminosilicates, defined by hyp-idiomorphic kyanite (finer grained than the first generation), overgrows the main foliation and is younger than sillimanite. Late growth of kyanite is also consistent with the observed quartz-kyanite knauer in the area of Val Lodrino, which developed late in the tectonometamorphic evolution of the area (see also Klein 1976, Allaz 2003). In several of these knauer kyanite was partially replaced by andalusite. The significance of andalusite is however uncertain, because this phase may be stabilised beyond it's actual stability field as a result of the incorporation of trace elements.

Discussion

Metamorphism of basic and pelitic rocks in the Cima-Lunga unit: Differences in the preservation of P-T information and the role of fluids

The preservation of P-T information in metamorphic rocks depends, besides of several other parameters, on equilibration kinetics. The above presented P-T data reveal several complexities: (1) In metapelites, mineral-paragenesis and related isopleths strongly depend on fluid-composition, which may not be well known. (2) Metaeclogites developed local chemical domains and may only have equilibrated on a small scale. (3) Basic and pelitic rocks document different segments of the whole PT-path, probably reflecting a different degree of preservation of the high-grade assemblage during exhumation.

Influence of fluid composition may be discussed by assuming fluid saturation and changing X_{H2O} of the fluid. In natural rocks, however, this approach may not be justified as it simulates open system behaviour. Due to the very limited pore space and the related extremely low permeability in high grade rocks, fluid may not buffer the solid assemblage, instead fluid-composition may be fixed by the latter. On the other hand, the retrograde history of a rock may be strongly controlled by the availability of fluids, because hydration reactions become important during cooling. In order to demonstrate for this effect, we calculate the modal abundance (in volume) of phases along the predicted P-T path of sample P88. The location of the "staurolite-in" and the amount of staurolite change systematically with the H_2O-content of the system (see Fig. 8). Because the extent of retrograde garnet consumption changes with the H_2O-content of the system, computed garnet composition changes as well (see small inset in Fig. 8b). As a result, garnet isopleths calculated for a fluid saturated system may become less reliable with increasing degree of fluid undersaturation. Attainment of fluid undersaturation in metapelitic systems does however not necessarily imply disequilibrium behaviour, because the major part of the reaction is water preserving (garnet + white mica = biotite + aluminosilicate). However, the exact location of garnet-isopleths will shift as soon as fluid undersaturation is reached, most probably near T_{max}.

Local equilibration of metaeclogite-subdomains testify for similar PT-conditions as reported for the surrounding metapelites (this study, Brouwer 2000). However, the retrograde evolution of basic rocks depends, similar to the metapelites, on the bulk fluid-content of the system, because reactions from eclogite to amphibolite facies-conditions are generally fluid consuming. Furthermore, oxygen fugacity may strongly influence stability relations and abundance of ferric-iron bearing phases like epidote, and as a result influence other faces that are in interaction with epidote. Therefore, modal abundance and phase-compositions in metapelites and metabasic rocks along the retrograde path are influenced by similar parameters. The low permeability of such gneisses and eclogites at 1.5-0.5 GPa, as well as the importance of retrograde hydration reactions, makes water undersaturation likely to be attained during ascent of the rocks. Because the PT-location where fluid undersaturation was reached may in general be only badly constrained, computation of phase diagrams and isopleths may be associated with additional uncertainties. Therefore, a multiphase equilibria approach (e.g. using program TWQ) may be able to better constrain equilibration conditions.

Tectonic evolution and the role of nappe dividers

Recognition and outlining of the different Alpine units in the Lepontine has been a major problem and topic since the start of Alpine research in this area. The well defined Mesozoic nappe dividers of the frontal part of the Lepontine nappes become, extremely reduced or are even missing in the study area. In addition, the metasediments of the southern Lepontine area are highly metamorphic and are no longer easily differentiable from older, polymetamorphic metasediments.

In order to separate the different units from each other, structural, petrographic, geochemical as well as metamorphic argumentr have been used. Depending on the metamorphic conditions during thrusting or stacking, the structural inventory may be of limited use only, because with increasing temperature, deformation becomes less strongly localised, and well defined mylonite horizons may no longer form. Nevertheless, based on the combined information, the nappe-succession of the study area can be defined with some certainty from bottom to top (see also above):

Leventina-unit
Simano-unit
Cima-Lunga unit (abundant HP-relics)
Maggia-nappe

Despite of a similar pre-Alpine history of Variscan granitoid intrusion into an older basement, Maggia and Simano-units are clearly separated from each other in the study area by the high pressure Cima-Lunga unit. In addition to the HP-relics that are found in this unit, its very inhomogeneous, fragmentary character (mélange of continental and oceanic fragments) points out the uniqueness of the Cima-Lunga unit. Cima-Lunga and Adula nappes have therefore been interpreted as Alpine subduction mélange or tectonic accretion channel (TAC; Engi et al. 2001; Trommsdorff 1990).

The Adula-unit which is located to the east of the study area, has the same tectonic position as the Cima-Lunga unit and an identical heterogeneous and fragmentary character, including various HP-relics. However, the two units differ considerably in their thickness. We constructed a thickness of ~2900 metres for the Adula nappe in upper Val Mesolcina (based on Nagel et al. 2002a), which is 6 times higher than the Cima-Lunga unit in Val Lodrino (~450 m). To the west of Valle Verzasca, the

Cima-Lunga unit becomes even thinner and its continuation remains ambiguous. This substantial change can be related to a continuous change in thickness from east to west, or alternatively, to a relatively sharp step in thickness. A more stepwise change could indicate that the Cima-Lunga unit represents only a single mélange-sheet emplaced in the nappe stack (Jenni et al. 1924). In contrast, the Adula consists of an assemblage of different mélange slices separated by slices of granitoid gneisses, which are emplaced as a package onto the nappe stack. A discontinuous or continuous change in thickness along strike may be caused by the pre-subduction geometry of the former plate boundary (see e.g. Goffe et al. 2003). Thus, the final shape and thickness of the mélange units depend on local stresses along a bent plate boundary.

Significance of this study for the geodynamic evolution

The investigated section of the Cima-Lunga unit contains several HP-relics similar to those reported for the adjacent northern Cima-Lunga- and Adula-nappe (e.g. Heinrich 1986, Pfiffner 1999). Both units have recently been utilised to discuss the dynamics of HP-exhumation (e.g. Brouwer et al. 2004, Froitzheim et al. 2003, Nagel et al. 2002a). Froitzheim et al. (2003) summarises the often-discussed models for HP-exhumation: erosion, extensional thinning, extrusion and extraction (see their Fig. 1). Although the latter author proposes extraction as the most important process, several other authors have suggested exhumation by extrusion as most likely (e.g. Greya et al. 2002, Roselle and Engi 2001, Burov et al. 2001).
Extruding, or upward flowing fragments may be individual, centimetre-meter sized boudins, or larger units of already mixed zones (e.g. Cima-Lunga unit). Although a strong deformation inside or around upward flowing fragments is clearly required, it remains ambiguous to decipher structures in the field that could be related to this process. Structures found today in classical-nappes as well as in TAC-units are concordant to each other, and are likely related to a final stage of nappe stacking. Structures attributable to the early development of the mélange may however be preserved in eclogite boudins (e.g. Tòth et al. 2001), although such structural data may not much help deciphering processes that acted in great depth. Fortunately, petrologic arguments on the P/T evolution of individual fragments and their matrix help deciphering the extrusion history of these units: After a high pressure phase, which is in part recorded in metabasic and metaultramafic rocks, the investigated basic and metapelitic rocks show a common stage of equilibration at around 0.6 GPa and 600-650˚C. Based on textural arguments (preferred orientation of mica, kyanite (1) and sillimanite, and overgrowth by a second kyanite (2) generation) we suggest that the major foliation became established in the course of this phase. Further post-D1/D2 retrogression, which is related to cooling and decompression, is visible in the outermost garnet rims, in rare kyanite (2) overgrowing the foliation, and in the development of late quartz-alumosilicate Knauer.
Combining this information with proposed P-T path form the adjacent Adula-nappe and the SSB (Nagel et al. 2002a, 2002b, Brouwer 2000, Grandjean 2001, Dale and Holland 2003) we can detect different P-T data and different segments of the paths (Fig. 7). Some data propose isothermal decompression, while others show combined cooling and decompression, followed by a late phase of reheating (Fig. 7). All P-T paths may be significant for individual fragments extruding along a tectonic accretion channel. Differences in the maximal reported pressure can be assumed if different fragments are incorporated at different times and depths inside the TAC. Furthermore, a different PT-history may be recorded, if the ascending fragments are of a contrasting size. The amount of hot, accreted material that extrudes and is emplaced on the nappe stack, may significantly influence the extent of late reheating.

Conclusions

This combined petrologic, structural and geochemical study addresses different aspects of the nappe stack in the Central Alps, and reveals information on its Variscan and Alpine history. Each of the studied nappes records a probably Variscan episode of igneous activity, and contains at least one extensive plutonic body, which may have influenced the future shape of the individual nappes. Alpine tectonic units can be reconstructed using petrologic and structural arguments. For the study area we propose the following sequence for the Alpine nappe stack: Leventina-, Simano-, Cima-Lunga-, and Maggia nappe. The Cima-Lunga nappe represent a relic of the former plate boundary that separated units from the European plate from those of the overlying Briançonnais unit (Maggia-nappe)
Inside the mélange unit, individual fragments record different stages of the P-T evolution. In detail, P-T relations are influenced by the amount and type of fluid present along the P-T path. In different rocks local equilibration are recorded from 1.5 GPa down to 0.6 GPa. At about 0.6 GPa and 600˚C all rocks followed the same exhumation path, indicating, that major movements were localised elsewhere at that time. Comparison between metapelites and basic rocks demonstrated that metapelites record a smaller segment of the whole PT-path, but nevertheless testify for conditions as high as 1.1 GPa.

References:

Allaz, J. & Maeder, X. (2003): Evolution tectonique et métamorphique de la nappe de Simano à l'Alpe Larecc, Valle Maggia (Tessin, Suisse). Thèse de Diplom. Université de Lausanne, 177 pp.

Bächlin, R. Bianconi, F., Codoni, A., Dalvesco, E., Knblauch, P., Kündig, E., Reinhard, M., Spaenhauer, F., Spicher, A., Trommsdorff, V. andWenk, E. (1974): Geologischer Atlas der Schweiz 1: 25000, Blatt 1313: Bellinzona. Geologische Kommision der Schweiz.

Berger, A., Rosenberg, C., and Schmid, S.M. (1996): Ascent, emplacement and exhumation of the Bergell Pluton within the Southern Steep Belt of the Central Alps. Schweiz. Mineral. Petrogr. Mitt., 76, 357-382.

Berman (1988): Internally-consistent thermodynamic data for minerals in the system Na_2O-K_2O-CaO-FeO-Fe_2O_3-Al_2O_3-TiO_2-H_2O-CO_2. J. Petrol., 29, 445-522

Bonin, B., Brändlein, P., Bussy, F., Desmos, J., Eggenberger, U., Finger, F., Graf, K., Marro, C., Mercolli, I., Oberhänsli, R., Ploquin, A., von Quadt, A., von Raumer, J., Schaltegger, U., Steyrer, H.P., Visona, D., and Vivier, G. (1993): Late variscan magmatic evolution of the Alpine basement, *in* von Raumer, J., and Neubauer, F., eds., Pre-Mesozoic geology in the Alps: Berlin, Springer, 171-201.

Burov, E., Jolivet, L., Le Pourhiet, L. & Poliakov, A. (2001): A thermomechanical model of exhumation of high pressure (HP) and ultra-high pressure (UHP) metamorphic rocks in Alpine-type collision belts. Tectonophysics, 342, 113-136.

Brouwer, F.M. (2000): Thermal evolution of high-pressure metamorphic rocks in the Alps: Utrecht, PhD University of Utrecht.

Brouwer, F.M., and Engi, M. (in prep): Staurolithe and other high-Alumina phase in Alpine eclogite: Analysis of domain evolution. Canadian Mineralogist .

Brouwer, F.M., van de Zedde, D.M.A., Wortel, M.J.R., and Vissers, R.L.M. (2004): Late-orogenic heating during exhumation: Alpine PTt trajectories and thermomechanical models. EPSL, 220, 185-199.

Casasopra, S. (1939): Studio petrografico dello gneiss granitico Leventina. Schweiz. Mineral. Petrogr. Mitt., 19, 449-708.

Dal Vesco, E. (1953): Genesi e metamorfosi delle rocce basiche e ultrabasiche nell' ambiente mesozonale dell' orogene pennidico. Schweiz. Mineral. Petrogr. Mitt., 33, 173-480.

Dale, J., and Holland, T.J.B. (2003): Geothermobarometry, P–T paths and metamorphic field gradients of high-pressure rocks from the Adula Nappe, Central Alps. J. Metam. Geol., 21, 813–829.

DeCapitani, C. (1994): Gleichgewichts-Phasendiagramme: Theorie und Software. Eur. J. Mineral. 6 Beiheft, 48.

Engi, M., Berger, A., and Roselle, G. (2001a): The role of the tectonic accretion channel in collisional orogeny. Geology, 29, 1143-1146.

Engi, M., Scherrer, N.C., and Burri, T. (2001b): Metamorphic evolution of pelitic rocks of the Monte Rosa nappe: Constraints from petrology and single grain monazite age data. Schweiz. Mineral. Petrogr. Mitt., 81, 305-328.

Froitzheim, N., Pleuger, J., Roller, S., and Nagel, T. (2003): Exhumation of high- and ultrahigh-pressure metamorphic rocks by slab extraction. Geology, 31, 925–928.

Gerya, T.V., Stöckert, B., and Perchuk, A.L. (2002): Exhumation of high-pressure metamorphic rocks in a subduction channel: A numerical simulation. Tectonics, 21, 1056.

Goffé, B., Bousquet, R., Henry, P., and Le Pichon, X. (2003): Effect of the chemical composition of the crust on the metamorphic evolution of orogenic wedges. J. Metam. Geology, 21, 123-141.

Grandjean, V. (2001): Petrographical evolution of mafic relics and their implication for the geodynamics of the Central Alps, PhD thesis, Bern, University of Bern.

Grond, R., Wahl, F., and Pfiffner, M. (1995): Mehrphasige alpine Deformation und Metamorphose in der nördlichen Cm. Lunga Einheit, Zentralalpen (Schweiz). Schweiz. Mineral. Petrogr. Mitt., 75, 371-386.

Gruskovnjak, A. (2002): Geologische und petrographische Untersuchungen im Lepontin im Grenzbereich von Maggia- und Simanodecke (Ticino) [Diplom thesis]: Bern, Universität Bern.

Heinrich, C.A. (1978) Metamorphose und Strukturen der Cima Lunga Serie I. Cima di Cagnone - Val Motto [Diplom thesis]: Zuerich, ETH Zuerich.

Heinrich, C.A. (1983): Die regionale Hochdruckmetamorphose der Aduladecke [PhD thesis]: Zuerich, ETH Zuerich.

Heinrich, C.A. (1986): Eclogite facies regional metamorphism of hydrous mafic rocks in the Central Alpine Adula nappe. J. Petrol., 27, 123-154.

Holland, T.J.B. and Powell, R. (1998): An internally consistent thermodynamic data set for phases of petrological interest. J. metam. Geol., 16, 309-343.

Hunziker, J. (1966): Zur Geologie und Geochemie des gebietes zwischen Valle Antigoriound Valle di Campo. Schweiz. Mineral. Petrogr. Mitt., 46, 473-552.

Hunziker, P. (2003): The stability of tri-octahedral Fe^{2+}-Mg-Al-chlorite. a combined experimental and theoretical study. PhD Thesis, University Bern, 119 pp.
Klein, H.H. (1976): Alumosilikatführende Knauern im Lepontin. Schweiz. Mineral. Petrogr. Mitt., 56, 435-456.
Leonardi, U. (2003): Zur Abgrenzung und Entwicklung der Cima Lunga und angrenzende Einheiten im Gebiet von Valle di Drosina - Valle di Lodrino (Kanton Tessin). Diplomarbeit, Universität Bern, 105 pp.
Liu, J., Bohlen, S. R. & Ernst, W. G. (1996): Stability of hydrous phases in subducting oceanic crust. EPSL,143, 161-171.
Nagel, T. (2000): Metamorphic and structural history of the Southern Adula nappe (Graubünden, Switzerland). Ph.D. Thesis, University of Basel.
Nagel, T., deCapitani, C., Frey, M., Froitzheim, N., Stünitz, H., and Schmid, S.M. (2002a): Structural and metamorphic evolution during rapid exhumation in the Lepontine dome (southern Simano and Adula nappes, Central Alps, Switzerland). Eclogae geol. Helv. 95, 301-321.
Nagel, T., deCapitani, C. and Frey, M. (2002b): Isograds and P-T evolution in the eastern Lepontine Alps (Graubünden Switzerland). J. metam. Geol., 20, 309-324.
Nimis, P., and Trommsdorff, V. (2001): Revised thermobarometry of Alpe Arami and other garnet peridotites from the Central Alps. J. Petrol. 42, 103-115.
Nussbaum, C., Marquer, D., Biino, G.G. (1998): Two subduction events in a polycyclic basement: Alpine and pre-Alpine high-pressure metamorphism in the Suretta nappe, Swiss Eastern Alps. J. Metam. Geol., 16, 591-605.
Maxelon, M. and Mancktelow, N.S. (2003) Synform or monocline - the structure of the Southern Steep Belt in the Central Alps of Switzerland VI. Alpine Workshop Sopron
Meyre , C., de Capitani, C. and Partzsch, J.H. (1997): A ternary solid solution model for omphacite and its application to geothermobarometry of eclogites from the Middle Adula nappe (Central Alps, Switzerland). J. Metam. Geol., 15, 687-700.
Pfiffner, M., and Trommsdorff, V. (1998): The high pressure ultramafic-mafic-carbonate suite of Cima Lunga Adula, Central Alps: Excursion to Cima di Gagnone and Alpe Arami. Schweiz. Mineral. Petrogr. Mitt., 78, 337-354.
Pfiffner, M.A. (1999): Genese der Hochdruckmetamorphen ozeanischen Abfolge der Cima Lunga Einheit (Zentralalpen), PhD thesis, Zürich, ETH.
Poli, S. (1993): The amphibolite-eclogite transformation: An experimental study on basalt. Am. J. Sci., 293, 1061-1107.
Preiswerk, H. (1918): Geologische Beschreibung der Lepontische Alpen. Beitr. geolog. Karte Schweiz N.F. 26, 80pp.
Preiswerk, H. (1921), Vom Gestein im Tessin, Die Alpen, 12, 441-461
Preiswerk, H. (1925): Tessinergneis. Eclog. geol. Helv. 19, 177-187.
Preiswerk, H. (1931): Der Quarzdiorit des Coccomassives. Schweiz. Mineral. Petrogr. Mitt. 11, 27-.
Preiswerk, H., Bossard, L., Grütter, O., Niggli, P., Kündig, E., and Ambühl, E., (1934): Geologische Spezielkarte Nr. 116; Geologische Karte der Tessinneralpen zwischen Maggia- und Blenio-Tal, Schweizerische Geologische Kommision.
Roselle, G.T., and Engi, M. (2002): Ultra high pressure (UHP) terrains: Lessons from thermal modelling. Am. J. Sci., 302, 410-441.
Rütti, R. (2003): The tectono-metamorphic evolution of the northwestern Simano nappe (Central Alps, Switzerland) , PhD thesis, Zürich, ETH Zürich.
Schermaier, A., Haunschmid, B., and Finger, F. (1997): Distribution of Variscan I- and S-type granites in the Eastern Alps: A possible clue to unravel pre-Alpine basement structures. Tectonophysics, 272, 315-333.
Steck, A. (1998): The Maggia cross folds: An enigmatic structure of the lower penninic nappes of the Lepontine Alps. Eclog. geol. Helv., 91, 333-343.
Taylor, S.R. and McLennan, S.M. (1985): The continental crust: its composition and evolution. Blackwell Scientific Publications, Oxford, 312 pp.
Tòth, T.M., and Engi, M. (1997): A new cluster analysis method for altered rock samples. Schweiz. Mineral. Petrogr. Mitt. 77, 439-447.
Tòth, T.M., Grandjean, V., and Engi, M. (2000): Polyphase evolution and reaction sequence of compositional domains in metabasalt: a model based on local chemical quilibrium and metamorphic differentiation. Geol. Journ., 1-21.
Trommsdorff, V. (1990): Metamorphism and tectonics in the Central Alps: The Alpine lithospheric melange of Cima Lunga and Adula. Mem. Soc. Geol. Ital., 45, 39-49.

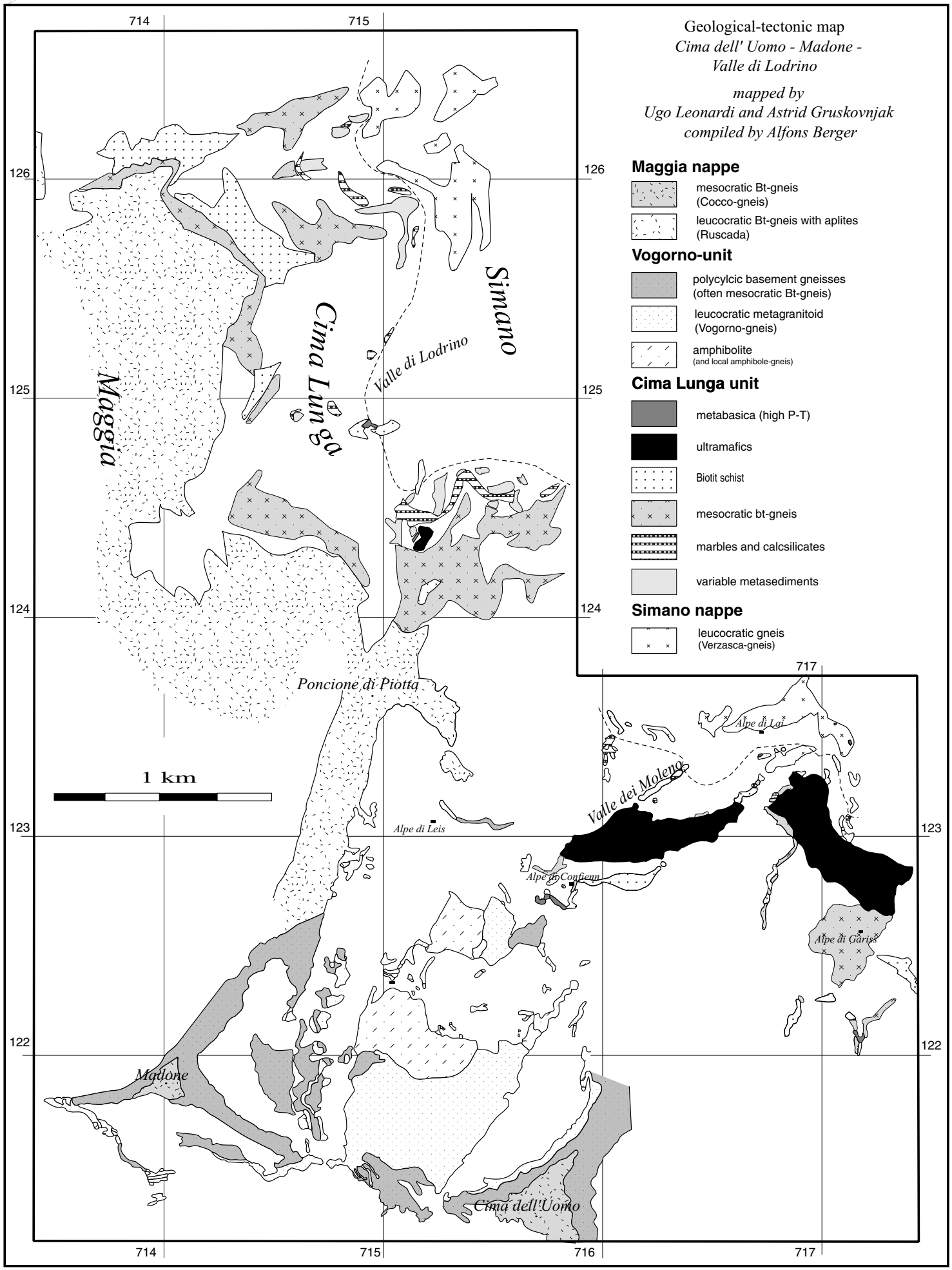

Plate 1. Geological map betweenCima dell' Uomo - Madone - Valle di Lodrino

Appendix

A1: TWQ-calculation:

Program-TWQ is used in combination with the internally consistent database of Berman (1992) (88, update 92). All solution models used are those included in the database, except for the clino-pyroxene model of Meyre et al. (1997).

Continuous lines denote reactions where all used endmembers have a high activity. Dashed lines those where one or several endmembers have a low to very low activity. Reaction-equations are only given for the first type of reactions.

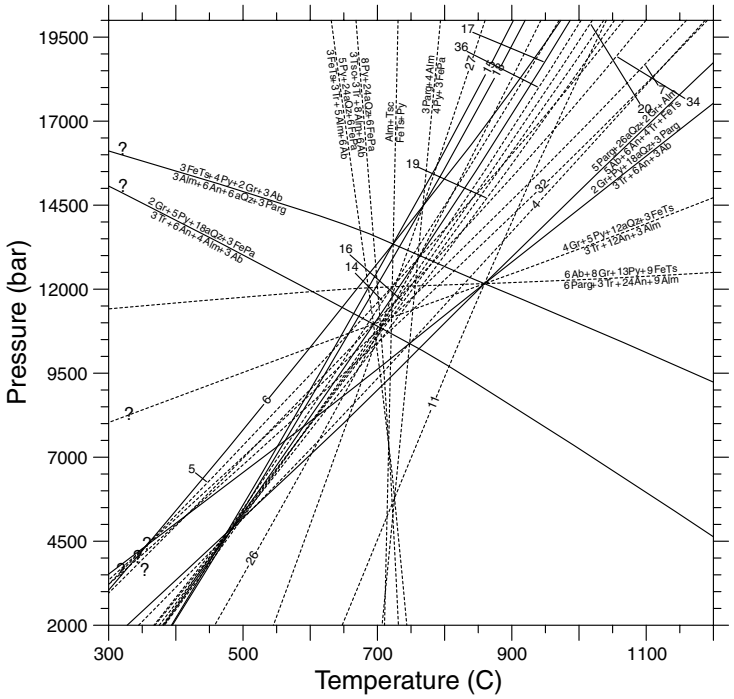

Figure A1: TWQ result of sample OS023AD

6: 3Ab+2Gr+Py+3Tsc = 3Parg+6aQz+6An
15: 3Ab+Alm+2Gr+4Tsc = 3Parg+FeTs+6aQz+6An
17: 6Ab+4Alm+8Gr+9Tsc = 3FePa+3Parg+3Tr+24An
18: 12Ab+4Alm+8Gr+12Tsc = 3FePa+9Parg+24aQz+24An

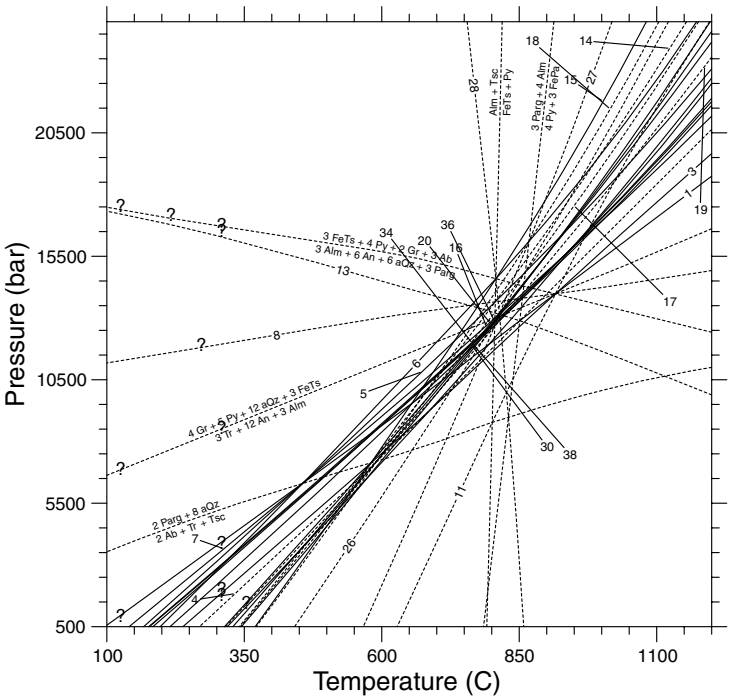

Figure A2: TWQ result of sample OS094

1: 2Gr+Py+18aQz+Parg = 3Tr+6An+3Ab
3: 5Parg+26aQz+2Gr+Alm = 5Ab+6An+4Tr+FeTs
5: 6Ab+8Gr+4Py+9Tsc = 6Parg+3Tr+24An
6: 3Ab+2Gr+Py+3Tsc = 3Parg+6aQz+6An
7: 4Gr+2Py+2aQz+3Tsc = 3Tr+12An
15: 3Ab+Alm+2Gr+4Tsc = 3Parg+FeTs+6aQz+6An
16: 2Alm+4Gr+12aQz+5Tsc = 2FeTs+3Tr+12An
20: 15Tsc+24aQz+16Gr+8Alm+6Ab = 48An+9Tr+6FePa
30: 3Parg+36FeTs+16Py+32Gr+24Ab = 96An+12Tr+27FePa

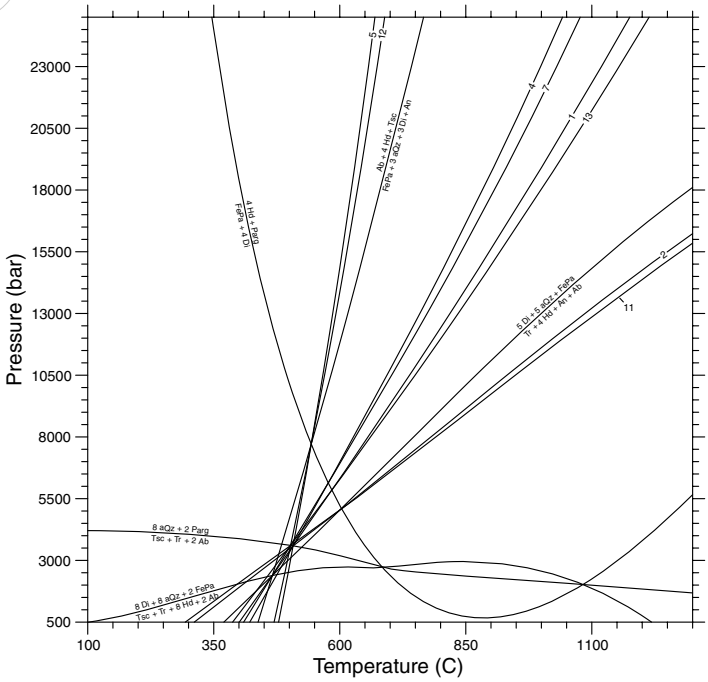

Figure A3: TWQ result of sample OS022AD

1: 2Di+2aQz+Tsc = Tr+2An
2: Di+5aQz+Parg = Tr+An+Ab
4: 2Ab+8Di+5Tsc = 2Parg+3Tr+8An
5: Ab+Di+Tsc = Parg+3aQz+An
7: 2Ab+8Hd+5Tsc = 2FePa+3Tr+8An
11: 4Hd+20aQz+5Parg = FePa+4Tr+4An+4Ab
12: 4Ab+4Hd+4Tsc = FePa+3Parg+12aQz+4An
13: 4Hd+4aQz+2Tsc+Parg = FePa+2Tr+4An

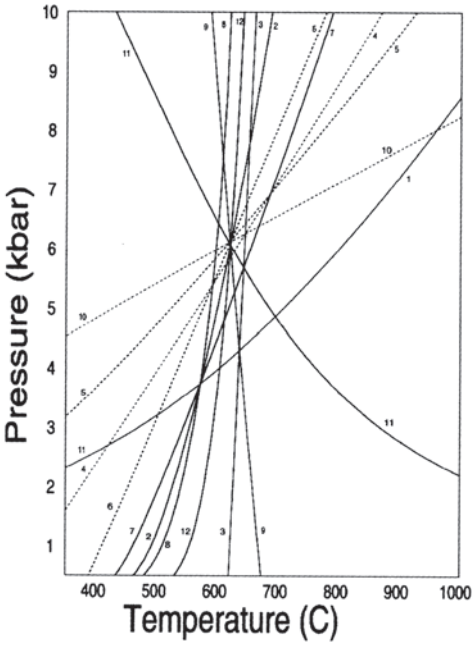

Figure A4: TWQ result of sample P88

1: Alm+Ms=Qz+2Ky+Ann
2: Pg+Qz=KyAb+H2O
3: Ann+Py=Phl+Alm
4: 4Alm+Gr+Ms=3An+Ann
5: 3An+Pg=3Ky+Gr+Ab+H2O
6: 2Ab+3An+2H2O=3Qz+2Pg+Gr
7: Alm+Ms+Pg=3Ky+Ann+Ab+H2O
8: 2Ab+Alm+Ms+2H2O=3Qz+2Pg+Ann
9: 2Ky+Phl+Qz=Py+Ms
10: 3An+Phl=Py+Ms+Gr
11: Ab+3Ky+Phl+H2O=Py+Pg+Ms
12: 2Pg+Phl+3Qz =Py+Ms+2Ab+2H2O

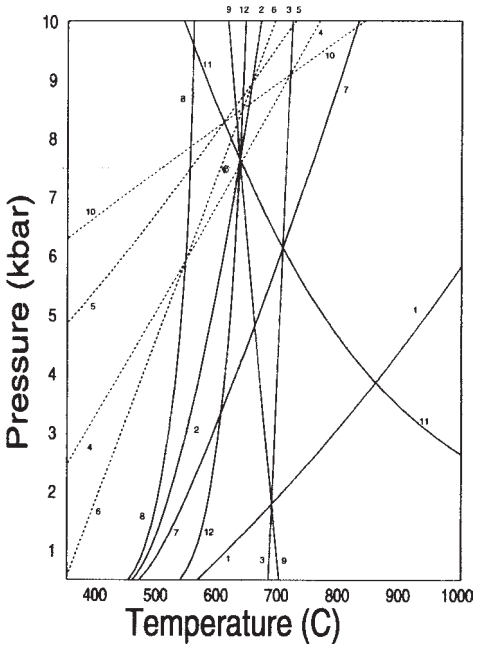

Figure A5: TWQ result of sample P86

1: Alm+Ms=Qz+2Ky+Ann
2: Pg+Qz=KyAb+H2O
3: Ann+Py=Phl+Alm
4: Alm+Gr+Ms=3An+Ann
5: 3An+Pg=3Ky+Gr+Ab+H2O
6: 2Ab+3An+2H2O=3Qz+2Pg+Gr
7: Alm+Ms+Pg=3Ky+Ann+Ab+H2O
8: 2Ab+Alm+Ms+2H2O=3Qz+2Pg+Ann
9: 2Ky+Phl+Qz=Py+Ms
10: 3An+Phl=Py+Ms+Gr
11: Ab+3Ky+Phl+H2O=Py+Pg+Ms
12: 2Pg+Phl+3Qz =Py+Ms+2Ab+2H2O

A2: Domino-calculation

For DOMINO calculations of metapelites we used the internally consistent database of Berman (88, update 92) with several recent updates in standard state data and solution models, fitted to this database. Added models are as follows:Chlorite, Hunziker (2003); Staurolite: Nagel et al. (2002b); Chloritoid: Nagel (2000); Clinopyroxene: Meyre et al. (1997); White mica: Keller et al. (in press)
For calulation of mafic rocks we used the internally consistent database of Holland&Powell (1998), due to the lack of an amphibole solution model in the Berman database.

Structures of the southwestern Lepontine: A working report

Thomas Burri and Alfons Berger

Introduction

Investigation on orogenic processes in high-grade mountain belts as the Central Alps of Switzerland and Italy involves combined petrographic, petrologic, isotopic and structural information. Whereas information on metamorphic conditions of the study area was given in the remaining chapters of this work, this chapter describes in some detail the petrography and structures of the Centovalli-, Onsernone-, Maggia- and Verzasca area, and introduces several working hypotheses on the significance of the observed structures in the context of subduction and collision. For discussion we have constructed a series of roughly SW-NE-striking profiles, using data from the literature and own survey data. The profiles show that the study area is defined by several syn- and antiformal structures. The report presents new data and concepts on the extent of the Maggia- and Antigorio nappes in the Valle Onsernone area, based on structural, petrographic and metamorphic evidence. It further discusses the relationships between observable structures, deformation phases and related tectonic context.

Short characterisation of the main tectonic units and structures

The southwestern Lepontine is composed of a stack of roughly flat-lying basement nappes, separated from each other by shear-horizons, by a sedimentary cover of Mesozoic or uncertain age, or by inhomo-geneously composed units of differing significance. Overall, four main deformation phases are found in the study area (see also Huber *et al*., 1980): D2 isoclinal folds refold a pre-existing D1-foliation. The axial planar foliation of D2 isoclinal folds is parallel to the D1-foliation, leading to a composite D1/D2 main foliation. We tentatively attribute these structural elements to subduction, delamination and nappe-stacking. D1/D2-structural elements (thus the nappe stack) were then refolded (D3) to the north and to the south, where two structural steep belts are observed (Milnes, 1974; Huber *et al*., 1980; Heitzmann, 1987; Schmid *et al*., 1989). To the south, this late phase of backfolding, which immediately preceded back-thrusting and associated rapid exhumation of the Lepontine, is classically termed post-nappe folding (Milnes, 1974), and has produced the dominant large-scale backfold-structure (Fig. 1). The backfolds grade towards the south into the Southern Steep Belt (SSB), which is a roughly east-west striking belt, dominated by vertical to overturned planar structures. In the Centovalli-Onsernone area, the backfold passes into the Onsernone-Antiform and Vergeletto-Synform (Fig. 1), which start as open folds in the west and get strongly compressed to the east. North of the Vergeletto-Synform, another open fold is recognised in the Valle Maggia area, the Maggia-Antiform. Further north, a major structure of the study area is encountered, the Maggia-Synform – Verzasca-Antiform pair (Preiswerk, 1921; Wenk, 1953; Grujic and Mancktelow, 1996; Steck, 1998). The Maggia-Synform, also called Maggia-Crossfold, bends from a north-south striking direction in the north into the E-W running SSB to the south (compare also with strike of the Maggia-unit in plate 1). This suggests that this synformal structure was refolded during formation of the SSB, similar to other folds to the east (Leventina-Antiform, Cressim-Antiform). Recent structural investigation has however questioned the importance of the Maggia-Synform, and has interpreted this structure as a nappe-internal complication of a combined Simano-Maggia-unit (Maxelon and Mancktelow, 2002). These new concepts reveal, however, how important a clear differentiation of the different tectonic units is, and that a correlation, based mainly on structural information, may lead to a tectonic interpretation strongly in contrast to another based mainly on petrography. The classical distribution into Alpine units or nappes (Schmidt *et al*., 1908; Preiswerk, 1918; Preiswerk *et al*., 1934) was based on the occurrence of (suggested) Mesozoic meta-sediments as well as on petrographic characteristics of the different units. Before we start with a detailed description of the structures, we therefore summaries petrography and some features of metamorphism of the different tectonic units of the Central Alps. Note that the E-W correlation of the different tectonic units in the Central Alps is complicated by the occurrence of the Maggia-Crossfold. To the east of this structure, the nappe stack is defined by the sequence (from bottom to top) Leventina nappe, inhomogeneous boundary series, Simano nappe, Cima-Lunga nappe and Maggia nappe; to the west by the sequence Antigorio nappe, MO-unit

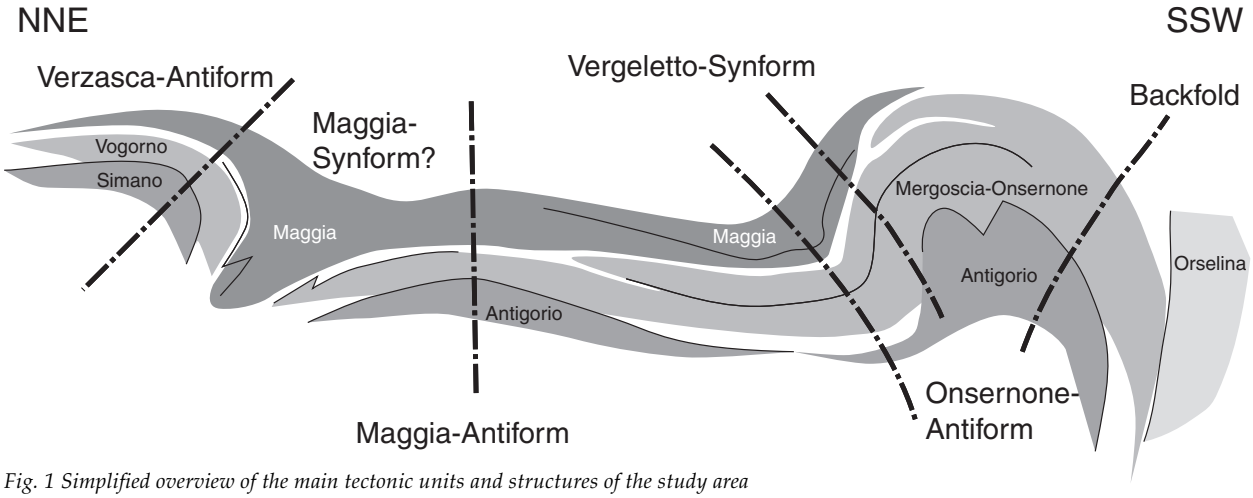

Fig. 1 Simplified overview of the main tectonic units and structures of the study area

(Mergo-scia-Onsernone-Someo unit) and Maggia unit. The different units show the following petrographic and petrologic characteristics:

Classical basement nappes

Leventina nappe: The Leventina nappe is dominantly composed of a relatively leucocratic one- (Bt), to two-mica (Bt+Ms) gneiss of granitic composition (Leventina-gneiss). At several localities in the top of this nappe, intrusive breccias may be observed (e.g. to the east above Biasca, also pers.comm. Rütti). Towards the north, the Leventina nappe is associated with the Lucomagno unit, which consists of metasedimentary basement with granitoid intrusions. The Leventina nappe shows Tertiary amphibolite-facies metamorphism, HP-relics are unknown.

Simano nappe: The Simano nappe consists of pre-intrusive basement and intruding igneous rocks. Intrusive rocks consist of a leucocratic two-mica gneiss (Verzasca-gneiss), and of coarse-grained leuco- to mesocratic augengneiss, both of granitic composition. Augengneiss dominates in the northern part of the nappe, whereas the Verzasca-gneiss dominates in the southern part. Both intrusive units obviously intruded a pre-Alpine basement. Intrusive breccias and migmatites are frequently observed in the Simano unit, as well as leucocratic and mafic dykes. Typical migmatites are usually metatexites, whereas the leucosome-rich agmatites are intrusive breccias rather than anatectic migmatites. The Simano nappe reached (Tertiary) amphibolite facies conditions, with Alpine anatexis restricted to the southernmost part of the nappe. Although elevated pressures of 12-15 kbar have been reported (Grand-jean, 2001, see also chapter eclogite; Rütti, 2003), unequivocal evidence of a Tertiary high-pressure overprint is absent.

Antigorio nappe: The nappe is dominantly composed of a granitic to granodioritic biotite-gneiss (Antigorio-gneiss), transected by various leucocratic dykes. Coarse grained augengneiss exist as well as finer grained varieties (Bevole). Though reported from the northern Antigorio (Huber, 1981), intrusive relations are usually absent. No high-pressure rocks have so far been reported from this unit, but note discussion of MO-unit below.

Maggia nappe: The Maggia nappe consists mainly of a metasedimentary basement, which is in part migmatitic and intruded by several larger intrusive bodies (Cocco- and Ruscada granitoids) and various dykes. Migmatites near larger intrusive bodies are in part diatexitic, leading to an almost continuous transition from migmatites into intrusives. No high-pressure relics have so far been reported from this unit.

Inhomogeneous units with high-pressure relics

Cima-Lunga unit: The Cima-Lunga unit, one of the classical HP-units in the Central Alps, has been interpreted as lithospheric mélange (Trommsdorff, 1990) or as part of the tectonic accretion channel (TAC, i.e. subduction channel) in the recent literature (Engi *et al*., 2001). Like the Adula-unit, the Cima-Lunga unit has a very inhomogeneous and fragmentary character, and contains as various rock types as granitoid orthogneiss, different types of meta-sediments as well as mafic and ultramafic rocks. Typical is the widespread occurrence of high-pressure relics in this unit. A large basement-slice (Vogorno-sheet), which appears to be part of the Cima-Lunga-TAC, shows macroscopic as well as geochemical characteristics identical to the underlying Verzasca-gneiss of the Simano. We propose that this sheet is a fragment of the Simano nappe, delaminated from this unit and sliced into the TAC-material.

Orselina-unit: The Orselina unit is part of the SSB and depicts characteristics very similar to that of the Cima-Lunga and Adula-units. Though very similar, Adula- as well as Cima-Lunga units cannot be directly combined with the Orselina unit (based on structural arguments), suggesting that all three units may be genetically related but represent different sections of the Alpine TAC. Up to date, no high-pressure relics have been reported from the Orselina unit west of Locarno, though such relics are known from the same unit east of Locarno (Wang, 1939). We note, however, that the western part of the Orselina unit shows much evidence of enhanced fluid and melt flow, what may have led to an effective resetting of

the unstable high-pressure assemblages.

Mergoscia-Onsernone "unit" (MO): The name is a combination of two units worked on by different authors: To the east, the unit was termed Mergoscia-Arbedo unit (Bächlin *et al*., 1981), in the lower Maggia and Onsernone area it is known as Onser-none unit (Pfeifer, 2004), and in upper Valle Maggia as Someozone (Gräter and Wenk, 2004). The MO-unit is again a fragmentary unit, however dominated by larger slices of granitoid orthogneiss (instead of metasediments), which are strongly migmatitic in the SSB ("Injektionsgneisse von Mergoscia" of the classical literature (e.g. Bächlin *et al*., 1981)), and intercalated with inhomogeneous and fragmentary trails (e.g. Cardada-trail, Gresso-trail, Vergeletto-trails). Because of their alike appearance, the granitoid orthogneiss of the MO-unit in the Maggia-Onsernone area cannot be well differentiated from the underlying Antigorio-gneiss, the only difference probably being a usually finer grain size of the MO-unit compared to the typical Antigorio gneiss. This complicates of course a clear delineation of the limit between the two units. MO- and Antigorio unit may however be distinguished based on petrologic arguments, because the MO-unit contains inhomogeneous trails of varying thickness, composed of metasediments, mafic and ultramafic rocks, with included relics of high-pressure metamorphism (see also chapter 5). Similar to our interpretation of the Vogorno-sheet, we interpret the MO-unit as slices of the Antigorio-unit, wedged into the TAC. The thickness of the inhomogeneous TAC-trails is usually relatively reduced, not overstepping a few tens of metres. The northernmost high-pressure relics are found in the upper Valle Maggia near Bignasco (see 5). As an alternative of the above interpretation of the MO-unit, it may be proposed that the MO-unit is integral part of the Antigorio unit, indicating that the complete Antigorio unit had experienced high pressure conditions at least in its southern part.

Inhomogeneous units without eclogite relics

Inhomogeneous boundary series between Leventina and Simano units: Consists of an inhomogeneous series of metasediments, mafic rocks, and slices of orthogneiss, the latter identical in type to the Simano-augengneiss (compare with Casasopra 1939, Bianconi (1971) and Keller *et al*. (1980)). No high pressure relics have so far been reported from this unit, despite of its petrographic similarity with the TAC-units.

Discussion of the profiles:

We have constructed two series of roughly N-S striking profiles, one series for the Maggia-Onsernone area, the other for the Verzasca-area (plate 1). Towards the north, the profiles bend to the east, as a function of the change in strike of the fold hinges and lineations (which are usually parallel in the study area), from an E-W into a N-S direction. This allowed a construction perpendicular to these linear elements. For construction we used own survey data, as well as data from published and unpublished literature (Kobe, 1956; Knup, 1958; Wenk, 1980?; Häuselmann, 1997; Burri, 1999; Gruskovnjak, 2002; Leonardi, 2003; Pfeifer, 2004; Gräter & Wenk, 2004). Structural measurements are denoted in blue, interpolated foliation traces in red. Foliation traces depict always the main foliation in an area, which may especially in the SSB be D3/D4-foliations rather than D1/D2-foliations (see below).

Delineation of the different tectonic units is based in part on own survey data (Onsernone-Maggia area) and on limits taken from the above cited authors. We point out, however, that the delineation of the Maggia from the MO-unit in the Vergeletto area is in part complicate, because unequivocal Mesozoic sediments are missing. Furthermore, a clear differentiation between Antigorio and MO-unit is almost impossible, based on the above mentioned similarities. Therefore the profiles in the Onsernone-Maggia area should mainly be used to infer structures of this area, and nappe boundaries should be taken as preliminary.

Maggia-Onsernone profiles

Profiles 1 to 6 lead through the Centovalli-Onsernone-Maggia area. As shown in figure 2, the profiles form a more or less continuous W-E section through the study area. Due to the occurrence of metaeclogite-bearing trails, we have interpreted the MO-unit as a stack of orthogneiss-slivers, delimited from each other by discontinuous inhomogeneous trails and/or shear horizons. Contacts of the individual sliver are drawn slightly discordant to the main schistosity (foliation traces). Discordance is however too small to be recognised in the field and may have been overprinted by D2. Because of the discontinuous and fragmentary character of these trails, the internal construction of the Onsernone unit is in part idealised. The main structure observed is the open D3-fold in the southern part of the area, where the Antigorio and the MO-units are backfolded from a roughly flat lying into a steeply inclined position. The north dipping axial plane foliation of the D3-fold is usually not well developed and is inferred from local parasitic folds in the order of centimetres to tens of metres. Structures in the Orselina unit keep up steepening towards the south until they get overturned. A structural discordance inside the Orselina unit is interpreted as a fault or an internal thrust (profiles 1-3), was however also interpreted as a synformal struc-

ture (Maxelon & Mancktelow, 2002). An alternative interpretation may be that refolded D2-foliations become completely overprinted by D4-foliations in the SSB in the south.

Towards the north, the following succession of syn- and antiforms is recognised on the profiles: In the westernmost profile 1, the open D3-backfold grades into the open Onsernone-Antiform and Vergeletto-Synform (the so called Vergeletto-Löffel (Wenk, 1953; Kobe, 1956; Knup, 1958)), followed by the open Maggia-Antiform and the larger scale Maggia-Synform - Verzasca-Antiform pair. In contrast to other folds of the area, the Verzasca-Antiform is not an open fold structure but a rather tight, strongly asymmetric fold with one overturned limb. Based on our own structural survey and on the structural data of the literature it remains ambiguous whether the Maggia-synform should really be considered as a synformal structure as proposed e.g. by Steck (1998). Our relatively restricted dataset in this area allows only the preliminary conclusion that the structures inside the Maggia-Synform become much more irregular compared to the structures observed to the SW and NE of this structure. Furthermore, the structural data shows a fan-like structure, with planar elements dipping gently to the NE in the SW (Maggia-Antiform), continuously steepening to the NE, and finally completely bending around the hinge of the Verzasca-Antiform, into a flat lying orientation. The fan structure is better visible when comparing profiles 3 and 4. The unsteady appearance of the foliations inside the "synform" suggests in our view a refolding of the D1 and D2 structures of the Maggia-nappe. Thus the Maggia-synform is interpreted as a D3-structure at least in respect to the Maggia nappe. The D3 folding of the Maggia-nappe may however be related to a D2-folding of the Simano unit. Although we remain unsure about the significance of the Maggia-Synform, we put forward that there is no doubt about the existence of the Verzasca-Antiform, as recently questioned by Maxelon & Mancktelow (2002). Recent investigations along a northern part of the antiform have confirmed the existence of an antiformal structure (Allaz and Maeder, 2003; Chevalier, 2005) as proposed some decades before by Keller (1968).

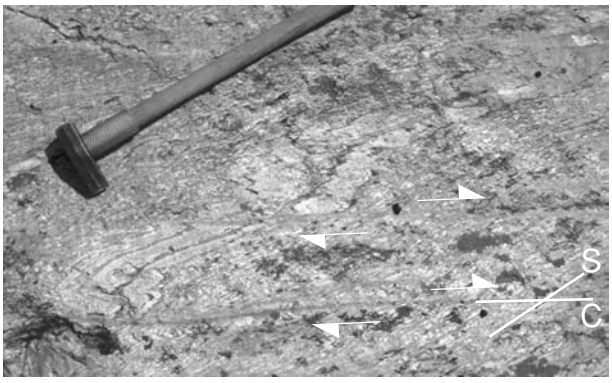

Fig. 2 Dextral shear-zones accompany the Pertusio-trail in Valle di Prato (locality Monti di Predee). The shear-zones transect and displace an augen- to cigar-gneiss of the boundary area (note displaced leucocratic veins, which have been folded prior to the displacement). Note S-Z relations between Alpine D2-foliation and D3-shear-zones. Hammer for scale.

The northernmost structure of significance in the context of this study is the so called Pertusio-trail. This trail was distinguished from the enclosing Simano- and Maggia-nappes based on its structural position close to the hinge of the Verzasca-Antiform, based on the occurrence of metasediments, and based on the change in lithology when overstepping this zone (Keller, 1968; Gräter & Wenk, 2004). Detailed survey in the Alpe Sambucco area (Val d'Osura), revealed that this zone is accompanied by an important shear-horizon, which increasingly changes the well preserved diatexitic migmatites of the Maggia-nappe into mylonitic banded gneisses of the boundary zone (Chevalier, 2005). These banded gneisses border against non-migmatitic, mesocratic meta/sediments of probably marly composition. The complete lack of features of migma-tisation in these metasediments suggests that they are younger than the Variscan migmatites, thus that they are of late Palaeozoic to Mesozoic age. Their marly composition indicate a Bünderschiefer-type protolith. The metasediments again border against mylonitic augen- to cigar- orthogneiss of the Simano unit, which grade into less deformed typical Simano-Augengneiss.

In our view, these observed features outline the Pertusio-trail as an important shear-zone between Simano- and Maggia-nappes. Observed linear elements are roughly horizontal, indicating a NW-SE directed transport direction in this part of the Pertusio-shear-zone, in line with the recent proposition of Pfiffner *et al*. (2002) that the Pertusio-trail has acted as a transcurrent shear-zone. All these features appear consistent with the interpretation of a nappe boundary zone. Further to the north of this trail, at Valle di Prato, this trail is characterised by the occurrence of metapelites and a few marbles, accompanied by a shear-horizon in granitoid gneisses, indicating dextral sense of shear (Fig. 2).

Deformation sequence

All so far mentioned syn- and antiforms are D3 structures, because they refold the respective local D1/D2-main foliation. This definition of the D3-structures does not imply an exact temporal coincidence of their formation; in contrast, these structures may even have formed in sequence (e.g. from E to W). However, all D3-structures are bent into the SSB, and/or are tightened towards the east, during a fourth phase of deformation (D4). This is well visible when proceeding from the western- to the easternmost profile: the above described sequence of antiforms and synforms remains roughly constant towards the east (profile 1-5), however all syn- and antiformal structures become tighter towards the east and converge inside the SSB near Locarno (see also plate 1). In the lowermost Valle Maggia, the differ-

ent folds appear tightly compressed, with fold-limbs synparallel to each other. Whereas in profile 5 still several syn- and antiforms may be inferred, they can no longer be differentiated in profile 6. The Maggia- and the Vergeletto-Synforms (seem to) coincide east of Locarno (see Vogorno-profiles), while the intermediate Maggia-Antiform disappears into depth. The MO-unit in the lowermost Valle Maggia is characterised by in part migmatitic granitoid gneiss with undulating, roughly vertical foliation (profile 6). Though relic fold hinge-structures are locally still visible, the Onsernone-Antiform, which grades into this structure, is no longer distinguishable. Obviously, the Onsernone-orthogneiss was strongly overprinted by a new-forming foliation in the SSB, which we also attribute to the D4-phase of deformation. Note that to the north of the Onser-none-Antiform in profile 5, a metasedimentary trail still reflects the structure of the antiform, while dominantly steep structures are observed in the underlying orthogneiss below the trail, and almost exclusively vertical structures in the same unit only a few kilometres to the east (profile 6). This strong overprint must be related to backthrusting and dextral transpression, which focused deformation into the SSB.
Note that in our interpretation the open D3-folds are related to backfolding, while the tightening and bending of the D3-structures (e.g. Onsernone-Antiform) as well as the strong overprint of D1-3-foliations by D4-structures in the SSB is related to backthrusting and compression in a transpressional regime.

Some points of discussion:

(A) The lower limit of the Maggia nappe in the Vergeletto-Onsernone area is not easy to map. As a result, the interpretation of the boundary changes considerably with the respective author (see nappe schemes in Preiswerk (1921), Kündig (1936), Kobe (1956), Knup (1958) and Spicher (1980)). Several authors have used the carbonate bearing inhomogeneous trails below Rosso di Ribia as the tectonic boundary between Maggia and Antigorio nappes. This attribution based however predominantly on the interpretation of these carbonates as Mesozoic nappe divides, neglecting the fact that other, very similar trails occur to the west as well as to the east of this trail, and that the orthogneiss in the footwall and hanging wall of the trail appear identical. An effect of this assumed boundary was a "bimodal Maggia nappe" in the Vergeletto area, with an upper "metasedimentary" unit, and a lower orthogneiss unit (with gneiss identical to the underlying Antigorio unit)"(see tectonic profile in Knup (1958)). In our view, rocks typical for the Maggia nappe first occur near Pizzo Molinera in the Vergeletto area, and to the east of this crest. This leads to an adjustment of the lower boundary of the Maggia unit in the Vergeletto area, as shown in the profiles and in figure 1.

(B) When comparing the northern and southern end of the Onsernone-Antiform, it appears that the Maggia nappe should meet the Orselina-unit somewhere in the air above Valle Onsernone. Based on petrography however, it can be excluded that Maggia and Orselina units have any genetic relationship (see description of different units above). Since there exists no indication of a reappearance of the Maggia nappe on the southern flank of Valle Onsernone, we conclude that the Maggia nappe must strike out in the air above Valle Onsernone. Similarly, the Orselina unit does not appear in the Vergeletto area, at least not in the same thickness as found in the Centovalli area. Instead, several inhomogeneous trails, in part with high contents of mafic rocks, occur to the north of Valle Vergeletto, intercalated with granitoid gneisses of Antigorio-type (MO-unit). Some of these trails have recently been found to contain relics of high pressure rocks (see chapter 5), and were therefore gathered, together with the surrounding orthogneisses, into the MO-unit (instead of being attributed to the Maggia nappe, as explained above). Nevertheless, when comparing the thickness of the inhomogeneous trails with that of the Orselina unit in the Centovalli area, the change in thickness is dramatic.
Our preliminary concept implies that the Antigorio-MO-nappe-stack got exhumed along the contact with the Orselina-TAC, suggesting that two different TAC-levels are now juxtaposed. One argument in favour of this hypothesis is the lack in high pressure rocks in the Orselina unit to the west of Locarno, indicating that the Orselina unit may represent a structurally higher TAC-level than the eclogite bearing (underlying) MO-unit. Note however that the Orselina unit west of Locarno shows many features characteristic of an enhanced melt and fluid flow, which may have promoted retrogradation of high-grade assemblages.
Of additional importance is the complete lack of high pressure rocks from the Maggia-nappe, which thus has never been subducted to considerable depth. The observed situation is similar to that in found in the Verzasca-profiles, where the Maggia-nappe overlies the high-pressure Cima-Lunga TAC, and gets into structurally ambiguous contact with the HP-Orselina unit to the south.
(C) In the Valle Verzasca-area, the Maggia nappe overlies the high pressure Cima-Lunga unit, which again tops the Simano unit. In the Maggia section, the Maggia nappe overlies the MO-unit, which grades into the underlying Antigorio unit. Thus, if the Maggia-Crossfold, as proposed (e.g. Steck, 1998), is a synformal structure, Antigorio and Simano-nappe are tectonic equivalents. Based on petrographic comparison of Simano and Antigorio nappes, this correlation is not straight forward (see description of the different units above). Furthermore, geochemistry shows that the plutonic bodies of the Simano nappe (leucogranite trend) are distinct

from those of the Antigorio nappe (calcalkaline trend) (see chapter Vogorno). However, Simano as well as Antigorio nappes contain abundant augen-gneiss in the northern half of the Lepontine area, the geochemistry of which could not be compared due to lack of data.
Recently, Maxelon & Mancktelow (2002) have proposed that Antigorio and Leventina nappes can be correlated using structural interpolation. Based on petrography this is feasible, since both, Antigorio as well as Leventina nappe dominantly consist of a relatively homogeneous orthogneiss. However, geochemistry again reveals differences between the two units, the Leventina nappe exhibiting a leucogranitic trend, and the Antigorio a calcalkaline trend. Thus, based on structural and geochemical arguments, the Antigorio nappe could be related to the Leventina nappe as good as to the Simano nappe, however with very contrasting consequences for the Maggia-Crossfold:
(a) If Antigorio and Leventina nappes are equivalents, the Verzasca-Antiform must denote the lateral, southwestern end of the Simano nappe. The Maggia-Synform would thus be related to the emplacement of the Simano nappe (D2 in Simano), which leads to a refolding of the Maggia nappe (D3 in Maggia). The down-bowing of the Antigorio nappe to the northeast of the Maggia-Antiform thus reflects a change in thickness of the nappe-stack as the Simano nappe appears to the NE. The Pertusio-shear-zone may thus be regarded as a lateral nappe boundary.
(b) On the other hand, if Antigorio and Simano nappes are tectonic equivalents, the Maggia-Synform must be related to a (D3) refolding of the whole nappe stack in the Lepontine area (Simano-Antigorio nappe folded around the hinge of the Crossfold). Note that because the Maggia-Synform is bent into the SSB, it must be older than the backthrust (D4) that is related to the transpressional phase. The crossfold must therefore be the expression of strong E-W convergence, preceding the N-S directed transpression.
(c) We favour a yet different alternative for the formation of the crossfold. We emphasise the unique fold style of the crossfold (overturned limb) and its association with the Pertusio-shear-zone. If we assume an internally pre-structured Antigorio - Simano nappe, deformation may concentrate into zones of high competency contrast (proto-Pertusio shear-zone). Further transpression may lead to the development of a nappe-internal lateral ramp, along which dextral shear as well as E-W convergence may be accommodated (Pertusio shear-zone). In our view, the Maggia-Crossfold has formed during emplacement of the Antigorio-Simano nappe, as a result of the formation of a nappe internal lateral ramp. The Pertusio shear zone thus acted as a nappe divide between Maggia and Antigorio-Simano nappe. The down-bowing of the Antigorio nappe to the NE is thus the expression of the lateral thrusting of the Simano nappe onto the Antigorio nappe.
In line with interpretations of Keller *et al*. (1980), but in contrast to other interpretations (Spicher, 1980; Grujic & Mancktelow, 1996; Steck, 1998, Preiswerk, 1934 #464), the Pertusio-trail cannot be connected to the north with the Mesozoic metasediments near Mogno (Valle Lavizzara), but strikes out in the air, parallel to the lineations and parallel to the folded base of the Maggia nappe. It is possible, though not necessary, that the unit in the Lago del Sambucco area (Valle Lavizzara) again belong to the Maggia nappe, which had then to be refolded along the front of the Simano-Antigorio nappe. Geochemical comparison of magmatic rocks of the Maggia nappe and of the Sambucco area revealed a strong correspondence, suggesting that the two units may have a common origin (Burri, 1999; Gruskovnjak, 2002). Note that we disagree with the interpretation on the Tectonic map of Switzerland ((Spicher, 1980)), which proposes a narrow connection between Maggia (s.s.) and Sambucco-unit. Due to structural arguments, every connection between the two units must strike out into the air, thus must have been eroded.
(D) Detailed survey in the Onsernone-Vergeletto area revealed that the Onsernone-Antiform shows evidence of internal thrusting, at least in the order of tens of meters (ductile shear-zones displacing the already folded structures of the Antiform). We have therefore tentatively introduced several thrusts into the interior of the Onsernone Antiform (profiles 2-5). This observation could also suggest that the Onsernone-fold grades into a thrust towards the east, as depicted in the hypothetic sequence sketched in figure 3. The sketch shows an E-W-, as well as a temporal development of the Onsernone-Antiform.

Vogorno profiles

Profiles 7-9 are situated in the Locarno-Verzasca area. Topography and several structural measurements are taken from unpublished profiles of Eduard Wenk. Again, the main structure visible in these profiles is the D3-backfolding of the nappe-stack into vertical to even overturned structures in the SSB. Maggia-, Simano- and Cima-Lunga units are folded around the marked, though very open D3-fold hinge. In contrast to older interpretations (Bächlin *et al*., 1981) the Maggia nappe reoccurs towards the north, e.g. in the area around Poncione dei Laghetti. The existence of the Maggia-nappe in this area has been confirmed by two recent studies, based on structural, petrologic and geochemical evidence (Gruskovnjak, 2002; Leonardi, 2003). Therefore, the nappe sequence in this area is defined from bottom to top by the Leventina, Simano (which appears astonishingly narrow in profile 7), Cima-Lunga and Maggia units. This shows that although now eroded, the Maggia-nappe must have topped the Simano-unit also in the upper Valle Verzasca sections (e.g. profiles 3-6), like it tops the Antigorio nappe in the Maggia area.

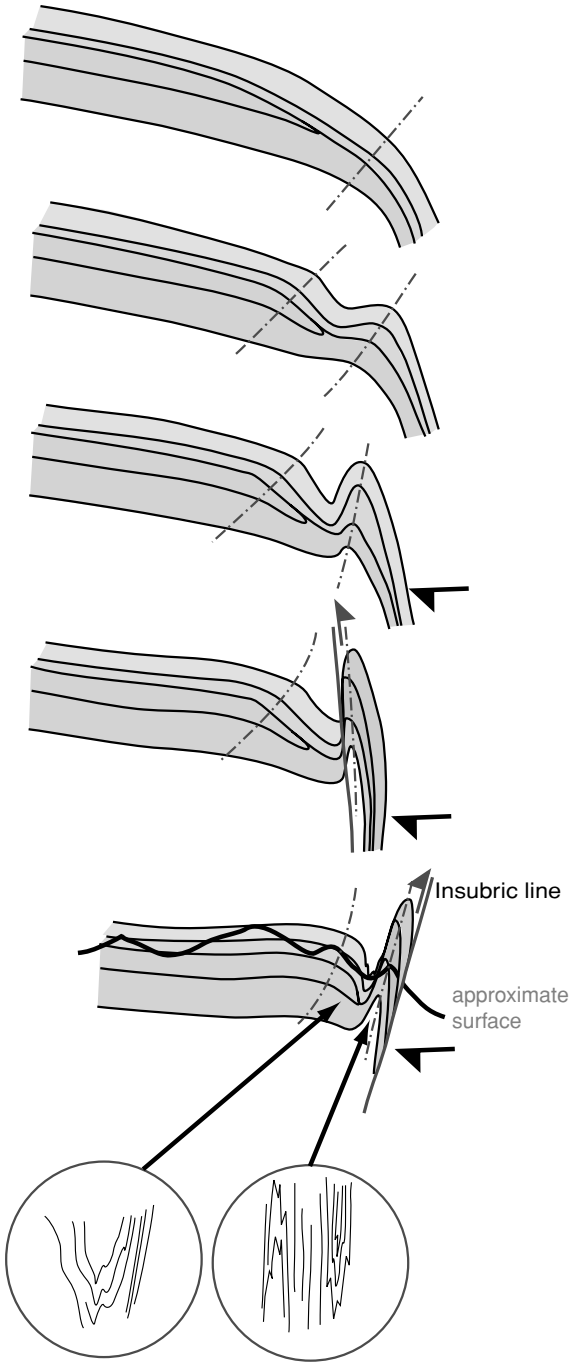

Fig. 3 Sketch depicting the formation of the backfold and the associated Onsernone-Antiform. The sketch can be interpreted as a W-E-profile as well as a kinematic scenario.

One complication in the Verzasca section is the appearance of the southwards thinning Vogorno-sheet, which is bent into the SSB along the D3-fold hinge, like the Simano and Cima-Lunga nappes. Based on its geochemical characteristics, the sheet cannot be distinguished from the underlying Simano unit, although separated from the latter by the HP-Cima-Lunga unit. We interpret the Vogorno sheet as a slice of the Simano nappe emplaced in the Cima-Lunga TAC-unit. The frontal fold of the sheet is well visualised by the structural measurements in profile 9. The position of the sheet on top of the Simano unit implies that the TAC was thrusted onto the Simano nappe. The sheet can probably be followed also on the western side of Valle Verzasca, where it dies out near Poncione di Piancascia (see plate 1, also in Gräter and Wenk (2004)).

Another complicating point is the structure of the Maggia nappe to the south. As we have shown above, Maggia- as well as Vergeletto-Synforms converge to the west and can no longer be differentiated in the Verzasca area. Although the generally vertical and tight structures do no longer allow a clear outline of the synformal structures in the Verzasca area, we have tentatively sketched a synformal structure. Based on the Verzasca profiles only, another interpretation would be that the Maggia nappe bends down into the SSB without forming a synformal structure, thus similar to the Leventina and Simano nappes. By contrast, we did not outline an antiformal structure in the MO-unit, as foliations are dominantly steep and lack evidence of an antiform, probably as a result of the strong D4-overprint.

Conclusion

In this study we have presented new structural profiles through the southwestern Lepontine area. We have discussed implications and consequences resulting from these profiles and have introduced some new concepts. Although the study may provide some insight into the tectonic characteristics of the study area, some of the structures remain ambiguous also after this study, wherefore we characterise this short contribution as a working report.

The structures of the study area can be attributed to four distinct phases of deformation. D1 and D2 are probably related to subduction and thrusting (or nappe emplacement), and have led to the dominant foliation in most of the study area. A third deformation phase, related to backfolding of the Central Alps, has led to the major D3-backfold along the SSB, as well as to several open syn- and antiforms. The Maggia-Crossfold, a major structure of the study area, is also attributed to D3. The fourth phase of deformation has led to further rotation of the D3-structures into parallelism with the SSB, and to tightening and convergence of the structures. In the SSB, the strong and focused transpressional deformation has strongly overprinted the D1-3 structures and has led to a new D4-foliation.

Based mainly on petrologic and petrographic evidence, we have proposed that the Maggia and the Antigorio nappes are separated from each other by the HP-bearing MO-unit, which has a position equivalent to the Cima-Lunga unit in the Verzasca area. The exact location of the boundaries is complicated by the fact that slices of Antigorio-type rocks are part of the MO-TAC, and that the inhomogeneous trails are often very reduced and discontinuous.

References

Allaz, J. & Maeder, X. (2003): Evolution tectonique et métamorphique de la nappe de Simano à l'Alpe Larecc, Valle Maggia (Tessin, Suisse). Université de Lausanne, 177 pp.

Bächlin, R., Bianconi, F., Codoni, A., Vesco, E. D., Knoblauch, P., Kündig, E., Reinhard, M., Spaenhauer, F., Spicher, A., Trommsdorff, V. & Wenk, E. (1981): Blatt 1313 Bellinzona. Geologischer Atlas der Schweiz ed. Schweizerische Geologische Kommission.

Bianconi, F. (1971): Geologia e petrografia della regione del Campolungo. Beiträge zur Geologischen Karte der Schweiz Nuova serie, 142°. Schweizerische Geologische Kommission, 238 pp.

Burri, T. (1999): Metamorphism and tectonics within the Vergeletto "Spoon" (Southern Valle Maggia, Ticino). Diploma Thesis, University of Berne, 112 pp.

Casasopra, S. (1939): Studio petrografico dello gneiss granitico Leventina. Schweiz. Mineral. Petrogr. Mitt. 19, 449-709.

Chevalier, G. (2005): Unpublished Masters thesis, in prep. Universität Bern.

Engi, M., Berger, A. & Roselle, G. T. (2001): Role of the tectonic accretion channel in collisional orogeny. Geology 29/12, 1143-1146.

Grandjean, V. (2001): Petrographical evolution of mafic relics and their implication for the geodynamics of the Central Alps. Dissertation, University of Berne, 103 pp.

Gräter, P. & Wenk, E. (2004): Geologischer Atlas der Schweiz, Blatt 1292 Maggia, draft version. Schweizerische Geologische Kommission.

Grujic, D. & Mancktelow, N. S. (1996): Structure of the northern Maggia and Lebendun nappes, Central Alps, Switzerland. Eclogae geol. Helv. 89/1, 461-504.

Gruskovnjak, A. (2002): Geologische und petrographische Untersuchungen im Lepontin im Grenzbereich von Maggia- und Simanodecke (Ticino). Diplomarbeit, Universität Bern, 87 pp.

Häuselmann, P. (1997): Zur Geologie des Val Vergeletto (Ti). Diplomarbeit, Bern, 98 pp.

Heitzmann, P. (1987): Evidence of late Oligocene/early Miocene backthrusting in the central alpine "root zone". Geodinamica Acta 1/3, 182-192.

Huber, M., Ramsay, J. & Simpson, C. (1980): Deformation in the Maggia and Antigorio nappes, Lepontine Alps. Eclogae geol. Helv. 73/2, 593-606.

Huber, M. I. (1981): Geologisch-strukturelle Untersuchungen im oberen Maggiagebiet (Tessin, Schweiz). Dissertation, Mitteilungen aus dem Geologischen Institut der ETH und der Universität Zürich, Neue Folge Nr 238, ETH Zürich, 221 pp.

Keller, F. (1968): Mineralparagenesen und Geologie der Campo Tencia-Pizzo Forno-Gebirgsgruppe. Beiträge zur Geologischen Karte der Schweiz Neue Folge, 135. Liegerung. Schweizerische Geologische Kommission, Bern, 71 pp.

Keller, F., Wenk, E., Bianconi, F. & Hasler, P. (1980): Geologischer Atlas der Schweiz, Blatt 1272 P. Campo Tencia. Schweizerische Geologische Kommission, .

Knup, P. (1958): Geologie und Petrographie des Gebietes zwischen Centovalli-Valle Vigezzo und Onsernone. Schweiz. Mineral. Petrogr. Mitt. 38/1, 236.

Kobe, H. (1956): Geologisch-Petrographische Untersuchungen in der Tessiner Wurzelzone zwischen Vergeletto-Onsernone und Valle Maggia. Schweiz. Mineral. Petrogr. Mitt. 36/1.

Kündig, E. (1936): Tektonischer Ueberblick über die gesamten Tessiner Alpen. Beiträge zur geologischen Karte der Schweiz 71.

Leonardi, U. (2003): Zur Abgrenzung und Entwicklung der Cima Lunga und angrenzende Einheiten im Gebiet von Valle di Drosina - Valle di Lodrino (Kanton Tessin). Diplomarbeit, Universität Bern, 105 pp.

Maxelon, M. & Mancktelow, N. S. (2002): Regional correlation of polyphase fold structures in the Central Alps - An approach based on 3D geometric modelling: Penrose Conference: Three-Dimensional Flow, Fabric Development, and Strain in Deformed Rocks and the Significance for Mountain Building Processes:New Approaches. Monte Verita, Switzerland.

Milnes, A. G. (1974): Post-Nappe Folding in the Western Lepontine Alps. Eclogae geol. Helv. 67/2, 333-348.

Pfeifer, H. R. (2004): Geologischer Atlas der Schweiz, Blatt 1312 Locarno, draft version. Schweizerische Geologische Kommission.

Pfiffner-O-A, Schlunegger-F & Buiter-Susanne-J-H (2002): The Swiss Alps and their peripheral foreland basin; stratigraphic response to deep crustal processes. Tectonics 21/2, 16.

Preiswerk, H. (1918): Geologische Beschreibung der Lepontinischen Alpen, Zweiter Teil. Oberes Tessin= und Maggiagebiet. Beiträge zur geologischen Karte der Schweiz 26/Spezialkarte 81, 43-81.

Preiswerk, H. (1921): Die zwei Deckenkulminationen Tosa-Tessin und die Tessiner Querfalte. Eclogae geol. Helv. 16/4, 484-496.

Preiswerk, H., Bossard, L., Grütter, O., Niggli, P., Kündig, E. & Ambühl, E. (1934): Geologische Spezialkarte Nr 116: Geologische Karte der Tessineralpen zwischen Maggia- und Blenio-Tal. Schweizerische Geologische Kommission.

Rütti, R. (2003): The tectono-metamorphic evolution of the northwestern Simano Nappe (Central Alps, Switzerland). Doctoral thesis, ETH-Zürich, 112 pp.

Schmid, S. M., Aebli, H. R., Heller, F. & Zingg, A. (1989): The role of the Periadriatic Line in the tectonic evolution of the Alps. In: Coward, M. P., Dietrich, D. & Park, R. G. : Alpine tectonics Geological Society Special Publication 45. Geological Society of London, , 153-171.

Schmidt, C., Preiswerk, H. & Stella, A. (1908): Geologische Karte der Simplongruppe mit Profilen und Erlauterungen. Beitr. XXVI

Spicher, A. (1980): Tektonische/Geologische Karte der Schweiz. Schweizerische Geologische Kommission.

Steck, A. (1998): The Maggia cross-fold; an enigmatic structure of the Lower Penninic nappes of the. Eclogae geol. Helv. 91/3, 333-343.

Trommsdorff, V. (1990): Metamorphism and tectonics in the Central Alps: The Alpine lithospheric mélange of Cima Lunga and Adula. Mem. Soc. Geol. It. 45, 39-49.

Wang, H. S. (1939): Petrographische Untersuchungen im Gebiet der Zone von Bellinzona. Schweiz. Mineral. Petrogr. Mitt. 19/1, 19-200.

Wenk, E. (1953): Prinzipielles zur geologischen Gliederung des Penninikums im zentralen Tessin. Eclogae geol. Helv. 46, 9-21.

Wenk, E. (1980?): Unpublished geological profiles through the Verzasca area, draft version.

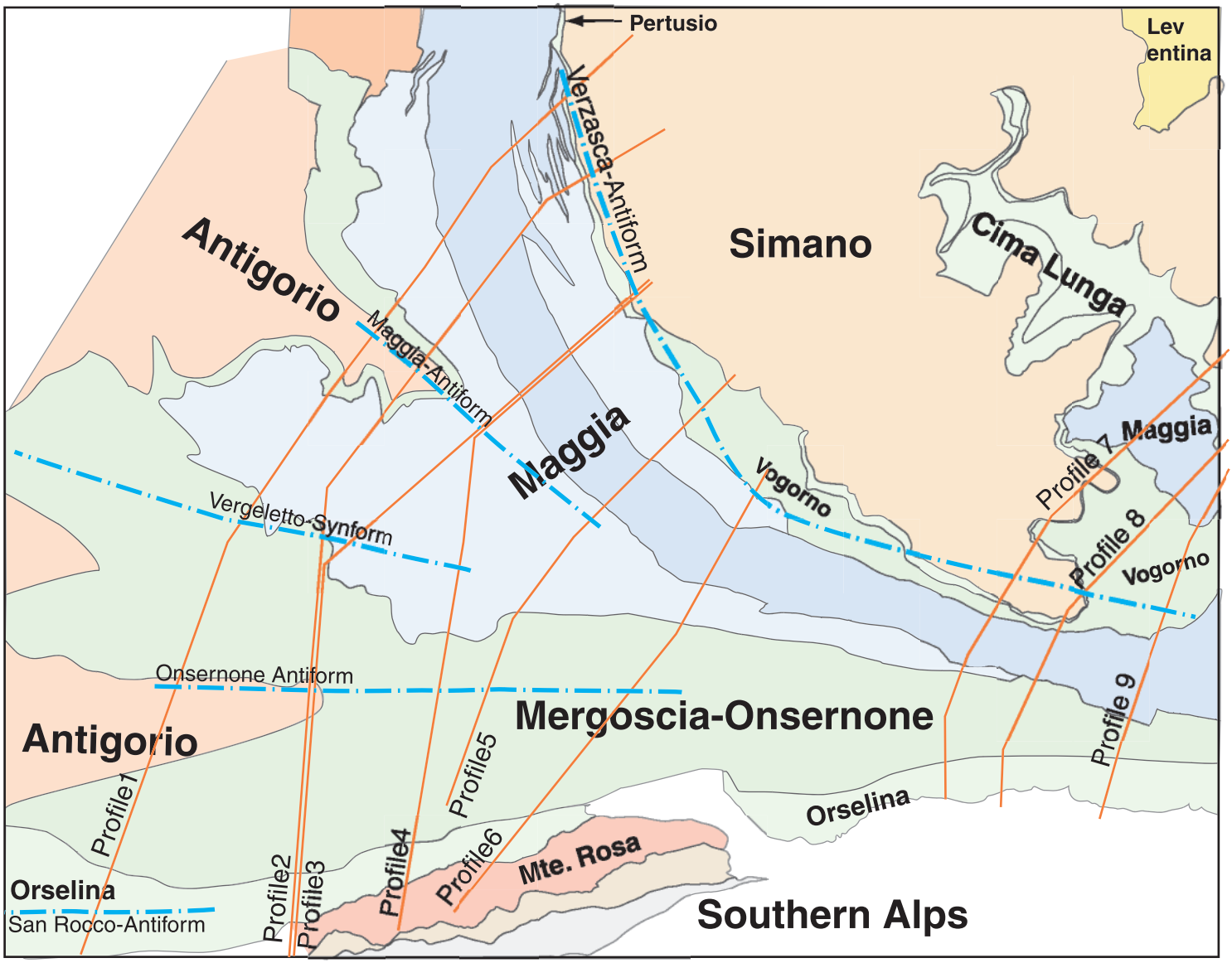
Pertusio
Lev
entina
Verzasca-Antiform
Antigorio
Simano
Cima Lunga
Maggia-Antiform
Maggia
Maggia
Vogorno
Profile 7
Vergeletto-Synform
Profile 8
Vogorno
Onsernone Antiform
Mergoscia-Onsernone
Antigorio
Profile 9
Profile1
Profile5
Orselina
Profile2
Profile3
Profile4
Profile6
Mte. Rosa
Orselina
San Rocco-Antiform
Southern Alps

Profile-Series
Maggia-Onsernone-Centovalli

- Simano-unit
- Vogorno sheet
- Pertusio-zone
- Monte Rosa-unit
- Orselina-unit
- Maggia-unit
- Onsernone-Mergoscia unit
- Antigorio-unit

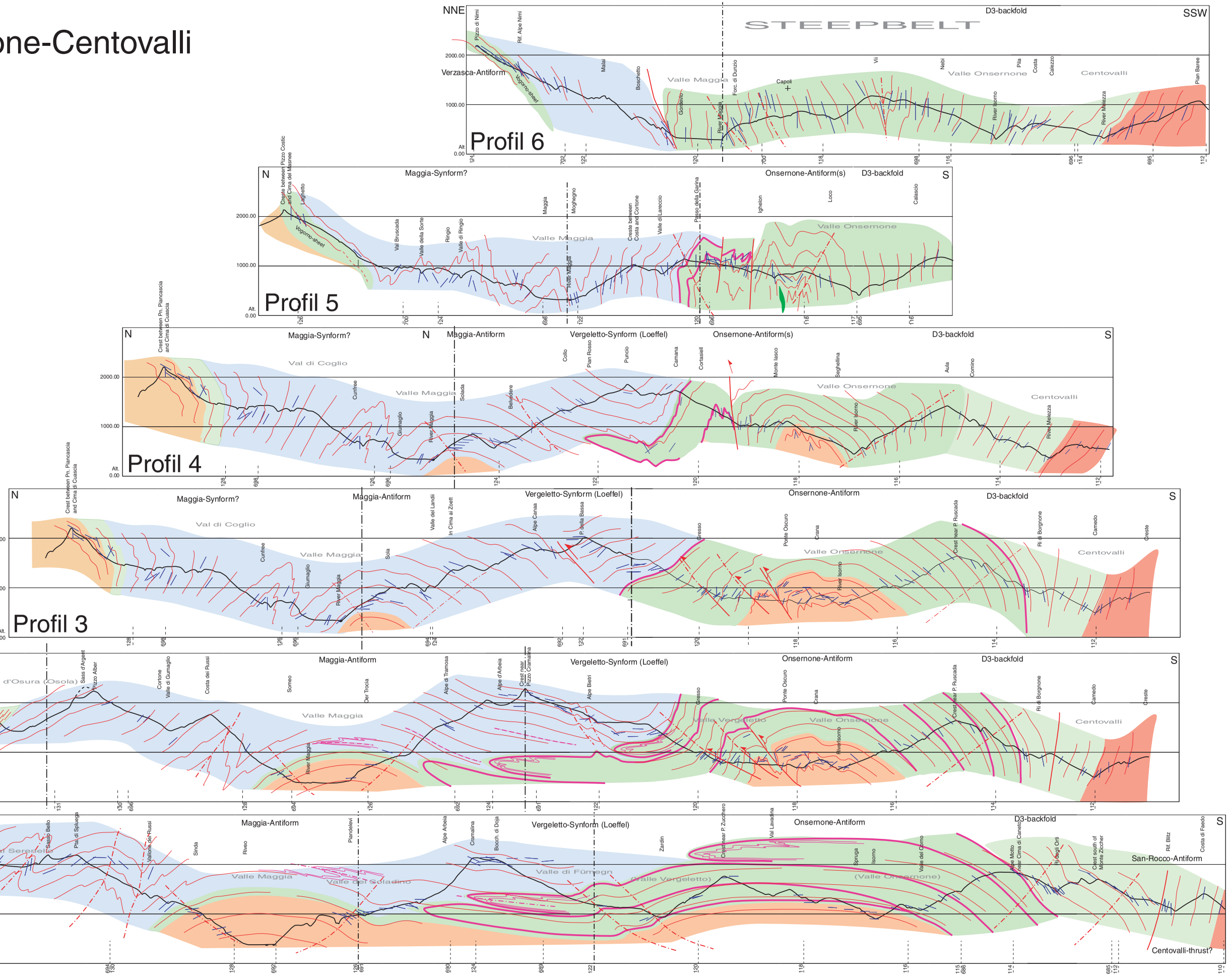

Plate 2

Profile-Series Verzasca